

HYDROTHERMAL ALTERATION AND MINERALISATION OF  
THE NIGERIAN ANOROGENIC RING COMPLEXES: WITH  
SPECIAL REFERENCE TO THE SAIYA SHOKOBO COMPLEX

Judith A. Kinnaird

A Thesis Submitted for the Degree of PhD  
at the  
University of St Andrews



1987

Full metadata for this item is available in  
St Andrews Research Repository  
at:  
<http://research-repository.st-andrews.ac.uk/>

Please use this identifier to cite or link to this item:  
<http://hdl.handle.net/10023/13407>

This item is protected by original copyright

**Hydrothermal alteration and mineralisation of  
the Nigerian anorogenic ring complexes:  
with special reference to the Saiya Shokobo Complex**

by

**Judith Ann Kinnaird**

**May, 1987**



ProQuest Number: 10171304

All rights reserved

INFORMATION TO ALL USERS

The quality of this reproduction is dependent upon the quality of the copy submitted.

In the unlikely event that the author did not send a complete manuscript and there are missing pages, these will be noted. Also, if material had to be removed, a note will indicate the deletion.



ProQuest 10171304

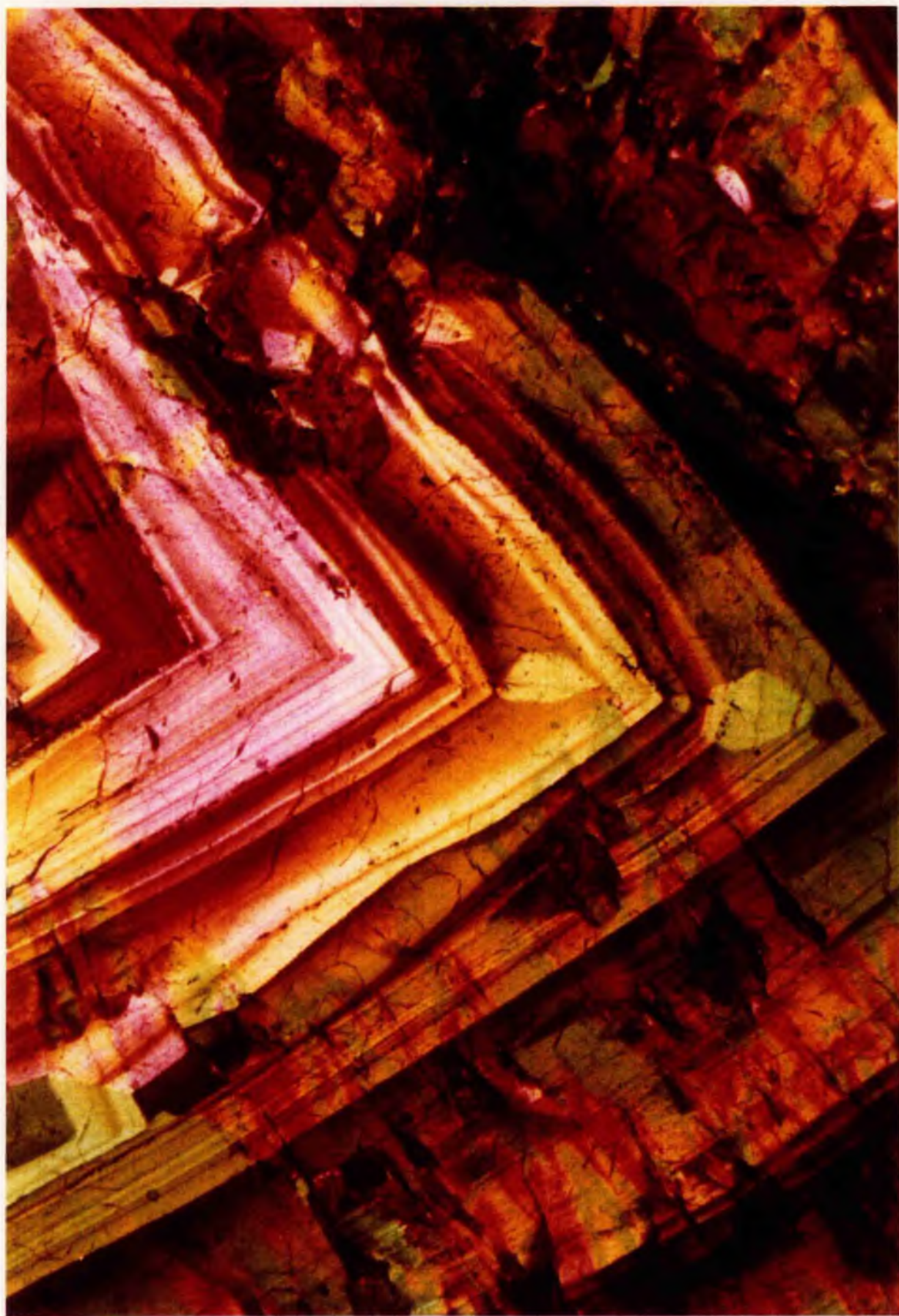
Published by ProQuest LLC (2017). Copyright of the Dissertation is held by the Author.

All rights reserved.

This work is protected against unauthorized copying under Title 17, United States Code  
Microform Edition © ProQuest LLC.

ProQuest LLC.  
789 East Eisenhower Parkway  
P.O. Box 1346  
Ann Arbor, MI 48106 – 1346

TW  
A 598



CERTIFICATE

I hereby certify that Judith A. Kinnaird has been engaged in research at the University of St. Andrews, that she has fulfilled the conditions of Ordinance No. 12 (St Andrews) and Resolution of the University Court, 1967 No. 1, and that she is entitled to submit this thesis in application for the degree of Doctor of Philosophy

I certify that the following thesis is of my own composition, that it is based on the results of research carried out by me, and that it has not been previously presented in application for a higher degree.

---

**For my parents**

Rocks, like everything else,  
are subject to change  
and so also are our views of them

Loewinson-Lessing, 1936

## ABSTRACT

The Nigerian anorogenic province is characterised by more than 50 complexes. In some complexes, the outer limits of the complexes are defined partly or completely by a ring dyke. This intrusion, generally composed of granite porphyry, was the chief structural element of the complex and controlled the distribution of both volcanic and subvolcanic magmatism at high levels in the crust.

The complexes are exposed at different erosional levels: in some complexes, particularly in the north, the volcanic products are preserved through caldera collapse. The majority of the volcanics are dominantly rhyolitic, some alkaline centres have preserved occasional successions of hawaiites, mugearites and trachytes confirming the dominantly alkaline trend from transitional ne-normative or hy-normative basalts. In other centres the volcanic cover has been removed so that the subvolcanic granites and syenites have been exposed.

The subvolcanic assemblages include minor gabbros, monzogabbros and syenites. However granitic rocks are overwhelmingly dominant with fayalite hedenbergite granites, amphibole granites and syenites, albite-rich and albite-poor aegirine arfvedsonite granites and biotite granites.

As far as the granites are concerned there was a natural progression from volcanic feeder intrusions to subvolcanic intrusions with fayalite and hedenbergite. The volcanic feeder intrusions were an important link during the caldera-forming stage between the subvolcanic roots and the overlying volcanic pile. They are represented by quartz and granite porphyries.

The mineralogical assemblages of many of these complexes however, is often the result of interaction with residual fluids. Fluids affected the late magmatic and particularly the postmagmatic (subsolidus) crystallisation history of a cooling subvolcanic pluton and to some extent the overlying volcanic pile. Such hydrothermal alteration has undoubtedly modified the original granite chemistry.

The residual fluids which were responsible for hydrothermal alteration also carried ore metals which were variously deposited at different stages of hydrothermal alteration. Mineralisation of a pluton generally occurred in the apical or marginal zones or in satellite dykes. Different styles of mineralisation tend to characterise different parts of a granite pluton and five separate zones have been recognised; the roof, marginal and contact zones of a pluton, the enclosing or overlying rocks and the surrounding ring dyke. Nine different styles of mineralisation have been identified including pervasive metasomatic disseminations; pegmatitic pods and lenses; stockworks and lodes. No particular type of hydrothermal alteration is restricted to one

particular style of mineralisation and it is possible to have disseminated sodic, potassic, acid or silica metasomatism and altered ring dykes may show the effects of all these processes.

The complexity of the subsolidus mineralogical re-equilibration has been appreciated by a detailed study of the Rishi area of the Saiya Shokobo complex. The Saiya Shokobo complex forms a distinctive hill mass in north central Nigeria which covers an area of approximately 250km<sup>2</sup>. The main structural feature of the complex is the elliptical fracture 17km in diameter which has largely determined the outline of the central massif of the Saiya Shokobo Hills and has controlled the emplacement of several of the intrusions of the complex. The complex is dominated by volcanic rocks which are confined within this elliptical fracture. During the latest stage of magmatic activity, the emplacement of a granite pluton moved beyond the confines of the main fracture and was intruded eccentrically to the north east of the main part of the complex. Thus the biotite granite intruded both its own volcanic pile and the basement hornblende biotite monzogranite.

The volcanic rocks are composed of crystal-rich ignimbrites with fractured and embayed quartz phenocrysts. The main feeder dyke, which occupies an early ring fracture, is also porphyritic. However, the phenocrysts are typically in synneusis-type aggregates and are modally less abundant. High in the volcanic pile arfvedsonite with minor amounts of aegirine developed in the groundmass of the ignimbrite. In samples collected close to the granite roof, the matrix consists of quartz and alkali feldspar with the development of sieve-textured brown biotite and with no amphibole.

The Rishi biotite granite was the final intrusive phase, emplaced to a high level within the Saiya Shokobo complex. The main granite mass covers an area of 13km<sup>2</sup> with small windows of granite exposed in the volcanics to the south. The main granite is commonly coarse- to medium-grained and cream or pink in colour when fresh. However there is a wide range of subtle coloration and grain size ranging from coarse- to fine-grained, and from equigranular to porphyritic and granophyric. The essential minerals are perthitic feldspar surrounded by clusters of glassy quartz crystals and ragged discrete flakes of biotite irregularly distributed throughout the granite. Accessory minerals include zircon, fluorite, and rutile which are widely distributed with columbite, cassiterite, sphalerite and other minerals locally.

Such textural and mineralogical variations are interpreted to be the result of rock-fluid subsolidus re-equilibration. In addition to the mineralogical and textural variations in the Rishi biotite granite, a sequence of alteration assemblages has been recognised which are indicative of continued fluid mobility at successively lower temperatures: small patches of saccharoidal white feldspar and lenticular zinnwaldite; local development of microcline; chloritisation of feldspar or biotite, greisen formation, silicification and late-stage alteration processes.

The processes of hydrothermal alteration are complex. They depend not only on the temperature and composition of the fluid, but also on the

initial rock type that was being affected, the extent of earlier rock-fluid reaction and on how long the fluids were retained. The different mineral assemblages indicate that alteration took place within an  $\text{Na}_2\text{O}-\text{K}_2\text{O}-\text{SiO}_2-\text{H}_2\text{O}-\text{F}$  system which produced albitisation, then microclinalisation of the feldspars during sodic and potassic alteration, and ultimately a destruction of the feldspars during acid metasomatism. This was followed by lower temperature silicification and late-stage alteration processes.

In addition to the alteration of the Rishi pluton itself, the host rocks which surround and overlie the pluton have also been affected. Thus the Pan-African basement monzogranite country rock which surrounds the Rishi biotite granite and the volcanic pile which overlies it have also been hydrothermally altered by volatiles escaping from the biotite granite cupola. For the first time, a sequence of alteration processes can also be recognised for the basement and to a more limited extent for the volcanic pile although the effects are not always as clearly defined in the basement or volcanic pile as they are for the biotite granite. Geochemically the basement monzogranites, the volcanic rocks and the Rishi biotite granite are distinctive in terms of their trace element assemblage such that each can be distinguished even when there has been intense hydrothermal alteration. Thus the basement monzogranite has higher Ba, V, Sr, Zr and Ce, slightly higher La with lower Nb, Y, Zn and Rb than the Rishi biotite granite. The volcanics can be distinguished by their enhancement of Ce, La, Zn and Zr contents compared with other rock types.

The PVTX nature of the fluids which were responsible for hydrothermal alteration have been monitored by a study of fluid inclusion characteristics in selected samples. The earliest fluids that were trapped in the quartz phenocrysts of the volcanic pile indicate that the fluids that separated from the silicate melt at a depth of around 6 km, were highly saline, probably at temperatures in excess of 750°C. Frequent boiling and loss of  $\text{CO}_2$  occurred in these early stages. Loss of  $\text{CO}_2$  appears to have been important for the deposition of columbite during sodic metasomatism. As the fluids cooled and lost  $\text{CO}_2$ , the condensate was responsible for potash metasomatism and the vapour phase caused acid metasomatism with later, cooler fluids responsible for silica and late-stage alteration.

The importance of boiling in the formation of the ore-deposits within the roof of the Rishi pluton must be emphasised.

## Acknowledgments

First and foremost thanks must go to my family for their tolerance and stoic acceptance of this thesis. Without their unfailing encouragement, sympathy and good humour, this thesis would never have materialised.

I would like to thank all the many people of Nigeria who have helped me over the period since 1973 when I first got involved with the project, whether it was for their hospitality, their company, their help or for useful discussion. Accommodation and logistical help was generously donated by the Amalgamated Tin Mines of Nigeria, especially D. Dent Young and his staff at Barakin Ladi. Additional advice and access to property was given by other mining companies including Bisichi-Jantar (Banke, Tibchi) and Gold and Base Ltd (Ririwai). Air photographs and maps were supplied by the Ministry of Lands and Surveys in Jos, Lagos and by the Lands and Survey Division in Tolworth Surrey. The Minister of Mines and Power Lagos and his staff in the regional offices are acknowledged for their advice and interest, particularly Bill Ford and Usman Turaki. I must also thank Gerry and Elizabeth Staley for their beer, beryls and preservation of my sanity. Mohammed Zakari's friendship and local knowledge proved invaluable and will always be treasured. The St. Andrews Younger Granite Research group consisted of a dozen individuals and all of them helped in some measure but special thanks must go to C. Abernethy, J. Bennett, E. Ike and S. Abaa who collected some of the samples used in the preparation of this work.

I would like to thank Andy Mackie, Alistair Reid, Angus Calder, and Donald Herd for the technical help they have given me over the years. Such help often goes unacknowledged, but without it no research of this nature can proceed. I am also grateful to Richard Batchelor for some of the geochemical data but especially for a sympathetic ear and useful discussion on many geochemical topics. Particular thanks to Jim Allan who worked under great pressure to produce the colour photographs for this thesis and to Kit Finlay who typed the Tables I didn't want to do!

I was introduced to the study of fluid inclusions in the laboratory of Bernard Poty of CRPG in Nancy and I am grateful to all those people in the lab. who helped me. The assistance of Jacques Leterrier, for guiding me through the intricacies of multicationic parameters was also appreciated.

I would like to thank staff at SURRC, East Kilbride, particularly John Whitley, Gus Mackenzie and Tony Fallick for the provision of isotopic data and their unfailing interest in Nigerian granites.

I would like to thank Françoise Blackburn for taking over the onerous burden of preparing a number of papers on African Geology for publication, thus enabling me to concentrate on completion of this thesis.

I greatly appreciate financial help from: The British Council for the award of a Visiting Fellowship to Ilorin University in 1983; The Overseas Development Ministry for the receipt of a Research grant R2679 and to the University of St. Andrews for a research scholarship during the period Oct. 1984 to September 1985.

Finally, no thanks would be complete without mention of Peter Bowden my supervisor for his help and encouragement. Both have been greatly appreciated.

## CONTENTS

PART 1	THE NIGERIAN ALKALINE ANOROGENIC PROVINCE	
Chapter 1	Introduction	2
	Historical background	2
	Regional setting	4
	Basement geology of Nigeria	6
	General geology of the ring complexes	9
Chapter 2	Petrology and geochemistry of the Nigerian Younger Granite Province	16
	Volcanic succession	18
	Volcanic feeder intrusions	20
	Subvolcanic rocks	21
	Geochemical characteristics	26
Chapter 3	Processes of hydrothermal alteration	39
	Sodic metasomatism	40
	Potassic metasomatism	48
	Acid metasomatism	50
	Silica metasomatism	56
	Late-stage alteration	56
Chapter 4	Geochemistry of the hydrothermal alteration processes	63
	Major element variations	64
	Minor and trace element variations	77
	Minor and trace element indicators of alteration	80
Chapter 5	Fluid inclusion studies	94
	Classification of inclusions	94
	Techniques of study	100
	Summary of thermometric data	103
	Discussion on fluid compositions	108
Chapter 6	Mineralisation and economic aspects of Nigerian ring complexes	114
	Styles of mineralisation	119
	Economic exploitation and future potential	133
	Summary of Part 1	136
PART 11	THE SAIYA SHOKOBO COMPLEX	
Chapter 7	The Saiya Shokobo complex	140
	Basement rocks	146
	Rishi biotite granite	152
	Mineralisation	155

Chapter 8	Petrology and geochemistry of the main rock types in the Rishi area	156
	Basement monzogranite	160
	Volcanic rocks and volcanic feeder intrusions	165
	Biotite granite	176
	Geochemistry	185
Chapter 9	Hydrothermal alteration and mineralisation in the Rishi area	196
	Zones of hydrothermal alteration and mineralisation	196
	Styles of mineralisation	202
	Sequence of hydrothermal alteration processes	209
	Geochemistry of the alteration processes	272
	Minor and trace element variations as indicators of hydrothermal alteration	310
	Chapter summary	316
Chapter 10	Mineral and Fluid Chemistry	322
	Sheet silicates	322
	Ore minerals	363
	Fluid inclusion data	382
	Summary of Part 11 and comparisons within Nigeria	409
Part 111	MINERALISATION - SOURCE OF FLUIDS AND ORE METALS	
Chapter 11	Heat flow, high heat production granites and radioelement variations	416
	Heat flow	416
	Heat production	417
	Heat production in the Nigerian anorogenic province	419
Chapter 12	Isotopic constraints on the source of the magma and the source of its fluids	425
	Origin of the magma	425
	Radiogenic isotope studies	425
	Stable isotope studies	439
	Origin of the fluids	443
PART 1V	COMPARISONS	
Chapter 13	Comparisons with other provinces	456
	Comparison with other anorogenic provinces	456
	Mixed alkaline provinces	466
	Tin provinces compared	472
Chapter 14	Summary and conclusions	478
References		484
Appendix		501

## LIST OF TABLES

	page	
1.1	Age determinations of the younger granites	3
1.2	Dated events in the Nigerian basement correlated with recognised events in West Africa	6
1.3	Pegmatite ages in the Pan-African reactivation zone of Nigeria	9
2.1	Major and trace element analyses of fayalite granites, syenites and quartz syenites	27
2.2	Major and trace element analyses of peralkaline granites	28
2.3	Major and trace element analyses of biotite granites	29
2.4	Correlation matrix for major and trace elements in the Niger-Nigeria anorogenic province	30
3.1	Characteristic mineral assemblage for each alteration process	41
3.2	Geochemical changes associated with each alteration process	42
3.3	Mineral assemblages generated during acid metasomatism	52
3.4	Mineralisation mineralogy of acid and silica metasomatised samples	55
3.5	Characteristic rock forming minerals related to each of the hydrothermal alteration processes	60
3.6	Accessory mineral assemblage of each of the hydrothermal alteration processes	61
4.1	Major and trace element analyses and normative compositions for sodic metasomatised rocks	65
4.2	Major and trace element analyses and normative compositions for potash metasomatised rocks	66
4.3	Analyses and normative compositions for acid metasomatised basement and volcanics	67
4.4	Major and trace element analyses of acid metasomatised potash-rich rocks	68
4.5	Major and trace element analyses of acid metasomatised perthite granite	69
4.6	Uranium-thorium concentrations in rocks from the Ririwai complex	84
4.7	Chemical data and rare-earth concentrations for some Ririwai rocks	87
4.8	Zr:Hf ratios for Nigerian granites and hydrothermal variants	89
4.9	Fluorine and chlorine concentrations in granitic rocks and minerals in the Nigerian granitoids	92
5.1	Selected phase data for salt-water systems	101
5.2	Summary table of fluid inclusion characteristics for selected Nigerian rocks	102
6.1	Columbite, cassiterite and zinc concentrations in the Rayfield Gona granite	123
6.2	Ore mineral assemblages related to styles of mineralisation	124
8.1	Modal composition of selected basement granite samples	163
8.2	Phenocryst population in the volcanics and volcanic feeder dyke of the Rishi area	168
8.3	Modal compositions of the five textural facies of the Rishi biotite granite	178
8.4	Chemical and normative compositions of selected basement granite samples from the Rishi area	186
8.5	Chemical analyses of basement granites from Nigeria	187
8.6	Chemical analyses and normative compositions of quartz feldspar porphyries	190
8.7	Chemical and normative compositions of Rishi biotite granite	193
9.1	Modal compositions of sodic metasomatised samples	212
9.2	Modal compositions of potash metasomatised samples	215
9.3	Modal compositions of acid metasomatised basement	225
9.4	Modal compositions of acid metasomatised volcanic rocks	230
9.5	Modal compositions of acid altered sodic-rich samples	233
9.6	Modal compositions of acid metasomatised microcline-rich rocks	235
9.7	Mineral assemblage characteristic of acid metasomatism of biotite perthite granite	240
9.8	Modal compositions of acid metasomatised biotite perthite granites: Stages 1 and 2	243
9.9	Modal compositions of acid metasomatised biotite perthite granites: Stage 3	244
9.10	Modal compositions of acid metasomatised biotite perthite granites: Stages 4 & 5	249
9.11	Modal compositions of SS80 with disseminated acid metasomatism	259
9.12	Summary of mineral assemblages generated during acid metasomatism of different rock types	261
9.13	Modal compositions of silica metasomatised facies	264
9.14	Modal compositions of late-stage alteration	267
9.15	Chemical analyses of sodic metasomatised facies of the Rishi area	275
9.16	Chemical analyses of potash metasomatised facies of the Rishi area	280
9.17	Chemical analyses of acid metasomatised monzogranite basement	285
9.18	Chondrite-normalised trace element patterns for hydrothermally altered rocks from the Rishi area	290
9.19	Chemical analyses of acid metasomatised albite-rich rocks of the Rishi area	292
9.20	Chemical analyses of acid metasomatised microcline-rich rocks of the Rishi area	294
9.21	Chemical analyses of acid metasomatised biotite perthite granite: Stages 1-3	298
9.22	Chemical analyses of acid metasomatised biotite perthite granite: Stages 4 & 5	300
9.23	Chemical analyses of silica metasomatised samples	305
9.24	Chemical analyses of late-stage alteration	307
9.25	K/Rb variations in acid metasomatised Rishi samples	311
9.26	Zr/Hf variation in acid metasomatised Rishi samples	315
9.27	Li content of Rishi samples	316
10.1	End-member compositions of the Li-Fe trioctahedral micas	323
10.2	Chemical compositions and structural formulae for micas from biotite granites	327
10.3	Chemical compositions and structural formulae for micas from biotite granites; continued	328
10.4	Chemical compositions and structural formulae for micas from biotite granites; continued	329
10.5	Chemical compositions and structural formulae for micas from hydrothermally altered samples	330
10.6	Mica compositional variations in Rishi samples	341
10.7	Microprobe analyses of compositional variations in biotite in SS67 and SS85b	342
10.8	Microprobe analyses of compositional variations of biotite in SS43	343
10.9	Microprobe analyses of compositional variations in biotite in SS64/1	347
10.10	Microprobe analyses of compositional variations in biotite in SS58/1	348
10.11	Microprobe analyses of compositional variations in biotite in SS53	349
10.12	Microprobe analyses of compositional variations in biotite in SS48	352
10.13	Microprobe analyses of compositional variations in chlorites	360
10.14	Classification of illite chemistry	361
10.15	Microprobe analyses of compositional variations in illite of SS20	362
10.16	Compositional variations within a zoned cassiterite	369
10.17	Compositional variations of genthelvite	372
10.18	Microprobe analyses of compositional variations in sphalerite from SS20/1 and SS102	375
10.19	Microprobe analyses of compositional variations in sphalerite from SS18, 6/1 and 20	376

10.20	Microprobe analyses of compositional variations in stannite	377
10.21	Microprobe analyses of compositional variations in pyrite	377
10.22	Microprobe analyses of compositional variations in chalcopyrite	378
10.23	Microprobe analyses of compositional variations in galena	380
11.1	Heat flow values for Precambrian shield areas	416
11.2	Radioelement variations and heat productivities for Nigerian anorogenic rocks	421
11.3	Radioelement variations and heat productivities for hydrothermally altered variants	422
12.1	Rb-Sr whole rock isotopic data (van Breemen et al, 1976)	427
12.2	Rb-Sr isotopic data (Rahaman et al, 1984)	428
12.3	Rb-Sr isotopic data (Dickin and Halliday 1987)	429
12.4	Lead isotopic compositions from some Nigerian Mesozoic rocks	431
12.5	Lead isotopic data	432
12.6	Sm-Nd isotopic compositions	437
12.7	Sulphur isotopes in co-existing sulphide assemblages	445
12.8	Temperature calculations from sulphide pairs	446
12.9	Oxygen isotopic compositions of whole rock and mineral separates	449
12.10	$\delta^{18}\text{O}$ geothermometry from co-existing mineral pairs	451
12.11	Mica-water hydrogen fluid compositions	452
12.12	Mica-water oxygen fluid compositions	453
13.1	Ore parageneses in carbonatites	471
14.1	Summary table showing metasomatic mineral assemblages	480
14.2	Summary table showing ore minerals characteristic of mineralised anorogenic complexes	481
14.3	Radioelement concentrations and heat productivities for selected granites	482

## LIST OF FIGURES

1.1	Schematic map of the major Precambrian units of West Africa	5
1.2	Generalised geological map of Nigeria	8
1.3	Location map for the major anorogenic igneous centres in Niger-Nigeria	10
1.4	Sketch map of the distribution of the Nigerian anorogenic ring complexes	12
1.5	Diagrammatic representation of the variation in age with distance calculated from the Hoggar	14
2.1	Schematic representation of the structural evolution of a typical ring complex	17
2.2	Summary Streckeisen diagram for Nigerian granitoids	23
2.3	Major element Harker variations	31
2.4	Summary Harker diagrams of averaged values of major and minor elements	32
2.5	Major element multicationic scheme for the classification of igneous rocks	34
2.6	Trace element Harker variations for the Nigerian granitoids	35
2.7	Nb-SiO <sub>2</sub> diagram	37
3.1	Composition of the amphiboles	43
3.2	Borehole log of the L13 core	47
3.3	Paragenetic sequence of ore minerals for each of the alteration processes	62
4.1	Q-Ab-Or plot of hydrothermal altered assemblages	70
4.2	AKFN diagram for Nigerian granites and hydrothermal variants	72
4.3	Q-F diagram showing trends during sodic, potassic, acid and silica metasomatism	73
4.4	QF diagram to show trends during acid and silica metasomatism	76
4.5	Chondrite-normalised trace element patterns for hydrothermally altered rocks	78
4.6	Chondrite-normalised rare-earth patterns for Ririwai rocks	79
4.7	Thorium-uranium concentrations in Nigerian volcanics, granites and metasomatised variants	85
4.8	Zr:Hf values for Nigerian granites and hydrothermal variants	90
5.1	Schematic explanation of petrological variations in granite roof zones	113
6.1	Anatomy of a hypothetical mineralised ring complex	116
6.2	Anorogenic ring complex map showing localities mentioned in the text	117
6.3	Geological sketch map of the Ririwai complex and cross-section of the lode	118
6.4	Location map of the mineralised localities of the Tibchi complex	129
7.1	Location map of the Saiya Shokobo Complex	139
7.2	General geology of the Zuku, Saiya Shokobo and Tongolo complexes	141
7.3	Topographic map of the Rishi field area	145
7.4	General geology of the Rishi area	147
8.1	Variations in quartz shape and intergrowth textures	157
8.2	Variations in feldspar (perthite) textures	158
8.3	Variations in mica textures	159
8.4	Sample localities in the Rishi area	162
8.5	Quartz-Alkali Feldspar-Plagioclase diagram showing the compositions of Nigerian basement rocks	164
8.6	Sample localities in the Dawa area	166
8.7	Distribution of the different textural facies within the the Rishi biotite granite	177
8.8	Chondrite-normalised trace element patterns for the different rock types of the Rishi area	188
8.9	Q-Ab-Or and Q-F plot for the major rock types of the Rishi area	191
9.1	Zones of ore deposition and the localities where the zones are exposed	198
9.2	Sample localities in the Rishi area for sodic metasomatised facies	203
9.3	Sample localities in the Rishi area for potash metasomatised facies	210
9.4	Sample localities in the Rishi area for acid metasomatised facies	223
9.5	Cross-section of locality SS106	253
9.6	Cross-section of locality SS108	257
9.7	Sample localities of silica metasomatised rocks and late-stage alteration	263
9.8	Q-Ab-Or plot of sodic and potash metasomatised samples	276
9.9	Q-F plot of sodic metasomatised samples	277
9.10	Chondrite-normalised trace element data for sodic metasomatised samples	277
9.11	Q-F plot of potash metasomatised samples	281
9.12	Chondrite-normalised trace element data for potash metasomatised samples	282
9.13	Chondrite-normalised trace element data for acid metasomatised rocks in the Rishi area	287
9.14	Q-F plot of acid metasomatised basement samples	288
9.15	Q-F plot of acid metasomatised volcanics	289
9.16	Q-F plot of acid metasomatised albite-rich samples	293
9.17	Q-F plot of acid metasomatised microcline-rich samples	295
9.18	Chondrite-normalised trace element data for acid metasomatised biotite perthite granite	302
9.19	Q-F plot of acid metasomatised biotite perthite granite	301
9.20	Q-F plot of silica and late-stage altered samples	306
9.21	Stability fields of K-feldspar, K-mica and kaolinite	309
9.22	Ce/Y versus silica diagram as a monitor of hydrothermal alteration	314
9.23	Summary Q-F plot for hydrothermally altered rocks of the Rishi area	319
10.1	Nomenclature diagram for the trioctahedral micas	324
10.2	Modified Rieder diagram for trioctahedral micas	325
10.3	R1-R2 compositional plot for trioctahedral micas (a) worldwide (b) Nigeria	331
10.4	Compositional variations in trioctahedral micas of the Afu complex on a modified Rieder diagram	333
10.5	Selected triangular compositional plots for the micas	335
10.6	Molecular proportions of Al/K against Fe <sup>2+</sup> /K	337
10.7	R1-R2 compositional plot showing colour variations	338
10.8	R1-R2 compositional plot of the micas from the Rishi biotite granite	344
10.9	Microprobe compositional variations within the mica of SS64	345
10.10	Microprobe compositional variations within the mica of SS48	351
10.11	R1-R2 bulk compositional plot of micas from hydrothermally altered rocks	354

10.12	Nomenclature for chlorite classification	359
10.13	Paragenetic sequence of ores	365
10.14	Th-salinity plot and Th-histogram for SS43 biotite perthite granite	389
10.15	Th-histograms for zinnwaldite albite granite and microcline pegmatites	391
10.16	Th-salinity plot for inclusions in quartz of SS109A SS109B	395
10.17	Th-histograms for SS 109C and silica metasomatised samples	398
10.18	Vector diagrams showing the effects of acidity and salinity in hydrothermal alteration	405
10.19	Summary of fluid inclusion data for the Rishi hydrothermal system	407
10.20	Summary Q-F cationic plots for the Afu, Banke, Tibchi and Ririwai complexes	412
10.21	Summary Q-F cationic plots for the Ropp, Jos Bukuru complexes and Rishi area	413
11.1	Heat flow sites in Africa	418
12.1	Strontium evolution plot	426
12.2	Initial strontium isotopic ratios for the Ririwai complex	426
12.3	Lead isotopic ratios	431
12.4	One model for the evolution of the principal units of the Ririwai complex	433
12.5	Initial lead isotopic compositions	434
12.6	Initial Pb versus initial Sr isotopic compositions	438
12.7	A compilation of $\delta^{18}\text{O}$ mineral and whole-rock analyses	440
12.8	$\delta^{34}\text{S}$ data for S-type, I-type and A-type granitoids	442
12.9	$\delta^{18}\text{O}$ analyses from hydrothermally altered samples	448
12.10	$\delta\text{D}$ versus $\delta^{18}\text{O}$ for fluids in equilibrium with greisen micas	454
13.1	The distribution of the alkaline complexes in Africa	458
13.2	Location map of global tin provinces	473



9.20	Phenocryst of perthite cut by veinlets of microcline in an altered porphyry feeder dyke	220
9.21	Altered porphyry feeder dyke	222
9.22	Altered basement monzogranite showing variation in colour and texture	222
9.23	Meshwork of monazite	226
9.24	Allanite and monazite	226
9.25	Large amoeboid-texture quartz in hornfels	228
9.26	Ghosts of twin lamellae of albite in mottled microcline	228
9.27	Altered ignimbrites	229
9.28	Photomicrograph of SS150 showing embayed crystals characteristic of the ignimbrites	229
9.29	Altered feeder dyke samples showing the textural variations	231
9.30	Euhedral prismatic apatite crystals and needles in SS176, altered porphyry feeder dyke	232
9.31	Photomicrograph of SS20/1a showing quartz replacement of perthite	232
9.32	Anhedral skeletal colourless cryolite in SS77	234
9.33	Cryolite with quartz, pale green mica and blood red sphalerite in SS77	234
9.34	Replacement of microcline by mica	236
9.35	Large patches of pinky-brown microcline remain within an otherwise mica-rich rock	236
9.36	Clustered green mica with zoned cassiterite and quartz	237
9.37	Spongy aggregates of very fine-grained blue-green coloured mica	237
9.38	Photomicrograph of SS44/1 showing the abundance of khaki-coloured mica	238
9.39	Discrete ilmenite occurs associated with clusters of blue-green mica	238
9.40	Photomicrograph of SS64/2 showing chloritisation along the k-lamellae in perthite	241
9.41	The same field of view as above, under crossed polars	241
9.42	Large quartz crystals encircled by small granules of topaz - chlorite encloses both	242
9.43	An enlarged magnification of chicken-wire textured chlorite	242
9.44	Photomicrograph of SS45/1 showing deep red sphalerite, quartz and chlorite accompanied by sericite	245
9.45	The same view as above under crossed polars	245
9.46	Small laths of pale green mica have developed from the fine-grained sericite in SS10/7	247
9.47	View as above under crossed polars	247
9.48	Zinnwaldite in SS8/3 with cleavage planes emphasised by chlorite	248
9.49	The same view as above in XPL	248
9.50	Clustered granules of topaz accompanied by granular quartz, traces of sericite and sphalerite	251
9.51	Similar view to above, under crossed polars	251
9.52	A quartz-chlorite assemblage of minerals in SS106A	254
9.53	A different part of the same sample - SS106A consists of a quartz-sericite assemblage of minerals	254
9.54	SS106B: a 2mm-wide vein of sphalerite cuts a quartz-chlorite mineral assemblage	255
9.55	Chlorite has replaced perthite, vestiges of which remain as pinky brown patches in SS106C	255
9.56	Microcline replaced by pale green sericite, SS80	260
9.57	The same as above under crossed polars	260
9.58	SS1 showing the development of siderite along the cleavages of the blue-green coloured mica	266
9.59	Siderite in cross-polarised light showing alteration to haematite, SS1	266
9.60	Small euhedral mica crystals developed between large mica books	268
9.61	Same view as above under crossed polars.	268
9.62	Brecciated vein, SS11/2	270
9.63	Photomicrograph of part of the vein above in cross-polarised light	270
10.1	Photomicrograph of a zoned zircon in zinnwaldite albite granite, SS64/1	366
10.2	Thin section showing ragged columbite and a lath of ilmenite in SS9/4	366
10.3	Large prismatic monazite crystal. Smaller crystals of monazite form a meshwork in the biotite	368
10.4	Zoned cassiterite in SS113 from near Dawa mining camp	368

#### Appendix 7

##### Linkam TH600 microthermometric system

- (a) the complete set-up
- (b) the inside of the heating/freezing chamber showing the central silver block with sapphire window

## INTRODUCTION

Part 1 of the thesis is an introduction to the petrology and geochemistry of the Nigerian province as a whole and is a review of work completed by several workers including the author. A great deal of data, some published, some unpublished, has been compiled on the hydrothermal alteration processes and a summary of the knowledge prior to the work of this thesis is given.

\*\*\*\*\*

The research carried out in Part II of the thesis is a detailed investigation of the mineralisation and hydrothermal alteration of the Rishi area of the Saiya Shokobo Complex. There are several reasons why this complex was chosen for study:-

1. There had been only two previous studies of the complex - one by Falconer in 1923 and one by Buchanan 1958-1960. The first of these formally identified the complex and the second completed detailed mineralogical mapping. However, little was published on the mineralisation.
2. The detailed mineralisation of the Ririwai and Jos-Bukuru Complexes had already been undertaken by the author and the Saiya Shokobo Complex had important comparisons and contrasts.
3. The Saiya Shokobo Complex, along with the nearby Banke Complex, is one of the few complexes where the effect of trapped volatiles on the volcanic pile can be studied, in addition to the hydrothermal alteration of both basement host and younger granite.

A range of techniques has been utilised to understand the sequential hydrothermal alteration processes and associated mineralisation. Field work, petrographic descriptions, major and trace element analyses, fluid inclusion microthermometry, ore petrology and microprobe analytical data have all been employed.

\*\*\*\*\*

In Part III radiogenic and stable isotopic studies have been used to investigate the heat-producing capacity of the Nigerian anorogenic granites, and to try to identify the source of the magma and ultimately the source of the fluid.

\*\*\*\*\*

In Part IV, the processes of hydrothermal alteration, the styles of mineralisation, the fluid evolution and the mineralisation of the Nigerian A-type granites are compared with other anorogenic complexes in Africa and briefly with other tin provinces.

## CHAPTER 1

### INTRODUCTION

#### Historical background

The anorogenic alkaline granites of Nigeria are a petrologically distinctive series of alkali feldspar granites, associated with minor syenites and gabbros, that were intruded in a sub-volcanic environment, beneath a dominantly ignimbritic pile.

These granites were first defined by Falconer (1911) who noted their undeformed, post-tectonic nature, called them younger granites, and contrasted them with the foliated calc-alkaline "older" granites of the basement. He described the younger granites as cross-cutting alkali granites with chilled margins, against the country rocks, containing riebeckite or biotite. In the first decade of the Geological Survey of Nigeria, which began in 1919, virtually all the younger granites were discovered and mapped in outline. This major feat was facilitated by the distinct topography of the rocky younger granite massifs which stand sharply in relief from the basement plains. During this mapping it was found that the younger granites include many textural and compositional variations. The main rock types described were granites containing either biotite, riebeckite or hornblende as the main ferromagnesian-bearing mineral, whilst porphyries, rhyolites and minor syenites and gabbros were also identified. In 1927, a generalised map of central Nigeria showing the location of most of the complexes was published.

The first detailed mapping of a younger granite massif by Bain (1934) at Kudaru, showed that the structure is controlled by ring-shaped intrusions. Following this, ring dykes were found in the Ririwai (Liruei) complex (Jacobson 1947) and at Neil's Valley near Jos (MacKay et al 1952). The work of MacLeod and others beginning in 1952, showed that the variations in granitic texture and composition noted by Falconer and other earlier workers and attributed to the proximity of the roof, usually occur as abrupt changes at igneous contacts rather than transitions within a single body. Many of the complexes therefore, were shown to consist of a series of distinct overlapping intrusions, often with a concentric arrangement.

By the mid 1960's, following a resurvey of the Plateau and adjoining areas by the Geological Survey- which began in 1952- a large number of the complexes had been mapped in detail and had been compared both structurally and petrographically with the White Mountain Magma Series of New Hampshire (Greenwood 1948).

Until 1962, the younger granites were regarded as being of late Precambrian age. However, Darnley et al (1962) published U/Pb and Th/Pb dates of about 160ma. This data was compatible with unpublished data that they quoted of a K/Ar age for biotite of 162ma and a <sup>206</sup>Pb/U age for pyrochlore of 204ma. A more

comprehensive study by Jacobsen et al (1963), using both K/Ar and Rb/Sr methods, confirmed a Jurassic age for the central Nigerian complexes (Table 1.1).

Table 1.1

AGE DETERMINATIONS - YOUNGER GRANITES

Specimen No	Material analysed and locality	Analytical details	Age million years			
		<b>RUBIDIUM/STRONTIUM METHOD</b>				
L. 365	Biotite from Rayfield-Gona biotite-granite. Rayfield (9°50'N, 8°54'E)	Rb per cent [0.527 [0.539	Radiogenic <sup>87</sup> Sr ppm 3.46 3.53			
X. 2040	Biotite from biotite-quartz vein in biotite-granite Banke (10°49'N, 8°28'E)	[0.562 [0.549 [0.572	3.67 3.62 3.67			
		<b>POTASSIUM/ARGON METHOD</b>				
L. 365	Biotite from Rayfield-Gona biotite-granite Rayfield (9°50'N, 8°54'E)	K per cent 7.56	Radiogenic <sup>49</sup> Ar ppm 0.091			
X. 2040	Biotite from biotite-quartz vein in biotite-granite Banke (10°49'N, 8°28'E)	7.98	0.096			
-	Biotite from Joe biotite-granite Joe (9°55'N, 8°54'E)					
		<b>LEAD/K METHOD</b>				
L. 185	Zircon from Shan fayalite-granite. Shan (9°45'N, 8°55'E)	Pb ppm 36	<sup>4</sup> mg/h 920			
	Zircon from alluvial concentrate. Near Rayfield, Joe/Dukuru Complex	24 19	512 430			
			104 104 107			
		<b>Lead Lead Method</b>				
		U per cent	Th Pb	Isotopic proportions <sup>204</sup> Pb <sup>206</sup> Pb <sup>207</sup> Pb <sup>208</sup> Pb	Apparent ages <sup>207</sup> Pb/ <sup>206</sup> Pb <sup>206</sup> Pb/ <sup>238</sup> U <sup>207</sup> Pb/ <sup>235</sup> U <sup>208</sup> Pb/ <sup>232</sup> Th	
	Pyrochlore from Keffo albite-riebeckite-granite Ririwai (10°43'N, 8°47'E)	2.892	1.316 1.235	1.27 29.50 20.13 49.09	- ve 205 59 160	?
	Fergusonite from alluvial concentrate Kuru (9°36'N, 8°20'E)	2.12	4.394 0.19	0.813 38.9 13.9 46.4	- ve 160 146 156	154
	Fergusonite from alluvial concentrate Takkoe (9°36'N, 8°48'E)	1.213	3.340 0.146	0.86 35.6 14.4 49.1	- ve 180 152 168	166

data from Jacobson et al, 1963

In 1971, the mapping resurvey, of these Jurassic ring complexes, which had been initiated in 1952, was published as Bulletin No. 32 of the Geological Survey of Nigeria. This was followed, in 1977 by Bulletin No. 33 which covered the geology of the Ririwai, Banke and adjacent complexes.

In 1973, a group of research students led by P. Bowden from St. Andrews and D.C. Turner, then of Zaria, began a programme of detailed mapping concentrating on complexes not already surveyed in detail, culminating in the production of three published maps. The last of these in 1981 was the first to show in some detail, all the younger granite complexes (Kinnaird 1981).

This latest phase of work for the first time, included systematic isotope geochemistry, mineral chemistry and mineralisation among the fields of research.

Examination of the textural features of granites related to tin mineralisation suggests that the rocks have been subjected to widespread pervasive hydrothermal alteration. The recognition of such pervasive alteration means that caution is required in interpreting geochemical data on the origin, fractionation history and isotopic signature of granites of this type.

It has long been known that the Nigerian alkali anorogenic granites and their associated mineralisation are the source of the country's alluvial ore deposits (Falconer 1911). Since 1905 when cassiterite production began, more than 700,000 tonnes of concentrate have been produced from alluvial deposits and since 1933 approximately 100,000 tonnes of columbite have been won from primary and alluvial sources. As these alluvial sources become exhausted, more interest will inevitably be centred on the primary ore distribution.

#### REGIONAL SETTING

The evolution of the west African anorogenic alkaline igneous ring complexes occurred in the period between the construction and initial fragmentation of Gondwanaland.

Accumulated palaeomagnetic and field evidence led Black et al (1979) to suggest the existence during the closing stages of the Pan-African, of a modern-type orogenic belt, involving the collision between the passive continental margin of the West African craton and the active continental margin of the Tuareg Shield to the east (Fig 1.1). Caby et al (1981), suggest that the West African craton was cold and rigid, and that the Tuareg Shield was an amalgam of relatively hot, and more ductile, microplates. Evidence in favour of a plate tectonic model is given by petrological assemblages characteristic of continental shelf, island arc and Cordilleran environments. Ophiolites have been recognised at Bou Azzer Morocco, situated along the northern margin of the West African craton (Leblanc 1976) and back arc basin facies and pillow lavas in the Anka and Zungeru belts, Nigeria (Fitches et al 1983) along the southern margin. However, the most convincing evidence in favour of an orogenic model, is the existence of distinctly paired metamorphic belts (Caby et al 1981). The high pressure - low temperature eclogitic rocks found on the margin of the West African craton, display mineral assemblages which strongly indicate that they formed in a subduction zone which was subsequently thrust onto the continental margin. Oceanic closure, around 600ma ago, (Caby et al 1981), is marked by a suture outlined by a string of positive gravity anomalies in the Tuareg Shield, corresponding to basic and ultrabasic complexes and perhaps ophiolites, which may be followed over a distance of 2000km along the eastern margin of the craton (Bayer and Lesquer 1978). The 600ma collision was accompanied by the translation of foreland nappes onto the West African craton and affected the entire Tuareg Shield. The reactivation of older gneissic terrains in the central and eastern part of the shield is marked by greenschist metamorphic overprinting, intense intraplate deformation, generation of granites and major lateral displacements along megashear zones (Caby et al 1981). The general pattern of shear belts in Nigeria (McCurry 1971,1973,1976, Grant 1978) and the whole of the Tuareg Shield,

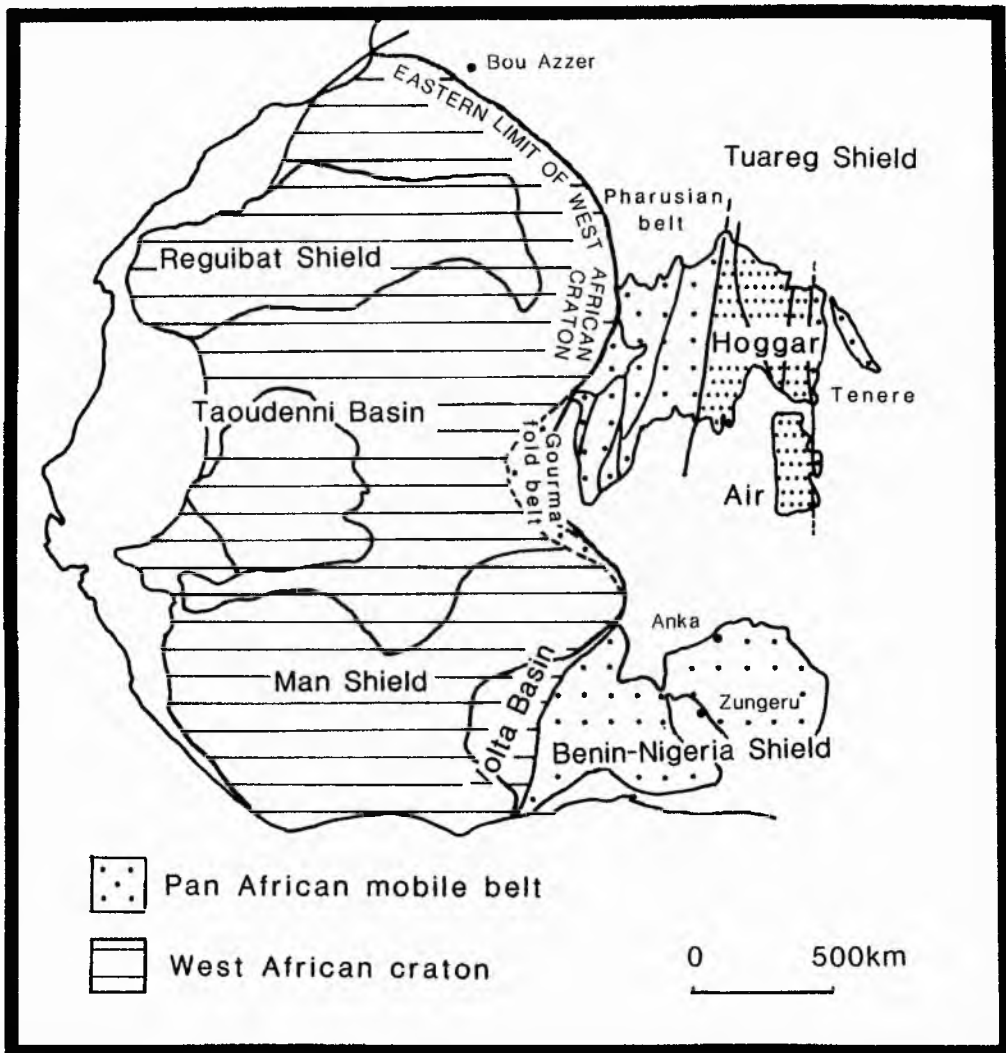


Fig 1.1 Schematic map of the major Precambrian units of West Africa (from Black 1984)

combined with the pattern of the Pan-African structures (Caby et al 1981), bears striking similarities to the tectonic pattern of Asia produced by the collision of India (Black et al 1979).

The size of the Pharusian ocean can be constrained by the palaeomagnetic data of Piper (1973) and McWilliams (1981). Thus the Upper Proterozoic ocean was about the size of the Red Sea or Mediterranean. Ocean closure coincided with a peak of plutonism which occurred in north central Nigeria about  $597 \pm 20$  ma (van Breemen et al 1977).

## Basement geology of Nigeria

The Nigerian basement has a complex history probably spanning the period from the Liberian orogenic cycle around 2800Ma, through to the Pan-African orogeny which occurred in late Precambrian to Cambrian (Table 1.2).

Table 1.2

Dated events in the Nigerian basement correlated with recognized events in West Africa

Dated events in Nigerian basement		Suggested terminology IGCP 108/144		
Rock type and radiometric age	Location	Reference and method	Orogenic cycle	Age range
Semi-concordant aplites in host banded gneisses 2,700 Ma	Ibadan SW Nigeria	OVERSBY, 1975 Pb-Pb (K-feldspar)	Liberian	3,000-2,400 Ma
Granite gneisses 2,200 Ma	Kaduna Ibadan	HURLEY <i>et al</i> 1966 GRANT 1969 Rb-Sr isochron whole rock	Eburnean	2,400-1,600 Ma
Granite gneiss 1,500 Ma	Ife, SW Nigeria	GRANT <i>et al</i> 1971a Rb-Sr isochron whole rock	Kibarian	1,600-900 Ma
Igneous and metamorphic rocks: 700-450 Ma	various	GRANT 1971a GRANT <i>et al</i> 1971b	Pan-African	900-450 Ma
Charnockites 553 ± 125 Ma*	Bauchi	VAN BREEMEN <i>et al</i> 1977, Rb-Sr whole rock		
Granite gneiss 610 ± 10 Ma	Panyam	VAN BREEMEN <i>et al</i> 1977, Zircon		
Granite gneiss 596 ± 23 Ma*	Panyam	VAN BREEMEN <i>et al</i> 1977, Rb-Sr whole rock		
Pegmatite 592 ± 15 Ma*)	Gubi	VAN BREEMEN <i>et al</i> 1977, Rb-Sr muscovite		
Metasedimentary rocks 550-490 Ma	Zaria, Funtua Maska, Kuseriki	HARPER <i>et al</i> 1973 K-Ar, mica and whole rock		
Calc-alkaline granite 508 ± 29 Ma* 445 ± 4 Ma*	Kuseriki Kuseriki	GRANT 1978 Rb-Sr whole rock Rb-Sr feldspar mica		
Pegmatites with tantalite, beryl etc 550-450 Ma	Jemaa, Wamba	TUGARINOV <i>et al</i> 1968 Pb-Pb (K-feldspar)		

\* ages recalculated to new decay constant  $\lambda 1.45 \times 10^{-11} \text{ Yr}^{-1}$

The oldest rocks, in southwest Nigeria consist of charnockitic rocks of unknown age and a gneissic complex comprising banded gneisses, migmatites quartzites, schists, amphibolites, leptynites and marbles metamorphosed to the almandine-amphibolite facies. These are cut by foliated granites which have

yielded lower Proterozoic ages. Younger metasediments of Upper Proterozoic age form north-south orientated metasedimentary belts of low grade psammitic to pelitic composition with locally developed calc-alkaline andesitic lavas. This basement complex is intruded by porphyritic granites, subordinate quartz-diorites and 2-mica granites which are considered to be Pan-African (Black 1984). These granites are most abundant in the central part of Nigeria which is the locus for the Mesozoic alkaline ring-complexes (Fig 1.2).

The granitic rocks associated with the Pan-African orogeny have contrasting petrological and geochemical compositions compared with the later Palaeozoic (Niger) or Mesozoic age (Nigeria) suite of alkaline ring complexes. However, in addition to granitic compositions typical of collision zones, the older suite does contain small A-type granites of short time duration.

The older granite intrusions were emplaced at different stages during the tectonic evolution of the collision zone. Early granitoids are foliated calc-alkaline granodioritic intrusions, whilst later undeformed post-tectonic intrusives are monzonitic, subalkaline to alkaline in character.

The early foliated granitoids are heterogeneous, fine- to medium-grained biotite + muscovite granodiorites with a highly irregular form. The later phase of post-tectonic intrusives are homogeneous, porphyritic, medium- to coarse grained biotite hornblende granites and monzonites with well defined intrusive form (MacLeod et al 1971).

A suite of pegmatites occurring as dykes and sheets cut Eburnean and early Pan-African metamorphic and igneous assemblages. Some pegmatites are barren and others richly enough mineralised to have been worked for tin, tantalite or other minerals. The barren pegmatites are found within and around the granodioritic plutons. These barren pegmatites, which are up to 100ma older than the mineralised Phanerozoic series of pegmatites, are not directly related to any apparent intrusive activity (Matheis and Caen-Vachette 1983). The mineralised pegmatites are distributed with a marked concentration in a broad zone, extending 400km northeast from the Ife area towards the younger granite province (Fig 1.2). It appears that the economically mineralised pegmatites occur within the north-south orientated younger metasedimentary belts composed of biotite schists and amphibolites.

The distinction of two separate ages for pegmatite formation (Table 1.3) can be interpreted in terms of the model proposed by Varlamoff (1972). The simple barren pegmatites which are small in size and occur within, or adjacent to granitic bodies, Varlamoff interpreted as granites that had intruded to shallow depth. In contrast, the mineralised pegmatites of his model are related to granites that crystallised at greater depth with the pegmatites not confined to the cupola zone. Instead, the pegmatites would be formed by hydrothermal fluids in the country rock above the cupola zone.

As the pegmatites changed from barren in late Proterozoic to mineralised in the Palaeozoic, it is reasonable to suggest that the earliest pegmatites are related to shallow depth calc-alkaline 'plate-collision' granitoids whilst the mineralised pegmatites may be related to late orogenic or even anorogenic older granites. In this case it is not surprising that the associated mineralisation should show similarities to the later anorogenic Mesozoic mineralisation.

Fig 1.2 Generalised geological map of Nigeria showing the location of the pegmatite zone

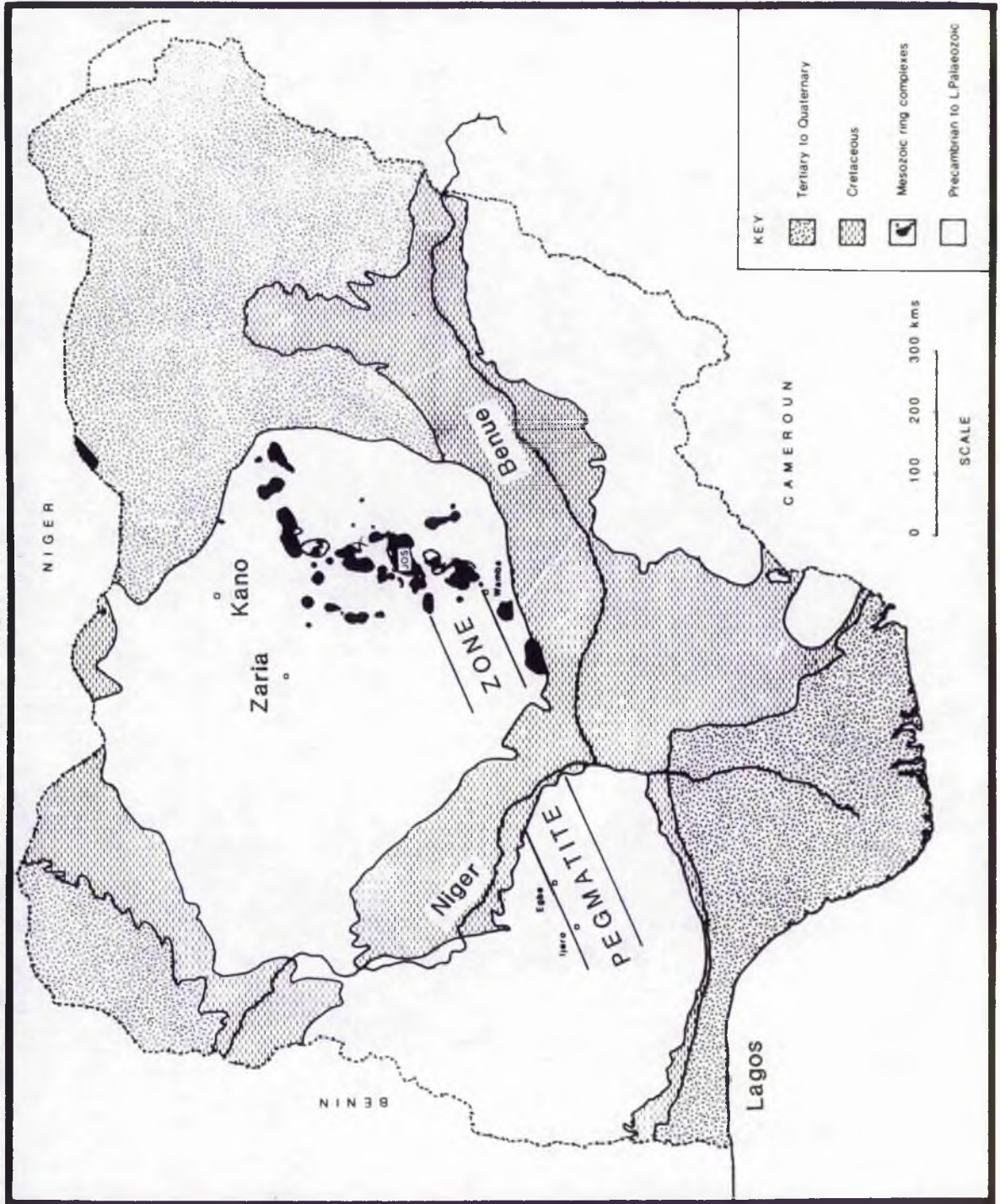


Table 1.3 Pegmatite ages in the Pan-African Reactivation Zone of Nigeria (after HARPER *et al* 1973, and MATHIES and CAEN-VACHETTE 1983).

Method	Age (in million years)	Locality	M = mineral, WR = whole rock
K-Ar	707 ± 13 Ma	Zaria	
K-Ar	555 ± 10 Ma	Zaria	
Rb-Sr	562 ± 12 Ma	Osu	WR - barren pegmatite
Rb-Sr	550 ± 15 Ma	Aramoko	WR - barren pegmatite
Rb-Sr	490 ± 14 Ma	Aramoko	M - muscovite
Rb-Sr	185 ± 6 Ma	Aramoko	M - biotite*
Rb-Sr	545 ± 10 Ma	Ijero	WR - mineralized pegmatite
Rb-Sr	487 ± 14 Ma	Ijero	M - muscovite
Rb-Sr	183 ± 5 Ma	Ijero	M - biotite*
Rb-Sr	523 ± 16 Ma	Ijero	M - oligoclase
Rb-Sr	534 ± 9 Ma	Egbe	WR - mineralized pegmatite
Rb-Sr	555 ± 5 Ma	Wamba	WR - mineralized pegmatite**

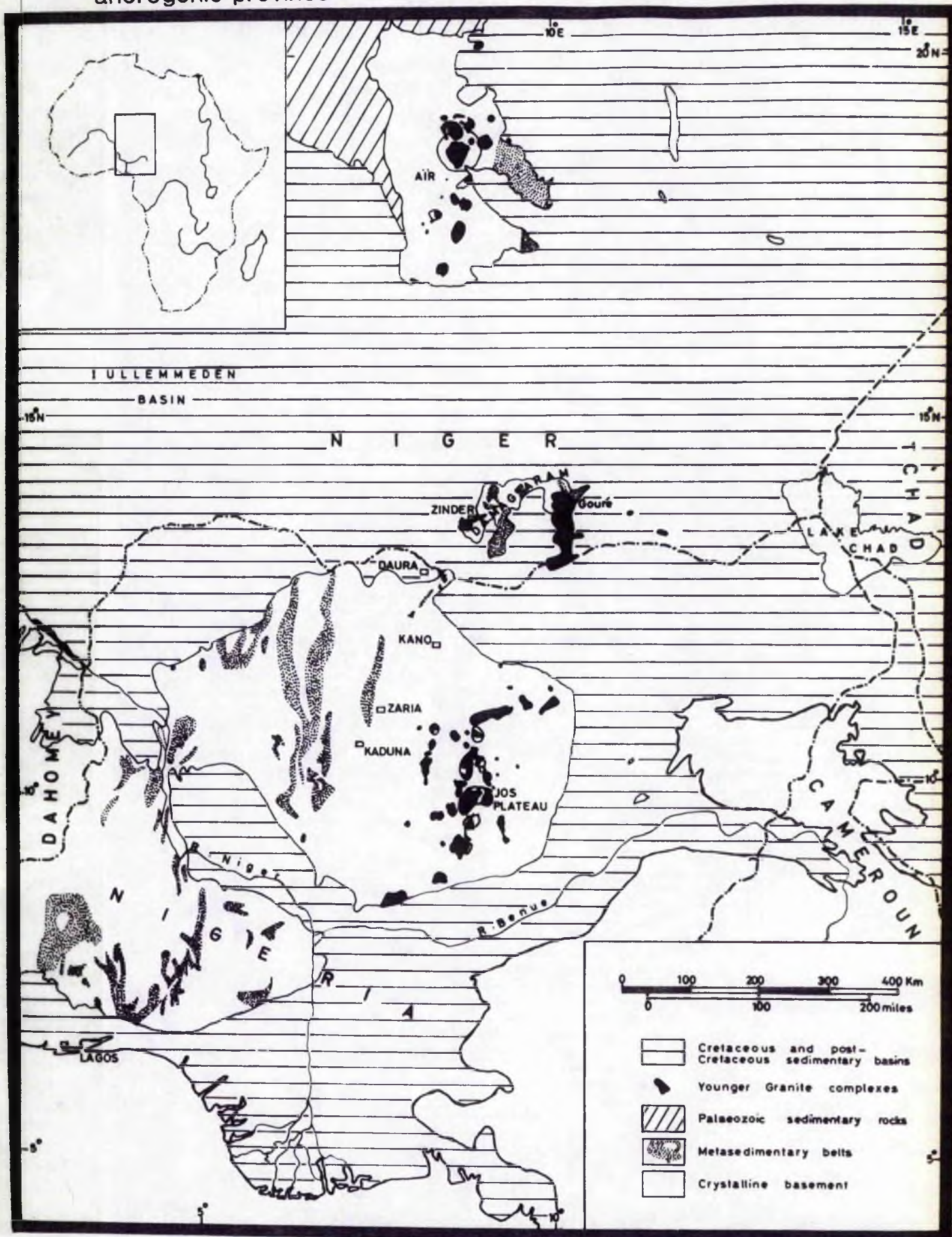
K-Ar ages from HARPER *et al* (1973) using new decay constants. Rb-Sr mineral and whole rock ages from MATHIES and CAEN-VACHETTE (1983). \* Biotite ages reflect onset of anorogenic magmatism in northern Nigeria. \*\* Includes point on isochron using related Pan-African monzogranite.

#### General geology of the ring complexes

The Mesozoic ring complexes of Nigeria form part of a wider province of alkaline magmatism. They occur in a zone 200km wide and 1600km long, extending from northern Niger to south central Nigeria (Fig 1.3). The alkaline complexes which constitute the Niger (Air) group were emplaced into the southern extremity of the Tuareg Shield whereas the Nigerian alkaline ring complexes were intruded into the northern segment of the Benin-Nigeria Shield.

Rb/Sr whole rock dating indicates that the complexes were episodically concentrated into three 60-70 million year periods; upper Ordovician to lower Devonian, Carboniferous to Permian and upper Triassic to Jurassic. Thus the

Fig 1.3 Location map for the major igneous centres in the Niger-Nigeria anorogenic province



oldest complex of Adrar Bous in the north of Niger is Ordovician in age, with progressively younger ages southwards (Fig 1.5). The most southerly ring complex of Afu is late Jurassic in age (Bowden et al 1976). In Nigeria, Rahaman et al (1984), have shown that the age migration of centres occurred along east-northeast - west-southwest and north north-east - south south-east lineaments (Fig 1.4); the ENE-WSW lineaments correspond to the direction of late Pan-African dextral transcurrent faults in the basement and are parallel to the marginal faults of the Benue Trough which has recently been interpreted as a pull-apart basin determined by sinistral shear (Benkhelil, 1982), and which contains transitional basalts and alkali rhyolite.

The location of the Palaeozoic and Mesozoic oversaturated alkaline provinces of Air, Southern Niger and Nigeria, in the former Pan-African mobile belts appears to be related to a regime of distension and reactivation of Pan-African shear zones and transcurrent faults. It is often at the intersection of north-south megashears and the NNW-SSE, NNE-SSW transcurrent fault systems that the ring complexes are located. Aeromagnetic anomalies suggest that a series of buried NE-SW lineaments of incipient rifts controlled the disposition of the individual complexes in Nigeria (Ajakaiye et al 1983) and it seems likely that emplacement of the younger granites was associated with epeirogenic uplift. Elsewhere in Africa Phanerozoic alkaline magmatism is likewise confined to Pan African domains.

More than 50 Nigerian ring complexes, which vary from <2>25 km in diameter (Kinnaird 1981), are intruded to high levels into the polymetamorphic amphibolite-granulite facies basement with the minimum of cataclasis. Metamorphic aureoles are frequently absent or very narrow (a few tens of metres) and reflect the high heat flow associated with subvolcanic emplacement. The ring complexes cover a total area of 7,500km<sup>2</sup> with individual massifs varying from 1000km<sup>2</sup> to <1 km<sup>2</sup>. The majority are between 100 and 250km<sup>2</sup> with circular or elliptical outline (Fig 1.4).

The Younger Granites are discordant high level intrusions with clearly defined cross-cutting contacts (Plate 1.1) which are sometimes rectilinear. They were emplaced by piecemeal stoping through the collapsed central block. These granites often rise steeply from the Pan-African Plain (Plate 1.2) and there is usually a close coincidence between the geological and topographical boundaries at the margins of the granites. The younger granites form continuous ranges and plateaux which rise 300 to 100m above the surrounding plain which is underlain by Older Granites, migmatites and metasediments of the basement complex. In the northern and southern parts of the province, the Younger granite complexes occur as rugged, isolated masses. In central Nigeria, however, the proximity of the complexes together with an abundance of resistant Older Granites in the intervening areas, has resulted in the formation of the Jos Plateau with an altitude generally over 1,350m.

Each of the ring complexes, whether they consist of overlapping centres such as Ningi-Burra or individual centres such as Tibchi, began as chains of volcanoes (Bowden and Kinnaird 1984a). Early ash fall tuffs and agglomerates were deposited from eruptions of explosive activity - abundant ignimbrites deposited from ash flows dominate the volcanics with only minor rhyolitic and thin basic flows. Erosion of the volcanic rocks in the southerly complexes has exposed the cupola zones of the underlying subvolcanic granites.



Plate 1.1

Contact between the Jos Bukuru complex (left) and the basement, showing the shallow outward-dipping nature of the contact. Photograph taken near Jos.



Plate 1.2

View eastwards across the basement towards the Sha Kaleri complex

Fig. 1.4. Sketch map of the distribution of anorogenic ring complexes in Nigeria with their Triassic-Jurassic ages in relation to the direction of major crustal lineaments shown by black arrows.



Ages from Rahaman et al (1984)

Volcanic feeders represent the link during the caldera-forming stage, between the subvolcanic magmas and the overlying volcanic pile. The fayalite hedenbergite quartz porphyry, which often has ignimbritic textures but intrusive form, is the ash flow material which failed to reach the surface and welded and consolidated in ring fissures (Ike 1983, Kinnaird et al 1985a).

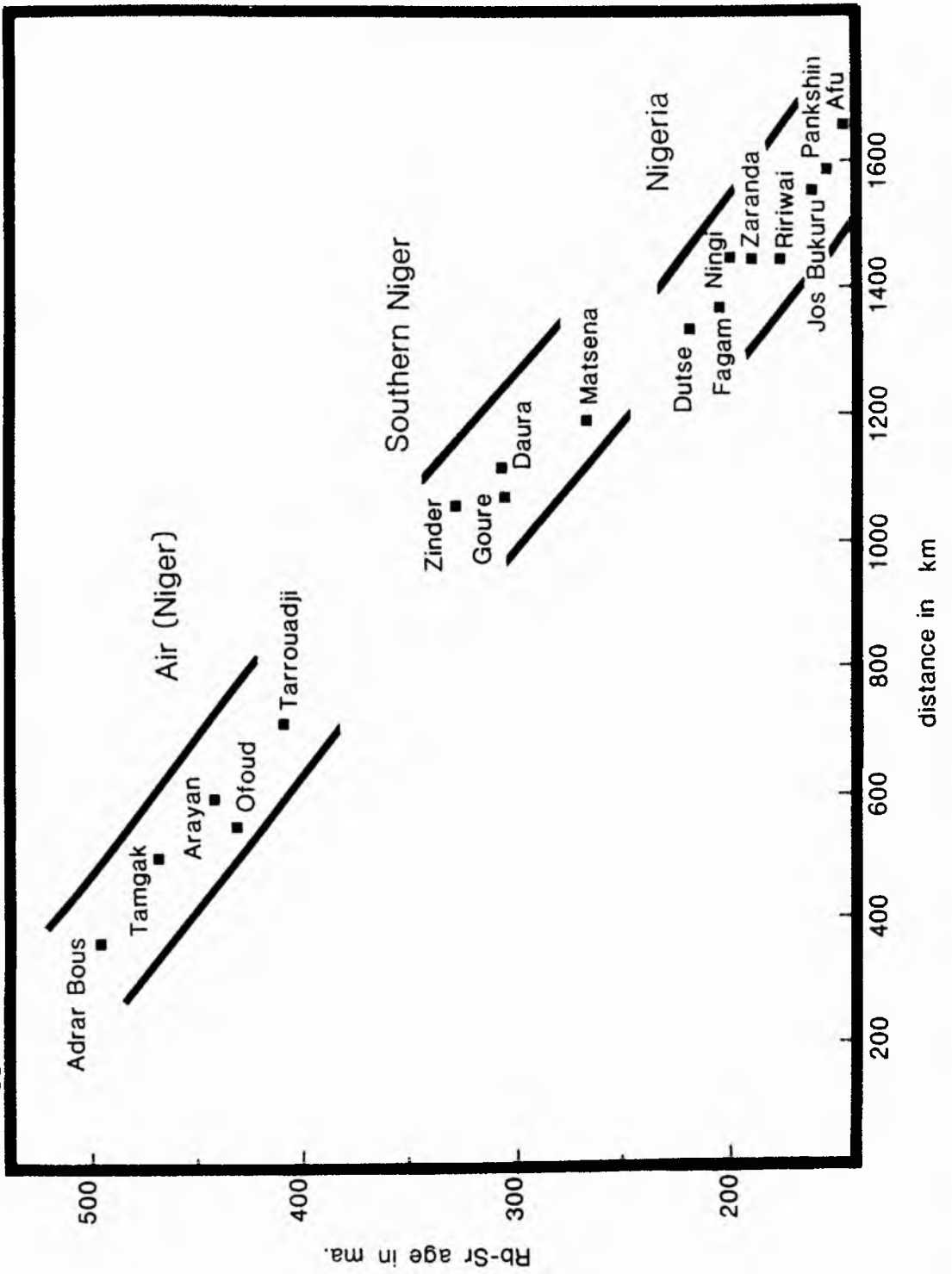
The granitoid suite is more than 95% granitic - intermediate and basic rocks, found in the Sara Fier, Sha Kaleri, Kila Warji and other complexes, constitute less than 5% of the area. There are several distinctive granite types:- metaluminous fayalite and hornblende bearing granites and porphyries; peralkaline granite and related syenites; and peraluminous biotite alkali feldspar granites and biotite syenogranites. These granites are chemically distinct from the suites of calc-alkaline and subalkaline granitoids intruded at the close of the Pan-African event some 600ma ago.

The various granite rock types are not uniformly distributed throughout the Province. Volcanic rocks are most abundant in the north where they form the major part of several complexes in particular the Ningi Burra Complex; in the Jos Plateau area of central Nigeria they only occur as small downfaulted remnants among the granitic intrusions; and volcanic rocks are absent from the southernmost complexes. This pattern of distribution as a first approximation must be due to the northern complexes being less deeply eroded than those of the south. The peralkaline granites have a similar pattern of distribution to the volcanic rocks; that is they are most abundant in the north, form a small proportion of certain complexes in the Plateau area and are absent from the southern complexes. The ring dykes reflect this distribution, so that in the northern complexes they are mainly peralkaline granite porphyries whilst those in the south are more often non-peralkaline. The bulk of the syenites and trachytes occur in the northeast of the Province where they are associated with peralkaline granites. Where they occur elsewhere in the province they are associated with fayalite granites. Biotite granites have a more limited distribution in the northern complexes than elsewhere, and where they do occur in the north, only their roof zones are exposed. In the central and southern group of complexes, massive intrusions of biotite- and hastingsite biotite granite are more common, with coarse, uniformly textured syenogranites - such as the Jos granite - becoming volumetrically more important in the central and southern group of complexes. The distribution of all the complexes in Nigeria, and their petrology, is shown in detail on the accompanying 1:500,000 scale map in the inset at the back of this thesis.

In the anorogenic ring complexes, a series of hydrothermal alteration processes with related mineralisation can be recognised (Kinnaird 1979). Early sodic metasomatism may affect all granite types. The effects of the later processes, beginning with potassic metasomatism are only well documented for the biotite granites. Subsequent acid metasomatism resulted in the process of greisenisation and silicification. Each hydrothermal process is characterised by a clearly defined sequence of ore deposition. Chloritisation, argillisation and zeolitisation are important but more restricted processes.

These hydrothermal processes affect all the granites. Where these processes have been extensive, disseminated and vein deposits of columbite, pyrochlore, cassiterite, and sphalerite, with sulphides of Cu, Fe, Mo and Bi developed in and around the roof and marginal zones of medium or fine-grained granite cupolas,

Fig 1.5 Diagrammatic representation of the variation in age (corrected to Rb-Sr decay constant  $\lambda = 1.42 \times 10^{-11} \text{ y}^{-1}$ ) with distance. Distances are calculated from the Hoggar (start of the Phanerozoic anorogenic magmatism) and projected onto the 9th meridian



with veins extending up to 2km out into the country rock. Such mineralisation is most extensive in biotite granites. In Niger, similar mineralisation has been noted, but it occurs on a much more limited scale owing to the predominance of peralkaline granites over biotite granites (Raulais 1946, 1948, 1957, 1959; Perez, 1985 ).

#### Present Study

The work carried out in this thesis is a detailed study of the mineralisation and hydrothermal alteration within the Nigerian younger granite province, with special emphasis on the Rishi area of the Saiya Shokobo Complex.

As the alluvial ores become exhausted, more interest will inevitably be centred on primary ore distribution. This thesis attempts to review the processes responsible for the introduction of the ore, the fluid chemistry responsible for hydrothermal alteration, the type of ore deposits, their structural setting, the origin of the magma and ultimately, the origin of the fluids.

CHAPTER 2  
PETROLOGY AND GEOCHEMISTRY OF THE NIGERIAN  
YOUNGER GRANITE PROVINCE.

## Introduction

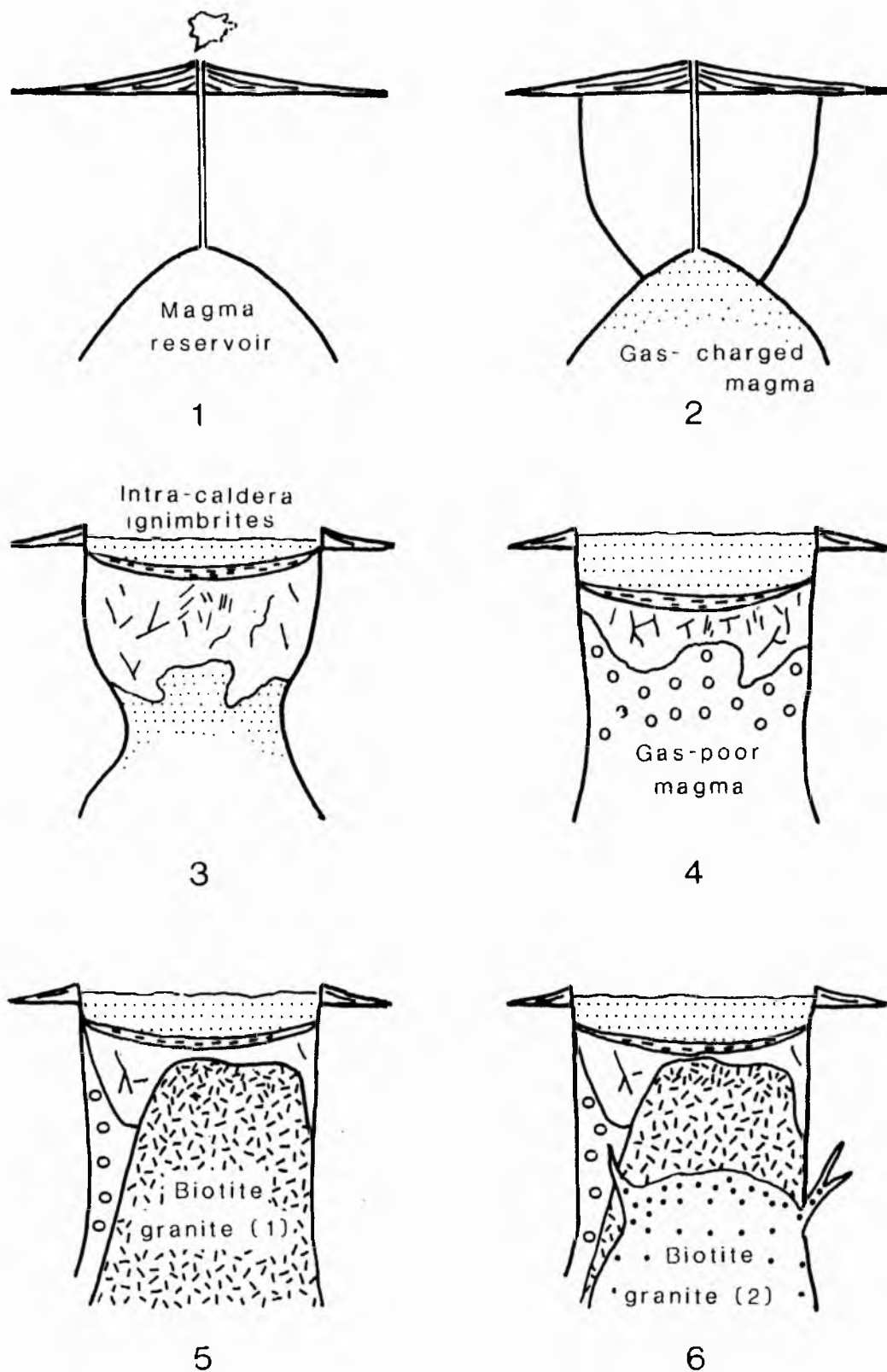
Most of the alkaline anorogenic centres are composed of chains of complexes often arranged concentrically as roots of volcanoes. The outer limits of most Younger Granite complexes are defined partly or completely by a ring dyke. This intrusion, generally composed of granite porphyry, is the chief structural element of the complex, controlling the distribution of both volcanic rocks and subvolcanic magmatism. Throughout the province all levels of erosion of the complexes can be studied from the volcanic centres of the north to the eroded centres of the Jos Plateau and southern Province. A schematic representation of the structural evolution of a typical ring complex is shown in Fig. 2.1. It illustrates the form of the volcanic and subvolcanic products found at different erosional levels, as well as the types and styles of extrusion and intrusion. Such a structural evolution of the Nigerian complexes, is typified by Ririwai (Kinnaird et al 1985a) and Tibchi (Ike 1983).

The frequency of occurrence and the coarse nature of the fragmentary ejecta suggests that the earliest igneous activity was violent and eruptive, dominated by pyroclastic products. Eruptive material formed a central shield volcano built on an updomed terrain (Stage 1 in Fig 2.1). At a later stage, a master cone-fracture was formed, which was inward dipping at depth but steepening to almost vertical towards the surface (Stage 2 in Fig 2.1). This ring fracture provided access to the surface for a fluidised granite magma. The sudden emptying of the magma chamber caused surface cauldron subsidence of the volcanic edifice and the concomitant extrusion of intra-caldera ignimbrites (Stage 3). The feeders to the ignimbrites were frozen as quartz fayalite porphyries (Stage 4). The granite porphyry of the ring dyke corresponds to the gas poor magma which partially displaced the quartz porphyry in the ring dyke fracture by stoping and marked the transition to the subvolcanic (plutonic) phase of activity (Stage 5).

In contrast to the early explosive volcanic activity, the phase of granite porphyry emplacement was quiescent and fracture controlled. The granite porphyry emplacement was by means of piecemeal stoping through the collapsed central block of basement. Subsequent granite intrusives stoped to high levels into the volcanic pile causing local contact metamorphism and hydrothermal fluid retention at the contact. In some complexes such as Banke and Tibchi, there was a single phase of granite emplacement but in the Kwandonkaya, Jos Bukuru, Tongolo and other complexes (Fig 1.4) the cycle of granite intrusion was repeated (Stage 6 in Fig 2.1). These intrusions commonly have an elliptical or semi-circular outline and often exhibit a centripetal arrangement of successive phases, with each of the subsequent intrusions having progressively smaller diameters. This phenomenon that can readily be explained by successive episodes of cauldron subsidence (Jacobson et al 1958). However, the pattern formed by successive granites can be profoundly eccentric and probably reflects shifts in

Fig. 2.1 Schematic representation of the structural evolution of a typical ring complex. Stages are described in the text.

(based on Kinnaird 1977 and Ike 1979)



the centre of magmatic activity with time (Bennett et al 1984). This migratory magmatic behaviour in the province has been discussed for the overlapping magmatic centres of the Sara Fier complex by Turner (1963) and for the Ningi Burra complex by Turner and Bowden (1979). Since, in general, individual magmatic centres in the province tend to have similar diameters, and activity at one centre ceased before a new centre was initiated, Turner (1963), suggested that a discrete high level magma chamber directly underlay each magmatic centre.

At certain erosional levels the volcanic products are preserved through caldera collapse following the classical caldera model based on Glen Coe. However, for the centres of the Jos Plateau and southern Province there is abundant evidence of resurgent caldera formation (Valles caldera model) so that the updomed volcanic cover has been eroded leaving a boss-like promontory of biotite granite. In some cases the granitic magma has not erupted onto the land surface but has been confined to a series of sheets and ring complexes, often referred to as underground cauldron formation.

#### VOLCANIC SUCCESSION

Most of the ring complexes in Nigeria, irrespective of whether they consist of isolated centres, or overlapping complexes, began as chains of volcanoes. Erosion of the complexes, particularly in the south, has removed much of the volcanic evidence. Where the volcanic rocks have been preserved by downfaulting of the caldera the magmatic evolution of the complexes can be established from preserved volcanic sequences. Even where the volcanics are well preserved in the northern complexes they are invariably confined within the major peripheral ring dykes.

The volcanic sequences are dominated by rocks of rhyolitic composition with thin basic horizons mainly in the lower parts of the volcanic succession. Igneous breccias containing a melange of acid and basic material (Plate 2.1), indicate that both types of magma must have been available at the time of ring fracturing. Evidence from the Ningi Burra complex (Turner and Bowden 1979), suggests that early volcanic evolution of the Nigerian ring complexes may have been similar to rift related activity.

The basic volcanic rocks, which account for less than 5% of the volcanic sequence, are olivine tholeiites with transitional basalts containing less than 3% modal hypersthene.

The intermediate suite of volcanic rocks, which are also volumetrically insignificant but petrologically important, can be divided into two suites (Bowden and Kinnaird 1984a). The alkaline suite of intermediate rocks includes hawaiites, mugearites and trachytes. The andesitic suite are volcanic compositions which may have resulted from the mixing of acid and basic components of successive pulses of magma.

The rocks of rhyolitic composition include ash-fall tuffs, agglomerates, minor lavas and abundant ignimbrites (Plate 2.2). The early ash-fall tuffs and agglomerates contain lithic fragments derived from underlying rock types. The ignimbrites, which range from finely crystalline to coarse, are characterised by broken crystals of quartz, phenocrysts of feldspar, and lithic fragments.



Plate 2.1      Fragmental volcanic rocks

Left    AP8      Agglomerates from the Ampan complex  
Right   BK3      Volcanic breccia from the Birnin Kudu complex



Plate 2.2      Ignimbrites with well developed fiamme

Left              Comendite from the Ririwai complex  
Right    B81      Welded tuff from the Banke complex

Lavas of rhyolitic composition form only a small portion of the acid volcanic pile. Their extrusion during the volcanic cycle may have occurred when volatile pressures had fallen from the pressures associated with ignimbrite eruption (Turner and Bowden 1979). Some ignimbrites contain sodic amphibole or pyroxene and have an agpaite coefficient greater than 1, giving them a peralkaline composition. These ignimbrites generally have structural and textural features which correspond to pantellerites and comendites.

In some complexes the volcanic rocks show the effects of post depositional devitrification or hydrothermal alteration and are occasionally strongly impregnated with haematite.

#### VOLCANIC FEEDER INTRUSIONS

The volcanic feeder intrusions which are the link between the subvolcanic intrusions and the overlying volcanic pile are all acid in nature. Structurally, the volcanic feeder intrusions take the form of cone sheets and ring dykes.

Thin, inward dipping cone sheets, often only a metre or two thick, occur around a number of central and northern complexes but are absent in the southern group of complexes. The cone sheets range from rhyolites, felsites and quartz porphyries to granophyres and microgranites.

The outer limits of most complexes are defined, either partially or completely, by a steep, outward-dipping ring dyke which is up to 2km wide. These ring dykes may be polygonal, circular or elliptical in outline with diameters ranging from 5 to 25km. Most ring dykes fractures have been filled by quartz or granite porphyry although some fractures may be filled by intrusions ranging in composition from granitic to syenitic and in texture from porphyritic to equigranular.

The quartz porphyries, often with ignimbritic textures but intrusive forms, represent part of the ash-flow material that froze within the ring fissures or cone sheets. Arrested growth forms of hedenbergite, feldspar and quartz phenocrysts are often visible in thin section.

The granite porphyries (Plate 2.3) represent the gas poor magma that followed behind the quartz porphyries emplaced into the ring fractures (Bowden and Kinnaird 1984a). In these rocks, variations in the composition and activity of the alkaline residual phase is observed by the appearance of Ca-Na amphibole replacing hedenbergite and fayalite, or a more sodic assemblage with arfvedsonite, aenigmatite and riebeckite together with annitic mica. Often with more continued reactions with residual fluids, the porphyritic texture was modified, the groundmass mineralogy coarsened and resulted in the formation of an equigranular texture of the biotite and peralkaline granites.

There is therefore a natural progression from porphyritic volcanic feeder intrusions to subvolcanic intrusions with equigranular textures.

## SUBVOLCANIC ROCKS

### Introduction

The subvolcanic intrusions, which are the terminal phase of magmatic activity occur either within the steep-sided ring fractures or as shallow dipping sheets or cupolas. Geophysical evidence (Ajakaiye 1968), indicates that the shallow dipping intrusions may extend beyond the confines of the ring fracture. However, there is generally a continuous sequence of intrusive forms from narrow ring dykes to large irregular plutons.

The subvolcanic intrusions are overwhelmingly syenitic to granitic in composition, with acid rocks accounting for more than 95% of the areal extent. Minor occurrences of basic and intermediate plutons are restricted to the Sha Kaleri, Sara Fier, Kila Warji complexes and a description of these is outside the purpose of this thesis. Basic rocks form less than 1% of the province and syenites around 4%. In every case, the basic intrusions are composed of rounded masses of gabbro net-veined with granite.

The syenites and alkaline granites have textural, petrological and chemical characteristics which are distinctly different from other granitoids and related rocks (Lameyre and Bowden, 1982). They form part of the A-type spectrum where A stands for anhydrous, alkaline and aluminous as well as anorogenic, to distinguish them from the well-known I and S types of Chappell and White. The alkaline granites which are the most abundant rock type in the Province, are defined partly on the dominant ferromagnesian minerals and on the Streckeisen modal classification. The mafic minerals are Fe-rich (eg fayalite, hedenbergite, annite etc) in keeping with the low Mg content of the rocks. The alkali feldspars range in structural state from orthoclase to maximum microcline - representing an increasing degree of post magmatic alteration. There are several distinctive granite types:-

- i) Metaluminous fayalite and hornblende bearing granites, syenites and porphyries with amphiboles or biotite plot in the granite field of Fig 2.2
- ii) Peralkaline granite and related syenites (with alkali or calcic amphibole in the compositional range ferrichterite to arfvedsonite in the granites and ferroedenite to ferroactinolite in the syenites) plot close to the Q-A join in the Streckeisen Q-A-P plot Fig 2.2.
- iii) Peraluminous biotite alkali feldspar granites and biotite syenogranites which plot close to the boundary between the two fields on the Streckeisen diagram.

### Fayalite and pyroxene-amphibole granites

Fayalite-bearing granites (Plate 2.4) and syenites are restricted in outcrop and are found in only eight complexes, whereas the pyroxene-amphibole bearing granites are found in a number of ring complexes. When fresh the fayalite granite contains a primary assemblage of fayalite and hedenbergitic clinopyroxene with orthoclase microperthite. Subsidiary reactions led to the



Plate 2.3 Hastingsite granite porphyries

Left KD1 from the Kudaru complex  
Right Sho39a Sho porphyry from the Ropp complex

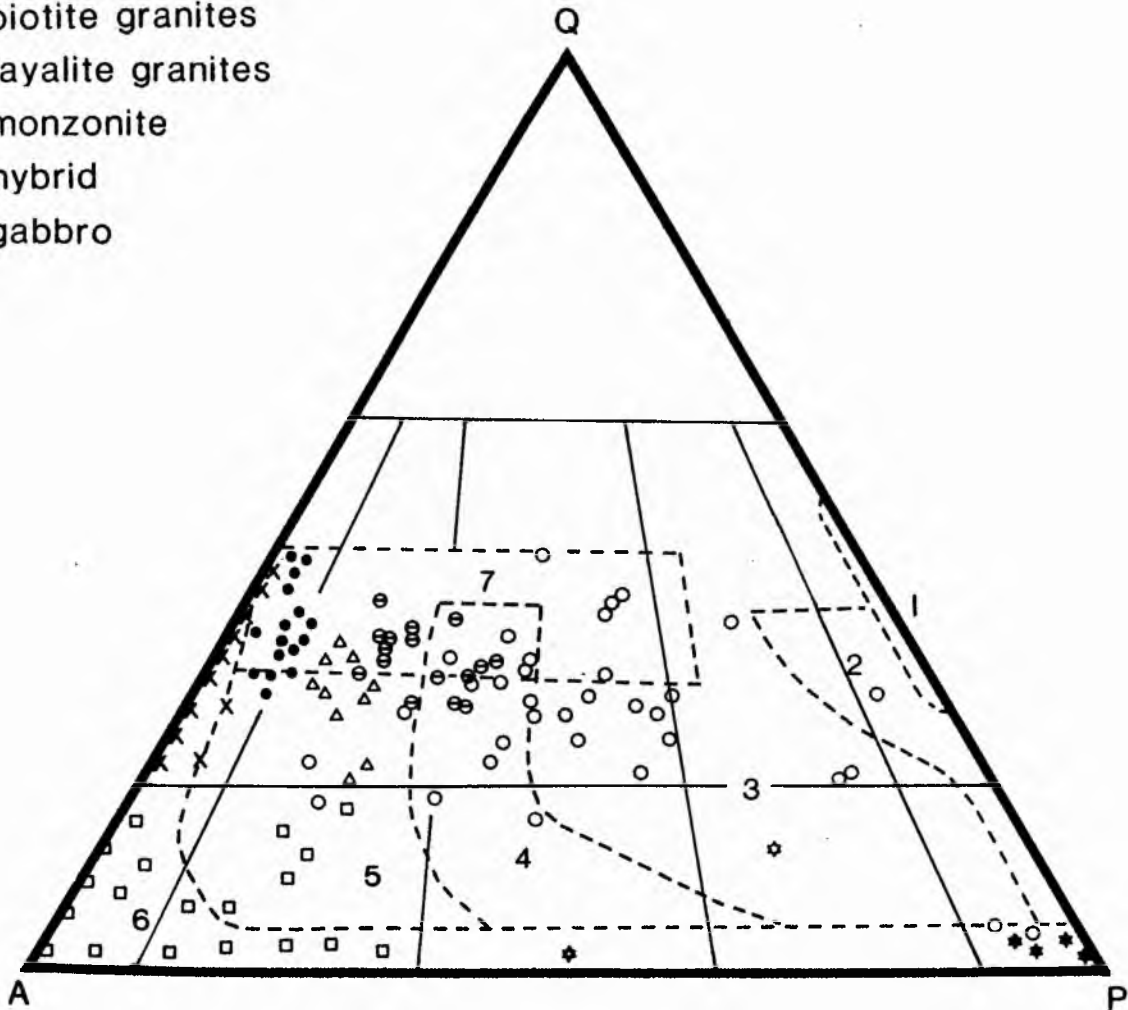


Plate 2.4 Fayalite granites

Left R20 Yelwa pyroxene fayalite granite from the Ropp complex  
Right JBJ200 Shen pyroxene fayalite granite from the Jos Bukuru complex

Fig 2.2 Summary quartz-alkali feldspar-plagioclase Streckeisen diagram showing the compositions of the Nigerian basement granitoids, the Niger/Nigerian ring complex granitoid suite (Bennett 1981) and the A-type granites of Australia (Collins et al. 1982), relative to the important fields of various global granitoid series, as defined by Lameyre and Bowden (1982).

- × peralkaline granites
- syenites
- biotite granites
- △ fayalite granites
- ⊛ monzonite
- ⊛ hybrid
- ⊛ gabbro
- A-type granites of the Lachlan fold belt
- Nigerian basement granitoids



conversion of the primary mafic assemblage to amphibole that belongs, either to a ferro-actinolite - ferroedenite trend in less evolved intrusions, or a ferro-actinolite - ferro-richterite trend in the more evolved intrusives (Ike et al 1985). The mafic assemblage, which occasionally includes biotite, is accompanied by quartz and microcline microperthite.

#### Peralkaline granites

The peralkaline granites and syenites, which are more abundant in the northern complexes, exhibit a wide variation in colour and texture (Plate 2.5). The granites are characterised by Na-Fe silicates such as aegirine and arfvedsonite. Ferrichterite arfvedsonite granite is volumetrically the most important member. The ferrichterite-arfvedsonite is mantled and replaced by aegirine, this transformation being the most striking in the granites. Minor zircon and riebeckite are occasionally associated with aegirine. The ferromagnesian minerals are accompanied by microcline perthite and interstitial albite laths. The riebeckite annite granites which occur in only five complexes, contain poikilitic riebeckite and ragged annite flakes in varying proportions. In the more peralkaline facies these may be accompanied by astrophyllite. The feldspar is microcline perthite with dentate intergranular margins of albite laths. The albitised peralkaline granites have a distinctive mineralogy and accessory mineral assemblage which is discussed in detail later in the thesis.

#### Biotite granite

The biotite granites are the most volumetrically abundant rock type of the province. The granites may occur within ring dykes, as circular plutons, cupolas and sheets. Although the biotite granites are mildly corundum normative, and peraluminous, they do not contain cordierite, muscovite or garnet as found in 2-mica leucogranites. Instead the excess alumina is partly linked with Li to form a series of trioctahedral micas varying from annite through siderophyllite and zinnwaldite to lepidolite and rarely trilithionite.

The biotite granites vary in texture from equigranular to porphyritic and sometimes granophyric. They range in grain size from very fine-grained to very coarse-grained (Plate 2.6). Textural variations even within one pluton characterise many of the biotite granites and such textural variations are often randomly arranged.

Commonly the biotite granites contain one feldspar occasionally as an albite-orthoclase but commonly as perthitic intergrowths and correspond to the hypersolvus granites of Tuttle and Bowen (1958). These one feldspar granites from high level, subvolcanic environments, have been interpreted as forming where cooling was relatively rapid and where the degree of unmixing of the two components in the perthitic intergrowths was slight. However, many of these perthites show lamellar, patchy or braided textures which are clearly related to lower temperature subsolidus processes.

Quartz is invariably the low temperature alpha form which occurs as irregularly shaped, composite grains sometimes interstitial to the feldspar, sometimes lobed into it. In the more potassic varieties containing large microclines, some quartz forms relatively small rounded inclusions in the latter, but some is moulded upon the microcline. Finally, quartz occurs as an



Plate 2.5 Peralkaline granites

- |        |      |   |
|--------|------|---|
| Left   | DT26 | Chilled margin of arfvedsonite granite from the Dutse complex       |
| Middle | RP11 | White equigranular biotite riebeckite granite from the Ropp complex |
| Right  | SH88 | Coarse arfvedsonite granite from the Shira complex                  |



Plate 2.6 Biotite granites

- |             |        |   |
|-------------|--------|---|
| Top left    | AF22/7 | Medium-grained biotite granite from Igo, Afu complex                          |
| middle      | AF10A  | Fine-grained Odegi biotite albite granite from the Afu complex                |
| right       | JB145  | Fine-grained Rayfield Gona biotite albite granite from the Jos Bukuru complex |
| Bottom left | JB128  | Coarse-grained Jos granite from the Jos Bukuru complex                        |
| right       | AF59/4 | Pink porphyritic biotite albite granite from the Afu complex                  |

anhedral mosaic that often shows strained extinction and frequently forms delicate myrmekitic intergrowths along feldspar boundaries.

## GEOCHEMICAL CHARACTERISTICS

### Introduction

The Nigerian granites have chemical characteristics that are distinct from the I and S types of Chappell and White (1974) or the 'magnetite series' and 'ilmenite series' proposed by Ishihara (1977) and fit into the group designated 'A type' by Loiselle and Wones (1979). Compared with typical I-type granitoids of similar silica contents, the A-type granitoids contain lower abundances of MgO, CaO, TiO<sub>2</sub> and P<sub>2</sub>O<sub>5</sub> but high K<sub>2</sub>O + Na<sub>2</sub>O. Probably the most significant chemical feature is that slight differences in the ratio of Na+K to Al can produce striking changes in the mineralogical composition of the suite. According to the agpaitic coefficient (Na+K/Al), the granites can be classified chemically into peralkaline, metaluminous and peraluminous. Peralkaline granites are characterised by Na-Fe silicates such as aegirine and arfvedsonite, metaluminous granites by fayalite and hedenbergite, and peraluminous granites by trioctahedral micas (Bowden and Kinnaird 1984a, Bowden 1985). The suite varies in differentiation index from

85.42 - 94.83 for fayalite granites  
83.58 - 96.37 for peralkaline granites  
89.03 - 98.37 for biotite granites

The peralkaline granites contain up to 13.11% ac in the norm whilst the peraluminous granites contain up to 4.65% normative corundum. Selected analyses for the different granite types are given in Tables 2.1 to 2.3.

### Major element chemistry

On the basis of 300 whole-rock analyses, Bennett et al. (1984), showed a negative correlation against silica for TiO<sub>2</sub>, MgO, Al<sub>2</sub>O<sub>3</sub>, CaO and total Fe. Harker diagrams constructed for this thesis on nearly 500 whole-rock analyses of granites and syenites confirm the negative correlation against silica for these elements and for MnO and P<sub>2</sub>O<sub>5</sub>. In addition the data for Na and K versus silica, not included in the Bennett et al compilation, has also been included. Here the picture is much less clear and the anticipated positive correlation against silica is not obvious (Table 2.4 gives a correlation matrix for major and trace element data in the Niger-Nigeria Younger Granite Province.) Although the data of Bennett et al (1984) indicates that there is a continuous evolution from compositions with 50% silica to granitic rocks with over 70% silica this is not strictly the case. If the number of samples are plotted as histograms of frequency then there does appear to be a "Daly" gap between compositions of less than 50% silica and compositions of greater than 60% silica. By selecting only one in six samples to illustrate Fig 2.3 (and in 2.6) this gap is highlighted.

The generalised variation in major and oxides with fractionation as recorded by increasing silica can be seen in Fig. 2.4. In general the data shows a smooth progression from gabbros through syenitic rocks to granites. With increasing silica, TiO<sub>2</sub>, MgO and CaO show a marked initial depletion in the metaluminous rocks which is thought to reflect incorporation of MgO and CaO into early pyroxene and CaO into apatite and feldspar, whilst in the case of TiO<sub>2</sub> and P<sub>2</sub>O<sub>5</sub>

Table 2.1 Major and trace element analyses and CIPW compositions of some Nigerian fayalite granite porphyries (AP5-T180) syenites (KW6) and quartz syenites NGL7-PN119

	Ampan AP5	Birnin Kudu BK11	Ririwai N96	Jos-Bukuru JBJ151	Mada MD35	Wase WS13	Zigau ZGI	Tibchi TIO8	Ningi-Burra NGL7	Kila Warji KWL	Pankshin PN119	Kila Warji KW6
SiO <sub>2</sub>	72.70	74.20	71.40	76.00	76.60	75.20	71.40	72.90	62.20	62.20	67.10	59.70
TiO <sub>2</sub>	0.07	0.10	0.28	0.10	0.10	0.20	<0.10	0.30	0.99	0.77	0.21	0.96
Al <sub>2</sub> O <sub>3</sub>	14.30	12.78	13.39	12.07	12.59	12.49	13.72	11.38	14.58	14.95	16.24	15.20
Fe <sub>2</sub> O <sub>3</sub>	0.42	1.73	1.58	0.88	0.34	0.91	1.17	2.82	1.93	3.65	0.75	1.83
FeO	1.58	0.28	2.30	0.59	1.49	2.19	2.62	0.98	6.13	3.91	2.38	6.74
MnO	0.05	0.05	0.15	0.04	0.04	0.09	0.11	0.08	0.17	0.18	0.06	0.17
MgO	0.02	0.07	0.04	0.01	0.06	0.01	0.13	0.12	0.88	0.66	0.04	1.26
CaO	0.62	0.71	0.74	0.54	0.56	0.49	0.89	0.83	3.47	2.97	1.21	4.11
Na <sub>2</sub> O	5.15	3.75	4.02	3.26	3.72	4.49	4.54	4.07	4.13	4.62	4.94	4.63
K <sub>2</sub> O	4.87	4.88	5.17	4.45	4.92	4.67	5.13	5.10	4.92	4.66	5.67	3.97
P <sub>2</sub> O <sub>5</sub>	0.01	0.01	0.04	0.01	0.01	0.01	0.05	0.03	0.15	0.31	0.11	0.47
H <sub>2</sub> O <sub>t</sub>	0.35	0.64	0.37	0.48	0.28	0.28	0.74	0.98	0.80	0.90	0.36	0.89
F											0.15	
O=F											-0.06	
Total	100.14	99.20	99.48	98.43	100.71	101.03	100.50	99.59	100.35	99.78	99.16	99.93
A/CNK	0.96	1.00	0.99	1.08	1.01	0.94	0.94	0.83	0.79	0.83	0.99	0.78
R1	1818.7	2414.5	2007.7	2821.2	2576.7	2232.48	1851.00	2111.3	1281.6	1293.4	1298.6	1146.0
R2	348.2	330.5	344.2	295.4	310.2	298.3	371.00	318.3	701.2	644.1	450.5	800.7
Li	9	3	24	153	40	9	33	21	11	9	7	5
Be	8	5	5	4	30	10	2	4	4	4	9	1
Cu		6	134		4			12				
Zn	93	134	177		129	102	109	157	135	110	56	91
Rb	157	167	137	542	238	140	75	100	72	60	107	50
Sr	3	19	10	4	13	10	22	33	208	181	21	300
Y	84	131		159	98	109	23		59	54	153	51
Zr	653	318	830	157	254	847	581	460	1114	703	533	617
Nb	106	88		162	95	189			38	53	41	43
SnO <sub>2</sub>	0	19	17	84	20	0		7	0	8	13	13
Ba	0	65		12	0	29		472	1136	895	149	1108
La	75	89		100	61	120		143	99	113	43	86
Ce	163	187		159	93	242		259	208	222	98	170
Hf	18	9		6	194	20		11	20	13	11	11
Pb	21	41	30	54	8	26		34	15	20	11	17
Th	30	7	20	64	38	30			1	13	17	7
TTDI	94.30	92.68	90.06	92.62	94.35	94.83	90.83	89.94	74.72	77.56	88.47	68.29
Qu	21.97	32.13	25.51	38.76	33.81	29.26	22.12	29.67	9.04	10.96	13.19	5.67
Ortho	28.77	28.83	30.55	26.29	29.07	27.59	30.31	30.13	30.01	27.53	33.50	23.46
Alb	43.56	31.72	34.00	27.57	31.46	37.97	38.40	30.14	45.67	39.07	41.78	39.16
Anor	1.53	3.46	3.23	2.61	2.71	0.14	1.92		1.24	6.30	4.26	8.98
Cor		0.07		0.94	0.15				0.84		0.42	
Ac												
Wo								3.77				
di & Wo								1.11				
& En	0.62		0.07			0.93	0.91	0.52		2.68		3.48
& Fs	0.01					0.01	0.08	0.30		0.93		0.90
Hy & En	0.68		0.08			1.04	0.93	0.20		1.82		2.77
& Fs	0.04	0.17	0.10	0.02	0.15	0.02	0.25		1.27	0.72	0.10	2.23
Ol & Fo	1.85		2.65	0.27	2.36	2.06	2.95		8.87	1.41	3.52	6.83
& Fa								2.20				
Mag	0.61	0.78	2.29	1.28	0.49	1.32	1.70		2.23	5.29	1.09	2.65
Haem		1.19										
Il	0.13	0.19	0.53	0.19	0.19	0.38	0.19	0.57	1.33	1.46	0.40	1.82
Ap	0.02	0.02	0.09	0.02	0.02	0.02	0.12	0.07		0.74	0.26	1.11
Water	0.35	0.64	0.37	0.48	0.28	0.28	0.74	0.98	0.52	0.90	0.36	0.89
Fluor											0.29	

Table 2.2 Major and trace element analyses and CIPW normative compositions of some Nigerian peralkaline (arfvedsonite) granites

	Shere SRN13	Dutae DUT23	Shira SH5	Zaranda ZAN46	Afu AF97	Fagam FGI2	Kila Warji KW19	Matsena MI	Ningi NG1	Pankshin PAN127	Ririwai N80	Ririwai N83
SiO <sub>2</sub>	74.70	74.00	74.95	72.20	76.41	76.50	71.20	73.50	76.70	72.00	76.30	76.50
TiO <sub>2</sub>	0.10	0.10	0.16	0.34	0.20	0.10	0.33	0.40	0.06	0.08	0.18	0.14
Al <sub>2</sub> O <sub>3</sub>	12.56	11.92	9.11	13.68	11.78	11.17	11.41	11.75	11.69	14.73	10.41	11.09
Fe <sub>2</sub> O <sub>3</sub>	1.97	1.75	1.94	1.34	1.57	1.31	4.98	1.49	0.43	3.49	1.49	1.63
FeO	0.99	1.82	4.01	1.71	0.00	0.96	0.72	1.80	1.33	0.00	0.74	0.80
MnO	0.03	0.08	0.10	0.07	0.05	0.04	0.08	0.06	0.04	0.07	0.05	0.05
MgO	0.01	0.01	0.07	0.01	0.04	0.01	0.04	0.02	0.01	0.02	0.03	0.01
CaO	0.17	0.26	0.29	0.21	0.46	0.24	0.27	0.24	0.25	0.42	0.35	0.25
Na <sub>2</sub> O	4.44	4.55	4.19	4.81	3.70	3.78	5.44	4.21	4.26	4.07	3.68	3.77
K <sub>2</sub> O	4.03	4.70	4.79	5.31	5.21	4.20	4.95	4.82	4.46	5.73	5.18	4.97
P <sub>2</sub> O <sub>5</sub>	0.01	0.01	0.01	0.01	0.02	0.01	0.03	0.01	0.02	0.00	0.01	0.01
H <sub>2</sub> O <sub>t</sub>	0.39	0.26	0.28	0.06	0.34	0.22	0.17	0.38	0.31	0.00	0.56	0.48
F	0.33	0.00	0.00	0.08	0.00	0.00	0.00	0.00	0.00	0.07	0.24	0.22
∑F	-0.14	0.00	0.00	-0.03	0.00	0.00	0.00	0.00	0.00	-0.03	-0.10	-0.09
TOTAL	99.29	99.46	99.92	99.80	99.78	98.54	99.62	98.68	99.56	100.65	99.12	99.83
A/CNK	1.05	0.91	0.72	0.97	0.94	1.00	0.77	0.93	0.95	1.08	0.85	0.92
R1	2355.7	2116.0	2217.0	1768.8	2511.5	2707.3	1499.5	2174.9	2502.3	1920.2	2500.2	2526.5
R2	265.4	262.5	211.0	291.7	282.6	245.6	255.0	257.5	256.9	335.3	243.4	245.1
Li	118	33	58	32	22	130	23	50	130	13	90	83
Be	6	8	9	6		10	10	8	9	7	27	8
V	0	1		0		0	0	0	0	0	0	0
Cu										39	117	117
Zn		165	166	71	98	275		160	315	318	235	478
Rb	212	116	219	82		291	181	140	361	129	298	411
Sr	1	5	<8	4		4	4	16	0	27	9	5
Y	136	76	16	22		254	66	92	104	98	114	590
Zr	689	869	666	423		685	1594	880	587	554	565	815
Nb	192	86		47		210	114	135	185	139	158	245
SrO <sub>2</sub>		8			54	46	8	20	34		25	17
Ba	0	33		8		0	0	138	0	64	40	0
La	74	102		149		155	116	35	32	145	111	139
Ce	163	231		286		213	221	98	86	297	215	286
Hf	22	17		7		23	38	18	20	15	20	26
Pb	55	18		3		93	29	33	95	21	70	55
Th	18	10		2		23	21	19	53	31	111	61
TTD1	94.48	91.73	83.58	95.13	96.49	94.47	83.86	91.93	95.41	93.99	91.82	94.59
Qu	33.12	28.83	35.09	23.08	34.41	37.69	23.49	29.85	33.76	25.71	36.51	35.85
Orth	23.81	27.77	28.30	31.37	30.78	24.81	29.25	28.48	26.35	33.85	30.60	29.36
Alb	37.55	35.14	20.19	40.68	31.29	31.99	31.13	33.60	35.30	34.42	24.71	29.37
Ancr		0.00		0.06	0.16	1.11				1.57		
Ac		2.94	5.61				13.11	1.77	0.65		4.31	2.21
Wo					0.51							
Di & Wo		0.51	0.57	0.14	0.12		0.48	0.47	0.46			
& En		0.01	0.02		0.10		0.08	0.01	0.01			
& Fs		0.57	0.63	0.16			0.44	0.52	0.52			
Hy & En	0.02	0.02	0.16	0.02		0.02	0.02	0.04	0.02	0.05	0.07	0.02
& Fs	0.08	2.15	6.65	1.45		0.58	0.12	1.51	1.73		1.15	0.62
Mag	2.86	1.06		1.94		1.90	0.65	1.28	0.30			1.25
Haem					1.57					3.49		
Il	0.19	0.19	0.30	0.65	0.11	0.19	0.63	0.76	0.11	0.15	0.34	0.27
Titan					0.35							
NB			2.07								0.36	
Ap	0.02	0.02	0.02	0.02	0.05	0.02	0.07	0.02	0.05		0.02	0.02
Water	0.39	0.26	0.28	0.06	0.34	0.22	0.17	0.38	0.31	0.00	0.56	0.48
Fluor	0.22			0.16						0.14	0.47	0.33

Table 2.3 Major and trace element analyses and CIPW normative compositions of some Nigerian biotite granites

	Amo AMN24	Ririwai RN75	Pankshin PAN112	Jos-Bukuru JON147	Banke B37	Mada MD33/3	Ningi NG208	Tibchi T15A	Ropp DR11	Dutsen Mai DW1	Fagari FG5	Kuduru KD12
SiO <sub>2</sub>	72.60	75.90	73.90	73.20	76.30	75.40	76.70	74.30	76.70	78.03	77.44	76.50
TiO <sub>2</sub>	0.29	0.11	0.15	0.18	0.04	0.10	0.20	0.08	0.14	0.06	0.08	0.10
Al <sub>2</sub> O <sub>3</sub>	14.07	12.85	14.88	14.18	12.10	13.33	13.18	11.74	13.36	12.14	11.99	12.83
Fe <sub>2</sub> O <sub>3</sub>	0.90	0.33	0.43	0.67	0.00	0.01	1.48	0.33	0.00	0.33	0.38	0.35
FeO	1.73	1.05	0.80	1.19	1.45	0.96	0.01	0.89	1.16	0.89	0.87	0.84
MnO	0.07	0.05	0.02	0.02	0.03	0.02	0.03	0.02	0.03	0.01	0.02	0.02
MgO	0.43	0.02	0.67	0.08	0.08	0.04	0.09	0.01	0.05	0.09	0.07	0.07
CaO	1.01	0.24	0.43	0.73	0.49	0.34	0.44	0.26	0.33	0.52	0.49	0.46
Na <sub>2</sub> O	3.36	3.91	3.98	3.45	3.95	4.26	3.41	3.98	4.41	4.59	3.89	4.17
K <sub>2</sub> O	5.74	4.31	5.17	5.32	4.86	4.53	5.10	4.59	3.58	3.56	4.45	4.85
P <sub>2</sub> O <sub>5</sub>	0.07	0.01	0.02	0.03	0.00	0.01	0.01	0.01	0.02	0.01	0.01	0.01
H <sub>2</sub> O <sub>t</sub>	0.35	0.52	0.45	0.51	0.32	0.20	0.66	0.64	0.34	0.42	0.34	0.34
F	0.12	0.36	0.16	0.47	0.00	0.00	0.00	0.00	0.00	0.00	0.00	0.00
O=F	-0.05	-0.15	-0.07	-0.20	0.00	0.00	0.00	0.00	0.00	0.00	0.00	0.00
Total	100.69	99.51	100.99	99.83	99.62	99.20	101.31	96.75	100.12	100.65	100.02	100.08
A/CNK	1.04	1.12	1.15	1.11	0.96	1.06	1.11	0.99	1.14	0.98	0.99	1.03
R1	2221.23	2617.36	2262.01	2350.85	2500.2	2419.27	2661.41	2461.32	2668.12	2698.69	2699.01	2551.94
R2	405.79	279.12	371.58	360.63	294.1	300.23	310.46	258.95	300.25	298.59	291.44	304.73
Li	34	391	25	32	110	158	13	122	558	138	67	56
Be	5	7	8	14	20	8	16	12	15	10	13	9
V	9	0	0	0	4	0	2	3	4	0	0	0
Cu		120				9		7				
Zn	61	376		126	117	68	70	61	103	77	42	48
Rb	185	979	192	296	422	620	318	502	966	389	347	283
Sr	100	15	28	38	1	0	29	1	0	22	3	4
Y	63	696	117	227	150	139	75	86	87	356	189	144
Zr	246	399	234	330	217	129	186	166	81	207	161	147
Nb	57	214	88	118	210	78	80	132	119	205	148	96
SnO <sub>2</sub>	8	40	19	39	25	0	34		76	10	10	
Ba	362	109	80	264	0	0	151	0	0	71	43	4
La	59	234	189	218	70	28	83	166	88	169	64	27
Ce	144	296	195	251	116	79	156	153	149	275	117	62
Hf	6	28	7	8	11	9	7	7	9	10	8	6
Pb	22	56	22	38	48	70	57	37	47	16	27	41
Th	27	111	25	41	50	66	63	69	61	42	39	36
TTDI	90.24	94.47	93.42	92.66	94.81	94.60	95.29	93.03	94.20	95.89	95.38	95.09
Qu	27.91	35.94	29.21	32.05	32.69	31.80	36.32	33.10	35.75	36.03	36.18	33.89
Orth	33.91	25.46	30.55	31.43	28.71	26.76	30.13	27.12	21.15	21.03	26.29	25.94
Alb	28.42	33.07	33.66	29.18	33.41	36.03	28.84	32.82	37.30	38.82	32.90	35.27
Anor	3.72	0.00	0.84	0.00	0.94	1.62	2.12	1.07	1.51	2.02	2.12	2.22
Cor	0.97	1.76	2.43	2.75		0.83	1.28	0.00	1.68	0.00	0.00	0.41
Hy & En	1.07	0.05	1.67	0.20	0.15	0.10	0.22	0.02	0.12	0.19	0.16	0.17
& Fs	2.08	1.57	0.90	1.37	2.01	1.63	0.00	1.19	1.95	1.09	1.10	1.13
Mag	1.30	0.48	0.62	0.97		0.01	0.00	0.48	0.00	0.48	0.54	0.51
Haem	0.00	0.00	0.00	0.00		0.00	1.48	0.00	0.00	0.00	0.00	0.00
Il	0.55	0.21	0.28	0.34	0.08	0.19	0.09	0.15	0.27	0.11	0.15	0.19
Ap	0.17	0.02	0.05	0.07		0.02	0.02	0.02	0.05	0.02	0.02	0.02
Water	0.35	0.52	0.45	0.51	0.32	0.20	0.66	0.64	0.34	0.42	0.34	0.34
Fluor	0.23	0.32	0.33	0.96	0.00	0.00	0.00	0.00	0.00	0.00	0.00	0.00

Table 2.4 Correlation matrix for major and trace elements in the Niger-Nigeria Younger Granite Province (taken from Bennett 1981)

	TiO <sub>2</sub>	Al <sub>2</sub> O <sub>3</sub>	Fe <sub>2</sub> O <sub>3</sub>	FeO	MnO	MgO	CaO	Na <sub>2</sub> O	K <sub>2</sub> O	P <sub>2</sub> O <sub>5</sub>	H <sub>2</sub> O <sup>+</sup>	Li	Zn	Rb	Sr	Y	Zr	P.I.	K/Rb
SiO <sub>2</sub>	-0.84	-0.76	-0.46	-0.90	-0.47	-0.84	-0.93	0.14	0.71	-0.72	-0.56	0.22	0.15	0.40	-0.89	0.19	0.08	0.73	-0.53
		0.49	0.45	0.82	0.37	0.72	0.82	-0.25	-0.70	0.64	0.47	-0.19	-0.14	-0.35	0.85	-0.17	-0.05	-0.60	0.55
		Al <sub>2</sub> O <sub>3</sub>	0.12	0.58	0.27	0.57	0.66	0.05	-0.46	0.46	0.35	-0.12	-0.20	-0.26	0.65	-0.17	-0.30	-0.74	0.34
			Fe <sub>2</sub> O <sub>3</sub>	0.29	0.26	0.27	0.34	-0.01	-0.27	0.31	0.29	-0.25	0.02	-0.32	0.41	-0.11	0.42	-0.14	0.40
				FeO	0.54	0.76	0.85	-0.19	-0.70	0.78	0.51	-0.15	-0.15	-0.34	0.80	-0.18	-0.10	-0.64	0.51
					MnO	0.34	0.38	-0.12	-0.30	0.51	0.36	-0.11	-0.01	-0.18	0.36	-0.08	0.02	-0.25	0.31
						MgO	0.91	-0.37	-0.81	0.50	0.45	-0.13	-0.16	-0.26	0.73	-0.13	-0.17	-0.74	0.28
							CaO	-0.36	-0.81	0.66	0.51	-0.19	-0.20	-0.36	0.90	-0.19	-0.17	-0.81	0.40
								Na <sub>2</sub> O	0.25	-0.17	-0.25	0.28	0.37	0.29	-0.30	0.21	0.22	0.57	-0.02
									K <sub>2</sub> O	-0.52	-0.45	-0.02	0.05	0.11	-0.75	0.09	0.10	0.76	-0.14
										P <sub>2</sub> O <sub>5</sub>	0.57	-0.12	-0.11	-0.27	0.64	-0.10	-0.03	-0.41	0.41
											H <sub>2</sub> O <sup>+</sup>	-0.14	-0.07	-0.21	0.48	-0.01	-0.04	-0.44	0.21
												Li	0.58	0.76	-0.20	0.36	-0.01	0.18	-0.37
													Zn	0.66	-0.18	0.40	0.39	-0.32	-0.27
														Rb	-0.37	0.47	0.15	0.31	-0.56
															Sr	-0.19	-0.12	-0.76	0.48
																Y	0.20	0.24	-0.28
																	Zr	0.33	-0.01
																		P.I.	-0.25
																			K/Rb

Fig 2.3. Harker diagrams showing major oxides for samples from the Niger/Nigeria Province. Symbols as in Fig 2.2. All figures are in percent values.

Data derived from Batchelor (1983) and this thesis.

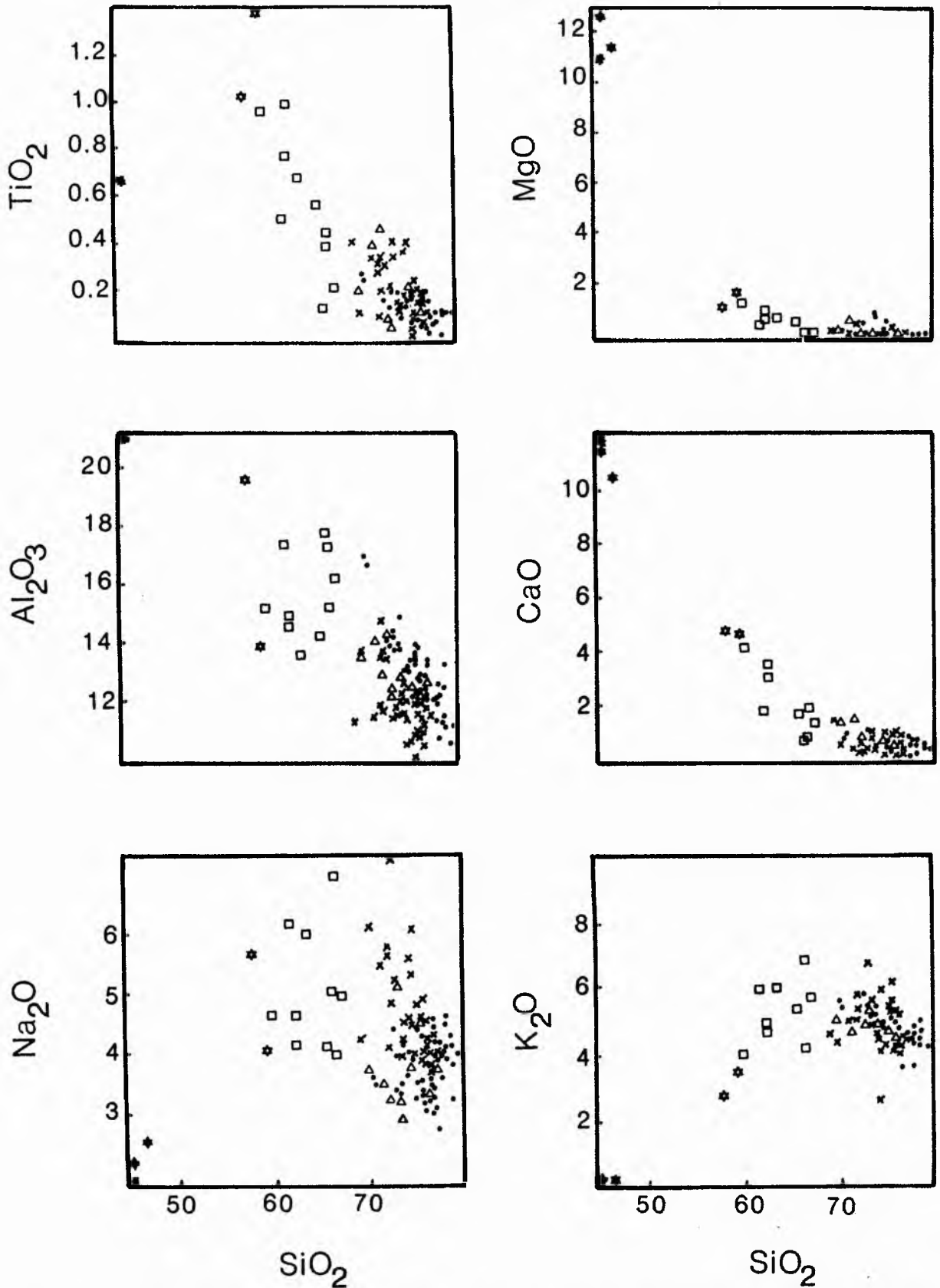
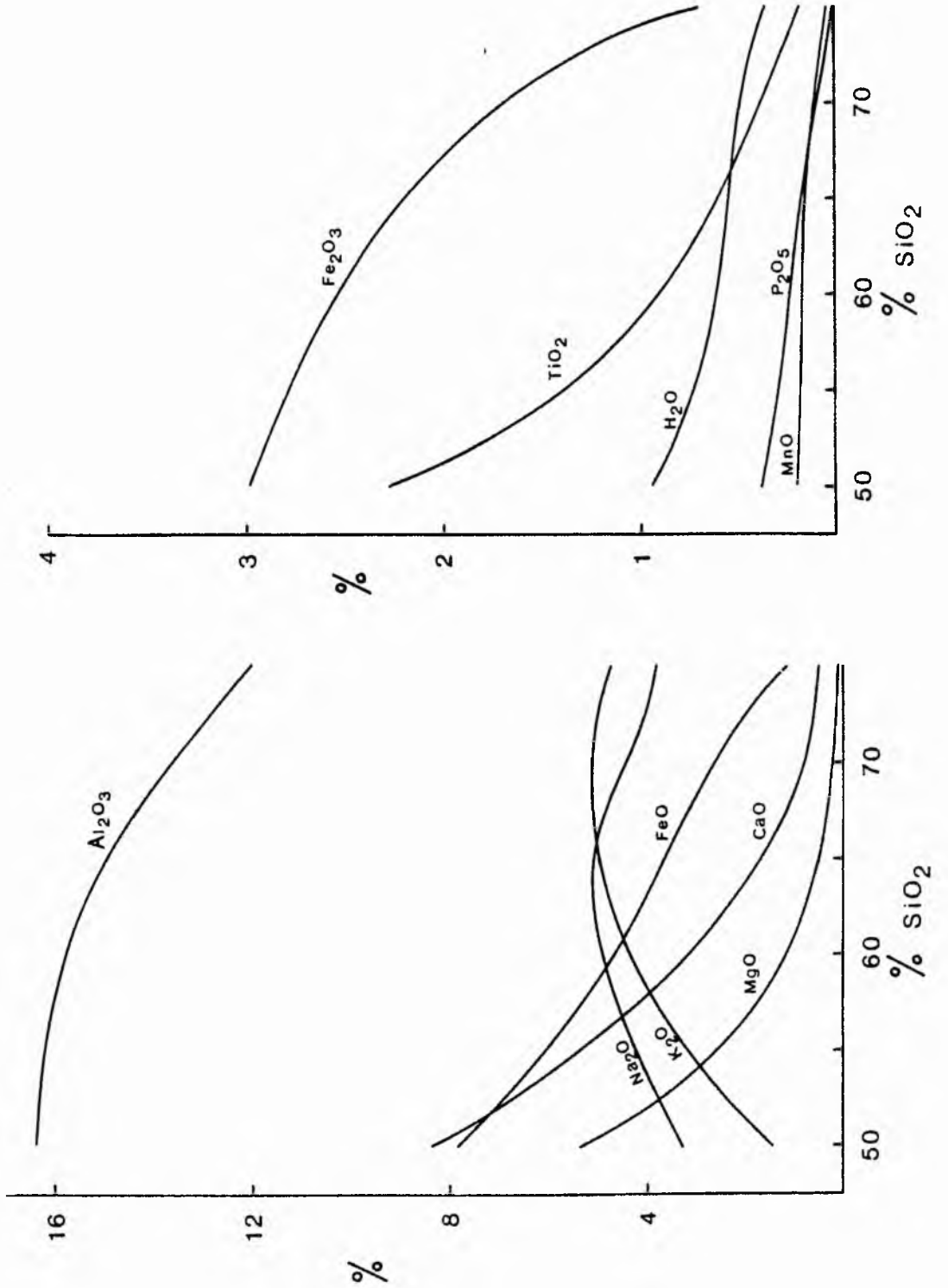


Fig 2.4. Summary Harker diagrams of averaged values for the major and minor elements in the alkaline rocks of the Niger-Nigeria anorogenic province



the fractionating phases were Fe-Ti oxides and apatite. There then follows a much more modest reduction in these oxides against silica concentration. In contrast the total iron content has a more or less linear decline against silica; the  $Al_2O_3$  content remains steady up to 60% silica (i.e. the intermediate stage) and then declines. When the variation in the suite as a whole is considered, however, fractional removal of such mineral phases denoted above has only made a limited contribution to the overall evolution of the magmas. Fractional crystallisation alone cannot account for granites with silica enrichment higher than that of a minimum melt and other factors must therefore be involved. In addition, the data for Na and K does not show the anticipated positive correlation against silica clearly, either for the peralkaline or peraluminous granites. This is because subsequent hydrothermal alteration and fluid phase transfer has undoubtedly modified part of the original granite chemistry.

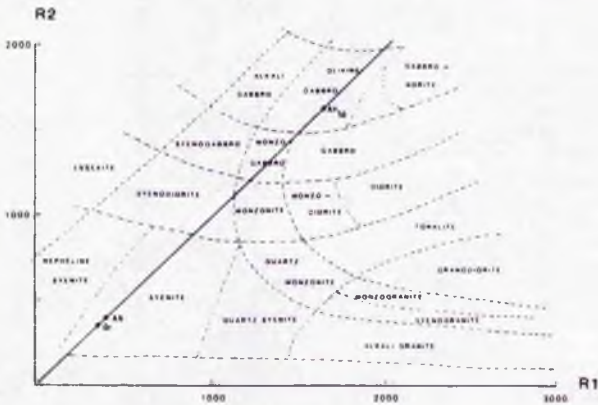
The major element chemistry of all the Nigerian rock types has been calculated using the R1-R2 multicationic scheme of de la Roche (1978) and the data are presented in Fig 2.5. The cationic data for most chemical analyses of the Nigerian volcanic rocks (Fig 2.5a), defines an alkaline magmatic lineage. This curvilinear trend on the diagram ranges from olivine basalt and hawaiite through mugearite and trachyte to alkaline rhyolite. In contrast, trachyandesites lie on a different trend which has been interpreted as mixing between basaltic and rhyolitic magma (Bowden and Kinnaird 1984a). The cationic proportions of the major oxides plotted for the subvolcanic rocks (Fig 2.5b and c), shows that the basic intrusives, the syenites, quartz syenites and fayalite granites lie on the volcanic trend. In contrast the alkaline syenites, the arfvedsonite granites, the zinnwaldite albite granite and some biotite granites do not lie on the volcanic trend. The major element chemistry of this group of granites has been interpreted as due to hydrothermal alteration by Bowden and Kinnaird (1984b). Thus the multicationic diagrams display not only the magmatic series of rocks of the Nigerian anorogenic province but also those rocks influenced by postmagmatic processes.

#### Trace element chemistry

Trace element data, when plotted against  $SiO_2$  (Fig 2.6) show increased Li, Rb, Zr, Zn, Sn, Nb, Y and F in the range 45-70%  $SiO_2$  and a marked increase in all these elements in the range 70-80% silica with corresponding decreases in Ba & Sr. In fact there is virtually a linear decrease in Sr with increasing silica. The granitoids display flat or HREE-enriched trends on chondrite-normalised diagrams with attendant strong Eu depletion. There is an enrichment in large ion lithophile (LIL) elements and high field strength (HFS) elements, particularly Nb, Sn, Hf, Zr and Ga, increases in Zn, Pb, Y and low abundances of the transition metals V, Ni, Co and Cr.

The trace elements together with most major and many minor elements therefore, show continuous variation trends from early to late-stage rocks. Although most LIL elements, especially Rb show a predictable increase in abundance with increasing degree of differentiation, some such as Ba show a regular decrease. The trends observed on the Harker diagrams (Fig 2.6) may be interpreted as paths of evolution towards successively more silica enriched and total iron-, MgO-,  $TiO_2$ -, and  $Al_2O_3$ -depleted liquid compositions. Fractional crystallisation involving plagioclase, biotite, magnetite and ilmenite could be responsible for

Fig 2.5 Major element multicationic scheme for the classification of igneous rocks



The de la Roche R1-R2 diagram showing petrographic divisions (Ab = albite; An<sub>50</sub> = plagioclase An<sub>50</sub>; Or = orthoclase). After de la Roche (1980).

Calculation of R1-R2 parameters

	Weight percent oxide	Molecular weight, M.W.	Number of cations	Cationic proportions	Millications per 100 g
SiO <sub>2</sub>	73.60	60.09	x 1	1.225	1,225
TiO <sub>2</sub>	0.10	79.90	x 1	0.001	1
Al <sub>2</sub> O <sub>3</sub>	13.17	101.96	x 2	0.258	258
Fe <sub>2</sub> O <sub>3</sub>	0.99	159.69	x 2	0.012	12
FeO	1.61	71.85	x 1	0.022	22
MgO	0.06	40.30	x 1	0.001	1
CaO	0.70	56.08	x 1	0.012	12
Na <sub>2</sub> O	3.69	61.98	x 2	0.119	119
K <sub>2</sub> O	5.38	94.20	x 2	0.114	114

$$R1 = 4Si - 11(Na + K) - 2(Fe + Ti) = 4900 - 11(233) - 2(12 + 22 + 1) = 2267$$

$$R2 = 6Ca + 2Mg + Al = 72 + 2 + 258 = 332$$

(a) The R1-R2 diagram depicting trends of volcanic compositions for Niger and Nigeria. Tibchi mixing trend calculated from chemical analyses of basalt (T53) and rhyolite (T153) taken from Ike (1979). Closed stars represent original compositions. Open stars are 80/20 and 60/40 mixes: partially closed star represents 50/50 mixing.

(b) The R1-R2 diagram depicting subvolcanic granite and syenite compositions found in granitoids from Niger and Nigeria (after Batchelor and Bowden, 1985). Note the arfvedsonite granite and alkaline syenite compositional fields do not lie on the volcanic trend.

(c) The R1-R2 diagram depicting compositional fields for biotite granite and riebeckite biotite granite. aag = albite granites, including arfvedsonite albite granite and zinnwaldite albite granite.

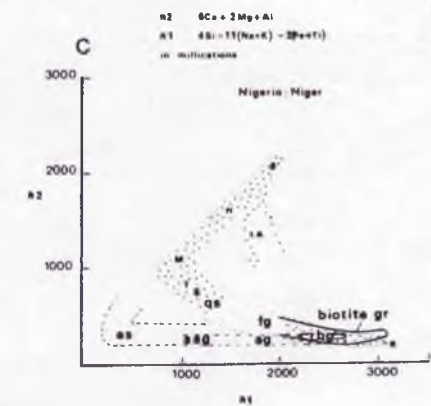
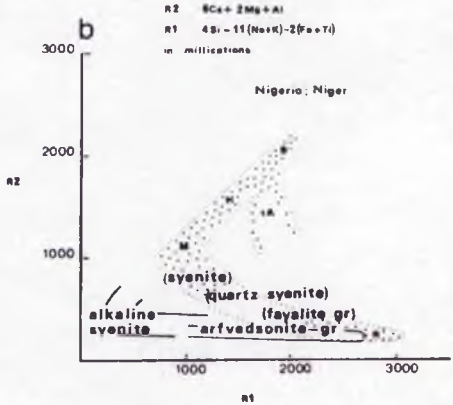
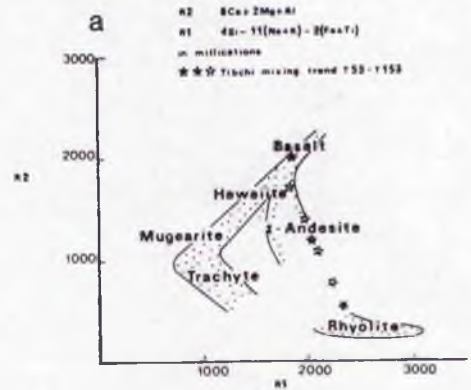
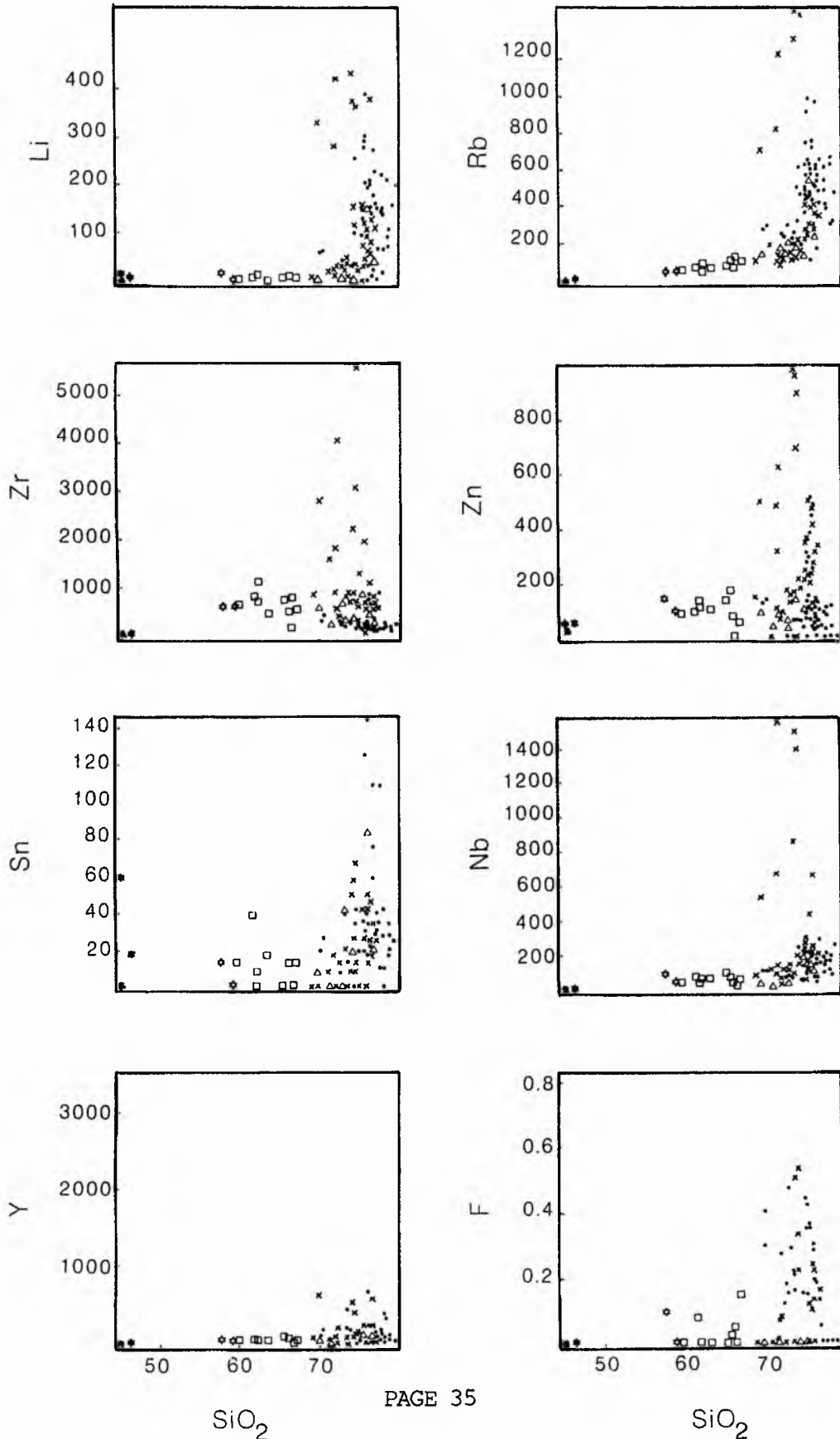


Fig 2.6 Trace element Harker diagrams for granitoids of the Niger Nigeria Province.

Symbols as in Fig 2.2, page 23. All values in ppm except fluorine and silica which are in per cent. Data derived from Batchelor (1983).



such variations.

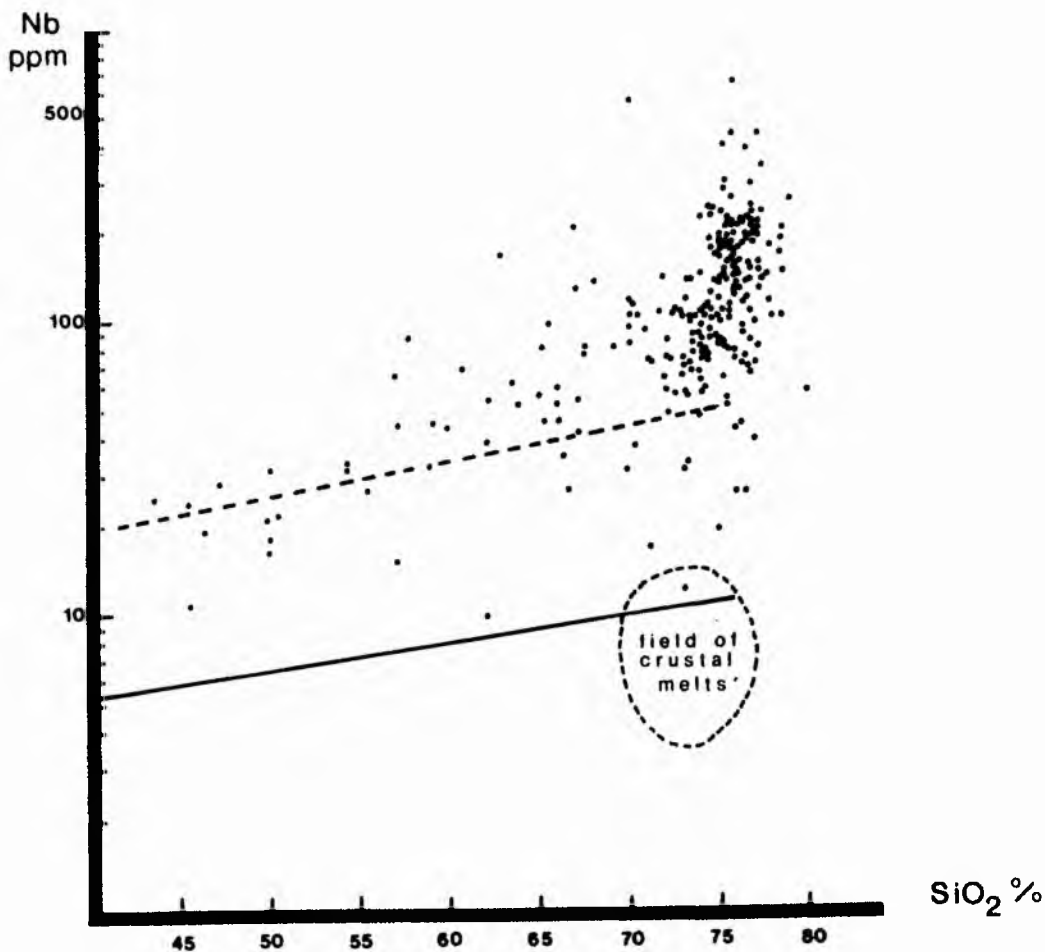
#### Petrogenetic considerations

Both geochemical and petrological characteristics have been used to discriminate between various granitoid series. A petrological interpretation of granitoid evolutionary series has been defined by Lameyre and Bowden (1982). Using the Streckeisen modal plot, they distinguished different plutonic series and their fractionates (Fig 2.2). The diagram discriminates between granitoid compositions which have evolved by fractional crystallisation of a basaltic parent and those which have formed by crustal fusion. Such a distinction clearly has tectonic implications. On the Lameyre and Bowden diagram, the peralkaline granites and syenites of the Nigerian orogenic province show affinities with granitoids associated with continental rifting (eg Oslo, Gardar, Ethiopia). The biotite and fayalite granites plot in the field defined as aluminous granitoids found in alkaline provinces. These granites are different in their peraluminous mineralogy from granites of orogenic affinities since they do not contain minerals such as muscovite, andalusite or garnet. In contrast the majority of the Nigerian basement granitoids, some of which do contain muscovite, plot in the field of calc-alkaline orogenic granites. The ring complex, A-type granites of Nigeria therefore, which are related to doming and failed rifting, are distinct and contrast with the A-type granites of the Lachlan fold belt in Australia (Collins et al 1982) which are related to the terminal phase of an orogeny (Bowden 1985). This is also indicated from the plot of Nb against silica (Fig 2.7 Pearce and Gale 1977) since the Nigerian granitoids plot in the field defined as within plate magmatism. However, certain care must be taken in interpretation of Nb values which are related to postmagmatic rather than magmatic influences.

Within such A-type provinces, some workers had found it difficult to explain the range of alkalinity as reflected by mineralogy and geochemistry. Each mineralogical granitic variant was considered by earlier workers to represent sequentially fractionated pulses of granitic magma. Each mineralogical variant was believed to display the petrological and geochemical characteristics inherited from magmatic processes. However, for a complex like Ririwai, considerable difficulty was encountered in explaining how fluctuating aluminous or peralkaline granites could be generated as part of an evolutionary sequence (Kinnaird et al 1985a).

The petrogenesis of such specialised granites has in the past been attributed to extreme differentiation or continued fractionation of a granite magma. However, once the magma composition has reached the granite minimum it is not possible to generate specialised granite by magmatic processes. More recently it has been suggested that alkaline granite magma can crystallise in the subsolidus under the influence of residual fluids. Mustart (1972) and Taylor (1979), postulated that crystallising granite magmas exsolve a peralkaline fluid phase on cooling. The effect of alkali loss or retention, which is well documented for peralkaline volcanic series, has also played a major role at subvolcanic levels. The distinctive mineralogical and chemical changes which can be observed in many of the subvolcanic granites, can only be explained satisfactorily by postmagmatic processes. Such changes are essentially the result of hydrothermal fluid interaction with an original magmatic assemblage of minerals. These have re-equilibrated with the residual fluids to give new mineral assemblages

Fig 2.7. Nb-SiO<sub>2</sub> diagram showing the division between within-plate magmatism and volcanic arc magmatism.



Solid diagonal line gives lower limit for within-plate volcanic rocks; dashed diagonal line gives upper limit for volcanic arc magmatism. Estimate of Nb-SiO<sub>2</sub> range of crustal melts derived from sediments metamorphosed up to and including amphibolite facies is superimposed on the diagram.

(from Pearce and Gale 1977)

accompanied by varying accessory minerals. Furthermore, with boiling fluids, the compositions of vapour and liquid can change dramatically during cooling and consolidation of the volcanic pile or the underlying subvolcanic intrusions. Such processes, can be demonstrated in the volcanic successions as well as in the peralkaline and biotite granites.

Thus if the range in mineralogy and bulk chemistry is linked to changes in the subsolidus, due to loss or gain of alkaline fluids, then the different granite and syenite types can be characterised by different assemblages of major, accessory and ore minerals. Such variations can be noted in the modal data and normative constituents and is reflected in the appropriate chemical diagrams.

The hydrothermal alteration has also been important for the introduction of a whole spectrum of minor and trace elements and such altered granites are characterised by high concentrations of Sn, Be, Li, U, Zr, Nb, Th, K, Rb, Mo, Zn, F, W, by low K:Rb, Sr:Y; and high Rb:Sr and K:Ba ratios. Chondrite normalised REE patterns show marked negative europium anomalies and enrichment in rare earths when compared with barren granites from Nigeria. The generation of a fluid phase at the late magmatic stage, possibly enriched in fluorine, is thought to have played a major role in determining geochemical trends during subsequent cooling. The presence of such a fluid would also have had a fundamental influence on the behaviour of certain elements that form stable fluoride complexes in aqueous fluids.

All the acid extrusive volcanic rocks show the effects of devitrification by hydrothermal alteration. Similarly hydrothermal effects can be seen in virtually all the subvolcanic rocks. It is only the fayalite granites and quartz porphyries which seem to have been relatively unaffected by late-stage fluid reactions and mineralisation. Thus the mineralogy and geochemistry of the porphyries provides important information on the dominantly magmatic features of anorogenic magmatism with only a partial imprint of subsolidus reactions.

## CHAPTER 3

### PROCESSES OF HYDROTHERMAL ALTERATION

#### Introduction

The rock type which most closely resembles the original granite magma is the quartz porphyry. It has a quenched porphyritic texture with embayed quartz and feldspar phenocrysts accompanied by an essentially anhydrous ferromagnesian mineralogy of fayalite and hedenbergite. All other granitic rock types represent the effects - to differing degrees - of fluid interaction which partially or totally modified the original granite magmatic mineralogy. These fluids are magmatic-hydrothermal in origin. Various minerals in the granites act as monitors of these fluid reactions (Bowden and Kinnaird 1985). Orthoclase ordered to microcline; ordered albite formed at intergranular boundaries - and ultimately pervaded the whole rock - and new subsolidus Li-Al micas grew at the expense of K-feldspars or late-magmatic Fe-rich micas. Depending on the alkalinity of the fluid phase, peralkaline minerals like riebeckite, arfvedsonite, aegirine and astrophyllite may also have been generated in the subsolidus.

Sub-solidus alteration by hydrothermal fluids has affected the cupola zone of many of the granites and their overlying volcanic piles. Such processes have been important for the introduction of ore elements within the granite cupolas.

#### Definition of hydrothermal processes

The simplest way to define an alteration process is a field term reflecting the most obvious or abundant mineral. Terms such as silicification, chloritisation, sericitisation, fluorisation etc. may be used in this way (Baumann et al 1974). Alternatively, it is possible to classify a process by the dominant chemical changes involved during alteration, such as soda metasomatism, although several elements may be introduced or removed simultaneously (Hemley and Jones 1964)

A further method of classification is based on the mineral assemblage generated during alteration and reflects temperature, pressure and chemical composition. A variety of terms for types of alteration have been used such as potassic, sericitic, argillic etc. to designate assemblages of minerals. Unfortunately, the terminology which is well defined for porphyry copper deposits, can be used differently by different authors and does not readily translate to paragenetic associations in tin deposits.

Rose and Burt (1979), suggest that a complete list of the mineral assemblage is necessary with the minerals catalogued in order of abundance. This too can be cumbersome and time consuming. Also any process of alteration will be controlled by the host rock that is being modified. It seems unreasonable therefore, to regard as different, two processes in which temperature, pressure conditions are the same and where the initial composition of the fluid is also the same, but where differing mineral assemblages are generated because of fluid interaction

with host rocks of differing chemistry.

For this reason, this work has chosen to define the processes of alteration on the dominant chemical change in composition although the modified mineral assemblages are also listed. In practise, a long list of minerals in the order of abundance is not needed to categorise or name any particular process - the chemical composition and structural state of the feldspar (eg ordered microcline), combined with the mica composition is sufficient to adequately define the alteration process (Table 3.1). Difficulty arises from this method where one process of alteration is superimposed on already altered rocks to give mineral assemblages that defy definition. Nevertheless an attempt has been made to distinguish which phases of alteration have occurred and how the mineral assemblages define the process.

The sequence of subsolidus hydrothermal alteration processes that have modified the original mineralogy of the granites can be recognised by local textural and colour variations, by structural changes in the alkali feldspar (Table 3.1), by the growth of new micas, by changing compositions of the opaque minerals (Kinnaird 1985, Kinnaird et al 1985a), by the assemblage of accessory minerals (Table 3.1) and by whole rock geochemical variations (Table 3.2). Those granites emplaced as ring dykes in polygonal or circular fractures with steep-sided contacts, display limited, but often locally important, hydrothermal subsolidus alteration assemblages. It is only in the granite cupolas with shallow outward dipping contacts where fluids were retained that metasomatic reactions were more intense (Bowden and Kinnaird 1984b).

On textural and field evidence, the earliest process of alteration was sodic metasomatism which involved the conversion of original perthitic feldspars into albite. Sodic metasomatism was largely independent of faulting and jointing of granites but was concentrated in the roof zone. This early sodic metasomatism may affect both peralkaline and biotite granites. The effects of the later processes are only known in detail for the biotite granites. In some areas sodic metasomatism was followed by  $K^+$ ,  $H^+$ ,  $Si^+$  metasomatism and argillic alteration. Initially, the reactions were widespread and pervasive, but as the solidifying granite cooled and contracted, a series of microfractures and later Q, F and P joints provided more localised access and channelways within the intrusive body for circulating fluids. It is important to emphasise, however, that there is considerable variation from complex to complex in the subsolidus assemblages and the sequential changes related to the different processes of alteration. In most complexes only one or two stages developed to a small degree and in the Saiya Shokobo Complex the major alteration process was acid metasomatism.

#### Sodic metasomatism

The mineral assemblages generated during sodic metasomatism depended on the intensity of rock-fluid interaction; the strongly peralkaline granites showing the greatest effect (Bowden and Kinnaird 1984a). The process is responsible for the pervasive alteration of perthitic feldspar to albite, desilication when the process becomes intense, and enrichment in trace and rare elements. If the sodic process continued to lower temperatures then mineral assemblages characteristic of propylitic alteration (Rose and Burt 1979), have occasionally been generated. Such assemblages include albite, epidote, chlorite and siderite and examples of epidote-rich joint planes can be seen in the Harwell paddock of the Rayfield

Table 3.1 Characteristic mineralogy assemblage for each alteration process

Process	Common Texture	Colour	Style of mineralisation	Characteristic feldspar	Characteristic mica	Ore minerals	Other Accessories
Sodic metasomatism	Saccharoidal	white or grey	disseminated process affecting the cupola zone	perthitic feldspar altered to ordered albite	pale coloured: in the compositional range Li-annite-petrolithionite - zinnwaldite - cryophyllite to trillithionite	pyrochlore with monazite and molybdenite in peralkaline facies columbite with cassiterite rutile, thorite, ilmenite monazite + uraninite + sphalerite in peraluminous facies ferrousomite in metaluminous facies	aegirine, amphiboles in range riebeckite to lithian arfvedsonite, villiamite, cycloite, amblygonite, thomsonolite, astrophyllite, chevkinite, narsarsukite and zircon in peralkaline facies zircon, fluorite, genthelvite and cryolite in peraluminous facies allanite and zircon in metaluminous facies
Potassic metasomatism	miarolitic	pink or red	restricted to miarolitic cavities in contact zones, or to fissure margins	perthitic or albitised feldspar altered to intermediate or maximum microcline	chloritisation of original mica: new mica in the range annite-siderophyllite	cassiterite, monazite, molybdenite, wolframite + sphalerite	amphibole in the range ferrosiderite to arfvedsonite in peralkaline facies: zircon in both peralkaline and peraluminous facies
Chloritic alteration	fine-grained	dark green, grey to black	at contact zones and within zones in unaltered biotite granite	destabilisation of feldspar to micaceous aggregates	chlorite + sericite	sphalerite, cassiterite, chalcopyrite, monazite, pyrrhotite, stannite, pyrite, allanite	fluorite, zircon + topaz
Acid metasomatism	'granitic'	green or grey	may be a pervasive process in the cupola zone or occur in tabular zones, or infill fissures	destabilisation of feldspars into topaz/sericite or chlorite/sericite aggregates:	new mica in the compositional range siderophyllite - zinnwaldite	cassiterite, monazite, wolframite, rutile, molybdenite, thorite sphalerite	zircon, quartz, topaz, sometimes fluorite, cryolite, siderite and genthelvite
Silica metasomatism	quartzose	colourless or milky quartz	may be a pervasive process in the cupola zone or form veins	vestiges of feldspar altered to clay minerals or zeolites	no new mica	sphalerite, chalcopyrite galena, cassiterite, wolframite, pyrite, pyrrhotite, stannite, molybdenite, cubanite, mackinawite etc	quartz, haematite
Argillic alteration	chalky	white or red-stained clays	restricted to cupola zones that have already been extensively sodic metasomatised	feldspars converted to kaolinite (or montmorillonite)	chlorite	haematite; supergene alteration of sphalerite, chalcopyrite and other sulphides to secondary ores.	epidote, siderite

Source of reference: Kinnaird *et al* 1985, Ewer 1986, Bennett 1981, Bowden and Kinnaird 1984a and b, Kinnaird 1979, Martin and Bowden 1981, Kinnaird 1985

Table 3.2 Geochemical changes associated with the hydrothermal processes

Sodic metasomatism	<p> <math>\ll</math>Na which may exceed 6%  <math>\ll</math>Fe  <math>&gt;K_3</math>  <math>Fe:Fe^2</math> ratio increases                 </p>	<p> <math>&lt;</math>LIL, HFS and associated                      elements such as Zn, Y, Be                      and F  <math>&gt;</math>Ba, Sr  <math>&gt;</math>in Th:U ratio                 </p>	<p>                     enrichment in all rare                      earths particularly in the                      peralkaline facies                 </p>
Potassic metasomatism	<p> <math>\ll</math>K  <math>&gt;</math>Na                 </p>	<p> <math>&gt;</math>LIL, HFS and associated                      elements compared with                      sodic metasomatism  <math>&lt;</math>Sn, W, Zn  <math>&lt;</math>in Th:U ratio                 </p>	<p>                     whole rare earth spectrum                      is depleted - rare earths                      must be released from                      host minerals to the                      hydrothermal fluids                 </p>
Acid metasomatism	<p> <math>&lt;</math>(Fe), (SiO<sub>2</sub>)  <math>&gt;</math>K, Al                 </p>	<p> <math>&lt;</math>LIL, HFS                      elements compared with                      potash metasomatism                      particularly U, Th, Ce                      and Y  <math>&lt;</math>Zn, Pb, W and Cu  <math>&lt;</math>Th:U ratio                 </p>	<p>                     whole rare earth spectrum                      including Eu is enriched                      compared with potash                      metasomatism                 </p>
Silica metasomatism	<p> <math>\ll</math>Si  <math>&lt;</math> Fe  <math>&gt;</math> in all other elements                 </p>	<p>                     LIL, HFS and associated                      elements selectively                      depleted with increase                      Sn, Zn, W, Bi, Cu, Pb &amp; MO                      ? <math>&gt;</math>in Th:U ratio                 </p>	<p>                     Rare earths selectively                      depleted                 </p>

Source of reference: Bennett 1981, Martin and Bowden 1981, Bowden and Kinnaird 1984a, b, Bowden 1985, Kinnaird *et al* 1985, Kinnaird 1985.

area of the Jos Bukuru Complex (see 1:500,000 map - inset at back of thesis). Sodic metasomatism is economically important for the introduction of Nb bearing ore minerals occurring as columbite in biotite granites and as pyrochlore in the peralkaline granites and of less importance as fergusonite in metaluminous hornblende biotite granites (Table 3.1).

- In the peralkaline granites, which are characterised by normative acmite and petrographically by blue sodic amphibole, the process of sodic metasomatism was characterised by a range of subsolidus modifications. The deep blue sodic amphibole, occasionally with green-blue cores together with aegirine, exhibits a wide variation in colour and texture. Arfvedsonite granites range from equigranular to porphyritic full of drusy cavities, and in colour from pink to white. With increasing modal content of albite they grade into arfvedsonite albite granites. The alkali amphiboles therefore belong to a continuously varying series ranging from ferrorichterite to arfvedsonite (Fig 3.1)

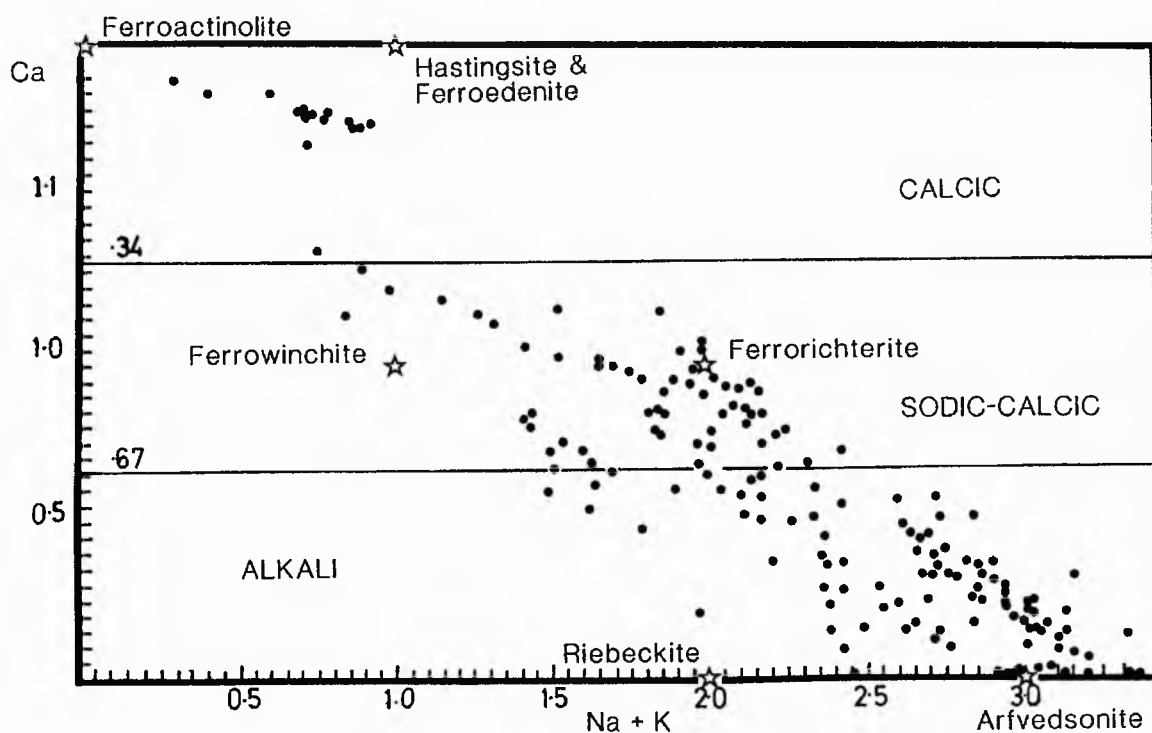


Fig 3.1. Composition of the amphiboles in Nigerian peralkaline granites, syenites and porphyries.

Often amphiboles may show two distinct forms, one as euhedral prisms of ferrorichterite, the other as irregular interstitial masses of Li-arfvedsonite of late subsolidus recrystallisation. Aegirine may have replaced, or been replaced by, arfvedsonite suggesting that there were fluctuating

physico-chemical compositions in the subsolidus. Arfvedsonite and aegirine are accompanied by accessory aenigmatite and traces of annitic mica with secondary iron titanium oxides. In addition to changes in amphibole composition during sodic metasomatism, the original perthitic feldspars were progressively altered, first by the gradual coarsening of the albite and microcline domains within perthite and ultimately by the growth of new albite laths. In the arfvedsonite albite granites (Plate 3.1), the major silicate minerals are accompanied by pyrochlore, Th-rich monazite, cryolite, stellate clusters of astrophyllite, cloudy prisms of uraniferous or Hf-rich zircon and sometimes by narsarsukite and chevkinite (Bennett 1981).

In the Tibchi Complex Ike (1979), describes a peralkaline sodic syenite, which is the result of sodic metasomatism. The rock which is white in colour and medium-grained, consists mostly of alkali feldspar microperthite, with minor amounts of mafic minerals and traces of quartz. Accessory minerals include bright green prismatic aegirine-augite, dark blue ferrorichterite partially replacing the aegirine-augite, fluorite and intergrown magnetite-haematite.

- In biotite granites cupolas, slight sodic metasomatism resulted in coarsening domains in perthite as described above, together with changing mica compositions. The albitisation process was characterised by a textural change from medium- or fine-grained equigranular or porphyritic perthitic granite to a saccharoidal fine-grained zinnwaldite albite granite or more rarely a lepidolite albite granite with increasing fluid reactions (Plate 3.2). In these extensively modified facies, thin sections show a "snowball" texture in which abundant laths of ordered albite are surrounding and enclosing larger anhedral crystals of untwinned turbid intermediate microcline and unstrained alpha quartz (Plate 3.3). Remnant cores of annitic or siderophyllite mica may have been overgrown by zinnwaldite mica but it is not unusual to find that all the original mica has been completely replaced. As a result of sodic metasomatism there was a destruction of original Ti-Fe oxides, enrichment in uranium, and the introduction of columbite and cryolite with minor cassiterite, thorite, xenotime, Th-rich monazite and Hf-rich zircon. Epidote, chlorite and siderite were formed when the process continued to low temperatures.

Surface samples of the Ririwai biotite granite compared with drillcore samples, (Fig 3.2) show that there is a diminishing proportion of albite within replacement perthite as depth increases (Kinnaird et al 1985b). At a depth of 295m the biotite granite consists of quartz, microcline perthite - showing little or no evidence of albitisation- and annitic mica (Kinnaird 1984). In contrast, at 400m, in the roof zone of another biotite granite an albite rich, almost monomineralic rock is encountered (Plate 3.4). This evidence therefore suggests that sodic metasomatism is concentrated in the apical region of a granite, although in many of the complexes the petrological evidence is not well preserved. Such a lack of evidence is probably due either, to erosion well below the apical zone, or to continued fluid reactions which have overprinted the earlier sodic metasomatism.

Sodic metasomatism may also have affected the metaluminous granites to a limited extent. In the hornblende biotite alkali feldspar granites the perthitic feldspar domains have dentate margins with small intergranular grains of ordered albite. Fergusonite, a rare earth niobate, is common in placer deposits derived from these rocks. The best known localities are in the Sara Fier and Jarawa complexes.

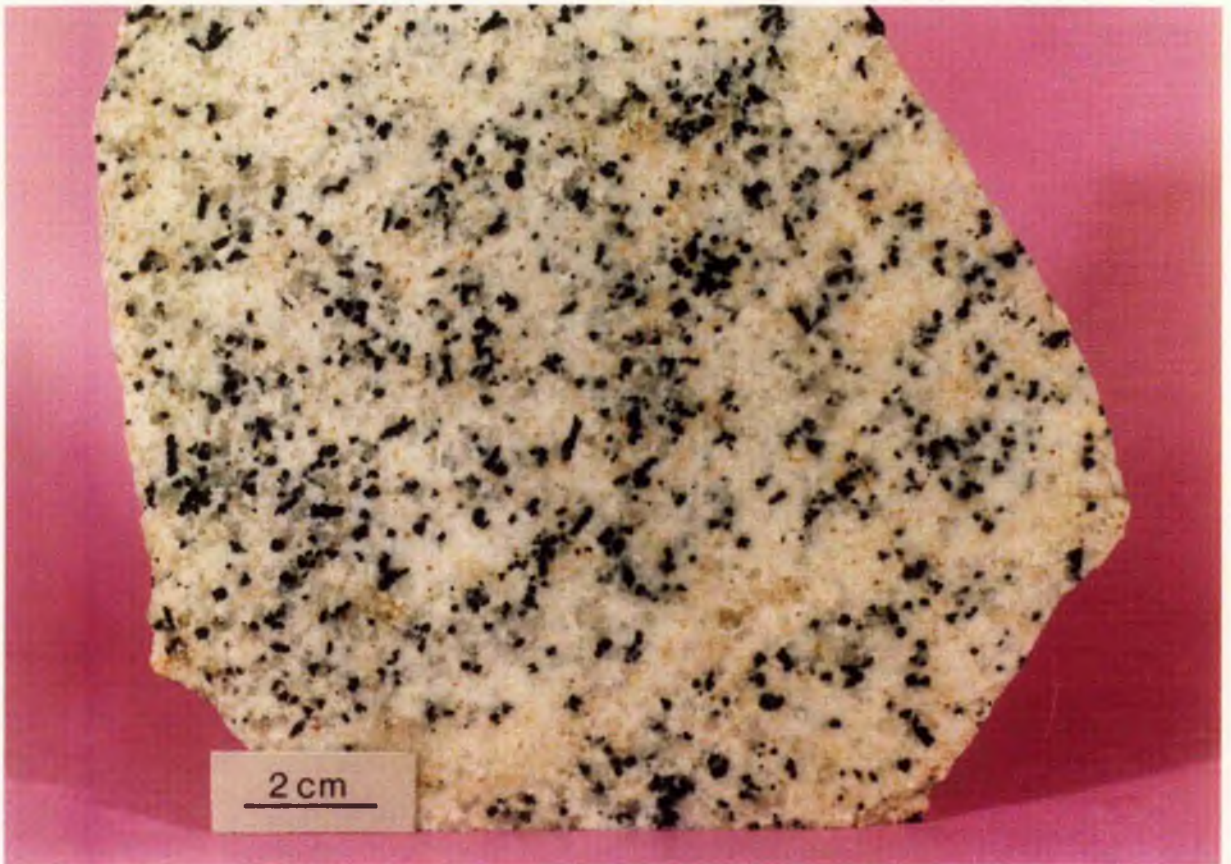


Plate 3.1 Arfvedsonite albite granite from the Kaffo valley of the Ririwai complex



Plate 3.2 Zinnwaldite/lepidolite albite granites

- |        |       |  |
|--------|-------|--|
| Left   | AF59  | Odegi zinnwaldite albite granite from the Afu complex                |
| Middle | AF110 | Lepidolite albitite, Agwalende, Afu complex                          |
| Right  | JB125 | Rayfield Gona zinnwaldite albite granite from the Jos Bukuru complex |



Plate 3.3

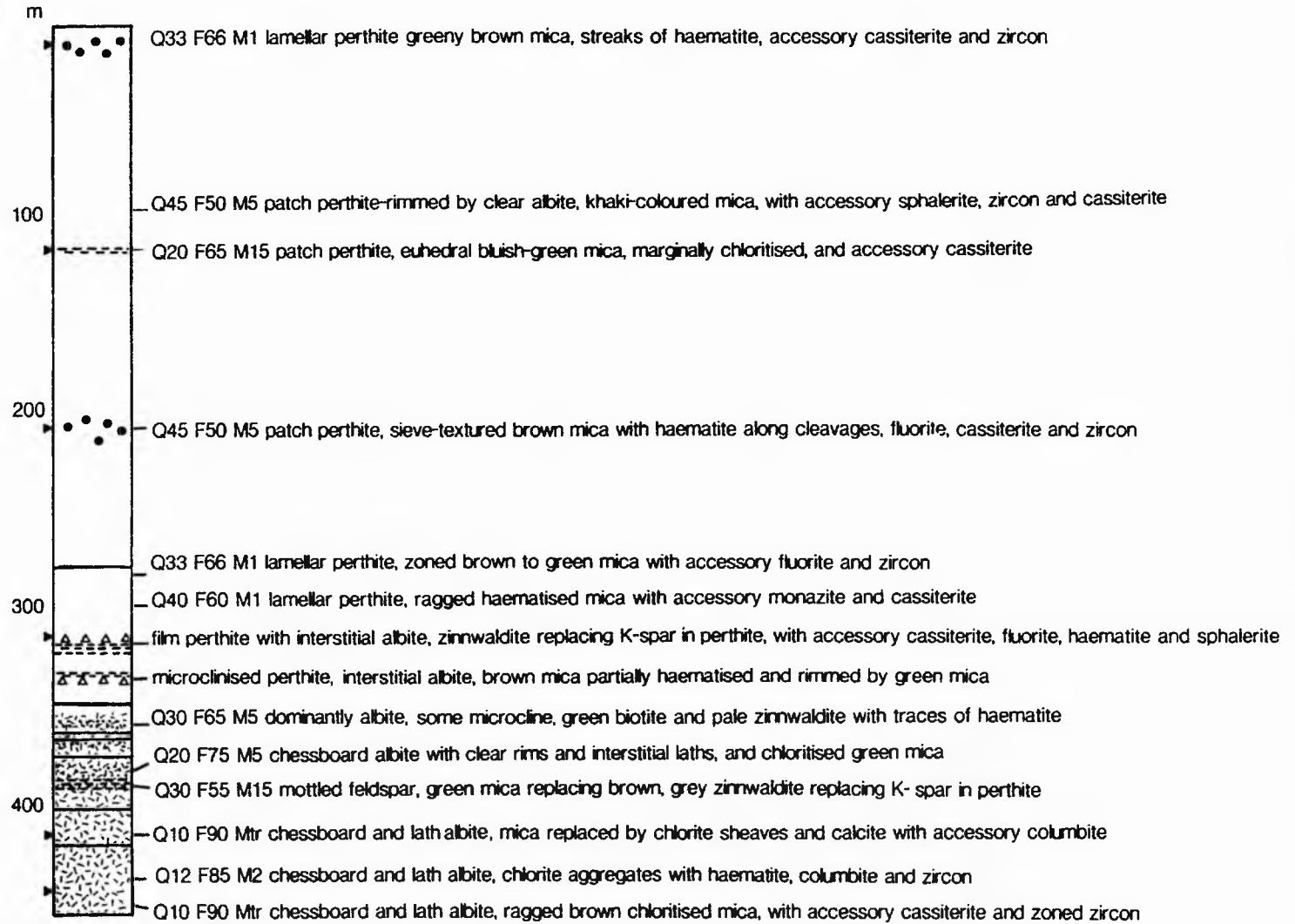
Zinnwaldite albite granite in thin section showing zinnwaldite (mottled), quartz, albite laths and microcline (without twinning); crossed polars. Field width 7.5mm.



Plate 3.4

Zoned zircon with chlorite (mottled, centre) surrounded by laths of albite. From the albitite at 436m depth in L13 core, Ririwai lode. Field of view 3mm.

L 13 CORE



KEY

- |   |   |                           |                         |
|---|---|---------------------------|-------------------------|
| microgranite                            | coarse-grained biotite perthite granite             | albite band               | greisenised zone        |
| medium-grained biotite perthite granite | albitised granite with abundant miarolitic cavities | potash metasomatised zone | geochemical sample site |

Fig 3.2. Borehole log of the L13 core from the Ririwai Complex showing lithological and modal variations.

## Potassic Metasomatism

Potassic metasomatism was characterised by the partial to complete replacement of sodium by potassium in the feldspars of the biotite granites, the development of intermediate to maximum microcline, growth of new mica in the compositional range from annite to siderophyllite and chloritisation of original mica (Bowden and Kinnaird 1984a). Accessory monazite, zircon, cassiterite,  $TiO_2$  minerals, molybdenite and occasionally wolframite are associated with phyllosilicate minerals (Kinnaird et al 1985a and Table 3.1).

As with sodic metasomatism there was desilication when the potassic process became intense. When the potassic process was extreme the desilication produced a honeycomb textured microcline (Plate 3.5). The microcline produced in this manner does not have the tartan twinning which is characteristic of the reconstructive transformation of orthoclase to microcline. Instead, it forms a turbid, mottled, low-relief mineral which is difficult to recognise without experience or confirmation by X-ray diffraction and has mistakenly been identified as kaolinite in some previous literature. At the same time as K for Na exchange, iron was released from the feldspar lattice and formed minute haematite rods which give a characteristic distinctive red coloration to the microcline (Plate 3.6). Structurally this feldspar is intermediate microcline. Where the process of potassic metasomatism was less intense, a monomineralic rock was not produced; the original perthitic feldspar was altered to reddened microcline, the quartz remained and the original biotite of the granite was modified. The modification may have taken the form of chloritisation; or, pale coloured overgrowths of new Li-Al rich mica rim the original Fe-Ti rich dark green/brown biotite. Zircons trapped in biotites during near-solidus crystallisation are dissolved in the fluids depositing the rim of ferrous siderophyllite. If these pervasive reactions continued to lower temperature then mica compositions changed to lithian siderophyllite accompanied by the breakdown of alkali feldspar to give topaz and sericite.

The process of microclinisation in biotite granites occurs at different stages in different complexes. In the Ririwai and Tibchi complexes it is a wallrock alteration process along major fractures and the process is only locally intense enough to produce a desilicated microcline syenite in the biotite granite adjacent to the fissure filling system. Elsewhere, potash metasomatism may be restricted to greisen bordered pockets at biotite granite margins or immediately beneath the volcanic cover. In the Afu, Ririwai and Saiya Shokobo complexes microcline pockets containing no quartz may reach several centimetres in size. The pockets are clearly related to an early stage of vapour separation. They are lined by small pink microcline crystals which may be accompanied by euhedral cassiterite up to 2mm diameter and tiny transparent spheres of fluorite (Martin and Bowden 1981). In other complexes, as with the albitisation process, erosion may have removed the roof and marginal zones so that the evidence of a dispersed potassic process has been removed.

The potassic process, like the subsequent hydrothermal alteration, affected only the biotite granites to any great extent. However, in the peralkaline facies, some amphibole compositions like ferrorichterite may also be an indicator of dispersed potash metasomatism and two peralkaline samples appear to have been affected. One (N84) is from the Ririwai complex and the composition of the amphibole is unknown. The other sample from the Tibchi Complex (T34B)



Plate 3.5 Honeycomb textured microcline developed adjacent to the Ririwai lode. Field of view 2.5cm.

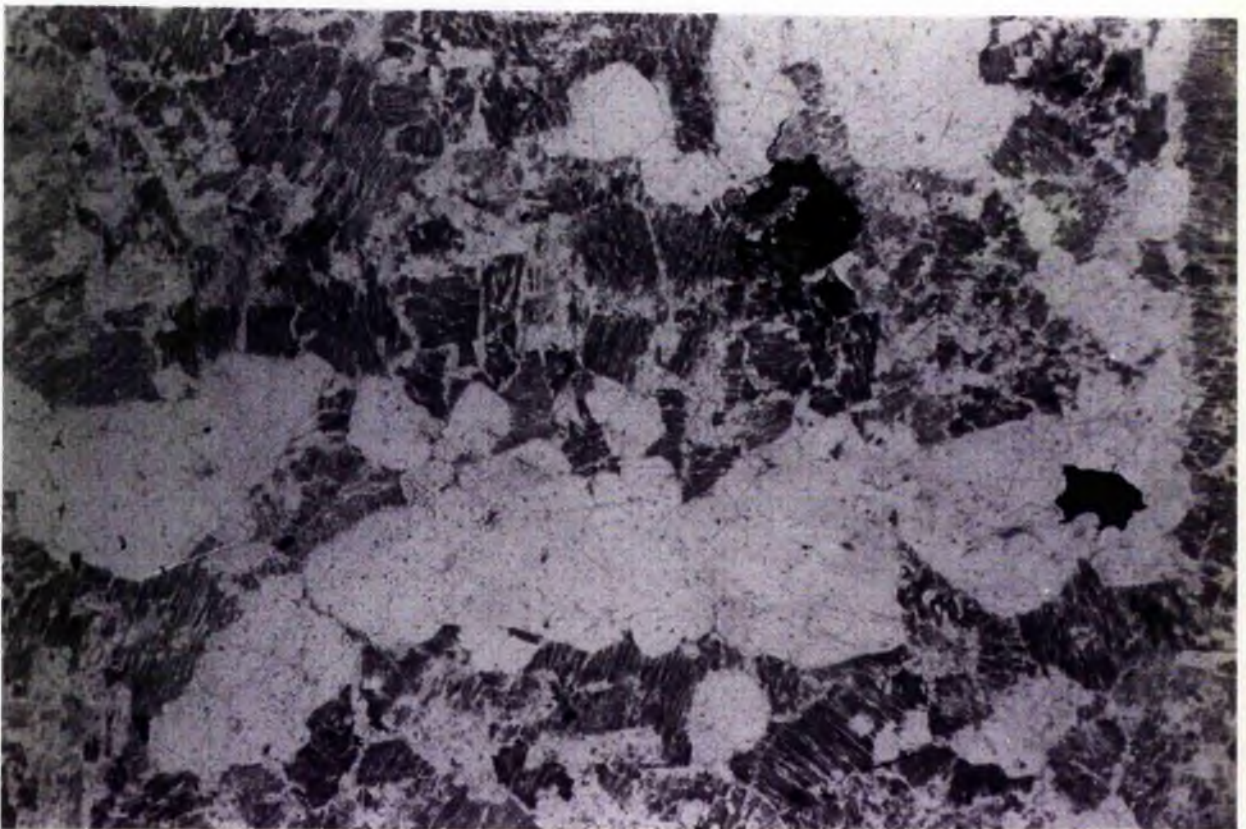


Plate 3.6 Beaded quartz in microclinised granite from the Adit area in the Ririwai complex. The microcline appears dark in PPL because of the red coloration imparted by haematite. x50

illustrates the effect of superimposition of the potassic phase on a wallrock already affected by an earlier sodic phase of activity. In the Tibchi Complex Ike (1979), describes a peralkaline potassic syenite, which is the result of potash metasomatism of the sodic syenite described above. The rock which is brownish-pink in colour and medium-grained is similar in appearance to the sodic syenite. However, like the microclinised biotite granite the sample shows reddening due to the development of haematite at the potash metasomatism stage. The essential minerals of the rock are microcline microperthite and dark blue amphibole transitional in composition from ferrichterite to arfvedsonite. The crystallisation of turbid K-feldspar along the perthite interface is analogous to that of intra-crystal albite produced during sodic metasomatism. The ferrichterite is pleochroic from golden yellow, through blue-black to dark blue and relict aegirine augite is almost completely altered to haematite. Accessory fluorite and traces of quartz occur accompanied by magnetite-haematite intergrowths which replace the amphibole pervasively. Magnetite is dominant over haematite. This differs from the oxide assemblage developed in the biotite granites at this stage. Any magnetite present in the biotite granites was usually associated with  $TiO_2$  minerals and is undergoing alteration to haematite. An extreme example of breakdown of all opaque minerals to haematite is given by a brick red phase of this syenite in which the alkali feldspar is maximum microcline and the amphibole is optically and chemically close to end member arfvedsonite. This is clearly the extreme version of potash metasomatism in peralkaline rocks. However, it must be stressed that only two examples of potash metasomatism in peralkaline rocks have so far been recorded.

In addition to potash metasomatism of the anorogenic granites, the basement host rock to the complexes may have been altered particularly where they are in contact with a ring dyke. Microcline-rich veins and wallrocks show a similar mineralogical assemblage to that in the biotite granites. There was an alteration of feldspar to microcline or pale coloured micaceous aggregates, the introduction of appreciable iron, reduction in silica and the transformation of annitic biotite and sometimes feldspar to chlorite as the process became more acid.

#### Acid (hydrogen ion) metasomatism and hydration

There may have been a gradual change in the mineral assemblage generated during lower temperature metasomatism in response to the changing  $K^+/H^+$  ratio in the fluid (Rose and Burt 1979). Such acid metasomatism was characterised by the breakdown of granitic minerals to produce a new mineral assemblage. However, since acid metasomatism can be superimposed on various earlier mineral assemblages the petrological characteristics depended on the intensity of earlier sodic or potassic metasomatism. Acid metasomatism of an unaltered perthitic alkali feldspar granite resulted in the formation of a mica-topaz-quartz assemblage conforming to a classic greisen (Plate 3.7). In contrast, in granites affected by sodic metasomatism, albite destabilised to form fluorite, cryolite and topaz with some montmorillonite. In granites affected by potash metasomatism, microcline was transformed into micaceous aggregates (Plate 3.8), chlorite or more rarely kaolinite where the cation/ $H^+$  ratio was low enough to enter the kaolinite field (Hemley and Jones 1964). Thus the effect of the acid metasomatism and the resulting mineral assemblage depended on the initial mineral assemblage (Table 3.3) and on the degree of acid

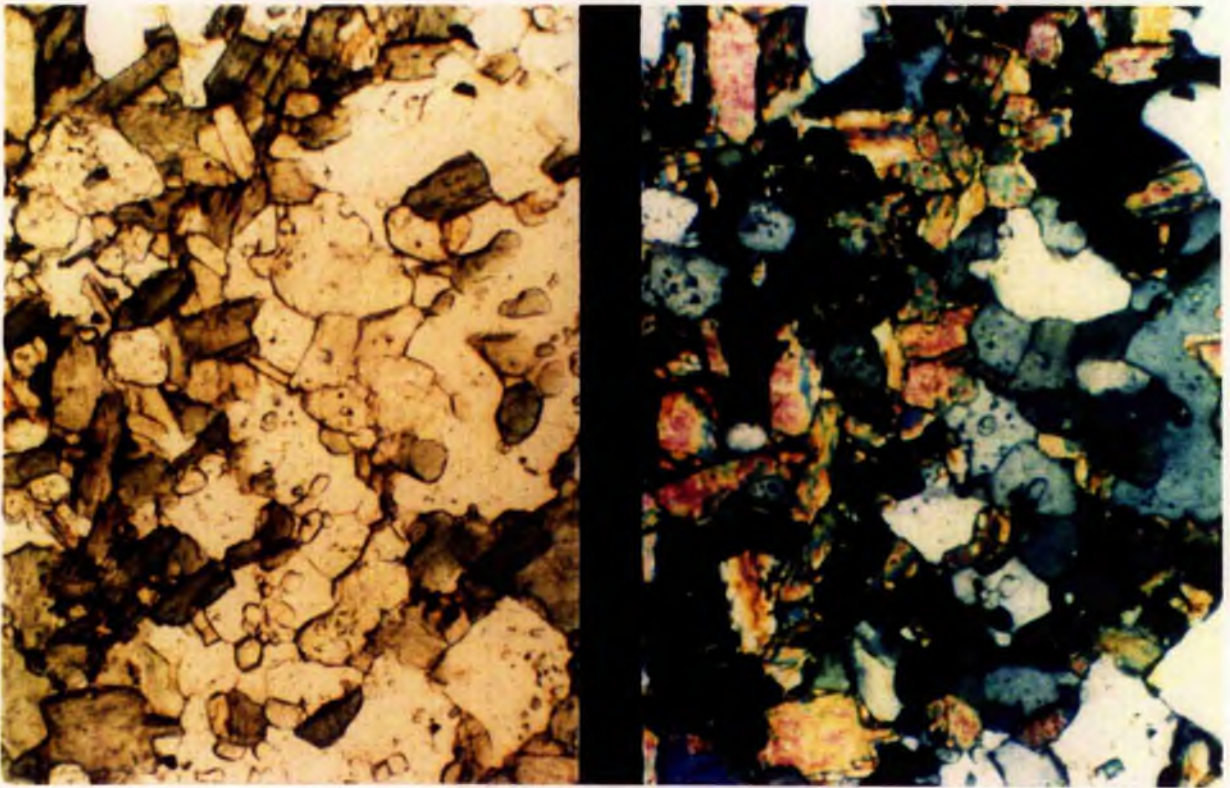


Plate 3.7

Greisen

Photomicrograph showing the classic greisen mineralogy of quartz, rounded topaz and green siderophyllite mica.  
 Left: PPL Right: XPL x50

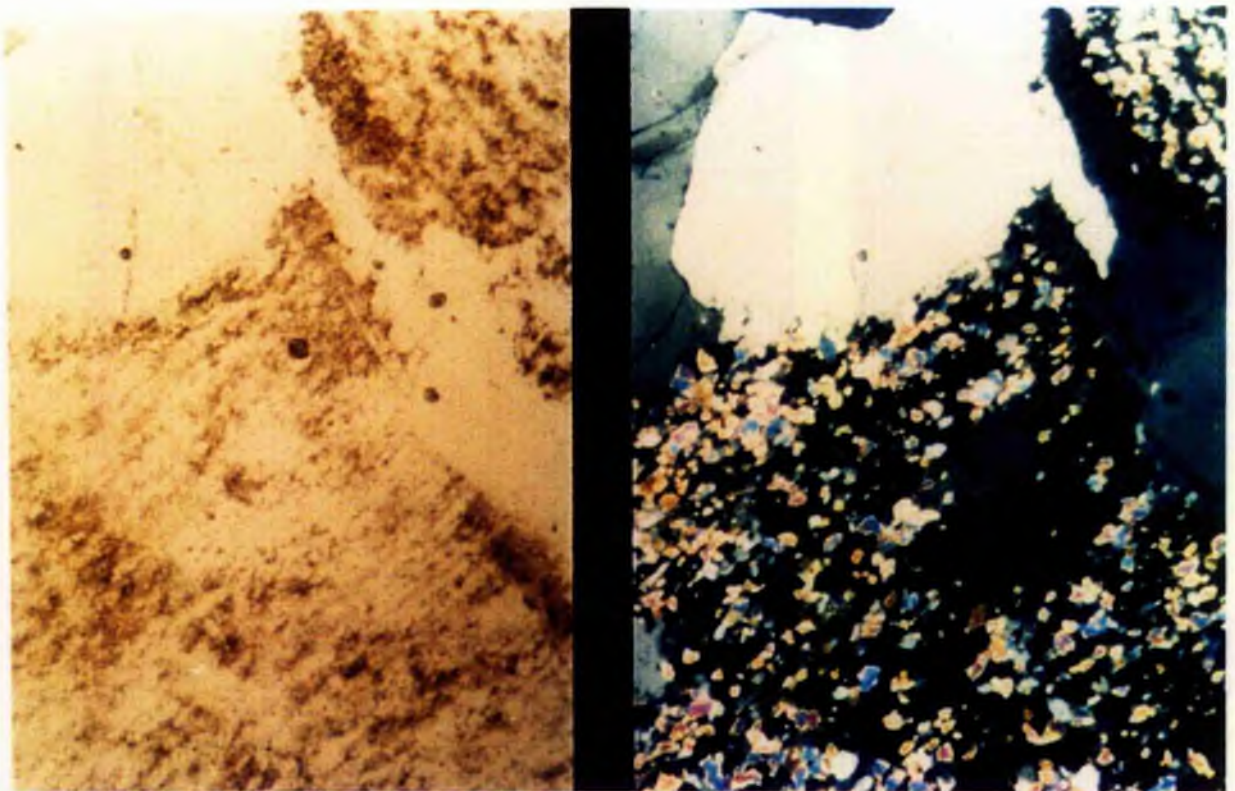


Plate 3.8

Acid metasomatism of biotite granite.

Microcline has been partially replaced by micaceous aggregates during acid metasomatism of biotite granite.  
 Left: PPL Right: XPL x50

TABLE 3.3. Mineral assemblages generated during acid metasomatism

Original rock type	New mineral assemblage
Pan-African porphyritic plagioclase granite	chlorite, fluorite, quartz, Li-Fe siderophyllite
unaltered biotite perthite granite	chlorite, siderophyllite-protolithionite mica, topaz, quartz
albitised biotite perthite granite	major sericite, fluorite, siderophyllite- protolithionite mica, quartz, cryolite
albitite	fluorite, cryolite, siderophyllite -zinnwaldite-lepidolite mica, topaz with some montmorillonite
microclinised perthite granite	sericite, chlorite, Li-siderophyllite mica, fluorite, topaz, quartz
microcline	Li siderophyllite-protolithionite mica, chlorite, quartz and occasionally kaolinite
slightly albitised microclinised granite	sericite, siderophyllite-zinnwaldite mica, topaz, fluorite, genthelvite, quartz

metasomatism. It is obvious from this figure that in addition to variations in mineral assemblages, the mica compositions generated during acid metasomatism also depended on the original material that was being metasomatised. Siderophyllite was generated by acid metasomatism of perthitic granites, forming first as a rim around original more annitic mica and later independently within the K rich zones of the perthite and ultimately as independent crystals of more uniform optical properties similar to siderophyllite first described from Pikes Peak in Colorado (Barker et al 1975). Protolithionite, zinnwaldite and lepidolite are associated with acid metasomatism of albite rich roof facies whilst lithian siderophyllite was generated from the microcline facies. Thus the term greisenisation is a useful general term to cover a whole series of mineral assemblages. The petrological characteristics and extent of greisenisation therefore depended upon the intensity and retention of earlier stages of albitisation and/or microclinisation, and the timing of fracturing and fissuring in the roof zone.

The acid metasomatism may have been a disseminated process throughout a biotite granite cupola or may have formed pervasive pockets associated with microcline; it may have diffused along zones (Plate 3.9) or may have occurred in fissure-filling veins.

Greisenisation that was pervasive used incipient microfractures in the host rock to penetrate and transform the original mineral assemblage (Plate 3.10). Occasionally the acid fluids may also have greisenised the surrounding country rock and/or volcanic cover. One particular feature of pervasive greisenisation is that the greisen may have retained the texture of the original host rock - for example at Gindi Akwati in the Ropp Complex greisenisation of the country rock preserved the Pan-African foliation. All stages of pervasive greisenisation can be recognised from zones of arrested pervasion (sheeted or multiple greisens) to partial or complete coalescence. More commonly pervasive greisenisation has occurred in the roof zones of granite cupolas superimposed on albitic variants. Other instances of pervasive greisenisation occurred following microclinisation of the albitised roof zone e.g. at Uwar Gida on Ginshi Hill in the Ririwai Complex.

Vein-controlled greisenisation is restricted to the border zones of fissures or joints which allowed limited penetration of fluids into the host rocks. Mineralogically they are similar to pervasive greisens with quartz, mica (compositions towards zinnwaldite), fluorite and topaz.

Acid metasomatism may also have affected the basement. This process is characterised by the chloritisation of original mica and feldspar in a type of alteration described as propylitic by Meyer and Hemley (1967). Chloritic alteration tends to be strongest in granitic basement rocks adjacent to younger biotite granite contacts. The intensity of alteration is greatest at the contact, grading outwards to merge with normal deuteric or metamorphic alteration phenomena. There is often an abundance of fluorite associated with chloritic alteration. The calcium was probably derived from the alteration of the calcic feldspar phenocrysts and combined with fluorine in the hydrothermal fluids. The low percentage of quartz in some of these zones also suggests that there has been some silica removal in HF rich fluids. Abundant sulphide deposition, dominated by sphalerite and chalcopyrite, occurred where there was a strong fluorisation process.



Plate 3.9 Greisenisation along diffuse zones in B65, Banke complex



Plate 3.10 Disseminated acid metasomatism  
left JBJ64H Jos Bukuru complex  
right SS26/4 Saiya Shokobo complex



The accessory minerals associated with acid metasomatism are commonly concentrated in the mica clustsers. The assemblage of ore minerals is mainly of oxides (Table 3.4) but in the later stages of deposition, sulphide minerals are introduced.

---

Table 3.4 Mineralisation mineralogy of acid and silica  
metasomatised facies

---

acid metasomatism

cassiterite  
 wolframite  
 sphalerite  
 molybdenite  
 monazite  
 rutile  
 pyrite  
 arsenopyrite  
 genthelvite  
 phenakite  
 stannite  
 chalcopyrite  
 pyrrhotite  
 bismuth  
 bismuthinite  
 galena  
 siderite  
 zircon  
 marcasite  
 greenockite  
 gold  
 argentite

silica metasomatism

cassiterite  
 wolframite  
 sphalerite  
 TiO<sub>2</sub> minerals  
 bismuth  
 bismuthinite  
 bismuthite  
 haematite  
 chalcocite  
 covellite  
 galena  
 stannite  
 pyrite  
 marcasite  
 chalcopyrite  
 cubanite  
 pyrrhotite  
 mackinawite  
 blaubleibender-covelline  
 tetrahedrite  
 greenockite  
 bornite

---

## Silica metasomatism

Several of the mineralogical reactions that took place during the earlier stages of hydrothermal alteration involved the release of silica. This was particularly the case during feldspar breakdown. The silica that was generated by such reactions dominated the later stages of hydrothermal alteration. Such silica metasomatism is characterised by an increase in the modal proportion of quartz relative to all other minerals in the altered rock. Like potash and hydrogen ion metasomatism, the process may have been pervasive or vein-controlled. Quartz may have been pervasively deposited in a cupola in vugs created by the earlier potash or hydrogen ion metasomatism (Plate 3.11), or it may have replaced all earlier formed minerals (Plate 3.12). Even more common are the quartz fissure-filling veins which are found in virtually all biotite granite masses.

There is a major sulphide deposition of ores dominated by sphalerite associated with quartz vein development, particularly in lodes at Ririwai and Tibchi. Early cassiterite, was followed by abundant dark brown sphalerite, chalcopyrite, galena and sometimes arsenopyrite or pyrite with a wide range of minor ores (Table 3.4).

Late stage alteration:

### Argillic alteration

Argillic alteration is a late stage process, characterised by the formation of clays in the kaolinite and montmorillonite groups at the expense of the feldspars. During sodic metasomatism of perthitic feldspars, ion exchange of Na for K lead to an 8% reduction in the molar volume of an alkali feldspar, which caused weakness to the individual feldspar grains, an increase in the porosity and a significant decrease in its physical resistance (Martin and Bowden 1981). Only in the three areas where sodic metasomatism has been most intensive in the biotite granites (Odegi in the Afu Complex, Jantar and Harwell in the Jos Bukuru Complex) was the argillic alteration a significant process. Argillic alteration has been economically important in these three areas, not so much for the clay formation but for ore extraction. Since these three areas have had a process of argillic alteration superimposed on the sodic metasomatism, the clays produced by the argillic process can be easily worked for the oxide ore assemblage introduced during sodic metasomatism.

In all three areas, SEM studies by E.K. Walton (pers. comm) have shown that the only clay mineral generated was kaolinite. The well developed hexagonal platelets of kaolinite are accompanied by sub-microscopic acicular crystals of zeolite - suggested to be mordenite.

Montmorillonite has been identified by Oyawoye and Hirst (1964) in the Kaskara biotite granite of the Ropp Complex. The biotite granite is normally a uniformly fine-grained texture, but marginally the texture becomes highly irregular consisting of pegmatitic knots and veins in which euhedral aggregates of microcline, quartz and less commonly biotite are found developed in cavities of varying sizes. The montmorillonite is found only in this border facies and occurs as an interstitial phase between the earlier-formed minerals in the

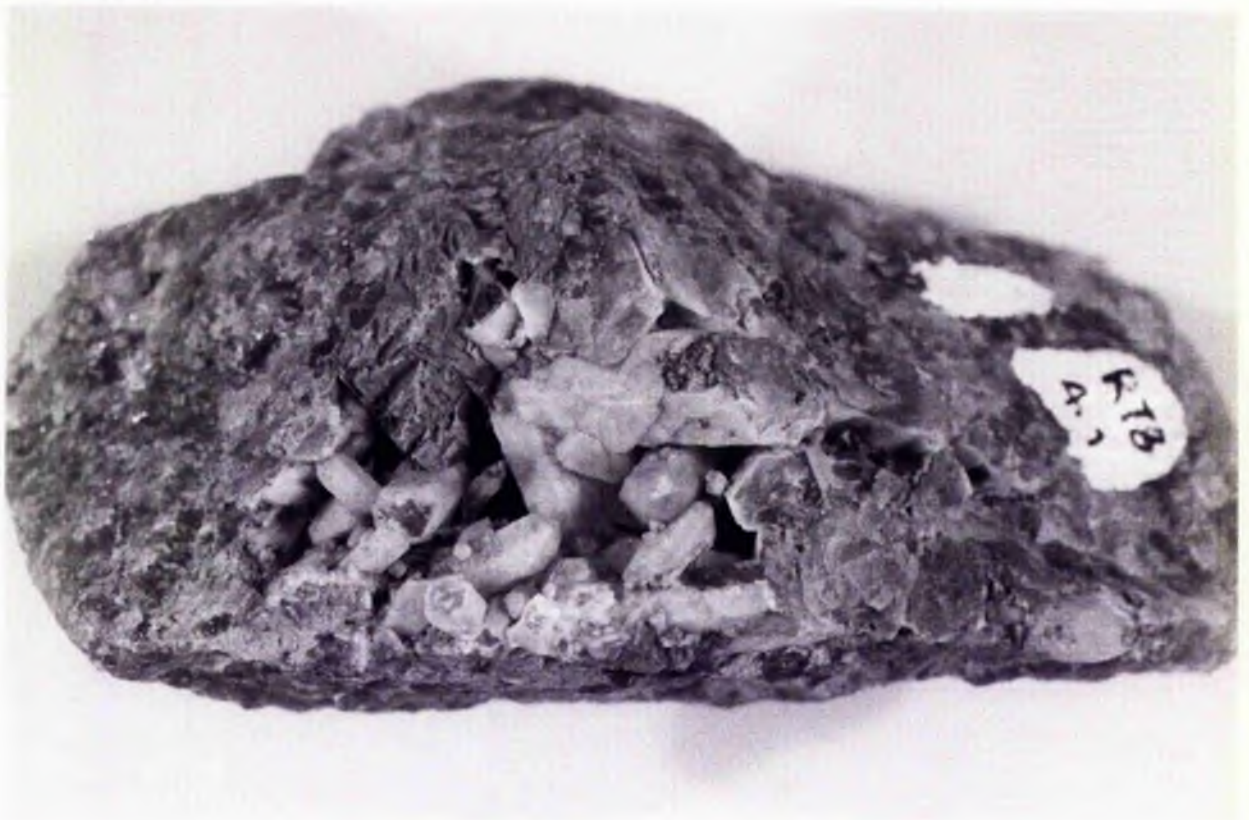


Plate 3.11            Miarolitic cavity developed in microcline adjacent to the Ririwai lode. Cavity partially filled by quartz crystals. Note the two generations of quartz: the centre of the crystal is clear and glassy, the rim is of milky quartz. Sample R78 4.7

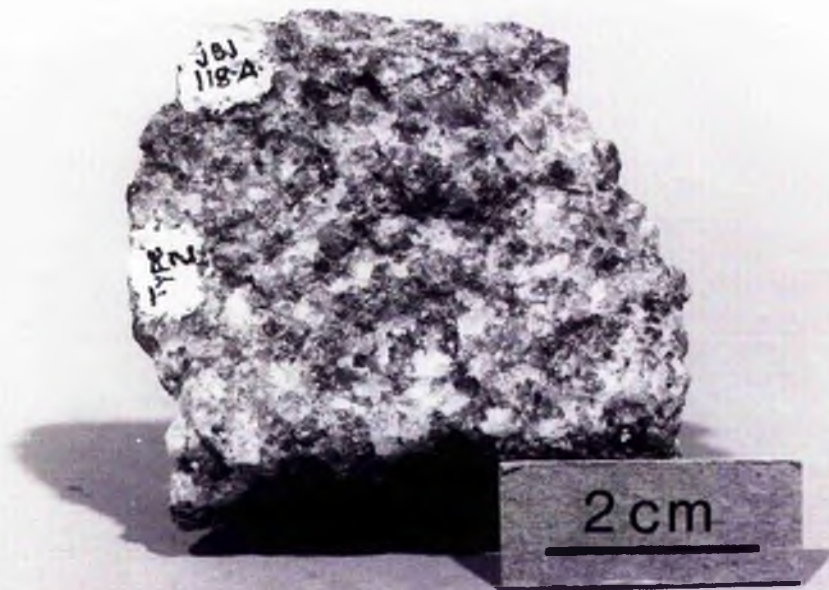


Plate 3.12            Mineralised sample from a silicified zone in the Sabon Gida South biotite granite composed of quartz, chlorite with 2% galena. JBJ118A Jos Bukuru complex.

TABLE 3.6 Accessory mineral assemblage of each of the hydrothermal alteration processes

sodic	potash	acid	silica	late-stage
pyrochlore	cassiterite	cassiterite	cassiterite	smithsonite
columbite-tantalite	wolframite	wolframite	wolframite	goethite
cassiterite	zircon	sphalerite	sphalerite	limonite
zircon	columbite	molybdenite	TiO <sub>2</sub> minerals	jarosite
galena	monazite	monazite	bismuth	haematite
thorite	ilmenite	pyrite	bismuthinite	cerussite
xenotime	rutile	arsenopyrite	bismuthite	pyromorphite
ilmenite	molybdenite	genthelvite	haematite	bornite
magnetite	powellite	phenakite	chalcocite	azurite
cryolite	sphalerite	stannite	covellite	malachite
bastnaesite	stannite	chalcopyrite	galena	chalcanthite
synchysite	chalcopyrite	pyrrhotite	stannite	pyrolusite
genthelvite	arsenopyrite	bismuth	pyrite	
gargarinite	genthelvite	bismuthinite	marcasite	
apatite		galena	chalcopyrite	
chevkinite		siderite	cubanite	
wikite		zircon	pyrrhotite	
uraninite		marcasite	mackinawite	
		greenockite	tetrahydroite	
		gold	blaubleibender-covellite	
		argentite	greenockite	

cavities. The monmorillonite which is of an olive green colour with a soapy lustre, occurs in a dense cryptocrystalline mass. Chemically this clay mineral is characterised by high alumina and iron and low  $K_2O$ , and based on chemical, X-ray and differential thermal examination, Oyawoye and Hirst (1964) considered it to belong to the beidellite-nontronite series. They suggested that the mineral was formed from late-stage magmatic fluids in which  $Fe^{3+}$ ,  $Al^{3+}$  and  $Si^{4+}$  have been concentrated with respect to  $K^+$ .

Elsewhere the formation of clay groups minerals is very patchy. Clay minerals may occur interstitial to quartz in pale green coloured massive quartz veins, or clays may infill vugs in major veins, or coat crystals and infill intra-crystal voids in smaller veins. An argillic alteration halo or zone which is commonly associated with porphyry copper deposits (Meyer and Hemley 1967) does not surround similar mineralised veins in Nigeria.

It seems likely that secondary ore minerals formed at this stage although very little supergene alteration is in fact present. Smithsonite forms white porous earthy coatings to sphalerite crystals; cerussite forms similar chalky coatings to galena, although pyromorphite has been recorded from the Ropp complex, presumably as an alteration product of galena. Chalcantite, chalcocite, malachite, azurite and even native copper formed at the expense of earlier copper-rich phases; dendritic pyrolusite and acicular or botryoidal haematite was produced by the breakdown of wolframite; pyrite and pyrrhotite has altered to limonite and jarosite and other sulphides to covellite and blaubleibender covellite (Iyer in Kinnaird et al 1985a). Such secondary mineral production is clearly still continuing and white coatings of smithsonite on sphalerite can be observed on stockpiles of ore at Ririwai and on the walls and roof of the galleries within the Ririwai mine. Secondary enrichment of ore minerals, which is so important in the development of ore bodies in porphyry copper deposits, is not of economic significance in Nigeria.

#### Zeolitic alteration

Zeolitic alteration has been identified both in the Shira Complex (Bennett 1981), in the Jos Bukuru Complex and Saiya Shokobo Complex. The zeolite of the Shira and Saiya Shokobo complexes, which is probably natrolite, occurs as white or colourless radiate sheaves or laths within pegmatitic pods or cavities. The zeolite is always associated with microcline and may have grown at the expense of the feldspar. From the SEM data described above it is clear that zeolitic alteration of feldspars described from the Jos Bukuru Complex also occurs in argillic altered zones. The zeolites probably formed at a late stage, although the author can offer no guide as to which process followed which, or whether they were contemporaneous. By analogy with the work of Savage et al (1985), coupled with the knowledge that zeolites are common in hot spring environments (White 1955), it seems likely that this type of alteration is a very late-stage process induced by circulating meteoric water.

Such zeolitic alteration in other environments, is usually accompanied by other minerals of the propylitic assemblage.

However, despite a search in this and similar material, these minerals have yet to be identified in alteration assemblages in Nigeria. Their existence however, is quite possible and it is likely that they, and the zeolites have been overlooked in the past.

## Summary

The mineralogical assemblage of many of the anorogenic complexes is often the result of reactions with residual fluids. Fluids affected both the late magmatic and particularly the postmagmatic (subsolidus) crystallisation history of cooling subvolcanic plutons and to some extent the overlying volcanic pile or surrounding basement. Such hydrothermal alteration has undoubtedly modified the original granite or host-rock chemistry and has been responsible for the introduction and dispersion of ore minerals. The sequence of subsolidus hydrothermal alteration processes that modified the original mineralogy of the granites can be established both from feldspar, mica (and amphibole) compositions (Table 3.5), and from the accessory mineral assemblage (Table 3.5, 3.6 and Fig 3.3).

Sodic metasomatism was responsible for the albitisation of the original perthitic feldspar in either biotite- or amphibole-bearing granites and resulted in enrichment of niobium-bearing ore minerals.

Potash metasomatism, which was almost entirely restricted to biotite granites, resulted in the microclinisation of original perthite or the albite produced during the earlier sodic metasomatism. Cassiterite and wolframite mineralisation were introduced at this alteration stage.

Acid metasomatism resulted in the breakdown of feldspar and new mica was generated from the potash released during this process. The mineralogical assemblage generated during acid metasomatism depended on the nature and degree of earlier alteration. Whatever, the mineral assemblage produced, it was invariably accompanied by accessory cassiterite plus other oxides and sphalerite accompanied by other sulphides (Table 3.5).

Silica metasomatism is a widespread process resulting from the liberated silica from feldspar breakdown, replacing both major and accessory minerals. Silica metasomatism is accompanied by a major ore deposition in two complexes.

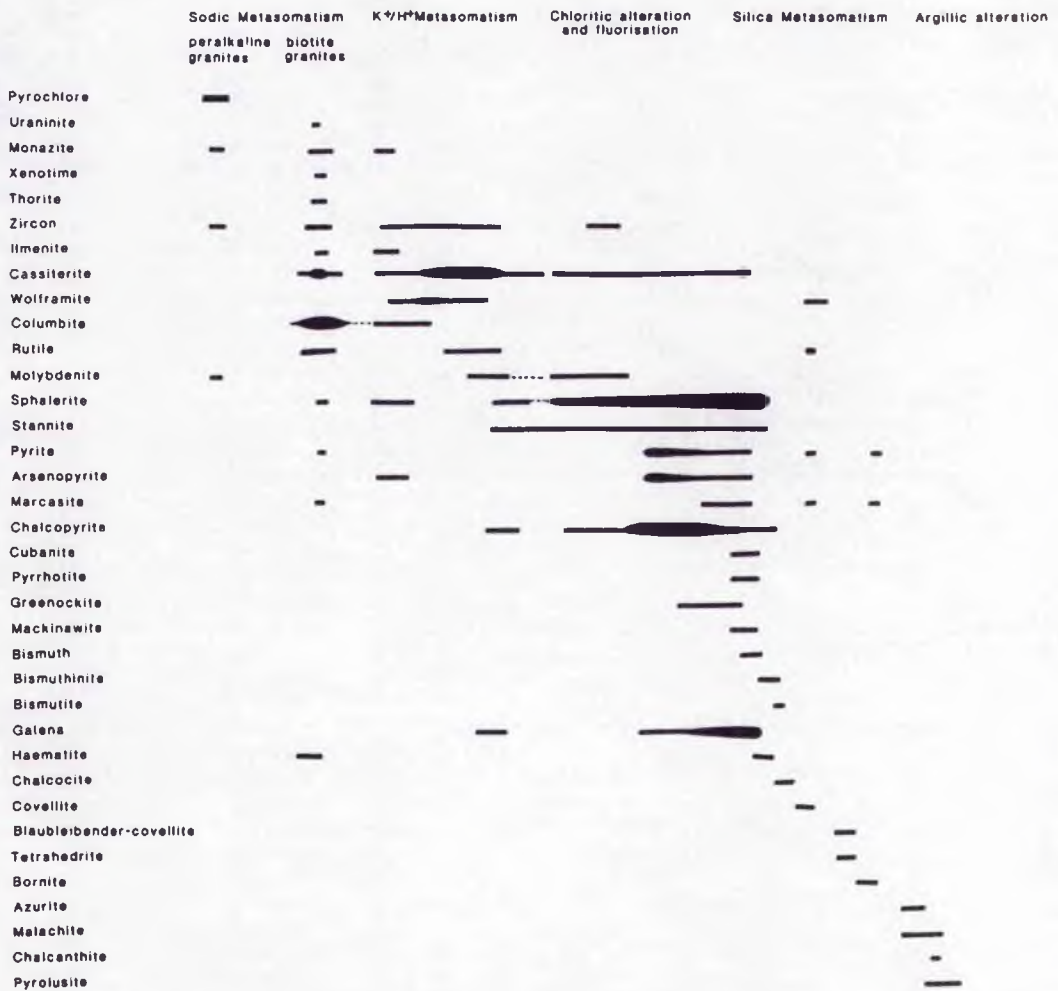
Other processes of chloritic alteration, argillic alteration and zeolite growth are minor, but locally important processes.

Clearly, if each of the processes of hydrothermal alteration is characterised by a different mineralogical assemblage then bulk rock chemistry must be different for each assemblage. The next two chapters examine the changes both in the major element and trace element chemistry related to each of the changing processes, together with a study of the nature of the fluid responsible for hydrothermal alteration.

Table 3.5. Characteristic rock-forming minerals related to each of the hydrothermal alteration processes

	sodic	peralkaline	peraluminous	potash	acid	silica	late-stage
	peralkaline						
	albite		albite	microcline	quartz	quartz	kaolinite
	ferrorichterite -		zinnwaldite-	chlorite	zinnwaldite-	siderite	montmorillonite
	Li-arfvedsonite		lepidolite	annite-	siderophyllite-	haematite	epidote
	aegirine		zircon	siderophyllite-	annite		chlorite
	aenigmatite		cryolite	zinnwaldite	sericite		siderite
	amblygonite		epidote	lepidolite	chlorite		
	astrophyllite		chlorite		topaz		
	chevkinite		siderite		zircon		
	narsarsukite				fluorite		

Fig 3.3 Schematic paragenetic ore sequence related the alteration stages.



Source: Kinnaird, 1985

## CHAPTER 4

### GEOCHEMISTRY OF THE HYDROTHERMAL ALTERATION PROCESSES

#### Introduction

In the previous chapter the mineralogical assemblages generated at different stages of hydrothermal alteration were presented. The geochemical data shows that the various mineralogical effects of sodic, potassic, acid, silica and late-stage metasomatism can be monitored by major and trace element variations. It is essential to consider that the hydrothermal fluids may have affected not only a granite cupola, but also overlying volcanics or surrounding basement rocks. The chemistry of the rock type that is being re-equilibrated with hydrothermal fluids, controls the composition and evolution of the fluid. Similarly many different rock types within a complex, from the quartz or granite porphyry ring dyke, to the different granite plutons, may have been mineralogically modified to varying degrees by the hydrothermal processes.

For many granites, slight subsolidus modifications may not be obvious either in hand specimen or thin section. Significant chemical variations however, often indicate that mineralogical re-equilibration with fluids has occurred. For example, the major element data of the granites in Table 2.1 - 2.3, together with the CIPW norms indicate that many of the 'unaltered' granites have undergone subsolidus fluid reactions. In hand specimens changing colourations or changing textures may be the first sign of such alteration. One very characteristic feature of these reactions in hand specimens of biotite granite, is the development of small "blotches" of haematite, often formed by the oxidation of opaque minerals and biotite. The development is verified by  $hm$  in the norm and by relatively high  $Fe^{3+}/Fe^{2+}$  ratios. The biotite granites are characterised by normative  $c$  which is absent in the peralkaline facies. Generally there is a decrease in  $an$  and a concomitant increase in  $c$  with the intensity of hydrothermal alteration. For the peralkaline spectrum as a whole  $ac$  is characteristic, usually accompanied by  $ns$ . There is however, an important increase in  $ns$  and  $ab$  associated with pyrochlore mineralisation.

#### Geochemical techniques

Major element chemistry was carried out using established rapid wet chemical techniques, followed by Atomic Absorption Spectrophotometry (AAS) for Ti, Al, Fe, Mn, Mg, Ca, Na and K, visible spectrophotometry for P and Si; redox titration for FeO, and gravimetry for total H<sub>2</sub>O. Trace elements were determined by XRF based on the Norrish and Hutton (1969) technique, with the exception of Li, Be and SnO<sub>2</sub> which were determined by AAS. All the analyses were undertaken in St. Andrews either by, or supervised by R.A. Batchelor. Further details of geochemical techniques are given in Appendix II, III and IV.

## GEOCHEMISTRY OF THE PROCESSES

The geochemical data of Tables 4.1 - 4.5, indicates that each of the hydrothermal alteration processes is characterised by a change in silica content, in alkali element ratios, accompanied by an enrichment or depletion in specific trace elements. Each process has also been distinguished by normative variations in Q-Or and Ab (Fig 4.1, Kinnaird et al 1985a, Kinnaird 1985).

### Major element variations during hydrothermal alteration

During sodic metasomatism major element variations (Table 4.1) show that there was an increase in Na and Fe and a decrease in K and Si when the process became intense. There was a dramatic increase in normative albite during sodic metasomatism, balanced by a decrease in normative quartz (Fig 4.1). Norm calculations show that for the Ririwai complex there is an increasing **ab** in the biotite granites from 32 to 69%. In Fig 4.1, the open circles represent samples from drill core L13, taken at different depths. The albitite samples - L13-411 and 440, shown as circles within a cross, plot closest to the albite pole. In the peralkaline granites there is an increase in **ab** from an average of less than 30% to over 50% in sample N90 (Table 4.1).

During potash metasomatism there was an increase in K and a concomitant loss of Na. This has been interpreted as K for Na exchange (Martin and Bowden 1981). At the same time as K replaced Na in the feldspars, iron was released from the feldspar lattice and formed a haematite coating to individual crystals. Norm calculations show there was a dramatic increase in normative **or** balanced by a decrease in **ab** so that in the Q-Ab-Or diagram (Fig 4.1), the salic compositions plot away from the central biotite granite field towards the Q-Or join and are represented by open diamonds. There are two trends on this plot however. The trend marked (iii) is shown by samples in which the microclinisation process was extreme and which suffered a desilication process to produce a microclinitic or microcline syenite. Where the process was less intense and a monomineralic rock was not produced then the trend marked (iv) on Fig 4.1 is followed. The mineralogical assemblage of samples which plot on this trend consists of quartz and reddened microcline accompanied by biotite and/or chlorite.

Chemically hydrogen ion metasomatism was characterised by a marked decrease in potash and alumina, due to feldspar breakdown, and sometimes by increases in  $Fe_2O_3$  and  $SiO_2$ . Norm calculations for vein greisens show a distinct decrease in **or** with a substantial decrease in **ab** and a concomitant increase in **q**. In the Q-Ab-Or plot of Fig 4.1, they are represented by closed inverted triangles which lie on the Q-Or join towards the Q pole. In contrast, the pervasive greisenisation recorded at Uwar Gida in the Ririwai Complex, is superimposed on remnant albitisation and partial microclinisation of the biotite granite adjacent to the volcanic cover. Here norm calculations reflect the more intense albitisation and the open inverted triangles can be seen to plot towards the Ab-Q join close to the Q pole in Fig 4.1.

Thus the plotting position of greisenised material on the Q-Ab-Or diagram, depends on the intensity of earlier processes; samples that were albitised and subsequently greisenised plot towards the Q pole on the Ab-Q side of the

Table 4.1 Major and trace element analyses and normative compositions of some sodic metasomatised samples from Nigeria

	PERALKALINE GRANITES AND SYENITES									biotite granites and syenites												Jos Bakuru RG5	Riahi SSS5/8	Dutsen Wai DW1
	Shere SHN10	Dutsen DM11	Wai DW13	Ririwai N86	N87	N88	N89	N90	Ropp RP2	Tibchi T34C	Ririwai L13-411	Afu L13-440	AF24/3	AF59/3	AF59/4	AF96/1	AF102	AF124						
SiO <sub>2</sub>	74.41	72.20	71.90	71.60	74.10	74.50	74.30	70.00	69.90	67.30	68.12	69.29	59.60	72.82	69.16	74.24	77.86	72.39	74.52	76.10	78.40	78.03		
TiO <sub>2</sub>	0.10	0.19	0.27	0.23	0.14	0.36	0.13	0.27	0.10	0.05	0.09	0.11	0.05	0.01	0.02	0.02	0.11	0.02	0.02	0.10	0.05	0.06		
Al <sub>2</sub> O <sub>3</sub>	11.92	11.61	11.83	13.54	12.19	10.45	11.47	14.50	13.60	17.16	16.13	15.02	16.76	13.37	15.69	14.06	11.74	15.32	13.55	10.95	12.40	12.14		
Fe <sub>2</sub> O <sub>3</sub>	1.96	1.88	1.68	1.85	1.79	2.14	1.89	1.63	1.39	1.07	0.51	0.78	0.25	1.65	1.27	1.23	1.55	1.02	0.46	0.00	1.26	0.33		
FeO	2.69	1.23	1.70	1.05	1.15	0.66	0.83	0.39	1.28	0.25	1.48	1.54	0.00	0.00	0.00	0.00	0.00	0.00	1.03	2.29	0.00	0.89		
MnO	0.04	0.06	0.09	0.07	0.07	0.09	0.01	0.13	0.05	0.02	0.08	0.08	0.01	0.04	0.03	0.02	0.02	0.02	0.02	0.03	0.02	0.01		
MgO	0.01	0.14	0.41	0.01	0.01	0.01	0.08	0.13	0.14	0.01	0.11	0.13	0.01	0.09	0.20	0.02	0.01	0.03	0.10	0.03	0.00	0.09		
CaO	0.12	0.36	0.39	0.01	0.04	0.02	0.32	0.44	0.44	0.46	0.52	0.42	8.38	0.33	0.52	1.02	0.14	0.62	0.12	0.65	0.23	0.52		
Na <sub>2</sub> O	6.05	7.23	5.74	6.79	5.56	6.04	5.28	5.97	6.09	7.32	9.95	8.43	9.84	5.29	6.14	5.08	4.46	6.35	4.98	3.89	4.40	4.59		
K <sub>2</sub> O	2.55	4.97	4.93	3.79	4.56	4.55	4.38	3.91	4.31	5.86	2.46	2.39	0.13	3.94	4.56	3.60	3.80	3.63	4.03	4.91	4.24	3.56		
P <sub>2</sub> O <sub>5</sub>	0.01	0.03	0.06	0.01	0.01	0.01	0.02	0.09	0.01	0.01	0.06	0.06	0.01	0.01	0.01	0.01	0.01	0.01	0.01	0.01	0.00	0.01		
H <sub>2</sub> O <sup>+</sup>	0.47	0.70	0.91	0.38	0.41	0.55	0.51	1.00	0.74	0.54	0.24	0.22	0.44	0.52	0.42	0.00	0.48	0.00	0.53	0.54	0.00	0.42		
F <sup>-</sup>	0.22	0.45	1.73	0.94	0.50	0.53	0.81	0.94			0.26	0.32		1.17					0.07					
OPF	-0.09	-0.20	-0.73	-0.39	-0.21	-0.22	-0.34	-0.39			-0.11	-0.13		-0.49					-0.02					
Total	100.46	100.60	99.91	99.88	100.32	99.69	99.69	99.00	98.05	100.05	99.90	98.66	95.48	98.75	98.02	99.30	100.17	99.41	99.44	99.50	101.00	100.65		
A/CNK	0.92	0.65	0.76	0.89	0.86	0.70	0.82	0.98	0.88	0.89	0.81	0.87	0.53	0.99	0.98	1.00	1.01	0.99		0.85		0.98		
R1	2089	993	1501	1390	1814	1672	1975	1569	1412	478	373	999	437	2008	1327	2267	2764	1690	2211	2471	2634	2699		
R2	248	274	295	268	244	208	264	338	321	387	378	347	1226	302	374	386	246	368	283	286	268	298		
Q	162	57	104	97	134	121	144	108	94	7	-2	56	-90	145	82	159	205	112	165	184	200	202		
F	-134	-134	-87	-138	-83	-99	-83	-117	-113	-119	-278	-229	-464	-93	-110	-106	-65	-139	-77	-33	-56	82		
Ba	0	10	103	0	0	0	0	44	0	0	0	0	0	0	0	0	0	0	0	65	0	71		
Be	9	20	20	45	75	49	31	30	118	6	5								11	10		10		
Ce	115	376	888	232	197	221	260	534	156	49									253	119	275			
Co				0.7			0.04																	
Cs				6.7			143																	
Cu		58	4	110	114	108	103		15	7	4										20			
Hf	9	146	63	103	89	258	127	148	90	5										12	7	10		
La	53	135	759	70	65	64	83	414	60	23										120	73	169		
Li	155	421	283	400	435	369	376	301	331	46	30	34								34	194	138		
Nb	187	1549	664	1604	854	1388	1494	1910	532	53										139	139	205		
Pb	80	82	202	103	311	254	485	536	77	71	25	37								37	16	16		
Rb	158	1224	819	1226	1303	1442	1450	1483	708	586	164	26								274	796	389		
Sb				0.6			2.85																	
Sc				0.2			0.1																	
Sn	26	0	0	50	50	67	58	126	46											34		10		
Sr	3	35	3	0	0	0	0	0	16	29	8	4								15	0	22		
Ta				312		282																		
Tb	11	62	128	126	217	128	318	356	86	42	73	69								34	60	42		
U		96	39	145	60	105	105																	
V	0	3	0	0	0	0	0	0	2	5														
Y	149	212	3469	144	549	154	414	1653	633	40	51	56								0	4	0		
Zn	696	624	485	766	988	900	968	500	282	164	26									163	127	356		
Zr	299	4045	1826	3071	2224	5552	3073	3674	2815	77	285	309								397	162	207		
Zr/Hf	33	28	29	30	25	22	24	25	31	15										33	18	20		
Ce/Y	0.77	1.77	0.26	1.61	0.36	1.44	0.63	0.32	0.25	1.23										0.15	0.94	0.77		
quartz	28.46	24.22	24.21	19.85	26.95	32.18	29.75	20.14	17.92	3.98	7.35	13.01	0.00	26.86	14.79	28.76	37.17	20.33	29.05	34.35	36.11	36.03		
ortho	15.07	29.36	29.13	22.39	26.94	26.88	25.88	23.10	25.46	34.62	14.53	14.12	0.77	23.28	26.94	21.27	22.45	21.45	23.83	29.01	25.05	21.03		
albite	47.11	32.05	31.40	48.54	37.31	28.42	34.61	50.49	45.94	55.64	69.27	63.95	67.28	44.74	51.93	42.96	37.64	53.71	42.16	28.99	37.21	38.82		
anorth	0.00	0.00	0.00	0.00	0.00	0.00	0.00	0.00	0.00	0.00	0.00	0.00	1.19	1.79	4.94	0.63	2.59	0.58			1.14	2.02		
nephel	0.00	0.00	0.00	0.00	0.00	0.00	0.00	0.00	0.00	0.00	0.00	0.00	8.64											
cordun	0.00	0.00	0.00	0.00	0.00	0.00	0.00	0.45	0.00	0.00	0.00	0.00		0.41										
scandite	3.57	5.44	4.86	5.35	5.18	6.19	5.47	4.62	0.00	1.48	2.26										0.16			
wollas	0.00	0.00	0.00	0.00	0.00	0.00	0.00	0.00	3.10				16.74						0.79					
di hvo	0.00	0.66	0.64	0.00	0.00	0.00	0.00	0.00	0.88	0.56	0.14			0.30	0.02					1.32		0.21		
di sen	0.00	0.10	0.18	0.00	0.00	0.00	0.00	0.00	0.13	0.39	0.01			0.26	0.02					0.09		0.03		
di ffs	0.00	0.62	0.50	0.00	0.00	0.00	0.00	0.00	0.84	0.02	0.14									0.07		0.03		
hy sen	0.02	0.24	0.84	0.02	0.02	0.20	0.32	0.22	0.41	0.26	0.32	0.22		0.24	0.03	0.02				1.46		0.19		
hy ffs	4.25	1.44	2.35	1.68	2.01	0.78	1.33	0.00	1.44	0.00	2.58	0.79								0.05		0.19		
magnet	1.05	0.00	0.00	0.00	0.00	0.00	0.00	0.90	0.00	0.00	0.00	0.00							1.75	2.63		1.09		
haemat	0.00	0.00	0.00	0.00	0.00	0.00	0.00	1.01	0.00	0.00	0.00	0.00		0.10	0.04	0.01			0.67			0.48		
ilmen	0.19	0.36	0.51	0.44	0.27	0.68	0.25	0.51	0.19	0.09	0.17	0.21	</											

Table 4.2 Major and trace element analyses and normative compositions of some potash metasomatised samples from Nigeria

	PERALKALINE GRANITE				BIOTITE GRANITE								BASEMENT				
	Tibchi T34	Ririwai RN84	N58a	N58C	RS14A	RS19A	RS19B	RI/20A	RI/20B	RI/23B	R2/1A	R2/1B	Ropp GAD17	GAD215	GAE58	GAE6	GAD318
SiO <sub>2</sub>	62.80	77.20	76.20	76.00	76.24	76.92	60.63	76.89	77.74	77.75	76.52	79.38	41.24	50.61	43.06	62.60	48.45
TiO <sub>2</sub>	0.05	0.15	0.08	0.07	0.06	0.07	0.04	0.08	0.06	0.07	0.07	0.07	1.44	0.36	0.78	0.26	0.59
Al <sub>2</sub> O <sub>3</sub>	15.76	11.60	10.89	10.69	11.12	10.86	10.51	11.49	10.07	9.89	12.25	9.68	13.05	17.46	19.45	13.65	16.39
Fe <sub>2</sub> O <sub>3</sub>	5.02	2.62	1.96	1.34	2.92	1.15	7.55	1.24	2.20	3.03	1.42	1.95	23.09	10.36	16.04	7.18	10.64
FeO	1.84	0.01	0.00	0.00	0.00	0.00	0.00	0.00	0.00	0.00	0.00	0.00	0.00	0.00	0.00	0.00	0.00
MnO	0.15	0.03	0.06	0.03	0.07	0.03	0.23	0.02	0.03	0.06	0.02	0.03	0.19	0.19	0.21	0.09	0.14
MgO	0.03	0.03	0.01	0.01	0.05	0.01	0.01	0.01	0.02	0.01	0.02	0.02	7.12	1.51	2.86	1.79	1.63
CaO	0.34	0.06	0.05	0.19	0.05	0.05	0.04	0.29	0.26	0.24	0.28	0.27	1.05	4.61	1.22	2.95	4.15
Na <sub>2</sub> O	5.58	2.70	0.01	0.98	0.39	0.24	0.08	2.79	0.24	0.22	2.37	0.74	1.12	1.13	4.11	2.06	1.12
K <sub>2</sub> O	7.20	4.59	9.76	9.78	8.15	8.72	5.40	5.02	7.78	7.39	6.82	7.02	8.81	7.52	7.13	5.48	8.26
P <sub>2</sub> O <sub>5</sub>	0.01	0.01	0.06	0.07	0.02	0.01	0.01	0.01	0.01	0.01	0.01	0.01	0.18	0.16	0.42	0.22	0.30
H <sub>2</sub> O <sup>+</sup>	0.54	0.83	0.37	0.30	0.43	0.58	0.54	0.62	0.44	0.60	0.75	0.60	1.24	1.25	2.11	2.07	2.64
F <sup>-</sup>		0.05	0.17	0.24								1.64	3.79	1.78	1.35	4.53	
Q <sup>+</sup>		-0.02	-0.07	-0.10								-0.69	-1.59	-0.75	-0.57	-1.90	
Total	99.32	99.86	99.55	99.60	99.50	98.64	85.04	98.46	98.85	99.27	100.53	99.77	99.48	97.39	98.42	99.13	96.94
A/CNK	0.90	1.22	1.02	0.85	1.16	1.09	1.74	1.09	1.08	1.12	1.04	1.04	0.98	0.95	1.17	0.93	0.89
Q	11	243	214	180	236	233	218	226	255	264	199	264	-7	30	-60	129	8
F	-33	9	206	173	160	177	111	11	153	146	63	120	132	41	-3	-3	65
Ag					2	1	45		5	1	2	2					
Ba	223	81	1	0	39	39	0	21	19	15	31	30					
Be	230	11	3	2	5	4	15	2	4	4	2	1	26	101	142	39	9
Cd					2	8	148		18	14	8	4	1	44	1	2	48
Ce	298	22	98	115	39	147	293	83	98	85	76	74					
Cu		4	21	10	16	38	27	12	27	7	77	23	3	87	4	3600	184
Hf	7	31	11	11	14	13	14	12	13	14	11	13					
La	184	14	50	59	17	86	0	58	52	51	47	43					
Li	310	5	340	209	1200	600	740	159	540	1100	420	600	1853	1664	1638	1122	4207
Nb	168	285	170	157	170	155	12	217	171	136	143	121					
Pb	202	82	182	142	249	5400	68300	270	2400	80	80	160	30	138	18	18	30
Rb	1131	421	1203	1254	1545	1186	1020	368	1178	1232	997	1089					
Sr	70	40	160	100	315	125	2130	118	350	470	110	335	130	3100	130	22130	110
Sn	80	3	0	0	0	1	1	5	1	0	1	0					
Th	89	57	66	60	74	91	343	54	78	47	29	53	2	10	54	7	4
U														4	6	18	6
V	3	0	0	0	6	5	3	4	5	5	6	5					
W			1320	720													
Y	85	99	43	142	13	1	1	75	107	130	131	129					
Zn	882	100	292	331	164	850	5100	3700	2500	2100	690	390	613	6372	347	341	12460
Zr	210	883	238	199	209	181	1	162	224	243	192	194					
Zr/Hf	30	29	22	18	15	14	0.8	18	17	17	17	15					
Ce/Y	3.51	0.22	2.28	0.81	3.00	147	293	1.11	0.92	0.65	0.58	0.57					
quartz	3.39	43.90	38.79	35.78	42.67	42.07	39.43	40.86	46.02	47.70	36.05	47.64	0.00	13.02	0.00	25.50	7.91
ortho	42.54	27.12	57.66	57.78	48.15	51.52	31.90	29.66	45.97	40.29	41.48	52.05	44.43	42.13	32.38	48.80	
albite	40.98	22.84	0.08	0.54	3.30	2.03	0.68	23.60	2.03	1.86	20.04	6.26	0.13	9.56	12.41	17.42	9.47
anorth	0.00	0.00	0.00	0.00	0.12	0.18	0.13	1.37	1.22	1.13	1.32	1.27	0.00	0.00	0.00	3.46	0.00
nephel	0.00	0.00	0.00	0.00	0.00	0.00	0.00	0.00	0.00	0.00	0.00	0.00	5.06	0.00	12.11	0.00	0.00
corund	0.00	2.19	0.31	0.00	1.62	0.96	4.49	0.97	0.81	1.12	0.49	0.40	1.67	7.49	4.97	3.06	5.61
acmite	5.48	0.00	0.00	3.91	0.00	0.00	0.00	0.00	0.00	0.00	0.00	0.00	0.00	0.00	0.00	0.00	0.00
hy ten	0.02	0.07	0.02	0.02	0.12	0.02	0.02	0.02	0.05	0.02	0.05	0.05	0.00	3.76	4.46	4.06	
hy kfs	0.29	0.00	0.00	0.00	0.00	0.00	0.00	0.00	0.00	0.00	0.00	0.00	0.00	0.00	0.00	0.00	0.00
ol kfs	0.00	0.00	0.00	0.00	0.00	0.00	0.00	0.00	0.00	0.00	0.00	0.00	12.42	0.00	4.99	0.00	0.00
magnet	4.53	0.00	0.00	0.00	0.05	0.00	0.63	0.00	0.00	0.00	0.00	0.00	0.00	0.00	0.00	0.00	0.00
haemat	0.00	2.62	1.96	0.00	2.88	1.15	7.11	1.24	2.20	3.03	1.42	1.95	23.09	10.36	16.04	7.18	10.64
ilmen	0.09	0.09	0.13	0.06	0.11	0.06	0.08	0.04	0.06	0.13	0.04	0.06	0.41	0.41	0.45	0.19	0.30
rutile	0.00	0.11	0.00	0.04	0.00	0.04	0.00	0.06	0.03	0.00	0.05	0.04	1.23	0.15	0.54	0.16	0.43
Na met	0.00	0.00	0.00	0.77	0.00	0.00	0.00	0.00	0.00	0.00	0.00	0.00	0.00	0.00	0.00	0.00	0.00
apatit	0.02	0.02	0.30	0.17	0.05	0.02	0.02	0.02	0.02	0.02	0.02	0.02	0.43	0.38	1.00	0.52	0.71
water	0.54	0.83	0.37	0.30	0.43	0.58	0.54	0.62	0.44	0.60	0.75	0.60	1.24	1.25	2.11	2.07	2.64
fluor	0.00	0.07	0.00	0.14	0.00	0.00	0.00	0.00	0.00	0.00	0.00	0.00	1.13	6.13	0.93	2.73	5.23
TTDI	86.91	93.85	96.53	94.11	88.01	95.62	72.01	94.11	94.02	93.22	96.39	95.37	52.18	67.01	54.54	75.30	66.18

Table 4.3 Major and trace element analyses of acid metasomatised basement (Trend 1) and acid metasomatised volcanic or roof facies (Trend 2)

ACID METASOMATISED BASEMENT Trend 1									ACID METASOMATISED ROOF FACIES Trend 2			
Ropp (Gindi Akwati)									Ririwai			
GAD18	GAD319	GAD323	GAD424	GAD426	GAE1	GAE2	GAE4	GAE540	Af22/5	Af60	T22	
SiO <sub>2</sub>	23.69	54.29	53.64	56.71	51.67	41.35	43.56	55.40	54.74	69.80	81.10	76.50
TiO <sub>2</sub>	0.29	0.36	1.02	0.14	0.52	0.30	1.70	0.51	0.52	0.10	0.02	0.16
Al <sub>2</sub> O <sub>3</sub>	6.53	20.75	16.29	17.50	13.96	15.91	14.33	16.83	16.99	16.65	10.24	11.17
Fe <sub>2</sub> O <sub>3</sub>	5.33	6.55	9.41	5.85	12.67	17.34	15.94	6.45	7.36	4.72	1.35	0.66
FeO												2.84
MnO	0.11	0.10	0.22	0.11	0.26	0.26	0.32	0.11	0.12	0.04	0.04	0.04
MgO	1.32	1.04	3.26	0.93	1.51	1.51	8.61	2.33	2.13	0.07	0.01	0.04
CaO	39.30	1.70	3.98	3.04	5.81	8.79	4.81	4.17	3.26	2.22	0.04	0.85
Na <sub>2</sub> O	1.72	5.81	5.55	7.60	5.31	3.26	2.60	5.60	5.12	0.08	3.70	4.16
K <sub>2</sub> O	2.59	4.47	3.60	2.02	1.98	2.78	4.20	2.53	3.51	1.88	3.33	1.45
P <sub>2</sub> O <sub>5</sub>	0.15	0.18	0.34	0.11	0.16	0.31	0.24	0.13	0.16	0.00	0.01	0.00
H <sub>2</sub> O	0.88	1.20	0.59	1.80	2.00	0.91	0.43	0.49	1.93	0.00	0.12	1.04
F <sup>2</sup>	17.60	1.49	1.67	2.77	2.97	4.84	2.71	2.55	3.75			
O=F	-7.39	-0.63	-0.70	-1.16	-1.25	-2.03	-1.14	-1.07	-1.57			
Total	92.12	97.31	98.87	97.42	97.57	97.53	98.31	96.03	98.02	95.66	99.96	98.91
A/CNK	0.08	1.19	0.80	0.87	0.65	0.65	0.82	0.86	0.94	2.69	1.05	0.75
Q	-446.5	-1.7	-5.6	-10.0	3.9	-39.6	11.1	23.0	24.9	318.4	259	251
F	-701.0	-122.8	-173.5	-256.5	-232.8	-202.8	-80.4	-201.3	-148.7	-2.2	-49	-119
Ag												
Ba												
Be	102	5	63	66	69	194	30	57	9	3		26
Cd	4	3	3	43	21	100	12	2	5			
Ce												
Cu	50	6889	10	470	516	766	41	6	1060			14
Hf												
La												
Li	34	535	521	935	67	156	407	1133	4217	192		21
Nb												
Pb	822	30	40	15	10	12	40	20	45			67
Rb												
Sn	2230	6200	530	450	250	1330	110	150	2400	100		50
Sr												47
Th	10	15	8	2	7	8	2	27	11			
U	5	6	15	6	13	16	6	22	22			
V												
W												
Y												
Zn	583	908	1100	9636	4100	19600	2400	497	1200	1000		196
Zr										1028		425
Zr/Hf												
Ce/Y												
quartz	0.0*	1.86	0.36	3.42	8.33	6.77	0.00**	9.15	8.37	57.88	46.78	42.85
ortho		26.41	21.27	11.93	11.70	16.42	24.81	14.95	20.74	11.11	19.67	8.57
albite		49.14	49.94	64.28	44.91	27.57	21.99	47.36	43.30	0.68	31.29	35.18
anorth	2.45		5.52		6.14	6.35	2.61	1.25		11.01	0.13	4.22
nephel												
corund		6.36	1.24	2.82	0.84	5.21	4.55	4.42	4.77	10.45	0.50	1.21
acmite												
wo	11.72											
di	3.80											
hy	3.29											
hy		2.59	8.12	2.32	3.76	3.76	16.17	5.80	5.30	0.17	0.02***	0.10
hy												
ifs												
ol												
ifo												
magnet											0.07	0.96
haemat	5.33	6.55	9.41	5.85	12.67	17.34	15.94	6.45	7.36	4.72	1.30	
ilmen	0.24	0.21	0.47	0.24	0.56	0.56	0.68	0.24	0.26	0.09	0.04	0.30
rutile		0.25	0.77	0.02	0.23	0.01	1.34	0.39	0.38	0.05		
Na met												
apatit	0.36	0.43	0.81	0.26	0.38	0.74	0.57	0.31	0.38		0.02	
water	0.88	1.20	0.59	1.80	2.00	0.91	0.43	0.49	1.93		0.12	
fluor	36.14	2.04										
TTDI	76.28	77.41	68.57	79.63	64.94	50.77	46.80	71.47	72.42	69.17	97.75	86.60

\* includes 0.28 pervsk, 7.75 Ca, Or 7.88 Ne, 12.00 Leuc.

\*\* includes 3.69 Ol% Fo

\*\*\* plus 4.48 hy %Fs

Table 4.4 Major and trace element analyses of acid metasomatised potash rich granites and microclinites Trend 3

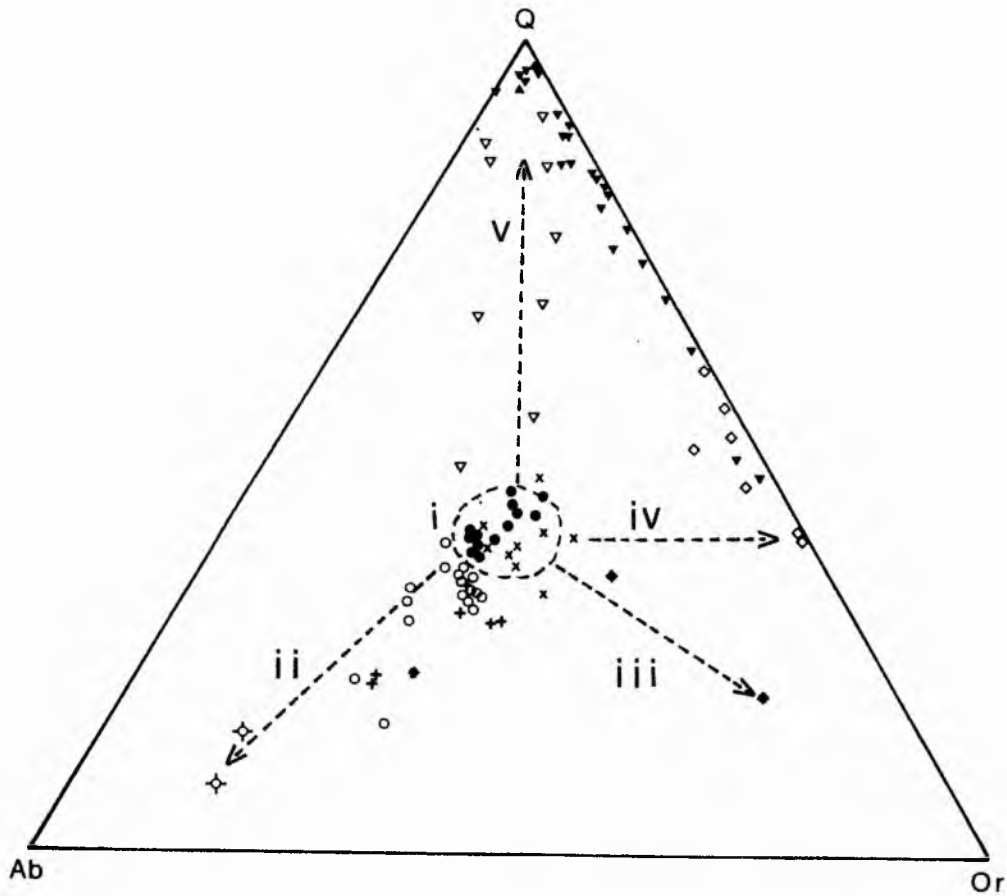
	Ririwai											
	AF21/2	N58B	R1/4	R1/18	RS14B	R1/22	R1/23A	R1/23C	R1/35	R2/1C	RS164	RS16C
SiO <sub>2</sub>	75.10	84.40	76.34	80.46	78.19	76.27	72.50	80.75	77.20	66.39	78.00	82.95
TiO <sub>2</sub>			0.08	0.44	0.06	0.04	0.06	0.08	0.06	0.12	0.05	0.07
Al <sub>2</sub> O <sub>3</sub>	7.34	4.28	11.62	8.51	8.75	11.99	3.03	7.10	12.10	10.78	7.50	5.47
Fe <sub>2</sub> O <sub>3</sub>	10.89	7.71	2.31	2.96	6.13	1.47	2.65	5.52	1.31	11.77	7.12	5.06
FeO												
MnO	0.06	0.18	0.02	0.03	0.18	0.02	0.06	0.10	0.01	0.26	0.16	0.12
MgO	0.09	0.01	0.13	0.07	0.01	0.04	0.07	0.01	0.05	0.01	0.01	0.01
CaO	0.65	0.18	0.25	0.01	0.05	0.11	0.18	0.20	0.35	0.34	0.04	0.04
Na <sub>2</sub> O	0.29	0.01	2.72	0.01	0.07	2.78	0.29	0.15	4.23	0.08	0.06	0.04
K <sub>2</sub> O	3.71	1.58	4.81	6.15	4.66	5.17	1.55	3.97	4.37	5.17	3.32	2.40
P <sub>2</sub> O <sub>5</sub>	0.01	0.08	0.01	0.01	0.02	0.01	0.01	0.01	0.01	0.02	0.01	0.01
H <sub>2</sub> O <sup>5</sup>	1.08	1.20	0.60	0.40	0.69	1.00	0.92	0.98	0.40	0.95	0.47	0.82
F <sup>-</sup>	na	0.77		na	na	na	na	na	na	na	na	na
O=F		-0.32										
Total	99.23	100.25	98.89	99.05	98.81	98.90	81.32	98.87	100.09	95.89	96.74	96.99
A/CNK		2.09	1.15	1.27	1.67	1.16	1.22	1.45	0.98	1.70	1.99	2.00
Q	320.3	431.6	230.1	314.8	331.4	221.8	357.3	355.9	194.4	251.5	359.3	406.9
F	57.8	30.0	9.9	130.1	95.8	18.1	20.3	75.9	-49.9	101.1	67.8	49.0
Ag					2		2	2		2	2	3
Ba		0			21		0	46		61	0	0
Be	13	5			9		3	4		16	11	7
Cd					2		58	6		10	16	40
Ce		159			30		65	96		150	66	74
Cu		49			12		21	7		190	1700	850
Hf		11			13		11	9		16	25	20
La		85			3		43	58		103	5	17
Li	327	150			2900		665	1600		5900	3200	2300
Nb		87			136		217	165		156	136	104
Pb		717			210		283	330		190	8230	4530
Rb		682			1653		368	967		2428	1503	1031
Sn	2540	350			1100		3470	870		3380	8190	945
Sr		1			0		5	0		14	51	0
Th		158			82		44	54		155	249	132
U												
V												
W		860										
Y		125			10		75	92		160	0	0
Zn	1900	2436			264		11000	1500		1900	1800	4100
Zr	1920	171			196		162	155		240	217	186
Zr/Hf												
Ce/Y												
quartz	57.72	78.28	85.75	56.77	59.89	40.06	64.42	64.27	35.21*	45.46	64.88	73.46
ortho	21.92	9.33	2.19	36.34	27.53	30.55	9.16	23.46	25.82	30.55	19.62	14.18
albite	2.45	0.08	3.72	0.08	0.59	23.51	2.45	1.27	35.78	0.68	0.51	0.34
anorth	3.16				0.12	0.48	0.83	0.93	1.13	1.56	0.13	0.13
nephel												
corund	1.69	2.55	0.14	1.84	3.55	1.65	0.57	0.22		4.48	3.76	2.76
acmite												
hy 1en	0.22	0.02	0.47	0.17	0.02	0.10	0.17			0.02	0.02	0.02
hy 1fs												
Ol 1fo												
magnet	0.17	0.09			0.41		0.02	0.09		0.50	0.38	0.19
haemat												
ilmen	0.02	0.32	0.04	0.06	0.11	0.04	0.11	0.15	0.02	0.23	0.09	0.13
rutile			0.04	0.41		0.02						
Na met												
apatit	0.02	0.19	0.06	0.06	0.05	0.02	0.02	0.02	0.02	0.05	0.02	0.02
water	1.08	1.20	0.60	0.40	0.69	1.00	0.92	0.98	0.40	0.95	0.47	0.82
fluor		0.10										
TTDI		87.70	91.66	93.17	88.01	94.12	76.03	89.00	96.81	76.68	85.00	87.98

\* includes 0.14 wo, 0.26 di, 0.12 titan

Table 4.5 Major and trace element analyses of acid metasomatised perthite granite: pervasive acid metasomatism of sodic/potash metasomatised samples (Trend 4) and silica metasomatised samples (Trend 5)

SiO <sub>2</sub> TiO <sub>2</sub> Al <sub>2</sub> O <sub>3</sub> Fe <sub>2</sub> O <sub>3</sub> FeO MnO MgO CaO Na <sub>2</sub> O K <sub>2</sub> O P <sub>2</sub> O <sub>5</sub> H <sub>2</sub> O <sup>+</sup> F Total	acid metasomatised perthite granite										pervasive acid metasomatism of Na <sup>+</sup> and K <sup>+</sup>										vein controlled silica metasomatism																																																															
	pervasive					perthite					Dutse					Fagun					Kuduru					Ririwei					RS6C					RS31/3B					RS31/3C					RS31/3A					RN74					SS17/5					JRI120					Ririwai					RI/14					RI/20C					RS16B			
JX122	JR164	JR118A	RS16	BE4	BE1	BE5	DUT32	FAG11	KOD1/3	RS5A	RS6B	RS6C	RS31/3B	RS31/3C	RS31/3A	RS5A	RS6B	RS6C	RS31/3B	RS31/3C	RS31/3A	RS5A	RS6B	RS6C	RS31/3B	RS31/3C	RS31/3A	RS5A	RS6B	RS6C	RS31/3B	RS31/3C	RS31/3A	RS5A	RS6B	RS6C	SS17/5	JRI120	Ririwai	RI/14	RI/20C	RS16B																																										
73.00	78.00	82.60	76.30	81.0	74.00	61.0	77.80	77.80	77.70	76.15	77.86	71.58	76.79	80.00	94.19	76.15	77.86	71.58	76.79	80.00	94.19	76.15	77.86	71.58	76.79	80.00	94.19	76.15	77.86	71.58	76.79	80.00	94.19	76.15	77.86	71.58	90.90	93.80	90.01	88.64	86.05																																											
0.10	0.10	0.30	0.10	0.30	0.30	0.10	0.20	0.30	0.10	0.07	0.08	0.08	0.05	0.11	0.06	0.07	0.08	0.08	0.05	0.11	0.06	0.07	0.08	0.08	0.05	0.11	0.06	0.07	0.08	0.08	0.05	0.11	0.06	0.07	0.10	0.01	0.06	0.05	0.05	0.05																																												
4.45	10.78	1.09	11.82	10.59	16.98	17.31	9.30	12.18	12.42	11.66	8.10	2.17	11.17	6.06	2.88	11.66	8.10	2.17	11.17	6.06	2.88	11.66	8.10	2.17	11.17	6.06	2.88	11.66	8.10	2.17	11.17	6.06	2.88	1.85	1.20	1.50	1.26	1.75	2.63																																													
17.50	5.08	1.66	8.77	5.85	6.90	8.85	7.89	8.75	8.73	1.72	2.67	5.67	1.28	7.70	1.34	1.72	2.67	5.67	1.28	7.70	1.34	1.72	2.67	5.67	1.28	7.70	1.34	1.72	2.67	5.67	1.28	7.70	1.34	3.40	0.64	1.76	2.44	2.74	2.74																																													
0.47	0.10	0.07	0.10	0.15	0.17	0.13	0.06	0.11	0.08	0.11	0.05	0.04	0.01	0.08	0.12	0.11	0.05	0.04	0.01	0.08	0.12	0.11	0.05	0.04	0.01	0.08	0.12	0.11	0.05	0.04	0.01	0.08	0.12	0.11	0.05	0.04	0.01	0.08	0.12	0.11	0.05	0.04																																										
0.11	0.05	0.01	0.02	0.01	0.11	0.17	0.01	0.01	0.01	0.09	0.17	0.21	0.01	0.03	0.01	0.09	0.17	0.21	0.01	0.03	0.01	0.09	0.17	0.21	0.01	0.03	0.01	0.09	0.17	0.21	0.01	0.03	0.01	0.09	0.05	0.02	0.19	0.01	0.01	0.01																																												
0.08	0.12	0.65	0.43	0.33	0.33	2.60	2.43	0.02	0.21	0.07	0.48	0.48	0.24	0.35	0.24	0.35	0.24	0.48	0.24	0.35	0.24	0.35	0.24	0.48	0.24	0.35	0.24	0.35	0.24	0.35	0.24	0.35	0.24	0.35	0.24	0.35	0.24	0.35	0.24	0.35	0.24																																											
0.16	0.17	0.17	0.09	0.05	0.05	0.05	2.43	0.03	0.05	3.07	2.17	0.87	3.72	0.86	1.32	3.07	2.17	0.87	3.72	0.86	1.32	3.07	2.17	0.87	3.72	0.86	1.32	3.07	2.17	0.87	3.72	0.86	1.32	3.07	2.17	0.87	3.72	0.86	1.32	3.07	2.17																																											
1.83	1.83	1.18	2.43	1.30	1.36	2.78	3.78	2.13	2.46	4.37	1.99	3.78	4.42	2.39	4.42	4.37	1.99	3.78	4.42	2.39	4.42	4.37	1.99	3.78	4.42	2.39	4.42	4.37	1.99	3.78	4.42	2.39	4.42	4.37	1.99	3.78	4.42	2.39	4.42																																													
0.01	0.01	0.01	0.03	0.00	0.00	0.12	0.00	0.01	0.00	0.01	0.02	0.01	0.05	0.02	0.02	0.01	0.02	0.01	0.05	0.02	0.02	0.01	0.02	0.01	0.05	0.02	0.02	0.01	0.02	0.01	0.05	0.02	0.02	0.01	0.02	0.01	0.05	0.02	0.02	0.01																																												
2.61	0.36	0.52	0.60	0.90	1.34	0.78	0.02	0.58	0.70	0.48	0.76	0.97	0.68	0.54	0.35	0.48	0.76	0.97	0.68	0.54	0.35	0.48	0.76	0.97	0.68	0.54	0.35	0.48	0.76	0.97	0.68	0.54	0.35	0.48	0.76	0.97	0.68	0.54	0.35																																													
98.66	96.58	87.06	100.66	100.46	101.44	95.15	101.51	101.91	102.32	98.00	94.16	80.47	98.42	98.14	101.26	98.00	94.16	80.47	98.42	98.14	101.26	98.00	94.16	80.47	98.42	98.14	101.26	98.00	94.16	80.47	98.42	98.14	101.26	98.00	94.16	80.47	98.42	98.14	101.26																																													
7.51	4.35	0.66	3.32	5.07	7.89	2.22	1.15	4.45	4.33	1.12	1.30	0.80	0.99	1.31	0.85	1.12	1.30	0.80	0.99	1.31	0.85	1.12	1.30	0.80	0.99	1.31	0.85	1.12	1.30	0.80	0.99	1.31	0.85	1.12	1.30	0.80	0.99	1.31	0.85																																													
394.8	386.4	440.6	362.2	415.7	357.6	246.4	272.2	382.4	375.8	226.1	315.7	354.6	208.8	360.6	461.0	226.1	315.7	354.6	208.8	360.6	461.0	226.1	315.7	354.6	208.8	360.6	461.0	226.1	315.7	354.6	208.8	360.6	461.0	226.1	315.7	354.6	208.8	360.6																																														
-3.0	31.2	-15.2	41.0	20.1	21.4	11.6	1.5	40.5	49.4	-12.3	-52.9	-28.3	-30.6	16.8	-31.4	-12.3	-52.9	-28.3	-30.6	16.8	-31.4	-12.3	-52.9	-28.3	-30.6	16.8	-31.4	-12.3	-52.9	-28.3	-30.6	16.8	-31.4	-12.3	-52.9	-28.3	-30.6																																															
0	0	0	30	5	315	329	0	1	7	2	2	2	1	2	2	2	2	2	1	2	2	2	2	2	1	2	2	2	2	2	2	2	2	2	2	2	2	2																																														
154	5	1	2	8	2	3	5	1	2	5	3	0	1	2	0	3	1	0	5	4	4	4	4	4	5	4	4	4	4	4	4	4	4	4	4	4	4	4																																														
107	28	328	84	97	34	7	644	109	24	99	112	109	82	109	86	99	112	109	82	109	86	99	112	109	82	109	86	99	112	109	86	99	112	109	86	99	112	109																																														
2	9	9	8	4	2	0	162	6	5	17	13	9	15	9	16	17	13	9	15	9	16	17	13	9	15	9	16	17	13	9	16	17	13	9	16	17	13																																															
65	13	90	35	41	20	0	255	91	11	74	107	70	54	75	58	74	107	70	54	75	58	74	107	70	54	75	58	74	107	70	54	75	58	74	107	70	54																																															
47	749	26	532	624	316	684	10	309	595	53	90	221	83	190	63	53	90	221	83	190	63	53	90	221	83	190	63	53	90	221	83	190	63	53	90	221	83																																															
109	121	47	93	116	14	6	359	134	86	158	251	136	170	165	101	158	251	136	170	165	101	158	251	136	170	165	101	158	251	136	170	165	101	158	251	136																																																
339	245	79000	87	311	92	208	84	64	103	20	48	20	807	967	152	20	48	20	807	967	152	20	48	20	807	967	152	20	48	20	48	20	48	20	48	20																																																
10	1149	4	105	524	684	1244	425	670	675	680	272	123	807	967	152	680	272	123	807	967	152	680	272	123	807	967	152	680	272	123	807	967	152	680	272																																																	
520	1000	120	210	890	81	550	62	240	240	1024	12200	17100	79	330	220	1024	12200	17100	79	330	220	1024	12200	17100	79	330	220	1024	12200	17100	79	330	220	1024	12200																																																	
6	3	0	18	16	62	114	7	1	6	8	53	52	1	0	2	8	53	52	1	0	2	8	53	52	1	0	2	8	53	52	1	0	2	8	53	52																																																
54	82	109	47	95	19	35	88	39	27	70	108	159	89	54	117	70	108	159	89	54	117	70	108	159	89	54	117	70	108	159	89	54	117	70	108																																																	
152	25	0	126	164	24	18	491	74	27	175	143	86	125	92	125	175	143	86	125	92	125	175	143	86	125	92	125	175	143	86	125	92	125	175	143																																																	
8200	400	19200	194	286	168	32000	32000	66	66	286	168	66	274	155	226	286	168	66	274	155	226	286	168	66	274	155	226	286	168	66	274	155	226	286	168																																																	
71.11	69.74	79.86*	65.53	75.01	67.64	49.15	69.04	67.83	67.83	40.75	56.81	64.03**	37.89	65.12	83.41***	40.75	56.81	64.03**	37.89	65.12	83.41***	40.75	56.81	64.03**	37.89	65.12	83.41***	40.75	56.81	64.03**	37.89	65.12	83.41***	40.75	56.81	64.03**																																																
1.00	10.81	1.06	14.36	7.68	8.04	22.33	12.58	14.53	14.53	25.82	11.76	2.30	26.11	14.12	4.31	25.82	11.76																																																																			

Fig 4.1. Q-Ab-Or plot showing (i) field of biotite and peralkaline granites: (ii) the vector towards the Ab pole of samples that have undergone sodic metasomatism: (iii) the vector towards the Or pole of syenites and pegmatites produced by intense potash metasomatism: (iv) the vector towards the Q-Or join of samples that have been microclinised but not de-silicated: (v) the vector towards Q on the Q-Or join of samples from greisen veins: (vi) the vector from granite composition towards the Q pole for samples that have undergone pervasive acid metasomatism.



- biotite granite
- × peralkaline granite
- albitised biotite granite
- + albitised peralkaline granite
- ⊕ albitite
- ◇ microclinised biotite granite
- ◆ microcline pegmatite
- ▽ pervasive greisenisation
- ▼ greisen vein
- ▲ quartz vein

diagram. In contrast, samples which were microclinised and then greisenised plot towards the Q pole but on the Or-Q side of the diagram and samples which have been subjected to all three processes plot close to the vertical Q+(Or=Ab).

The silicification process resulted from the release of  $\text{SiO}_2$  during earlier hydrothermal processes. The formation of albitites and microclinites, as in the Ririwai complex, released silica; this was also the case during the transformation of feldspar to mica at the acid metasomatism stage. Progressive loss of fluorine from the fluid would also have led to the deposition of silica. Thus the final major stage of alteration is the silicification process. Chemically this **silicification** process shows the obvious increase in silica, balanced by a decrease in all the other major elements except iron in some cases.

So far the major element changes have been represented on conventional Q-Ab-Or plots. However, this type of presentation is not strictly valid when greisenisation and silicification are being considered since both processes involve feldspar destruction. A different approach using the major element parameters has been used in the past by several authors most notably Meyer and Hemley (1967). However, they used Ca as one of their parameters, which has very low concentrations in many of the anorogenic granites. A similar presentation of data, using AKNF parameters ( $A = \text{Al}_2\text{O}_3 - (\text{Na}_2\text{O} + \text{K}_2\text{O})$ ,  $K = \text{K}_2\text{O}$ ,  $N = \text{Na}_2\text{O}$ ,  $F = \text{FeO} + \text{MgO} + \text{MnO}$ ) has been used by Jackson et al (1982) for Cornubian data. Using these AKNF parameters, the data of Table 4.1 - 4.5 have been plotted on Fig 4.2. Whilst the biotite granites define a fairly small field, similar in position and size to the one defined by the Cornubian granites (Fig 4.2a), the peralkaline granites show a much broader plotting range (Fig 4.2b). When the sodic metasomatised compositions are compiled and superimposed on the peralkaline field (Fig 4.2c), there is a large measure of overlap. The potash metasomatised facies plot in a different field of the AFN diagram from sodic metasomatised rocks, although there is a wide spread in the plotting positions (Fig 4.2d). In contrast, in the AKF plot, whilst many K metasomatised samples plot towards the K pole, there is a certain amount of overlap between  $\text{K}^+$  and  $\text{Na}^+$  metasomatised samples. For acid metasomatism, which is the equivalent of the phyllic alteration in Fig 4.2a, there is a wide spread of data in both AKF and ANF plots, even within one group of rocks that has been affected such as greisenised basement or greisenised potash-rich rocks for example. Obviously for the Nigerian Province such graphical representation of changing chemical compositions is not a useful technique.

An alternative approach is to use cationic molecular values, found in French classification schemes, which express whole-rock chemistry as cationic parameters in terms of mineralogical components. This approach was first devised by de la Roche (1964, 1978), de la Roche and Leterrier (1973) de la Roche et al (1980) to study the various Hercynian granitic rocks in France and more recently by Debon and le Fort (1983) and Batchelor and Bowden (1985) to test petrogenetic hypotheses. The multicationic parameters R1 and R2 were used in Chapter 2 to investigate the relationship between the volcanic and subvolcanic rocks. Such an approach is also valid in the study and graphical representation of major element changes during hydrothermal alteration.

In this chapter, the Q-F multicationic scheme is used in which analytical data are expressed in millications and plotted in relation to the mineral poles quartz, albite, mica and microcline (after de la Roche 1964 and Charoy 1979).

Fig 4.2 AKFN diagram for Nigerian granites and hydrothermal variants

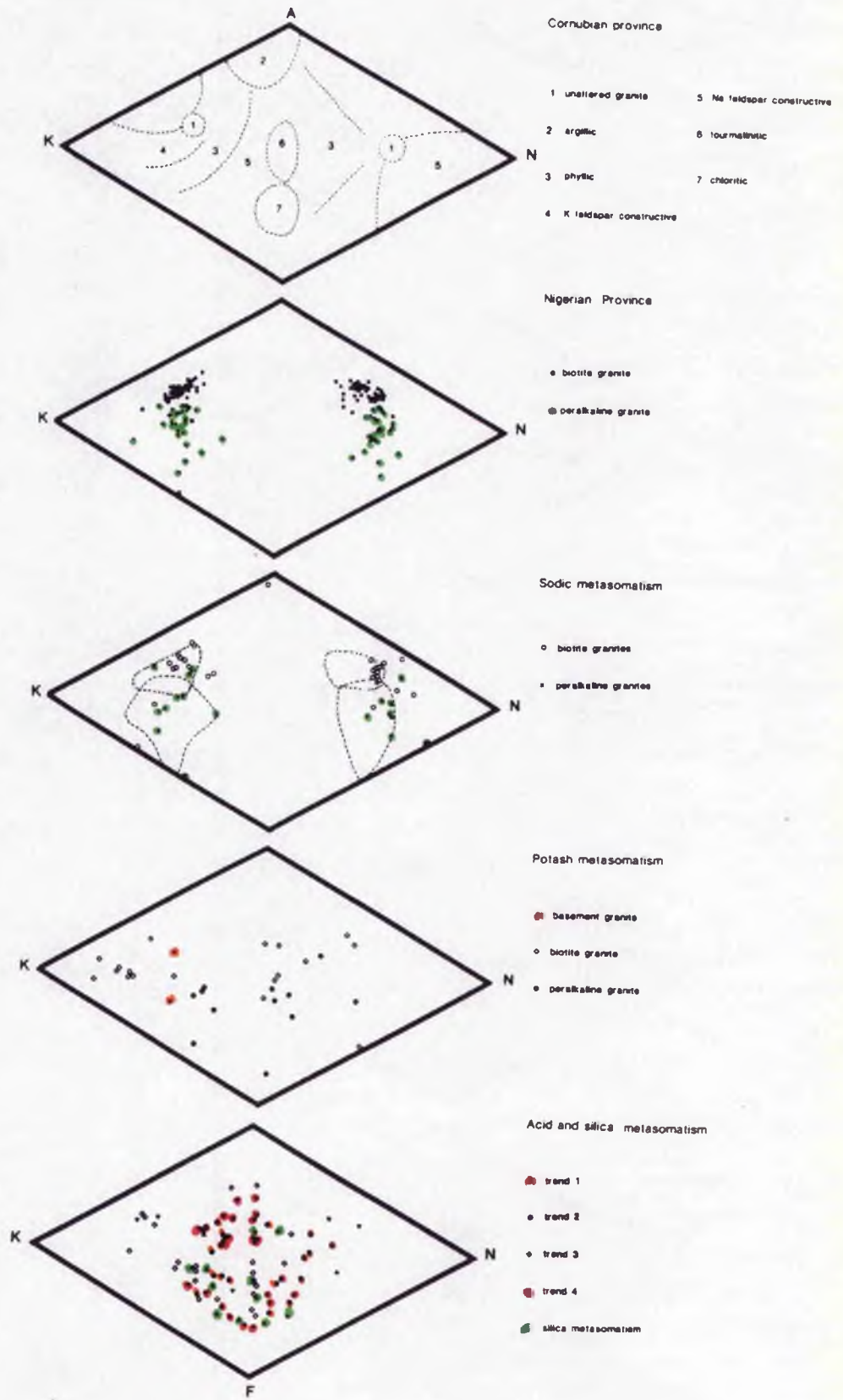
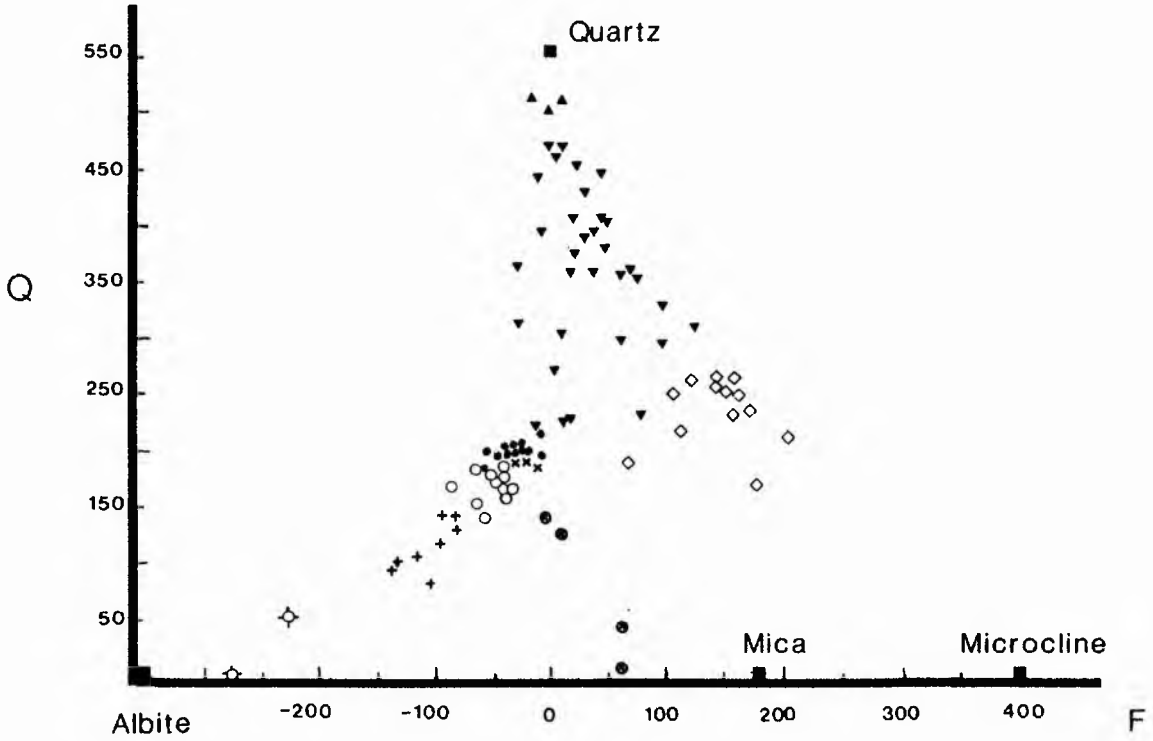


FIG 4.3. QF diagram (expressed in millications and plotted in relation to the mineral poles quartz, albite, mica and microcline) showing trends of sodic, potassic, acid and silica metasomatism.

$$Q = \text{Si}/3 - (\text{K} + \text{Na} + 2\text{Ca})/3$$

F = K - (Na + Ca) in millications



- biotite granite
- × peralkaline granite
- albitised biotite granite
- + albitised peralkaline granite
- ◊ albitite
- ◊ microclinised biotite granite
- ⊙ altered basement
- ▼ greisen
- ▲ quartz vein

This highlights changes in silica and alkali element ratios without regard to how the cations are distributed throughout the sample. Not only can salic components be displayed but mica analyses can be plotted into the diagram to define the greisenisation process between quartz-rich greisens and mica-rich greisens. The data presented on Figs 4.3 & 4.4, have been chosen from complexes throughout Nigeria. By calculating the multicationic components in terms of the parameters:

$$Q = 1/3Si - (K + Na + 2/3Ca) \text{ and}$$
$$F = (K - (Na + Ca))$$

for any granitic rock suites which have undergone varying degrees of subsolidus reactions, the degree of disturbance from granite minimum compositions can be clearly demonstrated. Furthermore, the dominant process of sodic, potash or acid metasomatism can be defined.

Samples have been selected which are unequivocal in interpretation in order to determine major element trends most clearly. The majority of samples however come from the Ririwai Complex and are discussed in Kinnaird et al (1985a) and Bowden and Kinnaird (1984a, b and c).

The granites that show little subsolidus modification cluster within a fairly small area of the diagram. The peralkaline granites shown as crosses on Fig 4.3, plot slightly nearer the F axis than the biotite granites shown as closed circles.

Sodic metasomatism facies have compositions which trend towards the albite pole. The peralkaline granites, shown as a plus sign, are arfvedsonite albite granites with pyrochlore. The biotite granites of the L13 core in Ririwai (Fig 3.1), show the greatest effect within the biotite granite facies, although the zinnwaldite and lepidolite albite granites of the Afu Complex also display this trend strongly. Most of the open circles on Fig 4.3, are sections of the L13 drill-core taken at different depths with varied textural and mineralogical facies. Samples L13-411 and L13-440 which are albitites, shown as a circle within a cross on Fig 4.3, are the most albitised facies of the biotite granite spectrum (two samples from the Afu Complex have negative Q values in addition to high negative F values).

Potash metasomatised facies have compositions which define a trend towards the microcline pole and these are represented by open diamonds in Fig 4.3. Samples selected to represent potash metasomatism have come from the reddened wallrock of the Ririwai lode, from microclinites and from microcline pegmatites within alteration zones of the Saiya Shokobo Complex. Potash metasomatised granite gneissic basement samples from the margin of the Gindi Akwati ring dyke in the Ropp Complex, show a distinctive but different trend. Compositions shown by a cross within a circle, plot in a trend from the granite field, towards the F axis, reflecting the nature of the basement. The bulk chemistry of the basement in Nigeria is variable, but the selected samples come from modified calc-alkaline compositions. Thus, because of the chemical parameters Q and F, any enrichment in Ca will displace compositions towards the base of Fig 4.3. The value of this multicationic diagram becomes apparent since other diagrams do not separate these altered basement rocks into a separate field.

During acid metasomatism in contrast, compositions plot towards the Q pole

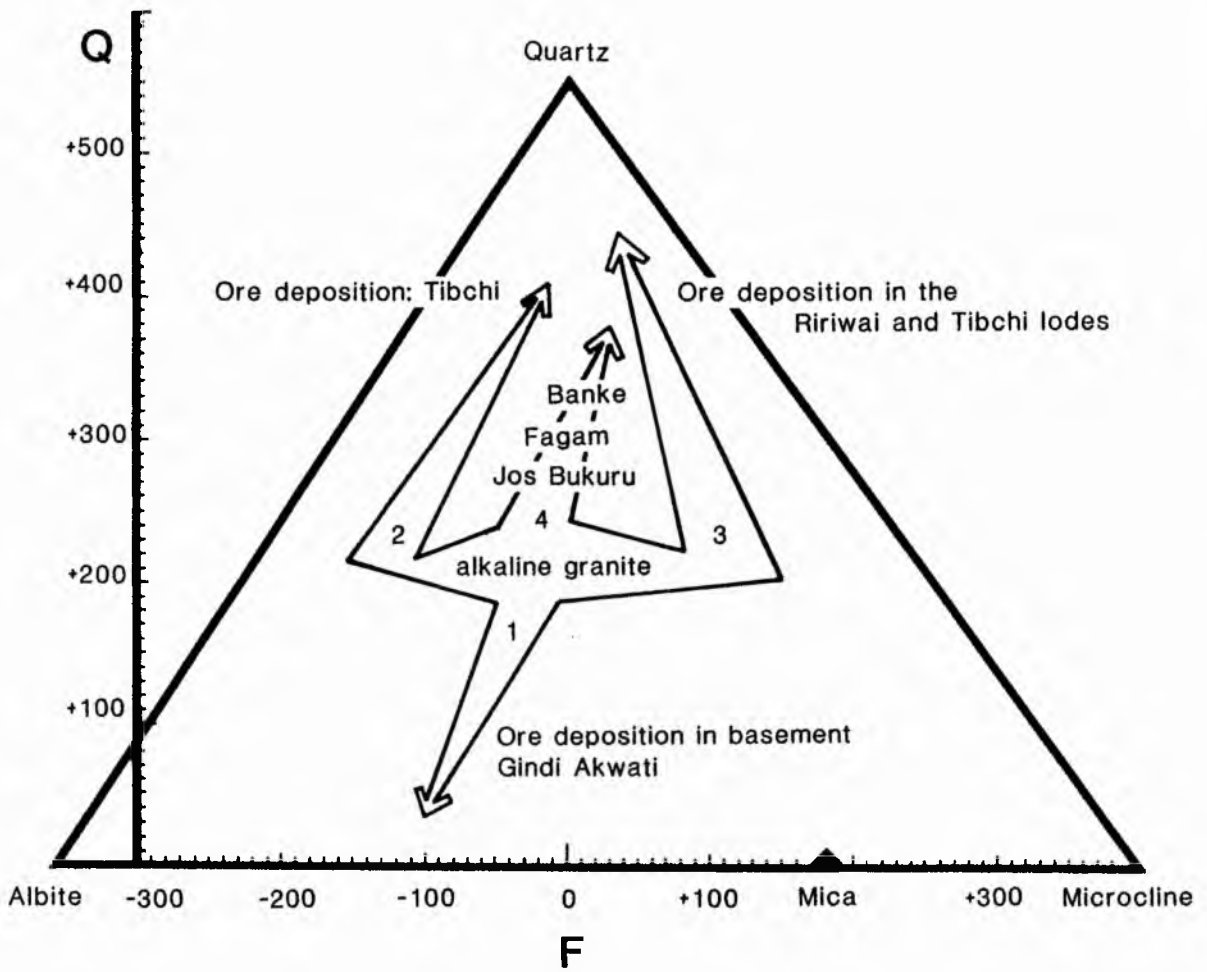
(Fig 4.3). However, there are several distinct trends towards the Q pole since the geochemical characteristics of acid metasomatism in Nigeria depends upon the intensity and retention of earlier stages of sodic and potash metasomatism, the bulk chemistry of the host rock, the composition pH, Eh, fS, fF, fCO<sub>2</sub>, fO<sub>2</sub> and the petrological characteristics and extent of greisen development. Since acid metasomatism may affect country rock, volcanics, perthite granite and metasomatised variants the chemical signature differs for each set of variables. The trends have been designated (1), (2), (3), and (4) in Fig 5.4. Trend 1 represents compositional trends during acid metasomatism of basement country rocks; trend (2) represents compositional variations during acid metasomatism developed in biotite granites close to the volcanic cover, such compositional variations reflect the acid metasomatism of albite-rich rocks; trend (3) represents compositional variations during acid metasomatism of microcline rich rocks and trend (4) represents compositional variations during pervasive acid metasomatism of previously unaltered perthite granites together with those granites that had already been affected by both sodic and potassic metasomatism.

Trend 1- Acid metasomatism of the basement has been studied in the Gindi Akwati area on the western perimeter of the Ropp Complex (Bowden and Kinnaird 1984b) and in the Dutsen Rishi area of the Saiya Shokobo Complex where acid metasomatism has also affected the volcanic cover. Quartz-poor and quartz-rich types of vein-controlled mineralisation are developed by fluid interaction on basement rocks. Much depends on the distance from the contact. Close to the contact quartz-poor veins rich in fluorite, sphalerite, chalcopyrite and other sulphides, are developed. These quartz-poor veins reflect the bulk chemical composition of the basement and its calcium-enrichment which displaces compositions towards the base of Fig 4.4. The trend of such samples (trend 1), is shown by a cross within a circle. Veins which penetrate well out into the basement are wolframite-bearing quartz veins. Obviously such quartz-enriched samples, regarded as monomineralic quartz greisens by Aubert (1969), will plot towards the Q pole along trend 4.

Trend 2- The apical region of a biotite granite may have undergone a process of sodic metasomatism already described. Thus acid metasomatism of such rocks will reflect this early sodic imprint. Similarly the volcanic cover to most biotite granites consists of rhyolitic ignimbrites some of which are mildly peralkaline. Acid metasomatism of such rocks will have been dominated by host rock chemical controls. Thus any greisens developed against or within the volcanic cover may show the sodic effect - with increasing silica effects as acid metasomatism gave way to silica metasomatism. This trend (trend 2) is well developed in the Tibchi rocks. Thus acid metasomatism of albite-rich roof rocks, which is usually a pervasive effect, plots parallel to the albite-quartz join in the quartz-albite-mica-microcline tetrahedra. This trend reflects the high initial alkali element enrichment of the altered facies.

Trend 3 -Vein-controlled acid metasomatism produced a greisen composed of quartz +mica+topaz+fluorite. Micaceous greisens and monomineralic mica rocks, developed from the breakdown of microcline in the roof zones during acid metasomatism of microcline-rich facies (trend 3 on Fig 4.4). Such mica-rich greisens plot on the quartz-mica join of the tetrahedra. Silica was released during microcline breakdown and compositions trend towards the quartz pole as silica metasomatism is superimposed on acid metasomatism. This trend has been described in detail for the rocks of the Ririwai lode in Kinnaird et al (1985a).

Fig 4.4. Summary Q-F diagram of the major trends of acid metasomatism and ore deposition for the Nigerian anorogenic province. Trends 1, 2, 3, and 4 are described in the text.



Trend 4 -The final trend is the pervasive acid metasomatism of perthitic granites that have not been affected by earlier metasomatism. This trend is characterised by thin marginal greisen veins from the Kudaru, Fagam, Jos Bukuru and Banke Complexes. Trend 4 is also the compositional trend for facies, such as that of the Uwar Gida area of the Ririwai Complex, where acid metasomatism had been superimposed both on remnant sodic and potassic metasomatism close to the volcanic cover. In this case the trend - as would be expected - bisects trends 2 and 3.

In conclusion therefore, it is clear that chemical data obtained from hydrothermally altered rocks, when plotted on the QF multicationic diagram, generate definite zones which can be correlated with known structural environments and known sequences of alteration. The QF diagram therefore, since it defines a series of trends for samples that have undergone acid metasomatism, is both a more useful and more valid method for the interpretation of hydrothermal effects than the Q-Ab-Or diagram.

#### Minor and trace element variations during hydrothermal alteration

Although it has been assumed in earlier literature that certain trace elements, especially the rare earths, are immobile under postmagmatic condition, recent research has shown that many trace elements have considerably different crystal-fluid partition coefficients compared with crystal-liquid values. Trace element variations therefore together with petrographic studies illustrate the geochemical modifications that have taken place in the subsolidus.

The chondrite-normalised plots of trace elements are grouped ranging from compatible to incompatible and distribution coefficients show distinctive trends during the alteration processes (Fig 4.5). Rock types like the quartz porphyries, fayalite granite and syenite show element distribution patterns that are governed by crystal-liquid partition coefficients. In contrast, all the chondrite-normalised plots show element distribution patterns that are governed by crystal-fluid distribution coefficients.

The granitoids display flat or HREE-enriched trends on chondrite-normalised diagrams with attendant strong Eu depletion. During hydrothermal alteration there was clearly REE mobility although the pattern of depletion or enrichment varies from that described for S.W. England (Alderton, Pearce and Potts 1980).

During sodic metasomatism there was a substantial enrichment in all REE's, particularly in the peralkaline facies (Bowden et al 1979). In the Nigerian province it was the albitised granites that have the highest lithium and uranium enrichment. In the peralkaline facies there was an increase in all trace elements including the high field strength elements Nb, Zr and Hf (Fig 4.6). In the biotite granites there was substantial enrichment in some of the LIL elements, an enrichment in Zn and particularly Sn and sometimes a depletion in Zr and Y.

During potash metasomatism, there was a depletion of the whole rare earth spectrum and compared with all other processes the potash-metasomatised wallrocks on Fig 4.6e, shown as open diamonds are significantly the most depleted. This was combined with a similar decrease in most of the trace element populations (Fig 4.5), although Rb, Li, Sn and Zn were increased. On

Fig 4.5. Chondrite-normalised trace element patterns arranged to show fluid-rock element partitioning. Elements to the left of each diagram have inferred bulk  $K_d$ 's partitioned to the rock while elements to the right of each figure have  $K_d$ 's partitioned to the fluid phase.

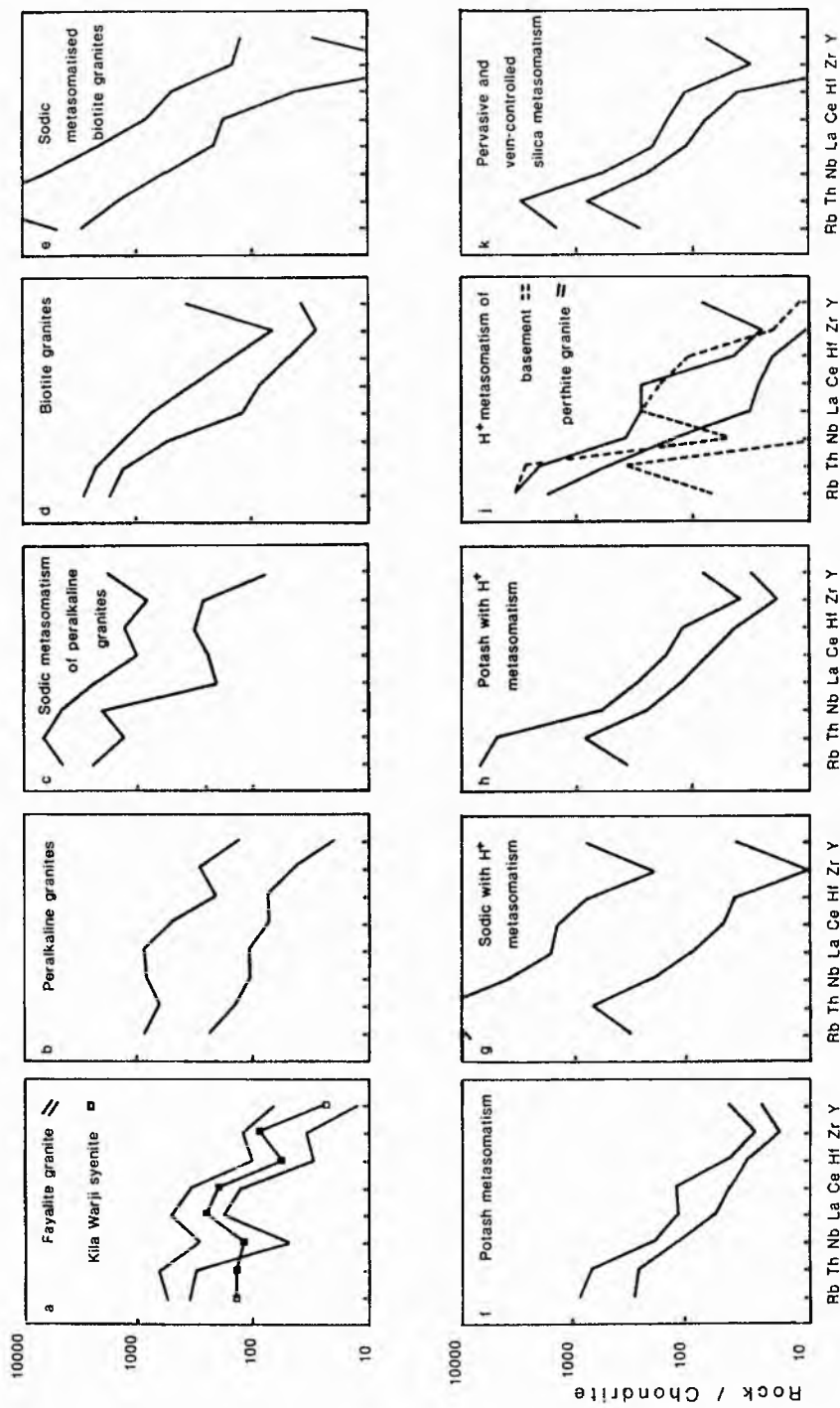
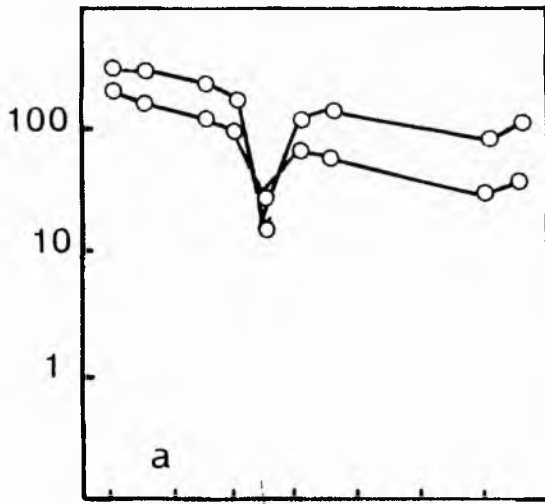
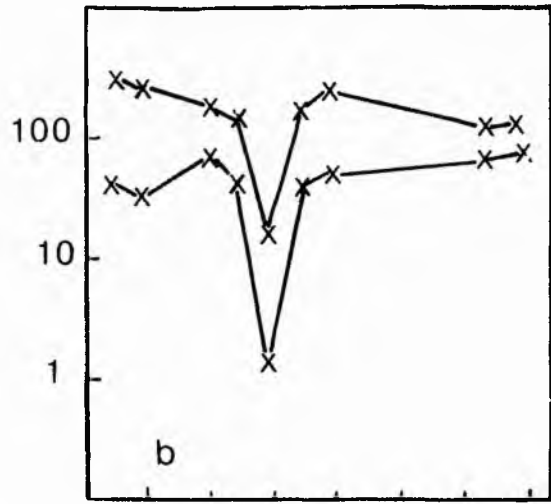


Fig 4.6. Chondrite-normalised rare earth element patterns for Ririwai rocks:-

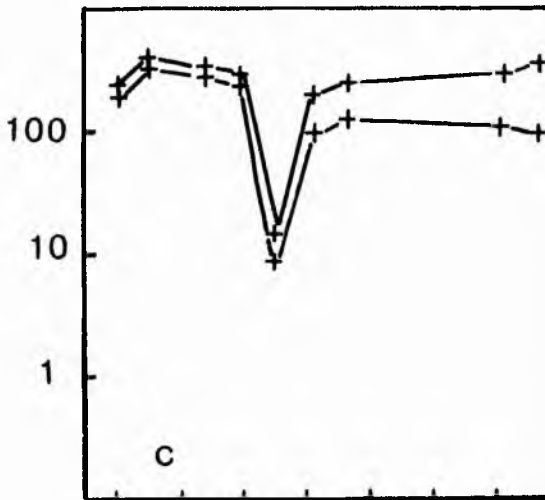
(a) volcanic rocks: (b) peralkaline granite: (c) arfvedsonite albite granite: (d) biotite granite: (e)  $H^+/K^+$  metasomatised rocks,  $H^+$ =triangles,  $K^+$ =diamonds: (f) "parental" syenite from Kila Warji (Bowden and van Breemen 1972, Bowden and Whitley 1974, Kinnaird et al 1984a and b).



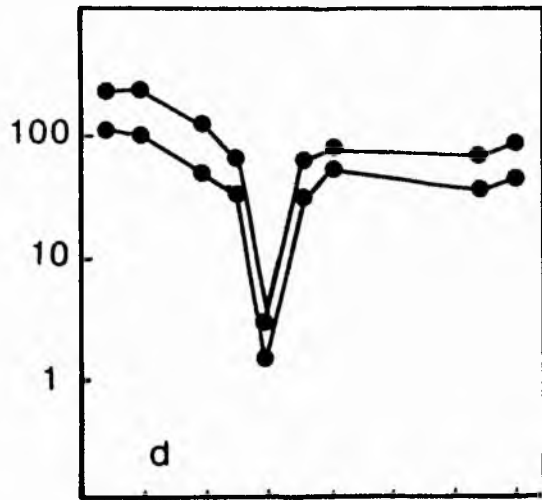
La Pr Sm Gd Dy Er Yb



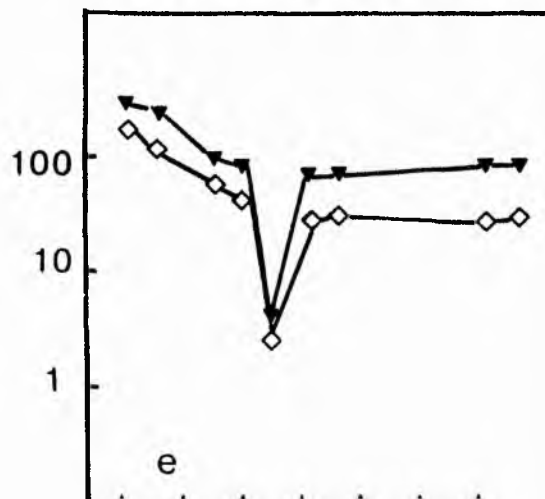
Ce Nd Eu Tb Ho Tm Lu



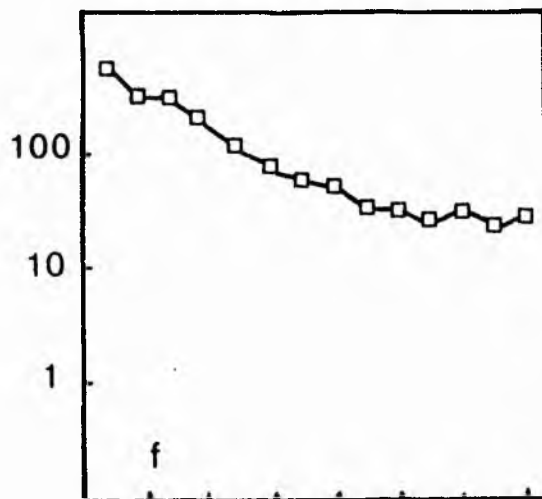
La Pr Sm Gd Dy Er Yb



Ce Nd Eu Tb Ho Tm Lu



La Pr Sm Gd Dy Er Yb



Ce Nd Eu Tb Ho Tm Lu

chondrite-normalised curves potash metasomatised wallrocks of the Ririwai lode show the most REE depletion (Kinnaird et al 1985a).

During acid metasomatism, the chondrite normalised plot of Fig 4.5, shows that there was a depletion in Zr relative to biotite granite and an increase in some of the trace element populations compared with potash metasomatism particularly in Th, Ce and Y. However, trace element patterns in greisens are very variable, since they are affected by earlier processes. Thus where H<sup>+</sup> metasomatism was superimposed on an earlier sodic effect, the chondrite normalised pattern (Fig 4.5g), shows a close similarity to that for sodic metasomatism and where superimposed on a potash effect (Fig 4.5h), the potash pattern is reflected. Where H<sup>+</sup> metasomatism was superimposed on an unaltered biotite perthite granite or basement, the chondrite normalised trace element patterns (Fig 4.5j), show a depletion most notably in Nb in the basement. The rare earths patterns (Fig 4.6), show that there was partitioning of the LREE to the greisen mineral assemblage, a slight enrichment of Eu coupled with increasing Yb and Lu with the interpolated HREE spectra of Dy, Ho, Er and Tm, partitioned slightly to the fluid. There was a marked increase of Li, which was accommodated in the new mica of the greisen and there was a substantial increase in the ore elements notably Sn, Pb, Zn, W, Cu and Fe - the latter element occurring within both the micas and the ore minerals.

No data exists for the rare earth behaviour during the silicification process but it is assumed that there was an overall decrease in REE's. The chondrite normalised plot (Fig 4.5), shows that whilst there was an overall decrease in the spectrum of many trace elements compared with biotite granite, there was a selective dilution, most notably in Zr. There was an increase in the ore elements during silicification particularly in Sn, Zn, W, Bi, Cu, Mo and Pb sometimes in appreciable quantities.

#### Minor and trace element indicators of hydrothermal alteration

A number of trace element patterns can be used to examine the processes of hydrothermal alteration. Several element pairs - K/Rb, Rb/Sr, <sup>87</sup>Sr/<sup>86</sup>Sr, and Th/U have already been considered by previous workers in addition to a discussion of rare earth element behaviour. In addition to these, the Ba/Rb and the Zr/Hf ratio can be considered, as can the concentrations of Li and F and the F:Cl and Ba:Rb. A study of such trace element assemblages shows that certain element pairs clearly indicate that fluid reactions have taken place even before any significant mineralogical changes can be detected.

#### The elements K, Rb, Sr and Ba

The element pairs K-Rb, K-Ba and Ca-Sr respectively have similar ionic properties. Therefore Rb and Ba are usually incorporated in potash-bearing minerals such as K-feldspar and biotite, and Sr is usually found in Ca-bearing minerals such as plagioclase. Since the CaO content of all Nigerian anorogenic granitoids is lower than the average for granitic rocks, strontium values will obviously also be lower. This is the case not only for fresh rocks but also the altered variants. More surprisingly however in view of the enriched potash levels in many of these granites, all the Nigerian granitoids are also low in Ba when compared with other low Ca-bearing granites.

During fractional crystallisation or partial melting, Rb was concentrated in the liquid phase. Such characteristics can be explained by the large ion size of Rb and its electronegativity which helps to define the differences in bond energy between K and O than between Rb and O. Thus K was preferentially removed whilst Rb tends to concentrate in the residual fluids. During late magmatic processes, Sr - which has a slightly greater ionic radius than Ca - was depleted relative to Ca in late stage processes. Thus, the geochemical behaviour of Rb and Sr show a greater sensitivity to late magmatic processes than either K or Ca. Thus Rb, Sr and Ba concentrations are initially controlled by processes of fractional crystallisation with Sr and Ba decreasing and Rb increasing in residual fluids with increasing crystallisation.

Therefore, the K/Rb, Rb/Sr, and Ba/Rb ratios are good indicators of the hydrothermal alteration processes:-

#### K/Rb

Rubidium was enriched in many Nigerian anorogenic granites but the amount of potash does not vary greatly unless there has been widespread potash metasomatism. Thus the K/Rb ratio or a plot of K against Rb reflects the degree of rubidium enrichment in the granitic rocks. The range in K:Rb ratio varies from complex to complex. There is a distinct negative correlation between K and Rb for all the Nigerian ring complex granites (Bowden and Kinnaird 1984c). Early explanations of this phenomena sought to explain the variations by extreme differentiation of a parental fayalite granite magma although the major element compositions do not vary widely even between the peralkaline, peraluminous and metaluminous variants. More recently, Bowden and van Breemen (1972) and Bowden and Turner (1974) suggested that Nigerian granites containing high Rb up to 1500ppm and low K/Rb ratios down to 35, had undergone substantial recrystallisation in the subsolidus during albitisation. Such a process may be recognised by a negative correlation of K against Rb (Bowden and Kinnaird 1984c). Thus the trend of K/Rb ratios to low values in Nigerian granites is believed to represent the degree of post magmatic adjustment in response to mineralising albite-rich fluids (Bowden and Kinnaird 1984c).

#### Rb/Sr

The Rb content of the anorogenic granites has been described by various authors but Bowden 1961, and Butler et al 1962 provided the first comprehensive study. Values for hornblende-bearing granites and porphyries are in the range 120-310ppm with peralkaline granites in the range 190-430ppm and biotite granites in the range 180-860ppm. A comparison of Rb-Sr ratios shows that for hornblende bearing granites and porphyries the average ratio of Rb to Sr is 200, for peralkaline granites the average ratio is 300 and for biotite granites the average ratio is 400:1. Rb/Sr ratios are high for the biotite granites of Banke and Ririwai compared to the mineralised granites of the Afu complex (Imeokparia 1981) The ratios for the altered facies of the Ririwai complex are even higher. Such high values recorded for the hydrothermally altered rocks are due to an increase in Rb associated with microclinisation and greisenisation. The ratio for unaltered Ririwai biotite granite is 268, for potash metasomatised rocks is 851 and for greisenised variants is 674 whilst even the sodic metasomatised albite arfvedsonite granite has a ratio of 310.

Rubidium-strontium isotopic studies on Ririwai rocks that have been carried out in Britain (van Breemen et al 1975) and France (Bonin et al 1979) suggests that the Rb/Sr system remained open until the circulation of mineralising hydrothermal fluids had ceased. Bonin et al (1979), suggest that the proportion of Rb-Sr in anorogenic alkali feldspars was controlled by fractional crystallisation of alkali feldspars in the magma chamber. After the emplacement of the granites, hydrothermal fluids mobilised Rb relative to Sr and therefore modified the relative proportions of Rb-Sr without any notable modification of the  $^{87}\text{Sr}/^{86}\text{Sr}$  ratio.

A consideration of the Rb-Sr systematics therefore could give a guide to the type of hydrothermal process that might have taken place.

#### Strontium ratios

The wide variation in initial  $^{87}\text{Sr}/^{86}\text{Sr}$  for the Nigerian anorogenic granites has been discussed by Bowden et al (1976) and more recently by Vidal et al (1979). The values range from 0.705 to 0.752 even from rock types from the same ring complex. In the past, this wide variation of initial strontium isotopic ratio has been used as an argument to suggest that there was a significant crustal involvement in the genesis of the anorogenic ring complexes. Clearly however, the initial  $^{87}\text{Sr}/^{86}\text{Sr}$  ratio offers no satisfactory definition of the source area of magma generation. Vidal et al (1979), compared the Nigerian continental anorogenic province with the oceanic equivalents in the Kerguelen Islands. They concluded that the data are isotopically consistent with an original mantle origin, but that some processes of modification have taken place to a larger extent in the continental setting. Bowden and Kinnaird (1984c), suggested that the mineralising fluids themselves in Nigeria may have had intermediate to high initial  $^{87}\text{Sr}/^{86}\text{Sr}$  ratios and that the wide variations in values noted for many Nigerian subvolcanic centres may be a measure of the degree of rock-fluid interaction. Thus, whereas in the Nigerian province rocks such as syenites with low initial ratios may be ascribed a mantle source, it does not necessarily follow that peralkaline granites with high initial ratios, have had any extensive involvement with the crust. Prior to this thesis, the stable isotopic data available (Borley et al 1976), on the peralkaline granite with the highest initial strontium ratio of 0.752, did not indicate any significant crustal input via a circulatory hydrothermal system in the cooling magma chamber.

#### Ba/Rb

The average Ba content of 19 syenites and monzonites is 466ppm (Table 2.1) but the levels decrease in the fayalite, and drop dramatically in the peralkaline and biotite granites (Tables 2.1-2.3). Since Ba levels are consistently low in most of the granites, the Ba/Rb ratio must also be low. The Ba/Rb values are higher in fresh rocks than altered ones and Rb was enriched relative to Ba during postmagmatic alteration. Thus for the Ririwai biotite granite the Ba/Rb ratio is 0.12, for potash metasomatised biotite granite the value is 0.08 and for acid metasomatised variants the value decreases to 0.01.

Studies in the Rishi area of the Saiya Shokobo Complex show that the volcanic pile and the biotite granite contain less than 10ppm Ba average, with concentrations decreasing to zero Ba in virtually all hydrothermal variants. In

contrast, Rb levels rose dramatically during potash metasomatism reaching nearly 7000ppm in a monomineralic mica rock produced by acid metasomatism of a microcline. The only rock types to show high Ba levels are the basement granitoids and the volcanic feeder dykes which cut the basement. Thus, since both the basement and the feeder dykes retain their high Ba, even on potash or acid metasomatism, the Ba/Rb ratio is perhaps a better guide as to the rock type that has been affected, rather than as a monitor of the process that has taken place.

#### Th/U

There are enriched levels of uranium and thorium in both the peralkaline and aluminous granites, with evidence of considerable mobility of both during periods of rock-fluid interaction (Bowden et al 1981; Ixer et al 1987).

Loss of uranium relative to thorium occurred during the leaching of the pile of rhyolitic ignimbrites. Similarly, surface samples of granites from the Ririwai complex (Kinnaird et al 1985b), show a progressive loss of uranium relative to thorium. This is interpreted as the result of uranium mobilisation to higher levels which have subsequently been eroded, with Th retained in accessory minerals (Bowden et al 1981). Surface samples contain less U and Th than those from depth which may be due to element mobility at lower temperatures (Chatterjee 1980). Samples from drill core L13 in the Ririwai complex show progressive increases in U and Th between 10m (L13-10) and 310m (L13-310) depth in the biotite granite (Table 5.6). Highest concentrations are encountered in samples from 411 and 440m depth which come from the albitic roof zone of the later biotite granite at depth. High levels of U and Th are therefore, clearly related to the albitisation process and the Th-U ratio is significantly decreased from the average for biotite granites (Fig 4.7). During the ensuing potash metasomatism, the uranium was remobilised and the Th therefore preferentially concentrated, resulting in an increased Th-U ratio. This reached a maximum in the greisen so the selective removal of uranium relative to thorium must have continued during hydrogen ion metasomatism. Combined neutron activation and particle track analysis, discussed in Chapter 12 shows that uranium was enriched during the early sodic and potash metasomatism whilst uranium was lost and Th therefore, preferentially enriched during greisenisation.

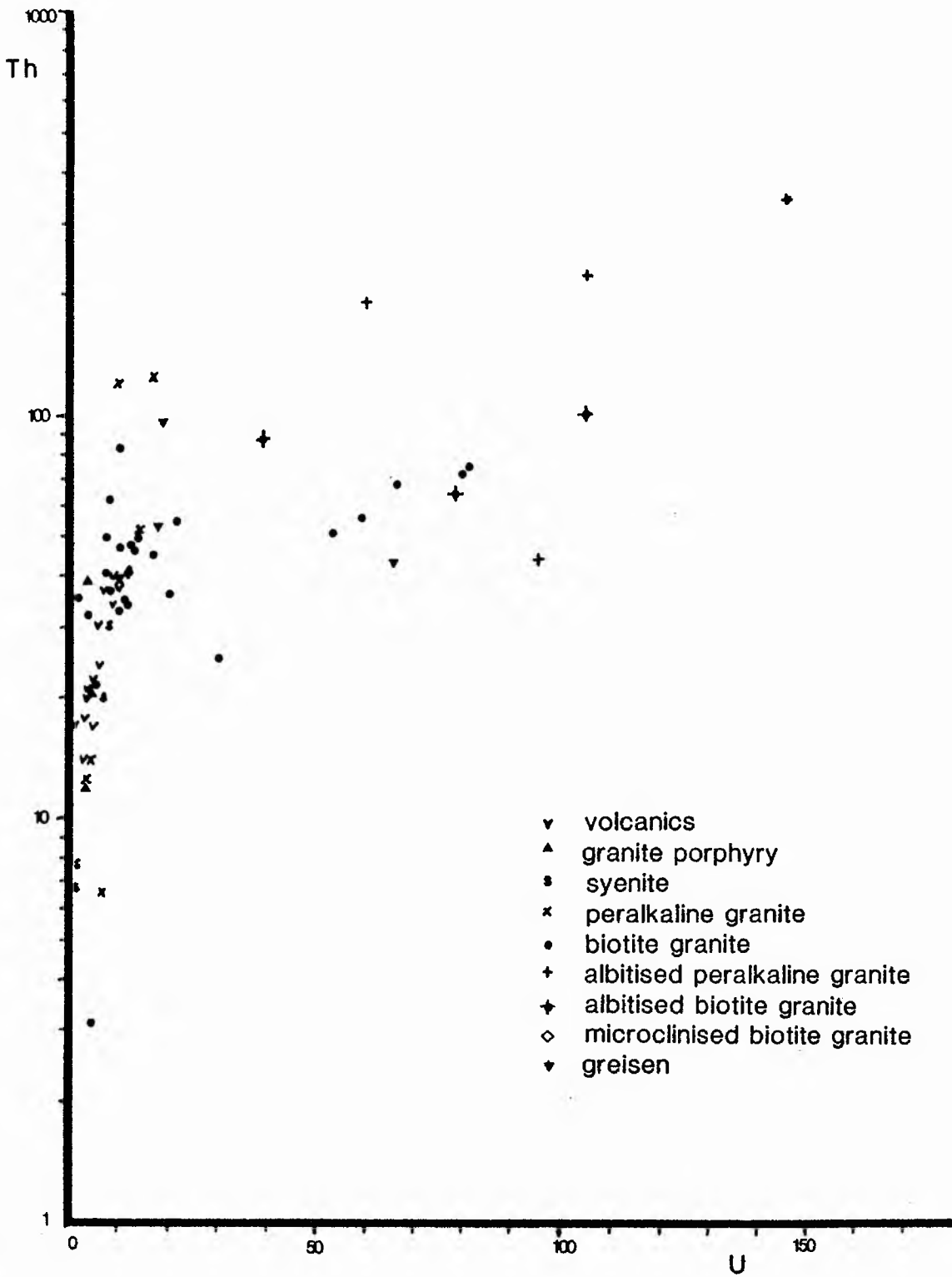
Thus hydrothermal processes have clearly modified the concentrations of U and Th depending on the location within the cupola, the relative concentration of U and Th, the intensity of fluid interaction, the composition of the fluid and type of fluid interaction e.g. albitisation, microclinisation etc. Hence the Th-U ratio may vary in Ririwai samples from 0.83 to 12 suggesting relative mobilisation of U in the subvolcanic roof zone.

A more recent detailed study of the L13 core material from Ririwai, undertaken by Ixer et al 1987, broadly concurs with these findings. They conclude that uranium was concentrated during crystallisation of the biotite granite, where it may have formed discrete minerals such as coffinite. Some additional uranium may have been introduced during sodic metasomatism, but was lost during potash and acid metasomatism and leached at the surface. Thorium too, may have been further introduced during albitisation, but its concentration was enhanced during greisenisation, and it was not lost by low temperature surface processes.

Table 4.6 Uranium/Thorium concentrations in rocks from the Ririwai Complex

Sample	Peralkaline granites	U	Th	Th/U
N83	arfvedsonite granite	14	15	3.6
N80	arfvedsonite granite	10	120	12
Biotite granites				
N77	biotite granite	7.5	41	5.5
N91	biotite granite	7.3	50	6.8
N92	biotite granite	8.0	62	7.8
N75	biotite granite	10.0	83	8.3
L13-10	biotite granite	30.0	25	0.83
L13-205	biotite granite	53.0	51	0.96
L13-310	biotite granite	58.0	56	0.97
Albitised granites (sodic metasomatism)				
N87	arfvedsonite granite	60	190	3.2
N88	arfvedsonite granite	105	100	0.95
N89	arfvedsonite granite	105	100	2.1
N86	arfvedsonite granite	145	350	2.4
L13-411	biotite albitite	81	73	0.90
L13-440	biotite albitite	66	69	1.05
Microclinised granites (potash metasomatism)				
R1-18	microcline-quartz wallrock	12.8	41.7	3.25
R1-35	microcline-quartz wallrock	10.2	38.8	3.80
Greisenised granite (acid metasomatism)				
R1-14	greisen vein	18.9	97.5	5.16

Fig. 4.7 Thorium-Uranium concentrations in Nigerian volcanics, granites and metasomatised variants



## Rare Earth Element behaviour

The Kila Warji syenite is regarded as a sample of the most 'primitive' rock type of the province from which the granitic magmas may have fractionated. It has therefore been taken as a standard reference against which all other rock types are compared. The chondrite-normalised REE spectrum (Fig 4.5), shows that there is a substantial variation not only in granitic variants, but also in the volcanic rocks and some volcanic feeder intrusions when compared with the Kila Warji syenite. There was an enrichment in the light rare earths, a substantial enrichment in heavy rare earths and significant Eu anomalies. The classical interpretation of Eu depletion was based on the effect of fractionating plagioclase and alkali feldspar preferentially removing Eu from the residual liquids. However, in Chapter 2, the fractionating magma model was discounted as an explanation to account for fluctuating aluminous or peralkaline pulses within one complex. An alternative interpretation was based on the behaviour of volatiles and fluid loss. The major part of the variation of chondrite-normalised rare earth patterns therefore, must be due to rare earth mobility at subsolidus temperatures. Thus the rare earth patterns can be attributed to a combination of magmatic and hydrothermal processes.

The absolute REE concentrations and the chondrite-normalised patterns for unmineralised amphibole or biotite granites shows a limited variation. When compared with the Kila Warji syenite (Fig 4.5f), the chondrite-normalised curves are distinctly flat, with significant negative Eu anomalies in all the granites the magnitude of which varies during the alteration processes.

From the evidence presented by Bowden et al (1979) in their text figure, Bowden and Kinnaird (1984c) made the following assumptions on the bulk distribution coefficients for rock-fluid interactions:-

(i) For rare earth elements as well as for other elements like Rb, the distribution coefficients for mineral-fluid are similar to mineral-liquid near the granite solidus (800-700°C).

(ii) From 700-500°C the light rare earths and Eu were partitioned towards the fluid. In contrast the heavy rare earths were partitioned towards the rock. A substantial subsolidus rare earth distribution occurred at these high temperatures which can be correlated with the process of albitisation and niobium mineralisation. It therefore infers that fluids involved in rock reaction caused sodic metasomatism resulting in a fluid that was enriched in Eu and light rare earths.

(iii) After the lower temperature rare earth depletion by potassic metasomatism, greisenisation along restricted fissures and joints was characterised by rock-fluid interactions where most rare earths were enhanced in the rock. The lower temperature fluid deposited the rare earth elements as accessory minerals in the greisens and zones of wallrock reaction. Any important concentration of fluorite will also contain Eu.

Ririwai and Tibchi examples:-

In the Ririwai complex the chondrite-normalised rare earth patterns for an aegirine crystal tuff, N82-69 (Table 4.7b), shows HREE enrichment compared with

Table 4.7a. Analyses and CIPW norms of volcanic rocks and porphyries from Ririwai

	N81-69 comanditic ignimbrite	X572 comanditic ignimbrite	N82-69 aegirine crystal tuff	X880 comanditic ignimbrite	X514 volcanic feeder	X1581 volcanic feeder	X669 volcanic feeder	X1363 volcanic feeder	N85-69 quartz porphyry	X592 granite porphyry	GP-N96 granite porphyry	N96 granite porphyry
SiO <sub>2</sub>	74.10	74.04	73.87	72.13	74.66	73.01	71.85	72.49	69.63	71.68	72.40	71.39
TiO <sub>2</sub>	0.20	0.17	0.35	0.16	0.17	0.06	0.08	0.35	0.45	0.30	0.28	0.28
Al <sub>2</sub> O <sub>3</sub>	10.88	11.95	11.96	10.57	11.50	11.13	12.12	12.51	13.97	12.04	12.35	13.39
Fe <sub>2</sub> O <sub>3</sub>	3.24	2.08	0.74	3.50	1.70	2.69	3.58	2.60	3.62	2.28	1.58	1.58
FeO	1.15	1.72	3.47	3.31	1.94	4.26	1.98	1.43	0.69	1.89	2.30	2.30
MnO	0.08	0.02	tr	0.46	0.02	0.35	0.23	0.07	0.05	0.13	0.09	0.15
MgO	tr	0.02	0.08	0.35	0.03	0.18	0.14	0.19	0.22	0.29	0.05	0.04
CaO	0.26	0.35	0.14	0.42	0.17	0.28	0.42	0.58	0.58	0.79	0.76	0.74
Na <sub>2</sub> O	4.43	4.46	4.48	4.64	3.16	3.49	3.84	3.91	3.62	4.36	4.44	4.02
K <sub>2</sub> O	4.09	4.76	4.51	4.14	5.30	3.98	4.68	5.13	5.42	5.12	4.87	5.17
P <sub>2</sub> O <sub>5</sub>	tr	0.05	0.01	0.02	0.66	0.02	0.04	0.05	0.14	0.07	0.04	0.04
H <sub>2</sub> O	0.31	0.65	0.41	0.29	0.52	0.29	0.43	0.25	0.70	0.61	0.24	0.24
H <sub>2</sub> O <sup>+</sup>	0.11	0.20	0.09	0.21	0.18	0.04	0.05	0.04	0.19	0.16	0.13	0.13
CO <sub>2</sub>		tr		0.06	0.03	tr	0.02	0.08		0.09		
ZrO <sub>2</sub>		0.27			0.30					0.11		
Cl		tr		0.03	tr	0.03	0.03	0.03		0.02		
F		0.11		0.07	0.11	0.12	0.26	0.03		0.12		
S		0.02		0.01	0.07	0.04	0.01	0.01				
Less O	98.85	99.87	100.19	100.37	99.92	99.97	99.76	99.75	99.28	100.06	99.29	99.47
		0.06		0.04	0.08	0.08	0.12	0.02		0.05		
	98.85	99.81	100.19	100.33	99.84	99.89	99.64	99.73	99.28	100.01	99.29	99.47
Fe <sub>2</sub> O <sub>3</sub>	0.74	0.68	0.18	0.51	0.47	0.39	0.64	0.65	0.84	0.55	0.41	0.41
FeO+Fe <sub>2</sub> O <sub>3</sub>												
Li												24
Be												5
Cu												135
Zn												175
Rb												125
Sr												13
Zr												830
Pb												30
U	8.9		7.3									4
Th	40		37									21
Q	33.25	29.51	28.13	27.67	35.10	34.26	30.97	29.02	26.67	25.53	26.06	25.50
Ox	24.16	28.12	26.65	24.46	31.31	23.51	27.65	30.31	32.02	30.25	28.77	30.55
Ab	33.19	34.96	36.41	31.32	26.73	29.52	32.48	33.07	30.62	33.42	36.41	34.00
An					0.57	0.94	0.74		1.43			3.23
C												
Ac	3.77	2.43	1.31	6.98								
Wo	0.25											
Di	0.62	0.57	0.55	1.28				0.73		3.04	1.01	
Hy		1.64	5.46	5.98	1.98	6.60	1.32	0.17	0.55	2.26	3.12	0.15
Hg	2.81	1.80	0.42	1.57	2.46	3.90	5.19	3.77	1.08	1.77	1.40	2.75
He									2.87	1.78	1.79	2.29
Il	0.38	0.32	0.66	0.30	0.32	0.11	0.16	0.66	0.85	0.57	0.53	0.53
Ap		0.12	0.02	0.05	0.14	0.05	0.09	0.12	0.33	0.17	0.09	0.09
water	0.42	0.85	0.50	0.50	0.70	0.33	0.48	0.29	0.89	0.77	0.37	0.37
fluor		0.22		0.14	0.13	0.24	0.51	0.05		0.23		0.00

Table 4.7b. Rare earth data for various rock types from the Ririwai complex. From Kinnaird et al 1985a.

	volcanic rocks /ignimbrites/		volcanic feeder N85-69	arfvedsonite granite			Biotite granite		Ririwai lode		
	N81-69 (comendite)	N82-69 (aegirine tuff)		N83	N86	N89	N78	N91	N58A	N588B	N58C
La	125	85.8	125	138	72.4	90	110	47.5	55.2	89.8	59.1
Ce	189	156	30	287	362	393	312	113	93.3	190	110
Pr	(20)	(25)	(25)	(25)	(36.9)	(49.2)	(25)	(9.8)	(8.6)	(3.1)	(9.8)
Nd	102	170	91	151	157	243	115	(37.8)	33.2	49.9	35.1
Sm	37.5	40.3	23.5	38.0	46.8	68.9	17.9	8.4	8.0	15.2	12.9
Eu	1.15	1.49	2.54	1.40	0.79	1.31	0.27	0.11	0.18	0.24	0.23
Gd	(41.4)	41.3	23.6	57.3	32.4	67.1	21.7	10.0	7.5	17.6	19.8
Tb	11.0	8.7	3.6	16.1	7.9	15.0	5.8	3.6	1.6	3.4	3.2
Dy	62	(51)	(17.1)	(86)	(58)	(93)	(31)	(21)	(8.6)	(5.8)	(20.6)
Ho	(11.7)	(10.1)	(3.5)	(21)	(11.7)	(23.4)	(6.6)	(4.3)	(2.0)	(1.3)	(4.7)
Er	(29.3)	(27)	(9.0)	(45)	(27)	(67.5)	(18)	(10.1)	(6.0)	(3.6)	(10.1)
Tm	(3.0)	(3.4)	(1.2)	(5.8)	(3.7)	(10.2)	(2.7)	(1.7)	(0.9)	(0.6)	(2.0)
Yb	20.1	22.7	8.0	33.5	25.6	82.0	19.6	9.9	6.1	17.3	13.5
Lu	4.47	1.88	1.64	5.3	3.7	15.3	4.0	2.1	1.01	2.84	2.23
Σ REE	658	645	636	910	856	1219	690	279	232	401	303
La/Sm <sub>n</sub>	2.0	1.3	3.3	2.2	0.78	0.80	3.8	3.5	4.3	3.6	2.8
Sm/Eu <sub>n</sub>	86	71	24	71	190	139	175	201	117	167	148
La/Lu <sub>n</sub>	2.9	4.7	7.9	2.7	2.0	0.6	2.8	2.3	5.6	3.3	2.7

( ) - interpolated values from rare earth curves; all ratios from chondrite normalised data

Analyst J E Whitley, SURRC, East Kilbride; instrumental neutron activation analysis.

the more primitive quartz porphyry feeder (N85-69). Such HREE enrichment was characteristic of the effect of a peralkaline imprint, and was accompanied by the appearance of  $ac$  in the CIPW norms (Table 4.7a).

For Tibchi Ike (1979), found that the REE pattern for the pristine unaltered quartz porphyry (T60) was identical to that of the granite porphyry ring dyke. All the other samples examined by Moyes (pers. comm. quoted in Ike 1979) for Tibchi are depleted in REE relative to the most pristine rock. The depletion is most noticeable in the LREE group. Plots of  $\Sigma REE$  and  $\Sigma Ce/\Sigma Y$  normalised to T60 (the most unaltered rock) against distance to the biotite granite show that the outcrop proximity to the contact cannot be correlated easily with the observed REE patterns. Both Moyes (quoted in Ike 1979) and Ike (1979) reached the conclusion that the quartz porphyries adjacent to the biotite granite contact have been affected by hydrothermal alteration. Moyes favoured the process of acid groundwater circulation. However, Ike favoured the important role of fluids escaping from the biotite granite as the only mechanism that could explain the localised variations.

#### Zr/Hf

The average crustal value for Zr/Hf is approximately 50 (Wedepohl 1969). In the Nigerian province the most "primitive" rock - the Kila Warji syenite (KW6 in Table 2.1) - together with the monzonites approximate to this value. All other rock types show a considerable range of ratios (Table 4.8 & Fig 4.8). Ratios calculated for more than 100 samples of different granite types indicate that fayalite granites range from 25-53, peralkaline granites from 25-65 and biotite granites from 9-46. This deviation from the crustal average is ascribed to differential mobilities of Zr and Hf during hydrothermal alteration. When the metasomatised variants of these rock types are examined, the Zr/Hf ratio deviates even further from the crustal average. Thus sodic metasomatised peralkaline and biotite granites show a range of 15-33, potash metasomatised facies show a range from 14-30 (with RS19B having a Zr/Hf ratio as low as 0.07) whilst values obtained for acid metasomatised samples are very variable. Acid metasomatised potash-rich facies show a Zr/Hf range of 5-15, whilst acid metasomatised samples that have already undergone both  $Na^+$  and  $K^+$  metasomatism range from 7-19. It was the pervasive acid metasomatic process that produced the greatest range of Zr/Hf values, which vary from 0.2-69. Samples from the Rishi area show an even wider range of values which will be discussed in Part 2 of this thesis. During silica metasomatism there was a further decrease in the Zr/Hf ratio with values ranging from 1.2-20. Thus the decreasing Zr/Hf ratio with increasing hydrothermal alteration is a clear indicator that postmagmatic fluid reactions have taken place.

#### Li

Lithium levels in most Nigerian anorogenic granites are higher than normal for barren granites. However, the anorogenic granites show an extreme range, which varies by a factor of over 100, from being low in the hornblende-bearing granites to high in the biotite granites (Bowden 1961). Lithium chiefly substitutes for  $Fe^{2+}$ ,  $Fe^{3+}$ , and  $Al^{3+}$  and occurs particularly in the micas, amphiboles, aegirine and astrophyllite.

The average Li content of hornblende-bearing granites and porphyries is 25ppm (Bowden 1961), while for peralkaline granite it is in the range 2 to 380,

Table 4.8. Zr:Hf ratios for Nigerian granites and hydrothermal variants

Fayalite granites, syenites and monzonites

	AP5	BK11	JB51	NSA84	WS13	TIO8	NG17	KW1	FN119	KW6	FN145	KW7
Zr	653	318	157	583	847	460	1114	703	533	617	544	565
Hf	18	9	6	11	20	11	20	13	11	11	10	11
Zr/Hf	36	35	26	53	42	42	56	54	48	56	54	51

Peralkaline granites

	SHN13	DUT23	ZAN46	FG12	KW19	M1	NG1	PAN127	N80	N83	KW21	NG103
Zr	689	869	423	685	1594	880	587	554	565	815	1287	503
Hf	22	17	7	23	38	18	20	15	20	26	24	19
Zr/Hf	31	51	60	30	42	49	29	37	28	31	54	26

Biotite granites

	AMN24	RN75	PAN112	JON147	B37	MD33/3	NG20B	T15A	DR11	DW11	FG5	KD12
Zr	246	399	234	330	217	129	186	166	81	207	161	147
Hf	6	28	7	8	11	9	7	7	9	11	8	6
Zr/Hf	41	14	33	41	20	14	27	24	9	19	20	25

Sodic metasomatism

	SHN10	DW11	DW13	N86	N87	N88	N89	N90	RP2	T34 <sup>*C</sup>	JB123	SS55/8	DW1
Zr	299	4045	1826	3071	2224	5552	3073	3674	2815	77	397	162	207
Hf	9	146	63	103	89	258	127	148	90	5	12	7	10
Zr/Hf	33	27	28	29	25	22	24	13	31	15	33	18	20

Potash metasomatism

	T34 <sup>*</sup>	RN84	N58A	N58C	RS14A	RS19A	RS19B	RI/20A	RI/20B	RI/23B	R2/1A	R2/1B
Zr	210	883	238	199	209	181	1	162	224	243	192	194
Hf	7	31	11	11	14	13	14	12	13	14	11	13
Zr/Hf	30	28	22	18	15	14	0.07	14	17	17	17	15

Acid metasomatism

	N58B	RS14B	RI/23A	RI/23C	R2/1C	RS16A	RS16C	JB122	JB164	JB118A	B36	B64	B91	DUT32	FG11	KD11/3
Zr	171	196	162	155	240	217	186	138	140	2	169	103	72	6820	84	142
Hf	11	13	11	9	16	25	20	2	9	9	8	4	2	162	6	5
Zr/Hf	15	15	15	17	10	5	9	69	15	0.2	21	26	36	42	14	28

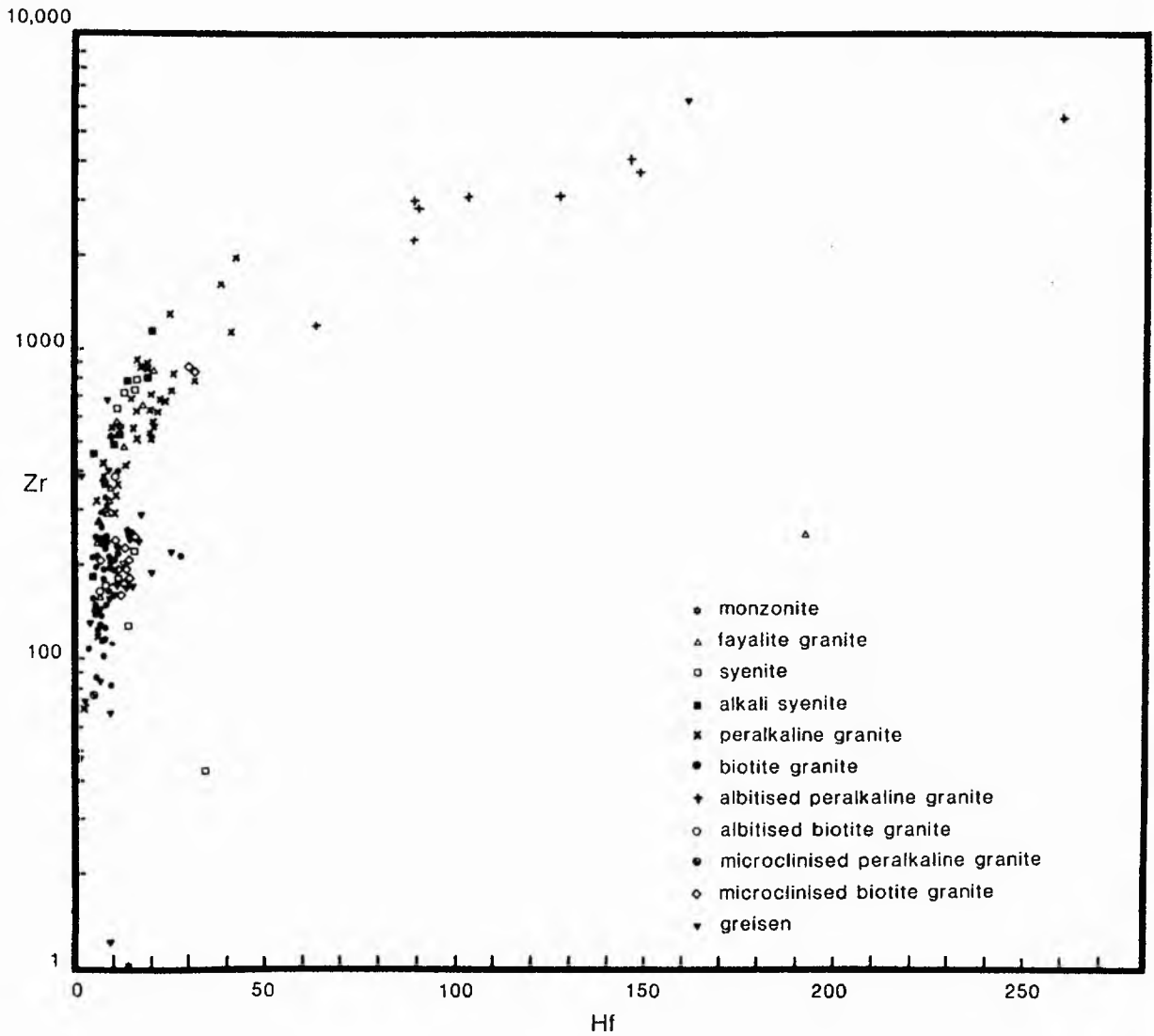
Silica metasomatism

	RS31/3A	RN74	SS117/5	JB120	RI/20C	RS16B
Zr	226	186	266	171	126	43
Hf	16	12	13	8	14	34
Zr/Hf	14	15	20	21	9	1.2

\* T34C is an albitite

\* T34 is a microclineite

Fig 4.8. Zr/Hf values for Nigerian granites and hydrothermal variants



averaging 135 and for a biotite granite from 1 to 558 ppm, averaging 210. During sodic metasomatism of both peralkaline and peraluminous granites this value rose. It is at a maximum in the peralkaline granites which have an average 363ppm Li. A further increase occurs during potash metasomatism. Of the 14 potash metasomatised biotite granite samples shown in Table 4.2 there is a range from 260-4270ppm with an average 1160ppm Li. There was a further increase associated with acid metasomatism to a maximum of 6000ppm in some greisens. This value then decreases during subsequent processes of silica metasomatism and argillic alteration.

#### Fluorine content and F:Cl ratio

The fluorine content of granitic rocks is important in prospecting since F is associated with Sn-W-Mo; Zn-Zr and Ta-Be deposits.

The Nigerian alkaline granites are particularly rich in fluorine. Although fluorite is a common accessory in all granite types there is little correlation between F-rich rocks and those high in Ca. In hydrothermally altered rocks however, any high values of Ca are invariably rich in fluorite. Fluorine values of the granitoids vary from an average 0.09% for syenites and peralkaline syenites (Table 4.9), through 0.19% for the fayalite and hornblende bearing granites and porphyries to 0.26% for the peralkaline granites (where the F is largely in the amphiboles) and 0.29% in the biotite granites (where the F is largely in the biotites). However, there is a wide variation in F values even for one rock type. For example, in a study of 35 biotite granite samples from the Jos Bukuru complex, Badejoko and Imeokparia (1979) found a wide range of F values, ranging from 0.12% to 0.82% which is much higher than the average 850ppm F for low Ca granites (Turekian and Wedepohl, 1961). However, they could find no consistent variation or increase from the older to the younger plutons, nor was there any correlation between F and SiO<sub>2</sub> content. However, they concluded that fluorine seems to be higher in those rocks that have been intimately associated with tin mineralisation and have suffered a high degree of albitisation and greisenisation.

In fact there was an increase in fluorine during all processes of hydrothermal alteration (with the exception of kaolinisation). Thus the increase in fluorine content alone is an indicator of hydrothermal alteration.

In contrast to the fluorine abundance of these granites, the chlorine content of the younger granites is always low and a study of 174 analyses of a variety of granitic rocks and hydrothermal variants shows little systematic variation. The highest chlorine content was found in early-formed calcic amphibole and the value decreased from an average 0.92% in the calcic amphiboles to an average 0.08% in later alkali amphiboles.

The fluorine to chlorine ratio however, because of the increasing fluorine during late magmatic and hydrothermal processes, is obviously a clear indicator of hydrothermal alteration.

Table 4.9, shows that the fluorine to chlorine ratio is at its lowest - 4.5 - in syenites and peralkaline syenites. The ratio increases to 6 in volcanic rocks and feeder intrusions and to 8.5 in fayalite and hornblende granites and porphyries. In peralkaline granites and biotite granites the ratio is

Table 4.9. Fluorine and chlorine concentrations in granitic rocks and minerals in the Nigerian granitoids.

Rock type	Fluorine range	mean of n	Chlorine Range	mean of n	Ratio F: Cl
Volcanic rocks and volcanic feeders	0.01- 0.36	0.12 25	0.01-0.03	0.02 9	6
Fayalite/hornblende granite and porphyries	0.03- 0.39	0.19 28	0.00-0.04	0.02 14	8.5
Syenites/peralkaline syenites	0.01- 0.18	0.09 8	0.00-0.02	0.02 4	4.5
Biotite granites	0.04- 1.06	0.29 54	0.00-0.04	0.02 11	14.5
Albitised biotite granite	0.16- 1.08	0.35 6	0.00-0.02	0.01 3	35
potash, metasomatised biotite granite	0.17- 0.24	0.20 2	-	-	
Greisenised biotite granite/basement	0.77-17.60	3.69 16	-	-	
Peralkaline granite	0.01- 0.52	0.26 21	0.00-0.06	0.02 10	13
Albitised peralkaline granite	0.10- 1.73	0.73 14	0.00-0.03	0.01 3	73
Calcic amphibole	0.29- 3.02	1.06 13	0.66-1.98	0.92 8	1.09
alkali amphibole	1.03- 3.31	2.00 15	0.01-0.18	0.08 13	25
biotite from hornblende biotite granite	0.86- 1.40	1.13 2	0.69-0.80	0.75 2	1.5
biotite from biotite granite	2.15- 4.70	3.03 15	0.02-0.20	0.13 12	23.3
protolithionite mica from greisen	4.40- 5.49	4.97 3	0.00-0.02	0.01 2	497

Source: Abaa 1976, Batchelor 1983, Borley 1976, Imeokparia 1984, MacLeod *et al.*, 1971.

approximately the same at 13-14. In hydrothermally altered variants of these rocks however, the ratios increased dramatically. In the albitised variants of these granites the ratio rises to 35 for the biotite granites and to 73 for the peralkaline granites. Clearly this enrichment of fluorine in late stage processes has important implications both for the transport of rare earth elements and for the mobility of tin. Eugster (pers. comm.) has shown that there is a strong partitioning of tin towards a fluoride phase. The increase in the fluorine to chlorine ratio is at its most dramatic where there has been an acid metasomatic process with the growth of fluorine-rich trioctahedral micas.

### Summary

Using major element multicationic parameters together with trace element monitors it can be shown that most of the granitic rocks within the Nigerian alkaline anorogenic province have been geochemically modified in the subsolidus. It is only the fayalite-bearing syenites and granites and some quartz porphyries which have been relatively unaffected by late-stage fluid reactions. From a geochemical viewpoint therefore, these intrusions can be used to assess the dominantly magmatic features of anorogenic magmatism since they have little imprint of subsolidus reactions. In contrast, alkali-amphibole- and biotite-bearing granites have been affected by a series of fluid reactions and several distinctive hydrothermal processes have been identified.

Each of these hydrothermal processes was characterised by enrichment or depletion in alkali element concentrations and silica abundance together with increased trace element concentrations, most notably in Li, Rb, Zr, Y and F. Each process can also be distinguished by normative variations in Q-Or and Ab.

In addition to the path-finder elements of Nb, Sn, Zn, W and F which are all increased in hydrothermally altered rocks, a number of other elements and pairs of elements can be used as monitors of potentially ore-bearing granitic rocks in Nigeria.

Thus the hydrothermally altered rocks are characterised by high concentrations of Sn, Be, Li, U, F, Zr, Nb, Th, K, Rb, Mo, Zn, F, W by low K:Rb, Ba:Rb, Sr:Y, and high Rb:Sr, K:Ba and F:Cl ratios. It is the significant variations in the Zr/Hf ratios that gives the most dramatic indication that postmagmatic fluid reactions occurred, even where there was no significant enrichment of ore metals.

## CHAPTER 5

### FLUID INCLUSION STUDIES

#### Introduction

In any study of a series of alteration processes and related mineralisation, it makes sense to study the fluids that were responsible for the alteration. This has been attempted by a study of fluid inclusions.

Fluid inclusions provide a sample of fluids that have existed at some time in the geological past. Later thermal or mechanical deformation may have caused the fluids to leak, although experimental work by Roedder and Skinner (1968), suggests that for most situations, leakage is of little significance. In the past, the ore-forming fluids were assumed to have been rich only in the constituents now present in the deposit, even in proportion to their abundances (Roedder 1984). However, most ore fluids contained, in addition to the ore elements deposited, large amounts of volatile constituents and soluble salts that passed through the ore deposit, leaving no trace apart from within the fluid trapped in the inclusions.

Various techniques are used to extract and analyse these fluids only at the expense of destroying the internal equilibrium. For certain transparent minerals, a great deal of information related to the pressure, temperature and the state of the fluid can be obtained by studying the reversible phase changes in the inclusion during controlled heating and freezing experiments. Therefore, in addition to a study of the size and shape of fluid inclusions under a normal petrological microscope, microthermometric measurements have been undertaken.

The equipment used for microthermometric analysis is a Linkam TH600 system (Shepherd 1981). A temperature controlled chamber has been designed for experiments over the dynamic range  $-180^{\circ}\text{C}$  to  $+600^{\circ}\text{C}$  with a maximum resolution of  $0.1^{\circ}\text{C}$ . Details and photographs of the equipment are given in Appendix 7, together with a theoretical basis to inclusion studies.

#### Classification of inclusions

Fluid inclusions can be divided into three types, depending on their time of entrapment. Primary inclusions are trapped by the sealing of growth irregularities in the host crystal. Healing of fractures formed during crystal growth yields pseudosecondary inclusions, whilst healing of fractures formed at some later time, forms secondary inclusions (Roedder 1984). For homogenisation temperatures it is essential to identify primary inclusions, that is those that were trapped as the host mineral was growing. In some cases, it is relatively easy to identify such inclusions where they follow growth zones or are parallel to crystal faces. For much of the vein quartz and almost all the granite and greisen quartz, however, there is no crystallographic form and it is more difficult to select primary inclusions.

Whilst it is possible to categorise inclusions into primary, pseudosecondary or secondary and to divide them into groups by morphology, a classification which indicates the nature of the trapped fluid is also possible. The adopted classification, modified from Weisbrod (1981), is based on phase composition. Glass inclusions are also regarded as fluid inclusions since most of these silicate melt inclusions were liquid at the time of trapping. Five types have

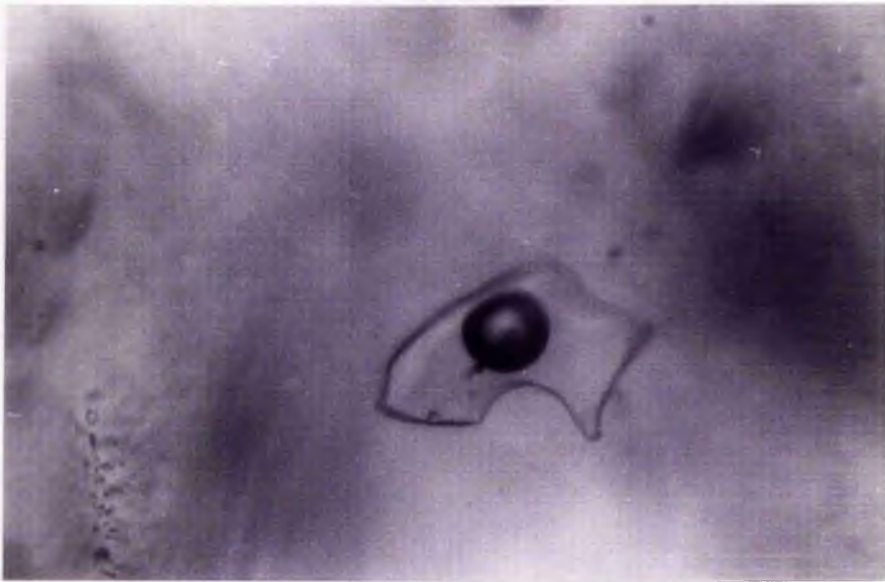
been distinguished:-

(i) Type L inclusions (Plate 5.1) contain an aqueous liquid phase, which is usually fairly low density, with a vapour bubble that occupies less than 50% of the inclusion. They are extremely abundant, up to 100 microns in size and account for 75% of the total inclusion population. Such inclusions are extremely abundant in quartz from the granite and hydrothermally altered variants. Many type L inclusions clearly belong to late fluid generations, as evidenced by their occurrence in secondary healed microfractures. The change in gas/liquid ratio in inclusions of different healed fractures within one mineral shows that a continuous fracturing process may have operated as fluids circulated. However, there is no clear gap between primary liquid-rich inclusions and late-stage inclusions. Clearly, the chemical and physical characteristics of the fluid were changing with time. At the latest stages of entrapment, monophasic aqueous inclusions (Plate 5.1c), which reach 40 microns in size, indicate that fluids were trapped at low temperatures (perhaps  $<70^{\circ}\text{C}$ ). Unlike the inclusions in the photograph, most of these late stage inclusions commonly are small,  $<10$  microns in size, and usually occur in planar arrays of secondary inclusions.

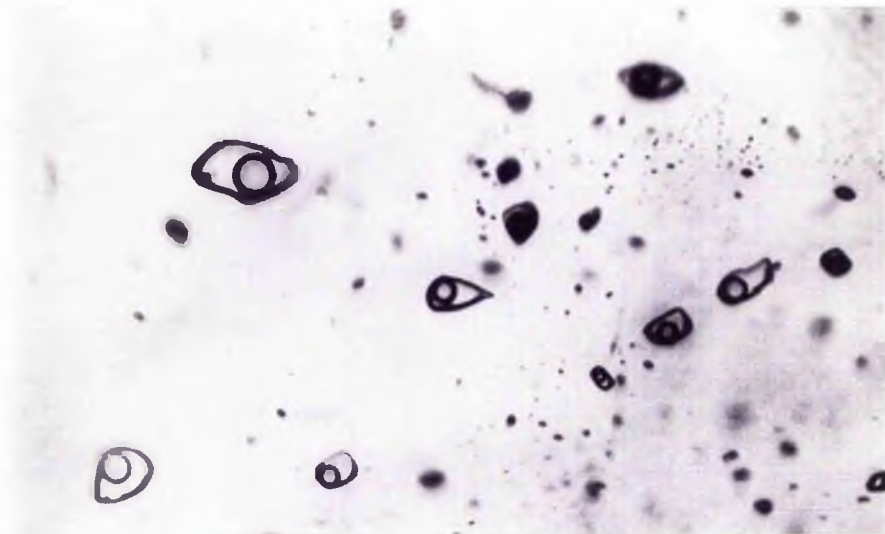
(ii) Type V inclusions (Plate 5.2a), are low density vapour-rich inclusions which contain a gas bubble which occupies more than 50% of the volume of the inclusion at room temperature. On heating these inclusions homogenise to the vapour phase. In addition to the large vapour phase, there is a varying proportion of a liquid phase, which sometimes only becomes evident on cooling. The accompanying aqueous fluid has a low salinity and solid phases are rare. Vapour-rich inclusions occur in most rock types and range from less than 5 microns to over 50 microns in size in some of the hydrothermally altered facies. The inclusion shape varies from that of negative crystals to complete irregularity. Such irregularly-shaped inclusions are very useful in determining the precise temperature of homogenisation of the inclusion into the vapour phase where the last stage of the expansion of the vapour bubble can be monitored.

The coexistence of vapour-rich and liquid-rich inclusions indicates that boiling (or effervescence) of the fluid was common. Often this has resulted in the trapping of inclusions with different proportions of liquid and vapour. In order to assume that boiling has occurred the homogenisation temperature of the vapour-rich inclusions should ideally be the same temperature as that at which the liquid-rich inclusions homogenise. This unfortunately is not always the case since small amounts of liquid may be trapped with the vapour and also gas may be trapped with the liquid. In both cases homogenisation temperatures will be erroneously high.

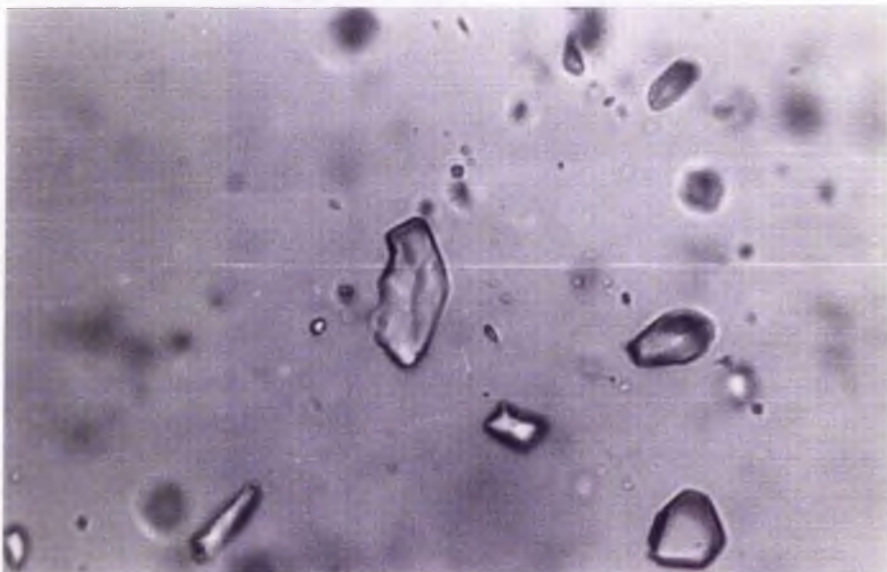
(iii) Type C inclusions possess, in addition to water, a second immiscible phase which is  $\text{CO}_2$  (Plate 5.2b) with traces of other gases such as  $\text{CH}_4$ ,  $\text{N}_2$  and  $\text{H}_2\text{S}$ . At high temperature, water and carbon dioxide mix in all proportions, but at lower temperatures, the mutual solubilities are very low and an inclusion that was originally a homogeneous mixed fluid, separated into two immiscible fluids, one rich in carbon dioxide and other gases, the other rich in water. Variable phase ratios of  $\text{CO}_2$  and water in some samples distinguishes a heterogeneous trapped fluid however, since there would be constant phase ratios at room temperature if the trapped fluid had been originally homogeneous. Below  $31^{\circ}\text{C}$ , where  $\text{CO}_2$  constitutes in excess of 6% by volume and is at more than 75 bars partial pressure, it may be recognised at room temperature by the "double bubble effect". Such inclusions account for only about 3% of the total population. They have been recognised in albitised granites and pegmatites and vary from  $<10$  to 50 microns in size.



(a) Irregularly-shaped inclusions in fluorite from the Afu complex. Inclusion size approximately 40 microns. AF23



(b) Plane of pseudosecondary inclusions in R1/44 quartz sample from the Ririwai lode. Maximum inclusion size is 50 microns.



(c) Liquid-filled inclusions in late-stage quartz from the Ririwai lode indicating low temperature formation. Inclusions up to 40 microns in size.



Plate 5.2a

Type V inclusions in vein quartz from the Banke complex.  
Inclusion length 20 microns.



Plate 5.2b

Type C inclusion in SS161 ignimbrite from the volcanic pile of the Saiya Shokobo complex. The inclusion contains a large inner vapour bubble of  $\text{CO}_2$  gas with a thin rim of  $\text{CO}_2$  liquid. The remainder of the inclusion is an aqueous fluid. Inclusion length 10 microns: photograph taken at  $25^\circ\text{C}$ .

(iv) Type S inclusions (Plate 5.3) have formed from fluids that were saline when trapped and contain a solid phase or phases which may occupy up to 30% of the total volume. In addition there is a high density aqueous phase which occupies a larger volume than the solid phase. Type S inclusions account for approximately 3% of the total population. Halite is the most common daughter mineral. It is cubic, or rounded, colourless, with high relief and is isotropic. Sylvite, a similar colourless isotropic mineral was distinguished by its more rapid solubility during heating. These inclusions are called three-phase when one solid is present - in addition to liquid and vapour - and multiphase when several solids occur. Multiphase inclusions are particularly abundant in aquamarine (Plate 5.3c) and topaz (Plate 5.3b) from marginal pegmatitic pods and may reach more than 1mm in size. The inclusions are often elliptical or elongate and their distribution is partly controlled by the crystallography of the host mineral, particularly in aquamarines.

In addition to halite a variety of other phases occur:-

a prismatic low birefringent mineral is possibly anhydrite ( $\text{CaSO}_4 \cdot 2\text{H}_2\text{O}$ ), rhombohedral crystals may be a carbonate or iron chloride, fibrous bundles of needles are probably dawsonite ( $\text{NaAl}(\text{CO}_3)(\text{OH})_2$ ).

The identification of the other phases is more questionable. Reddish hexagonal plates are believed to be haematite, and small pseudo-hexagonal crystals with a low refractive index may be cryolite. It is important to emphasise that not all S-type inclusions are halite-bearing but may contain several small unidentified phases that could include complex salts, alkali halides, carbonates, bicarbonates, sulphates and oxides.

Solid phases may also occur in inclusions by accidental trapping of already crystalline minerals in a droplet of fluid that was later incorporated in a mineral as a fluid inclusion. These should be distinguished from daughter crystals which have precipitated from a saline fluid. In a given sample, groups of Type S inclusions with very similar solid phase contents are common. Where this occurs, it is clear that the solids are daughter minerals even though they may not dissolve before homogenisation of the liquid and vapour phases during heating experiments.

(v) Type M inclusions, consist of globules of a silicate melt, trapped at a temperature above  $600^\circ\text{C}$  and at  $P > 1\text{kb}$ , which have cooled to form devitrified glass plus other fluid and solid phases. The inclusions can be identified by their devitrification texture, lack of ice formation on freezing, refractive index and sometimes by the presence of more than one vapour bubble. They are usually ovoid in form and they account for less than 1% of the total inclusion population. Rarely, such inclusions co-exist with dense saline globules of aqueous fluid which must have resulted from immiscibility between the saline brine and the silicate melt.



- (a) three-phase inclusions containing liquid, a gas bubble and a cube of halite. Inclusions are in B65, a wolframite-bearing quartz vein cutting basement in the Banke complex. Size up to 50 microns.



- (b) multiphase pseudosecondary inclusions in topaz, parallel to [001]. Each inclusion contains a large vapour bubble in the liquid plus several daughter minerals. Inclusions up to 100 microns in size. Amo complex.



- (c) multiphase inclusion in aquamarine from Igo in the Afu complex. Inclusion is 0.5mm long. This is one of a vast number of inclusions oriented along the *c* axis of the mineral.

## Techniques of the study

A study of a representative suite of samples from different granites and from each type of hydrothermal stage was undertaken prior to the commencement of this thesis. Twenty one samples were selected from six complexes: Afu, Amo, Banke, Jos Bukuru, Ririwai and Ropp. Four were chosen to represent the "magmatic" fluid; two each were chosen for sodic and potash metasomatised rocks and the remaining 12 samples were altered by acid or silica metasomatism or both (Table 5.2).

Topaz, beryl, fluorite and quartz, provided good fluid inclusion data, but no information was possible on any of the ores. Those that are transparent, such as sphalerite and cassiterite, either do not contain suitable fluid inclusions, or were too dark in colour to be usable for thermometric studies.

Virtually all samples contained more than one generation of inclusions and secondary inclusions are common as planes and trails of small rounded or elongate cavities. The inclusions may be extremely abundant, particularly in quartz. The size of the inclusions ranges from <1 micron, which is too small for thermometric study, to inclusions >1mm in topaz and aquamarines.

Polished wafers of the samples were prepared to a thickness of approximately 1mm although the eventual thickness was determined by the relative transparency of the mineral to be studied. These wafers were polished on two sides both to improve optical observations and to ensure good even contact with the heating/freezing block within the thermometric cell.

A number of thermometric measurements, usually between 50 and 200, were made on each sample and the data is summarised in Table 5.2. On freezing, ice crystals developed in all except glass inclusions. The first melting temperatures of this ice are commonly in the range  $-34$  to  $-23^{\circ}\text{C}$ , which is the eutectic temperature of the system  $\text{NaCl-KCl-H}_2\text{O}$  (Table 5.1). This indicates therefore, that in most inclusions, the bivalent cations of Ca and Mg are absent. Calculation of salinity from last ice crystal melting temperatures showed a complete salinity range from <1 to 23.3 wt% NaCl, whilst hydrohalite development on freezing also indicated fluid salinities in the range 23.3 to 26.3 wt% NaCl.

During heating experiments two sets of homogenisation data were measured. One, the partial homogenisation of the  $\text{CO}_2$  liquid and gas phases into a single phase, the other, the total homogenisation of all the phases in the inclusions. For the  $\text{CO}_2$  phases, homogenisation temperatures were within the range  $+14$  to  $+31^{\circ}\text{C}$ , with homogenisation to the liquid phase, corresponding to a density of 0.85 to 0.468  $\text{g/cm}^3$  (Valakovich and Altunin 1968).

Total homogenisation shows a frequency distribution that differs between granites and each hydrothermal alteration stage. In most inclusions, homogenisation is to the liquid phase. Also on heating the melting temperatures of halite were observed in the range 216 to  $391^{\circ}\text{C}$  and high salinity values of between 26 and 45 wt% NaCl were calculated from these melting temperatures.

Table 5.1 Selected phase data for salt-water systems considered most relevant to aqueous fluid inclusions

Salt system	Eutectic temp ( $^{\circ}\text{C}$ )	solid phases
$\text{H}_2\text{O}-\text{NaCl}-\text{CaCl}_2$	-55.0	ice + $\text{NaCl}\cdot 2\text{H}_2\text{O}$ + $\text{CaCl}_2\cdot 6\text{H}_2\text{O}$
$\text{H}_2\text{O}-\text{MgCl}_2-\text{CaCl}_2$	-52.2	ice + $\text{MgCl}_2\cdot 12\text{H}_2\text{O}$ + $\text{CaCl}_2\cdot 6\text{H}_2\text{O}$
$\text{H}_2\text{O}-\text{KCl}-\text{CaCl}_2$	-50.5	ice + $\text{CaCl}_2\cdot 6\text{H}_2\text{O}^*$
$\text{H}_2\text{O}-\text{CaCl}_2$	-49.5	ice + $\text{CaCl}_2\cdot 6\text{H}_2\text{O}$
$\text{H}_2\text{O}-\text{Na}_2\text{CO}_3-\text{K}_2\text{CO}_3$	-37.0	ice + $(\text{K},\text{Na})_2\text{CO}_3\cdot 6\text{H}_2\text{O}$ + $\text{K}_2\text{CO}_3\cdot 6\text{H}_2\text{O}$
$\text{H}_2\text{O}-\text{NaCl}-\text{FeCl}_2$	-37.0	ice + $\text{NaCl}\cdot 2\text{H}_2\text{O}$ + $\text{FeCl}_2\cdot 6\text{H}_2\text{O}$
$\text{H}_2\text{O}-\text{FeCl}_2$	-35.0	ice + $\text{FeCl}_2\cdot 6\text{H}_2\text{O}$
$\text{H}_2\text{O}-\text{NaCl}-\text{MgCl}_2$	-35.0	ice + $\text{NaCl}\cdot 2\text{H}_2\text{O}$ + $\text{MgCl}_2\cdot 12\text{H}_2\text{O}$
$\text{H}_2\text{O}-\text{MgCl}_2$	-33.6	ice + $\text{MgCl}_2\cdot 12\text{H}_2\text{O}$
$\text{H}_2\text{O}-\text{NaCl}-\text{KCl}$	-23.5	ice + $\text{NaCl}\cdot 2\text{H}_2\text{O}^*$
$\text{H}_2\text{O}-\text{NaCl}-\text{NaHCO}_3$	-21.8	ice + $\text{NaCl}\cdot 2\text{H}_2\text{O}$ + $\text{NaHCO}_3$
$\text{H}_2\text{O}-\text{NaCl}-\text{Na}_2\text{SO}_4$	-21.7	ice + $\text{NaCl}\cdot 2\text{H}_2\text{O}$ + $\text{Na}_2\text{SO}_4\cdot 5\text{H}_2\text{O}$
$\text{H}_2\text{O}-\text{NaCl}-\text{Na}_2\text{CO}_3$	-21.4	ice + $\text{NaCl}\cdot 2\text{H}_2\text{O}$ + $\text{Na}_2\text{CO}_3\cdot 10\text{H}_2\text{O}$
$\text{H}_2\text{O}-\text{NaCl}$	-21.2	ice + $\text{NaCl}\cdot 2\text{H}_2\text{O}$
$\text{H}_2\text{O}-\text{KCl}$	-10.6	ice*
$\text{H}_2\text{O}-\text{NaHCO}_3-\text{Na}_2\text{CO}_3$	- 3.3	ice + $\text{NaHCO}_3$ + $\text{Na}_2\text{CO}_3\cdot 10\text{H}_2\text{O}$
$\text{H}_2\text{O}-\text{NaHCO}_3$	- 2.3	ice + $\text{NaHCO}_3$
$\text{H}_2\text{O}-\text{Na}_2\text{CO}_3$	- 2.1	ice + $\text{Na}_2\text{CO}_3\cdot 10\text{H}_2\text{O}$
$\text{H}_2\text{O}-\text{Na}_2\text{SO}_4$	- 1.2	ice + $\text{Na}_2\text{SO}_4\cdot 10\text{H}_2\text{O}$

Eutectic temperatures as given by Borisenko (1977)

\* Data for  $\text{KCl}\cdot n\text{H}_2\text{O}$  hydrate uncertain.

Table 5.2. Fluid inclusion characteristics of selected samples from granites, hydrothermal pegmatites and different hydrothermal mineralogical assemblages

Complex	Sample No and Location	Mineral	Mineral assemblage	Mineralization type	Inclusion type	Primary Secondary or Pseudo Secondary	Size $\mu\text{m}$	Main Th range	Salinity wt% NaCl
Afu	Af 23 Rafin Gabee	fluorite	micro-quartz-fluorite sulphides	irregularly shaped replacement body	L, V, S	P, S	50 $\mu\text{m}$	300-420	13-17
	Rafin Gabee	quenezzine	quenezzine-quartz	pegmatitic pod	L, S	P, TS	100-1 $\mu\text{m}$	400-500	26
Amo	Tibbar creek	topaz	quartz-falderop-topaz beryl	pegmatitic pod	L, S	PS, S	1 $\mu\text{m}$	350-470 decrepitation occurs	26
Banke	B48 Babadamu	quartz	quartz, albite, beryl pegmatite	pegmatitic pod	L, V, S	P, S	3-8		-
	B64	quartz	quartz-mica-greisen	sheeted veins	L, V	P, S	10-45		-
	B65	quartz	quartz-wolfenite	quartz vein	V, L, S	P	8-50	300-400	<40
	B93	quartz	quartz-wolfenite	basement quartz vein	L, C, V, S		8-20	228-244*	-
	B4.3 Ginye Hill	quartz	quartz-wolfenite vein	basement quartz	L, C, V, S	P, S	8-50	150-380	
	B1.3 Zarze Quarry	quartz	quartz-fluorite-sulphide	mineralised ring dyke	L, V, C		2-20	300-350	<6-15
Jos-Bukuru	B222 Babagarami	quartz	quartz-chlorite	altered wallrock	L, V		50	300-350	3-15
	JBM1122 Bukuru SW	quartz	quartz-mica-chlorite disseminated ZnS and PbS	altered wallrock	L, V		20-30	300-350	3-15
	JB 100 Gyantagere Quarry	quartz	quartz-albite-microcline-mica	permissive sodic then potash then H <sub>2</sub> O metasomatism	L, V, C		10	310-500	5-20
	M151	quartz	quartz, perthite, muscovite	unaltered biotite granite	P, L	P, S	30	210-380	<16
	Anglo Jos	quartz	quartz, perthite, microcline, muscovite	altered wallrock	L	P		278-340	<10
Riviera	R3A.4 Nakota push	quartz	quartz-microcline wallrock	permissive potash metasomatism	L, S, V	P	30	360-460	<36
	R56 Umar Side	quartz	quartz, (albite), microcline mica, coesite, sulphides	permissive then potash, then H <sub>2</sub> O metasomatism	L, V	P, S		360-380	5-8
	R68 S of Kaffa Valley	quartz	quartz, arfvedsonite albite	permissive sodic disseminated mineralisation	L, V	P, S	10	260-360	2-12
	R10.7 near Adit in the lode	quartz	quartz, microcline, chlorite	potash metasomatism of altered wallrock	L, V	P	20	31-460	-
	R1/44 Riviera lode 30 m depth	quartz	quartz + apatite + galena + chalcocite etc	fracture filling quartz vein	L, V	P, S	10-100	360-380	6-11
	R514C Riviera lode-surface	quartz	quartz + galena + apatite + wolfenite	fracture filling quartz vein	L	P, S	80	340	7
Ropp	RP 130 Decimo	quartz	arfvedsonite albite + pyrochlore granite	permissive sodic; disseminated mineralisation	L, V, C, S, M	P, S	20	260-500	<20

## Summary of thermometric data

### Granites and pegmatites

The samples JBJ151, an unaltered biotite perthite granite, the pegmatitic topaz from the Amo complex, quartz from a pegmatite of the Banke complex and the aquamarine from the Afu complex were chosen in the belief that they represented magmatic 'unaltered' samples. The pegmatitic pods are ascribed to fluid separation from the silicate melt and were therefore expected to have trapped an early fluid.

Sample JBJ151 from the Jos Bukuru complex, which is a biotite perthite granite contained some recognisable silicate melt inclusions which did not contain vapour bubbles. Most inclusions however, seemed to be two-phase liquid-rich inclusions. A few of these Type L inclusions gave homogenisation temperatures as high as 500°C however, the main range of homogenisation temperatures was between 250-380°C. Even allowing for a pressure correction, this was considerably lower than had been anticipated.

The topaz crystals from the Amo complex which may be up to 100 microns in size, also give temperatures of homogenisation lower than expected. The inclusions are multiphase with as many as eight daughter phases in the inclusions (Plate 5.3b). Several of the solid inclusions in topaz and also in aquamarine, did not dissolve before the homogenisation temperature was reached. They are still regarded as daughter minerals crystallised from a saline fluid however, because of the similarity of phase ratio in most inclusions (Kinnaird 1985). In most inclusions only four daughter solids can be seen. This may be due to metastable conditions or simply the small size of some of the phases in inclusions less than 10 microns in size. None of the daughter minerals have been identified with certainty. One rounded mineral phase which consistently dissolved between 110 and 120°C may be sylvite, and another phase which melted around 370°C is probably halite. However a pale green, highly birefringent lath-shaped daughter mineral did not dissolve at the temperature of homogenisation which was within the range 350-420°C. Continued heating in an attempt to dissolve the other daughter minerals lead to decrepitation at temperatures above 420°C. Kelly and Turneure (1970) in a study of saline inclusions in quartz from Sn-W deposits of the eastern Andes also noted as many as eight daughter phases in inclusions, in particular they noted that a light green fibrous silicate(?) mineral which seemed not to dissolve on normal heating runs dissolved completely after 48 hours held at the homogenisation temperature and many of the daughter minerals dissolved close to the Th, suggesting trapping of fluids that were boiling and saturated with respect to those particular phases.

Both the topaz and aquamarine give homogenisation temperatures of 400°C or higher for saturated solutions which according to the data of Haas (1971) imposes a minimum depth of formation of 1150m and a minimum vapour pressure within the inclusions of 110 bars.

## Sodic metasomatism

The mineral assemblages which formed in response to sodic metasomatism depended on the intensity of rock-fluid interaction with the strongly peralkaline compositions representing the maximum effect. Samples JBJ300, a zinnwaldite albite granite and RP150 an arfvedsonite albite granite were selected as examples of sodic metasomatised rocks. Albite is an important constituent of both samples (>50%) and is accompanied by quartz and aegirine, arfvedsonite and pyrochlore in sample RP150 and by biotite and columbite in JBJ300.

Both samples are characterised by a variety of inclusions - rare melt inclusions together with Type S and vapour-rich inclusions. Such a variety is also found in some granites although for the sodic metasomatised rocks the most notable feature of this facies is the abundance of CO<sub>2</sub>-rich inclusions. The Type V inclusions often have a negative crystal shape and the measurement of the homogenisation temperature is not possible with any degree of accuracy. Homogenisation temperatures of the Type L inclusions are in the range 260-500°C, with the lowest temperatures being recorded in the peralkaline facies (Table 5.2). The salinity of these inclusions covers a wide range with dilute inclusions together with saline inclusions. This observation plus the occasional occurrence of Type S inclusions suggests that the fluid must have boiled at a temperature of <400°C. This would account for the range in salinity of the inclusions since the dilute inclusions would be condensates and the saline inclusions would equate with the high-density brine. This would also explain the inhomogeneous distribution of CO<sub>2</sub> in inclusions. The CO<sub>2</sub> inclusions homogenise to the liquid phase indicating high densities and total homogenisation of all the phases in the inclusions was >350°C for the few inclusions which did not decrepitate before this temperature.

Degassing of the fluid and loss of CO<sub>2</sub> at this early stage must have led to a very different composition for the remaining fluid which resulted in the deposition of columbite and associated minerals. Geochemically, high values of uranium are only recorded in albite-rich facies. Other similar elements like the HREE's, Th and Zr could have been transported and concentrated by similar processes linked with CO<sub>2</sub> loss from the fluid.

## Potash metasomatism

Samples R10.7A and R3A.4 from Ririwai were selected as potash metasomatised samples together with a sample from Anglo Jos in the Jos Bukuru complex. All samples are from microcline-rich wall rocks.

The first sample occurred adjacent to a major lode system in the Ririwai complex; R3A.4 came from a small vein system in the southwest of the same complex. In these samples, turbid microcline, accompanied by quartz and chlorite are the only essential minerals of the rock although there are variable amounts of sphalerite, wolframite and cassiterite. The fluid inclusion population is characterised by abundant small, often saline inclusions in feldspars. These saline inclusions are accompanied by vapour-rich and liquid-rich inclusions in quartz which is interpreted again as due to boiling of the fluids. No thermometric data has been obtainable on inclusions in feldspars. Those in quartz indicate homogenisation temperatures in a wide range up to 500°C

although there was a peak of homogenisation temperatures in the range 360-460°C. There are lower temperature homogenisation peaks however, with thermometric results identical with those from later quartz veins although in the quartz of the microcline-quartz assemblage they do not necessarily appear as secondary inclusions. This is interpreted as due to void-filling in the vuggy microclinised wallrock during later silicification.

For the wallrock sample L3A/4, from the Makota path veins, homogenisation temperatures were at a maximum of 360°C with a wide range in salinity up to 36 wt% and a fluid density of around 0.95 g/cm<sup>3</sup>. Dissolution temperatures of halite in the occasional Type S inclusions were very close to the temperature of total homogenisation, further substantiating the fact that the fluid was boiling and saturated with respect to NaCl. Since the fluids were boiling the data of Haas (1971) can be applied directly to suggest a depth of formation of 1030 metres and a confining pressure of >100 bars.

The sample from Anglo Jos contained small dilute Type L inclusions with homogenisation temperatures in the range 278-340°C which suggests a minimum depth of 1000m at the time of trapping.

#### Acid metasomatism

During acid metasomatism the granite minerals destabilised to give new subsolidus mineral assemblages. Several different samples were selected for study in this group in an attempt to see if any differences in character of the inclusions may help to explain the different mineralogical assemblages. All the selected samples have a wide range of fluid characteristics with inclusions up to 100 microns in size; often there is evidence of boiling and the inclusions may or may not contain daughter minerals. Homogenisation temperatures are in the range 230-420°C. The salinity may be from <10 to 35 wt% NaCl.

In sample AF23 from the mica-rich sulphide-bearing mineralised "pipe" at Igo in the Afu complex inclusions were investigated in fluorite. These ranged in size up to 50 microns and in shape from tubular to irregular. The inclusion population is dominated by Type L inclusions (Plate 5.1a) with Type V inclusions and Type S inclusions with several daughter minerals. Several of these dissolved at temperatures less than 220°C with the halite dissolution close to the temperature of total homogenisation. Homogenisation temperatures were overwhelmingly in the 300-420°C range although some temperatures were measured down to 279°C. As with many other samples a wide range of salinities were obtained from freezing experiments but the most consistent set of measurements indicated that the fluid had between 13 and 17 eq wt% NaCl with a maximum density of 0.83 g/cm<sup>3</sup>. From the data of Haas (1971) a minimum depth at the time of trapping would be 1275m corresponding to a confining pressure of 114 bars.

Sample RS6 from the Uwar Gida area of the Ririwai complex is a sample showing the effects of disseminated acid metasomatism. The sample came from the roof of the biotite granite pluton, close to the volcanic cover. The inclusion population in quartz is characterised by a mixed assemblage of Type L and Type V inclusions homogenising in the same temperature interval of 360-380°C. The Type L inclusions have a maximum density of 0.77 g/cm<sup>3</sup>. Since the inclusions were boiling at the time of trapping, the depth of formation was at least 1416m with a pressure of around 120 bars.

Also in the Ririwai complex, greisen veins from the Makota path area and the Ririwai lode were studied. Inclusions are invariably Type L or Type V with some monophasic liquid inclusions forming trails along healed fractures in the quartz. Salinity was low from 6-10 eq.wt% NaCl. Homogenisation temperatures were within the limited range 360-380° with maximum fluid densities of 0.72g/cm<sup>3</sup>. The homogenisation temperatures showed a considerable overlap between those found for potash and silica metasomatised rocks and is also similar to the pervasively greisenised roof rocks of the Uwar Gida area discussed above.

In the Jos Bukuru complex two samples from greisen assemblages had inclusions populations that contained co-existing Type L and Type V inclusions with homogenisation temperatures in the range 300-350°C (Table 5.2) and with moderately dilute fluids with a density of the fluid of around 0.82 g/cm<sup>3</sup>. Again these inclusions appear to represent boiling assemblages and from the data of Haas (1971) the depth of formation would have been about 900m with a confining pressure of 80 bars.

#### Silica metasomatism

Quartz veins both from within biotite granites and from wolframite-bearing veins in the basement were studied. These studies showed that silica metasomatism was often characterised by the trapping of large inclusions up to 50 microns in size which are dominantly liquid-rich.

In the Afu and Banke complexes, late stage wolframite-bearing quartz veins contain saline halite-bearing inclusions in addition to Type L, and vapour-rich inclusions. Field evidence suggests that there was a rapid release of this vapour when boiling occurred which has resulted in brecciation of the vein material;

At Zarara quarry in the Banke complex hydrothermal modifications are limited to narrow zones although the degree of reaction may have locally been intense. The granite porphyry contains feldspar phenocrysts showing arrested growth forms set in a fine-grained matrix. From the petrological point of view it is this matrix which substantially reacted with the fluids. With sudden pressure release, local marginal brecciation occurred and ore minerals were deposited in veins that cemented the brecciated blocks (see Plate 6.11). Mirolitic cavities containing elongate prismatic quartz crystals occur within and between the brecciated blocks of ring dyke porphyry which was recemented by late-stage quartz. Fluid inclusion studies on this late-stage quartz showed homogenisation temperatures with a wide range up to 430°C and with a broad variation in salinity values up to 20 eq.wt% NaCl. This wide range for both values is consistent with inhomogeneous trapping and it seems likely that boiling occurred at around 300-350°C since higher temperatures of homogenisation can be discounted because of inhomogeneous trapping. Low density inclusions can be explained as condensates.

Inclusions in a quartz sample B4.3, from a wolframite-bearing quartz reef in the basement of the Banke complex, also showed a wide variety of inclusion types. The inclusions were large and dominated by Type L inclusions with a moderately large vapour bubble, and these were accompanied by Type V inclusions, Type S inclusions and rare Type C inclusions. The Type L inclusions showed a

range of salinity with some inclusions giving a fluid salinity of 15-18 eq. wt% NaCl, whilst others with last ice crystal melting temperatures equivalent to <6 eq. wt%. These were assumed to be condensates from the boiling saline brine. Type S inclusions showed a large halite crystal (Plate 5.3a) which gave dissolution temperatures up to 332°C corresponding to a maximum salinity of 40 eq. wt% NaCl. These dissolution temperatures were close to the total homogenisation temperature of 350-380°C. For a fluid of ~15 eq. wt% NaCl boiling at ~350°C, with a density of 0.83 g/cm<sup>3</sup> the depth at the time of trapping would have been ~1300 metres with a confining pressure of more than 120 bars (Haas 1971).

Sample B4.3 just described came from the quartz reef at the base of Genya Hill. In contrast sample B93, from the top of the same hill less than a 100m higher, gave homogenisation temperatures that were significantly lower - 228-244°C with very dilute salinities.

Wolframite-bearing quartz veins from locality B65 also contain a mixed population with Type L inclusions, Type V inclusions with a vapour bubble that may occupy up to 85% of the volume of an inclusion, rare Type C inclusions and Type S inclusions with one or more solids. The bulk of the homogenisation temperatures are within the range 300-400°C but there is a wide range in the salinity values. Type S inclusions with halite (Plate 5.3a) gave dissolution temperatures for the halite of up to 363°C corresponding to a maximum salinity of the fluid of 40 eq. wt% NaCl.

A detailed study was undertaken on sample R1/44 collected from a depth of 30 metres from the major quartz vein of the Ririwai lode (Kinnaid et al 1985a). The inclusions were large, Type L inclusions, up to 50 microns in size (Plate 5.1b) and with consistent temperatures of homogenisation between 360 and 380°C with occasional lower homogenisation temperatures as low as 269°C. These later lower temperature inclusions had slightly lower salinities than those with homogenisation temperature above 350°C. Clearly the quartz of the lode must have formed over a range of temperatures since fluid inclusions in vein quartz containing galena and wolframite in sample R514C, collected at the Adit in the western end of the Lode have slightly lower salinities and lower temperatures of homogenisation than R1/44. Salinity varied little at around 7.8 eq. wt% NaCl with the majority of inclusions giving homogenisation temperatures between 338 and 342°C.

In some samples from the quartz veins of the Ririwai lode there are clearly two stages of quartz formation. Euhedral transparent prismatic crystals of early quartz up to 5cm long are surrounded by a milky-white rind up to 2mm thick. This opalescent rim contains a myriad of tiny inclusions around 5mm in size occasionally reaching 40 microns in size (Plate 5.1c). Few show vapour bubbles on account of metastability within such small inclusions. However, repeated heating and cooling runs caused vapour bubbles to nucleate in several inclusions. Homogenisation temperatures obtained from these inclusions show that the fluid was trapped at <120°C and that it had an extremely low salinity with fluid density close to 1gm/cm<sup>3</sup>.

For silica metasomatism as a whole therefore, the salinity as determined from the last ice-melting temperatures in fluid inclusions was in the range 6-12 eq. wt% NaCl. However, where the fluids boiled as at Zarara quarry in the Banke complex, fluid inclusions also indicate wide ranges in salinity from <5 to >35 eq. wt% NaCl. Such a salinity range can be explained by boiling. Quartz

deposition clearly took place over a wide range of temperatures from 380° to less than 70°C. Sulphide deposition took place in the range 220-380°.

#### Late-stage alteration

Because of the difficulty of obtaining fresh material from kaolinised cupolas, the homogenisation temperatures from the late-stage quartz deposition, described above, are equated in this work with argillic alteration.

#### Ore deposition

The temperature of cassiterite deposition determined from inclusions in accompanying quartz was from low CO<sub>2</sub>-bearing fluids which were initially highly saline (>35wt% NaCl) at temperatures as high as 500°C. However, cassiterite deposition continued to temperatures as low as 250°C from fluids which ranged in density to almost 1g/cm<sup>3</sup> at the later stages. The sulphide ore minerals were deposited from more dilute fluids at temperatures <420 and usually in the range 220-380°C with low fluid densities. Tungsten deposition also occurred over a wide temperature interval and in some cases was demonstrably from CO<sub>2</sub>-bearing fluids (Banke) and in other complexes (Adit, Ririwai lode) from non-CO<sub>2</sub>-bearing fluids. Homogenisation temperatures range from 228-400°C with a peak of temperatures around 350°C and a salinity often between 15-18 eq.wt% NaCl.

#### Discussion of thermometric data and fluid compositions

##### Introduction

Few fluid inclusions appear to have been trapped from late magmatic fluids. However, this does not mean that all the inclusion data is from secondary minerals. Where minerals such as quartz have been recrystallised and deposited to low temperatures, many of the inclusions will have been trapped as primary fluids in equilibrium with the mineral as it grew. Such re-equilibration in the granites occurred because at high levels in the crust the granite was no longer in equilibrium with the fluids. Although the nature of the late magmatic fluid therefore is still a matter of speculation a discussion on the source, composition and evolution of the fluids is nevertheless possible on the basis of the available fluid inclusion data, geochemical, petrographic and field evidence.

However, before considering the various lines of evidence it is important to consider the mechanics of emplacement of a water-bearing magma. Most fresh granitic rocks contain less than 1 wt % H<sub>2</sub>O and although the solubilities of the volatile components increase with increase in pressure, there is a major solubility gap between water and granitic melts throughout crustal pressures. At pressures of greater than 400 bars the solubility of water in magmas is greater than 1 wt%. Therefore, if magmas are not dramatically undersaturated in water throughout much of their crustal history, they will lose a major part of their original hydrogen content during their rise through the crust (Sheppard 1977). For a felsic magma to reach high levels in the crust the initial water content cannot be greater than about 3 wt%. If such a magma becomes saturated in water, it does so at depths of less than about 4km. Magma with a higher initial water content would become completely crystallised, after boiling off most of its

volatiles, at a depth of several kilometres. Petrological observations indicate that a part of many high level plutons crystallised before the residual magma became saturated in water. Thus 3 wt% water is probably substantially higher than the initial water content of most high level plutons. The amount in excess of the final 0.6 - 1 wt% will form the magmatic hydrothermal part of the system unless it was directly lost to the atmosphere (Sheppard 1977).

The results of the emplacement of granites to high levels does not just depend on the composition of the magma and its degree of saturation but also on the country rock and its saturation both at the magmatic and post-magmatic stages. In fact the emplacement of an intrusion may generate fractures and permeability in the host rock itself leading to localised hydrothermal convective cells which collapsed into the granite stock on cooling. Rejuvenation of these cells may have occurred depending on the heat production capacity of some of these granite plutons.

#### Field evidence

From field evidence it is obvious that the Nigerian granites were emplaced high in the crust, as many of the complexes in the north have associated volcanic rocks. Since the main control on depth of crystallisation of a rising body of granitic magma is its H<sub>2</sub>O content (Burnham 1979, Wyllie 1979), the magmas of the ring complexes must have been relatively H<sub>2</sub>O poor, although the high fluorine content of the magma would have increased the solubility of H<sub>2</sub>O (Bailey 1977). The field evidence of miarolitic cavities and pegmatitic pods in the cupola and contact zones into which crystals could grow seems indicative of the early separation of a gas phase. Variations in the mineral assemblage within the pegmatitic pods also indicates the importance of volatiles in the process of hydrothermal alteration. Further evidence on the importance of a volatile stage is based on the occurrence of brecciated zones in the Banke, Afu and Saiya Shokobo complexes.

#### Geochemical evidence

The initial fluids were clearly rich in carbon dioxide, fluorine, chlorine, and probably also hydrogen and nitrogen. The abundance of fluorine which is more soluble than water in the melt (Burnham 1979), probably enhanced REE mobility since thermodynamic calculations indicate that the REE forms more stable compounds with fluorine than with chlorine. Also, HCl is less soluble in the melt than water (Wyllie and Tuttle 1964), which is reflected in F:Cl ratios for minerals and rocks (Table 4.9 page 92). However, despite the general high ratio of F:Cl from analyses, fluid inclusion studies show that Cl was available particularly during late stage quartz vein formation.

#### Combined evidence from fluid inclusion, geochemical and field data

Fluid inclusion studies monitor the complete spectrum of fluid evolution from a silicate melt/saline separation, through gas to aqueous liquid composition. The varied inclusion populations with contrasting homogenisation temperatures, even within one granite or vein, indicate the wide range of re-equilibration in the subsolidus.

Since the granites are known to have been intruded to shallow depth, a small pressure correction needs to be applied to the homogenisation temperature to

give the true temperature of trapping. For Ririwai, where fluids were boiling during lode formation, a depth of formation of at least 141m, with a pressure of around 120 bars, can be interpreted from the data of Haas (1971). If the fluids were not boiling this hydrostatic pressure would involve a temperature correction ( $\Delta T/^\circ\text{C}$ ) of approximately  $50^\circ\text{C}$  for a 10% eq.wt NaCl solution (Klevtsov and Lemlein, 1959). Elsewhere, pressure corrections range from  $20-70^\circ\text{C}$  for  $\Delta T/^\circ\text{C}$ .

Experimental and textural evidence suggests that the earliest fluid inclusions were trapped at the late magmatic stage. Melt inclusions trapped at the magmatic stage are found in quartz crystals in albite granites and it therefore seems likely that the albite granites represent crystallised examples of residual granite magma plus trapped fluids. All subsequent mineralogical variants resulted from differing degrees of interaction of escaping fluids on originally magmatic rocks or host. The coexistence of melt inclusions with daughter-bearing inclusions suggests that initially there was a separation of dense saline brine from the residual melt, followed by vapour phase separation from the brine to form a low density aqueous fluid.

The saline fluid trapped as inclusions within aquamarine and topaz crystals from marginal drusy pegmatitic pods in some of the biotite granites may represent the fluid which evolved from the melt. Inclusions show saline fluids at high temperatures, with abundant daughter minerals in addition to gas and aqueous phases. Homogenisation temperatures for these inclusions range up to  $500^\circ\text{C}$ , which allowing for a pressure correction, indicates that trapping of fluids must have begun at temperatures in excess of  $570^\circ\text{C}$ . Experimental work by Manning (1982) suggests that for granites rich in fluorine, there is a change in the minimum liquidus temperature from  $730^\circ\text{C}$  for a fluorine free granite to  $630^\circ\text{C}$  for the system with 4 wt% F at 1 kbar. The younger granites are clearly fluorine rich with up to 6% F. Many contain fluorite as an accessory, particularly the biotite granites, and many of the silicate phases are also F-rich. Large topaz crystals also occur in some pegmatitic pods. The existence of pegmatitic pockets in which large crystals could grow seems indicative of the early phase separation of a gas and it can be assumed that effervescence or boiling occurred locally. Variations in the mineral assemblage within the pegmatitic pods indicates the variable occurrence of vapour phase generation. Clearly such volatile rich granites can be expected to have depressed the granite minimum. Further, Manning (1981) has found glass in experimental charges down to  $550^\circ\text{C}$  overlapping the corrected Th for the fluid inclusions from aquamarine and topaz.

Miarolitic cavities indicating vapour phase separation, in Nigeria are often associated with brecciation. Local concentrations of calcite with albite, or microcline formation and siderite in greisens, may represent periods of  $\text{CO}_2$  effervescence related to decreasing solubility of  $\text{CO}_2$  with falling temperature.

Previous evidence indicates that the early fluid, responsible for sodic metasomatism must have been rich in albite components accompanied by high U, Th, Nb, Zr and HREE). Loss of  $\text{CO}_2$  appears to have been an important precursor to columbite or pyrochlore formation and appears to lead to "insolubility" of uranium which is incorporated into monazite, thorite, xenotime or zircon (Kinnaird 1985, Kinnaird et al 1985a). The early loss of  $\text{CO}_2$  was accompanied by albite - or albitite- formation.  $\text{CO}_2$  degassing of the high temperature residual fluid could have transported U and Nb into the roof zones of granite cupolas since important concentrations of uranium are found in the cover to some

Niger-Nigeria granite complexes (Bowden et al 1981). Furthermore, subsequent lower temperature postmagmatic reactions may have mobilised uranium and carried it to higher levels. Geochemically high uranium values are only recorded in granites retaining their record of albitisation. From experimental studies (Luth 1976, Kovalenko 1976, Manning 1982) it appears that there may have been a continuum from residual magma to hydrothermal fluid for alkaline provinces without involving immiscibility or phase separation. However, should degassing or boiling have occurred then the resultant fluid compositions would have been drastically different. Since boiling selectively removed  $\text{CO}_2$  and other volatiles from the liquid, the pH and K/H of the remaining fluid would have increased, moving out of the stability field of albite (Rose and Burt 1979) and resulting in the formation of potassium feldspars at the expense of the earlier more sodic feldspar.

According to the work of Fournier (1976), the change from soda to potash metasomatism was probably also assisted by pressure release. Fournier has shown that, when a given fluid is more enriched in soda than potash, sodic metasomatism will prevail at higher temperatures and pressures. As the pressure drops below 220 bars, salts rich in sodium will precipitate and the fluid becomes enriched in KCl. As the pressure drops still further, the potassic process will dominate.

During hydrogen ion metasomatism coexisting vapour rich and fluid rich inclusions give homogenisation temperatures from 300-380°C for greisens in the granite and volcanics and down to 220°C for greisens in the basement. The oxide and co-existing sulphide assemblage help define the conditions of alteration and ore deposition during this acid metasomatism. Molybdenite, sphalerite and other sulphides may accompany the oxide assemblage dominated by cassiterite. The presence of pyrite and chalcopyrite accompanied by haematite and rarity of magnetite and pyrite-bornite (Rose and Burt 1979) suggest relatively high  $\text{fO}_2$  and  $\text{fS}_2$ , at temperatures of 500-600°C with an appreciable portion of oxidised sulphur in the fluid. These temperatures are higher than those suggested from fluid inclusion evidence. At 300°C however, reduced sulphur appears to dominate. This same sequence of fluid evolution has been described in porphyry copper deposits (Rose and Burt 1979).

During silica metasomatism, the temperature of the fluid fell below 400°C and sulphide ores were deposited in the temperature range 220-380°C. Fluid salinity varied widely as a result of fluid boiling. A second generation of quartz, believed to be contemporaneous with argillic alteration, was deposited at temperatures below 120°C and a minor secondary ore mineral assemblage may have been produced in response to these fluids.

## Summary

Effervescence, (unmixing of  $\text{CO}_2$ ) or boiling may have taken place at different stages during the evolution of the fluid, leading to divergent pathways of fluid reactions represented by contrasting assemblages in miarolitic cavities, granite roof facies and during greisenisation. Although boiling of fluid may have occurred at any stage it was during hydrogen ion metasomatism that it was most critical. If boiling was retarded, greisenisation was pervasive. When boiling occurred and phase separation took place, quartz-greisen veins developed. As with the deposition of columbite or pyrochlore related to  $\text{CO}_2$  unmixing, it

appears that boiling and release of a vapour phase was needed to precipitate the ore metals. For example, during the early stage of mineralisation, disseminated columbite distribution was related to CO<sub>2</sub> loss from saline fluids that were rich in Na, Fe, Nb, U, Th, Zr and HREE.

The schematic explanation of petrological variations in the roof facies of Nigerian granite cupolas is shown in Fig 5.1. This provides a useful summary compilation which emphasises the importance of successive periods of boiling in a multicomponent fluid as a result of decreasing pressure, to generate ore deposits. The sequence A-C-E-G represents a series of roof facies variations generated in response to fluid reactions with changing Na, KF and HF activities during falling temperature. Contrasting petrological sequences, generated by sudden pressure release, effervescence, or boiling of the fluid, are indicated by path variants A-B, C-D, E-F and G-H. Substantial ore formation of economic importance was associated with models D, F and H. Thus the schematic model displayed in Fig 5.1 is dependent on physical and chemical changes that took place in fluid composition to generate the ore deposits. Should drastic phase changes not have occurred the fluid evolution and petrological variations followed the falling temperature path A-C-E-G. It was only when sudden pressure variations occurred that paths A-B, C-D, E-F, G-H could appear. From the economic standpoint it was the constraining pressure release that generated the abundant ores, and the characteristic mineral assemblages. Further, it seems clear that without the separation of a vapour phase, ore deposits cannot be generated (Roedder, 1977).

#### Explanation of Fig 5.1

The sequence A-C, E-G represents a series of roof facies variations generated in response to fluid reactions with changing  $\mu_{NaF}$ ,  $\mu_{KF}$  and  $\mu_{HF}$  activities during falling temperatures. Contrasting petrological sequences, generated by successive periods of boiling in a multicomponent fluid as a result of decreasing confining pressure, are indicated by paths:- A-B, C-D, E-F and G-H. Substantial ore formation of economic importance is associated with model D, F and H.

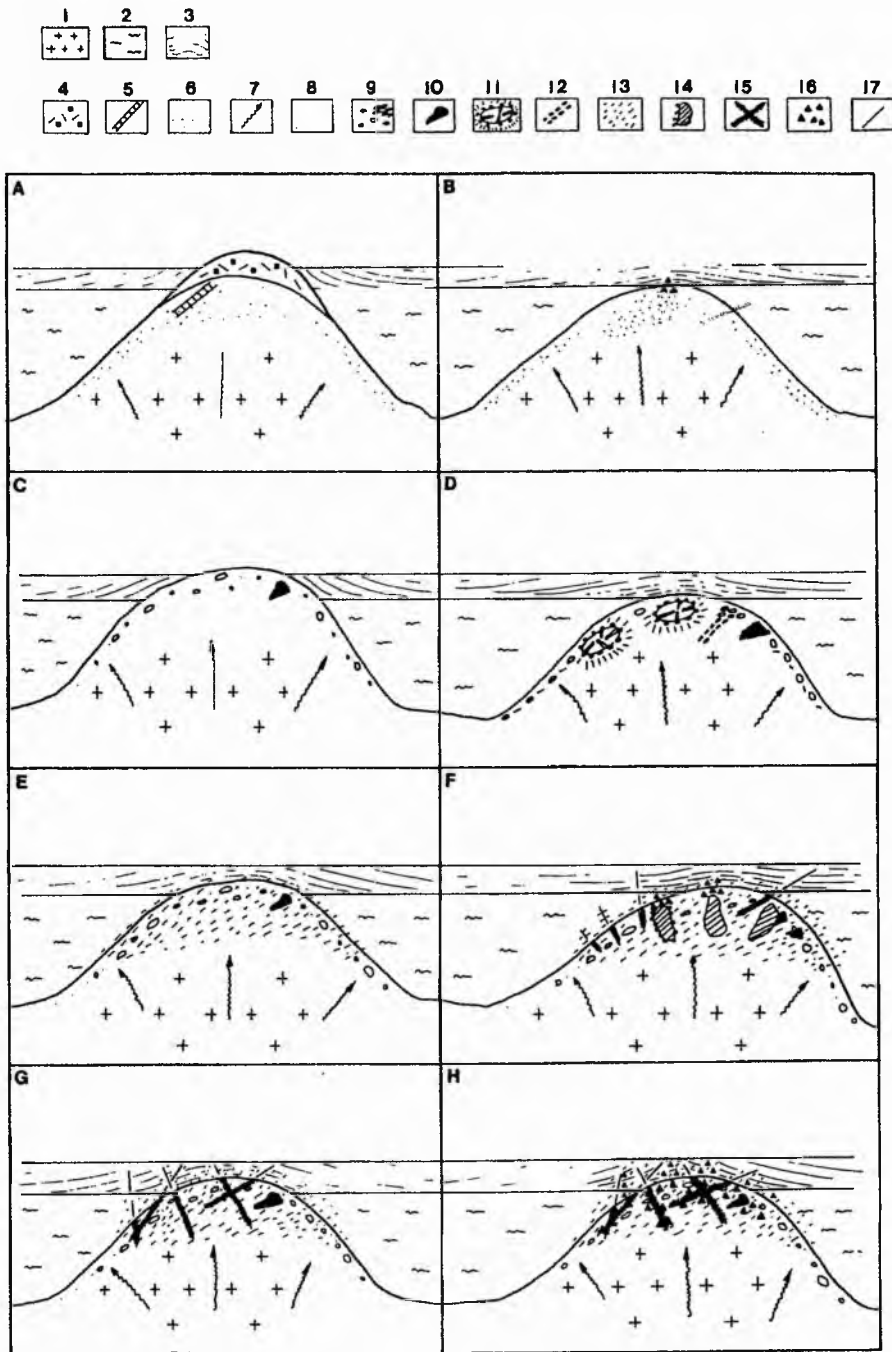
#### Key:

- 1 - biotite granite and biotite syenogranite cupola.
- 2 - Pan-African basement
- 3 - volcanic cover of the anorogenic centre

#### Petrological variants caused by fluid interaction

- 4 - genthelvite quartz albite pegmatite
- 5 - quartz albite aplite
- 6 - albitisation (sodic metasomatism)
- 7 - movement of residual fluids
- 8 - albitite veins (note albitite concentration in B)
- 9 - microclinisation (potash metasomatism)

Fig 5.1 Schematic explanation of petrological variations in the roof zones of Nigerian biotite granite cupolas



- 10- gem pockets with beryl or topaz
- 11- miarolitic cavities lined with microcline and filled with alpha quartz
- 12- microclinite veins
- 13- pervasive greisenisation
- 14- greisen pocket associated with local concentrations of microclinite
- 15- greisen vein filling local fissures with quartz, and limited zones of wall rock reaction
- 16- breccia zones generated by vapour pressure release on boiling of multicomponent fluid
- 17- wolframite-bearing quartz vein in Pan-African basement and volcanic cover.

## CHAPTER 6

### MINERALISATION AND ECONOMIC ASPECTS OF NIGERIAN RING COMPLEXES

#### Introduction

The hydrothermal processes may have affected all rock types. Where these processes have been extensive, disseminated and vein deposits of Sn, Zn, W and Nb with Cu, Fe, Bi, U and REE are developed in and around the roof and marginal zones of medium or fine-grained granite cupolas, with veins extending up to 2km out into the country rock. Such hydrothermal alteration and mineralisation has made the Nigerian province a major world producer of columbite and cassiterite since early this century although the economic importance of ore production has declined in the last decade. Since 1905 when records began, more than 700,00 tonnes of cassiterite concentrate and 100,000 tonnes of columbite have been produced. The economic potential varies according to the style of mineralisation and the mineralogical association. Two distinctive mineralogical associations can be recognised: a pyrochlore-columbite type with rare earth enrichment and an oxide-sulphide assemblage with cassiterite, wolframite and sulphides. Of these associations the pyrochlore-columbite type is restricted to pervasive disseminations in granite cupolas although concentrations may occur in pegmatitic sheets and veins. The oxide-sulphide assemblage however, characterises a wide range of styles of mineralisation.

#### Styles of mineralisation

- (i) late magmatic pegmatitic pods with quartz, topaz, beryl and feldspar
- (ii) pervasive metasomatic disseminations with columbite or pyrochlore + cassiterite
- (iii) pre-joint and post-joint pegmatitic lenses with albite or microcline, genthelvite, uraninite, columbite and thorite
- (iv) quartz rafts, stockworks, sheeted greisen veins and pervasively altered hostrock with cassiterite, wolframite and sulphides
- (v) fissure filling veins or lodes with cassiterite, wolframite and sulphides
- (vi) irregularly shaped replacement bodies with cassiterite and sulphides
- (vii) quartz veins with wolframite or scheelite, bismuth minerals, sometimes abundant cassiterite and/or sulphides
- (viii) mineralised margins of ring dykes, with cassiterite and sulphides
- (ix) alluvial and eluvial deposits of columbite, cassiterite, zircon etc.

No particular type of hydrothermal alteration is restricted to one particular style of mineralisation and the classification is somewhat oversimplified. Thus it is possible to have disseminated sodic, potassic, acid or silica

metasomatism; altered ring dykes may show the effects of all the processes; pegmatitic pods may be generated at any hydrothermal alteration stage and fissure filling lodes may show all types of hydrothermal alteration with earlier alteration assemblages overprinted by later ones.

The different processes of fluid reaction, alteration and associated mineralisation characterise different parts of a granite pluton. These different structural environments of deposition can be regarded as five separate zones (Fig 6.1). In some complexes all the different zones may show some alteration and mineralisation. In the majority of complexes however, one or two zones may show evidence of mineralisation. Figs 6.2 and 6.3 show the location of mineralised areas mentioned in the text.

### Zones of deposition

**The roof zone.** The roof zone of an intrusion is characterised by disseminated mineralisation related to sodic, potassic or acid metasomatism, quartz rafts and sheeted vein systems, pegmatitic pods and veinlets, irregularly shaped replacement bodies and fissure-filling veins in the apical region eg. at Baban Damu, Banke (Fig 6.2) and at Ginshi Hill adit area, Ririwai (Fig 6.3).

**The marginal zone.** The marginal zone of the intrusion may extend over a horizontal distance of 200-500m inside the granite contact. It is characterised by stockworks, sheeted veins, associated wallrock alteration and pegmatitic pods containing a complex paragenesis of oxides and sulphides with greisenisation and silicification eg. at Rishi, in the Saiya Shokobo Complex.

**The contact zone.** The contact area occupies a zone ca. 20m on either side of the granite contact. The zone is characterised by stockworks, fissure-filling veins and intense alteration. If the country rock is basement, chloritic alteration is often very intense and massive sulphide deposits may occur. Beneath a volcanic cover, pegmatitic quartz, feldspar and genthelvite may occur.

**The country rock.** Where the country rock is basement, mineralisation occurs in quartz veins and stringers, or sometimes in marginal greisens. The quartz veins are wolframite- or scheelite-bearing with occasional bismuth minerals and sometimes abundant cassiterite or sulphides.

The country rock may consist of an ignimbritic pile which is poorly jointed. Mineralisation is restricted to thin stringers with cassiterite and sulphides. If the country rock consists of intrusions of earlier granites, thin, sheeted vein systems may occur where individual veins are of the order of 2mm-1cm wide. Often these veins are unmineralised, greisenised granite, although occasionally they contain cassiterite and sulphides.

**Ring dykes.** Circular, elliptical or polygonal granite porphyry ring dykes characterise many of the ring complexes. Mineralisation may occur as disseminations within the porphyry groundmass, along joint planes and along the inner and outer margin of the ring dyke. The mineralisation which is always sporadic and economically insignificant, is characterised by cassiterite together with a sulphide assemblage of ores dominated by sphalerite, chalcopyrite and galena.

Fig 6.1 Anatomy of a hypothetical mineralised ring complex

Country rock                      Roof zone                      Ring dyke  
Marginal zone                      Contact zone

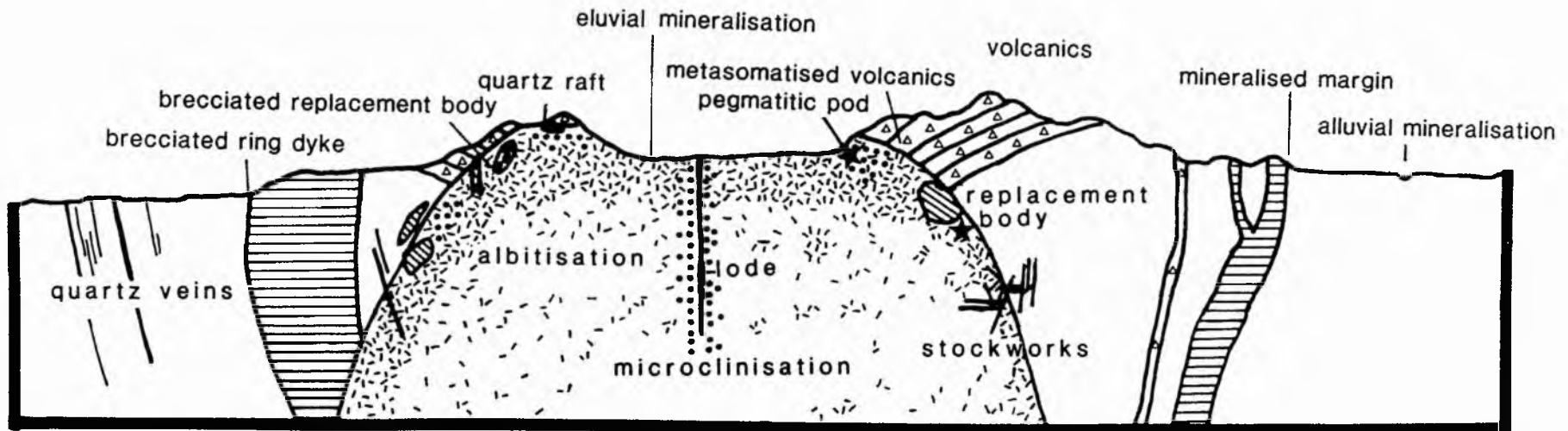


Fig.6.2 Younger granite complex map showing localities mentioned in the text

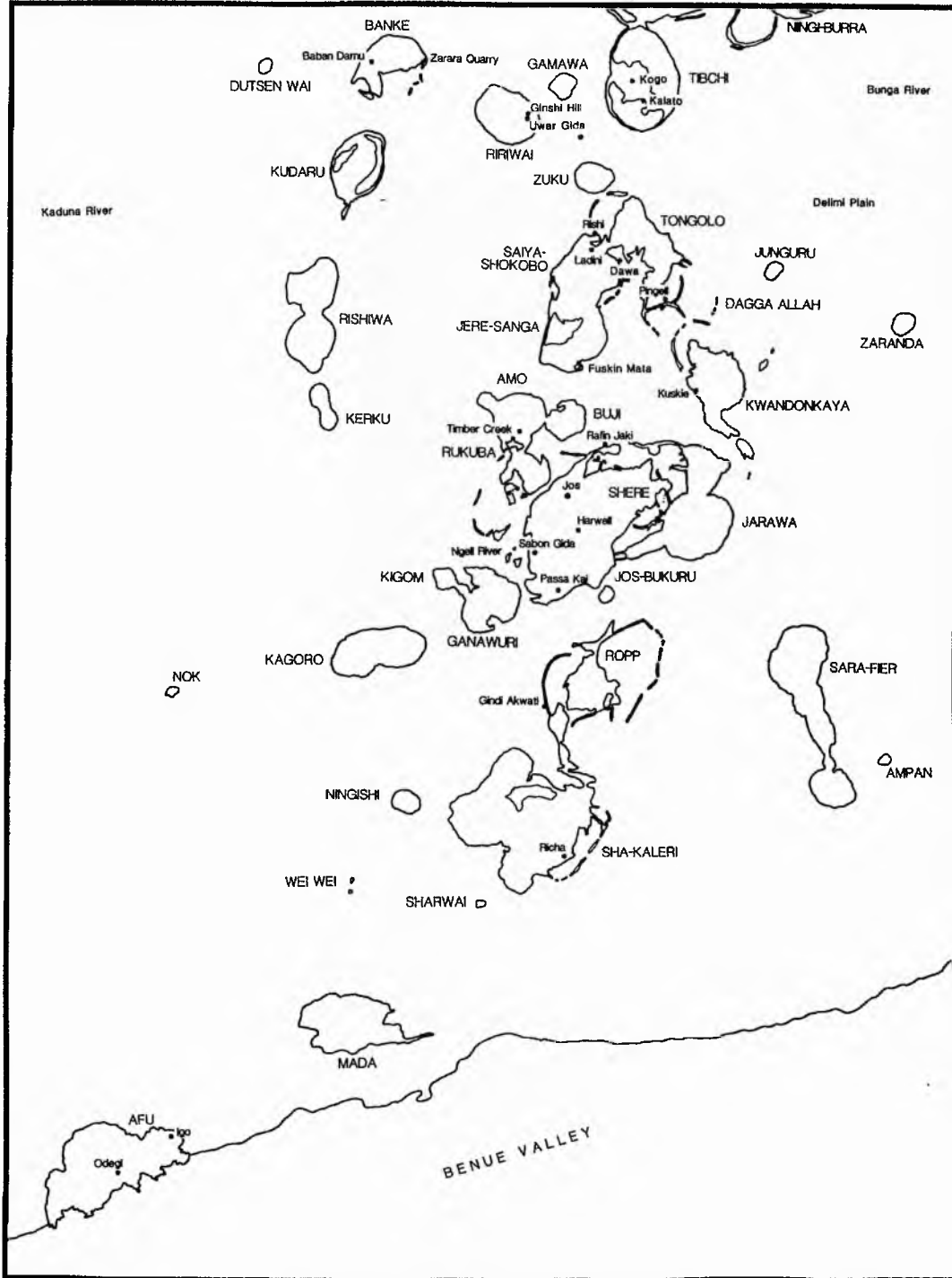
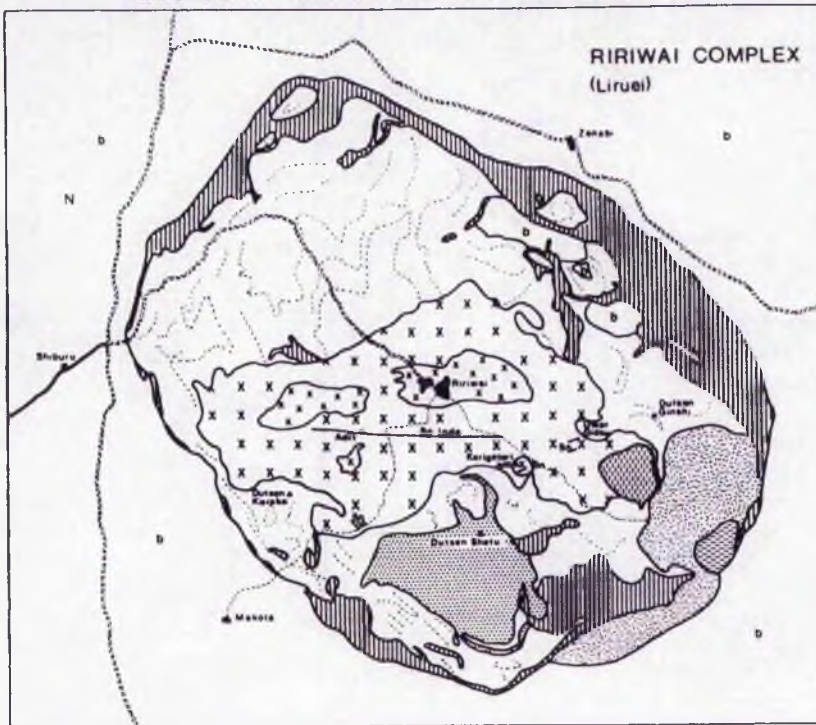


Fig 6.3 Generalised geological map of the Ririwai complex and schematic cross-section of the lode

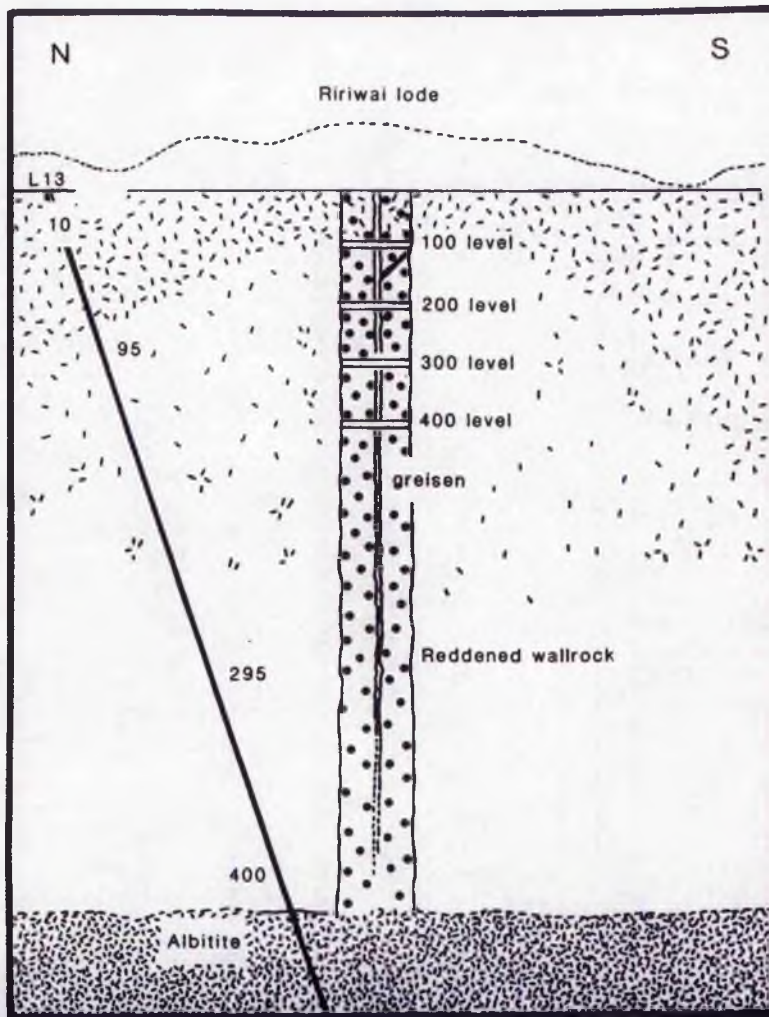


KEY

- Vein controlled Zn-Sn mineralisation
- Arvedsonite albite granite
- Biotite microgranite
- Biotite granite
- Arvedsonite aegirine granite

Scale 0 1 2 kms  
0 1/2 miles

- Arvedsonite granite porphyry
- Granite porphyry with calcian arvedsonite (inner fayalite and hedenbergite)
- Quartz fayalite porphyry with ferrohedenbergite and ferrichterite
- Agglomerates, rhyolitic ignimbrites and lavas locally intercalated with plagiophytic basalts
- Basement



## Styles of mineralisation

### (i) Pegmatitic pods and vugs (miarolitic cavities)

Generally the margins of the granites are not characterised by extensive pegmatitic development in miarolitic cavities. Where this does occur the resultant pods are sporadic and usually only of the order of a few centimetres or less (Plate 6.1). In the biotite granites these pegmatitic pods may be composed of clear or smoky quartz with long prism faces, alkali feldspar sometimes twinned, blue-green beryl, often of gem quality aquamarine, and colourless to pale blue topaz, also often of gem quality (Plate 6.2). Crystals rarely exceed 8cm in size but crystals of topaz and beryl are commonly 5cm.

The best known localities are at Timber Creek at the contact between the Tega biotite granite of the Amo Complex and the Teria biotite granite of the Rukuba Complex (Fig 6.2); near Kalato in the Tibchi Complex and near Kuskie in the Kwandonkaya Complex (Fig 6.2). Staley (pers comm) reports single aquamarine crystals growing in vugs in biotite granite near Igo in the Afu Complex (Fig 6.2).

### (ii) Pervasive metasomatic disseminated mineralisation

The most important phase of disseminated mineralisation was related to sodic metasomatism since disseminated potash metasomatism was not a widespread process and fracturing and fissuring of granites usually led to the channelling of late stage fluids into distinct tabular zones.

Disseminated mineralisation related to sodic metasomatism is characterised by the pyrochlore-columbite association of ore minerals which has been of major economic importance. Whilst the two minerals have been recorded together, one or the other is always vastly dominant so that pyrochlore is predominant in albitised peralkaline granites and columbite is dominant in albitised biotite granites.

a) The pyrochlore-bearing granites occur in six localities in Nigeria in the Ririwai, Dutsen Wai, Shere, Buji, Ropp and Kigom Complexes. The uranium-enriched pyrochlore forms distinct irregularly-distributed, honey-coloured octahedra accompanied by Th-rich monazite, cloudy prisms of uranium-, thorium- and hafnium-enriched zircon, amblygonite, stellate clusters of astrophyllite, cryolite, thomsenolite, villiaumite and sometimes narsarsukite and chevkinite. At each of these localities, the albitised peralkaline facies covers only a small area. The pyrochlore may contain up to 5%  $U_3O_8$ , but despite localised high concentrations, the heterogeneous dispersed nature of mineralisation over such small areas has proved to be too difficult and expensive to attract mining interest so far.

b) The columbite-bearing granites are more widespread than the pyrochlore-enriched type. Many of the alkali biotite granites of Nigeria show slight sodic metasomatism and enrichment in a series of oxide ores, principally columbite and cassiterite (Table 6.1), throughout the apical zone. Subsequent unroofing by erosion of these ore-rich apical zones has resulted in the

formation of economically important eluvial and alluvial ore deposits. Eluvial deposits are concentrated in soils which lie above or close to the source rock, whereas alluvial deposits have been transported, deposited and sometimes re-worked, by surface waters.

The most intense albitisation and highest primary enrichment of columbite occurs in localised parts of the Jos Bukuru complex and the Odegi area of the Afu complex. In these areas the granite has been decomposed to the consistency of clay by late stage argillic alteration (Plate 6.3). This allows the extraction of ore minerals by the use of monitors and gravel pumps. At Passa Kai, 12km south of Jos, the white granite forms sills and irregularly branching dykes, feathering out upwards into small white veinlets cutting the dark coloured schistose basement. There is a very large variation in columbite content from <30 to >2200ppm  $Nb_2O_5$  (Table 6.1)

In the Jos Bukuru complex at Harwell, 5km northeast of Bukuru (Fig 6.2), the columbite rich facies also contains abundant thorite, xenotime and monazite with traces of ilmenite, magnetite, and zircon. The zircon which forms brown, almost opaque crystals, contains up to 5% Hf. There is a substantial enrichment in heavy rare earth elements and also uranium in the ores, particularly in the thorite, xenotime, monazite and zircon (Table 6.2).

Another example of intense albitisation occurs in the Odegi area of the Afu complex (Fig 6.2). A white fine-grained, columbite-rich zinnwaldite albite granite forms an elliptical outcrop surrounded by pink perthite granite. It is approximately 3000m long and 1400m wide trending NE-SW with the greatest decomposition and columbite enrichment along the northern and southern margins. The average grade described by Jones (1953) is equivalent to 1200 ppm, with an average  $Nb_2O_5:Ta_2O_5$  ratio of 13:1. This grade has decreased with depth of working.

In general however, the petrological evidence of sodic metasomatism is not well preserved in many complexes. This is due, either to unroofing of the granite to a depth below the sodic metasomatised apical zone, or because continued fluid reactions through falling temperature and changing fluid composition have overprinted this earlier process.

### (iii) Pegmatite pods and lenses

Pegmatitic pods and lenses can occur at any stage of hydrothermal alteration, with albite, microcline, Li-Fe biotite or quartz as the main mineral depending on the stage of formation. These pegmatites are sporadically distributed and unimportant in economic terms. They are <1.5 m in maximum diameter or width and are traceable over outcrop distances of less than 100 m. The largest bodies occur as lenses which are characterised by abundant albite or microcline feldspar. At Harwell in the Jos Bukuru complex (Fig 6.2), both albite and microcline pegmatites occur cutting the decomposed columbite-bearing zinnwaldite albite granite in a disused mining paddock. The earlier of the two types, the albite pegmatite, is commonly sinuous in form and <1.5 m in width. It contains occasional patches of genthelvite, associated Li-siderophyllite and accessory thorite and columbite. The later microcline pegmatites are strongly tabular in form (Plate 6.4), commonly only a few centimetres wide and are characterised by green amazonite as a major constituent with some quartz, Li-siderophyllite,



Plate 6.1 Pegmatite pod

with quartz and siderophyllite - margin of Rishi biotite granite



Plate 6.2 Minerals from pegmatite pods

left to right: twinned microcline, topaz, aquamarine and smoky quartz





Plate 6.3 Argillised paddock (quarry) floor

The floor of paddock 8838 showing the intense argillic alteration and veins of kaolinite. Jos Bukuru complex.



Plate 6.4 Microcline pegmatite

Microcline pegmatite in the Harwell pegmatite which in addition to green 'amazonite' contains a little quartz, zinnwaldite, genthelvite and microlite. Jos Bukuru complex.

Table 6.1 Columbite, cassiterite and zinc concentrations in the Rayfield Gona biotite albite granite from the Jos Bukuru Complex

Harwell Area				Jantar Area			
	Nb <sub>2</sub> O <sub>5</sub>	SnO <sub>2</sub>	Zn	PCP	Nb <sub>2</sub> O <sub>5</sub>	SnO <sub>2</sub>	Zn
8838	90	25	108	10A	40	20	108
88A	770	200	100	10B	30	20	100
88B	510	165	105	10C	30	20	105
88C	460	165	315	10D	900	520	137
88D	470	70	174	10E	2290	1450	132
88E	610	140	249	10F	1200	68	87
88F	55	50	117	10G	30	20	135
88G	470	130	113	10H	1280	350	128
88H	770	50	84	10J	1720	430	100
88J	520	56	203	10K	750	360	104
88K	1115	50	158	10L	500	20	183
88L	590	120	419	10M	1050	28	193
88M	630	120	nd	10N	820	20	173
88N				100	320	20	100
88/1127B				10P	40	20	95
A	100	-	nd	10Q	40	20	142
B	1300	1433	nd	10R	430	20	84
C	1140	830	nd	10S	33	20	100
D	1000	650	nd	10T	33	20	126
				10U	450	20	206
				GPA	50	50	107
				B	33	-	131
				C	33	-	50
				D	50	-	151

All values in ppm  
Data from Kinnaird 1977

Table 6.2 Ore mineral assemblages related to styles of mineralisation

style	major minerals	accessory minerals	ore assemblage
i) late magmatic pegmatitic pods	quartz-alkali feldspar	beryl, topaz	
ii) pervasive metasomatic disseminations	quartz-albite quartz-microcline quartz-mica	thorite, xenotime, monazite, zircon zircon,	columbite, ilmenite, cassiterite pyrochlore cassiterite, wolframite, molybdenite cassiterite
iii) pre-joint and post-joint pegmatitic lenses	quartz-albite quartz-microcline	genthelvite, protolithionite, thorite zinnwaldite or protolithionite, beryl, genthelvite	columbite uraninite, microlite
iv) quartz rafts, stockworks, sheeted greisen veins and altered wallrock	quartz quartz-mica	genthelvite topaz, fluorite	cassiterite, haematite cassiterite, sphalerite, chalcopyrite
v) fissure filling veins or lodes	quartz - microcline - mica	monazite, thorite, xenotime, zircon	cassiterite, columbite, wolframite, rutile, sphalerite, molybdenite, stannite pyrite, arsenopyrite, chalcopyrite, pyrrhotite, bismuth minerals galena
vi) irregularly shaped replacement bodies	quartz-mica	fluorite, siderite, chlorite	cassiterite, wolframite bismuthinite, sphalerite, chalcopyrite, pyrite
vii) quartz veins	quartz	haematite	wolframite, cassiterite, bismuth minerals
viii) mineralised margins of ring dykes	quartz-microcline-mica	fluorite	sphalerite, chalcopyrite and galena with pyrite, pyrrhotite, stannite arsenopyrite, molybdenite and cassiterite
ix) eluvial and alluvial deposits	quartz	zircon, monazite, xenotime, thorite fergusonite, allanite, sphene	cassiterite, columbite, ilmenite, magnetite, rutile, pyrochlore

The list of accessory and ore minerals is rarely complete at one locality. Instead the list is intended to convey the impression of what might be found.

genthelvite and microlite (Kinnaird 1977).

A uraninite-bearing albite pegmatite with quartz and genthelvite occurs in the Saiya Shokobo Complex. Uraninite forms as small black crystals approximately 1 mm in size, clustered on the feldspar crystals. The pegmatite is associated with greisens that have developed along both horizontal and vertical joints. A similar relationship between pegmatite and greisen occurs in the Baban Damu area of the Banke Complex, 5 kms WNW of Banke school. Here, sinuous quartz, albite, green-mica pegmatites, containing knots of blue-green aquamarine, lie approximately parallel to horizontal greisens which are interlinked by vertical greisens.

In the northern complexes where peralkaline granites predominate pegmatitic lenses have also been noted in amphibole-rich granites. In these, the mineralogy is limited to feldspar accompanied by amphiboles up to 5cm in size (Plate 6.5).

(iv) Quartz rafts, sheeted greisen veins and stockworks

Quartz rafts characterise the roof zone of a biotite granite cupola. They occur at the contact zone between the granite and the overlying volcanic pile where the volcanics have not fractured to allow fluid escape. They are not common throughout the Province possibly because the right erosional level is exposed in so few complexes. Nor are they richly mineralised although there does seem to be an enrichment in ore minerals beneath the rafts. The best developed is at Uwar Gida near Ginshi Hill, Ririwai. Here in the roof zone, the biotite granite is very reddish in colour: this is partially due to microclinisation of feldspars but also due to the abundance of genthelvite in the roof zone. Between genthelvite-rich microgranite and the banded volcanics lies a zone of pure massive, milky quartz up to 2 m thick, linked to vertical quartz veins which cut the genthelvite microgranite (Plate 6.6). Although the quartz is only slightly mineralised, the underlying stockwork within the top 30 m of the granite roof is richly mineralised and has been worked by trenching and adits, mainly for cassiterite. The sulphides, which have not been worked, appear to be disseminated below the main cassiterite horizon.

Sheeted greisen veins and stockworks characterise the marginal and contact zone of a biotite granite. Sheeted greisen veins consist of a series of thin, subparallel veins (Plate 6.7). They are found in many complexes but are particularly well developed in the Ladini area of the Saiya Shokobo Complex and in the Banke Complex. The sheeted veins may be subhorizontal as at Baban Damu, Banke (Plate 6.8), or steeply dipping as at Saiya Shokobo. These steeply dipping sheeted greisen veins look very similar to the sheeted veins of Cligga Head, Cornwall. Individual veins may vary from 1 mm to 0.5 m and usually consist of a greisen assemblage of quartz-siderophyllite, occasionally with a thin central stringer of quartz. The stockworks are similar to the sheeted veins except that they do not occur as parallel veins but as a series of anastomosing ramifications within the marginal or contact zone of a granite intrusion. Mineralogically the veins systems are characterised by quartz, pale or green coloured Li-Al or Li-Fe mica usually with abundant topaz and fluorite, cassiterite, or more rarely traces of sulphides.

The stockworks and sheeted vein systems are much smaller and have a much simpler paragenesis than the fissure filling lode systems.



Plate 6.5 Peralkaline pegmatite.

Large crystals of arfvedsonite with alkali feldspar and quartz in a pegmatite from the Shira complex.



Plate 6.6 Quartz vein cutting genthelvite-rich mineralised granite in the roof zone of the Ririwai biotite granite at Uwar Gida. Immediately above this a 2m wide quartz raft separates the granite from the volcanics.

6.5



Plate 6.7 Steeply dipping sheeted veins from the Banke complex (B64)



Plate 6.8 Horizontal sheeted veins near Baban Damu, Banke complex

6.7



Plate 6.9

The adit at the western end of the Ririwai lode has exploited a series of braided ore-bearing quartz and greisen veins for cassiterite and wolframite. The reddened 'microclinised' wallrock also contains cassiterite, wolframite and sphalerite. The width of the lode here is about 6m.



Plate 6.10

Bladed wolframite crystals up to 1.5cm long, oriented perpendicular to the strike of the vein. B65, Banke complex.

69.

(v) Fissure filling lodes.

Only two major lodes have been noted in Nigeria and these occur in the biotite granites of the adjacent complexes of Tibchi and Ririwai. In both complexes the central biotite granites have an elliptical shape and the lodes tend to follow the central axis. In the Tibchi complex the elliptical intrusion has a long axis orientated northwest-southeast whereas in Ririwai the axis of the ellipsoid intrusion lies east-west with an east-west orientation to the lode (Fig 6.3 & 4).

In both complexes the lodes are the product of several alteration processes with fluids channelled in enlarged steeply dipping tectonic master joints, which opened during the continued uplift stage. There were several phases of deposition of the major ore minerals during successive phases of hydrothermal alteration and mineralisation was repeatedly emplaced in the same lode system.

The Ririwai lode extends for a distance of 5 km in an east-west direction and to over 400 m depth and dips to the south at  $85^{\circ}$ . The maximum surface width of the lode system is 8 m. The lode, which is extensively mineralised, consists of a series of parallel to subparallel or braided quartz veins enclosed by zones of grey greisen grading outwards through reddened microclinised wallrock into the pale pink equigranular biotite perthite granite (Plate 6.9).

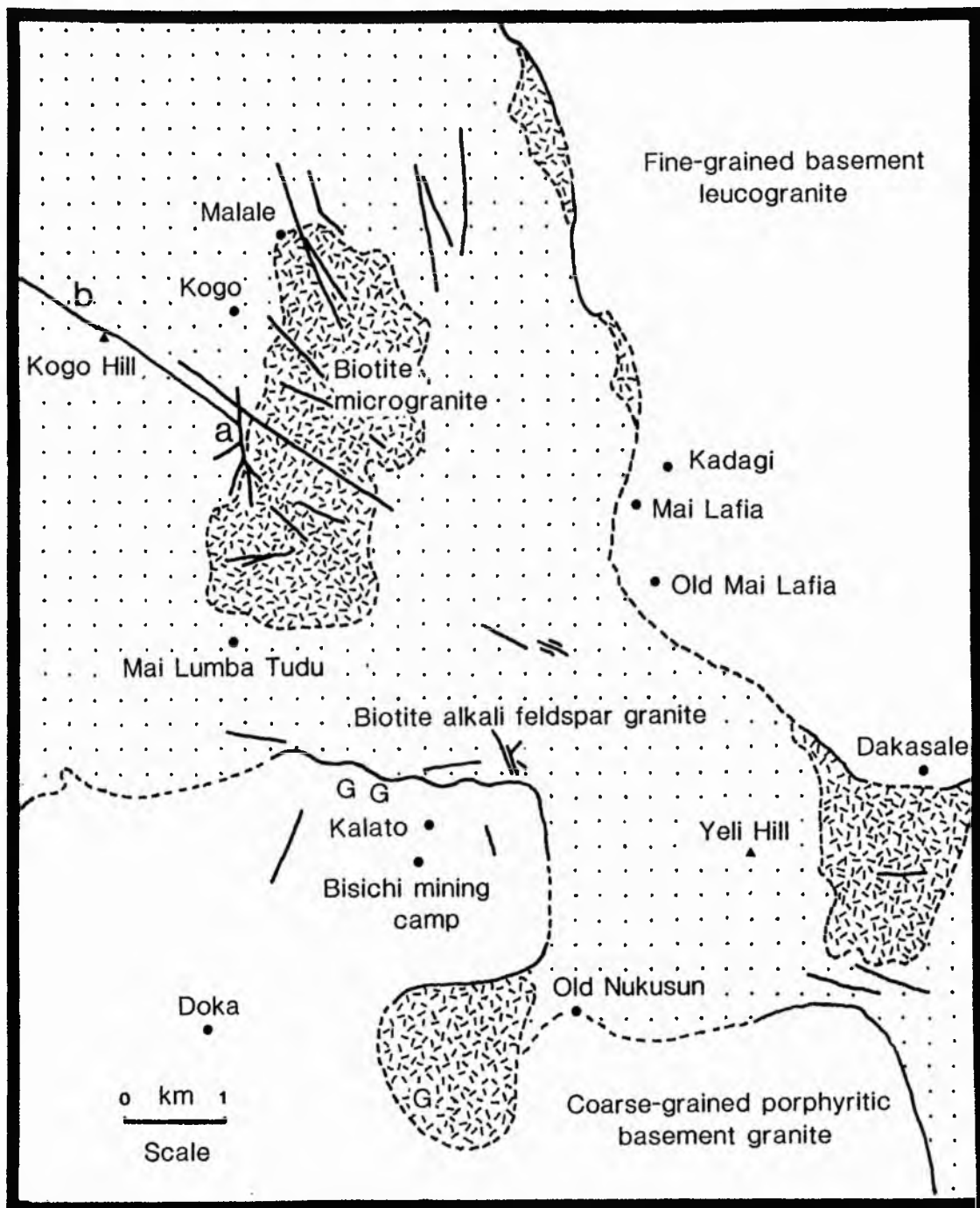
There are two lode systems in the Tibchi complex forming a letter Y. One orientated north-south (labelled (a) on Fig 6.3, between 3 and 15 m wide and strike length of at least 1 km (Rockingham 1951); the other (labelled (b) on Fig 6.4), is orientated northwest-southeast, with similar dimensions and a strike length of over 2 km. The north-south lode consists in the south of reddened quartz veins rich in cassiterite and wolframite with an almost complete absence of sulphides. The northwest-southeast lode follows the main axis of the elliptical biotite perthite granite. It is similar to Ririwai with a reddened microcline rich outer facies grading through a greenish grey greisen to fissure filling quartz, which is sometimes massive and milky, sometimes well crystallised. The lode is well exposed on Kogo hill which rises 100 m above the surrounding biotite granite.

Unlike the Ririwai complex, the Tibchi mineralised veins extend out into the basement which overlies the biotite granite but in both complexes the lode system is confined within the outer ring dyke.

The lodes are rich in cassiterite and wolframite and have been surface mined on a small scale for many years. About 50 tons of wolframite were extracted from the Ririwai lode during 1939-1945. At depth, a sulphide assemblage of ores is also abundant but the weathering and decomposition of the sulphides at the surface has given a false impression of the relative abundance of the sulphide and oxide ore assemblages. In both complexes sphalerite is the major ore mineral. In Ririwai this is about 1.5%, followed by cassiterite with 0.5%.

The Ririwai lode has been opened up as an underground mine and is currently being assessed for future production of primary cassiterite as alluvial ores are depleted. It is estimated that when in production the mine will produce 1600 tonnes of tin metal a year and 6000 tons of zinc metal. The Tibchi lode has been drilled and assessed for ore producing potential but has not yet been opened up

Fig 6.4 Location map of the mineralised localities in the Tibchi Complex (based on Ike, 1979)



underground.

(vi) Irregularly shaped replacement bodies

Irregularly shaped replacement zones containing massive or disseminated ore may occur in the roof and contact zones of biotite granite bodies. Generally they are composed of mica-rich greisens formed by acid metasomatism of granite already altered by potash metasomatism. The green coloured mica is in the compositional range Fe siderophyllite to Li siderophyllite and is accompanied by quartz-fluorite-siderite with cassiterite and sulphides. The best examples occur in the Rishi biotite granite and at Igo in the Afu Complex.

At Igo the host granite is coarse-grained biotite perthite granite. In the mineralised zone, deposition of cassiterite and wolframite accompanied by siderite was followed by massive sphalerite and chalcopyrite, with pyrite and green fluorite formation. The dark iron sphalerite with up to 17% Fe forms massive well twinned crystals <25 cm in size which are brecciated and re-cemented by late stage wolframite bearing quartz veins. Brecciation probably took place during sphalerite formation as the chalcopyrite exsolution blebs within the sphalerite are elongated into rods. The sphalerite clasts often have a thin crust of quartz crystals. The ore bodies were first worked by opencast techniques and a block of cassiterite weighing 9 tonnes came from here. The area was also a major source of wolframite during the 1940-45 war.

vii) Quartz veins

The quartz veins are generally vertical and vary from massive milky veins 30m wide to clear comb-textured veins, 1 cm wide. Virtually all the granites of the Province show late-stage quartz veining but only those granites which have disseminated mineralisation have ores within the quartz veins. Mineralised exogenetic quartz veins also occur in the basement within 1 km of a younger granite.

Wallrock alteration may occur marginal to the quartz veins or the veins may infill fissures in a lode system with mineralised greisen, as at Tibchi and Ririwai. Also the quartz veins may cut the granite or country rock without any marginal alteration.

The quartz veins that occur in the basement are generally characterised by wolframite of ferberite composition (Plate 6.10). The wolframite occurs sporadically as bladed crystals, at the margin or vein centre, orientated parallel or perpendicular to the strike of the vein. The wolframite is accompanied by some cassiterite and minor sulphides and often by bismuth minerals. Well cleaved leaves up to 2 cm in size of native bismuth have been found in several complexes. South of Richa scheelite occurs in quartz veins with selvages of greisen which cut basement granitoids.

The wolframite-rich quartz veins of the Dagga Allah area occur at a greater distance from the younger granites than is usual. It seems likely that they are related to younger granite which may exist at shallow depth within the Dagga Allah ring dykes. Geophysical prospecting supports this possibility (Ajakaiye et al 1983).

The quartz veins within the younger granites such as in the Ririwai lode, may contain a wider spectrum of ore minerals than those of the basement.

#### viii) Mineralised ring dyke

In many complexes, the ring dyke fractures have been intruded by granite porphyry with phenocrysts of pink or white feldspar showing arrested growth forms, set in a fine-grained matrix. Fluids escaping along these steeply dipping fractures locally reacted with, and mineralised the porphyry. Where fluid interaction has occurred, the fine-grained matrix has been largely altered to a greisen assemblage leaving the perthite phenocrysts unaltered or partially transformed to microcline. Often these petrological changes are limited to narrow zones although the degree of reaction may be locally intense (Bowden and Kinnaird 1984a). Examples of mineralised granite porphyries are known from Zarara Quarry in the Banke Complex, near Pingell in the Dagga Allah complex, at Rafin Jaki in the Jos Bukuru complex, from Gindi Akwati in the Ropp complex and south of Richa in the Sha Kaleri complex.

The mineralisation is characterised by a sulphide assemblage of ores dominated by sphalerite, chalcopyrite and galena, with pyrite, pyrrhotite, stannite, arsenopyrite and molybdenite together with scheelite at the Richa locality.

At Zarara quarry, the porphyry of the outer margin of the eastern ring dyke of the Banke Complex has been brecciated and cemented by mineralising fluids and late stage vein quartz. Mirolitic cavities lined with microcline contain elongate prismatic quartz crystals (Plate 6.11).

At Gindi Akwati in the Ropp Complex the ring dyke has brecciated, metamorphosed and permeated an earlier basic dyke. The breccia has been cemented by pale coloured mineralised veins in which quartz or fluorite may be the main gangue.

#### ix) Alluvial and eluvial mineralisation (Plate 6.12)

During the partial unroofing of mineralised granite cupolas due to uplift and erosion, the ore minerals have been removed only to be redeposited in eluvial and alluvial deposits. The richest alluvial concentrations occur within the vicinity of granite cupolas that have only undergone shallow erosion.

Uplift of the central part of Nigeria which began in Neogene (Kogbe 1981) led to the formation of an upstanding area known as the Jos Plateau, in the Jos-Bukuru area. The Plateau, which rises >400 m above the surrounding basement plain, has an above average rainfall for this part of Nigeria, resulting in more rapid denudation of the granite cupolas. The Plateau region forms a major watershed so the ore minerals eroded from the granites are widely distributed in the modern river systems and are readily worked due to the almost perpetual availability of water.

During the Pleistocene in Nigeria, thick deposits of cassiterite and columbite-bearing alluvium were laid down in broad shallow valleys on the Jos Plateau. These deposits are the target for extensive mining activity especially in the Ngell River area, 12km southwest of Jos. Large reserves of high grade



Plate 6.11 Mineralised porphyry from Zarara quarry, Banke complex. The porphyry of the eastern ring dyke has been brecciated. Greisen and quartz veins carry cassiterite and chalcopyrite with fluorite.



Plate 6.12 Mining in paddock 1373, Jos Bukuru complex.

6.11

placer deposits are still preserved beneath Quaternary to Recent basalt flows which filled some of the broad shallow valleys. More than 95% of Nigeria's tin export is produced from alluvial deposits. These alluvial placer deposits occur as gravel pockets in both ancient and modern stream channels. Grades may have been as high as  $1.5 \text{ kg m}^{-3}$ , but are nowadays nearer to one-tenth of this.

Columbite is also an important alluvial ore mineral in Nigeria, although production is much less than that of cassiterite. Whilst there is a small production of pegmatitic columbo-tantalite from the basement, the vast bulk of the material has been derived from primary, eluvial and alluvial deposits associated with sodic metasomatism of some of the anorogenic granites.

Alluvial monazite, thorite, zircon, pyrochlore, ilmenite, magnetite and xenotime separates from these placer deposits have all been sold sporadically according to world price with annual combined exports from 0 to 1000 tonnes.

Most of Nigeria's tin production has come from alluvial deposits derived from an area within a radius of 50km of Jos and because alluvial workings are situated principally on the Jos Plateau, it has often been incorrectly assumed that mineralisation is restricted to this small area in northern Nigeria. In fact similar alluvial mineralisation related to many of the complexes has been recognised in Nigeria, together with the petrologically similar, but chronologically older anorogenic granites in Niger. The pre-eminence of the Jos Plateau as a tin and columbite producer therefore is due to the abundance of granitic plutons, the physiography and radial drainage of the Plateau, combined with an abundant all-year round water supply to work the deposits.

#### Economic exploitation and future potential

Nigeria has long been known for its cassiterite and columbite production. Production of cassiterite was of the order of 10,000 tonnes annually for many years. Between 1905 and 1971 about 630,000 tonnes of cassiterite was exported (Kogbe and Obialo 1976) with maximum production in 1946 when 14,225 tonnes of concentrate containing between 72 and 74% tin was produced. Production declined in the 1970's to a little over 3800 tonnes in 1979 and by 1983 had fallen to about 1700 tonnes. Virtually all the cassiterite was exported as concentrate until 1962 when a tin smelter was commissioned in Jos. Since then the tin is exported as tin metal.

Prior to 1965, 95% of the world's columbite consumption was supplied by Nigeria and since 1933 approximately 100,000 tonnes of columbite have been extracted from primary and alluvial sources and production fluctuated between 100 and 2000 tonnes annually. Peak production was in 1963 when 3334 tonnes were exported. Since the mid-1970's production declined dramatically to less than 400 tonnes in 1981.

There is future potential for minerals of both the pyrochlore-columbite association and the oxides-sulphide assemblages:-

Pyrochlore introduced during sodic metasomatism of peralkaline arfvedsonite granites in Nigeria could have an economic potential. The pyrochlore may contain up to 5%  $\text{U}_3\text{O}_8$ , but despite localised high concentrations, the albitised peralkaline facies covers only a small area and the heterogeneous dispersed

nature of mineralisation over such small areas has proved too difficult and expensive to attract mining interest so far. In addition cryolite which forms several modal percent in some of the albitised facies may become a commercial proposition. In addition to large tonnages of disseminated Nb, rare-earths, zirconium, yttrium, thorium and uranium clearly have potential although commercial primary values are on a small-scale and too sporadically distributed to envisage any economic exploitation in the near future.

In Niger uranium occurs in upper Palaeozoic and lower Mesozoic continental basins west of the Air mountains. Bowden et al (1981) have shown that the original source of the uranium was alkaline ignimbrites preserved in Palaeozoic anorogenic complexes. The original ignimbrite was enriched in uranium, a considerable portion of which was leached during weathering of the volcanic pile. Tectonic uplift, anorogenic plutonism, followed by weathering and erosion of the volcanic cover, with sedimentation in nearby basins, have all contributed to the uranium mineralisation which is exploited at Arlit in Niger. The geochemical and petrological similarities between the complexes in Niger and Nigeria suggests that there is potential in Nigeria for secondary uranium deposits if the tectonic and sedimentological controls were favourable. Enriched U/Th concentrations occur in the Nigerian granites with the pyrochlore-columbite type of mineralisation and veins and pegmatitic pods with traces of uraninite also occur. The most likely hosts for secondary uranium mineralisation would seem to be the Cretaceous-Tertiary sedimentary sequences in the Benue trough (Fig 6.2), but no significant deposits have been found so far. Uranium deposits could still be discovered particularly in the drainage systems entering the Chad basin.

The greatest potential for the immediate future however, is for the minerals of the oxide-sulphide association:-

In Nigeria total reserves of cassiterite and columbite are estimated to be in the order of 140,000 and 70,000 tonnes respectively, sufficient only for several years production at existing rates. There is the potential for exploitation of sub-basaltic tin deposits of the Ngell Valley near Jos. As the alluvial ores become exhausted and tin prices rise, more attention will inevitably be centred on the primary ore distribution. The major lodes of the Ririwai and Tibchi complexes may well present an attractive commercial proposition. Already a pilot mine has been set up by the Nigerian Mining Corporation at Ririwai and preliminary exploitation has been completed at Tibchi. As cassiterite is accompanied by sphalerite and galena in these lodes the commercial prospect will be improved with the availability of a smelter linked to lead-zinc production in the Benue Valley. Further into the future, mineral potential may well be located in granite cupolas still unexposed beneath a volcanic cover.

Wolframite occurs in many of the complexes. However, unlike many of the other oxide ores wolframite does not survive in the alluvial deposits and is extracted only from primary deposits. In most cases although the wolframite is locally abundant, large areas of the veins are barren which makes prospecting and comparison of tungsten values difficult. In Nigeria, production reached a peak in 1939 when 240 tonnes were produced. During the period 1950-1960, 77 tonnes were exported but since then the payable deposits have been exhausted and production has virtually ceased.

In Nigeria there may also be a future potential for molybdenum. Small flakes

of molybdenite are common in mineralised veins and altered granite throughout the province, but the only large scale occurrence is in the riebeckite aegirine granite in the Kigom Hills. The molybdenite occurs near the vertical contact between a riebeckite aegirine granite and the basement. It is scattered through the granite in rich clusters of skeletal rosettes several centimetres across and in small disseminated flakes; it also forms a coating on joint surfaces. Although small pockets of granite are rich in molybdenite, the average concentration is low. During the period 1962-1972, 33 tonnes of molybdenite was produced from the Kigom locality. In 1967 Chartered Mining Limited undertook an investigation on the molybdenite deposit and more recently the same deposit has been prospected by Billiton International. However, no further development has taken place and molybdenite production has ceased. Near this molybdenite-bearing granite a galena-rich vein, rich in silver has been worked in the Kigom river valley. Most of the galena throughout the province is argentiferous but again deposits are so far too small to warrant interest.

Gold may accompany minerals such as bismuthinite etc. in late-stage alteration assemblages in replacement bodies and quartz veins. Placer deposits derived by erosion may occur in and around some complexes and have economic potential for the future, although this seems unlikely.

The economic prospects for the future will obviously depend on world market price. However, local development of infrastructure is also important. As road networks increase and accessibility is improved more remote areas of mineralisation, previously unworkable may become economically viable.

#### Summary

There is a wide range of styles of mineralisation ranging in size from small-scale pegmatitic pods to major disseminated ore deposits. From the economic viewpoint the most important styles are the disseminated columbite deposits associated with pervasive metasomatism and the placer deposits of alluvial and eluvial cassiterite, columbite and other ores.

However, even within these two economically important different styles of mineralisation there is a wide range of accompanying ore minerals and these are summarised in Table 6.2.

## SUMMARY OF PART I

The Nigerian anorogenic province is characterised by more than 50 complexes. In some complexes, the outer limits of the complexes are defined partly or completely by a ring dyke. This intrusion, generally composed of granite porphyry, was the chief structural element of the complex and controlled the distribution of both volcanic and subvolcanic magmatism at high levels in the crust.

The complexes are exposed at different erosional levels: in some complexes, particularly in the north, the volcanic products are preserved through caldera collapse; in other centres the volcanic cover has been removed so that the subvolcanic granites and syenites have been exposed.

Where the volcanic rocks have been preserved by downfaulting of the caldera the magmatic evolution of the anorogenic centres can be clearly established. Although the majority of the volcanics are dominantly rhyolitic, some alkaline centres have preserved occasional successions of hawaiites, mugearites and trachytes confirming the dominantly alkaline trend from transitional ne-normative or hy-normative basalts.

The subvolcanic assemblages include minor gabbros, monzogabbros and syenites. However granitic rocks are overwhelmingly dominant with fayalite hedenbergite granites, amphibole granites and syenites, albite-rich and albite-poor aegirine arfvedsonite granites and biotite granites.

As far as the granites are concerned there is a natural progression from volcanic feeder intrusions to subvolcanic intrusions with fayalite and hedenbergite. The volcanic feeder intrusions were an important link during the caldera-forming stage between the subvolcanic roots and the overlying volcanic pile. They are represented by quartz and granite porphyries.

The mineralogical assemblages of many of these complexes however, is often the result of interaction with residual fluids. Fluids affect the late magmatic and particularly the postmagmatic (subsolidus) crystallisation history of a cooling subvolcanic pluton and to some extent the overlying volcanic pile. Such hydrothermal alteration has undoubtedly modified the original granite chemistry and has been responsible for the introduction and dispersion of ore minerals.

Using geochemical data, particularly the trace element monitors of Zr/Hf, together with petrographic studies, it can be shown that many of the rock types of the alkaline complexes have been geochemically modified in the subsolidus. The acid volcanics show effects of devitrification by hydrothermal alteration. Similarly, hydrothermal effects can be seen in virtually all the subvolcanic rocks and it is only the fayalite granites and quartz porphyries which seem to have been relatively unaffected by late-stage reactions. From a geochemical point of view these feeder intrusions can be used to assess the dominantly magmatic features of anorogenic magmatism since they show only a slight imprint of subsolidus modifications. It is only in the granite cupolas with shallow outward-dipping contacts where fluids were retained, that metasomatic reactions were most intense.

There were four periods of hydrothermal alteration that were important economically; sodic metasomatism (albitisation), potassic metasomatism (microclinisation), acid metasomatism (greisenisation) and silica metasomatism (silicification). Later lower temperature processes of alteration such as zeolitic or argillic alteration also occurred but they were more restricted in occurrence and limited in economic importance since no new ores were added at these stages.

On textural and field evidence the earliest process of alteration was sodic metasomatism. This process occurred before joining or faulting of the granites and its effects were therefore disseminated throughout a granite roof zone. The mineral assemblages generated depended on the intensity of rock-fluid reaction and on the initial mineralogy of the original rock type. In both the peralkaline and biotite granites however, the process was characterised first by the coarsening domains in perthite and with increasing rock-fluid reaction, laths of albite were generated at the expense of the perthite.

Potash metasomatism which followed sodic metasomatism may also have been a disseminated process. In other instances it was restricted to alteration pods in the granite margins and immediately beneath the volcanic cover, whilst in the Ririwai and Tibchi complexes, potash metasomatism affected fissure wallrocks. Mineralogically the process was characterised by microclinisation of feldspar due to the partial or complete replacement of sodium by potassium in the feldspars.

Feldspar alteration was linked to the growth of new mica and as the process of acid metasomatism succeeded potash metasomatism, there was a progressive breakdown of perthite or microcline feldspar which produced further Li-Al or Li-Fe micas. This mica-quartz assemblage development, which is universally known as greisenisation, may have been locally pervasive within a granite roof zone, or it may have been concentrated along fissures and fractures as in the case of sheeted veins or lode systems.

The final major process of hydrothermal alteration and ore formation was silica metasomatism. Like potash and acid metasomatism, the process may have been pervasive or vein-controlled. Quartz was deposited in vugs or fissures or replaced all earlier formed minerals.

Each of the processes of hydrothermal alteration was characterised by a different assemblage of ore minerals. Sodic metasomatism generated a pyrochlore-columbite association whilst a varying oxide-sulphide assemblage of ore characterised the later hydrothermal processes.

The PVTX nature of the fluids which were responsible for hydrothermal alteration have been monitored by a study of fluid inclusion characteristics in selected samples. During sodic metasomatism loss of  $\text{CO}_2$  appears to have been important for the deposition of uranium-enriched pyrochlore. Fluids were saline and ranged in temperature from  $>600^\circ\text{C}$  to less than  $300^\circ\text{C}$ . Potash metasomatism occurred over a similar range of temperatures although much of the  $\text{CO}_2$  had been lost from the fluid by this stage. The process cannot have been entirely temperature dependent and the  $\text{Na}^+/\text{K}^+$  ratio in the fluid must have been largely responsible for determining which process operated. Pervasive acid metasomatism resulted from fluids that were in the temperature range  $420\text{--}220^\circ\text{C}$  and which were

subject to periodic boiling particularly in the temperature range 350-380°C. A minimum depth of 0.1km has been assessed for the pervasive acid metasomatism of the Ririwai complex. Vein-controlled acid metasomatism generally took place in the temperature range 270-380°C from Na-Cl-F fluids that boiled as pressure was released in fissures and along incipient fractures. Major cassiterite deposition took place from 380-300°C in greisens from fluids that were boiling. Silicification occurred at less than 380°C with deposition of quartz down to temperatures less than 70°C from fluids that were gradually decreasing in salinity.

The residual fluids which were responsible for hydrothermal alteration also carried ore metals which were variously deposited at different stages of hydrothermal alteration. Mineralisation of a pluton generally occurred in the apical or marginal zones or in satellite dykes. Different styles of mineralisation tend to characterise different parts of a granite pluton and five separate zones have been recognised.: the roof, marginal and contact zones of a pluton, the enclosing or overlying rocks and the surrounding ring dyke. Nine different styles of mineralisation have been identified including pervasive metasomatic disseminations; pegmatitic pods and lenses; stockworks and lodes. No particular type of hydrothermal alteration is restricted to one particular style of mineralisation and it is possible to have disseminated sodic, potassic, acid or silica metasomatism and altered ring dykes may show the effects of all these processes.

The economic potential varies according to the style of mineralisation and the mineralogical association. The pyrochlore-columbite association with rare earth enrichment has been economically important; the majority of the columbite has been extracted from eluvial and alluvial sources and from extensively decomposed primary rocks. Of the oxide-sulphide assemblage with cassiterite, wolframite and sulphides, cassiterite is the most important ore mineral. It has been mined almost exclusively from alluvial deposits. Wolframite has been extracted from stockworks and quartz veins in the past. At the current time however, there is no mining of either wolframite or sulphides although there are plans to extract sulphides in the near future from the lodes of Ririwai and Tibchi.

The early chapters in this thesis are a summary of research work by the Nigerian Younger Granite Research Group led by Dr. P. Bowden during the years 1973-1981. The author's contribution towards the Group's investigations centred on hydrothermal alteration and mineralisation. Therefore, a substantial part of Chapters 3 & 4 is the author's work and the entire Chapters 5 and 6. For the investigations of each of the phases of hydrothermal alteration and mineralisation examples were drawn from a number of complexes. For example, the Afu, Ririwai, Ropp, Jos Bukuru and Dutsen Wai complexes provided samples for the study of sodic metasomatism. In total material from fourteen complexes provided the data on which the conclusions were based. With the exception of the Ririwai complex, no one complex had been studied in great detail from the point of view of hydrothermal alteration and mineralisation. It was for this reason that this research chose the Saiya Shokobo complex for a detailed study of the processes involved in subsolidus rock-fluid reactions. The Saiya Shokobo complex, along with the nearby Banke complex, is one of the few complexes where the effects of the trapped volatiles on a volcanic pile can be studied, in addition to the hydrothermal alteration of both the surrounding basement and younger granite. Part II of this thesis therefore seeks to extend the ideas derived in Part I with a view to modification or amendment as necessary.

## Part II Saiya Shokobo complex

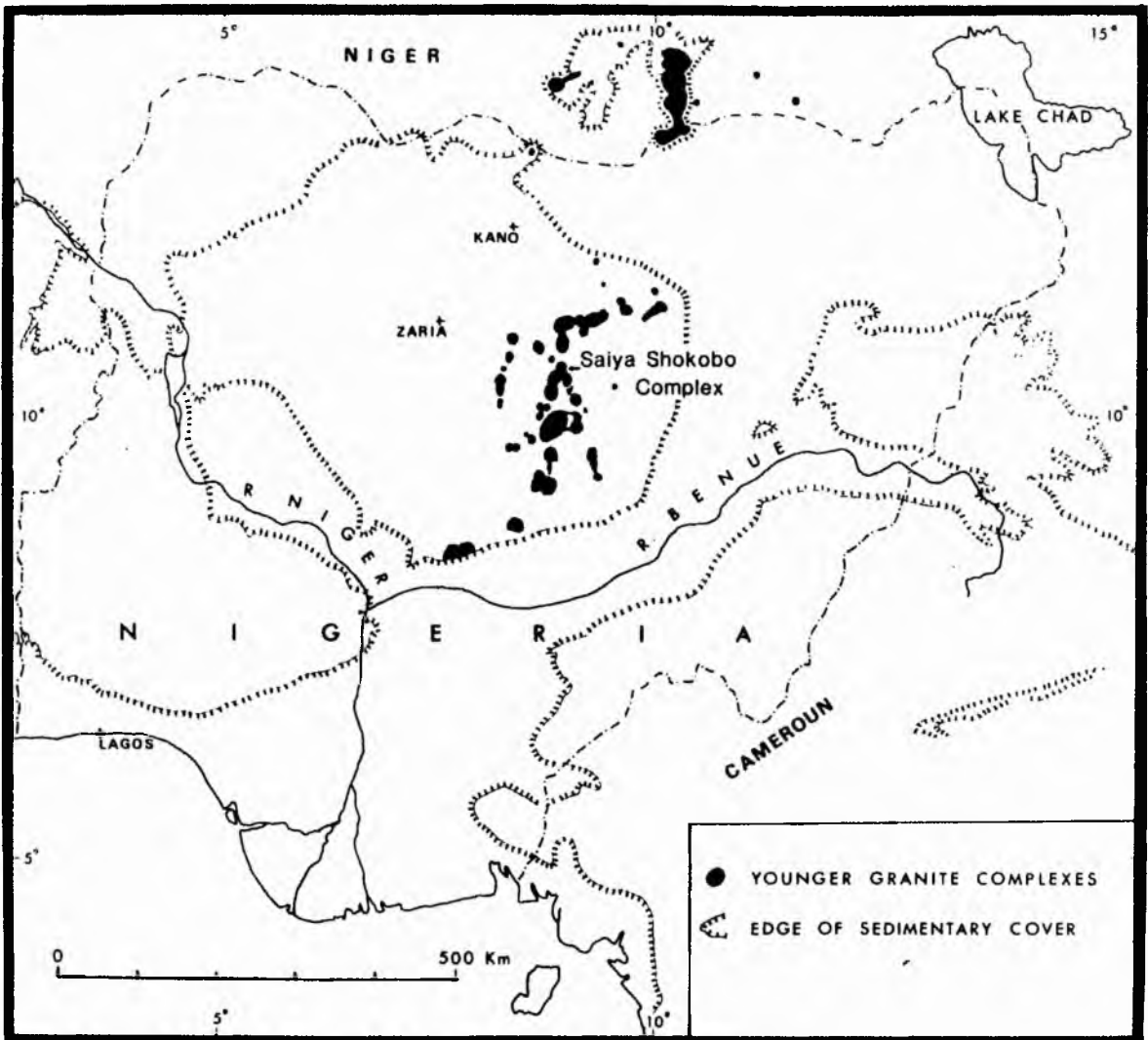


Fig 7.1 Location map of the Saiya Shokobo Complex

## CHAPTER 7

### THE SAIYA SHOKOBO COMPLEX

#### Introduction

The Saiya Shokobo Complex is situated at the boundary between Plateau, Bauchi, Kaduna and Kano States and is one of the northern ring complexes of Nigeria (Fig 7.1). The Rishi area lies between the main part of the Saiya Shokobo complex to which it belongs and the Tongolo Complex to the north (Fig 7.2). Both complexes are named after prominent peaks (Dutsen Saiya 1360m, Dutsen Shokobo 1315m and Dutsen Tongolo 1340m).

The Saiya Shokobo Complex forms a distinctive hill mass, (Plate 7.1) isolated from the main Jos Plateau, and covers an area of approximately 250km<sup>2</sup>. It is contiguous with the Jere Sanga Complex to the south and the Tongolo Complex to the north-east and lies immediately to the south of the small Zuku peralkaline complex. The Saiya Shokobo complex is elliptical in outline with the longer axis trending roughly north northeast - south southwest for a distance of approximately 17km from the Rishi Hills in the north to the Shokobo Hills in the south. It is an area of rugged topography and poor access with a maximum altitude of 1680m rising 650m above the surrounding plain.

The Tongolo Complex to the north and east of the Saiya Shokobo Complex also forms a prominent hill mass and covers an area of approximately (130km<sup>2</sup>). To the southeast of the main complex it is contiguous with the polygonal granite porphyry ring dyke system of the Dagga Allah area which extends to the Kwandonkaya complex. The complex is roughly rectangular in outline extending nearly 30km from northwest to southeast and approximately 20km in the northwest southeast direction. At the present level of erosion a ring pattern is not particularly apparent. It is an area of poorly vegetated rugged hills rising to a maximum of 1340m on Dutsen Tongolo which lies 470m above the Delimi Plain to the east.

The Rishi area forms a gap between the two prominent hill masses (Fig 7.3) and provides access into both complexes (Plate 7.2). A reasonable quality dirt road from Fuskin Mata to Ningi allowed access to Rishi, although by now (1987), a metalled road will have been opened. Further access into the complexes is by footpath alone.

The drainage from the Saiya Shokobo and Tongolo complexes is radial. Rivers draining to the north and east eventually link with the perennial Bunga river and drain to the Chad basin whilst those draining to the west and southwest join up with the Kaduna River and ultimately, the River Niger.

Climatically the area has a dry season from October to mid-May and a wet season between the months of May and September. Rainfall is approximately 1200mm per annum although most of this falls in July and August. The rainfall, combined with the high Sudan Savanna-type grassland means that it is impossible to do fieldwork in the area during these months. Since much of the area has only a thin soil cover with sparse perennial vegetation the streams dry up shortly

**JERE-SANGA (N. Part)**

- JS1 Vent agglomerates, ash-fall tuffs, crystal-poor ignimbrites
- JS2 Intra-caldera crystal-rich ignimbrites
- JS3 Quartz fayalite porphyry
- JS4 Ferroaugite hastingsite syenomonzonite and porphyry

**SAIYA-SHOKOBO**

- SS1 Dolerite
  - SS2 Hastingsite syenite
  - SS3 Pre-caldera rhyolites: mainly ignimbrites
  - SS3' Basalt
  - SS4 Shokobo caldera: hedenbergite arfvedsonite quartz porphyry
  - SS5 Arfvedsonite granite ring dyke
  - SS6 Saiya intra-caldera volcanics: mainly crystal-rich peralkaline ignimbrites
  - SS7 Arfvedsonite granite porphyry ring dyke; includes minor bodies of arfvedsonite granite and also aegirine porphyry
  - SS8 Arfvedsonite granite
  - SS9 Biotite granite
- M. S. Buchanan (2b)

**TONGOLO**

- T1 Pre-caldera rhyolites: mainly crystal-poor ignimbrites
- T2 Intra-caldera rhyolites: mainly crystal-rich lithic ignimbrites
- T3 Granite porphyry: with hedenbergite and hastingsite or arfvedsonite
- T4 Arfvedsonite and aegirine arfvedsonite granites
- T5 Biotite granites
- T6 Albite biotite granite

R. Black and M. S. Buchanan (2b). N. of lat 10°30'. photogeology by D. C. Turner (1)

**ZUKU**

- ZK1 Vent agglomerates
  - ZK1' Other pre-caldera rhyolitic rocks
  - ZK2 Hedenbergite quartz syenite porphyry
  - ZK3 Aegirine arfvedsonite granite ring dyke
  - ZK4 Aegirine granites
- Jacobson & MacLeod (2a)

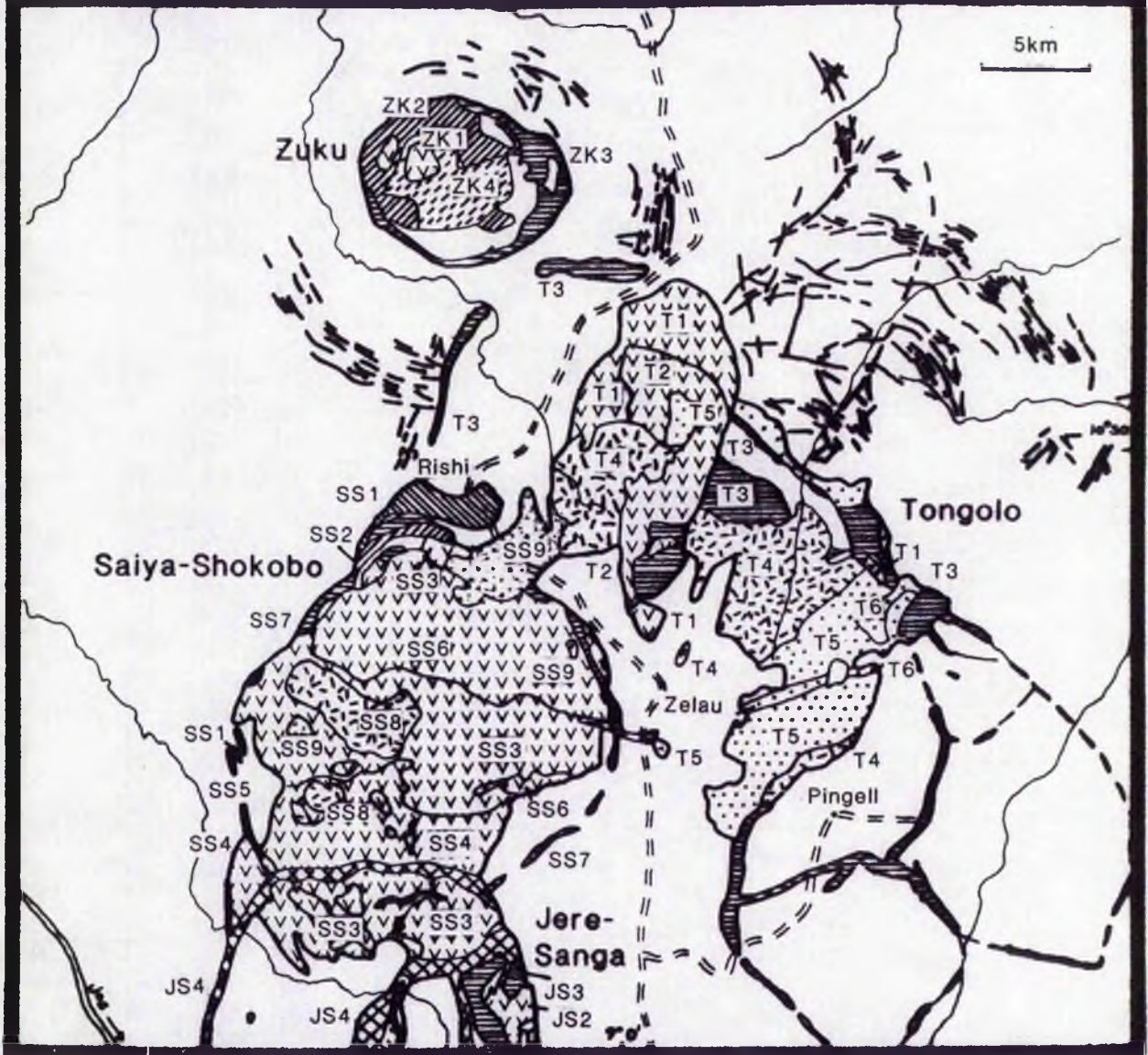


Fig 7.2 General Geology of the Zuku, Saiya Shokobo and Tongolo Complexes

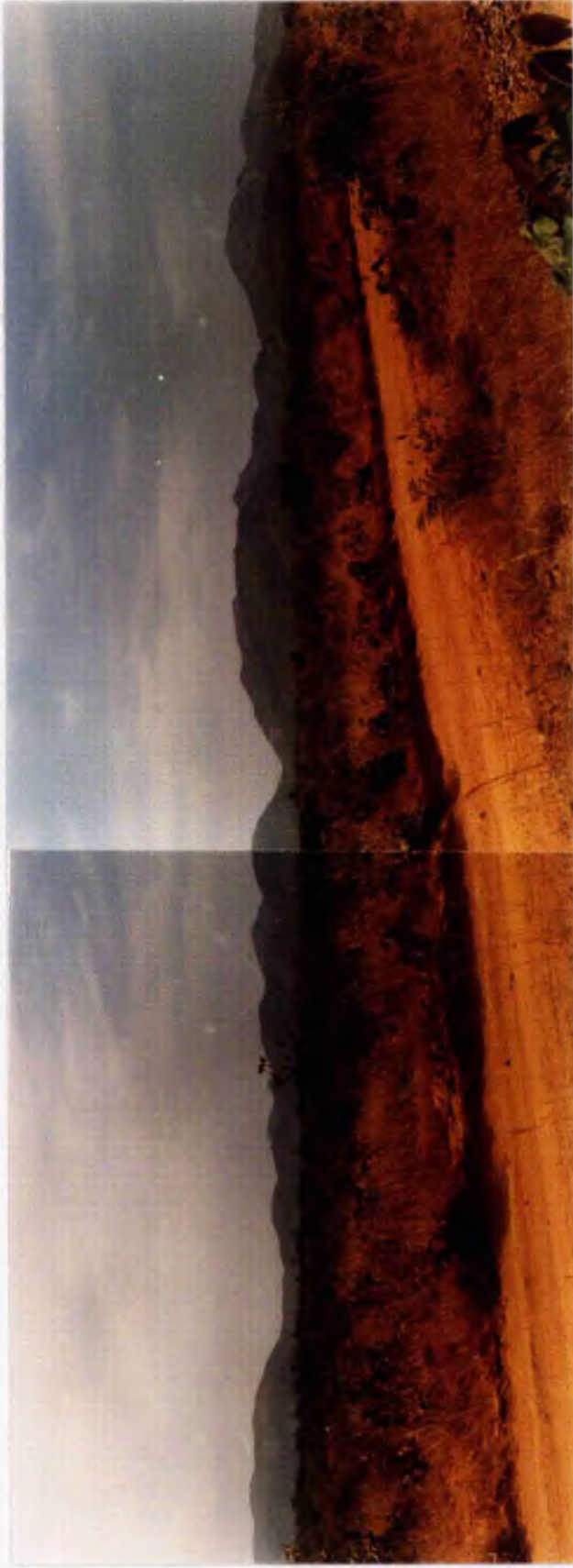


Plate 7.1

Saiya Shokobo complex

View northeastwards towards the distinctive hill mass of the Saiya Shokobo complex



Plate 7.2

Panoramic view of part of the Saiya Shokobo complex

View from the volcanic cap of Dutsen Rishi (loose rubble) and biotite granite (immediate foreground) across the Rishi gap to the volcanic hills to the south

after the rains have ceased and field work can be resumed in late October. During March and April when the sun is overhead both temperature and humidity rise, making working conditions more difficult.

#### Previous work

Falconer and Raeburn (1923), first described the Saiya Shokobo and surrounding complexes which were shown on the Geological Tinfields map of Nigeria, published in 1927. The Saiya Shokobo Hills and Tongolo Hills were described and the Rishi-Neli Hills (the northwest part of the Tongolo complex) were discussed as a separate area. The Rishi granite - the subject of Part II of this thesis - was described as building

" a small portion of the northern front of the Saiya Hills and is clearly intrusive into the overlying porphyries".

In addition to an identification of the main rock types, they also remarked on the similarity between the basic intrusives of the Rishi area and the rocks of the Kofai complex. They recorded the presence of granite inliers within the volcanics and also briefly described the tin occurrences in the Dawa area.

The study by Buchanan in the years 1958-1960 identified the main structural features of the complex and mapped the lithological units at the scale of 1:100,000. A detailed mineralogical description of these units was given in Buchanan et al.(1971).

#### Structure

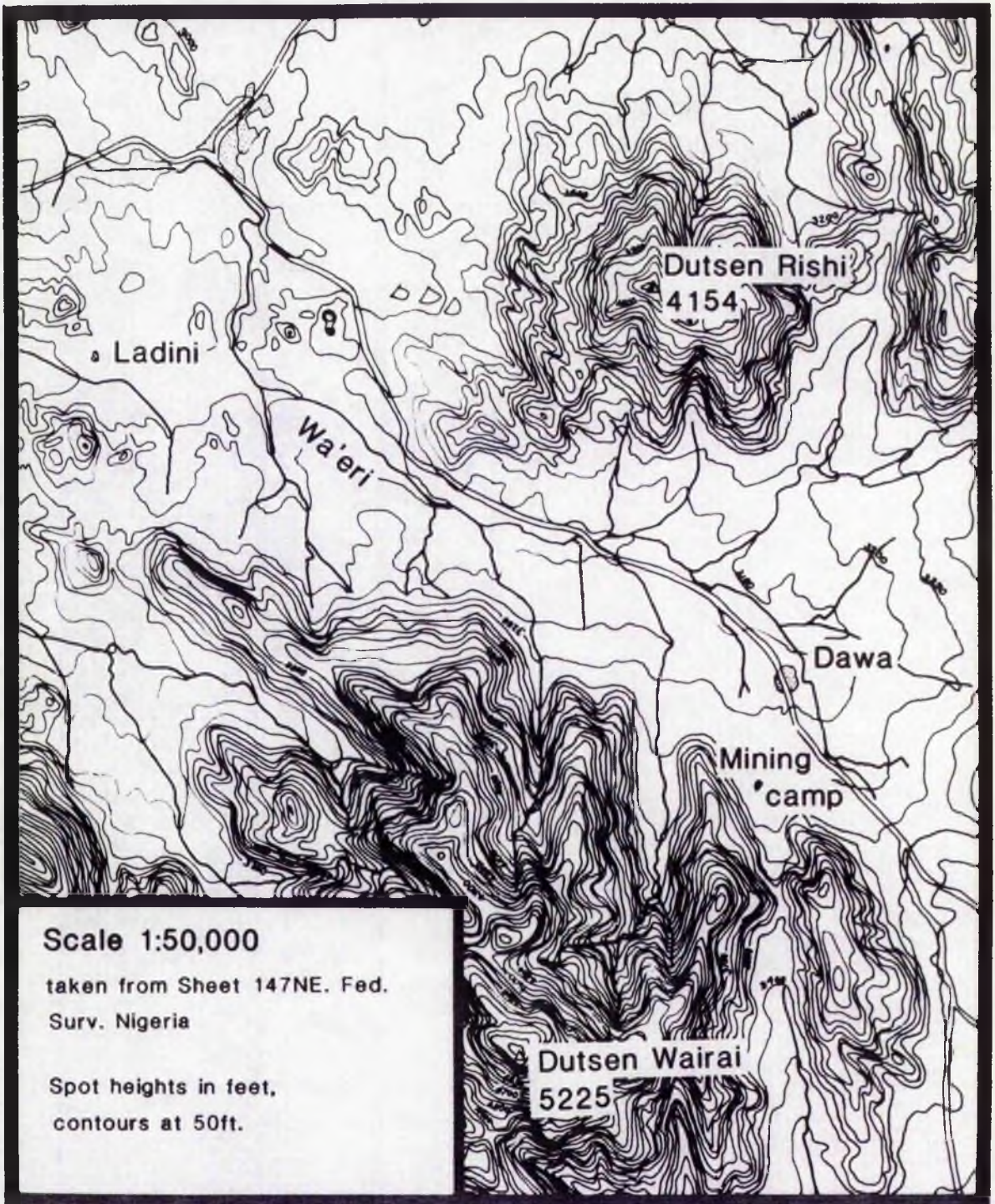
The main structural feature of the complex is the elliptical fracture 17km in diameter (Fig 7.2), which has largely determined the outline of the central massif of the Saiya Shokobo Hills and has controlled the emplacement of several of the intrusions of the complex. The volcanic rocks are confined within this elliptical fracture. During the latest stage of magmatic activity, the emplacement of the granite moved beyond the confines of the main fracture and was intruded eccentrically to the north east of the main part of the complex.

#### Field Geology

The Saiya Shokobo Complex is dominated by volcanic rocks consisting of agglomerates and ignimbrites (Fig 7.4) with the earliest intrusive phase formed by an arcuate doleritic ring dyke showing net veined acid/basic assemblages. Later intrusives became peralkaline in nature with the development of arfvedsonite-bearing granites and porphyries. A notable feature of the southern part of the complex is the intrusion of the Limoro syenite ring dyke which cuts the Shokobo Hills. The dyke which is elliptical in plan is centred on the Jere Sanga complex to the south (Fig 7.2).

Within the Saiya Shokobo Complex MacLeod et al (1971) distinguished fourteen separate petrological phases which have been condensed into nine phases on the enclosed 1:500,000 scale map due to the small size of five of the phases. The complex is intruded into porphyritic biotite hornblende older granites.

Fig 7.3 Topographic map of the Rishi field area



In contrast with the Saiya Shokobo complex the Tongolo area is dominantly granitic. Ignimbrites occur to the north east of Rishi in the northwest of the Tongolo complex and beneath these lie the granite cupola zones. MacLeod et al (1971) distinguished 15 separate phases, two volcanic and thirteen intrusive. These have been reduced to six phases on the 1:500,00 scale map.

The field area selected for detailed study was in the Rishi - Dawa area of the Saiya Shokobo complex. The area extends from  $8^{\circ}55'E$  to  $8^{\circ}59'E$  and from  $10^{\circ}24'N$  to  $10^{\circ}30'N$  (Fig 7.4). Field mapping of the area was accomplished using aerial photographs at a scale of 1:40,000 together with an excellent topographic map, an unusual feature for this part of Nigeria! Both photographs and map were supplied by the Directorate of Overseas Surveys and paid for by the Overseas Development Ministry. Field information was transferred from photograph overlays on to the 1:50,000 contoured map using a radial line plotter. The Rishi area was visited four times, amounting to a total of six weeks in the complex. Sampling was concentrated on the biotite granite and the adjacent rock types and more than 300 samples were collected.

### The Rock Types

Since the work reported in this thesis is related to hydrothermal alteration and mineralisation the petrological descriptions which follow are selective. It is not the intention to give a complete petrological picture of the individual units. This has already been done by Buchanan in MacLeod et al (1971). The principal rock units are detailed in Fig 7.2, but only those rock types of the Rishi area that have been altered to some extent by hydrothermal fluids, are described.

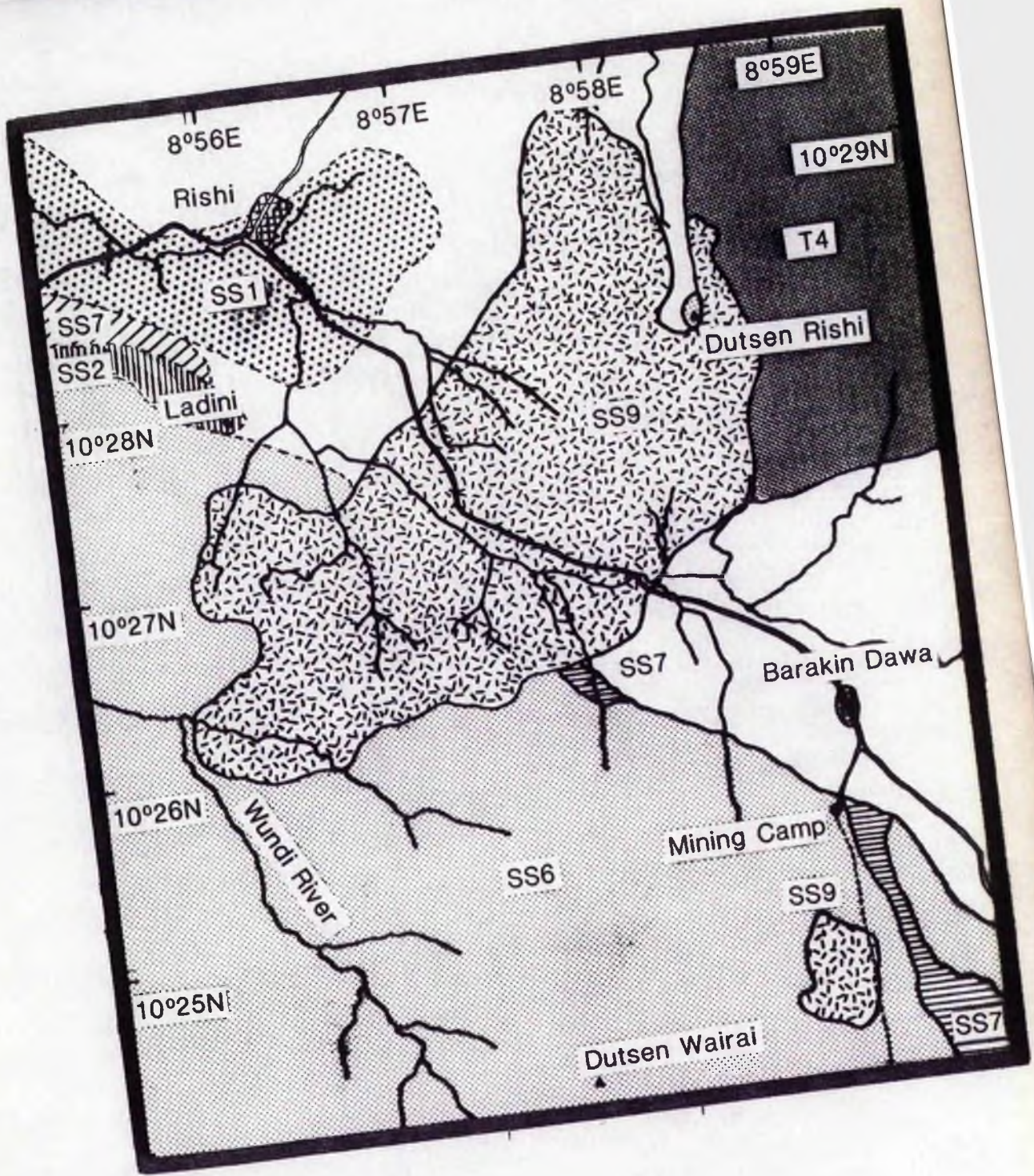
## BASEMENT ROCKS

### Introduction

In the Rishi area the basement is composed of two porphyritic biotite hornblende granites. The Tongolo granite to the southeast is well exposed in the river bed on the road between Dawa village and Rishi, while the Zelau-Rishi granite is well exposed both along the new road construction southwest of Rishi, and immediately to the north of Dutsen Rishi. Both are typical porphyritic older granites, similar to many in the vicinity of the Jos Plateau, with large tabular plagioclase feldspar laths up to 5cm long set in a dark, medium grained matrix of quartz, plagioclase, microcline, biotite and hornblende (Plates 7.3 and 7.4). Jointing is widely spaced so the outcrops form smooth boulders or flat slabs in stream beds, that are difficult to sample. Both granites appear largely unfoliated but with the exception of the areas described, the exposures are generally poor. Macleod et al (1971), consider that both the Zelau-Rishi granite to the northwest and the Tongolo granite to the southeast are intrusive masses into the granite gneiss.

### Contact relationships

Along the greater part of their boundaries the Rishi and Tongolo Older granites are in contact with fine and medium-grained biotite and biotite-muscovite granites. Macleod et al (1971) records no actual contacts are



Scale 0 km 1

Fig 7.4 General Geology of the Rishi area for key see Fig 7.2

Plate 7.3 (right) and  
Plate 7.4 (below) :

Greisen veins  
in Zelau Rishi  
megacrystic monzogranite

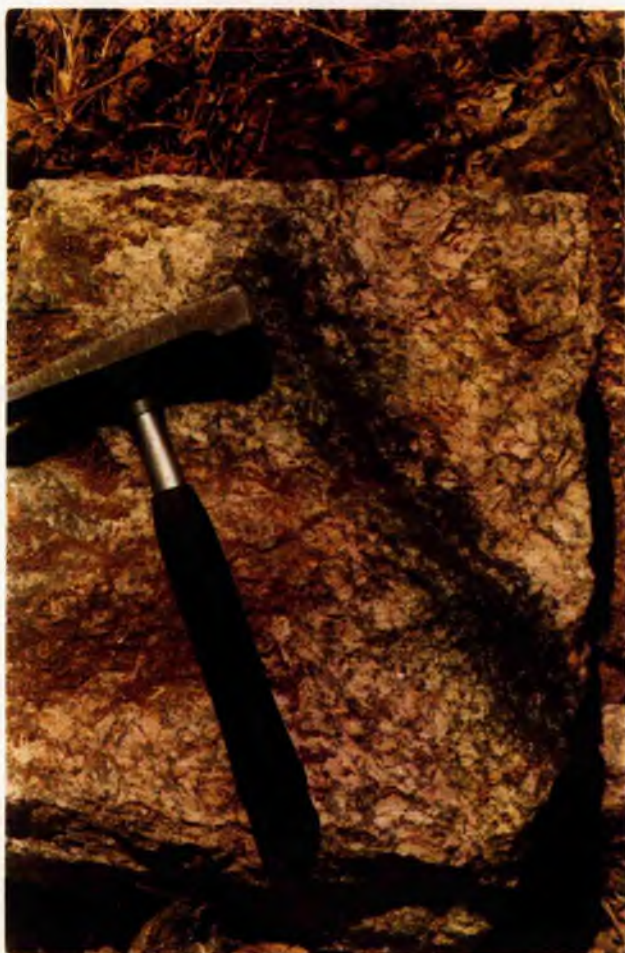




Plate 7.5

Volcanic pile and feeder dyke

View southwards from Dawa. The hill to the right is composed of crystal-rich ignimbrites while the one on the left is the quartz feldspar porphyry feeder dyke.

## Contact relationships

The volcanic pile has sharp contacts with the basement which are clearly marked by a distinct change in slope when the contacts are not well exposed.

The granite window south of Dawa reaches an elevation of almost 1000m indicating that the granite rose up to quite high levels in the volcanic pile. Here the contact appears gradational because of extensive hydrothermal alteration both of the granite and overlying volcanics. There are also several smaller windows of the granite exposed over a wide area, most notably in the Ladini area, but here too there has been substantial subsolidus modification of the original mineralogy of both the granite and volcanic pile.

## Volcanic feeder dyke

The volcanic feeder dykes which are generally discontinuous, sometimes branching or double, cut both the volcanic pile and the basement, sometimes enclosing screens of these rocks between parallel feeders. The main feeder dyke which is remarkably persistent, occupies an early ring fracture which controlled ring complex formation. The feeder dyke is elliptical in plan with a radius of 8.5km. Although the feeder dyke is often discontinuous in outcrop the most continuous section which is approximately 12km long, is in the chosen field area. Both sets of samples collected from the feeder dyke, came from miners pits which were dug either to exploit cassiterite-mineralised stringers or pervasive mineralisation of the groundmass.

Like the porphyritic volcanic material, the volcanic feeder dyke contains quartz and feldspar phenocrysts but they are typically in synneusis aggregates and they are modally less abundant than in the volcanics. The ratio of quartz to feldspar phenocrysts is similar in both however, varying from 1:1.5 to 1:3. whereas in the complexes further north there is a quartz to feldspar ratio of 1:4 in the feeder dyke compared with 1:1 in the volcanic pile. The pink and white feldspar phenocrysts are set in a fine-grained microcrystalline groundmass which is bluish grey in colour and which may have originally been glassy (see Chapter 8). The feeder dyke is described by Buchanan et al (1971) as containing "crystals of blue riebeckite in all but the most chilled varieties" but no amphibole was observed in any hand specimens or in any thin sections and the only ferromagnesian mineral noted was biotite.

## Contact relationships

Although the feeder dyke is a narrow intrusion, averaging 150m and thinning to only a few metres wide in places, it none the less occurs as a persistent ring dyke, which can be traced as discontinuous outcrops encircling the whole complex (Fig 7.2). Contact relationships with the other rock types however, are not clear as where they are exposed in the field area there has been extensive hydrothermal alteration along the contact zone (Plate 7.5)

## RISHI BIOTITE GRANITE

### Introduction

The Rishi biotite granite, (shown in inset 3 on the 1:500,000 scale map), is the final intrusive phase, emplaced at a high level within the Saiya Shokobo complex. The main mass of the granite occupies an elongated area trending from northeast to southwest and it covers an area of 13km<sup>2</sup>. There are two further important outcrops south of Barakin Dawa. The larger of these is shown on the inset 3 of the 1:50,000 scale map and Fig 7.4. Windows of the Rishi granite appear in the volcanics and basement over a wide area and Buchanan (in Buchanan et al 1971) believes it may form part of the same intrusion as the medium grained biotite granite of the Tongolo Complex. If so, a dome-shaped intrusion with a diameter of 20km must underlie much of the area between the two complexes. The gravity data of Ajakaiye (1977), suggests that there is one granite body with a negative gravity anomaly of -80mgal centred on this postulated body. The exposed granite is therefore a high level, highly specialised granite. The Rishi biotite granite is well exposed to the south of Dutsen Rishi and in the Ladini area. However, between Dutsen Rishi and Yelwa Rishi the granite forms long smooth whaleback ridges which are difficult to sample (Plate 7.6). The exposed granite lacks cognate xenoliths or restite phases.

The main granite is coarse- to medium-grained and cream or pink when fresh. Perthitic feldspar with patches of late albite, forms aggregated clusters up to 1cm or more and these are surrounded by chains or clusters of glassy quartz. Biotite forms discrete ragged interstitial laths or late stage aggregates up to 4mm in diameter. Accessory fluorite and zircon are common together with cassiterite, columbite and rutile. The coarse grained facies occurs in the centre of the exposed mass, where erosion has cut down into the main granite body. Towards the margins it becomes medium-grained, equigranular or porphyritic and occasionally granophyric. At the contacts it becomes fine-grained to microgranitic. This microgranitic phase is generally cream or whitish in colour. The mica is pale in colour, approaching zinnwaldite in composition and rich in small zircon crystals. Fluorite is a common accessory in association with the mica. These microgranitic patches are widely distributed but with a marked concentration in the marginal areas. Texturally however, there is a wide variation within the exposed area from fine to coarse-grained and from porphyritic to equigranular (Plate 7.7). However, each of these facies variants form part of the main granite and there are no internal mapable contacts. Within each of the different facies there is often further textural and mineralogical variations and there is evidence of fluid mobility from such textures. This is often characterised by feldspar phenocrysts showing alteration along thermal cracks, late hydrothermally developed biotite, usually in clots and often interleaved with fluorite, and late hydrothermally grown quartz.

Superimposed upon this mineralogical and textural variation is the sequence of alteration process assemblages, indicative of continued fluid mobility at successively lower temperatures: local patches of saccharoidal white feldspar indicative of albitisation, pink coloration of microclinised feldspars, removal of quartz to form microclinites, chloritisation of feldspar or biotite, greisenisation, silicification and late-stage alteration processes.



Plate 7.6

General view of the central part of the Saiya Shokobo complex. View southwards from Dutsen Rishi across the biotite granite to the volcanic hills west of Dawa.



Plate 7.7                      Textural variations within the Rishi biotite perthite granite

left to right :

- |         |   |
|---------|---|
| S23/13  | granophyre  |
| SS40    | porphyritic biotite granite with occasional feldspar phenocrysts >1cm in size |
| SS43    | coarse-grained Rishi granite  |
| SS55/8  | medium-grained Rishi granite  |
| SS49/2b | fine-grained Rishi granite  |

## Contact relationships

There is no cataclasis of country rocks by the biotite granite emplacement and no evidence to suggest other than passive, permissive emplacement. Where the contact is exposed there is no evidence of basic enclaves, cognate xenoliths, or xenoliths of country rock within the outer aureole of the biotite granite. However, no detailed structural interpretation of the mechanism of emplacement has been undertaken.

The biotite granite contact with the overlying volcanic pile is characterised by extensive hydrothermal alteration and mineralisation. Sheeted vein systems and stockworks also occur and these have been worked extensively in the past for cassiterite which sometimes occurs in knots weighing several kilos. Sphalerite is the dominant sulphide which is accompanied by chalcopyrite in both disseminated and vein-controlled mineralisation.

## MINERALISATION

### Introduction

Economically the Rishi biotite granite has been important for the extraction of primary wolframite and cassiterite and for the mining of alluvial columbite and cassiterite shed from the biotite granite. However, when last visited in December 1983 all mining activity had ceased even on the local scale. In addition to these oxide ores there is abundant sphalerite and chalcopyrite accompanied by minor molybdenite, galena, pyrite and other sulphides. The mineralisation is concentrated in the contact zone between the biotite granite cupola and the overlying volcanics or basement. Predominantly, the mineralisation occurs on the granite side of the contact. The overlying rocks have clearly acted as a seal to fluid migration and where escape has occurred the change in bulk rock chemistry has been responsible for rapid ore deposition. Eight hundred metres to the south of Dawa mining Camp escaping ore rich fluids have utilised vertical fractures infilled by quartz porphyry feeders, resulting in the formation of a mineralised porphyry, the groundmass of which has been extensively altered whilst the phenocrysts remain largely intact.

## CHAPTER 8

### PETROLOGY AND GEOCHEMISTRY OF THE MAIN ROCK TYPES in THE RISHI AREA

#### Introduction

More than four hundred samples were collected in the Rishi area, from 200 sites. These localities are shown on Fig 8.4 for the Rishi area and Fig 8.6 for the Dawa area. A brief description of each of the samples is given in appendix 1. Samples 1-86 were collected by C.A. Abernethy and the remaining material was collected by the author.

The petrology of all the rock types in the Rishi area, whether they are from the basement, the volcanic pile, the biotite granite, or hydrothermal variants, is dominated by the minerals feldspar, quartz and mica. These minerals show a wide range in size, form and textural relationships. Before entering into descriptive petrology therefore, it is necessary to briefly explain the terminology that has been utilised to describe both the forms and textural relationships that appear throughout this and ensuing chapters.

#### Mineralogical and textural introduction

The textures of igneous rocks depend upon crystallinity, granularity, crystal shapes and mutual relationships between crystals. However, several textures encountered in the Rishi rocks are not typically igneous and are therefore not discussed in the "Atlas of igneous rocks and their textures" by Mackenzie et al (1982).

With regard to crystal form, two kinds of terms are used to describe crystal shape according to McKenzie et al (1982):-

-Terms indicating the quality of the development of crystal faces, i.e. euhedral, subhedral and anhedral.

-Terms specifying the three-dimensional shape of individual crystals which include skeletal, dendritic or embayed crystals.

In the first category such terms need no further explanation. However, in the second category, to this terminology has been added clustered, beaded, amoeboid and angular. Sketches indicating the nature of these terms are given in Figs 8.1

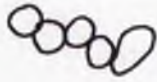
For the mutual relationships between mineral phases, it is the intergrowth textures that are of most interest. The terminology includes consertal texture, micrographic, granophyric and myrmekitic textures together with micropertthitic textures. Sketches of these are shown in Figs 8.1. For the perthitic feldspar, existing terminology has been adapted and extended for describing the mutual relationships between the two phases of alkali feldspar in the perthites. The terminology used is explained in the sketches of Fig 8.2.

The textural variations in the micas are very varied particularly in the hydrothermally altered rocks and the terminology used is shown in the sketches of Fig 8.3.

Fig 8.1 Variations in quartz shape and intergrowth textures



clustered



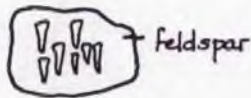
beaded



embayed



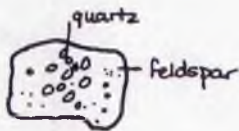
consertal



micrographic



granophyric



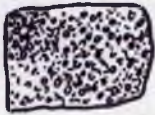
myrmekitic



spherulitic



amoeboid



SIEVE-TEXTURED



LAMELLAR PERTHITE - typical regular alternations of perthitic lamellae of probable exsolution origin



LAMELLAR PERTHITE transition to patch perthite. Often phenocrysts may show a core of lamellar perthite while the outer margins have coarsened to patch perthite



PATCH PERTHITE - irregular domains of dark grey microcline and clear albite



BRAIDED PERTHITE - there is no single type of braided perthite, this description is used for any perthite that involves albite lamellae crossing each other on {111} or {110} faces.



FILM PERTHITE - very fine lamellae have nearly straight or lensoid textures parallel to {601}. Often film textures developed in one of the separate domains.



INTERGRANULAR ALBITE - small laths of albite developed in the interstices between larger crystals.

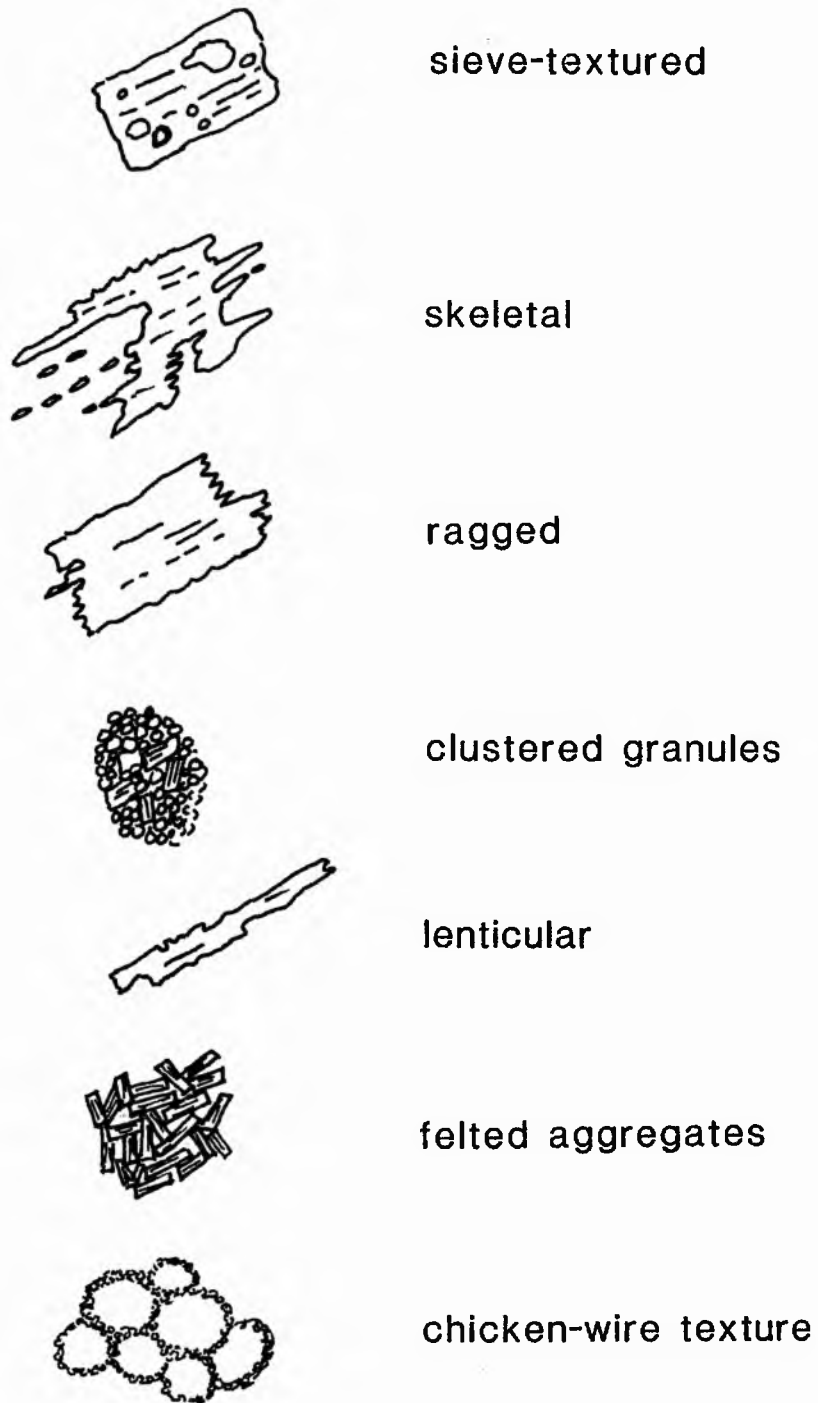


CHESSBOARD ALBITE - developed due to sodic metasomatism of perthite (or microcline)



SNOWBALL TEXTURE - abundant laths of albite are surrounded and enclosed by large anhedral crystals of untwinned turbid intermediate microcline

Fig 8.3 Textural variations in micas



## BASEMENT GRANITE

### Introduction

The basement granites are typical coarse to very coarse-grained, porphyritic, poorly jointed, late Pan-African (older) granites. Both the Tongolo and Zelau-Rishi granites are unfoliated and are characterised by large, white, tabular feldspar laths up to 5cm long set in a dark, medium grained matrix of quartz, microcline, plagioclase, biotite, hornblende and iron-titanium oxides (Plate 8.1). The location of the samples selected for study are shown in Fig 8.4.

### Petrology

The essential minerals are microcline, quartz, oligoclase, biotite and hornblende in approximate order of abundance. Modal analyses have been made of seven thin sections of the granites but the coarse grain size precludes an accurate determination of mineral percentages by the usual point counting assessment. Nevertheless the modal compositions of quartz, alkali feldspar and plagioclase are given in Table 8.1 and are plotted on the Streckeisen modal diagram (Fig 8.5).

Accessory minerals include apatite, zircon, allanite, epidote, sphene, sericite, chlorite, fluorite and opaque oxides.

The feldspar megacrysts are dominantly microcline perthite with film or patch perthitic texture. Mottled perthite (Plate 8.2), may contain oligoclase ghosts. Sericitic alteration is common with occasional alteration to epidote and pale brown biotite. Albite-oligoclase megacrysts are common in some samples, the twin lamellae have been almost obliterated by sericitic alteration in some cases.

The quartz occurs as clustered grains, often with consertal texture. They range in size up to 2cm and may be anhedral, rounded or lobed. Commonly they show strain extinction, strong fracturing and sutured margins. They also contain an abundant assemblage of complex fluid inclusions which accounts for the dusty nature of the quartz grains.

The biotite forms small, khaki- or sometimes tan-coloured, randomly orientated, clustered prismatic laths, pleochroic through brownish shades, to straw yellow. The biotite is distributed between and around the feldspar megacrysts and sometimes occurs as a replacement after the microcline perthite. The cleavage traces are rarely bent.

Occasional clustered crystals of deep blue-green edenitic hornblende varying from anhedral to euhedral, occur between or within the feldspar megacrysts. The hornblende displays good cleavage and is often quite fresh. Allanite occurs as anhedral to euhedral metamict crystals. Apatite forms small, glassy, euhedral prismatic crystals occurring as discrete crystals in mica clusters, feldspar or quartz. Occasionally it occurs as aggregates in groundmass quartz and in sample SSl80 it forms a prismatic crystal 3mm long. Zircon is ubiquitous, but never abundant and occurs as small, euhedral clear prismatic crystals that have no associated metamict halo. It is associated with allanite and particularly



Plate 8.1            Basement monzogranite

SS179 Coarse, porphyritic monzogranite with megacrysts of feldspar set in a dark, medium-grained groundmass of quartz, microcline, plagioclase, hornblende and Fe-Ti oxides. Cross-cutting granophyric vein is related to the intrusion of the Rishi biotite granite.

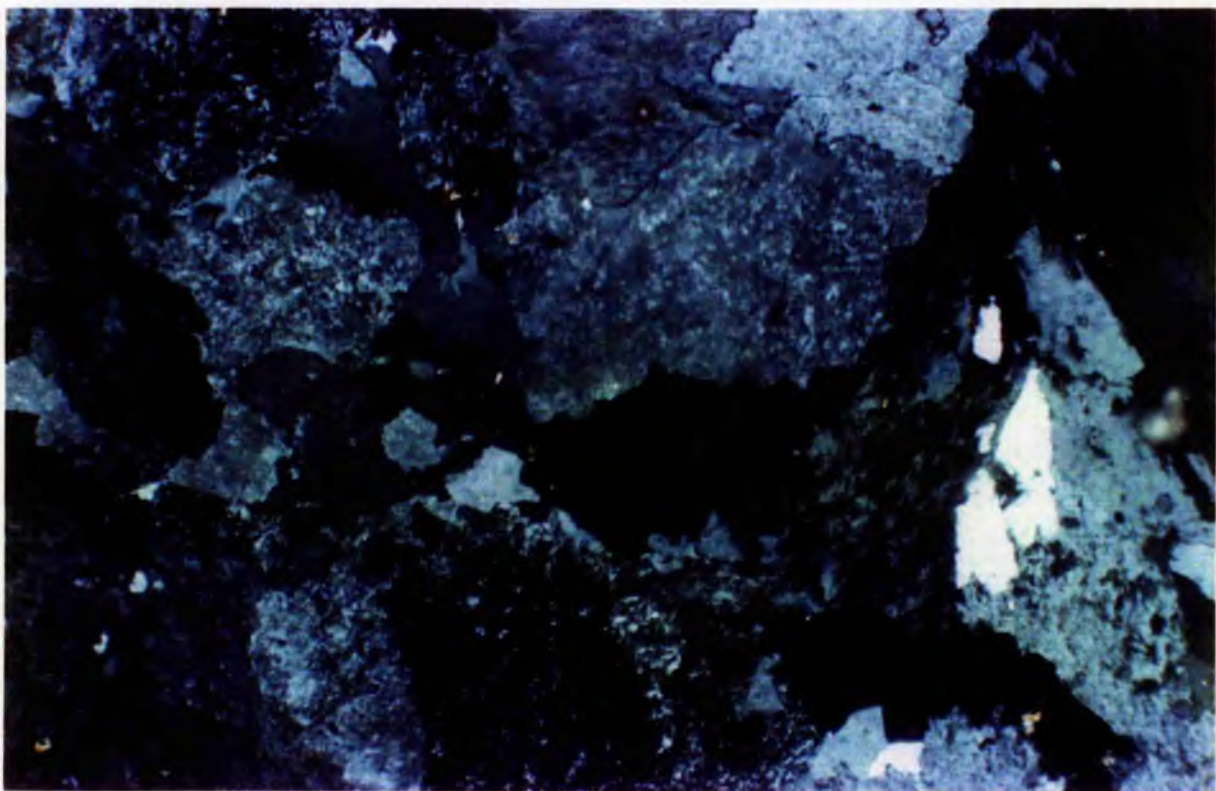
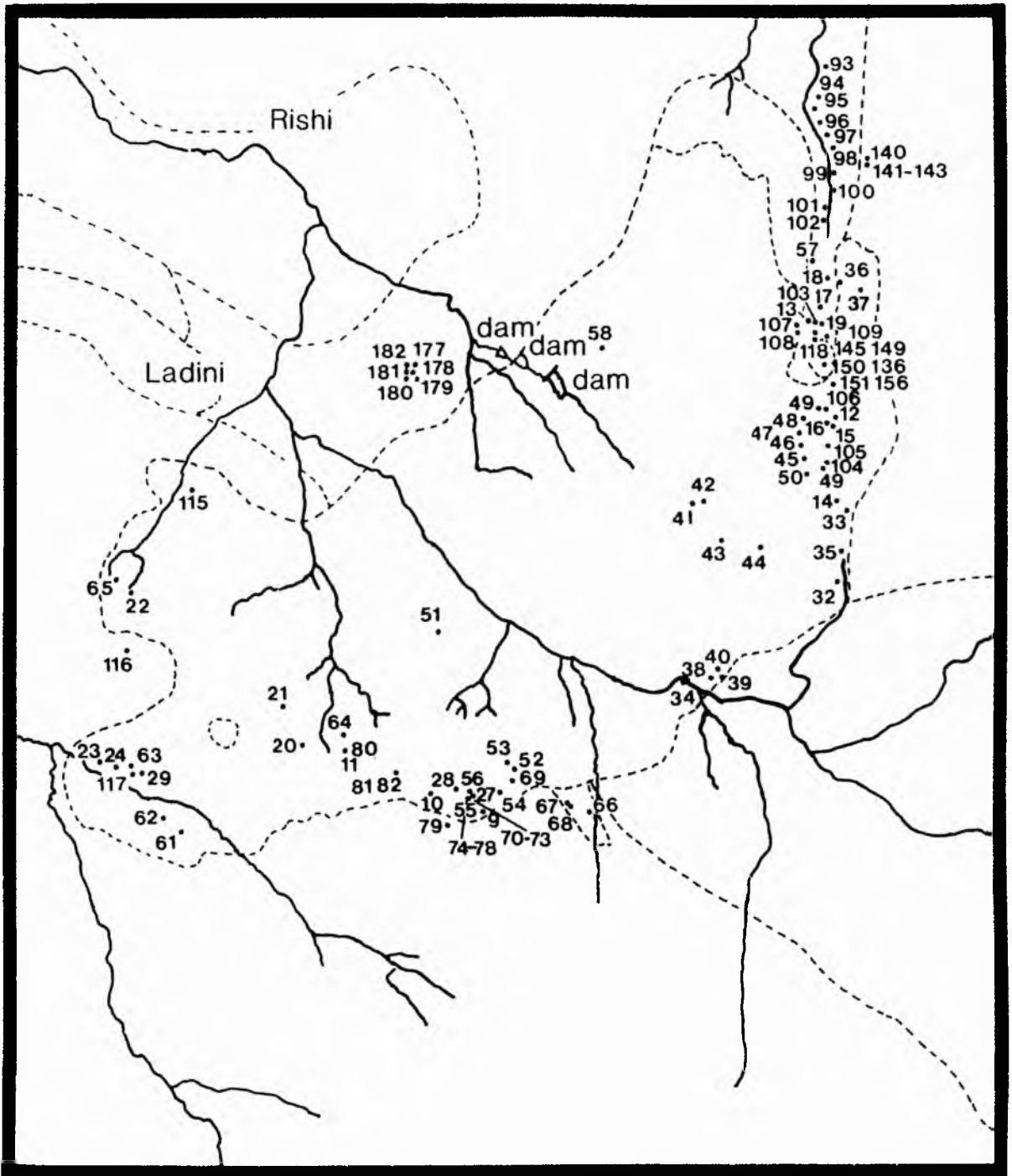


Plate 8.2            Basement monzogranite in thin section

SS177 showing microcline megacrysts with a mottled texture x50



Scale 0 km 1

Fig 8.4 Sample localities in the Rishi area

apatite within the mica clusters. Fluorite also occurs occasionally as colourless, rounded interstitial grains associated with the opaques within the mica clusters. The opaques form irregular, skeletal or sieve-like textured crystals or "blebs" usually associated with the clusters of mica. The sieve-textured example (SS179), poikilitically encloses apatite, feldspar or sphene. Close to the contact with the biotite granite the basement has been hornfelsed and mineralised north of Dutsen Rishi. This will be discussed in detail in Chapter 9.

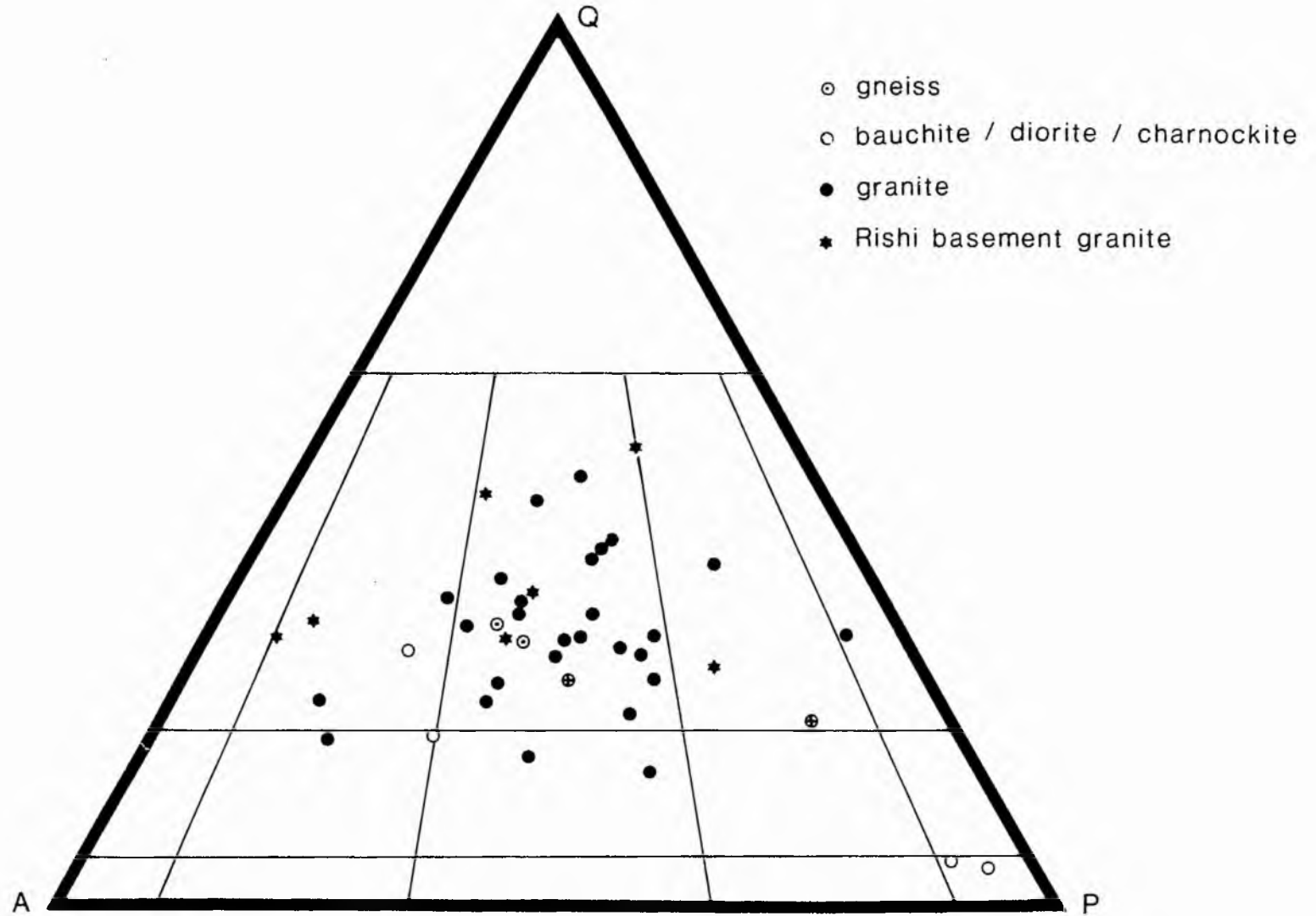
Table 8.1 Modal composition of selected basement granite samples

Mineral/No	SS57/14	SS177	SS178	SS179	SS180	SS181	SS182
Quartz	42.8	23.6	49.7	38.3	31.4	27.5	31.0
Microcline	30.0	19.6	14.4	30.4	56.5	56.5	35.0
Plagioclase	18.0	48.8	28.5	16.9	9.4	7.5	22.1
Biotite	0.2	4.7	4.4	7.5	0.9	6.2	5.1
Chlorite	7.2	0.2	0.8	2.0	0.4	0.2	4.2
Hornblende				0.2	0.1		0.1
Fluorite	0.1	0.3	0.4	0.2	0.1	0.4	0.1
Opagues	0.9	1.8	0.8	2.9	0.3	0.8	1.2
Apatite		0.7	0.2	0.9	0.8	0.5	0.8
Zircon	0.7	0.3	0.2	0.3	0.1	0.2	0.2
Sphene	0.1		0.4	0.4		0.1	0.3
Epidote						0.1	

#### Discussion

According to the Streckeisen diagram, these late Pan-African granites are strictly monzogranites. They are members of the subalkaline or high K calc-alkaline series and regarded as calc-alkaline monzonites by Lameyre and Bowden (1982). They compare with Pitcher's post-collision uplift granites which are independent of subduction related processes. Previous research on these late-Panafrican granites indicates a significant crustal component. Pitcher (1982) envisages that a possible model for magma generation of this nature is that partial melts derived from crustal or sub-crustal rocks were produced during adiabatic decompression consequent on the end of uplift and erosion at a time when such rocks were rapidly elevated into low pressure zones. He further suggests that melting was concentrated in the pressure-release zones provided by deep faults, which might also have brought hot mantle rocks into juxtaposition with cooler crustal rocks. The existence of such major deep-seated faults and shear zones is known for Nigeria and particularly Niger (Black 1984, Black et al 1985). It has been suggested by Bowden et al (1986), that it was the exploitation and reactivation of such Pan-African shear zones and transcurrent faults during the fragmentation of Gondwanaland that controlled the locations of Phanerozoic intra-plate magmatism in West Africa. This magmatism began with the voluminous eruption of an ignimbritic pile.

Fig 8.5 Quartz-Alkali feldspar-Plagioclase diagram showing the compositions of Nigerian basement rocks



## VOLCANIC ROCKS AND VOLCANIC FEEDER INTRUSIONS OF THE RISHI AREA

### Introduction

The earliest units of the volcanic sequence were pre-caldera vent agglomerates and ignimbrites exposed as a broad band across the southern part of the complex. Across the northern part of the complex, in the Rishi area, there is a thick volcanic pile, which was fed from depth by the quartz feldspar porphyry feeders, and preserved by subsidence of a semi-circular block. The units of interest are:-

the **volcanic pile**, since there are localised patches of hydrothermal alteration caused by fluids escaping from the granite into the base of the pile

the **quartz feldspar porphyry** ring-dyke, as fluids escaping from depth utilised these steep-sided fractures and modified the original mineralogy of the porphyries.

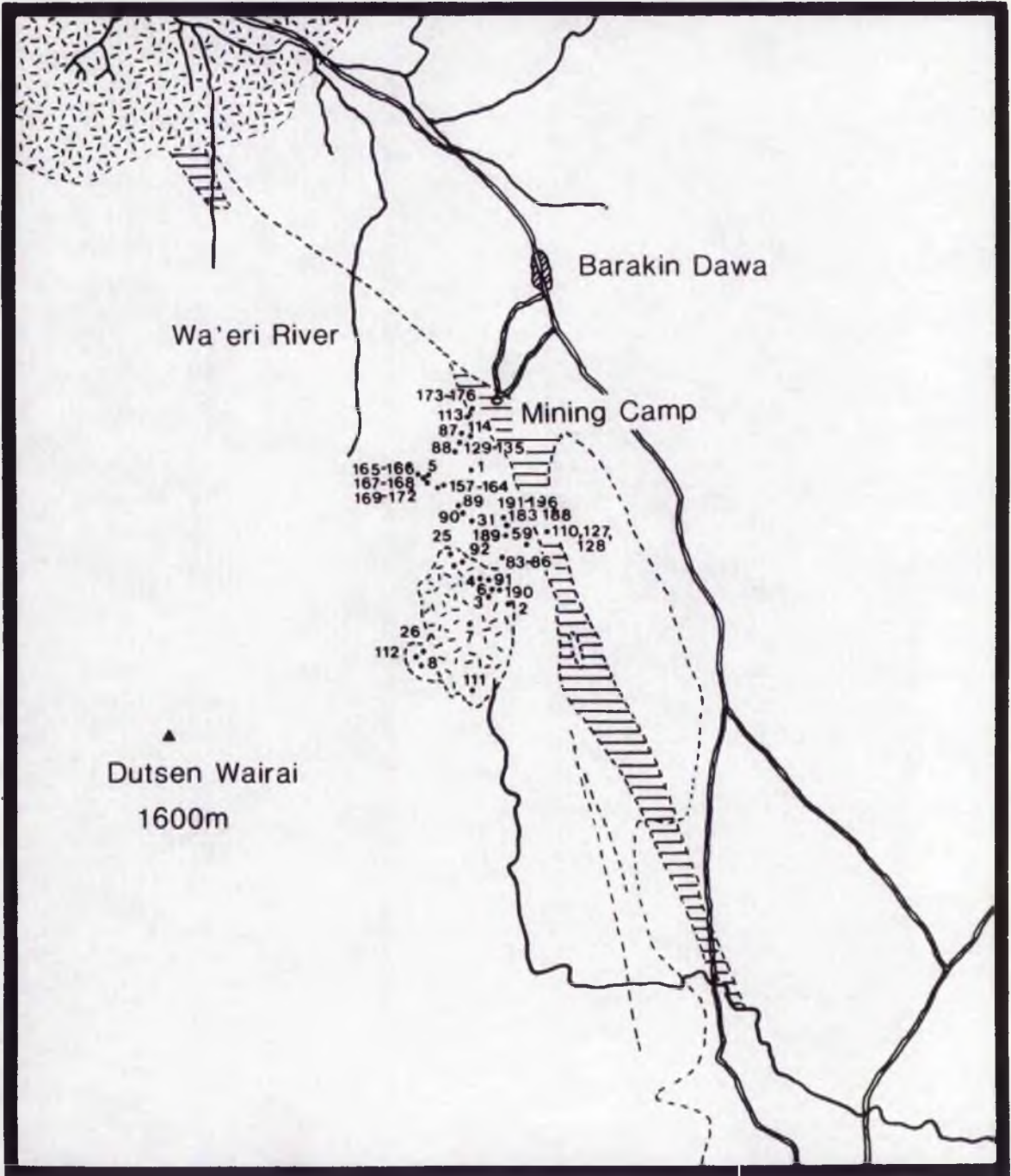
Hand specimens of the ring-dyke are identical to the crystal-rich volcanics of the Dawa Hill area and the ring dyke is therefore interpreted as a feeder dyke to the volcanic pile.

Sampling of these rock types consisted of vertical traverses in two areas, one in the volcanic pile of Dawa Hill and one through the porphyry feeder-dyke several hundred metres to the east of the Hill (samples 110-128, Fig 8.6). The traverses were intended to collect pristine specimens and transitional specimens through to hydrothermally altered samples close to the contact with the biotite granite.

The most pristine material from the volcanic pile is petrographically a quartz feldspar porphyry. It varies from grey to almost blue-black in colour, with irregularly-shaped to euhedral phenocrysts of colourless, cream or pink-coloured alkali feldspar and colourless glassy quartz, set in a microcrystalline groundmass of finely crystalline alkali feldspar, plagioclase, quartz and accessory minerals (Plate 8.3). In the marginal zones, the rock has a dark blue-black devitrified glassy matrix with a phenocryst population of around 20%. Towards the centre of the mass however, the groundmass is coarser in texture, the porphyry is lighter in colour and phenocrysts constitute up to 60% of the rock.

### Petrology of the volcanic pile in the Dawa-Ladini area

In the **volcanic pile** there is a series of welded crystal tuffs, which are grey in hand specimen with clearly identifiable phenocrysts of quartz and feldspar. The feldspar phenocrysts are generally larger in size than those of quartz with maximum phenocryst sizes of 7mm for the feldspar and 4mm for the quartz. In sample SS157 however, the feldspar and quartz phenocrysts are similar in size. The phenocrysts are often fragmental especially the feldspars. The crystal content varies between 38 and 48 % by volume and averaging 41% (Table 8.2).



Scale 0 km 1

Fig 8.6 Sample localities in the Dawa area

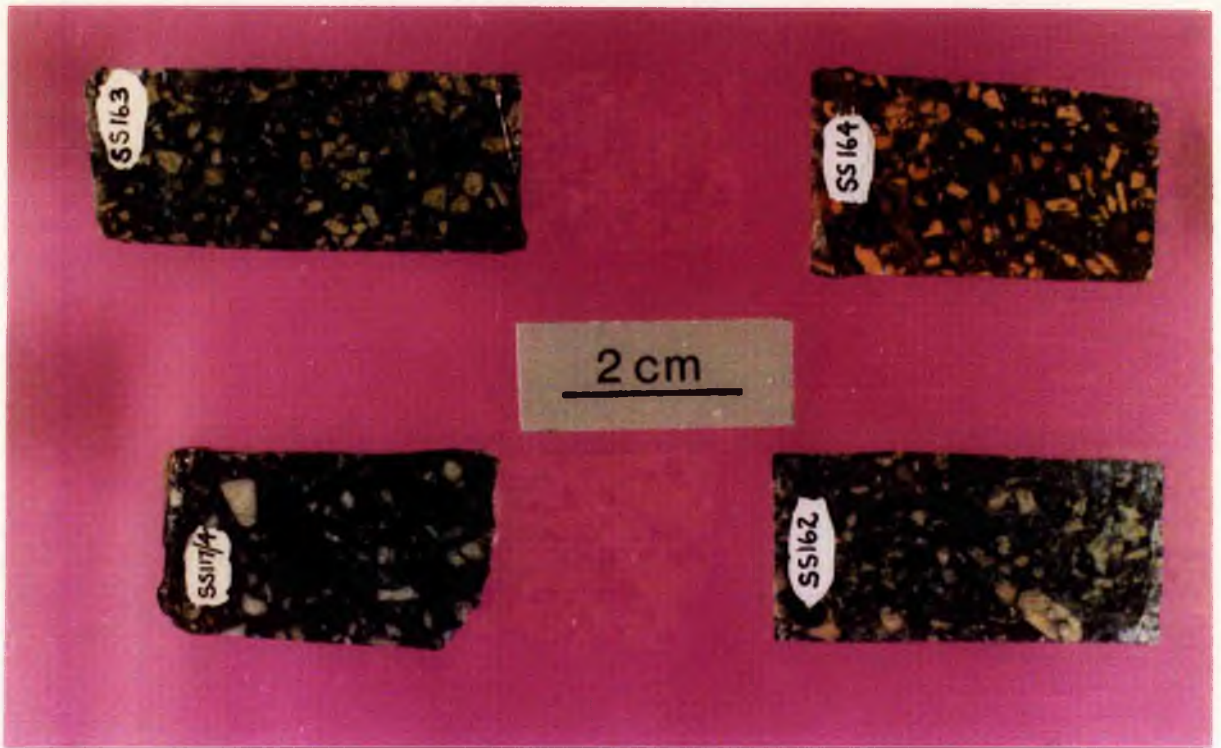


Plate 8.3 Quartz feldspar porphyry from the volcanic pile

The porphyry contains white, cream or pink feldspar phenocrysts and glassy quartz crystals set in a microcrystalline groundmass

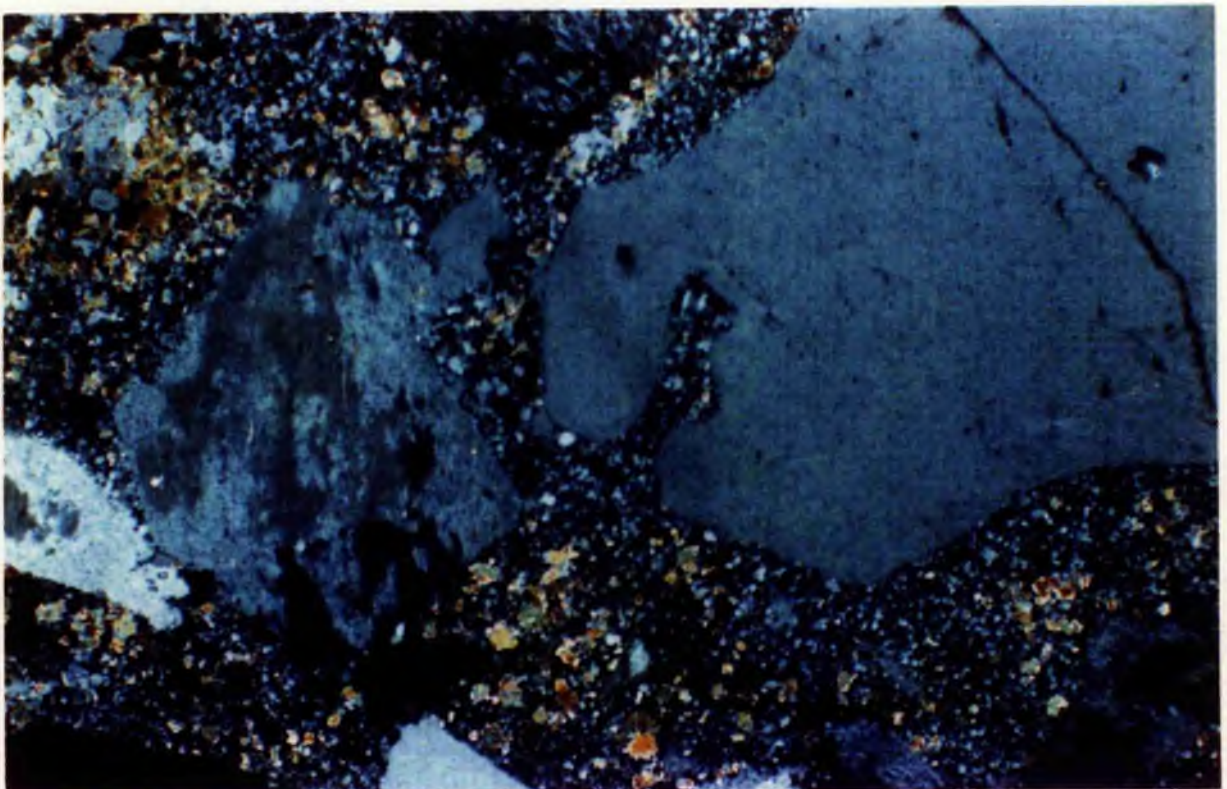


Plate 8.4 Quartz and feldspar phenocrysts in thin section

Embayed quartz crystal x50

Table 8.2 Phenocryst population in the volcanics and volcanic feeder dyke.

	volcanics									
	SS116	117/4	SS157	SS158	SS160	SS161	SS162	SS163	SS167	feeder SS175
Quartz	8.4	9.9	15.9	14.8	15.1	9.9	9.6	10.3	12.8	7.8
Feldspar	36.0	24.5	22.7	28.9	33.6	30.9	33.4	24.4	28.9	16.7
Groundmass	55.5	65.3	61.4	55.6	51.3	58.9	56.8	65.3	58.3	75.5
Total Phenocryst Population	42.4	34.4	38.6	43.7	48.7	40.8	43.0	34.7	41.7	24.5

A recount of SS160 to check precision gave quartz (15.1%), feldspar (34.1%) and groundmass (50.8%).

The quartz phenocrysts which vary in size from 2-4mm in diameter, show both rounded and bi-pyramidal forms. The stubby hexagonal bipyramidal habit is of high  $\beta$  quartz which has spontaneously inverted to low alpha quartz at 570°C but which has retained the high quartz structure. Often these quartz phenocrysts are embayed or skeletal in form, indicating rapid crystallisation (Plate 8.4). Resorption features have also been noted. Sometimes also the phenocrysts are fractured and broken, which is interpreted as due to explosive eruption and volatile loss (Plate 8.5). The quartz phenocrysts are clear, unstrained and evenly distributed. Occasionally, groundmass crystals occur within the quartz phenocrysts or their embayments. These are interpreted as having filled voids in the phenocrysts at the same time as growth of myrmekitic rims to feldspar phenocrysts, during groundmass crystallisation. There are abundant fluid inclusions, some are gas rich, others are fluid-rich with moderate-sized vapour bubble and some contain birefringent daughter minerals.

The feldspar phenocrysts vary from 2-7mm in length, are regularly distributed throughout the rock, and are euhedral in shape. The phenocrysts of feldspar in hand specimen are sometimes glassy with small cracks generated by thermal shock on cooling. These cracks are characterised by the development of white or pink turbid areas. They may show Carlsbad twinning, sometimes they are broken and embayed. In thin sections SS116 and S117/4 from the southwest margin, rare feldspar phenocrysts have clear cores and turbid margins traversed by cloudy zones in which faint micropertthite lamellae can be distinguished (Plate 8.6). The cracks, which cross the twin plane boundaries, were generated by thermal

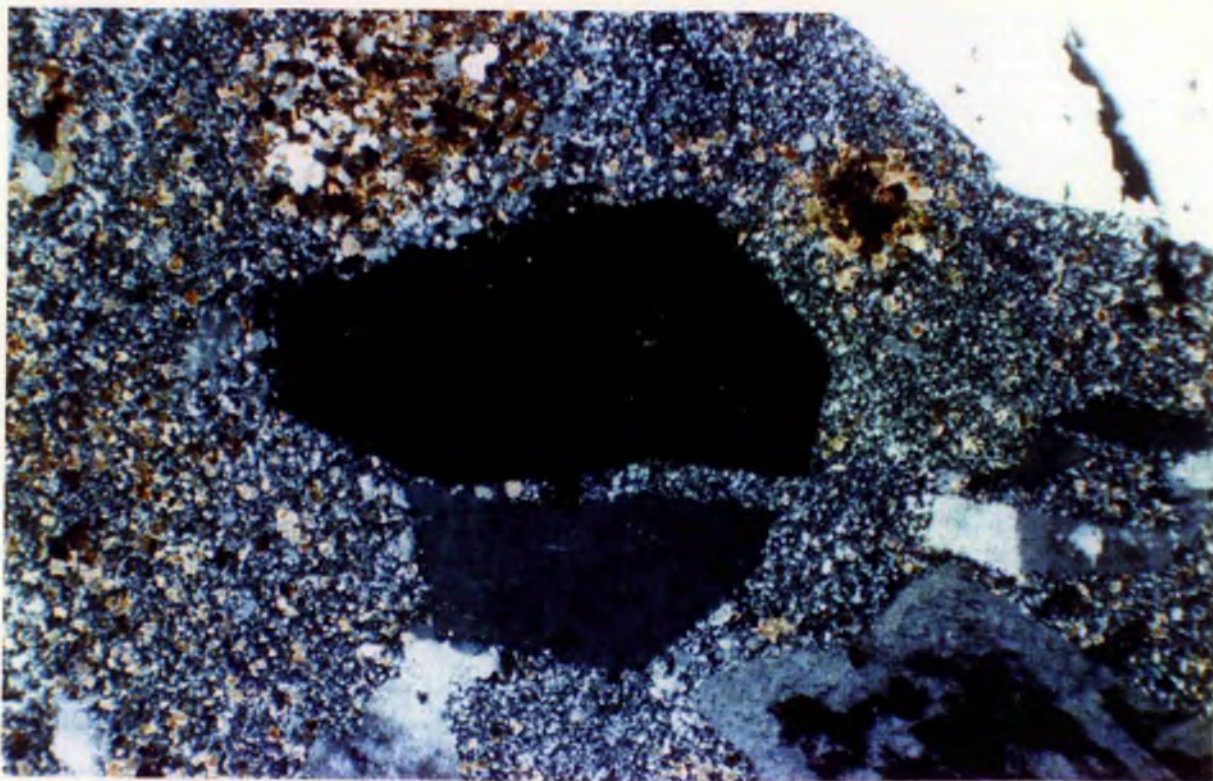


Plate 8.5 SS157 Fractured quartz phenocryst set in a fine-grained groundmass with clots of biotite. Quartz feldspar porphyry. x50

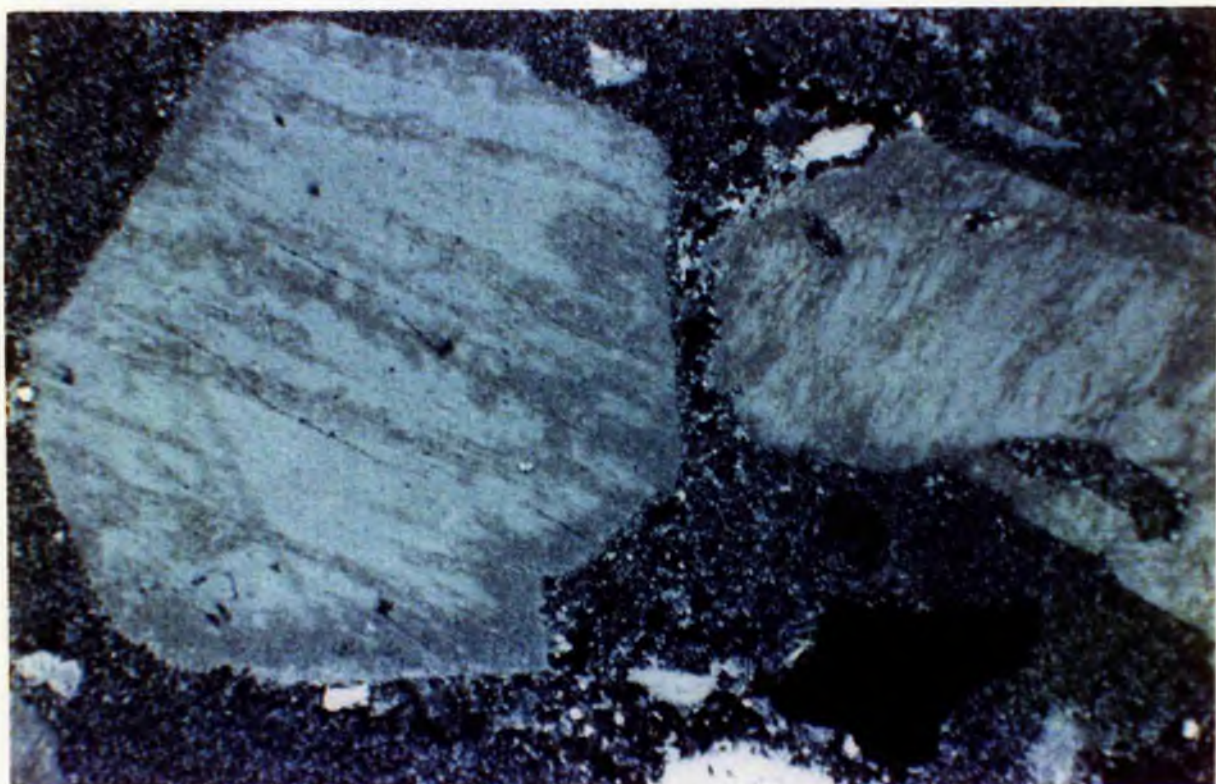


Plate 8.6 SS117/4 Orthoclase phenocryst with turbid zones of microcline set in the fine-grained groundmass of the quartz feldspar porphyry. x50

shock on cooling. Residual fluids have exploited these cracks, producing reaction zones in which microperthite has developed. Feldspar in the groundmass has also reacted with the fluid and its increased ordering is reflected in its turbidity. More commonly however in the samples examined, the whole feldspar population is perthitic. Initially, the perthite contains regular alternations of lamellae of probable exsolution origin. In slightly altered samples, the lamellae gradually coarsen and then break down into irregular domains of intermediate microcline (dark grey) and albite (white), to give a patch perthite (Plate 8.7). Film perthite develops from the patch perthite in more hydrothermally affected specimens from the Dawa area. Myrmekitic intergrowths of quartz occur along phenocryst margins. As this overgrowth occurs even in fragmental phenocrysts, and as it is in continuity with the groundmass, it is assumed that the overgrowth was contemporaneous with groundmass crystallisation. By analogy with the work of Ike (1979) on the feldspars of the quartz porphyry of the Tibchi complex, it is believed that the transparent feldspar is orthoclase cryptoperthite and the turbid zones with exsolved albite consist of a three-phase assemblage of a dominant orthoclase component with subordinate amounts of intermediate microcline and low albite.

The matrix is variable depending on the location:-

- In samples collected at Dawa, the matrix consists of quartz and alkali feldspar. The recrystallisation of the groundmass has resulted in the formation of clots of sieve-textured, khaki-coloured biotite - poikilitically enclosing rounded quartz (Plate 8.8) - accompanied by occasional streaks, lenses and blebs of fluorite, crystals of zircon, prismatic apatite and irregular patches of opaque iron-titanium oxides, probably representing recrystallised earlier mafic minerals. In addition to the biotite clusters there are rounded granules of biotite in the groundmass. Usually these are isolated, but they sometimes form beaded chains. These granules are greeny brown to tan in colour, pleochroic to straw yellow. Rare euhedral flakes of greeny brown mica, less than 0.1mm in size and also pleochroic to pale straw colour also occur in the groundmass. These flakes are most abundant in SS160 which also has the coarsest groundmass texture.

The accessory mineral assemblage is quite varied. Allanite, zircon and apatite occur in groundmass mica clusters. Cassiterite and sphalerite may occur in grains up to 0.5mm across, opaque ores - ilmenite, magnetite and haematite - are scattered in blebs through the groundmass with ilmenite laths up to 2mm recorded.

- In samples from the Ladini area, the groundmass mineralogy is rather different. The matrix which shows less recrystallisation than at Dawa is finer grained. It consists of quartz, feldspar and arfvedsonite with minor amounts of aegirine and no biotite. In sample SS116, the original mafic mineralogy has been completely destroyed and the only remains are clusters of opaques and rarely chlorite. In SS117/4 however, there is an amphibole whose probable composition is in the range richterite to arfvedsonite. It occurs as minute rounded discrete granules which are extremely abundant in the groundmass, less common spongy clusters up to 0.3mm in size, which are largely altered, prismatic laths, <0.004mm long in the groundmass, larger laths which are replaced by iron oxides, and rare skeletal, sieve-textured crystals up to 0.3mm in size (Plate 8.9). It is intensely pleochroic from dark blue-black through blue-green to khaki. Minute yellow-green prismatic crystals of aegirine, seen

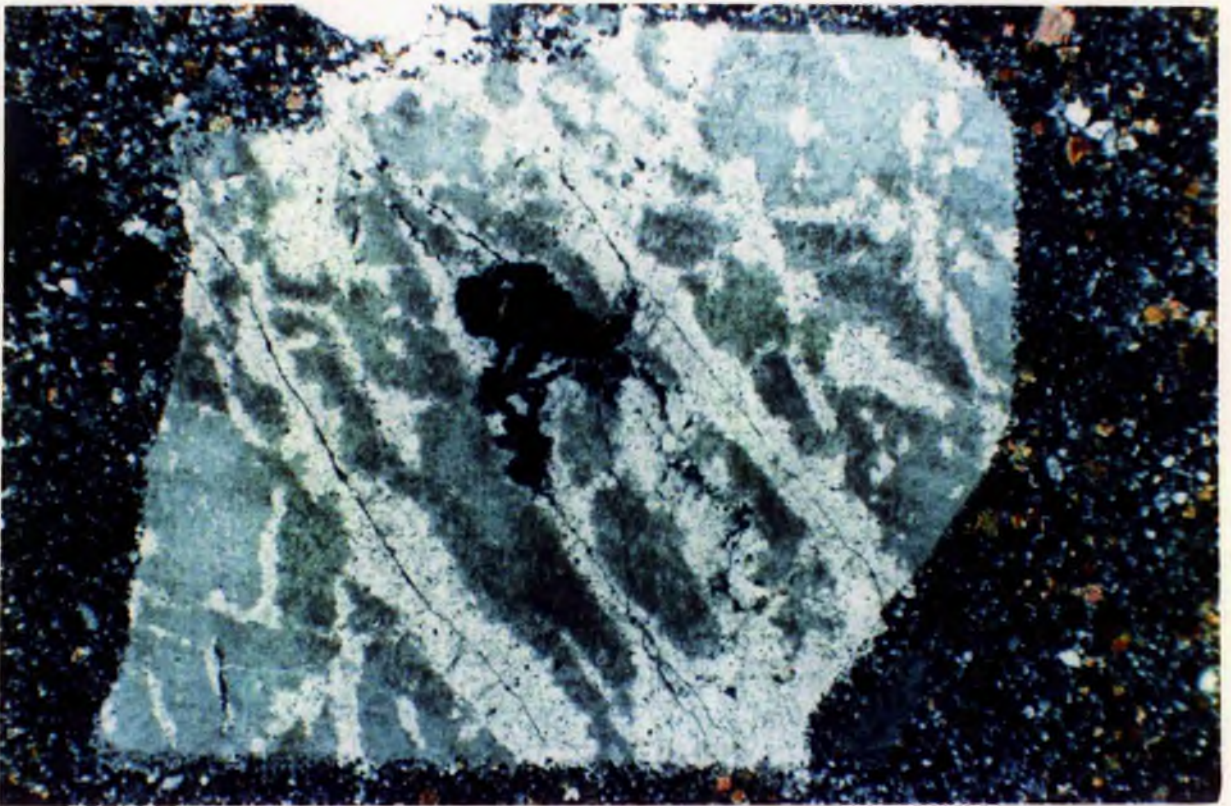


Plate 8.7 Lamellar perthite altering to patch perthite in the quartz feldspar porphyry. SS162, XPL x50

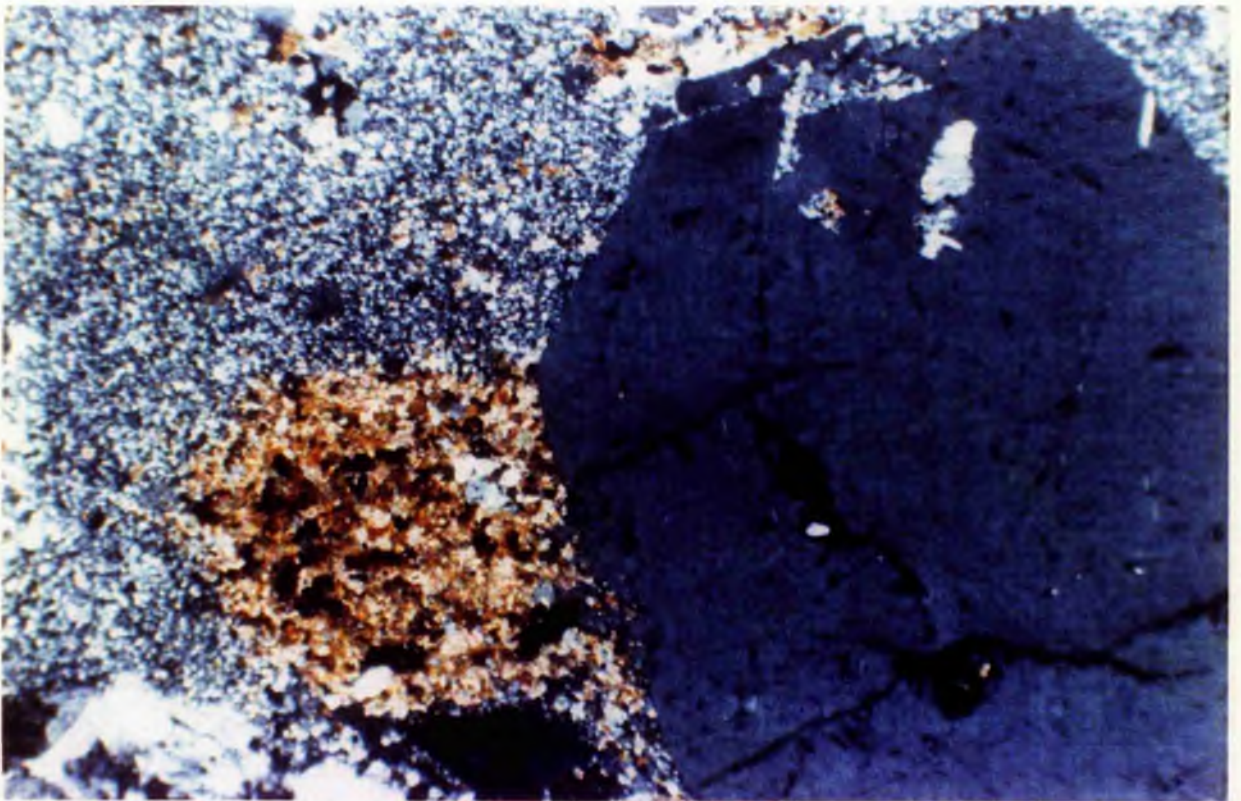


Plate 8.8 Recrystallised groundmass in SS157 with a clot of khaki-coloured biotite. XPL x50

3.7

8.8

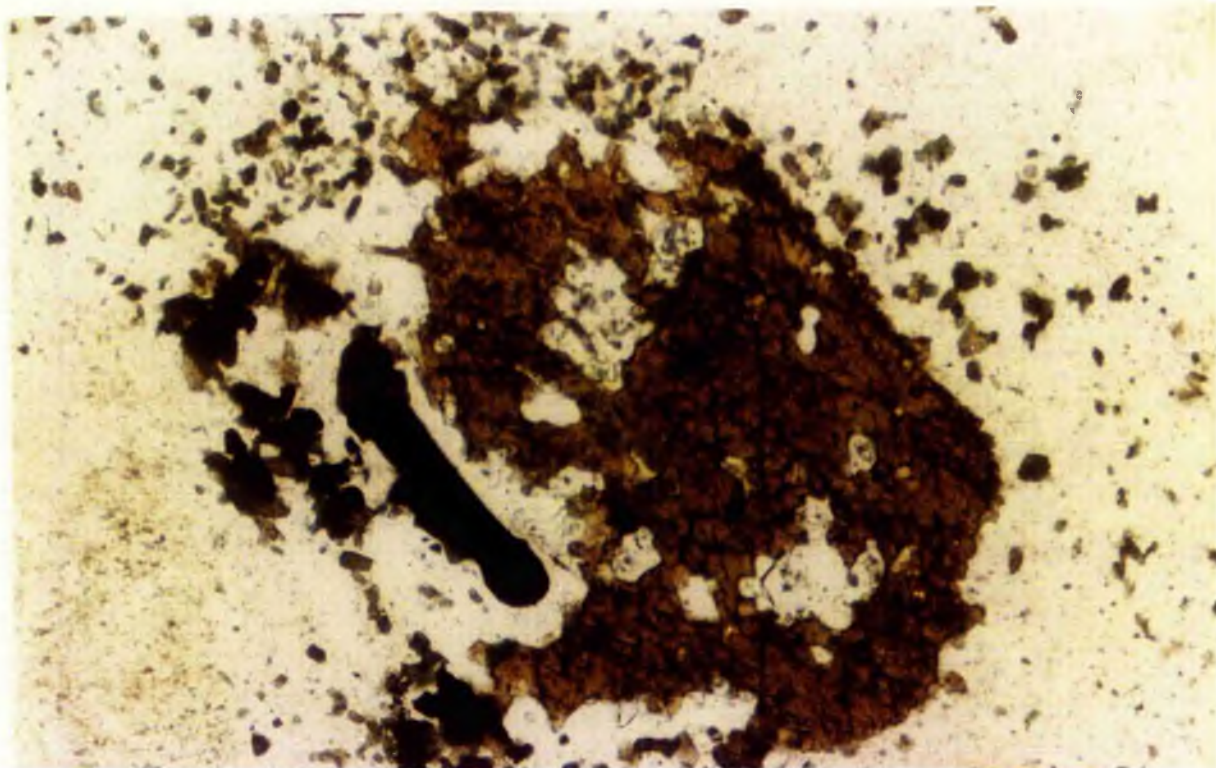


Plate 8.9 Arfvedsonite in the quartz feldspar porphyry

SS117/4 Skeletal, sieve-textured arfvedsonite with small granules of aegirine x125

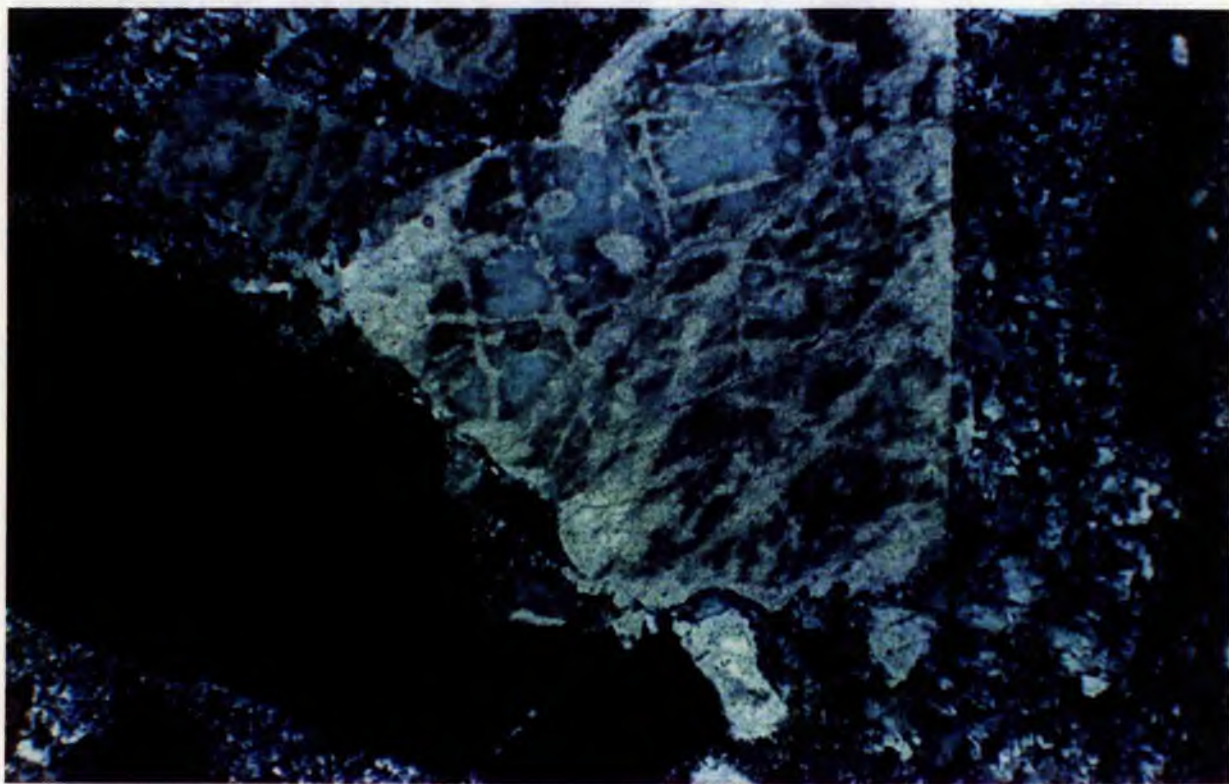


Plate 8.10 Quartz feldspar porphyry feeder dyke

Aggregates of patch perthite are set in a groundmass which is coarser textured than that of the volcanic pile. x25

only under highest magnification, occur within or around the arfvedsonite granules. There is no trace of biotite development. Apart from the iron and iron-titanium oxides, accessory minerals are less abundant than in the Dawa samples. Occasional zircon, fluorite, apatite and calcite occur.

The groundmass which was probably once isotropic in nature, has been completely recrystallised. Usually the groundmass is a fine grained mosaic but occasionally patches of coarsening texture are observed, becoming most abundant in SS160. Shards and pumice fragments are replaced by relatively coarse grained quartz with alkali feldspar and albite, sometimes showing spherulitic or myrmekitic texture. These are accompanied by the skeletal biotite already described and the iron oxides. Only ghostly relics of fiamme can be seen which therefore distinguishes this rock as a crystal tuff rather than as a porphyritic rhyolite. This recrystallisation is attributed to the nearness of the granite intrusion and the detailed effects and chemical changes associated with fluid phase reactions will be considered in more detail in the next chapter. Similar features of recrystallisation have been noted in the volcanics of the Tibchi Complex, close to the biotite granite contact (Ike 1979). However, unlike the welded crystal tuffs from other complexes, lithic fragments are rare in the volcanic pile at Dawa.

#### Petrology of the volcanic feeder dyke in the Dawa area

The quartz feldspar porphyry **feeder dyke** contains large phenocrysts of feldspar (Plate 8.10), and smaller rounded or ovate quartz phenocrysts (Plate 8.11), sometimes showing evidence of synneusis, set in a medium-grained groundmass of crystalline quartz which shows vestiges of a spherulitic texture. The groundmass texture is distinctly coarser than that of the volcanic pile. The phenocryst content is much lower than in the porphyritic volcanic material and occupies about 25% by volume compared with the 41% of the volcanics (Table 8.2).

The turbid feldspar phenocrysts are very variable in size from lmm to lcm, and are unevenly distributed. They are euhedral to ovoid in shape and may be embayed, but are never broken. They are dominantly patch perthite with some film perthite - often the perthite has been microclinised. The quartz is commonly rounded to ovate, and may be fractured and embayed, sometimes with strain extinction. The quartz contains abundant gas-rich and saline fluid inclusions. There is a much smaller percentage of quartz phenocrysts than in the volcanics. The porphyry feeder dyke also differs from the porphyritic volcanics in the absence of mica from the feeder intrusion. The groundmass is medium grained, with little variation and consists almost solely of quartz with occasional zircon and monazite and only traces of skeletal or anhedral iron oxides unless the porphyry has been hydrothermally altered. There are also traces of yellow sphalerite in the groundmass with anhedral to rounded grains of cassiterite not uncommon. Fluorite occurs within clusters of cassiterite crystals. These cassiterites vary from colourless to tan or reddish in colour and are commonly associated with late stage quartz veinlets. Sample SS175 is cut by quartz stringers up to lmm in width. The quartz in the stringers is tangential to the walls and contains reddish crystals of cassiterite. The feeder dyke appears to have been altered by mineralising late-stage fluids, escaping from depth, and utilising the ring-dyke fracture and in sample SS176, the feldspars have been completely destroyed resulting in haematite or limonite-lined cavities. Despite the extensive alteration of SS176, there is little evidence of ore minerals.

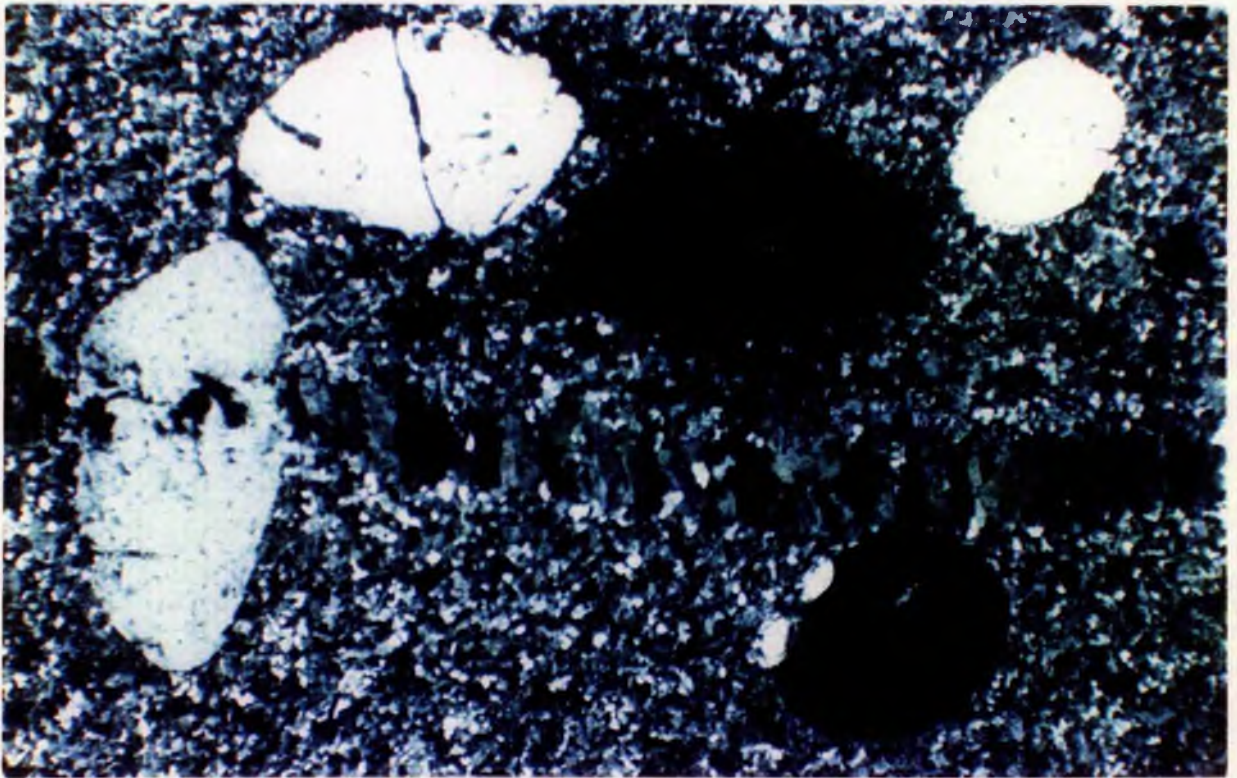


Plate 8.11 Porphyry feeder dyke

SS175 rounded phenocrysts of quartz in a medium-grained groundmass cut by a vein of microcline x125



Plate 8.12 Textural variants of Rishi biotite granite

- SS23/lb Granophyre
- SS38 Porphyritic texture
- SS14/1 Coarse-grained biotite granite
- SS55/8 Medium-grained biotite granite
- SS49/2 Fine-grained biotite granite

## Discussion

The deep embayments within both quartz and to a lesser extent the feldspar phenocrysts suggest rapid growth and "quench" crystallisation. Experimental work by Donaldson (pers comm) shows that deep embayments in quartz can only be created during skeletal crystallisation and are never formed by resorption. In contrast, slight curvature to normally angular faces, which is occasionally observed in some phenocrysts, may have resulted from resorption at a later stage.

There is a difference between the feldspar phenocryst assemblage from the Wundi river area and that from the volcanic pile at Dawa. Samples from the southwest in the Wundi river area, show occasional clear cores with turbid rims and cloudy zones traversing the phenocrysts. In the Dawa area however, the feldspars are mainly perthitic and clearly indicate greater fluid reaction. This is linked to a coarser-textured groundmass in the Dawa area.

The groundmass may have originally been dominantly glass, as suggested by occasional spherulitic textures but this has now been devitrified to a microcrystalline texture and partly re-equilibrated with the fluid exsolved from the underlying granitic intrusion. Under the influence of the fluids, new quartz clusters have grown in the groundmass.

The ferromagnesian mineralogy of the porphyry differs between the two areas studied. In the Wundi river area, there was abundant arfvedsonite, both within the groundmass and as occasional phenocrysts accompanied by minute aegirine. In the Dawa area however, the ferromagnesian mineralogy is solely of biotite and iron oxides. This is in sharp contrast to the porphyries from all other complexes where there are both amphibole phenocrysts and amphiboles in the groundmass - often of different compositions. This is also in contrast with the Tibchi Complex where Ike (1979) found that a peralkaline fluid evolved from the underlying biotite granite had resulted in the growth of new amphibole in both granite and quartz porphyries adjacent to the granite. Even samples taken very close to the biotite granite contact at Dawa however contain only biotite.

The absence of any evidence of synneusis of phenocrysts, coupled with the observation of broken crystals, faint relics of fiamme and traces of recrystallised shards suggests that the volcanic units are part of an ignimbritic pile. Such crystal rich ignimbrites are analagous to some described from the Ningi Burra complex (Turner and Bowden 1979), where although the crystal content ranges from 5-60%, the majority are crystal rich with 40-60% crystals. The eruptive mechanism of ash flows requires a build up of gas pressure and Turner and Bowden (1979), suggest that it is likely that favourable conditions for large eruptions were achieved only after substantial crystallisation had taken place. When more than 50-60% of the magma in a subvolcanic chamber was crystalline then eruptive activity ceased. By the caldera-forming stage therefore, a large high level reservoir capable of supplying crystal rich ignimbrites having volumes of the order of 50km<sup>3</sup> must have been developed. Turner and Bowden (1979) suggest, that once the gas-rich upper part of this had been erupted, accompanied by caldera collapse, the rest crystallised in situ as granite. If this is the case then there should be an overall similarity between the chemistry of the granite and the overlying volcanic pile. This comparison will be considered later.

## BIOTITE GRANITE

### Introduction

The main granite is medium to coarse-grained and cream or pinkish in colour when fresh. However there is a wide range of subtle colouration and grain size ranging from very fine to coarse with textural variations from granophyric or equigranular to porphyritic (Plate 8.12). The essential minerals are perthitic feldspar, quartz and biotite in order of abundance. Accessory minerals include zircon, fluorite and rutile, which are widely distributed with columbite, cassiterite, sphalerite, danalite and genthelvite locally. In the more hydrothermally altered facies of granite and microgranite the colour may vary from white, through cream, pale yellowish to pink and red. Intergranular patches of albite may occur and the perthitic feldspar and biotite is altered to some extent.

### Mineralogy

The main feldspar is of a microcline microperthite. These perthites show a variety of relationships of the sodic and potassic components. The most unaltered facies (SS 41/1a & SS58/1) show a lamellar distribution of phases with narrow albite lamellae in regular alternations with microcline lamellae (Plate 8.13). Such a texture is probably of exsolution origin. In granite samples where there has been limited hydrothermal alteration and subsolidus re-equilibration there is a gradation of lamellar perthite into patch perthite. With increasing hydrothermal alteration the distribution of the albite "patches" within the K-spar becomes completely random to give a patch perthite (Fig 8.2). The first signs of albitisation are the intergranular development of albite between perthite grains.

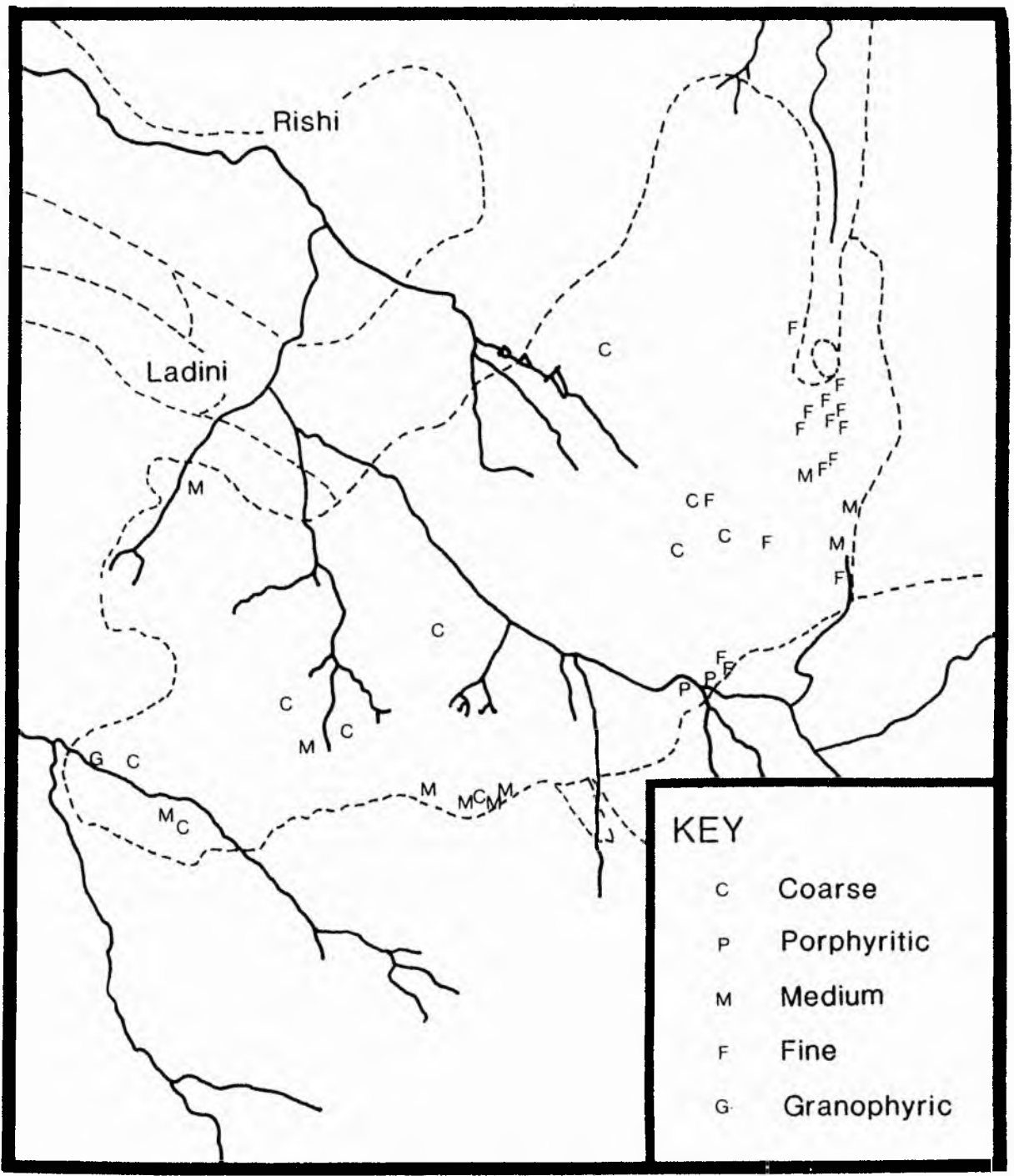
The quartz shows a wide range in crystal shape and texture. It varies from unstrained and isolated rounded crystals to clustered and beaded sometimes with consertal texture and often with strain extinction. Granophyric texture and micrographic intergrowths also occur in several samples.

The mica is the only ferromagnesian mineral of the granite. It is variable both in colour and texture. Such textures are shown in Fig 8.3.

### Petrology

There are five distinct textural types, a granophyric, a porphyritic, coarse-, medium- and fine-grained facies (Fig 8.7). Modally, the first four are indistinguishable (Table 8.3), but the fine-grained facies tends to show a hydrothermal modification either by sodic or pervasive acid (SS16/1) metasomatism.

Granophyres are represented by samples SS24/2, SS179 and SS23/13. Sample SS23/13 contains 29% modal quartz, 63% alkali feldspar and nearly 4% mica (Table 8.3). The texture varies from granophyric - in which intergrowths of quartz and turbid alkali feldspar extend outwards from a feldspar phenocryst (Plate 8.14) - to micrographic, in which there are intimate intergrowths of quartz and alkali



Scale 0 km 1

Fig 8.7 Distribution of the different textural facies within the Rishi biotite granite





Plate 8.13

Photomicrograph showing lamellar perthite and quartz in coarse-grained biotite granite. SS41/1a, XPL x50



Plate 8.14

Granophyric intergrowths of unstrained quartz and alkali feldspar together with lamellar perthite in sample SS23/13. XPL x50

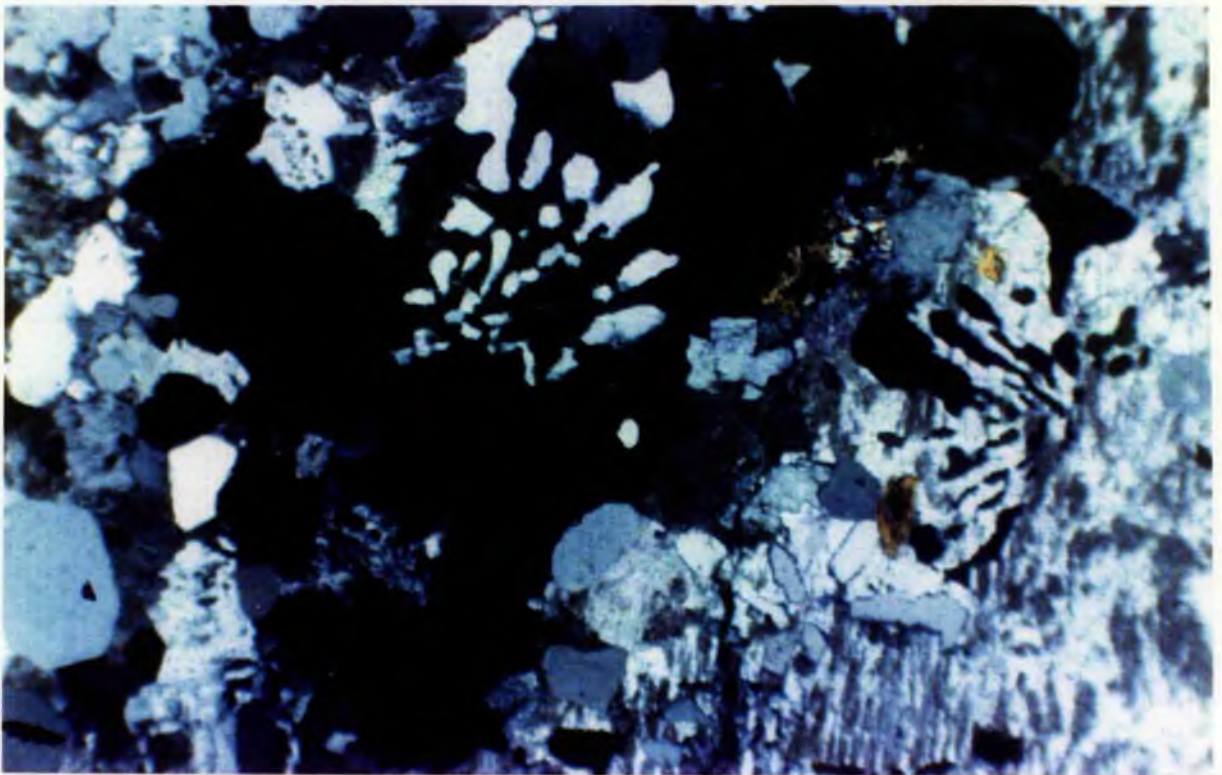


Plate 8.15                      Micrographic texture

Cuneiform intergrowths of quartz and alkali feldspar. Perthite shows patch texture (bottom right) and lamellar texture (right base). x50

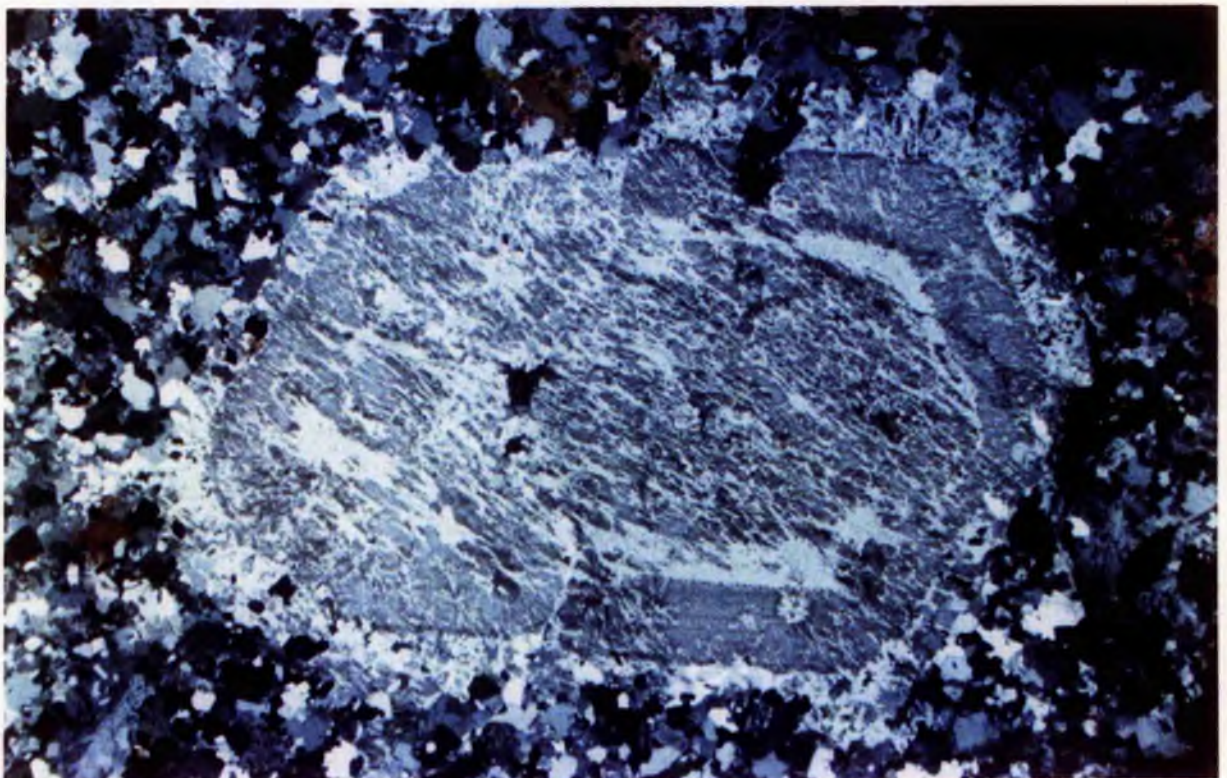


Plate 8.16                      Zoned feldspar

Large phenocryst with core of lamellar perthite separated from a rim of microcline by a thin clear zone of albite (SS40b) x15

feldspar. All the quartz is unstrained and rich in fluid inclusions. The feldspar sometimes shows lamellar, patch and occasionally braid perthite in the more "granitic" facies, becoming more mottled in the granophyric or micrographic facies. Occasionally there is slight alteration to albite or mica and in SS24/2 there is sometimes a limonitic staining of the feldspar. The main mica is very varied in texture ranging from skeletal and sieve textured to discrete ragged plates or clusters. It shows maximum absorption colours from grass green to deep greeny brown and is pleochroic to straw yellow or very pale green. Opaques are often associated with the mica where it has been chloritised. Discrete interstitial colourless fluorite is randomly disseminated and is not associated with mica distribution. In SS24/2, accessory genthelvite forms a skeletal, sieve-textured crystal 0.6mm in size. The genthelvite is a pale pink, high relief mineral which encloses globules of quartz and mica.

In the porphyritic facies, (SS34, SS38, SS40, SS42/1, SS53), modal quartz varies from 29-41%, perthite from 55-65% and mica from 2-5% (Table 8.3). Phenocrysts are of quartz or feldspar. The quartz phenocrysts are composite, up to 4mm in size, with strained extinction. Groundmass quartz is usually <0.5mm in size, and forms isolated, clustered, beaded or rounded grains, sometimes with consertal texture and with strained extinction. Occasionally, the groundmass quartz shows micrographic intergrowths with turbid alkali feldspar, especially in SS53 (Plate 8.15). The feldspar phenocrysts reach 2cm in size. The larger phenocrysts are often twinned and zoned (Plate 8.16). Larger phenocrysts have perthitic cores and margins with lamellar or patchy textures separated by a thin clear zone of albite in optical continuity with the albite of the perthite (SS38 and SS40). This zone of albite probably marks the beginning of a second stage of perthite growth. The perthite of the groundmass ranges from lamellar and patch textures which are dominant, through film perthite and myrmekitic or micrographic textures to intergranular albite laths. Both groundmass and phenocryst perthites show occasional mottled textures indicative of potassic alteration. The granophyric intergrowths of this facies and the granophyre indicate simultaneous growth of quartz and feldspar. The biotite varies from grass green through deep green to black in colour with little variation in any one section. It is nearly always skeletal in texture (Plate 8.17), with occasional discrete well-formed flakes or felted aggregates in SS42/1 (Plate 8.18). The skeletons have often enveloped rounded quartz and sometimes rounded or euhedral fluorite and more rarely zircon and monazite. There is no chloritisation and the cleavages, although distinct, are not characterised by extensive haematite development. Sample SS53 differs a little from the other four samples. There are colour variations within individual micas ranging from tan to deep green. Cleavages are emphasised by haematite development and occasional chloritisation.

In the coarse-grained facies, (SS41/1a, SS43, SS58/1, SS63/2 & SS64/1) the quartz varies from 29-36 modal per cent, perthite from 57-64% and mica from 1-9% (Table 8.3). The quartz is usually as rounded or irregular clusters 2-3mm in size, sometimes beaded, sometimes showing consertal texture and often with strain extinction plus occasional isolated subhedral to anhedral crystals. Usually the quartz is clear, sometimes it appears turbid due to the abundance of fluid inclusions. The feldspar forms clusters up to 1cm or more and these are surrounded by the chains or aggregates of glassy quartz. In several samples (SS41/1, SS43, SS58/1 for example) the perthite has a dominantly lamellar texture (Plate 8.19). In others (eg. SS27/2 & SS64/1) the lamellar texture has been broken down and patch perthite is dominant with some film perthite within

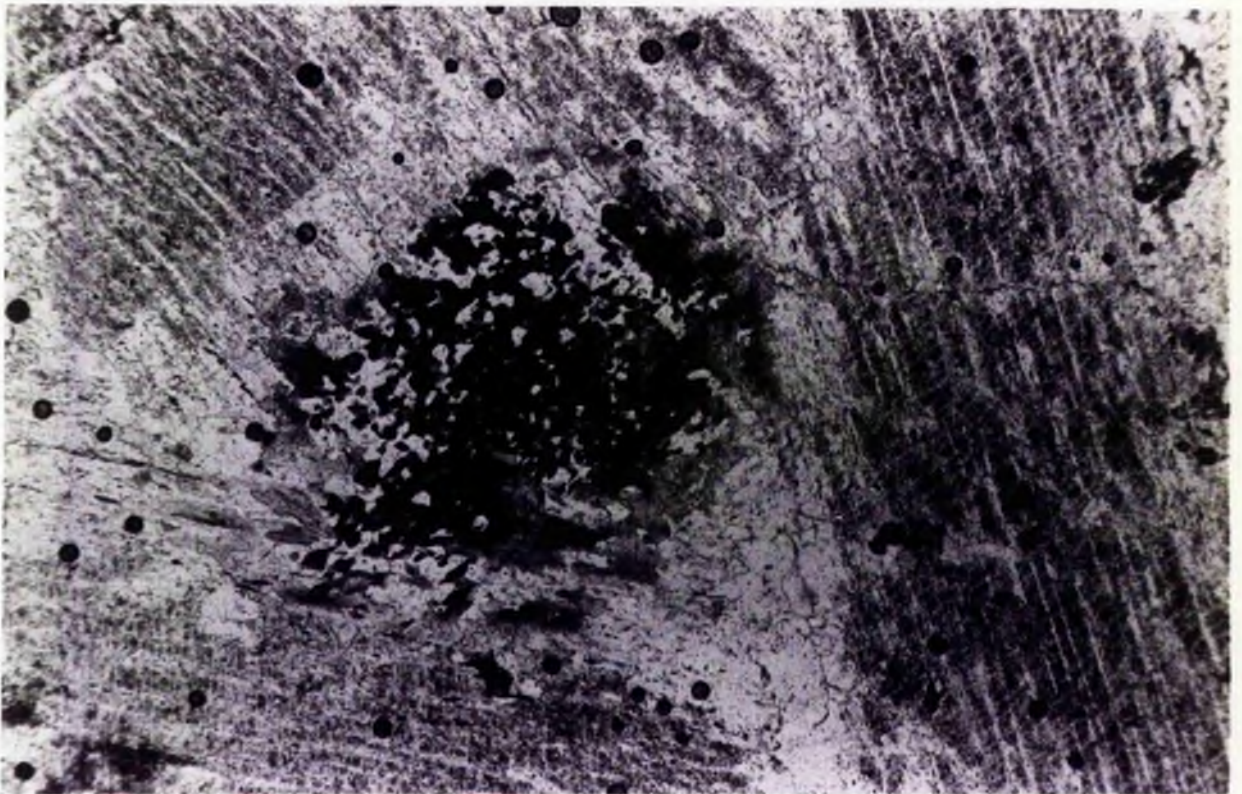


Plate 8.17

Photomicrograph showing skeletal mica with phenocrysts of lamellar perthite in porphyritic granite. SS40B, PPL x50



Plate 8.18

Felted aggregates of greenish brown mica in porphyritic biotite granites. SS42/1, PPL x50

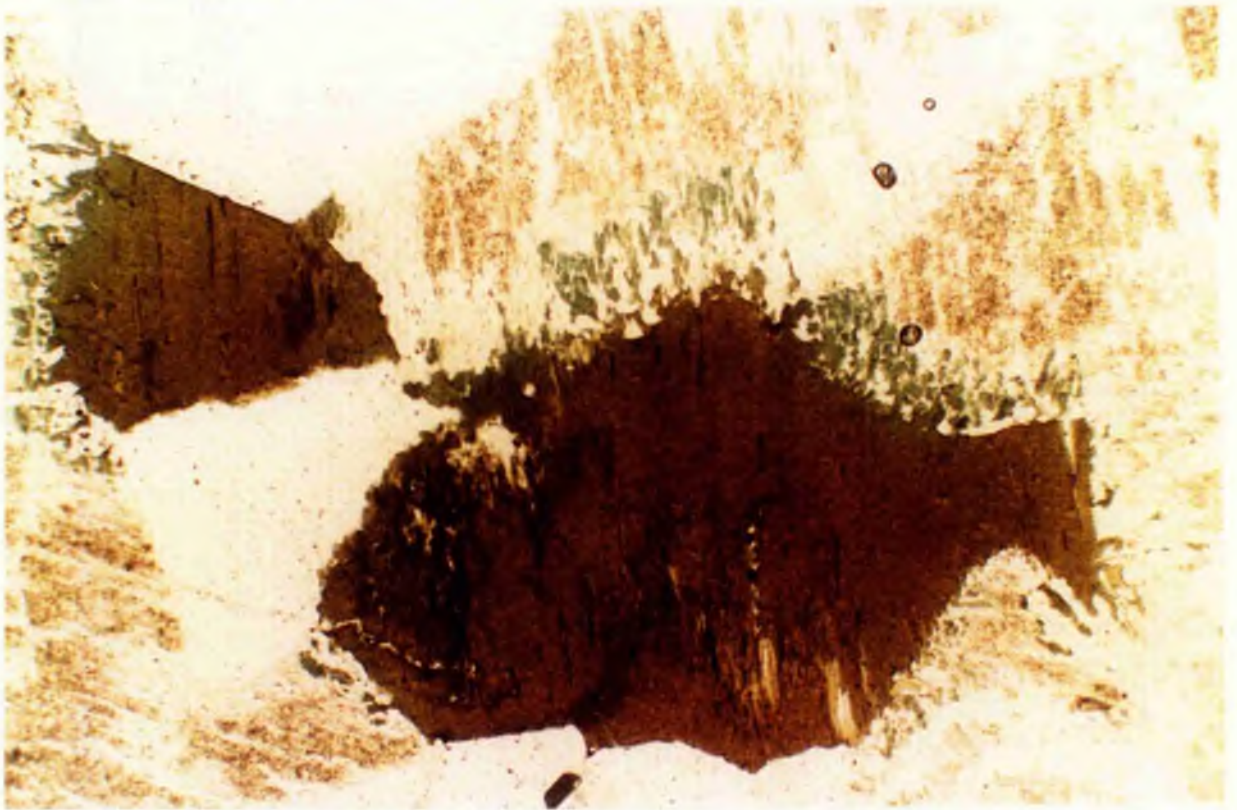


Plate 8.19 Pale green mica has grown along the potash rich zones of the lamellar textured perthite in SS43. PPL x50



Plate 8.20 Lamellar perthite rimmed by sieve-textured microcline. SS10/8, XPL x50

8.19.

one of the separate domains. Intergranular albite occurs in small amounts in most samples. Granophyric texture develops along feldspar boundaries. The degree of alteration either to sericite or chlorite is very limited.

In relatively unaltered granite, the biotite occurs as ragged, skeletal or sieve textured flakes or occasional aggregates up to 5mm in diameter, scattered irregularly through the rock. It varies from bluish green through khaki to deep bluey or brownish green or almost black and is pleochroic from pale green to yellow brown or khaki. Where the granite has been affected by late-stage alteration the biotite becomes paler in colour, often a pale bluey green and may be pleochroic from pale brown to colourless, or be pale grey. Pale green biotite which forms irregular fringes around existing biotite can often be seen growing at the expense of the K lamellae in perthites (Photo 8.19). This feature of new subsolidus biotite growth is particularly well displayed in SS43 and SS58/1). Pleochroic haloes surrounding monazite, zircon and occasional allanite are particularly noticeable in the paler varieties of mica. Fluorite often occurs, usually as rounded or subhedral masses within or around the mica and sometimes along the micas cleavage traces. In paler biotite, it is not uncommon to find haematite and rutile in minute rods associated with the fluorite along cleavage traces. In SS63/2 the cleavage traces are bent and heavily accentuated by opaques and limonitic streaks.

In the medium-grained facies, (SS9,10/8,12/3,33/8,35/1,36/2,50/2 and 55/8), modal quartz has a greater variation than in the coarse facies. It varies from 24-41% (Table 8.3), perthite from 51-68% and mica from 3-6%. The quartz is usually as rounded or irregular clusters up to 7mm in size but commonly 2-3mm across and sometimes it is much smaller and forms an interlocking mosaic. Sometimes it is beaded and both beaded and clustered quartz may show consertal texture and strained extinction. In addition there are occasional isolated subhedral to anhedral crystals. Usually the quartz is clear, sometimes it appears turbid due to the abundance of fluid inclusions. The feldspar forms discrete grains up to 5mm or more and these are surrounded by the chains or clusters of glassy quartz. In almost all samples the perthite is a mixture of lamellar or patch textures with some film perthite. Intergranular albite occurs in small amounts in most samples. Sometimes the perthite has myrmekitic integrowths of quartz. Also a granophyric texture develops along feldspar boundaries both at feldspar/quartz contacts and feldspar/feldspar grain boundaries. Several samples show incipient potassic alteration, and in SS10/8 lamellar perthite is rimmed by sieve-textured microcline (Plate 8.20). In other samples there has been slight acid alteration and chlorite may have been generated from either feldspar or mica alteration. The degree of alteration to chlorite however, is very limited. The biotite shows the same features of colour variation and texture described for the coarse grained facies above.

Biotite microgranite (SS16/2 and 49/2B), is commonly developed at the contact with the volcanics. In this fine grained facies the modal variation is greater than in the other textural variants, with either increased albite as a result of sodic metasomatism, traces of microcline replacing perthite, or increased biotite as a result of pervasive greisenisation. Only SS49/2B is a true fine-grained facies showing little hydrothermal alteration. The quartz occasionally forms rounded phenocrysts which may be up to 4mm in size and which sometimes shows strained extinction, set in a groundmass of small rounded or anhedral grains <0.5mm sometimes with very irregular amoeboid shapes. This does not show strained extinction, suggesting recrystallisation. Rare phenocrysts of

perthite, with Carlsbad twinning, are up to 4mm and show a patch texture. In SS16/2 the perthite shows traces of microclinisation. Groundmass perthites, less than 0.5mm in size, are also dominantly patch perthites. The mica is variable in colour from pale tan to deep chestnut - often within one sample - but the general tendency is towards a deep green colour.

All the biotite granite facies carry accessory zircon and fluorite, with minor genthelvite, haematite, ilmenite, columbite, pyrochlore, sphalerite and chalcopyrite.

## Discussion

The granophyric texture which is developed in several samples probably represents cotectic crystallisation of feldspar and quartz at the granite minimum temperature in a saturated medium. The samples that display both granophyric and micrographic textures are all from the roof facies of the granite, close to the contact with the volcanic pile.

Textural variations within other facies of the biotite granite reflect fluid phase development and rock-fluid interaction. It is probable that the resultant mineralogy is post-magmatic in origin. However, for the purpose of this discussion, the granites are regarded as "fresh", even though there are a number of petrographic and geochemical indicators that the fresh granite has been modified. This is particularly evident in the microcline rims to perthite, the subsolidus growth of biotite along K-lamellae in perthites and the development of chlorite.

## GEOCHEMISTRY

### Basement

Three samples of the porphyritic megacrystic monzogranite have been analysed, all from the Zelau-Rishi granite (Table 8.4). They have a range of silica content from 68.5-70.7%, an average 14.3% alumina, a range of 2.4-3.8 ferric iron and low MnO and MgO concentrations. CaO values range from 1.2-1.8%, Na<sub>2</sub>O content is from 3.0-3.4% and they are potash enriched, with K<sub>2</sub>O concentrations from 5.3-6.3%

Compared with other analyses of porphyritic older granites from Nigeria (Table 8.5), which show a surprisingly narrow range of values for each of the major element, there are no appreciable differences. The older granites from the Rishi area are very close in composition to the average of 39 samples taken from southwest, central and northern Nigeria.

Chondrite-normalised values (Fig 8.8a) of selected trace elements for the Zelau-Rishi basement granitoids are compared with the range for 22 samples from north central Nigeria. Values for the Zelau-Rishi granite fall within the range for the basement granites as a whole, with the exception of one Rb value, which exceeds other recorded values. However most of the Rishi samples clearly contain trace element concentrations towards the upper limits for all the elements.

Table 8.4 Chemical analyses and normative compositions of the Zelau-Rishi Older Granite

	SS17/2	SS180	SS181
SiO <sub>2</sub>	70.66	68.56	70.23
TiO <sub>2</sub>	0.20	0.49	0.50
Al <sub>2</sub> O <sub>3</sub>	14.30	14.27	14.26
Fe <sub>2</sub> O <sub>3</sub>	2.37	3.64	3.84
MnO	0.02	0.04	0.04
MgO	1.46	0.43	0.49
CaO	1.23	1.69	1.80
Na <sub>2</sub> O	2.95	3.34	3.40
K <sub>2</sub> O	6.27	5.40	5.30
P <sub>2</sub> O <sub>5</sub>	0.04	0.22	0.19
Total	99.50	98.08	100.05
R1	2128	2014	2122
R2	485	482	497
Q	149	137	146
F	16	-23	-29
Ba	1879	725	712
Be		13	
Ce	67	224	208
Cr	0	1	12
Cu	25	15	14
F		1300	
Hf	2	7	6
La	51	121	115
Li		36	
Mo		14	
Nb	15	18	20
Ni	8	5	4
Pb	54	32	33
Rb	397	222	225
Sn		27	
Sr	245	157	166
Th	13	25	23
V	18	16	14
Y	34	40	41
Zn	270	94	101
Zr	121	323	329
Zr/Hf	61	46	55
Ce/Y	2.0	5.6	5.1
quartz	24.83	24.84	26.14
ortho	37.04	31.9	31.31
plagio	24.95	28.25	28.76
anorth	5.84	6.95	7.69
corund	0.52	0.39	0.12
hy %en	3.63	1.07	1.22
haemat	2.37	3.62	3.84
ilmen	0.04	0.09	0.09
rutile	0.18	0.44	0.45
apatit	0.09	0.52	0.45
TTDI	86.82	85.00	86.21

Table 8.5 Chemical analyses of Nigerian Basement Granitoids

	1	2	3	4	5	6	7	8	9
SiO <sub>2</sub>	71.45	65.70	72.45	67.46	68.34	67.73	69.80	68.45	67.07
TiO <sub>2</sub>	0.32	0.43	0.25	1.11	0.80	0.95	0.66	0.78	0.75
Al <sub>2</sub> O <sub>3</sub>	14.26	15.75	14.05	15.29	14.55	14.40	14.48	14.24	14.53
Fe <sub>2</sub> O <sub>3</sub>	0.18	0.26	0.17	0.60	0.60	0.40	0.70	1.13	1.70
FeO	2.34	3.98	1.71	4.15	3.39	3.79	2.67	3.21	3.23
MnO	0.10	0.13	0.05	0.08	0.05	0.06	0.05	0.06	0.08
MgO	0.82	0.59	0.57	1.22	0.85	0.85	0.76	0.86	0.68
CaO	1.84	2.19	1.40	2.81	2.03	1.95	2.08	1.68	2.32
Na <sub>2</sub> O	3.57	3.92	3.18	2.96	3.06	2.78	2.66	2.60	3.20
K <sub>2</sub> O	4.64	5.94	5.75	4.68	5.23	5.35	5.61	6.33	5.44
P <sub>2</sub> O <sub>5</sub>	0.12	0.12	0.16	0.47	0.31	0.35	0.21	0.26	0.23
H <sub>2</sub> O <sup>+</sup>	0.55	0.65	0.47	0.00	0.00	0.00	0.00	0.00	0.34
H <sub>2</sub> O <sup>-</sup>	0.04	0.05	0.04	0.00	0.00	0.00	0.00	0.00	0.04
CO <sub>2</sub>	0.11	0.24	0.20	0.00	0.00	0.00	0.00	0.00	0.30
Cl <sup>2</sup>	0.02	0.02	0.02	0.00	0.00	0.00	0.00	0.00	0.00
F	0.02	0.02	0.02	0.00	0.00	0.00	0.00	0.00	0.00
S	0.02	tr	tr	0.00	0.00	0.00	0.00	0.00	0.00
Total	100.40	99.99	100.49						
Less O	0.02	0.01	0.01						
Total	100.38	99.98	100.48	99.09	99.21	98.51	99.68	99.60	99.91

	10	11	12	13	14	15	16	17
SiO <sub>2</sub>	67.86	65.59	62.28	73.60	66.78	67.84	71.97	72.24
TiO <sub>2</sub>	0.61	0.81	0.24	0.08	0.85	0.74	0.22	0.36
Al <sub>2</sub> O <sub>3</sub>	14.90	14.49	20.31	13.92	13.94	14.60	13.76	14.10
Fe <sub>2</sub> O <sub>3</sub>	0.73	3.96	0.67	0.17	1.28	1.22	0.13	0.39
FeO	3.24	1.53	0.75	0.52	4.43	3.26	1.82	1.59
MnO	0.06	0.10	0.04	0.01	0.09	0.05	0.06	0.02
MgO	0.55	0.71	0.32	0.12	0.73	0.67	0.37	0.37
CaO	2.15	2.37	1.60	1.24	2.66	2.24	1.16	1.18
Na <sub>2</sub> O	3.32	3.28	5.71	3.62	3.32	3.45	3.30	3.93
K <sub>2</sub> O	5.72	5.14	7.03	5.12	4.52	4.97	5.50	4.88
P <sub>2</sub> O <sub>5</sub>	0.19	0.26	0.08	0.03	0.31	0.27	0.08	0.11
H <sub>2</sub> O <sup>+</sup>	0.44	1.08	0.35	0.46	0.68	0.60	1.01	0.65
H <sub>2</sub> O <sup>-</sup>	0.03	0.17	0.04	0.08	0.04	0.04	0.14	0.09
CO <sub>2</sub>	0.16	0.47	0.09	0.93	0.27	0.09	0.49	0.06
Cl <sup>2</sup>	0.00	0.00	0.00	0.00	0.00	0.00	0.00	0.00
F	0.00	0.00	0.00	0.00	0.00	0.00	0.00	0.00
S	0.00	0.00	0.00	0.00	0.00	0.00	0.00	0.00
Total	99.96	99.96	99.51	99.90	99.90	100.04	100.01	99.97

Analyses 1-3 MacLeod et al 1971

4-8 Kayode 1976

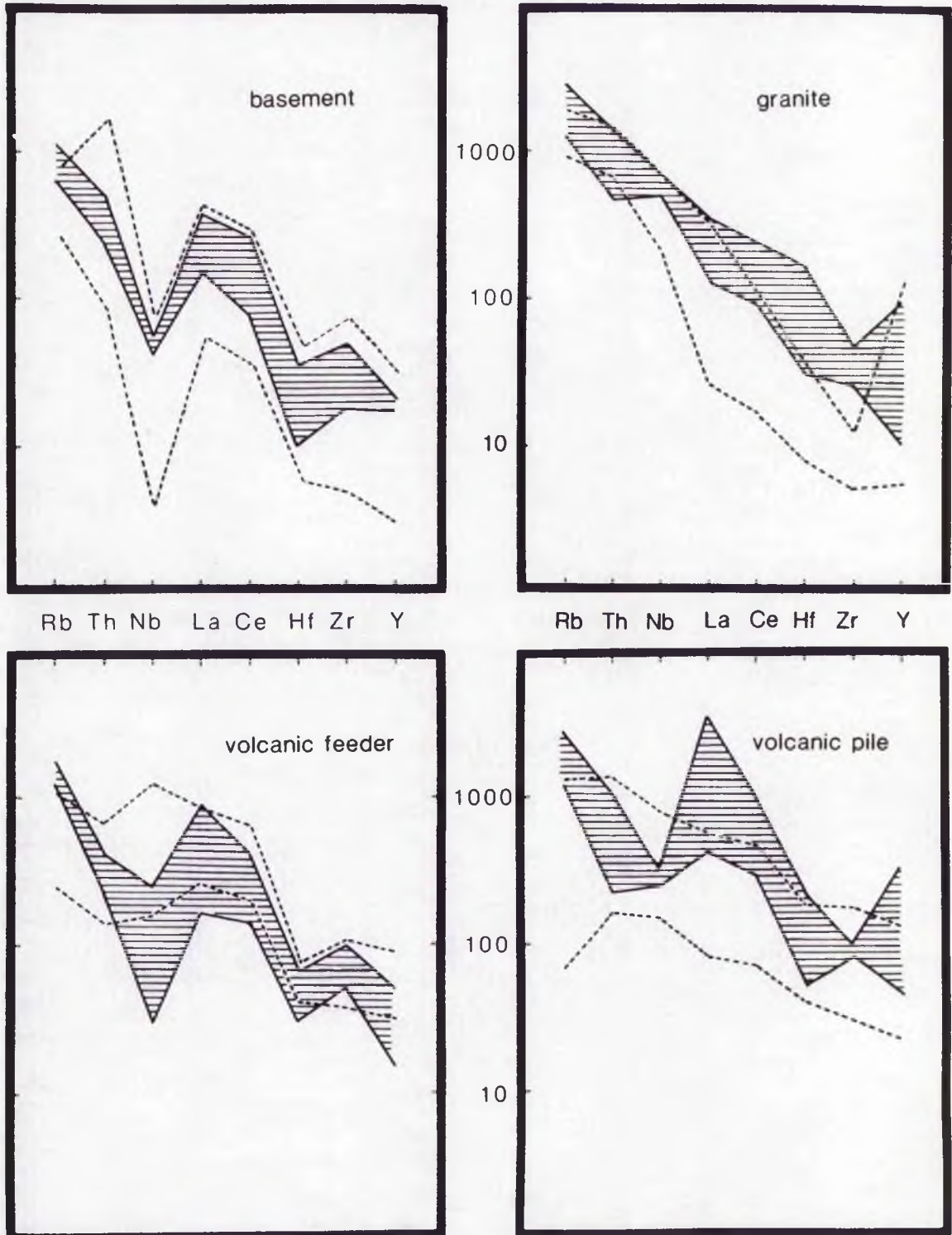
9-17 Olarewaju 1978

## Older Granite analyses:

- 1 Medium-grained Gora biotite granite, north central Nigeria
- 2 Medium- to coarse-grained hornblende biotite granite
- 3 Fine- to medium-grained Assob biotite muscovite granite
- 4-8 Porphyritic granites of the Igbo Ora complex, SW Nigeria
- 9 Porphyritic granite from Kayarda, north central Nigeria
- 10 Porphyritic granite from Saminaka, north central Nigeria
- 11 Porphyritic granite from Dan Alhaji, north central Nigeria
- 12 Fine-grained leucogranite from Dan Alhaji
- 13 Fine-grained leucogranite along Banke-Dogoa road, north central Nigeria
- 14 Porphyritic granite along Falgore-Kano road, north central Nigeria
- 15 Porphyritic granite along Falgore-Kano road
- 16 Medium- to coarse-grained granite from Mai-Lumba area, north central Nigeria
- 17 Fine-grained leucogranite near Mai-Lumba

Fig 8.8 Selected chondrite-normalised trace element data for the different rock types of the Rishi area.

The shaded zone covers the range of concentrations found in the Rishi area; the dotted zone is the range for similar rock types elsewhere in Nigeria based on 22 samples for the basement, 20 samples for the volcanic feeder intrusion, 22 samples for the volcanic pile and 68 for the biotite granites



The chondrite-normalised values of trace element concentrations within the basement rocks, have important implications for the petrogenesis of the younger granites.

The granite is corundum normative and is shown as crosses on the Q-F cationic plot and Q-A-P normative diagram (Fig 8.9).

### Volcanic rocks

Ten volcanic rock samples have been analysed, eight from the volcanic pile and two from the volcanic feeder intrusions (Table 8.6). Those from the volcanic pile, have a silica content averaging 74% which is standard for volcanic rocks of the province as a whole. The alumina and ferric content of these rocks however, at 12.7% and 2.9% respectively, is higher than the average for the province. The soda content, which averages 3.7% is about average for Nigerian volcanic rocks but the most noticeable chemical feature is the enhancement of potash in these volcanics compared with the province as a whole. The average of 5.2% for Rishi rocks is considerably higher than the 4.5% for the Nigerian province. Clearly, the normative compositions show that these volcanic rocks are peraluminous in character with normative corundum.

Trace element values are very variable in both the volcanic pile and feeder dyke, for example Ba values are zero for seven out of the ten samples with values up to 1835 ppm (SS173) in the remaining three. Selected chondrite normalised trace element values are plotted on Fig 8.8 and compared with other acid eruptive rocks (Fig 8.8d) or porphyry feeders (Fig 8.8c) from the Nigerian Province as a whole. Rather surprisingly, when the trace element patterns of the volcanic pile at Rishi are compared with the province as a whole there is a significant difference. It had been expected that the range of values for the Rishi area would fall within the range for samples collected from the Province as a whole, but as Fig 8.8c shows, this is not the case. Rishi samples are more enriched in most elements especially in Rb, La and Ce compared with other complexes.

Since only two samples of the porphyry feeder dyke were analysed, the actual range of trace element concentrations may be greater than indicated. However, when compared with porphyry feeder dykes from other complexes in Nigeria the pattern is broadly similar. With the exception of Rb, there is a slight depletion of the whole trace element spectrum within the Rishi samples, which is most noticeable for Nb.

There is a marked difference in the chondrite-normalised pattern of selected trace elements for the Rishi volcanic pile and the porphyry feeder dyke. This is due to the relative depletion of Nb in the volcanic feeder and the relative enrichment of La in the volcanic pile. This must indicate that there have been post magmatic changes in elemental concentrations either in the volcanic pile or the porphyry, or perhaps both. The enrichment in Rb in both the volcanic pile and feeder dykes compared with similar rock types elsewhere in Nigeria reflects the higher K content of the Rishi samples.

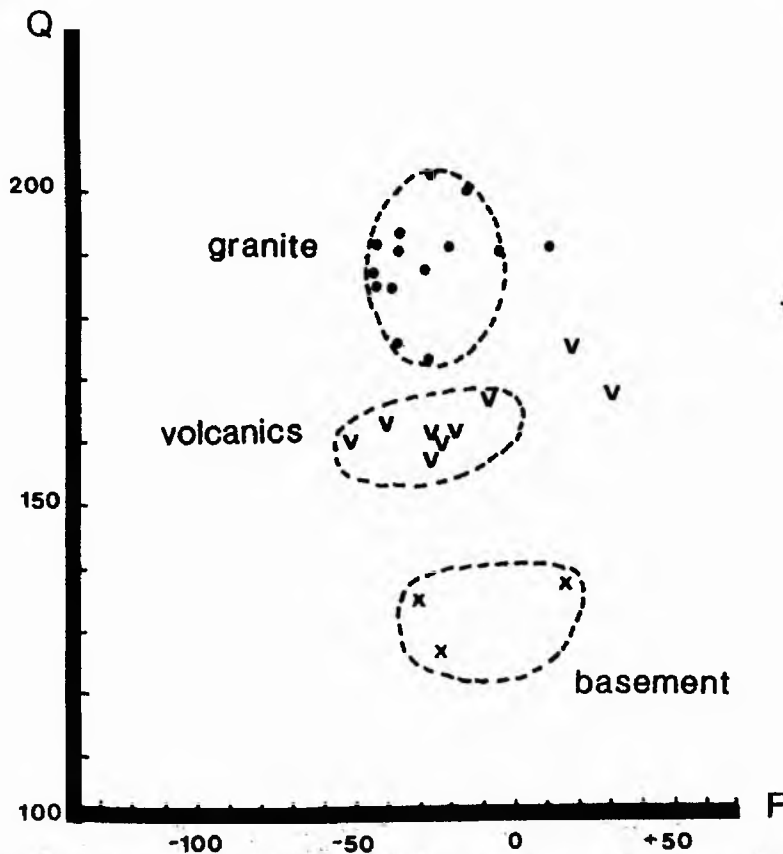
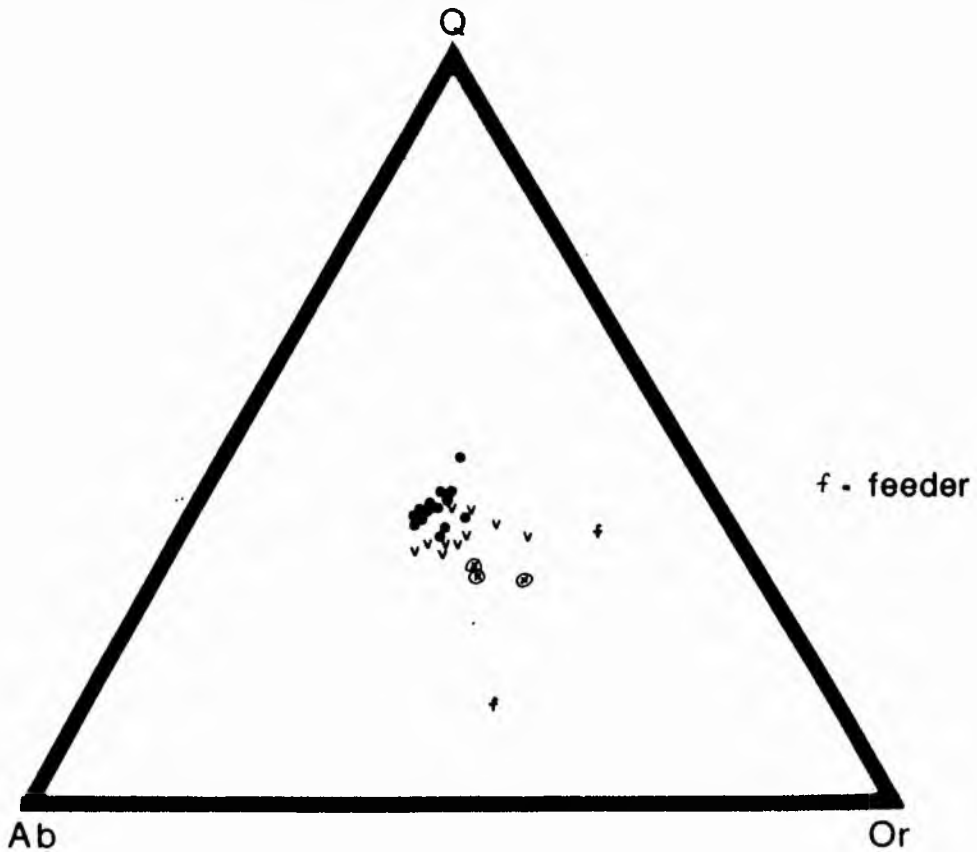
Table 8.6 Chemical analyses and normative compositions of the Quartz-feldspar Porphyries

	SS84	SS85/2	SS157	SS158	SS160	SS161	SS162	SS167	feeder dyke	
									SS173	SS175
SiO <sub>2</sub>	74.75	75.82	74.20	74.48	74.44	73.45	74.35	74.36	62.73	74.94
TiO <sub>2</sub>	0.20	0.20	0.18	0.21	0.20	0.28	0.20	0.21	0.93	0.23
Al <sub>2</sub> O <sub>3</sub>	12.62	12.32	13.05	12.74	13.34	13.04	12.78	12.80	18.53	12.87
Fe <sub>2</sub> O <sub>3</sub>	2.66	2.83	2.66	3.08	3.07	3.40	2.91	2.70	3.32	0.80
MnO	0.03	0.03	0.00	0.06	0.04	0.03	0.05	0.03	0.05	0.02
MgO	0.09	0.25	0.03	0.10	0.02	0.00	0.01	0.03	1.66	0.02
CaO	0.42	0.57	0.66	0.57	0.60	0.63	0.54	0.59	2.94	0.85
Na <sub>2</sub> O	3.10	3.45	3.69	3.88	4.06	4.19	3.51	3.91	3.69	1.86
K <sub>2</sub> O	5.84	4.91	5.31	5.11	4.79	4.50	5.45	5.22	6.30	7.65
P <sub>2</sub> O <sub>5</sub>	0.01	0.03	0.01	0.02	0.01	0.01	0.01	0.02	0.37	0.04
Total	99.72	100.41	99.79	100.25	100.57	99.53	99.81	99.87	100.52	99.28
R1	2440	2600	2318	2304	2314	2259	2353	2270	1288	2516
R2	297	315	328	316	327	323	309	316	760	344
Q	185	198	171	172	172	169	177	168	60	183
F	16	-17	-18	-27	-40	-51	-7	-26	-38	87
Ba	0	0	0	0	0	83	0	0	1853	21
Ce	256	249	387	275	420	842	278	329	120	360
Cr	0	0	0	0	6	30	0	0	16	4
Cu	80	0	17	17	12	19	10	16	6	11
F					5600				3900	
Hf	10	42	12	12	11	11	10	12	6	13
La	148	168	257	145	431	1112	154	183	52	296
Li					398				36	
Mo					14				33	
Nb	113	111	101	103	94	112	100	97	10	86
Ni	97	72	7	6	9	10	10	7	13	9
Pb	32	159	45	163	56	442	56	17	21	423
Rb	855	959	473	585	667	436	679	648	453	606
Sn					408				27	
Sr	7	9	13	9	12	12	9	9	337	38
Th	52	36	24	23	32	24	26	34	11	21
V	0	0	0	0	0	0	0	0	102	0
Y	88	95	110	88	168	641	86	137	27	95
Zn	446	317	353	1500	4967	1706	1616	1159	162	1001
Zr	637	660	631	616	563	683	599	632	341	668
Zr/Hf	64	16	21	51	51	62	60	53	57	51
Ce/Y	2.9	2.6	4.7	3.1	2.5	1.3	3.2	2.4	4.4	3.8
quartz	33.38	35.47	31.00	31.15	31.23	30.55	31.95	30.59	9.45	33.12
ortho	34.50	29.01	31.37	30.19	28.30	26.59	32.20	30.84	37.22	45.20
albite	26.22	29.18	31.21	32.82	34.34	35.44	29.69	33.07	31.21	15.73
anorth	2.02	2.63	3.21	2.26	2.91	3.06	2.61	1.97	12.17	3.95
corund	0.46	0.37	0.06	0.00	0.41	0.16	0.15	0.00	1.18	0.08
di %wo	0.00	0.00	0.00	0.00	0.00	0.00	0.00	0.09	0.00	0.00
di %en	0.00	0.00	0.00	0.00	0.00	0.00	0.00	0.07	0.00	0.00
hy %en	0.22	0.62	0.07	0.25	0.05	0.00	0.02	0.00	4.13	0.05
haemat	2.66	2.83	2.66	3.08	3.07	3.40	2.91	2.70	3.32	0.80
ilmen	0.06	0.06	0.00	0.13	0.09	0.06	0.11	0.06	0.11	0.04
rutile	0.17	0.17	0.18	0.02	0.15	0.25	0.14	0.00	0.87	0.21
titan	0.00	0.00	0.00	0.31	0.00	0.00	0.00	0.43	0.00	0.00
apatit	0.02	0.07	0.02	0.05	0.02	0.02	0.02	0.05	0.88	0.09
TTDI	94.10	93.66	93.58	94.16	93.86	92.58	93.84	94.50	77.88	94.05

Fig 8.9

(a) Q-Ab-Or normative values for the different rock types to show variations in salic constituents between v = volcanic rocks, f = volcanic feeder dyke, cross within a circle = basement monzogranite, solid circle = biotite granite

(b) the same data samples plotted on a Q-F diagram to show the different fields occupied by the major rock types



## Biotite granite

Like the volcanic rocks the biotite granite is peraluminous with the molecular proportion of alumina greater than that of sodium and potassium oxides combined. The main mineralogical expression of this peraluminous character in these anorogenic biotite granites is a trioctahedral lithium-iron mica. The only other aluminous phase, topaz, is restricted to greisenised granites, which are more aluminous than other granites because of the removal of alkalis during the greisenisation process.

Fifteen samples were analysed from the fine, medium, porphyritic and coarse facies (Table 8.7). The overall chemistry shows a remarkably constant silica composition which varies between 75.52 and 77.73% and averages 76.86%. The highest silica enrichment is in the fine-grained facies but there is otherwise no general correlation between variation in grain size and silica percentage. There is an equally limited range of alumina which is restricted to the range 11.94-12.93%. There is similarly a very tight range of alkali and iron compositions. Chondrite-normalised trace element variations, shown on Fig 8.8b have a very limited range of values.

This limited range of major and minor element chemistry - which lies close to the granite minimum - is not surprising as the previous rock types considered also show a limited range. Perhaps what is surprising is the narrow range of trace element values. When compared with the average for biotite granites from the province as a whole however, all the trace element concentrations shown in Fig 8.8b are enhanced compared with other complexes. For example, Rb values within the Rishi biotite granite, which average 664 ppm (15 samples), are consistently higher than the average for Nigerian biotite granites as a whole, which is 464ppm (68 samples). Also tin values are much higher than the average of 22ppm given by Olade (1980).

## Discussion

A comparison of the chemistry of all the rock types shows that the basement granites have the lowest silica (70%), the volcanics have intermediate values (75%), while the biotite granite is silica enriched (77%). In contrast alumina values are lowest in the biotite granites and highest in the basement granitoids. Calcium values are highest in the basement granitoids, low in the younger granite and very variable in the volcanic sequence. Soda values are broadly similar in all rock types whilst potash values are high in all rock types, most notably in the volcanic sequence (up to 7.66%). Because of the different silica concentrations the different rock types occupy different fields on a Q-F plot (Fig 8.9).

It is a comparison of the trace element data however, that proves the most interesting as far as petrogenesis is concerned. The porphyritic older granites of the basement are clearly distinguishable from the younger granites on trace element abundances. Most notably they have higher Ba, V, Sr, Zr and Ce, slightly higher La with lower Nb, Y, Zn and Rb. This contrast is very valuable in distinguishing basement granitoids that have been extensively altered from younger granites which have also been extensively modified. The altered basement

Table 8.7 Chemical analyses and normative compositions of the Rishi Biotite Granite

	coarse		porphyritic					medium					fine		
	SS27/1	SS43	SS58/1	SS64/1	SS34	SS38	SS40/1	SS9	SS10/8	SS12/3	SS35	SS35/1	SS50/2	SS85/1	SS86
SiO <sub>2</sub>	77.16	77.04	77.58	77.16	77.07	77.08	77.41	77.45	76.91	76.31	75.44	76.10	75.52	76.83	77.73
TiO <sub>2</sub>	0.07	0.00	0.08	0.07	0.00	0.01	0.06	0.01	0.07	0.01	0.05	0.07	0.08	0.13	0.05
Al <sub>2</sub> O <sub>3</sub>	12.21	12.14	11.94	12.14	12.25	12.14	12.14	12.18	12.16	12.93	13.04	12.91	12.75	12.58	12.47
Fe <sub>2</sub> O <sub>3</sub>	1.43	1.63	1.69	1.43	1.56	1.63	1.54	1.69	1.81	1.61	1.42	1.45	1.63	1.81	1.03
MnO	0.01	0.02	0.03	0.02	0.02	0.02	0.01	0.02	0.03	0.18	0.00	0.01	0.02	0.03	0.01
MgO	0.06	0.24	0.01	0.03	0.22	0.00	0.04	0.04	0.09	0.24	0.02	0.03	0.01	0.09	0.05
CaO	0.31	0.36	0.34	0.30	0.23	0.25	0.29	0.26	0.40	0.57	0.76	0.73	0.62	0.07	0.37
Na <sub>2</sub> O	4.18	3.45	3.59	4.05	3.89	4.12	4.03	2.97	3.67	3.65	3.71	3.88	3.40	3.34	3.45
K <sub>2</sub> O	4.34	4.63	4.52	4.35	4.52	4.45	4.39	4.43	4.72	4.96	4.94	4.91	4.72	5.44	5.40
P <sub>2</sub> O <sub>5</sub>	0.01	0.00	0.00	0.00	0.01	0.08	0.01	0.00	0.03	0.01	0.01	0.01	0.00	0.00	0.00
H <sub>2</sub> O	0.00	0.00	0.00	0.00	0.42	0.36	0.00	0.30	0.00	0.00	0.00	0.00	0.00	0.00	0.00
Li <sub>2</sub> O	0.04	0.03	0.04	0.04	0.03	0.04	0.04	0.06	0.00	0.00	0.00	0.01	0.02	0.00	0.00
Total	99.82	99.54	99.82	99.59	100.22	100.18	99.97	99.41	99.88	100.47	99.39	100.11	98.75	100.32	100.56
R1	2601	2782	2790	2645	2655	2588	2657	3024	2668	2648	2514	2504	2675	2610	2661
R2	276	289	271	272	276	265	271	269	286	327	338	333	316	259	287
Q	197	213	214	201	202	197	202	236	203	199	184	184	201	202	200
F	-48	-19	-26	-44	-34	-43	-42	-6	-25	-28	-28	-34	-21	6	-3
Ba	0	1	0	0	0	58	0	42	0	0	0	0	0	0	0
Ce	112	178	121	123	115	123	123	114	125	132	113	100	129	174	78
Cr	0	0	0	9	0	0	38	0	1	0	0	0	0	0	0
Cu	15	4	15	10	4	4	24	6	14	5	20	20	13	0	0
F		5300	3100		3400	2800		3300		3100	3900				
Hf	7	9	8	6	11	11	6	10	8	8	6	6	7	32	24
La	74	110	72	64	65	71	74	68	81	76	56	50	68	88	42
Li	186	135	167	194	139	195	192	269	28	28	19	23	87		
Mo		<14	<14		<14	<14		<14		17	<14				
Nb	195	244	231	183	216	229	200	197	194	174	178	179	157		221
Ni	6	4	8	9	5	5	7	6	12	4	9	9	15	31	71
Pb	14	24	13	44	22	16	25	120	29	150	68	57	38	52	21
Rb	741	518	592	740	514	621	607	803	807	479	452	455	495	1135	994
SnO <sub>2</sub>		81	27		64	32		150		67	67				
Sr	3	6	5	3	5	9	4	3	5	3	5	5	17	0	4
Th	68	38	23	66	33	39	56	65	66	29	35	31	64	27	62
V	1	5	4	2	5	4	0	3	8	4	0	1	1	0	6
Y	129	188	139	120	133	132	128	127	127	150	166	153	144	19	138
Zn	119	211	354	183	165	193	245	231	653	367	589	565	299	344	386
Zr	180	227	219	172	177	278	222	189	187	188	193	191	186	466	305
Zr/Hf	28	25	27	29	25	25	37	19	23	24	32	32	27	15	13
Ce/Y	0.95	0.95	0.87	1.03	0.86	0.93	0.96	0.90	0.98	0.88	0.68	0.65	0.90	9.2	0.57
quartz	35.53	38.14	38.67	36.29	36.37	35.79	36.53	42.62	36.61	35.60	33.34	33.23	36.35	36.32	36.15
ortho	25.64	27.35	38.67	36.29	26.70	26.29	25.94	26.17	27.89	27.71	29.19	29.01	27.89	32.14	31.90
albite	35.35	29.18	30.36	34.25	32.90	34.85	34.08	25.12	31.04	30.87	31.38	32.82	28.76	28.25	29.18
anorth	1.47	1.79	1.69	1.49	1.08	0.72	1.37	1.29	1.79	2.76	3.70	3.32	3.08	0.35	1.84
corund	0.10	0.80	0.53	0.23	0.57	0.29	0.26	2.03	0.36	0.84	0.24	0.00	0.92	1.07	0.28
di fwo	0.00	0.00	0.00	0.00	0.00	0.00	0.00	0.00	0.00	0.00	0.00	0.01	0.00	0.00	0.00
di fen	0.00	0.00	0.00	0.00	0.00	0.00	0.00	0.00	0.00	0.00	0.00	0.01	0.00	0.00	0.00
hy fen	0.15	0.60	0.02	0.07	0.55	0.00	0.10	0.10	0.22	0.60	0.05	0.06	0.02	0.22	0.12
magnet	0.00	0.07	0.00	0.00	0.07	0.04	0.00	0.04	0.00	0.56	0.00	0.00	0.00	0.00	0.00
haemat	1.43	1.58	1.69	1.43	1.51	1.60	1.54	1.66	1.81	1.22	1.42	1.45	1.63	1.81	1.03
ilmen	0.02	0.00	0.06	0.04	0.00	0.02	0.02	0.02	0.06	0.02	0.00	0.02	0.04	0.06	0.02
rutile	0.06	0.00	0.05	0.04	0.00	0.00	0.06	0.00	0.03	0.00	0.05	0.00	0.06	0.10	0.04
titan	0.00	0.00	0.00	0.00	0.00	0.00	0.00	0.00	0.00	0.00	0.00	0.14	0.00	0.00	0.00
apatit	0.02	0.00	0.00	0.00	0.02	0.19	0.02	0.00	0.02	0.02	0.02	0.02	0.00	0.00	0.00
water	0.00	0.00	0.00	0.00	0.76	0.36	0.00	0.36	0.00	0.00	0.00	0.00	0.00	0.00	0.00
TTDI	96.52	94.68	95.74	96.24	95.98	96.93	96.56	93.91	95.54	94.18	93.91	95.06	93.00	96.71	97.23

granitoids can be recognised by their high V, Sr and Zr content and particularly by the higher levels of Ba. Clearly, these elements are not mobilised into the fluids during subsolidus recrystallisation and mineral growth.

If the volcanic rocks are examined within this framework of comparisons there is no clear trace element pattern:-

Ba values vary from 0-1843 ppm - some samples clearly have high basement values, others show depletions similar to the younger granites  
Rb, Hf and Th values are higher than the basement granites and similar to the younger granite  
Ce, La, Zn and Zr values are consistently higher than all other rock types  
Nb values are intermediate between the basement granitoids and the younger granites  
Sr, P and Ti values are very variable, some are low similar to the younger granite, others - particularly in the volcanic feeder dyke are high, similar to basement granitoids.  
Y content is also variable particularly in the volcanic pile, from higher than the younger granites to lower than the basement.

Thus the volcanics have a distinct chemistry, with higher Ce, La, Zn and Zr than other rock types, but nevertheless they tend to show some basement characteristics as well as some characteristics of the younger granites. Since the volcanic feeder dyke that linked the overlying volcanic pile to the magma chamber, undoubtedly cut through the basement, a signature of basement trace element patterns is not surprising in the volcanics. This is particularly evident in the contribution of Ba, Sr and Zr from the basement into some of the volcanic rock samples, most noticeable in samples SS161 and the feeder dyke sample SS173 and SS175.

The chondrite-normalised trace element data used in Fig 8.8 use only selected trace elements. It is usual in diagrams of this kind to include also the elements Ba, K, Sr, P and Ti in addition to Rb, Th, Nb, La, Ce, Hf, Zr and Y. However, because of the low values of Ba, Sr, P and Ti within the younger granite province, the complexity of the resultant plot obscured the contrasts in the other trace element assemblages between basement, volcanics, volcanic feeder and biotite granite. It was for this reason that only the selected elements were used.

However, as well as trace element patterns to compare and contrast the different rock types it is also important to consider what can be deduced about petrogenesis. In particular, the variation in Zr/Hf ratio was shown in Part I to have been a sensitive indicator of rock-fluid reactions. The average crustal value for Zr/Hf is around 50 (Wedepohl 1969). Values in the basement granite fall between 46-55, whereas the volcanic rocks vary from 21-62 with an average value of 50. In contrast however, the biotites granite show a more consistent but lower ratio which varies between 19 and 37, averaging 27. Such a variation from average crustal values indicates that even these apparently "fresh" rocks have been modified by fluid reactions. The variation is attributed to differential mobilities of Zr and Hf in a fluid-vapour medium. Such variations are further enhanced in samples where there is clear evidence of fluid reactions such as in the microclinisation or chloritisation of perthite.

Clearly the volcanic rocks of the ignimbritic pile have a different major element and trace element chemistry from the biotite granites to which they must be related. In addition to a wide range in Zr/Hf ratios, the biotite granite exhibit a wide range to high values for certain trace elements, notably F, Li, Nb, Sn and Zn. Such values are not compatible with simple crystal fractionation but can be explained by hydrothermal alteration. The Q-F plot (Fig 8.8b) also suggests that some of the original compositions have been modified. The Rishi samples so far discussed define a field for each rock type on the Q-F plot. Several samples (SS85/1, SS84 and SS172, together with both feeder dyke samples) plot outside these general fields and are explained as resulting from rock-fluid interaction. Such modifications form the basis of the next chapter.

## CHAPTER 9

### HYDROTHERMAL ALTERATION AND MINERALISATION IN THE RISHI AREA

#### Introduction

Hydrothermal alteration and mineralisation in the Rishi area was first described by Falconer and Raeburn (1923). They noted that quartz veins are abundant in the Rishi biotite granite and that "silicification and greisenisation are common throughout". They also described the window of biotite granite near Dawa:-

"the small outcrop of fine-grained granite on the floor of the Dower Valley ..., is much fissured and broken and crossed by alteration lines in the neighbourhood of which the granite is blackened and silicified, the change in colour being due to the replacement of the feldspars by quartz, topaz, and green mica. The altered rock itself carries tinstone but the latter is most abundant in thin quartz veins within the altered areas or in the unaltered rock adjoining. The rhyolites and quartz porphyries surrounding the granite are likewise crossed by alteration lines and blackened, silicified, and mineralised granite. The groundmass of the quartz porphyry of the neighbourhood is often completely micasised while quartz veins and stringers carrying tinstone are common throughout..... The clear demonstration of the occurrence of tinstone in the rhyolites and quartz porphyries is of considerable economic importance."

Economically, the Rishi biotite granite has been important. In addition to the occurrence of cassiterite, wolframite and sulphide rich veins, alluvial columbite and cassiterite derived from the biotite granite are mined in many of the local streams.

The mineralisation is concentrated in the contact zone between the biotite granite cupola and the overlying volcanics or basement. Predominantly the mineralisation occurs within the endocontact zone although locally there has been intensive hydrothermal alteration of the basement granites and overlying volcanics. There has also been hydrothermal alteration of the porphyry feeder dyke to the volcanics.

The overlying rocks in general, have acted as a seal to fluid migration resulting in extensive pervasive alteration of the cupola zone.

#### ZONES OF HYDROTHERMAL ALTERATION AND MINERALISATION

In chapter 4, four different zones of ore deposition were identified:-

- (i) The roof zone
- (ii) The marginal zone
- (iii) The contact area
- (iv) Ring dykes

Clearly in the Rishi biotite granite all the zones of deposition are exposed (Fig 9.1a)

The **roof zone** is exposed in the Dutsen Rishi area, the Ladini area and in the area to the south of Dawa Mining Camp Fig 9.1b. In the Dutsen Rishi area the overlying rock type is both basement and volcanics, whereas in the other two areas it is the volcanic pile only.

The **marginal zone**, which extends over a horizontal distance of 200-500m within the endocontact zone of the biotite granite, can be examined both in the Dutsen Rishi and Wundi river areas of the complex.

The **contact zone** which occupies a zone ca 20m wide on either side of the granite contact can be observed in several places. The contact zone with the basement can be examined in the Dutsen Rishi area and the contact zone with the volcanics is exposed at Dutsen Rishi, Dawa and in the Wundi River area (Fig 9.1b).

**Ring dykes** can be examined immediately to the north and south of Dawa mining camp.

(i) The roof zone

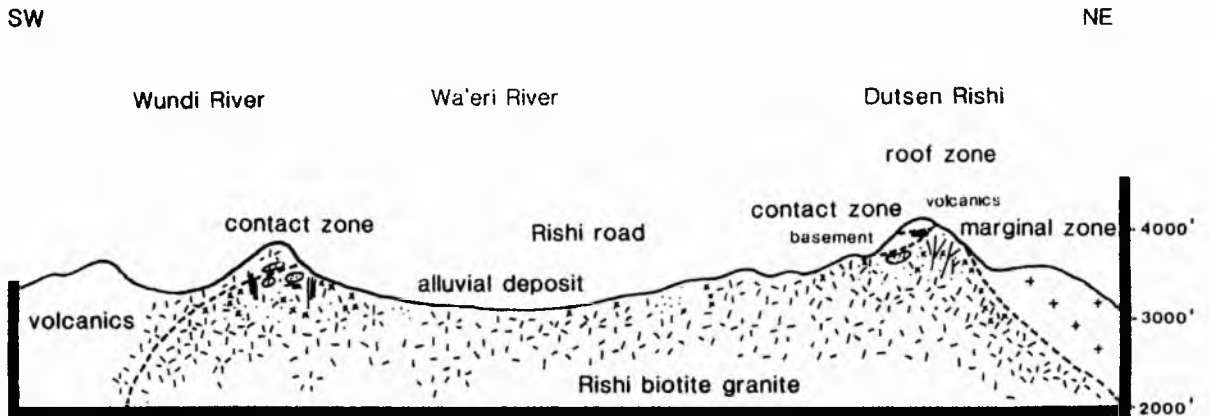
The roof zone is characterised by quartz rafts, disseminated mineralisation associated with pervasive metasomatism, sheeted veins and irregularly-shaped pods of alteration and mineralisation. To the south of Dawa, windows of exposed granite roof are white in colour and extremely friable due to extensive alteration. South of Ladini, the granite roof has been altered by sodic metasomatism, to a white saccharoidal, friable decomposed rock. This has been subsequently affected both by potash and acid metasomatism. The acid metasomatism has resulted in greisen formation which is largely vein controlled and has affected the flat lying q joints in the granite as well as forming vertical dyke-like bodies. The veins are generally light coloured and consist of anhedral quartz, coarse clustered blue green mica with abundant strongly zoned and twinned cassiterite concentrated in the mica clusters. Fluorite and haematite may form along the mica cleavages. Where the acid metasomatism follows the strong potash metasomatism a monomineralic mica rock develops.

(ii) The marginal zone

The marginal zone extends over a horizontal distance of 30m inside the granite contact. It is characterised by stockworks, sheeted veins and associated wallrock alteration, pegmatitic pods containing genthelvite and other minerals, and disseminated mineralisation. Within the marginal zone of the biotite granite south of Dutsen Rishi veins are quartz rich, with mica locally undergoing chloritisation of varying degrees and which also contain disseminated sulphides or cassiterite. The veins may also be zoned as at localities SS106 and SS109.

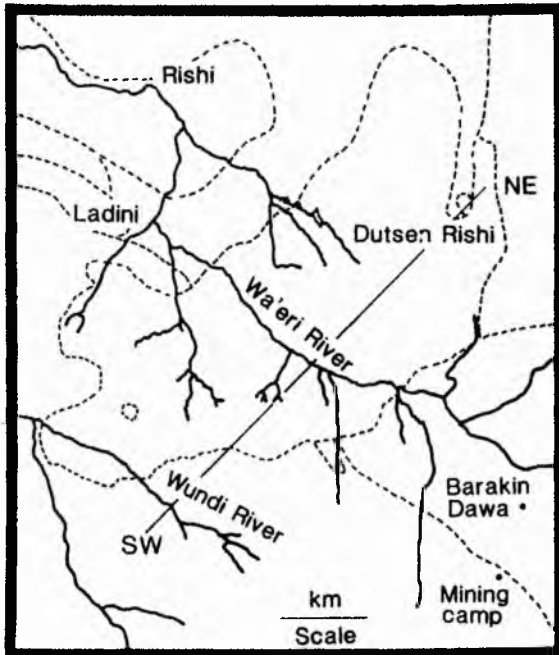
South of Ladini, the fine grained marginal facies of the granite along the southern margin of the Rishi biotite granite along the Wundi River, has been extensively altered and mineralised (Plate 9.1).

Fig 9.1 Zones of ore deposition and the localities where the zones are exposed



a) Cross-section of the Rishi biotite granite

b) The Rishi biotite granite showing the line of cross-section



KEY

- + peralkaline granite
- v volcanics
- ⊙ pervasive sodic metasomatism
- ⊙ pervasive potash metasomatism
- ⊙ pervasive acid metasomatism
- pegmatitic pod
- quartz raft
- ||| sheeted veins
- ⊙ stockworks
- ⊙ replacement body



Plate 9.1

Wundi River area south of Ladini

View across the fine-grained mineralised marginal facies of the Rishi biotite granite to the volcanic cover

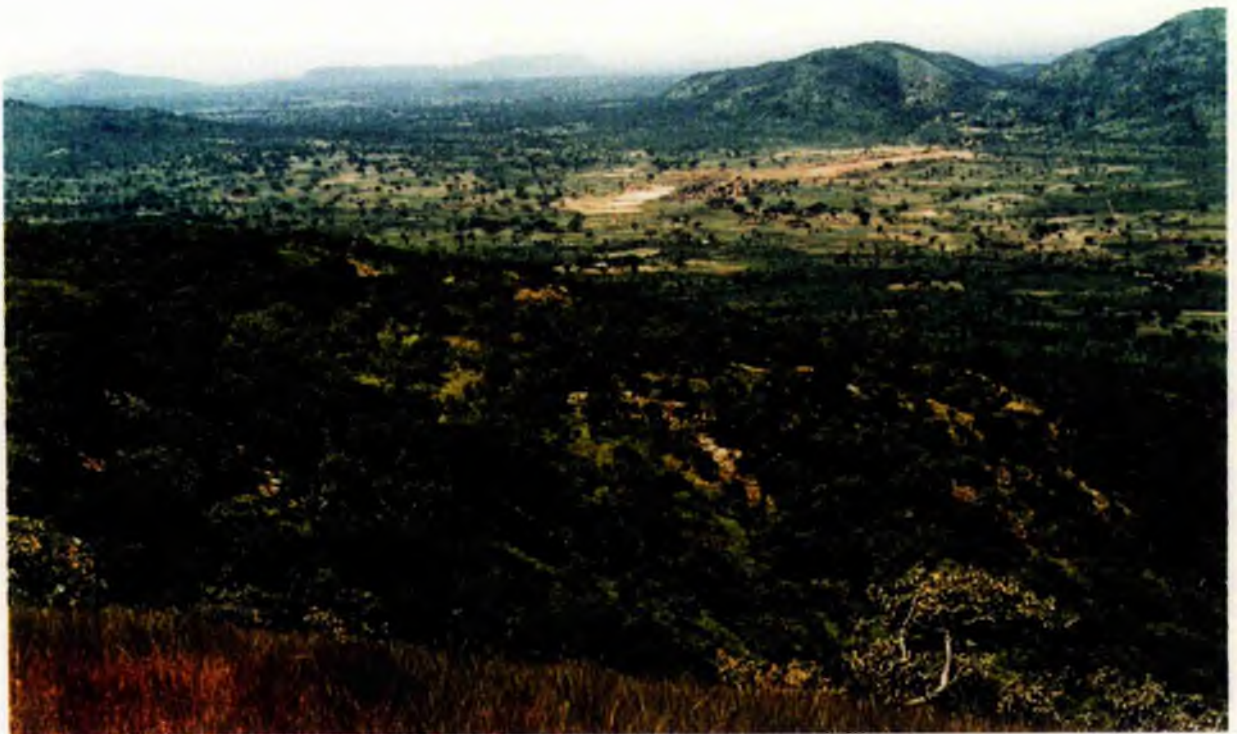


Plate 9.2

Dutsen Rishi contact zone

View from the grassy knoll of Dutsen Rishi looking down onto the tree-covered contact zone of the Rishi biotite granite

### (iii) The contact zone

The contact zone occurs over a distance of approximately 20m on either side of the contact. The zone is characterised by intense alteration, particularly where the country rock is basement. The contact zone of the biotite granite can be seen to the northwest of Dutsen Rishi, along the southeastern margin near the Wa'eri river and along the southwestern margin near the Wundi river (Fig 9.1b). Within the granite the zone is characterised by pervasive microclinisation, microcline-linedmiarolitic cavities and microcline (or amazonite)-mica pegmatitic knots, sulphide-rich micaceous pods and sheeted greisen veins or stockworks

#### The contact zone between granite and Basement

Early stages in the alteration of the basement granitoids can be observed on the Rishi road, just south of Rishi village suggesting the presence of the biotite granite at shallow depth. At locality SS179 a granophyric vein, believed to be an offshoot from the granite below, forms a pale 1cm wide vein cross-cutting the basement (Plate 8.1). Nearby there are thin dark-coloured, randomly oriented greisen stringers which suggest the beginnings of basement alteration.

Intense alteration occurs in a thin finger of basement which extends southwards from the surrounding plain, up a river valley on top of the granite roof, almost to the volcanic cap of Dutsen Rishi. Extensive stockwork mineralisation occurs either in the biotite granite endocontact zone - which occurs at a shallow depth of 30m and is exposed in pits - or within the endocontact zone of the overlying basement finger. In the endocontact zone, the mineralised veins forming a stockwork in the biotite granite are quite distinct from the veins in the overlying basement. Whereas the veins of the basement are dark in colour, sulphide-rich, quartz-poor and fluorite and chlorite-rich, the veins in the biotite granite are paler in colour, quartz-rich, with topaz instead of fluorite and sulphides that are disseminated and less abundant.

Mineralised veins within the basement are no more than 3m wide, generally vertical and localised. They are dark, almost black in colour, fine-grained and contain little quartz or topaz.

#### The contact zone between the granite and volcanic pile

The ignimbritic pile shows varying types of alteration. Thin stringers of ore-bearing quartz, with associated alteration halos do occur but more commonly the alteration affects the groundmass of the quartz feldspar porphyry. The hydrothermal effect on the volcanic pile was studied in the Dutsen Rishi, Dawa and Ladini areas

#### Dutsen Rishi

The summit of Dutsen Rishi is a smooth grassy knoll only 100m across, which is quite distinct from the surrounding rocky tree-lined slopes (Plate 9.2). The

rock is dark fine-grained, silica rich, slightly reddened and with occasional phenocrysts and represents the intensely altered volcanic capping immediately on top of the biotite granite.

#### Dawa area

Samples of the volcanic rocks were taken in a traverse from the biotite granite roof over a vertical distance of 200 metres. It was anticipated that alteration of the volcanic pile would be intense close to the contact and that such alteration effects would diminish with increasing height above the biotite granite. As will be discussed later, this was not found to be the case at all. The conclusion therefore, must be that fluids escaping from the biotite granite did not percolate upwards through the volcanic pile in direct fashion. Instead, the volatiles must have percolated upwards through zones of weakness in the volcanic pile and spread out laterally along certain more permeable horizons in the volcanic pile.

#### Dawa south

Potash metasomatism, resulting in microcline formation has been extensive. In addition to the slightly reddened wallrock adjacent to small stockworks, there has also been the development of microcline in miarolitic cavities. The cavities were formed by the escape of the vapour phase from the roof of the biotite granite. Later silicification also lined the miarolitic cavities with quartz.

There has been extensive greisenisation. Where microcline has been greisenised a monomineralic mica rock developed. Elsewhere the greisen is quartz-rich with sulphides. The mica occur either as small pale coloured flakes associated with topaz and quartz, or as large colourless or pale green euhedral crystals, often with haematite and fluorite along the cleavage traces. In other specimens the mica is brown, more iron rich and undergoing chloritisation. Siderite is a common accessory and fluorite is often abundant. Streaks of genthelvite are common in veins that lie within 30m of the contact. Phenakite has also been recorded (Taylor 1959). Sphalerite and cassiterite are common whilst pyrite and molybdenite are locally abundant. Galena is rare or absent.

#### Wundi River area

In the Wundi River area, small caps of volcanic material can still be found resting on the biotite granite at locality SS117 and elsewhere. At the contact between the two rock types there is rich stockwork mineralisation. Excavation for the ore minerals usually has obliterated the field relationships but the variety of specimens enables a reasonable reconstruction of the original geology to be made.

The biotite granite roof was clearly albitised. The granite is white, saccharoidal and very decomposed. Mineralised veins occur mainly within the biotite granite but occasionally extend into the overlying volcanic pile. The mineralised veins are characterised by quartz, chlorite and sericite or occasionally by quartz and coarse pale green mica. Sheeted veins occur at locality SS21 these consist of thin parallel greisen veinlets less than 1mm wide.

#### (iv) Ring dykes

Mineralisation may occur as disseminations within the porphyry groundmass, along joint planes and along the inner and outer margin of the ring dyke.

#### STYLES OF MINERALISATION

In Part 1, nine different styles of mineralisation were discussed. Not all of these styles are evident in the Saiya Shokobo complex, whilst others such as stockworks and sheeted veins are extremely well developed. The location of these different styles of mineralisation are shown on Fig 9.2 and compared with Part I below:-

##### (i) Late magmatic pegmatitic pods

The margins of the Rishi biotite granite are not characterised by late magmatic pegmatitic pods consisting of quartz and feldspar with topaz and beryl. They do however contain post magmatic metasomatic pegmatitic lenses which are described under (iii) below.

##### (ii) Pervasive metasomatic disseminated mineralisation

The most important phase of disseminated mineralisation in other complexes is related to sodic metasomatism. A process of sodic metasomatism has also occurred in the Rishi biotite granite and has been locally important for the introduction of columbite. Intense sodic metasomatism has occurred only in a few localities and its effect has largely been masked by a later overprinting of potash or acid metasomatism. Columbite enrichment is not as great as in other complexes with the same degree of hydrothermal alteration.

Unlike other complexes described so far however, there has also been a disseminated process of potash metasomatism and mineralisation in the Rishi biotite granite which has been responsible for some of the dispersed cassiterite.

##### (iii) Pegmatitic pods and lenses with albite or microcline

These pegmatitic pods and lenses are sporadically distributed and unimportant in economic terms. They have been noted at localities SS9,10,23,27,43,55,70 and 117. Usually they are simple and consist of quartz and K-feldspar or K-feldspar and mica. At the following localities however, the mineralogy is more complex (Plate 9.3)

At locality SS9, the pale grey equigranular medium-grained granite contains abundant small pegmatitic knots. Between the pegmatitic pods and the granite there is a usually a zone of greisen composed of quartz, green siderophyllite mica and sometimes pink K-feldspar, often with miarolitic cavities within the dark greisen zone. The pegmatite pods consist of a combination of quartz, mica, creamy K-feldspar and green or turquoise amazonite. The pegmatitic pods may themselves be zoned. Sample SS9/6 is zoned from biotite granite through a dark green quartz, mica, feldspar pegmatite to a centre consisting of monomineralic siderophyllite mica or feldspar crystals.

Fig 9.2 Sample localities reflecting different styles of mineralisation  
For key to geological units see Fig 7.4

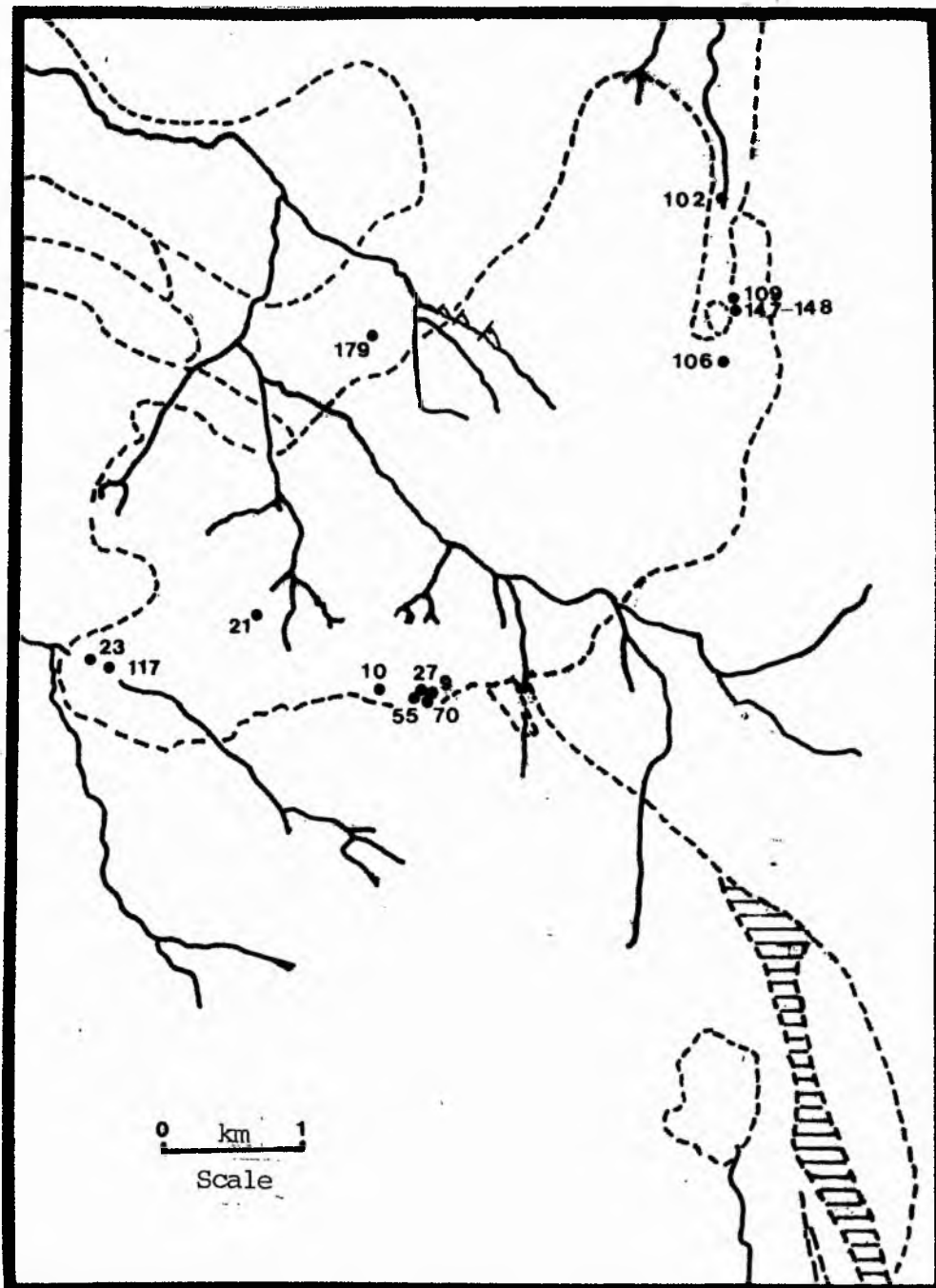




Plate 9.3 Hydrothermal pegmatites showing variations in mineralogy

left to right :

- SS117/3 genthelvite, quartz and albite with uraninite
- SS23/7 microcline and siderophyllite
- SS43 quartz and microcline
- SS23/4 siderophyllite



Plate 9.4 Sheeted veins

- SS21/1 Thin parallel veins with quartz and siderophyllite

At locality SS23, the white, equigranular medium to fine grained biotite granite also contains abundant zoned pegmatitic pods. The centre is often occupied by coarse cores of monomineralic green siderophyllite mica, or mica with K-feldspar. Also associated with the pegmatitic pods metasomatic syenites have developed. White or salmon pink microclinites surround pegmatitic knots of quartz.

At locality SS27, the dark greisen zone which surrounds the pegmatitic pod is extremely mica rich and also contains topaz and chalcopyrite.

A uraninite-bearing albite pegmatite with quartz and genthelvite occurs in the Wundi river area at locality SS117. Uraninite forms small black crystals approximately 1mm in size, clustered on the feldspar crystals. The pegmatite is associated with greisens that have developed along both vertical and horizontal joints in the contact facies of the granite.

Miarolitic cavities lined with microcline and quartz crystals are common, particularly in the Wundi river area.

#### (iv) Quartz rafts, sheeted veins and stockworks

Quartz rafts which characterise the roof zone of a biotite granite cupola and occur between the granite and overlying volcanic pile are poorly developed in the complex. At locality SS147 and 148 however, just below the volcanic capping of Dutsen Rishi, a small quartz raft is exposed. In parts it consists of massive quartz with small miarolitic cavities: locally it may consist of long prismatic quartz crystals associated with patches of pervasive greisenisation. Within these greisen patches there are vestiges of feldspar, and patches of haematite and chlorite developed from biotite breakdown. Although no ore minerals were observed, the existence of small pits at this locality suggests that ore minerals have been worked in the raft. Between the quartz raft and the altered volcanics of Dutsen Rishi the roof facies is a greisenised microgranite which is rich in ore minerals.

Sheeted veins and stockworks characterise the marginal and contact zones of the Rishi biotite granite. Sheeted veins consist of a series of thin parallel veins (Plate 9.4). They are particularly well developed in this complex most notably in the Ladini area. They are steeply-dipping or vertical. Individual veins may vary from 0.5 to 1mm and usually consist of a greisen assemblage of quartz-siderophyllite, occasionally with a thin central stringer of quartz.

The stockworks are similar to the sheeted veins except that they do not occur as parallel veins but as a series of anastomosing ramifications within the marginal or contact zone of the Rishi granite. They are particularly well exposed in deep pits around locality SS102 north of Dutsen Rishi (Plate 9.5). The pits expose the biotite granite beneath the basement rib. Mineralogically the vein systems are characterised by quartz, pale or green-coloured Li-Al or Li-Fe biotite usually with abundant topaz and fluorite, cassiterite or more rarely traces of sulphides.

#### (v) Fissure filling lodes

There are no examples of fissure filling lodes in the Rishi area. There is however, a small lode at Tabagindi in the Tongolo Complex. The absence of any



Plate 9.5                      Stockwork in the Rishi biotite granite

Anastomosing veins of greisen, sometimes with a central quartz vein, cutting the Rishi biotite granite north of Dutsen Ginshi



Plate 9.6                      Irregularly shaped replacement body

Mica-rich irregularly shaped patch of hydrothermal alteration in the Rishi biotite granite close to the contact with the volcanic pile

lode structure in the Rishi area indicates that major fracturing of the biotite granite did not take place. In other complexes, such fracturing may have been the result of subsequent intrusions of biotite granite at depth.

(vi) Irregularly shaped replacement bodies

The volcanic pile above the biotite granite locally formed a barrier to fluid migration and the change in rock type coupled with the decrease in permeability has clearly facilitated precipitation of ore minerals. The resulting mineralised pods tend to be sporadic and irregular in distribution and although localised ore-rich concentrations occur they have never proved economic. The pods are variable in size shape and distribution. Commonly they are mica-rich patches containing clusters of cassiterite and aggregates of zircon crystals (Plate 9.6). Unusually for Nigeria, these pods also sometimes occur on the volcanic side of the contact.

(vii) Quartz veins

The quartz veins are generally steeply dipping to vertical and vary from massive milky veins up to 3m wide in the basement north of Dutsen Rishi, to thin stringers less than 1mm wide. Where they occur within the biotite granite they carry an ore assemblage of cassiterite, and sulphides. Occasionally there are honeycomb-textured facies within zoned veins.

Quartz veins occur in the basement within 1km of the younger granite contact. They are characterised by an ore assemblage of wolframite with cassiterite and traces of sulphides. Between the quartz vein and the basement, particularly where the veins are <1cm wide, there may be a thin selvage of a pale-coloured micaceous greisen.

(viii) Mineralised ring dyke

Two hundred metres to the north of Dawa mining camp, the feeder dyke to the volcanic pile has been fractured by quartz-rich fluids carrying cassiterite. Thin quartz stringers, less than 0.5mm wide, cut the quartz feldspar porphyry. These stringers fracture phenocrysts so that the dyke was obviously quite consolidated before quartz veining occurred. The quartz grows tangential to the stringer margins and contains reddish crystals of cassiterite and traces of opaque minerals.

Eight hundred metres to the south of Dawa Mining Camp, escaping ore rich fluids have utilised vertical fractures related to the porphyry feeder dyke of the volcanic pile (Plate 9.7). The groundmass of the quartz feldspar porphyry has been extensively altered whilst the pink feldspar phenocrysts up to 1cm long show lesser degrees of alteration.

(ix) Alluvial and eluvial mineralisation (Plate 9.8)

Alluvial deposits of cassiterite and columbite have been mined in the area both by a major company - Jantar Bisichi - and by groups of local miners. Small eluvial deposits have been worked south of Dawa Camp where the erosion of the Dawa granite window has resulted in rich pockets of concentrate.

All mining company activity had ceased when last visited in December 1983 and very little sign of local activity was evident although a small number of bags

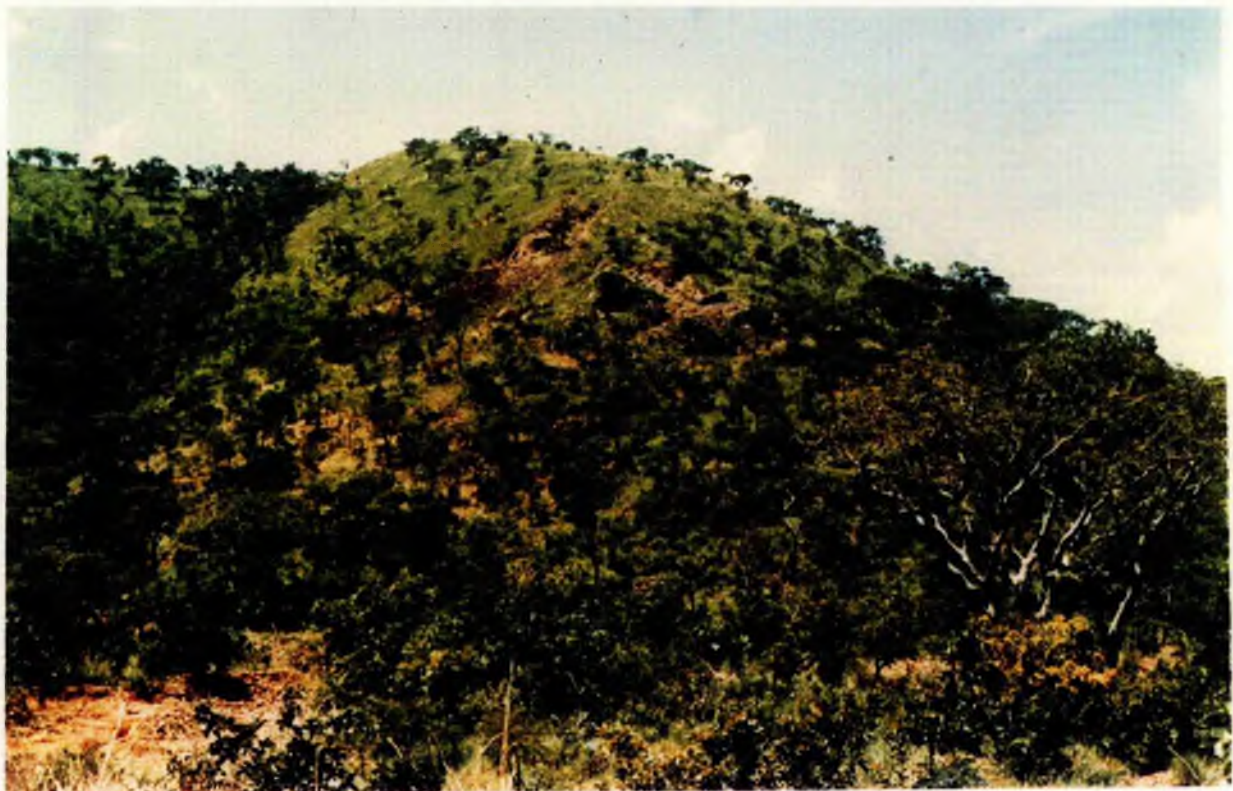


Plate 9.7 Mineralised ring dyke

The porphyry ring dyke has been extensively altered and mineralised. Small workings towards the top of the hill and also bottom left have exploited cassiterite. Locality SS112.



Plate 9.8 Alluvial ore deposits

View from Dutsen Rishi showing the commercial exploitation of the alluvial deposits of the Wa'eri River

of tin concentrate from the area were recorded by the Mining Corporation.

## SEQUENCE OF HYDROTHERMAL ALTERATION PROCESSES

### Introduction

The sequence of subsolidus hydrothermal processes determined in Chapter 3, can be related to the Rishi biotite granite. On textural and field evidence the earliest hydrothermal alteration was related to a disseminated sodic process. This was followed by a pervasive or vein controlled potassic process locally resulting in the formation of microcline pods. The process of hydrogen (acid) metasomatism which followed, was of economic importance for the deposition of an oxide and sulphide assemblage of minerals. Silica metasomatism was the final major process of economic importance. Argillic alteration was a very minor process in the Saiya Shokobo complex and the last process of zeolitisation, although it was responsible for the formation of secondary ore minerals, was not of economic significance.

Whilst all these processes can be recognised, it is often by no means easy to define the sequence of processes that have occurred. Moreover, when several processes have affected the same sample it can be difficult to assign the mineralogical parameters to a particular group. Usually, such samples are grouped under the heading of the latest process to have operated. However, where a later process has only had a slight effect and the mineralogical, textural or chemical signature identifies the earlier process, then it has been grouped with the appropriate assemblage.

As expected, such a detailed survey of alteration within one anorogenic centre, shows the complexity of hydrothermal alteration processes. For the first time it can be appreciated that the basement granite host may have been affected by sodic, potash or acid metasomatism or combinations of these processes. For example, the effects of sodic then acid metasomatised basement have been recognised. Similarly the volcanic rocks may have been altered by a combination of processes, although this is harder to define since there is so little trace of the sodic process remaining. The question of whether an early sodic process has been entirely overprinted, or whether it occurred at all, will be discussed in this chapter.

### Sodic metasomatism

Samples showing the effects of sodic metasomatism can be found throughout the roof facies of the main Rishi biotite granite and particularly in samples from windows exposed in the volcanics near Dawa mining camp (Fig 9.3).

The process of sodic metasomatism observed in samples (SS23/12, SS42/2, SS44/2, SS48/1, SS55/8, SS62, SS69, SS189 and SS190) is rarely intense. Only in SS48/1 is there the associated textural change which occurs in other complexes when sodic metasomatism has been a major process. In SS48/1 the original medium-grained equigranular or porphyritic texture of the granite has been lost so that the rock is a saccharoidal fine-grained albite granite (Plate 9.9). There is also a change from the typical pink coloration to white.

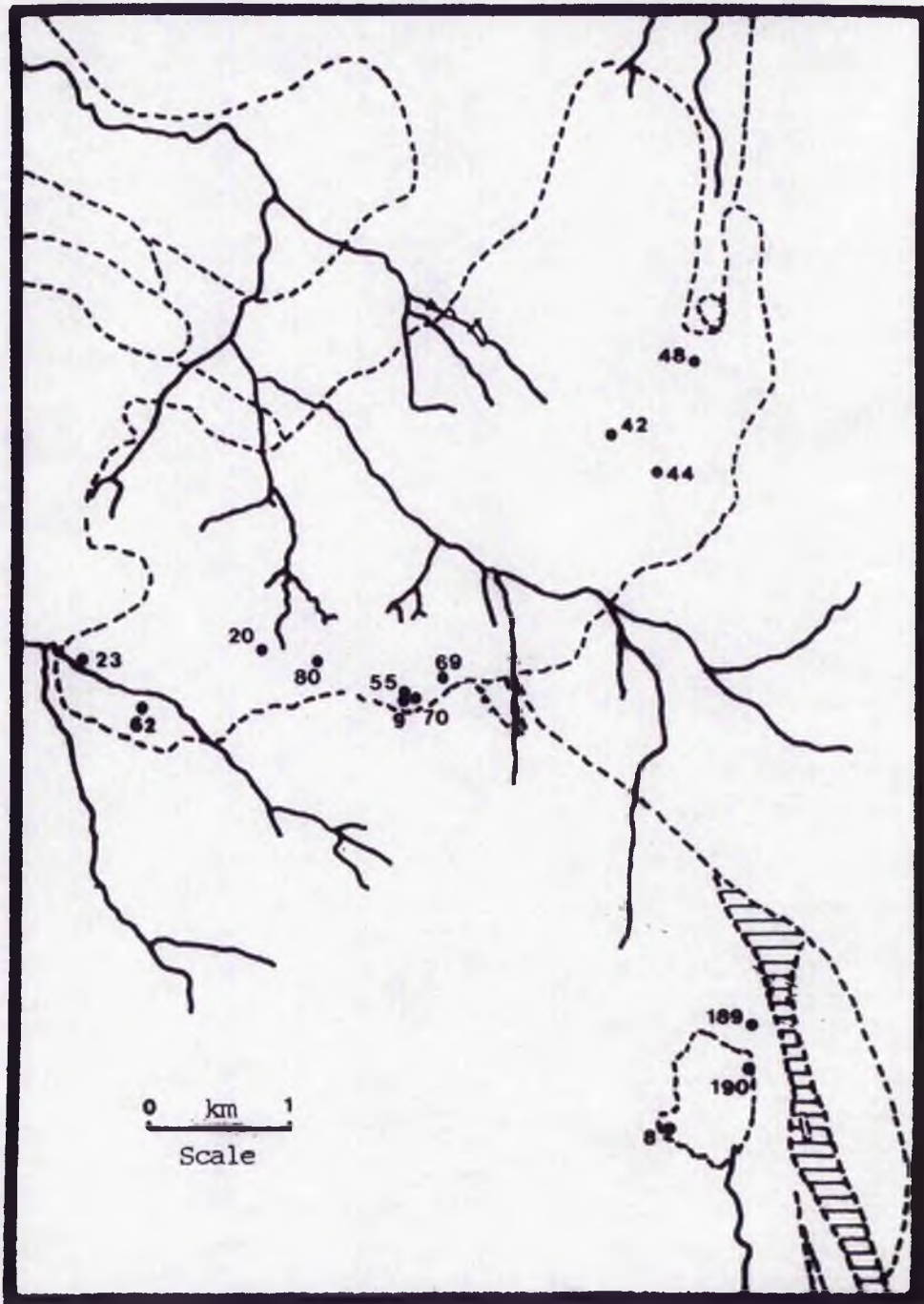


Fig 9.3 Sample localities of the sodic and potash metasomatised samples.  
For key to geological units see Fig 7.4



Plate 9.9                      Zinnwaldite albite granite

SS48                      Saccharoidal textured fine-grained albite granite  
with lenticular zinnwaldite

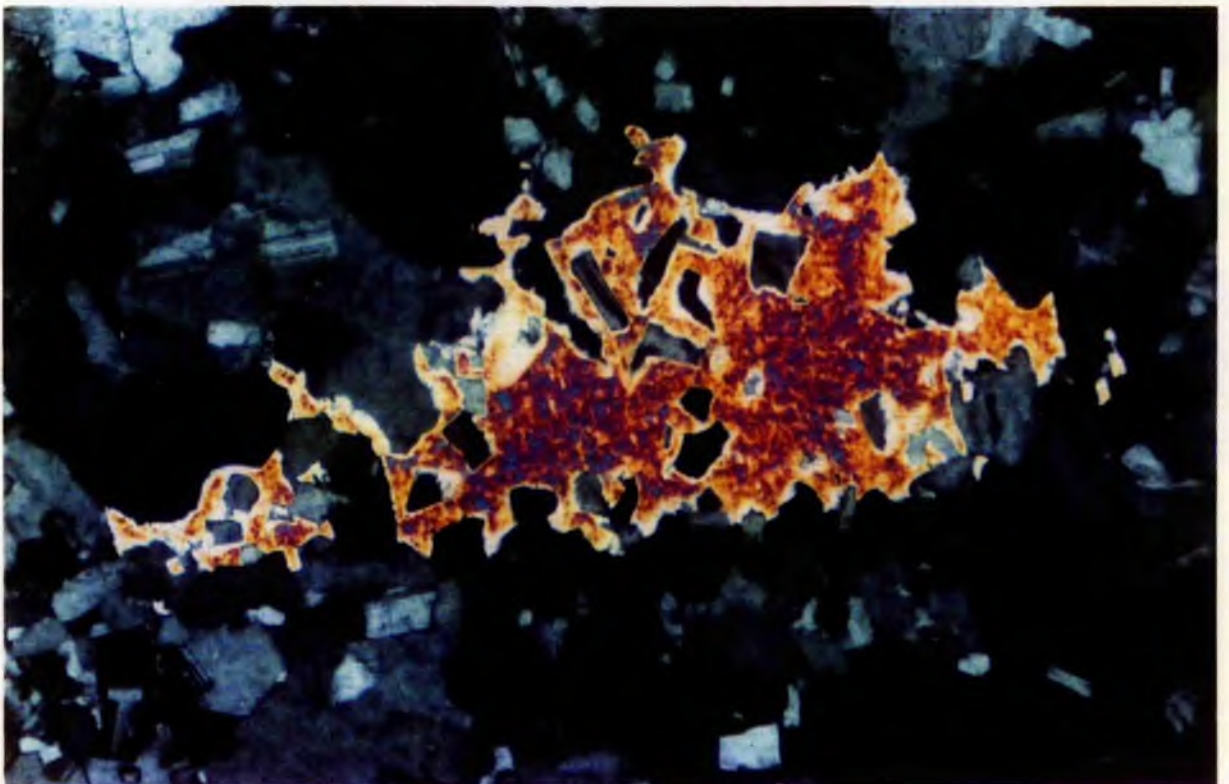


Plate 9.10                      Thin section of SS48

Short stumpy laths of albite forming a fine-grained mosaic. Sieve-textured zinnwaldite encloses quartz, albite and fluorite. x125

Mineralogically, sodic metasomatism is characterised by the albitisation of the original perthite, by the destruction of Ti-Fe oxides and the growth of new ferromagnesian phases, by the development of a new mica and by the introduction of an assemblage of oxide ore minerals similar to that observed in other complexes. Occasionally there are traces of perthite breaking down to epidote particularly in SS190.

In SS48/1 the whole rock has been recrystallised, unstrained quartz and short stumpy albite laths form a fine-grained mosaic (Plate 9.10). There is only a small amount of perthite remaining. In other samples of the same facies, albite develops both at perthite margins and within the cores of the original perthite. The perthite, which may occur as quite large glomeroporphyritic aggregates, shows complex grain boundaries. It may show traces of chloritisation whilst the original mica altered either to chlorite or iron oxides (SS62). The new mica is coarse, lenticular or sieve like in habit, and poikilitically encloses quartz, fluorite, albite and zircon. In SS48 it is a honey coloured zinnwaldite, compositional details of which are discussed in Chapter 10. In other samples the colour is often grass green and compositionally also lies close to zinnwaldite. The more the modal percentage of albite, the paler the mica. Accessory minerals include fluorite, zircon and euhedral skeletal cryolite (Table 9.1). The zircon formed at this stage is small <0.1mm, very dark in colour, often metamict and clearly rich in uranium and thorium. Ore minerals are rather sparse in the thin sections examined. Only in SS48/1 does columbite occur. However, increased Nb in several of the analyses of these rocks indicate that there has been some columbite mineralisation elsewhere in the complex.

Table 9.1 Modal compositions of sodic metasomatised samples

	SS23/12	SS44/2b	SS48/lb	SS55/8	SS190
Quartz	44.5	43.4	40.5	24.3	31.8
Microcline/Perthite	37.2	25.7	13.5	65.7	47.2
Albite	17.1	28.2	40.3	4.6	13.7
Biotite	0.1	1.5	4.1	4.6	5.1
Chlorite		0.6		0.4	0.9
Fluorite	1.0	0.5	0.6	0.2	0.4
Cryolite			0.8		
Columbite			0.1		
Opaques			0.1		0.3
Zircon	0.1	0.1	0.1	0.1	0.2
Monazite					0.4

Despite the fact that the textural and mineralogical evidence suggests that samples such as SS48/1 have undergone sodic metasomatism, it is not immediately apparent from the chemical data. Few of the sodic metasomatised facies contain more Na<sub>2</sub>O than K<sub>2</sub>O thus underlining the importance of a detailed petrographic study in determining the fluid processes.

Sample SS44/2 contains small beaded, consertal textured quartz with very frilled margins sometimes showing strain extinction. Also the quartz may occur

as discrete grains or micrographic interlocking mosaics with feldspar (Plate 9.11). The feldspar is very variable. Intergranular albite, up to 1mm in size is accompanied by occasional glomeroporphyritic blebs of very patchy perthite some of which appears to have subsequently been microclinised and chloritised. Sodic alteration appears to have been responsible for sericite development from perthite whilst the coarser mica which is more equant than in others samples of this facies is grass green to greeny brown in colour and pleochroic to khaki. Sometimes the cleavages are emphasised by ore mineral development and subsequent chloritisation may have occurred.

Sample SS23/12 has part which has been albitised and part which has been subsequently microclinised. In the albitised part of the sample, quartz granules have developed from perthite breakdown (Plate 9.12). Larger crystals which are anhedral, clustered and unstrained enclose albite laths. The process of sodic metasomatism has resulted in the coarsening of the original film perthite in addition to the albite growth. Accessory, dark-coloured metamict zircon is accompanied by 1 modal percent anhedral skeletal, colourless fluorite which is more abundant than in most other samples of this facies.

There is a diminishing proportion of albite with depth in the Rishi pluton. Sample SS44/2, which comes from the roof near the eastern margin of the main pluton, contains 28% modal albite and SS48/1 which comes from just beneath the volcanic cap of Dutsen Rishi, contains 40% modal albite. In contrast, sample SS40 although it comes from a contact zone, lies 300m below the Dutsen Rishi roof and shows only traces of albitisation. This evidence substantiates the findings of a drill core study of Ririwai described in Chapter 3, that sodic metasomatism is concentrated in the apical zone of granite. It also emphasises the point that albitisation is not a marginal feature.

It is clear from the QF diagrams discussed later that there must have been a sodic metasomatism of the basement. This resulted in an albitisation of the original feldspar. The effects of this sodic imprint however, are largely overprinted by later potassic and acid processes.

Several albitised samples have subsequently been microclinised and SS 23/12 records a transition from an albite-rich zone into a microcline.

#### Potash metasomatism

Potash metasomatism has been a widespread process within the Rishi biotite granite pluton. However, the mineralogical expression of this process has often been masked by the superimposition of later stages. Samples SS8/1a, SS8/1b, SS9/3, SS9/11, SS20/3, SS23/9, SS23/12 and SS70, retain the potassic assemblage of minerals (Fig 9.3). In addition to potash metasomatism of the biotite granite, potash metasomatised basement and volcanic rocks can also be recognised.

Potassic metasomatism is characterised by the development of intermediate to ordered microcline, often at the expense of perthitic feldspar. The microcline produced in this manner, as was explained in Chapter 3, does not show tartan twinning. Instead, it forms a turbid, mottled, low-relief mineral that accounts for up to 88 modal percentage of the rock (Table 9.2).

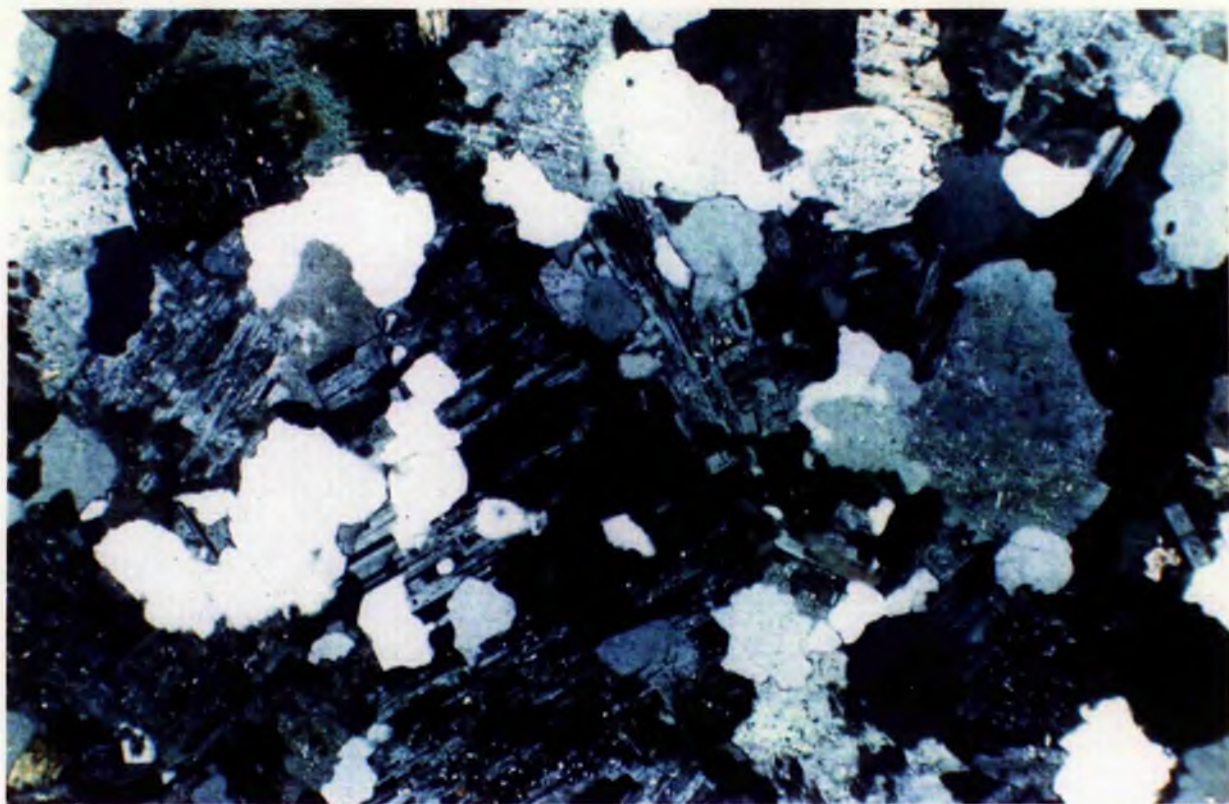


Plate 9.11      Consertal textured quartz with albite, remnants of perthite and mottled microcline (centre right). XPL x25

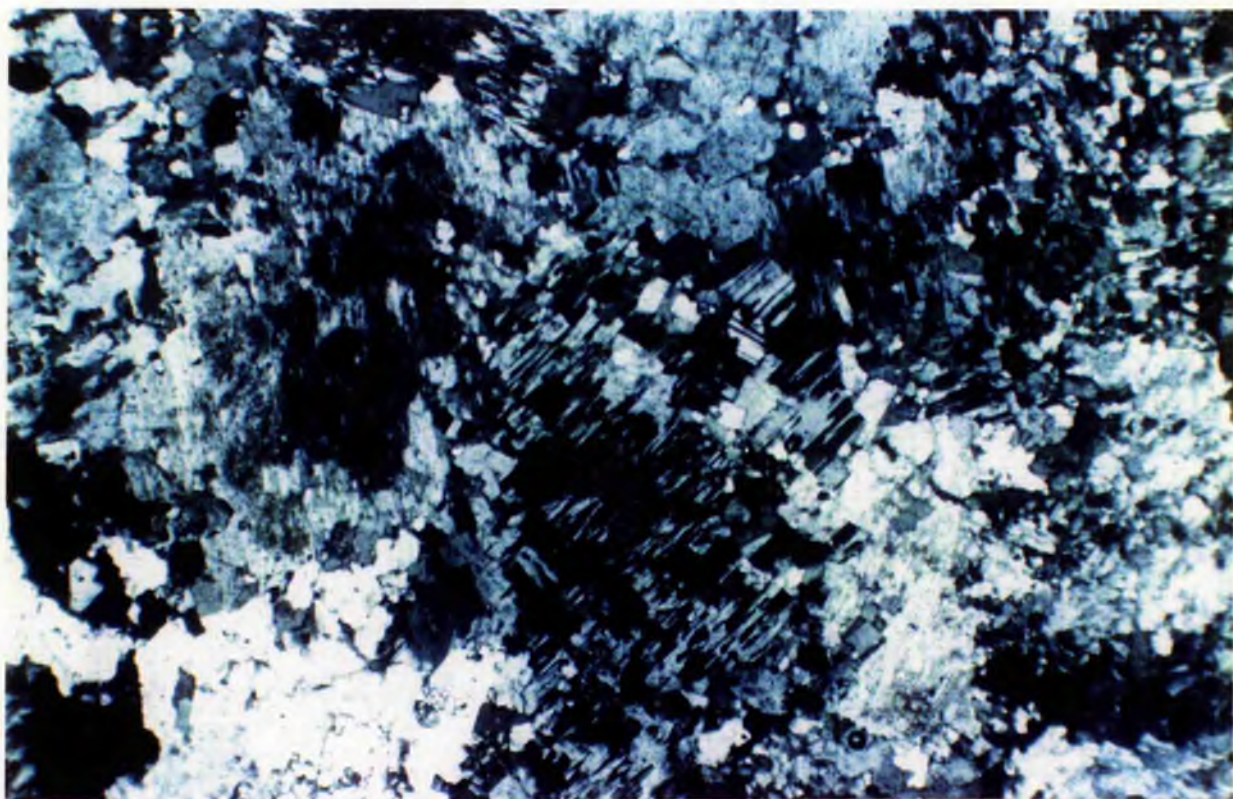


Plate 9.12      Small granules of quartz, film textured perthite and albite which is developing a chessboard texture. XPL x25

Table 9.2 Modal compositions of potash metasomatised samples

	SS8/1a	SS81b	SS23/9	SS9/3S	S12/2
Quartz	4.4	4.1	4.6	9.3	30.0
Microcline	80.2	53.6	88.1	57.9	59.8
Albite	8.2	3.9	5.3	11.6	
Biotite	0.1	33.6		20.8	7.2
Chlorite	2.1	1.3	0.3		1.3
Fluorite	0.1	0.2	0.5	0.3	0.6
Sphalerite	1.8	0.2			0.3
Cassiterite	2.7	2.5	1.0		0.1
Opagues		0.2	0.1		0.3
Zircon	0.1	0.3	0.1	0.1	0.3
Monazite	0.3	0.1			
Molybdenite					0.1

As with sodic metasomatism there is desilication when the potassic process became intense and when the potassic process was extreme the desilication produces a salmon-, or sometimes cream-coloured honeycomb-textured metasomatic microcline (eg SS8/1a, SS8/1b, SS23/9, SS23/12 - Plate 9.13). Unlike similar microclinites of other complexes, there was no brick-red colour development. Possible explanations as to the colour difference are discussed later. Within the turbid microcline of these microclinites, thin sections show some patches or film perthite remain as cores or irregular islands. Stubby laths of albite - occasionally up to 0.5mm in size - which are unaltered, may have grown from the soda released from K-for -Na replacement in the perthite, or may be all that remains of an albitite that has been microclinised (Photo 9.14). The microcline, is accompanied by subordinate amounts of interstitial unstrained quartz, fluorite and rare flakes of colourless mica. In SS8/1b, chlorite replaced an earlier mica. Its habit is reminiscent of the skeletal zinnwaldite generated during sodic metasomatism and it may therefore be that this sample has already undergone a sodic alteration process. Skeletal strongly coloured and zoned cassiterite is abundant in virtually all samples, with zircon, monazite and occasional fluorite. In SS8/1a there is also abundant skeletal, sieve textured sphalerite which is yellow in colour (Photo 9.15). Small miarolitic cavities 2 to 3mm across may contain a lining of quartz crystals, albite, cassiterite or traces of chlorite or zeolite sheaves. Sample SS8/1b, which is also classed as a microcline, in reality represents a transition between a microcline and a greisenised microcline. Large rare clear flakes of zinnwaldite up to 1.5mm across are growing at the expense of the microcline. Cleavages are often emphasised by chlorite. Discrete spongy chlorite probably represents the breakdown of an earlier generation of mica. Sample SS20/3 represents a further step in the greisenisation process and will be discussed under acid metasomatism.

Where the process of potassic metasomatism was less intense, and a microcline was not produced, eg in SS12/2, the original perthitic feldspar was altered to microcline, the quartz remained and the original biotite of the granite was modified. The modification may have taken the form of chloritisation, the development of a new blue-green or pale yellow-green mica,



Plate 9.13 Microclinites, showing the range of colour from white to pink and the variation in texture from fine- to medium-grained. Left to right: SS23/12, SS23/9, SS8, SS8/1



Plate 9.14 Photomicrograph of small stubby laths of albite (centre picture) in mottled microcline. SS23/12, XPL x50

or the development of pale coloured overgrowths of new Li-Al rich mica which formed rims around the original Fe-Ti rich dark green/brown biotite. The new mica is in the compositional range from annite through siderophyllite towards zinnwaldite. There was an introduction of accessory monazite, zircon, abundant dark reddy-brown cassiterite,  $TiO_2$  minerals, molybdenite and occasionally wolframite associated with phyllosilicate minerals.

Potash metasomatism may also have produced pegmatitic patches (SS9/11 and SS70), which apart from a coarser texture with individual crystals of mica, quartz or feldspar up to lcm in size, the mineralogical assemblage and features are similar to the potash metasomatised granite.

In addition to varying degrees of potash metasomatism of the perthite granites, it may also be possible to recognise a facies that represents potash metasomatised albitite. Samples SS23/9 and SS23/12 contain around 5% albite which forms large stubby unaltered laths. These albite laths however, may have resulted from the extreme potash process expelling Na from the perthite lattice, rather than representing vestiges of albite as remnants from the albitisation process. In effect both processes may have been involved. Quartz forms around 5 modal percent of these samples and is accompanied by clusters of chlorite, 0.3mm across, which entirely replace earlier mica. The accessory minerals include occasional clusters of purple fluorite, together with 1% cassiterite, which is deeply coloured and strongly zoned and pleochroic from pale grey to reddy-brown. Sheaves of chlorite/zeolite accompany quartz in the lining of miarolitic cavities.

The potassic metasomatism of the basement (SS17/3, SS18/25, SS57 and SS179a), resulted in a mineralogical assemblage similar to that generated in the biotite granite. The large feldspar phenocrysts of the basement were destroyed and microcline developed at the expense of the existing feldspar (Plate 9.16) whilst the original biotite was chloritised (Plate 9.17). Except in SS179a however, the effects of such potassic metasomatism were almost entirely masked by the later acid metasomatism which converted all the microcline generated at this stage into micaceous aggregates.

The potassic metasomatism of the volcanic rocks (Plate 9.18), as shown by samples SS84, SS85, SS86 and SS172 resulted in the microclinisation of the feldspar phenocrysts although as in the basement rocks, the later process of acid metasomatism and the growth of new micas in the groundmass, chemically and mineralogically tend to have obscured the potash process. However, even within the acid metasomatised variants, the microclinised feldspars are still distinct. The best example of the mineralogical and textural effect of potash metasomatism is in SS86 which comes from close to the biotite granite contact. Quartz phenocrysts are unaltered, feldspar phenocrysts which range in size up to 5mm, retain patch and film perthitic textures although some show the turbidity characteristic of microclinisation (Plate 9.19). However, it is in the groundmass that the effects of potash metasomatism are most obvious. The fine-grained groundmass of the porphyry has been lost, abundant microcline has developed, quartz has coarsened in texture and the appearance of the rock is of a porphyritic granite. It is only the fractures and embayed nature of the quartz phenocrysts that testifies to the original nature of the rock.

The porphyry feeder dyke has also been affected by potash metasomatism. In SS173 for example, the original perthite feldspar is extremely turbid and has

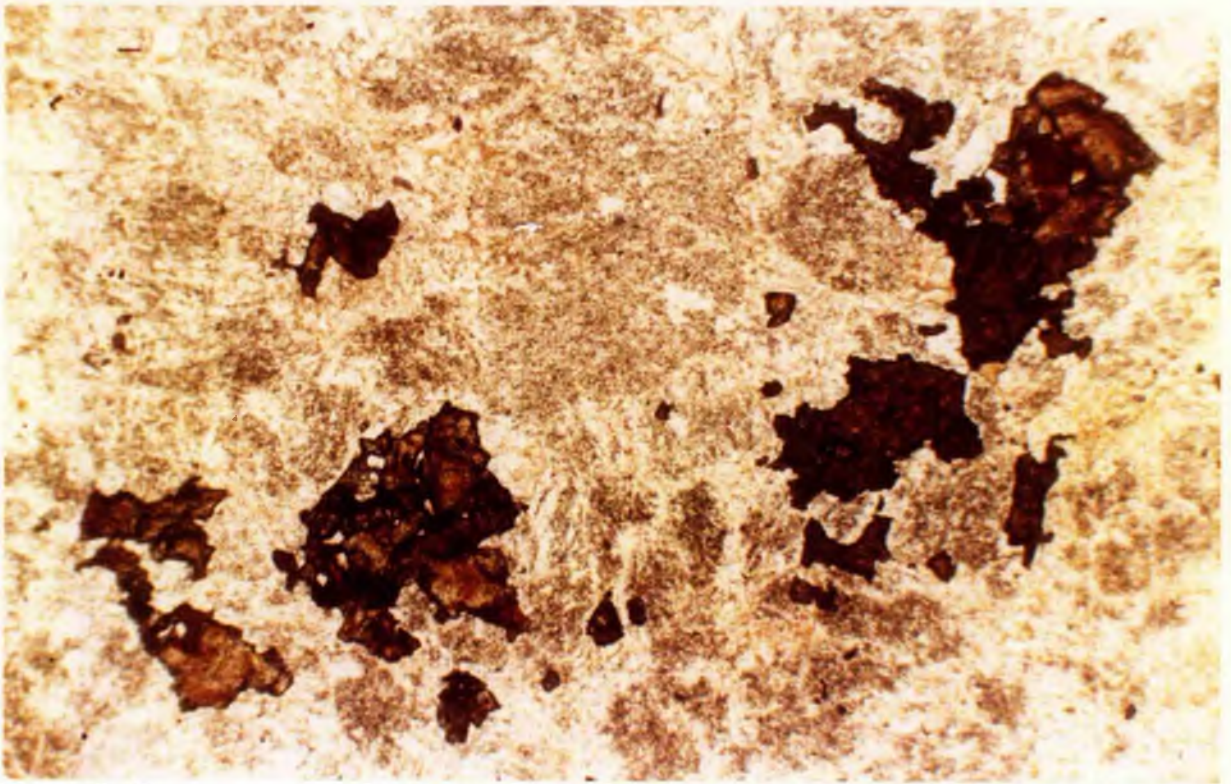


Plate 9.15

Sphalerite and zoned cassiterite in mottled microcline.  
SS8/1a, PPL x50



Plate 9.16

Large pink microcline phenocrysts in basement monzogranite  
undergoing extensive greisenisation

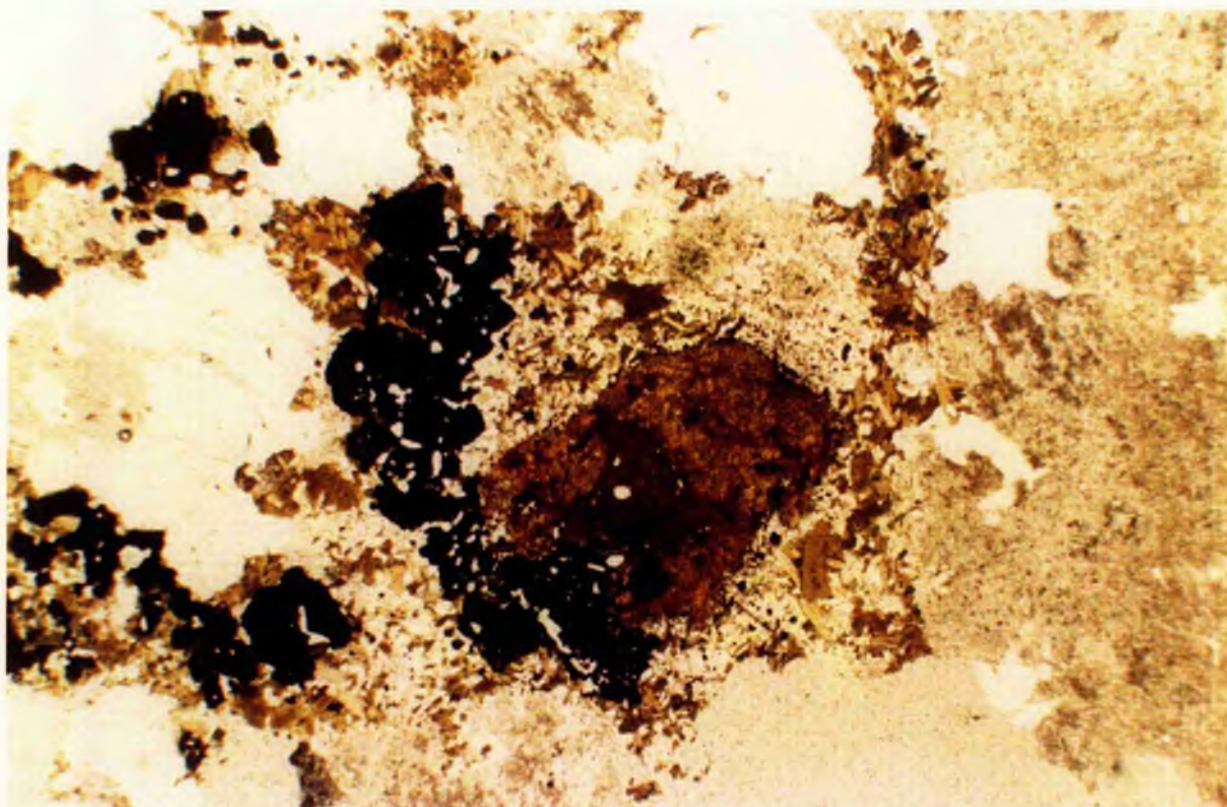


Plate 9.17 Altered basement with microcline feldspar, partially chloritised biotite and completely chloritised hornblende. PPL x25



Plate 9.18 SS85 : potash metasomatised quartz feldspar porphyry grading into potash metasomatised biotite granite

9.17

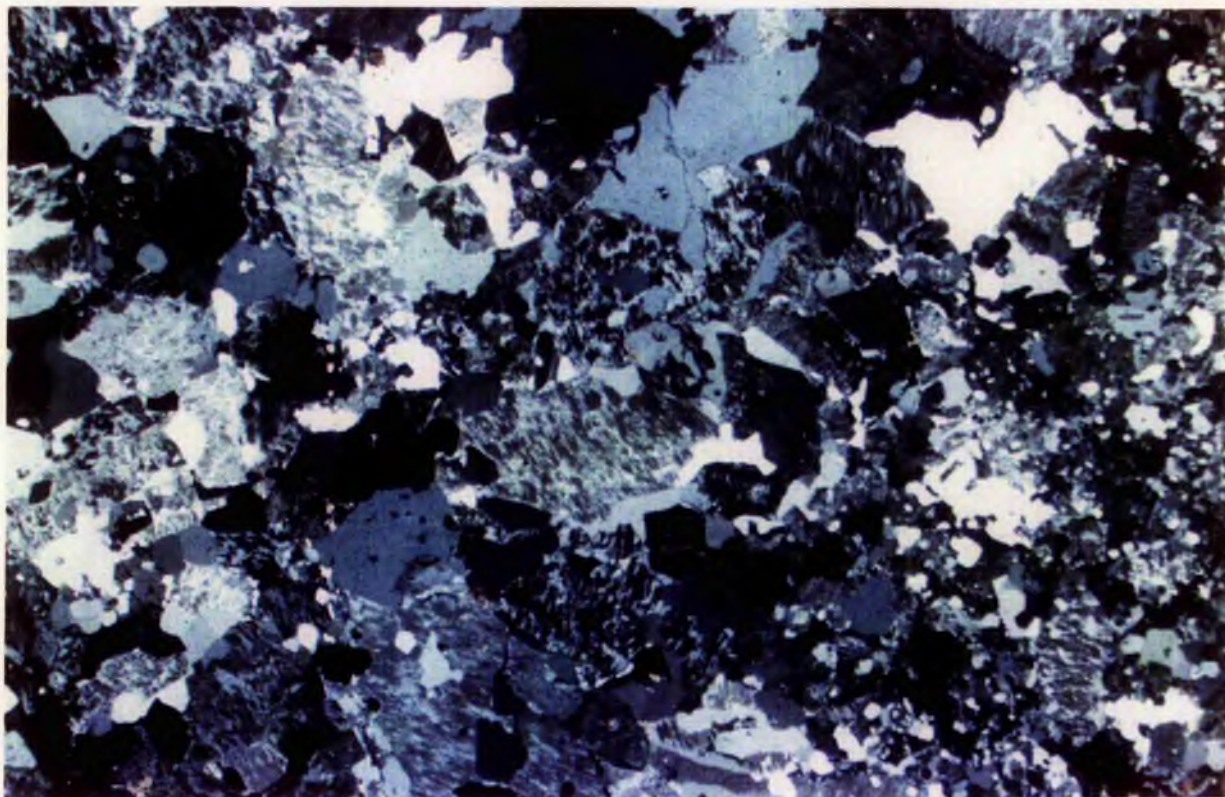


Plate 9.19

Amoeboid-shaped quartz and perthite showing both patch and film-textured arrangements of the albite and microcline components. Abundant turbid microcline occurs in the groundmass. Photomicrograph of SS86, XPL x15

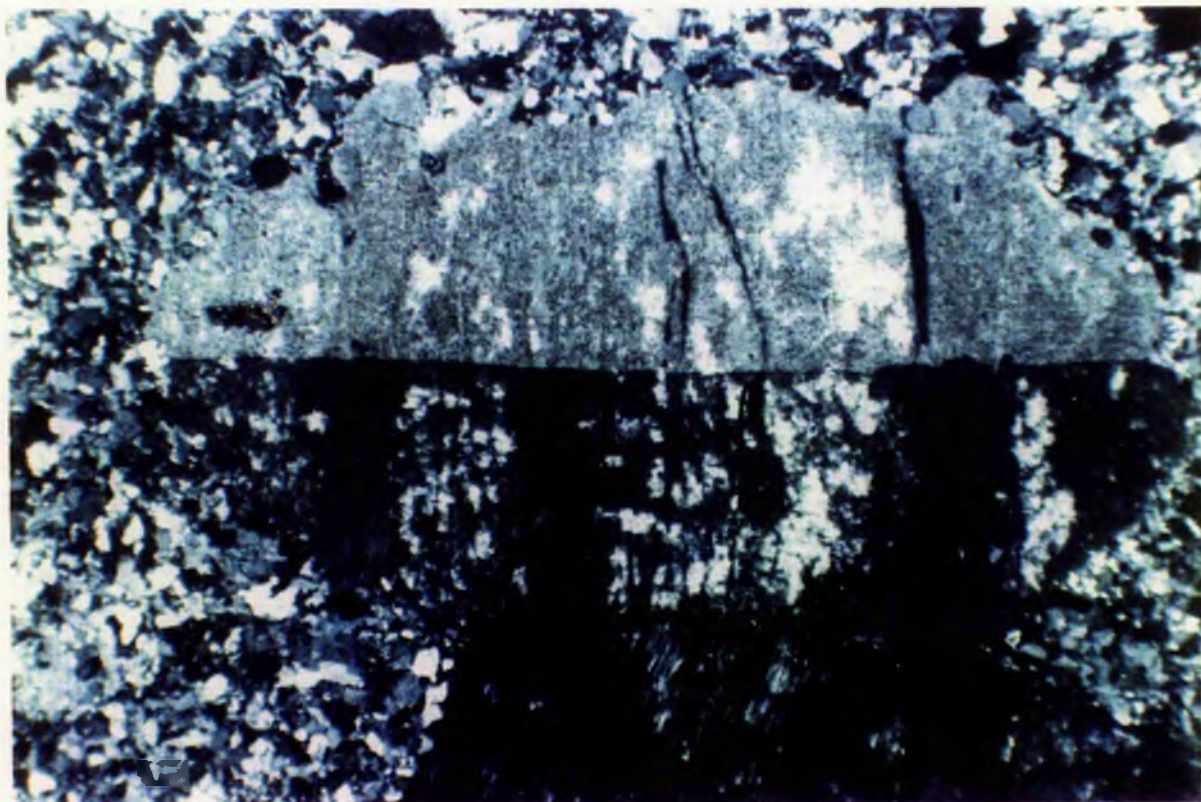


Plate 9.20

Turbid phenocryst of mottled microclinised perthite cut by veinlets of microcline in an altered porphyry feeder dyke. Photomicrograph of SS175, XPL x50

9.19

9.20

obviously undergone potash metasomatism. In SS175, the feldspar phenocrysts are very variable in size and unevenly distributed, sometimes in synneusis-type aggregates. Although these are dominantly patch or film-textured perthites, some show mottling due to microclinisation (Photo 9.20). In addition, veinlets of microcline with quartz, <1mm in width, cross-cut the groundmass and perthites phenocrysts. These veinlets carry small cassiterite crystals which vary from tan to reddish in colour (Plate 9.21).

Such a potash process within the volcanic pile and porphyry feeder dykes does not appear to have occurred in other complexes; where metasomatic effects have been observed in the volcanic rocks, they have been of a sodic nature. The question therefore arises as to whether the Rishi volcanic rocks also underwent a sodic process, which has been overprinted and obliterated by the dominant potassic process. Certainly the sodic process was weak in the Rishi area if niobium enrichment can be used as a measure of the sodic imprint. However, the geochemical evidence discussed later, together with the mineralogical evidence presented here, suggests that a wave of sodic metasomatism has passed upwards and outwards through the volcanic pile and the basement but has been overprinted and masked by later processes.

In summary, it has been possible to distinguish the different mineralogical assemblages generated by potash metasomatism, according to the rock type that is being metasomatised, and according to whether sodic metasomatism has or has not preceded the potash metasomatism.

#### Acid (hydrogen ion) metasomatism and hydration

##### Introduction

There may have been a gradual change in the mineral assemblage generated during lower temperature metasomatism in response to the changing  $K^+/H^+$  ratio in the fluid (Rose and Burt 1979). Such acid metasomatism was characterised by the breakdown of granitic minerals to produce a new mineral assemblage. Thus acid metasomatism was characterised by the gradual loss of original feldspar, the development of Li-Fe or Li-Al micas and gradual increase in quartz as acid metasomatism became more intense. The accessory minerals associated with acid metasomatism are commonly concentrated in the mica clusters. The assemblage of ore minerals is mainly of oxides, but in the later stages of deposition, sulphide minerals were also introduced.

This process of acid metasomatism may be disseminated within the roof of the Rishi biotite granite cupola or form pervasive pockets associated with microcline; it may diffuse along zones (Plate 9.4) to produce veins, sheeted veins and stockworks. The effect may also extend beyond the confines of the biotite granite to affect the volcanics and basement. It is a widespread process but at its maximum close to the contact and within the roof of the biotite granite (Fig 9.4).

Since acid metasomatism can be superimposed on various earlier mineral assemblages within the biotite granite roof zone and since it can also affect the basement or volcanic pile, the petrological characteristics of the process depend on the initial rock type and on the intensity of earlier sodic or potassic metasomatism.

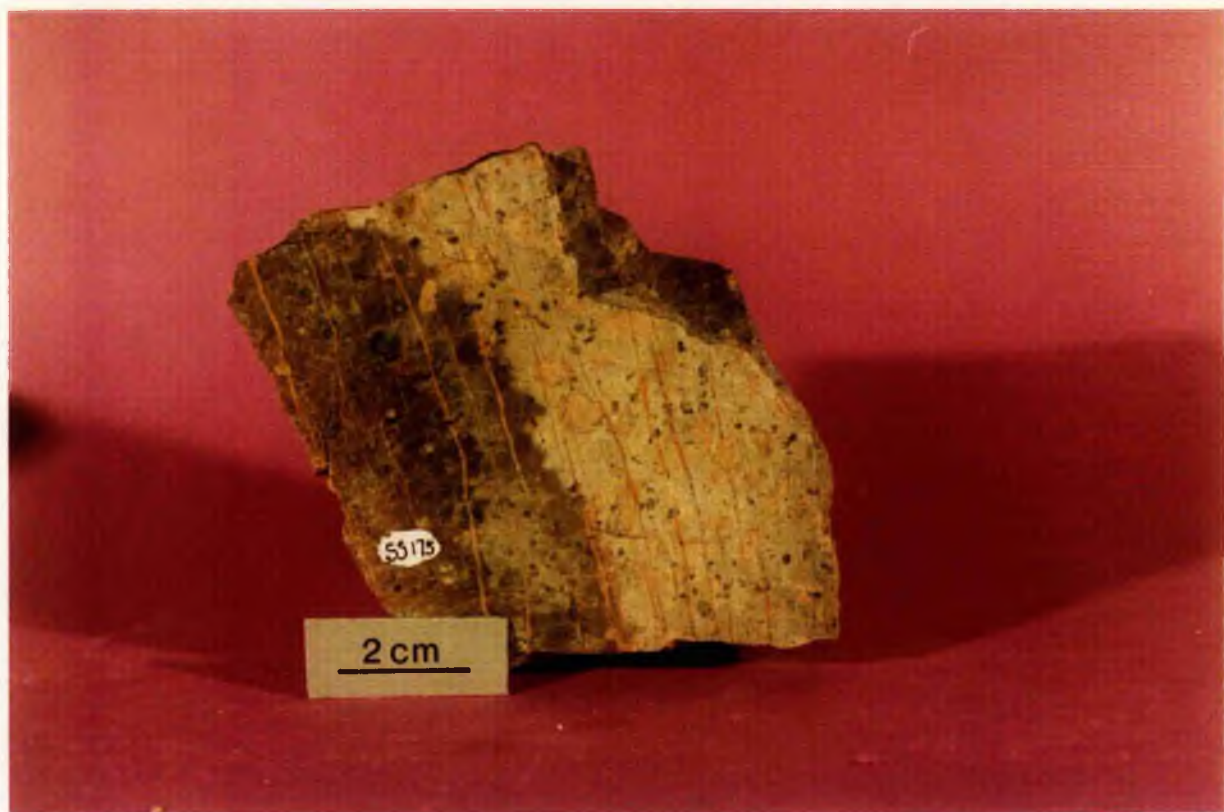


Plate 9.21 Altered porphyry feeder dyke

Thin veinlets of microcline cutting the altered porphyry feeder dyke. Locality SS175



Plate 9.22 Altered basement monzogranite

Variation in colour and texture of altered monzogranite showing the abundance of chalcopyrite and sphalerite in sample SS94 (right).

Samples from left to right: SS18/6, SS92, SS94

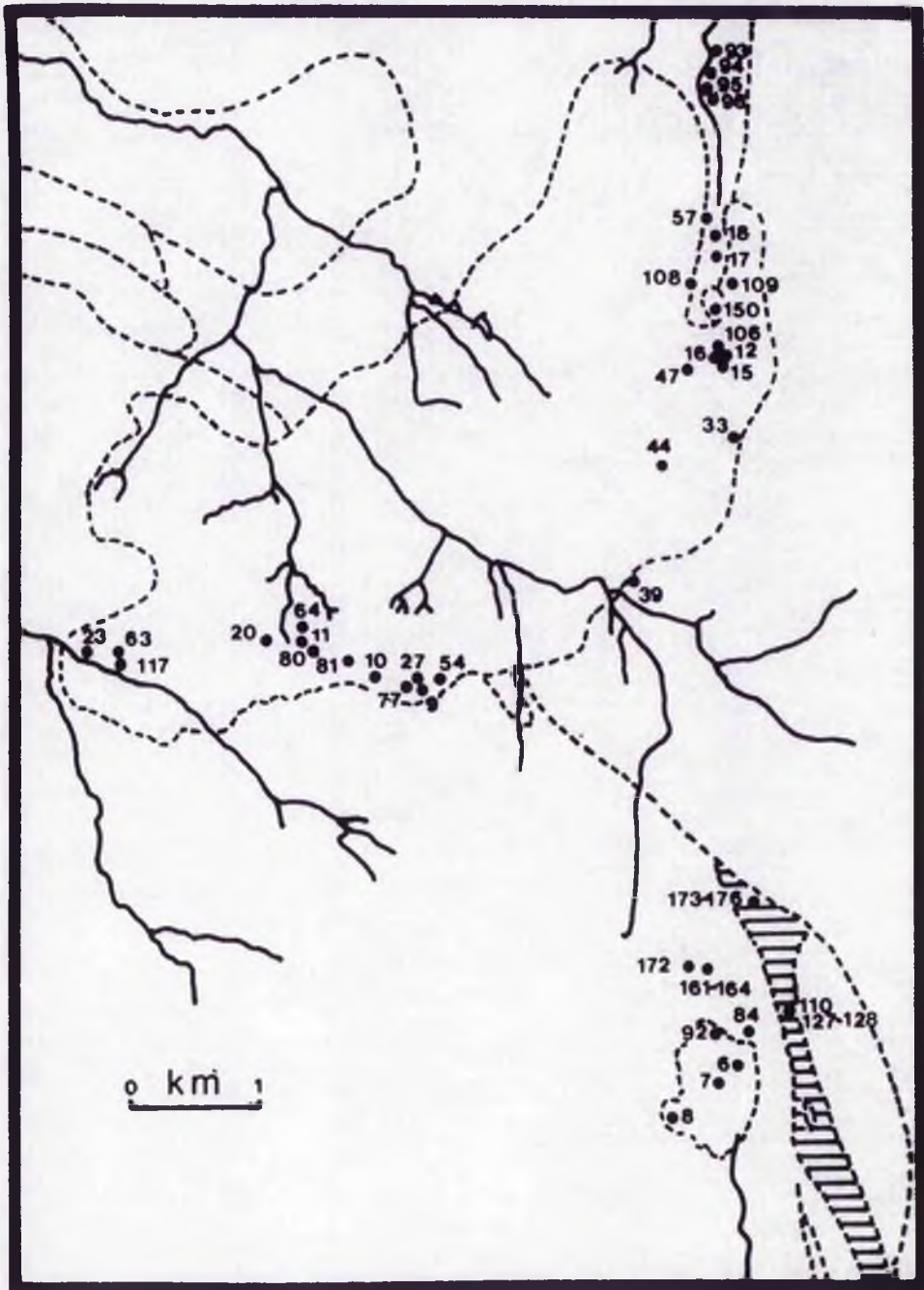


Fig 9.4 Sample localities of acid metasomatised facies.  
 For key to geological units see Fig.7.4

## Acid metasomatism of the basement

In part one of this thesis, on the data available from the Nigerian complexes as a whole, acid metasomatism of the basement was recognised and shown as trend 1 in Fig 4.4 on page 76). However, at Rishi it is clear that the process of acid metasomatism of the basement can be subdivided. Thus it is possible to distinguish acid metasomatised (greisenised) basement which may or may not have suffered potash metasomatism, described as Trend 1a below, from an acid metasomatised facies that had previously undergone sodic metasomatism (described as Trend 1b). Although the mineralogy is much the same in both cases, there is a marked textural difference, a difference in ore abundance, plus a distinction in major and trace element chemistry. It is in these altered basement granites that the most varied assemblage of ore minerals and accessories can be found.

### Ore-rich assemblage (Trend 1a)

The dominant process of acid metasomatism on the basement, affected basement megacrystic monzogranite which in places had also suffered an earlier potash metasomatism. The effects of the acid process can be examined in the hornblende biotite monzogranite north of Dutsen Rishi close to the Rishi biotite granite contact. The altered basement is fine-grained, almost black in colour, extremely micaceous and very ore-rich (Plate 9.22). Samples SS18a, SS18b, SS18/5, SS18/14, SS57/3, SS57/4, SS57/14, SS93, SS94 and SS102 show that the acid alteration was characterised by the chloritisation of annitic mica, alteration of K-feldspar to kaolinite or chlorite, the alteration of albite to pale coloured micaceous (sericitic) aggregates and the growth of large books of honey coloured zinnwaldite. The intensity of alteration was greatest at the contact, grading outwards to lesser altered basement in which the feldspar porphyroblasts can still be identified although the groundmass may be altered. There was a gradual progressive alteration in SS57/2 through SS57/3 to 57/4. In 57/2 there was no development of pale honey-coloured mica, in 57/3 it occurs in small clots associated with opaques whereas in 57/4 it forms abundant clusters, which may reach 2mm across, composed of lath-like crystals. Purple fluorite is abundant - the calcium was probably derived from the alteration of the calcic feldspar phenocrysts and combined with fluorine in the hydrothermal fluids. The low percentage of quartz in some of these samples indicates removal by the fluids which must therefore have been rich in Hf.

Texturally, the grain size of the altered basement is usually quite coarse with ore minerals often several centimetres in size. In SS57/14, which is still texturally and mineralogically recognisable as an older granite the feldspar phenocrysts show extensive sericitisation. In addition some perthites have been chloritised or altered to a mixture of epidote and biotite. Late-stage feldspathic veins cross-cut the altered perthites. SS57/14 is not extensively mineralised but the other samples are rich in sulphide ores (Table 9.3) with a small percentage of cassiterite. Sphalerite, is extremely abundant and may vary from small crystals which are yellow to orange in colour in thin section and rimmed with chalcopyrite, to large blood red crystals which are traversed by veins of chalcopyrite, whilst chalcopyrite is also exsolved along cleavages and partings in the sphalerite. Chalcopyrite, is also abundant as massive skeletal crystals, often poikilitically enclosing other minerals and occasionally forming small euhedral crystals 1mm in size. Cassiterite occurs sporadically often marginal to the sphalerite crystals. It varies in colour from colourless through shades of yellowish to reddish brown. Accessory fluorite, monazite and zircon

are ubiquitous. The zircons are small and commonly are surrounded by pleochroic haloes in biotite. Monazite forms discrete prismatic crystals up to 4mm in size (SS94), but more commonly occurs as a mesh of crystals or as rosettes (Plate 9.23). Dark brown, skeletal, prismatic crystals of allanite, up to 2mm in length occur associated with the monazite, particularly in SS57/4 (Plate 9.24). Alunite, barytes, calcite and smithsonite - which have not been noted before in the mineralogical assemblages of the alteration processes - occur as accessories in quantities too small to register in Table 9.3, together with occasional skeletal ilmenite. Small patches of a mineral believed to be jarosite occur in association with the sulphide ores in several samples. Also small amounts of a brown almost isotropic low relief mineral which occurs in association with chlorite in both the groundmass and in late veins is probably a clay mineral (?nontronite) and natrolite occasionally lines small miarolitic cavities.

Table 9.3. Modal compositions of acid metasomatised basement

	Ore-rich (Trend 1a)					Ore-poor (Trend 1b)			
	SS57/3	SS57/4	SS57/14	SS94	SS93	SS17/2	SS17/4	SS17/5	SS39
Quartz	19.7	46.7	42.8	2.9	0.9	33.8	17.8	8.4	33.6
Perthite						26.4	35.7	54.0	50.4
Microcline		0.1	29.9						
Albite			18.0						
Clay mins	0.5			6.6					
Sericite						0.1	2.5	3.4	3.2
Biotite	48.1	6.7	0.2	30.8	39.5	23.3	24.6	29.6	11.2
Chlorite	7.4	9.4	7.2	8.8	16.9	15.6	16.7		1.2
Fluorite	1.9	6.7	0.1	2.6	20.1		0.2		
Sphalerite	19.9	26.3		17.2	2.3				
Cassiterit	0.1	0.1		0.3	2.5		0.1	0.6	
Chalcopyrt	1.1	1.2		28.8	7.9				
Other ores	0.1	0.4	0.9	0.8	0.7	0.3	0.3		
Zircon	0.1	0.2	0.7	0.2	0.4	0.3		0.2	
Monazite	0.3	0.3		0.9	7.9		0.1		
Sphene			0.1						
Allanite		1.6			0.9				
Apátite			0.1	0.2				1.2	0.2
Zeolite	0.8								

The wide variation in modal percentage of the minerals in Table 9.3 reflects the coarse texture and sporadic occurrence, particularly of the ore minerals.

#### Ore-poor assemblage (Trend 1b)

In contrast, to the coarse ore-rich, acid metasomatised basement just described, acid metasomatism of basement which had already undergone sodic metasomatism produced a pale-coloured, fine-, even-grained micaceous rock. Samples SS17/2, SS17/3, SS17/5 and SS39 show these characteristics. The original quartz phenocrysts remain as anhedral crystals within clusters, occasionally up to 1cm in size, with strain extinction and sutured margins. Sometimes the quartz has been fractured and in SS 39, the granular texture of the quartz is typical

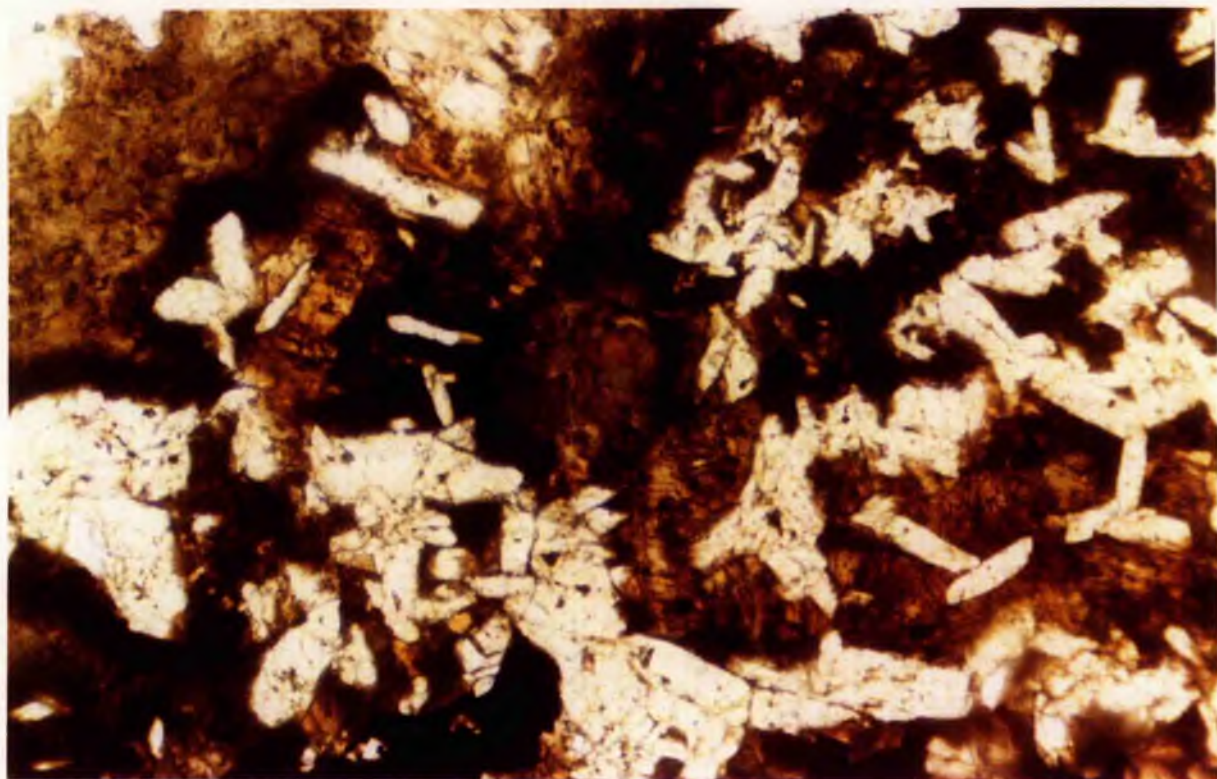


Plate 9.23 Meshwork of monazite

Abundant monazite crystals with dark brown mica which has been partially chloritised. Note the haloes which surround many of the monazite crystals. x250



Plate 9.24 Allanite and monazite

Dark brown prismatic crystals of allanite associated with monazite x50

of a hornfels (Plate 9.25). Perthite phenocrysts, showing a patch texture are partially replaced by sericite whilst the original albite has been totally replaced by a fine-grained mesh of sericite (Table 9.3). Ghosts of twin lamellae of the albite indicate the original feldspar composition (Plate 9.26). Chlorite, accompanied by opaques, replaced earlier ferromagnesian minerals and there was also a marginal alteration of perthite to chlorite. There was no development of large books of mica which characterised the veins described above, there was no major deposition of ore minerals and the assemblage of accessory minerals was limited to zircon, occasional cassiterite and monazite.

#### Acid metasomatism of volcanic rocks (trend 2)

The Q/F plot of the volcanic rocks (Fig 8.8), shows that two of the samples (SS84 and SS172) which do not appear altered in hand specimen, plot out of the general field of the volcanic rocks. Their position on the Q/F plot suggests that they have undergone acid metasomatism although the phenocryst assemblage of crystals is similar to other samples. However, it is in the groundmass that there is most evidence of fluid reaction and alteration. In thin section, there is a devitrification of the original glassy groundmass and a coarsening texture with biotite growth in response to fluid reactions. However, all the volcanic rocks show some microscopic evidence of groundmass coarsening and subsolidus biotite growth but in the two samples above, mica growth is more advanced than in other samples. Others like SS161/2 show dark patches of alteration in the groundmass, even in hand specimen (Plate 9.27). These patches may reach sizes of 2-3cm. In thin section the dark patches appear as fine-grained clustered granules of greeny brown to mid brown coloured mica, accompanied by rounded grains of cassiterite less than 0.1mm in size. The phenocrysts of quartz remain intact, whilst the feldspar phenocrysts which have been corroded, show several alteration features, in particular the destruction of a patch perthitic texture and increased turbidity due to microclinisation.

In addition to these samples, SS164 represents a further step in progressive alteration and in this case there is a reddening of the feldspar phenocrysts in hand specimens. In contrast to the previous samples, the mica does not form clusters but instead is evenly distributed as fine-grained granules throughout the coarsened groundmass although its modal percentage is much the same as in the other samples (Table 9.4). It is dark green or sometimes brown in colour and shows signs of alteration to chlorite and haematite. The feldspar phenocrysts have reacted with the residual fluid to a greater extent than in most samples of the volcanics, they are very turbid and almost completely microclinised.

In SS150 however, from the summit of Dutsen Rishi, there has been intense acid metasomatism of the volcanic pile immediately above the biotite granite roof. The small outcrop is very distinct because it is covered only with a poor grass vegetation in contrast with the heavily wooded slopes (Plate 9.2). In hand specimen the rock is fine-grained and micaceous and it is difficult to identify what it was originally (Plate 9.27). However, in thin section, its volcanic origin is evidenced by the quartz phenocrysts. These quartz phenocrysts which have rounded or bipyramidal form are sometimes fractured, often embayed and sometimes showing resorption features. (Plate 9.28). Such features are characteristic of quartz from the volcanic pile. Apart from the structural location of the specimen there is little remaining evidence to the original rock type although ghosts of feldspar phenocrysts are picked out by clustered mica

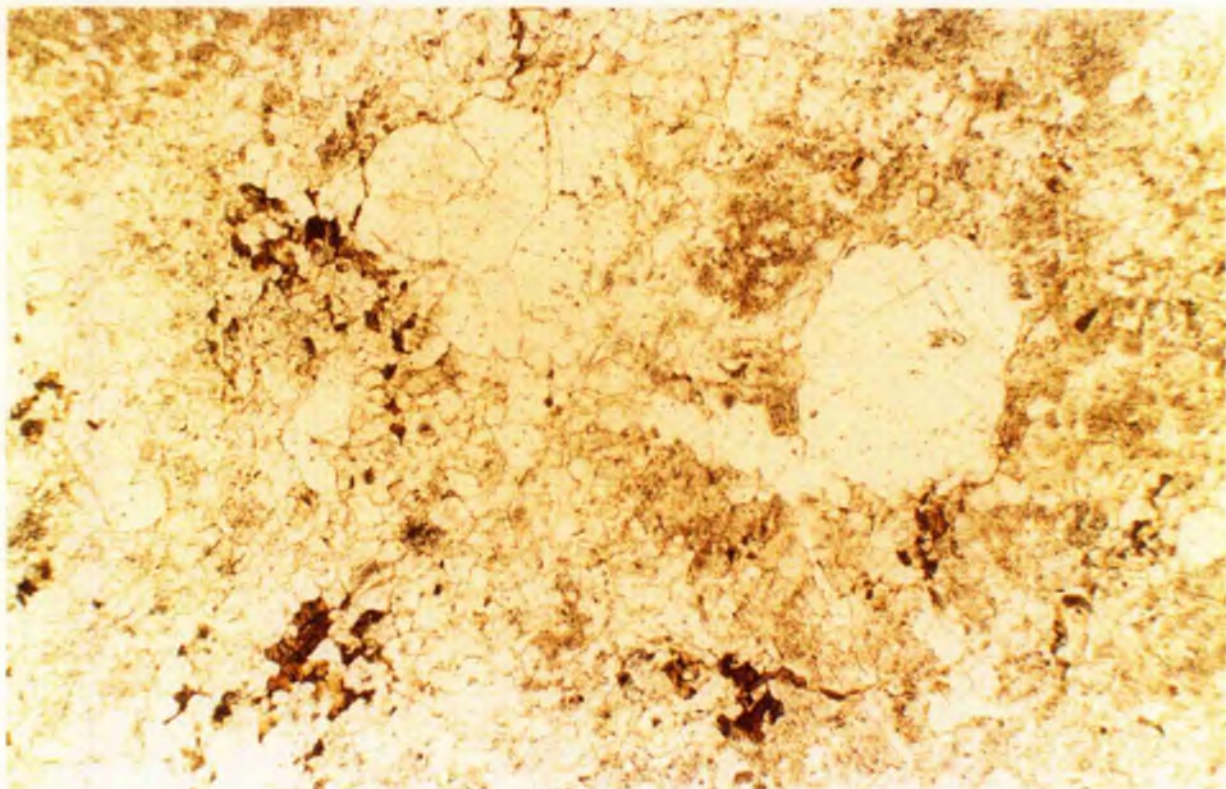


Plate 9.25 Large amoeboid-texture quartz in hornfels which is largely composed of granular quartz, perthite and wisps of chloritised mica. SS39, PPL x50.

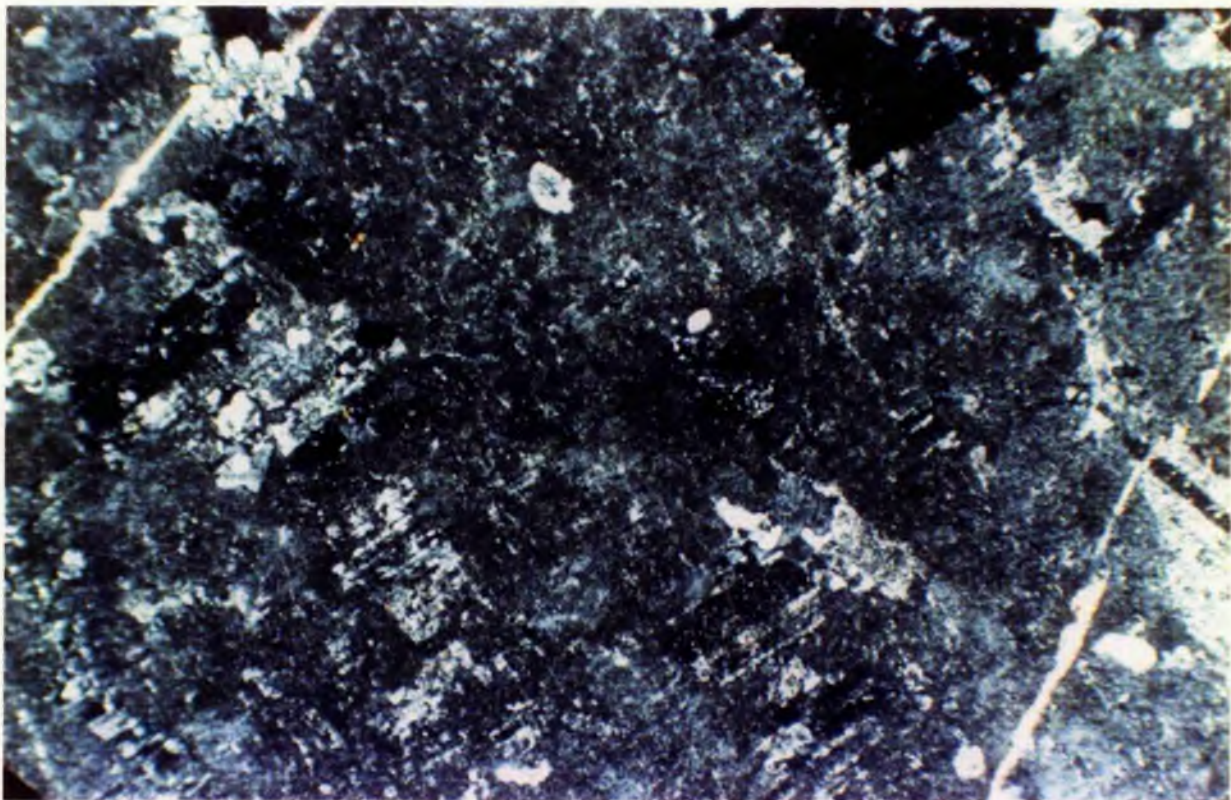


Plate 9.26 Ghosts of twin lamellae of albite in mottled microcline. More commonly the albite has been sericitised. SS17/2, XPL x50.



Plate 9.27 Altered ignimbrites: dark patches of felted biotite aggregates in SS161 to the right. On the left, SS150 from the summit of Dutsen Rishi has lost its volcanic character.

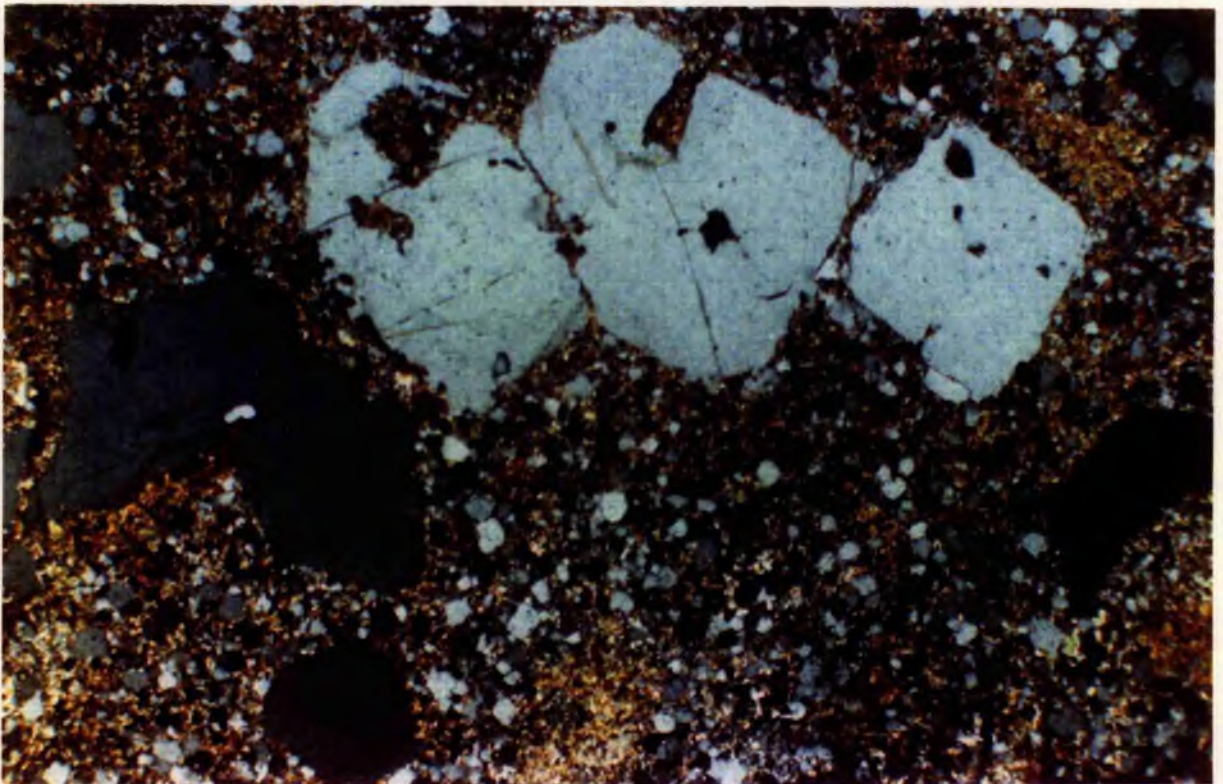


Plate 9.28 Photomicrograph of SS150 showing embayed crystals which are characteristic of the ignimbrites. XPL xl20.

granules. Traces of feldspar remain (Table 9.4), which are in various arrested stages of being replaced by extremely fine-grained aggregates of mica. The quartz-rich groundmass is even textured. Individual quartz grains are emphasised by a rim of greeny-brown biotite. Biotite is abundant and evenly distributed in the groundmass.

Table 9.4 Acid metasomatism of volcanic rocks

	volcanic pile			volcanic feeder	
	SS150	SS161/2	SS164	SS173	SS176
Quartz	63.0	25.2	49.0	68.7	14.1
Perthite	0.8	54.0	29.7	5.0	63.4
Albite		1.4			1.9
Biotite	34.2	18.9	18.6	3.0	14.3
Chlorite	1.2		0.7	0.8	0.7
Fluorite			0.1	0.8	
Cassiterite					0.3
Columbite			0.1		
Other ores	0.6	0.4	1.7	20.8	3.0
Zircon				0.1	
Monazite	0.2	0.1	0.1	0.1	
Apatite				0.5	1.8

Acid metasomatism of the feeder dyke has also occurred in many places. The mineralogical and textural changes are very varied (Plate 9.29). In SS173, the feldspar in the groundmass is extremely coarse and turbid and has obviously undergone a process of microclinisation followed by a partial alteration to a tan coloured mica. The mica occurs in clusters and as wispy interstitial trains. In addition stubby laths of albite up to 1mm long occur and these have undergone some sericitisation. Both feldspars also show traces of kaolinisation. In contrast in SS176, the feldspar phenocrysts which were probably more altered to mica than in SS173, are now almost completely altered to wisps, spongy, or angular-shaped orange-coloured limonite. This limonite coats vugs left by feldspar alteration. In addition, any mica that may have existed has also been altered to limonite. Despite the extensive alteration, there is little evidence of mineralisation. Accessory minerals include apatite which is common, along with zircon and monazite.

The apatite forms colourless euhedral prismatic crystals up to 0.2mm in size, which are disseminated throughout the rock (Plate 9.30). It is more abundant than in any other sample examined from Rishi.

In other areas, particularly at localities SS110, 127 and 128, the phenocrysts assemblage of the porphyry feeder dyke remains recognisable (Plate 9.29). Although the feldspars are altered it is in the groundmass that acid alteration is at its most extreme. The groundmass is largely khaki or tan coloured mica which is associated with cassiterite, sphalerite and genthelvite as accessory minerals.



Plate 9.29

Altered feeder dyke samples showing the textural variations.

In SS128 (left) the phenocryst assemblage of the porphyry remains recognisable. Although the feldspar phenocrysts are altered it is in the groundmass that acid alteration is at its most extreme. In SS176 (right) the feldspar phenocrysts have been altered to orange brown limonite and only a few feldspar phenocrysts remain.

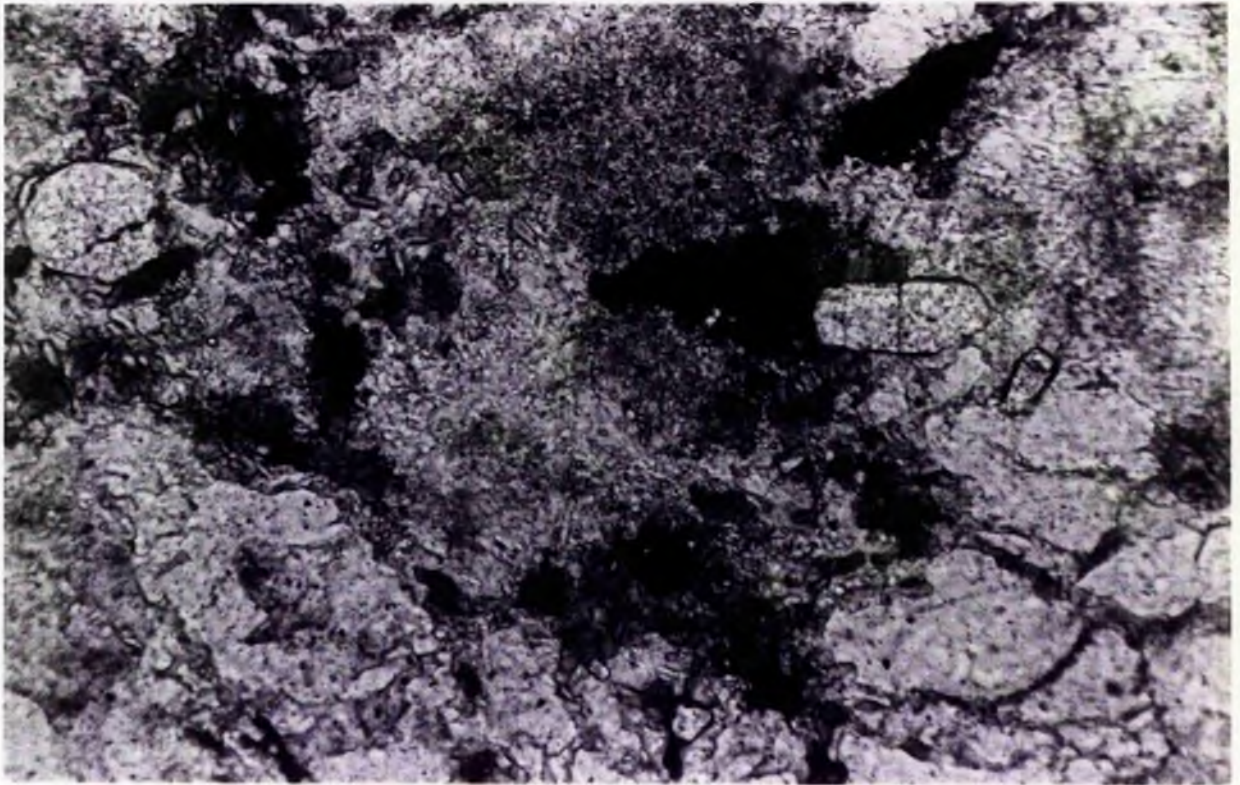


Plate 9.30 Euhedral prismatic apatite crystals and needles in SS176, altered porphyry feeder dyke. Photomicrograph in PPL x125

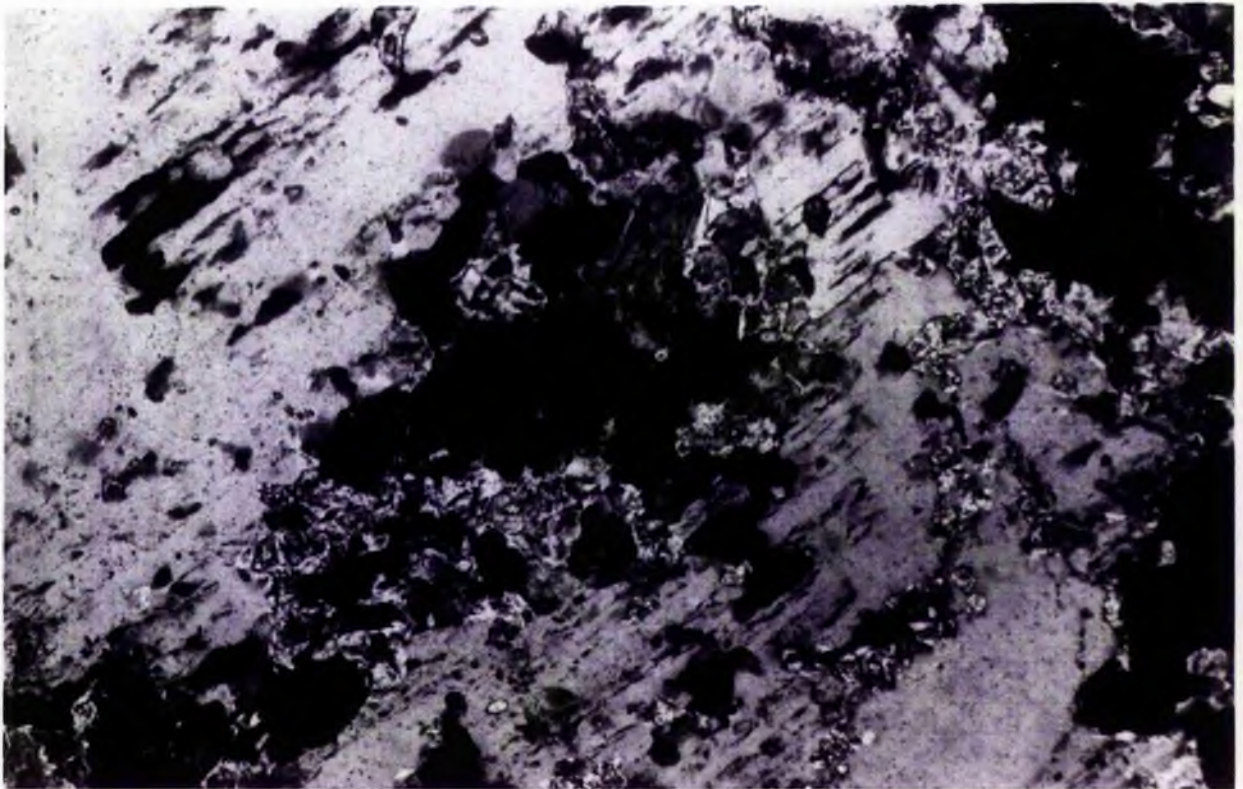


Plate 9.31 Photomicrograph of SS20/1a showing quartz replacement of perthite. Trains of fluid inclusions mimic inclusion-rich potash zones and vestiges of perthite remain. Also in the field of view is anhedra sphalerite together with sericite. XPL x125

## Acid metasomatism of albite-bearing facies

The samples which show acid metasomatism of albitised rocks (SS9/4, SS20/1, SS20/4, SS77 and SS117/6) come from the southern margin/roof zone of the Rishi biotite granite, close to the contact with the volcanic pile. Because the phase of sodic metasomatism was only weakly disseminated, the major mineralogical assemblage that is generated from acid metasomatism of sodic facies is very similar to that of acid metasomatised perthite granite containing minor albite, which is discussed in detail later. A good example of this group is SS20/1a. It consists of abundant sericite generated from albite breakdown and subordinate pale green mica, developed from unaltered perthite. In samples where albite was originally subordinate to perthite clustered laths of pale green mica dominate sericite development. Quartz must also have replaced feldspar. Parallel, linear trains of fluid inclusions mimic inclusion-rich potash zones in perthites (Plate 9.31). However, it is the accessory mineral assemblage that is the most interesting aspect of this facies because it reflects the sodic event. In SS77, cryolite comprises 2.5% of the sample (Table 9.5). It ranges in size from 0.1-1mm and forms skeletal, granular, sometimes equant crystals (Plate 9.32), which are always colourless and "greasy" in appearance, similar to topaz, from which it can be distinguished by negative R.I. and lower birefringence. The cryolite is accompanied by thorite, zircon, monazite, topaz and sphalerite (Plate 9.33), whilst in SS9/4 prismatic columbite is also an accessory. Chalcopyrite, which occurs in the modal percentage of SS20/1a, occurs only as an exsolved phase within sphalerite; no discrete chalcopyrite has been noted.

Table 9.5 Acid metasomatism of samples already affected by sodic metasomatism

	SS9/4	SS20/1a	SS20/1b	SS77
Quartz	57.3	40.4	42.0	54.0
Microcline/Perthite	8.4	3.3	2.0	3.7
Albite	4.2	0.3	0.6	4.1
Biotite/sericite	28.4	37.8	48.8	33.6
Chlorite	0.3	5.2	1.4	0.7
Topaz	0.3	0.2	0.4	0.1
Fluorite	0.7	0.5	0.8	0.2
Sphalerite		10.7	3.8	0.5
Chalcopyrite		1.2		
Other ores	0.1	0.2		0.2
Zircon	0.1	0.1	0.2	0.2
Monazite	0.1	0.1		0.1
Cryolite				2.5
Columbite	0.1			
Thorite				0.1

## Acid metasomatism of microcline rich rocks

Since the process of potash metasomatism has produced a range of microcline-rich rocks, which may vary from 50-90% microcline, the superimposed acid metasomatism will vary according to the degree of the earlier process.

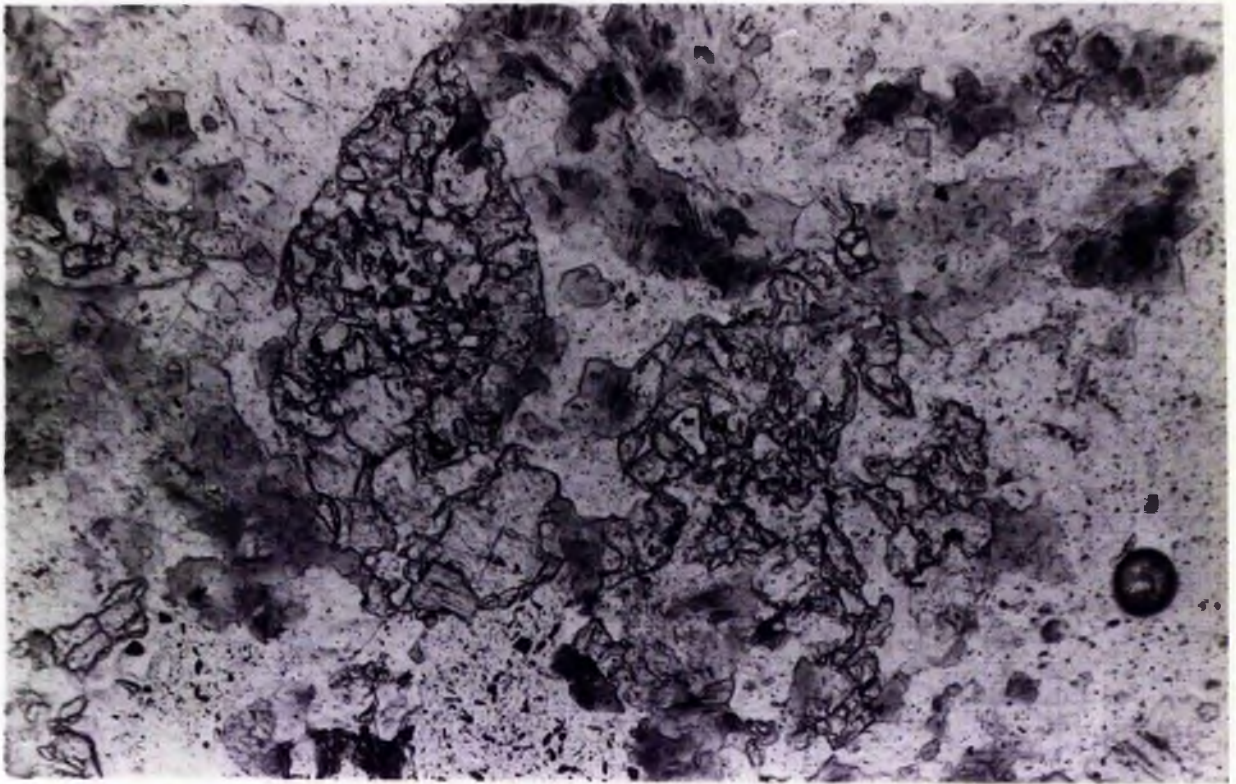


Plate 9.32 Anhedral skeletal colourless cryolite in SS77. PPL xl25

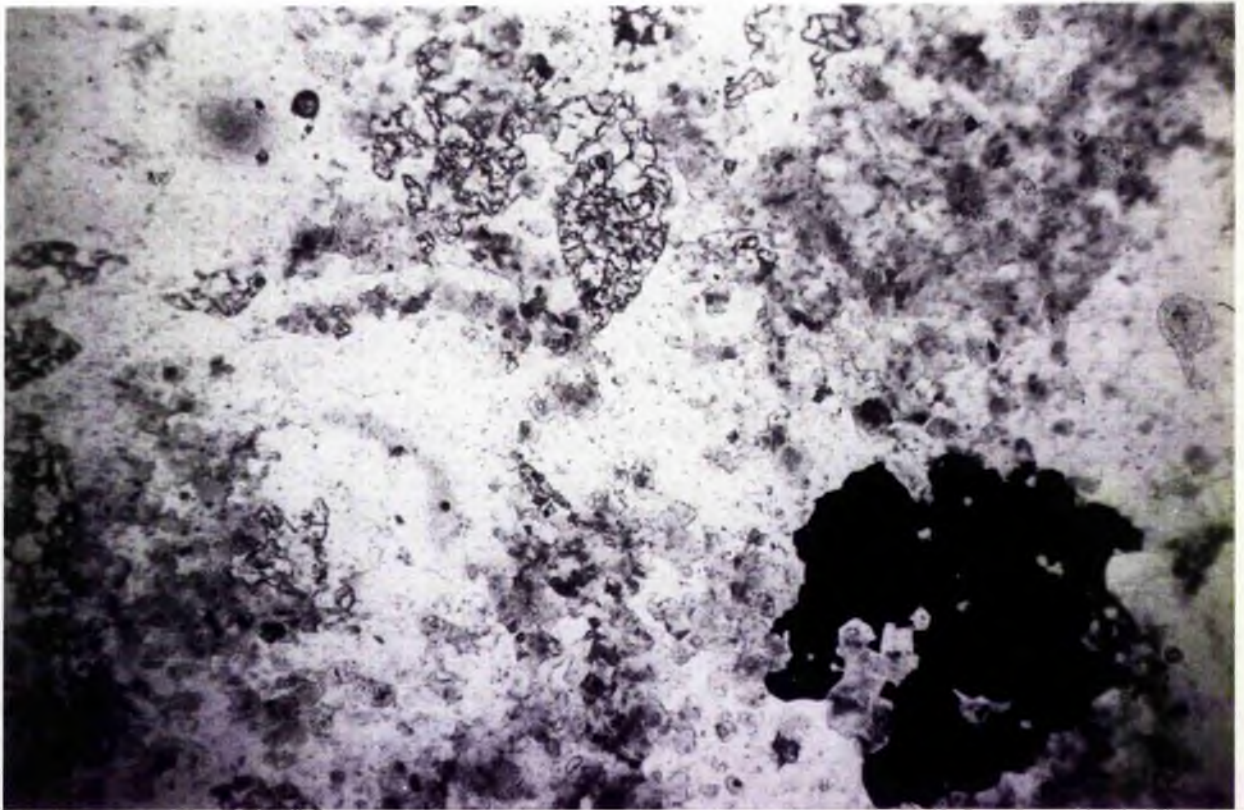


Plate 9.33 Cryolite with quartz, pale green mica and blood red sphalerite in SS77. PPL xl0

Essentially, since the cream or salmon-coloured microcline is altered to green siderophyllite or zinnwaldite mica at this stage, and the abundance of mica reflects the degree of earlier microclinisation, the coloration of the hand specimens is a guide to the intensity of alteration (Plate 9.34)

In SS20/2 there is a transition within the sample from a microcline through to a mica-rich rock, whereas in SS20/3, large patches of salmon pink microcline remain within an otherwise mica-rich rock. The mica in both SS20/2 and 20/3 forms spongy aggregates of very fine blue-green mica flakes (Plate 9.35), similar to SS64/3 described below. Mica clearly replaced the microcline and occasionally there is an associated sheaf-like development of chlorite. The pink microcline is very mottled and undergoing incipient alteration to topaz and chlorite in addition to mica. In SS20/2 the microcline is less turbid and sometimes shows microscopic development of cross-hatched twinning - a rare phenomena for Nigerian hydrothermal assemblages.

In other samples SS23/1, SS27/5, SS63/1, SS64/3, SS54/2, SS81 and SS117/5a, the rock is composed of varying proportions of quartz and siderophyllite, becoming a monomineralic mica rock in SS44/1 (Table 9.6). The mica forms clusters of euhedral crystals with plates typically 0.5mm across (Plate 9.36). Individual books may reach 4mm in diameter. The micas are never zoned although there may be vestiges of an earlier brown-coloured phase. The cleavages were often emphasised by haematite or ilmenite development associated with fluorite and in SS23/1 this was accompanied by the development of siderite. Interstitial mottled microcline remnants occur in a few samples and in SS23/1 these remnants have partially been altered to kaolinite, presumably at the same time as siderite development. SS64/3 differs from the other samples in that the mica occurs as spongy irregularly-shaped aggregates of extremely fine grained blue-green mica with no lath development (Plate 9.37). The monomineralic mica rock, SS44/1 has a slightly different coloured mica in that it is khaki in colour as opposed to blue-green (Plate 9.38). Where rare quartz occurs, it forms clustered anhedral mosaics, sometimes showing strain extinction and an abundance of gas-rich fluid inclusions.

Table 9.6 Acid metasomatism of microcline-rich rocks

	SS20/2	SS20/3	SS23/1	SS44/1	SS63/1	SS64/3	SS117/5A
Quartz	37.5	4.1	52.9	0.8	16.8	36.9	35.9
Microcline/Perthite	38.5	35.5	1.8		0.1		0.3
Albite	1.0						
Biotite	17.8	57.8	43.3	98.0	81.8	61.7	61.2
Chlorite	1.6	0.3		0.1		0.3	
Topaz	1.5						
Fluorite	0.6	0.6	0.7	0.1		0.1	0.2
Sphalerite	1.1	0.1					
Cassiterite	0.1		0.2	0.1	0.1	0.1	1.2
Ilmenite					0.2		
Haematite		0.5	0.7	0.5	0.8	0.8	0.5
Zircon	0.3	1.0	0.3	0.3	0.1	0.1	0.6
Siderite			0.1				
Monazite		0.1		0.1	0.1		0.1



Plate 9.34

On the left, spongy aggregates of fine-grained blue-green mica have almost entirely replaced microcline and only traces of pink microcline remain. In the other two samples microcline has only partially been replaced.  
 Left to right: SS20/3, SS20/2, SS23

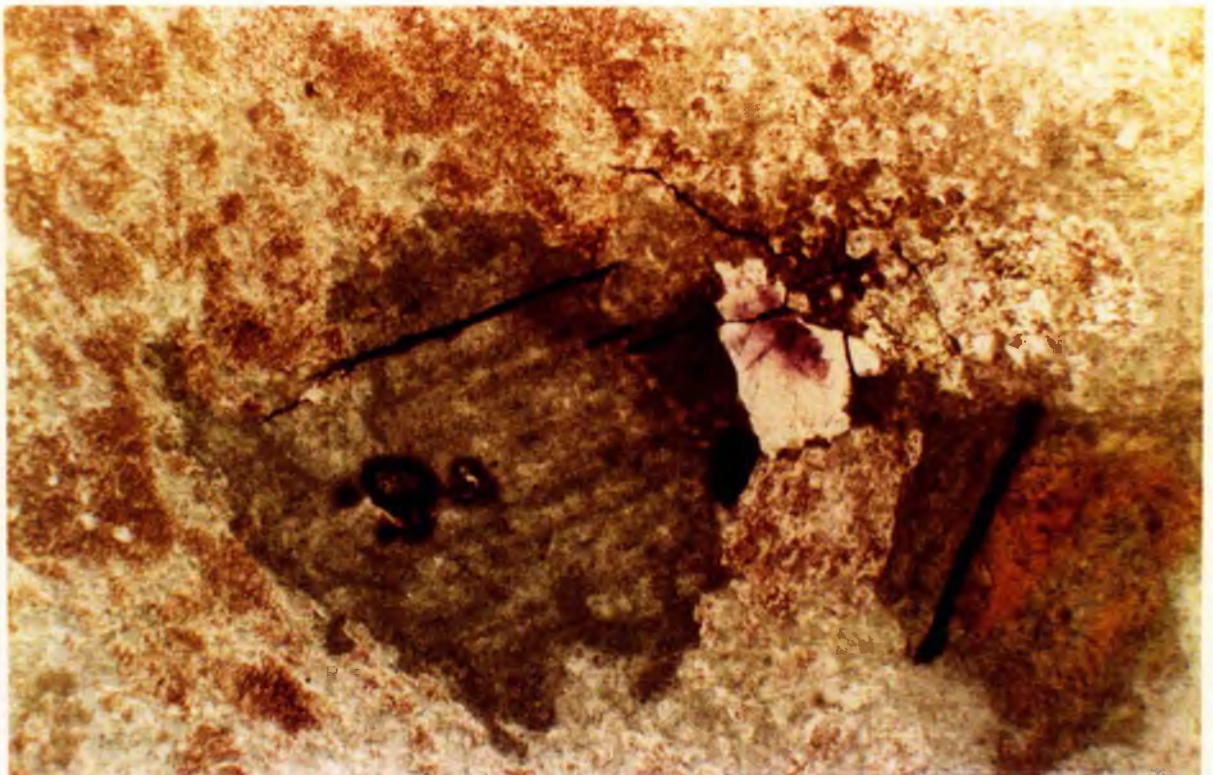


Plate 9.35

Large patches of pinky-brown microcline remain within an otherwise mica-rich rock with accessory fluorite. Most of the mica occurs as spongy aggregates and only rarely do large crystals occur. Note the zircons with pleochroic haloes and the haematite development along cleavages.  
 PPL x125



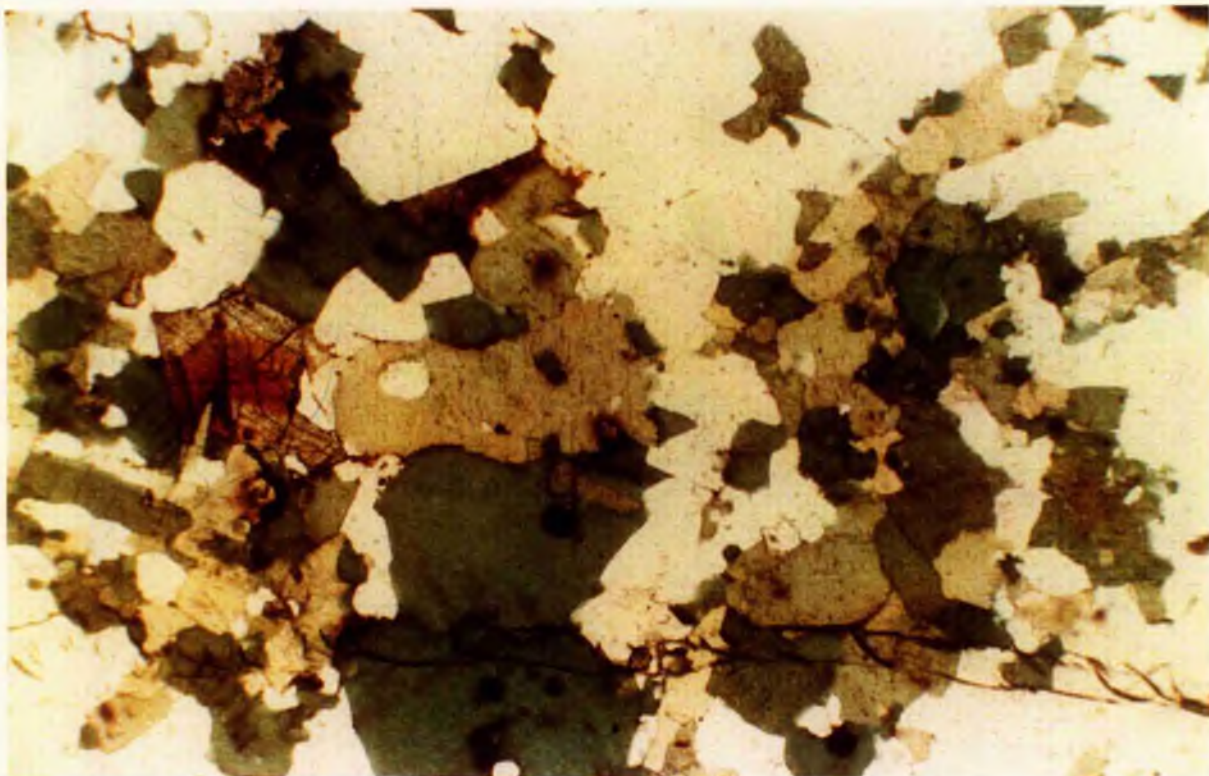


Plate 9.36

Clustered green mica with zoned cassiterite and quartz. The individual micas are up to 0.5mm in size. SS117/5a, PPL x125

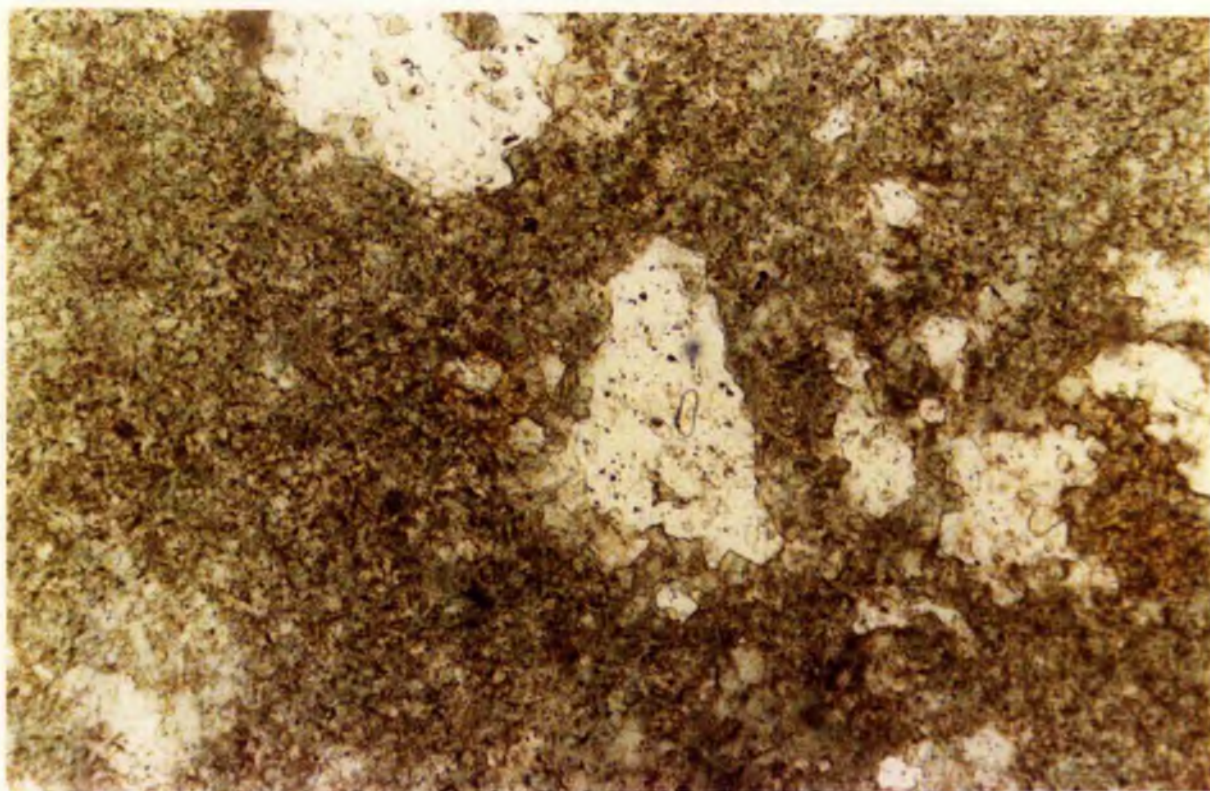


Plate 9.37

Spongy aggregates of very fine-grained blue-green coloured mica. SS64/3, PPL x50



Plate 9.38

Photomicrograph of SS44/1 showing the abundance of khaki-coloured mica. PPL x25

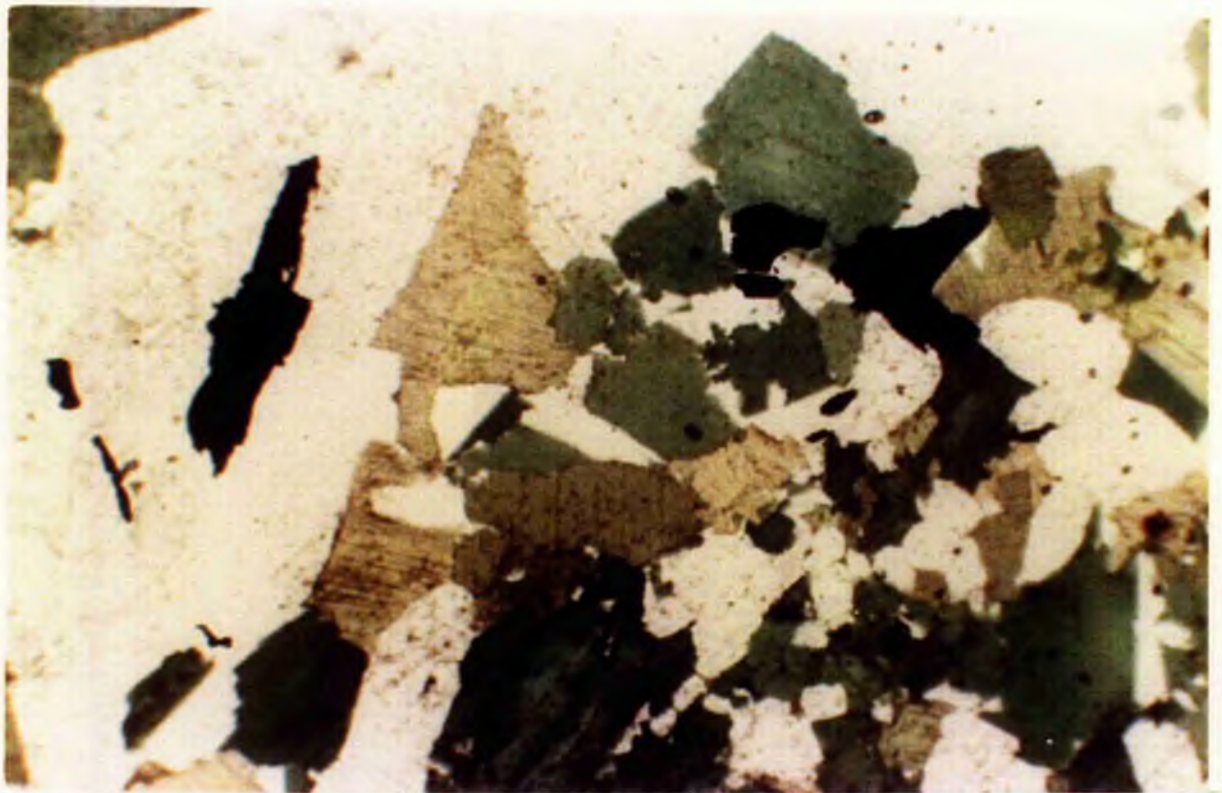


Plate 9.39

Discrete ilmenite occurs associated with clusters of blue-green mica in this photomicrograph of SS63/1. PPL x25

Accessory minerals are limited in range and sparse in abundance with fluorite, zircon, siderite, haematite, monazite, sphalerite, ilmenite and cassiterite particularly in SS117/5a where it forms 1.2% of the sample. The cassiterite is usually small, anhedral and deeply coloured, although twinned and zoned crystals do occur. These are brown at the centre and colourless towards the rim. Where fluorite is enclosed in mica a pleochroic halo has sometimes developed around the fluorite inclusion, indicating that the fluorite may be Th- or U-bearing. In SS63/1 there are several discrete crystals of ilmenite, usually associated with the mica clusters (Plate 9.39). The small percentage of cassiterite is particularly surprising in view of the fact that locals are actually working some of these monomineralic mica rocks for tin.

#### Acid metasomatism of perthite biotite granite

Acid metasomatism of an unaltered perthitic alkali feldspar granite is a progressive process. Most of the mineralogical changes have already been described such as destabilisation of perthite, albite and mica, but in this particular case there has not been any significant earlier hydrothermal alteration of these minerals. It is a very common type of alteration within the Nigerian biotite granites and the Rishi biotite granite is no exception.

Occasionally, as in SS80 which comes from the southern margin of the Rishi biotite granite, the acid metasomatism has been a disseminated process. More commonly, the acid metasomatic process appears to have occurred along incipient fractures. Initially a dark-coloured quartz, chlorite + topaz rock was produced but with continued acid metasomatism a quartz, topaz, siderophyllite - zinnwaldite assemblage was produced, which conforms to a classic greisen. Ultimately, as the acid alteration became more silicic, a quartz-topaz rock similar to the Australian silixites was produced. This then graded into monomineralic quartz rocks as the process of silicification became dominant. Although the alteration is a progressive process it is possible nevertheless, to divide it into stages in order to discuss the sequence of mineralogical changes that are observed (Table 9.7).

Table 9.7 Mineral assemblage characteristic of the different stages of acid metasomatism of a biotite perthite granite

Stage 1	Quartz-feldspar-chlorite
Stage 2	Quartz-chlorite+ topaz
Stage 3	Quartz-chlorite-sericite
	or
	Quartz-sericite-chlorite
Stage 4	Quartz-sericite or quartz+Li-Fe biotite + topaz
Stage 5	Quartz-topaz (silexite)

#### Stages 1 and 2

Samples such as SS12/2a, SS12/3, SS15b and SS64/2 represent the first stages in acid metasomatism of a biotite perthite granite. Vestiges of original ragged skeletal brown biotite remain, but most has been chloritised and is associated with fluorite, zircon and opaque minerals. Large phenocrysts of lamellar and patch perthite may be largely unaltered, as in SS12/3, or show various stages of alteration to chlorite. In SS64/2 there is a superb example of the lamellar perthite undergoing chloritisation along the potash lamellae within the perthite (Plate 9.40 and 41). Occasionally, quartz can be seen replacing perthite (SS12/2a) and granules of topaz were also generated at this stage from perthite alteration. Accessory minerals include deep orange-coloured sphalerite, molybdenite, zircon, monazite, fluorite and haematite (Table 9.8).

Stage 2 was reached when all the original feldspar had been chloritised and the original mica destroyed so that a quartz-chlorite assemblage + topaz was produced. There are many examples of this type of alteration in Rishi (SS15a, 16/4, 16/5, 16/6, 18/1, 18/6, 32/3b, 33/7, 35/2). In SS16/6, for example, discrete quartz crystals <0.5mm in size, with rare aggregates up to 3mm in size and showing strain extinction together with spongy clusters of chlorite are accompanied by discrete rounded colourless topaz, which forms 16% of the volume (Plate 9.42), together with accessory cassiterite. All original perthite and mica have been chloritised. An unusual chicken-wire spongy texture occurs where there is a high percentage of chlorite, in which discrete quartz is outlined by granular aggregates of chlorite (Photo 9.43). Deep red coloured sphalerite forms abundant skeletal crystals which poikilitically enclose quartz, chlorite and topaz and must therefore have formed late. SS18/1 has a similar mineralogy but the quartz grains are much larger than in SS16/6. The grain size of the quartz in such samples appears to be governed by the original texture in the biotite granite. Occasionally - as in SS15A - it is possible to find granules of topaz forming a beaded rim around quartz crystals. Accessory minerals include fluorite, zircon, monazite, chalcopyrite, sphalerite, cassiterite and topaz. The

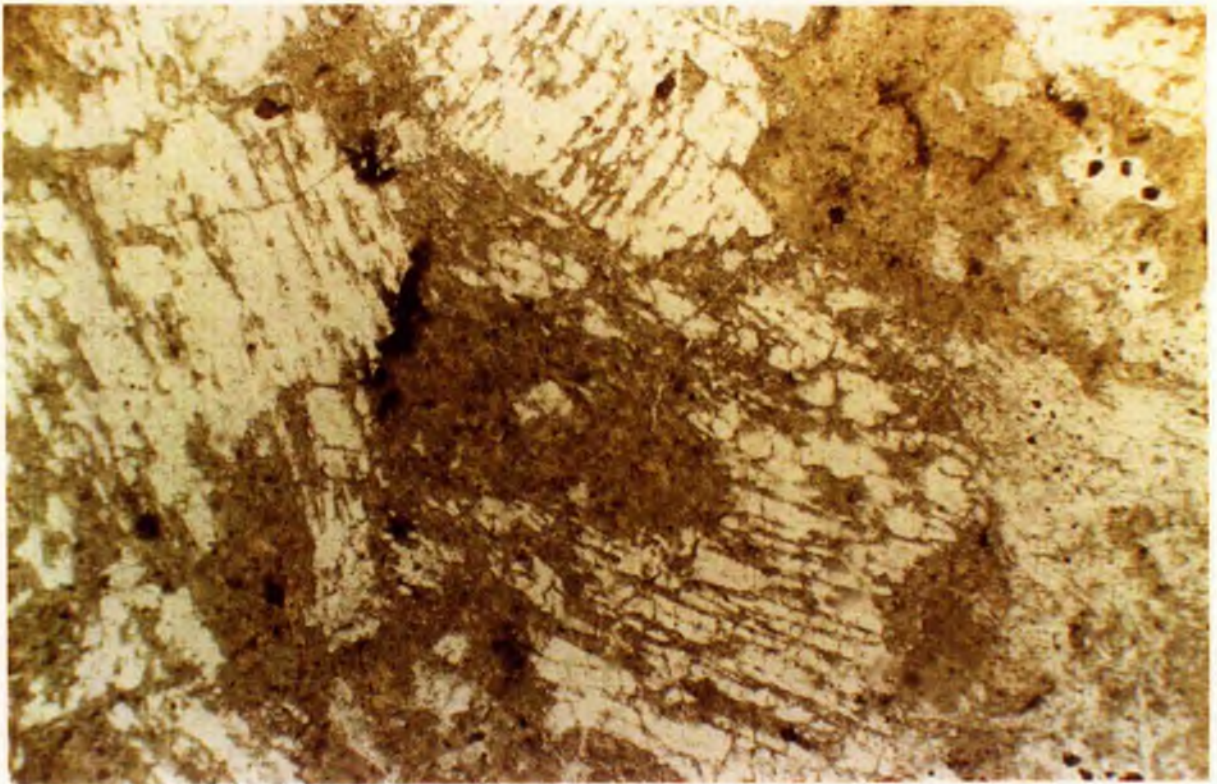


Plate 9.40                      Photomicrograph of SS64/2 showing chloritisation along the k-lamellae in perthite. PPL x125

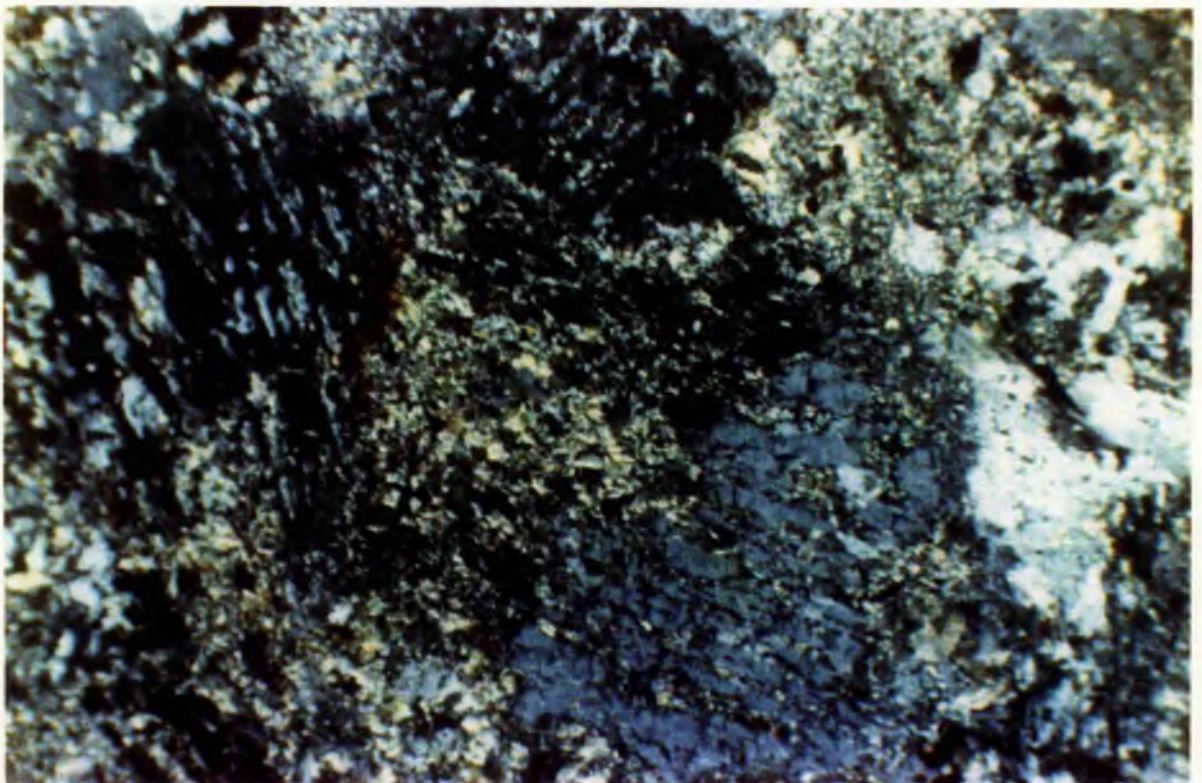


Plate 9.41                      The same field of view as above, under crossed polars.

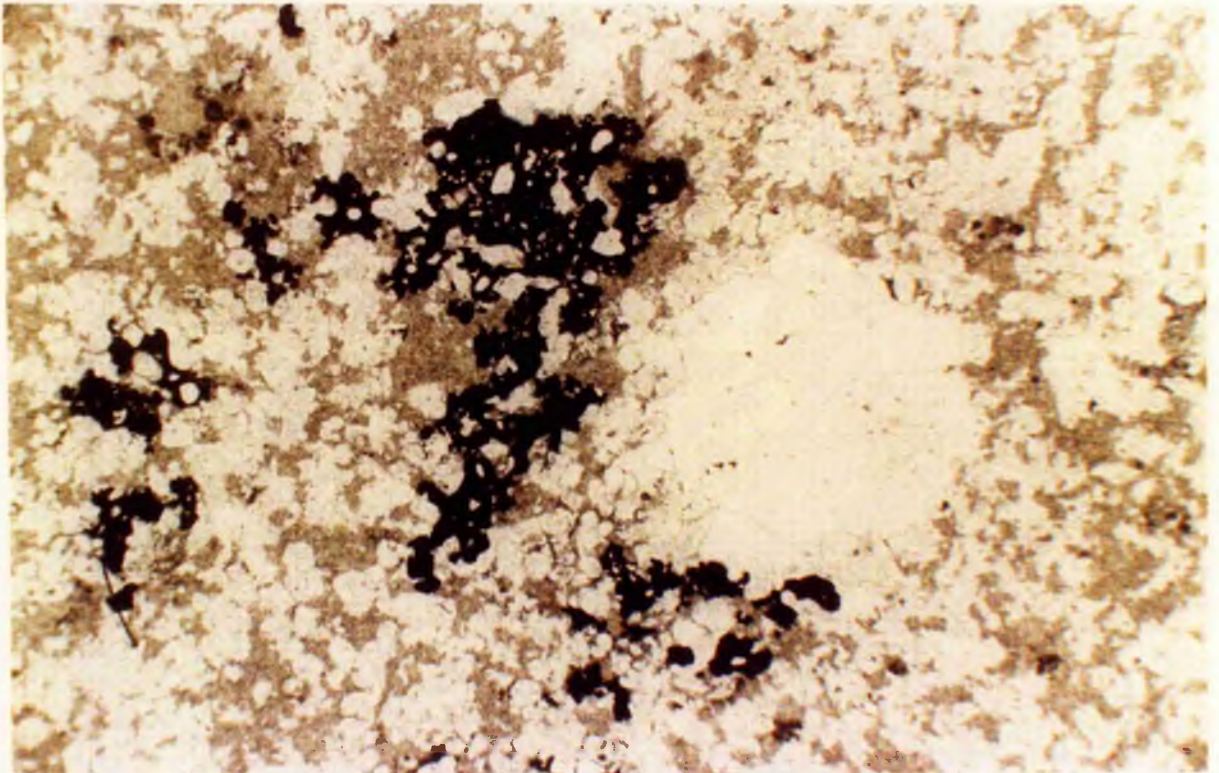


Plate 9.42

The large quartz crystals at the centre of this photomicrograph are encircled by small granules of topaz which is abundant throughout the sample. Chicken-wire textured chlorite encloses both topaz and quartz. Accessory sphalerite appears in this view although cassiterite is dominant in the specimen. SS16/6, PPL x25

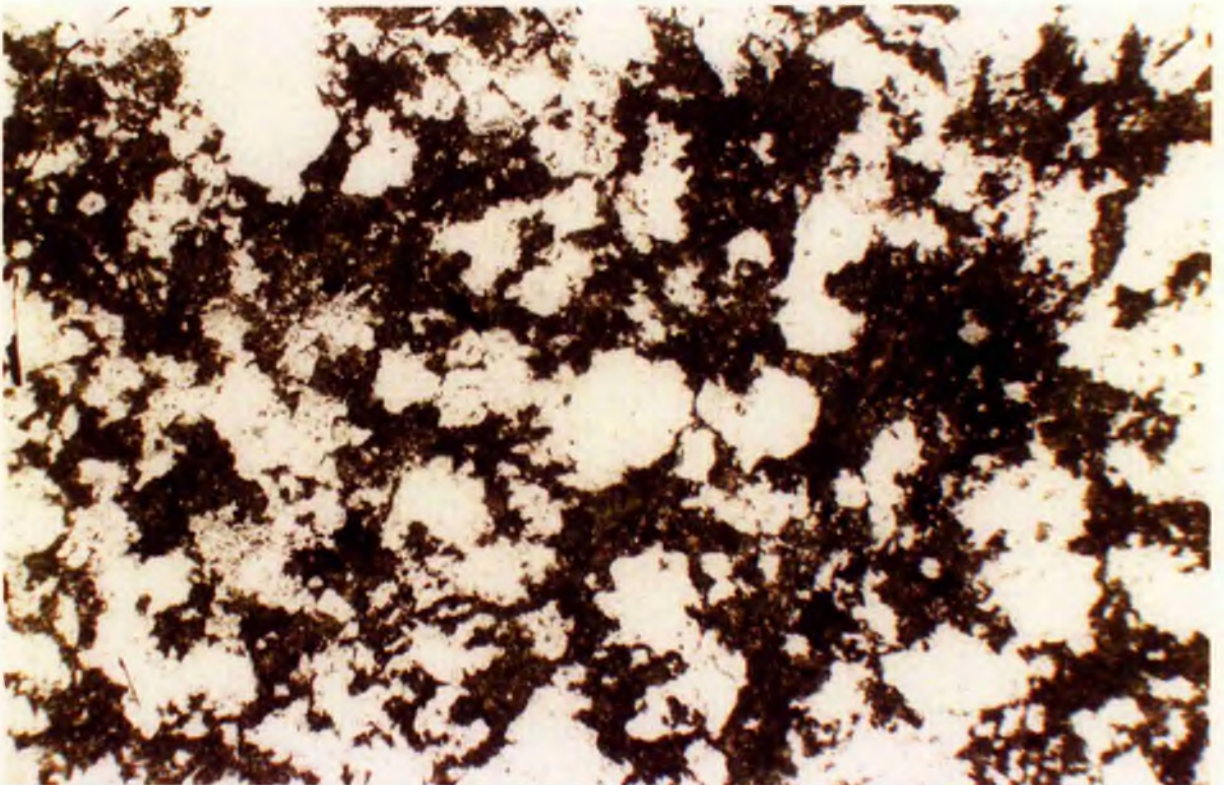


Plate 9.43

An enlarged magnification of chicken-wire textured chlorite, this time in SS33/7. The chlorite encloses quartz and is accompanied by deep red skeletal sphalerite.



topaz varies from rounded granules <0.1mm in size to euhedral crystals 1mm long with well developed 001 cleavage. The amount of topaz varies from less than 0.1% to over 16% and appears to be dependant on the modal percentage of perthite in the original granite. (If the perthite content was high then the alumina released from the original feldspar breakdown was in excess of that which could combine with the available Li and Fe to form mica. When this happened the excess alumina so released formed topaz.)

A similar mineral assemblage can be recognised in many of the Nigerian complexes where fluid reactions have not progressed beyond this stage.

### Stage 3

With further alteration the chlorite was progressively sericitised, resulting initially in a quartz-chlorite-sericite+topaz assemblage (eg SS12/6, SS15b, SS16/3) in which chlorite dominated and then to an assemblage where sericite abundance exceeded the chlorite percentage (e.g. SS45/1 and SS12/7 in Table 9.9).

Table 9.9 Acid metasomatism of perthite biotite granite - Stage 3

	SS12/6	SS12/7	SS12/8	SS12/9	SS16/3	SS33/4
SS45/1						
Quartz	55.8 57.5	55.3	52.3	50.6	54.5	65.0
Perthite			1.0	1.3		
Sericite	19.2 26.1	20.5	21.3	12.0	21.5	18.7
Chlorite	22.5 14.4	22.3	22.8	18.5	22.2	10.4
Topaz			0.6	15.3	0.1	
Fluorite	0.3 0.1	0.1	0.5			
Sphalerite	2.0 1.5	1.6	1.3	1.0	1.5	5.5
Chalcopyrite	0.3	0.1		0.1	0.1	
Haematite						0.1
Zircon			0.1	0.1	0.1	0.3
Monazite	0.1		0.1	0.1		
Molybdenite	0.2	0.1				

Sample SS12/6 contains roughly equal proportions of chlorite and sericite. The green-coloured chlorite, showing first order interference colours, is partially altered to colourless sericite which shows bright second order interference colours. Texturally it is similar to the previous stage, the chlorite/sericite intergrowths form a fine-grained spongy network of crystals which surround and emphasise the mosaic of quartz crystals. The individual quartz crystals, which may range in size up to 2mm, are generally around 0.3mm in diameter, commonly unstrained and rich in gas-filled inclusions.

In other thin sections the essential mineralogy is similar and only the proportion of chlorite to sericite varies (Table 9.9). Texturally there is a little variation, in some samples (SS33/4 and 45/1) the chlorite is clustered into aggregates up to 4mm across, of fine-grained crystals which coarsen to sheaf-like aggregates 0.5mm across occasionally (Plates 9.44 and 9.45). In

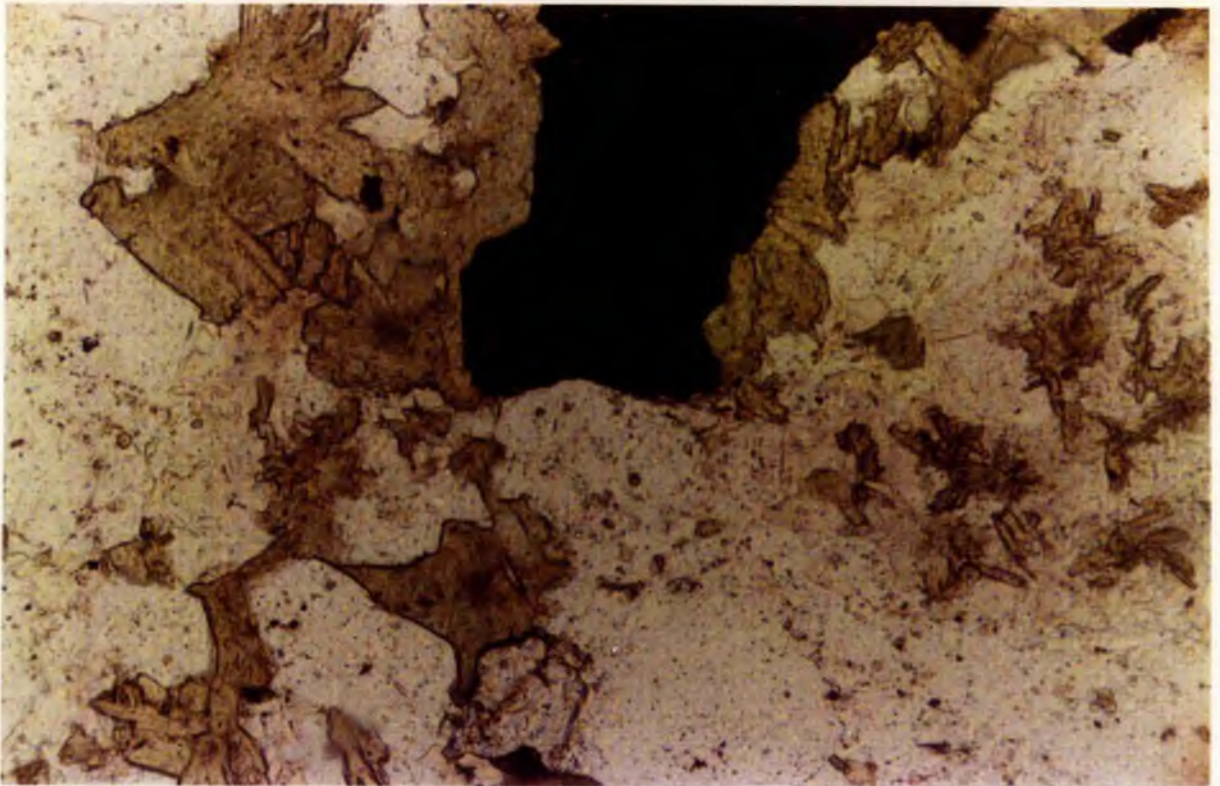


Plate 9.44

Photomicrograph of SS45/1 showing deep red sphalerite, quartz and chlorite which has developed in a sheaf-like form, accompanied by 'sericite'. PPL xl25



Plate 9.45

The same view as above under crossed polars.

SS16/3, microgranular mosaics of topaz (15.3%) surround and enclose quartz. This topaz appears to have developed from chlorite. Colourless anhedral accessory fluorite up to 0.5mm, is accompanied by abundant deep orange skeletal sphalerite, and traces of molybdenite. Accessory sphalerite may be intergrown with a small amount of chalcopyrite. Both sulphides enclose chlorite and sericite indicating a late-stage formation within the paragenetic sequence.

#### Stage 4

There was a change in both mineralogy and in texture as fluid processes continued. The mineral assemblage generated at this stage is characterised by the complete alteration of chlorite to sericite. Ultimately books of trioctahedral Li-Fe mica developed from the sericite clusters, with continued rock-fluid interaction. A large number of samples represent this stage SS6/1, 7/1, 8/3, 10/1, 10/2, 10/7, 10/10, 11/5, 11/8, 20, 23/6, 27/7, 47/3a, 47/4, 92, 95 and SS96.

At first there was only the noticeable mineralogical change as chlorite disappeared from the assemblage and abundant topaz developed (Table 9.10). Initially, the texture was similar to the previous stage with a spongy network of pale grass-green coloured sericite forming clusters and outlining the mosaic of quartz and topaz crystals (eg. SS47/4 and SS10/2). This sericite texture mimics the chicken-wire texture of the chlorite from the previous stage. The texture gradually changed and small mica flakes developed from the spongy sericite clusters. At first they were pale green in colour and small in size (eg. SS92 and SS10/7 - Plates 9.46 and 9.47). Gradually as the size of the flakes increased, the colour of the mica changed to a honey colour which in SS6/1 is rimmed by a pale blue mica. Ultimately large discrete flakes of colourless mica up to 1mm in diameter occurred, sometimes with slightly curved cleavage traces emphasised by chlorite (eg SS8/3 - Plates 9.48 and 9.49), and sometimes with vestiges of chlorite within the otherwise colourless mica (eg SS7/1). The modal percentage of topaz decreased as this new mica developed implying that the fluoro-aluminosilicate was taken up in the new mica.

At the same time as textural changes in the mica there were textural changes in the quartz. There was an increase in grain size from mosaics of crystals 0.1-0.2mm across to >1mm in SS6/1. Often this quartz has sutured margins and strong strain extinction. It is texturally very variable, sometimes the crystals are remarkably angular, sometimes consertal, occasionally amoeboid and sometimes lobed into other minerals which it replaced. The coexistence of both strain free and strongly strained quartz within one sample testifies to the existence of more than one generation of quartz within these rocks.

The assemblage of accessory minerals includes sphalerite, cassiterite, chalcopyrite, fluorite, haematite, zircon and monazite. However, there seems no systematic occurrence of any of the accessory minerals. Thus sphalerite may be abundant at any stage (up to 20% - see Table 9.10), or sparse, and similarly with cassiterite, although it never forms more than 5% of a sample. Chalcopyrite occurs as a discrete phase in some samples, whilst in others cases it appears to have resulted as an exsolution phase from sphalerite. Fluorite, may or may not occur - sometimes it is associated with mica distribution but in SS95 it appears closely associated with chalcopyrite. Zircon and monazite are never abundant but occur in most samples. One other accessory worthy of note is genthelvite, which forms 13% of SS11/5. It occurs as pale pink sieve-textured euhedral to subhedral

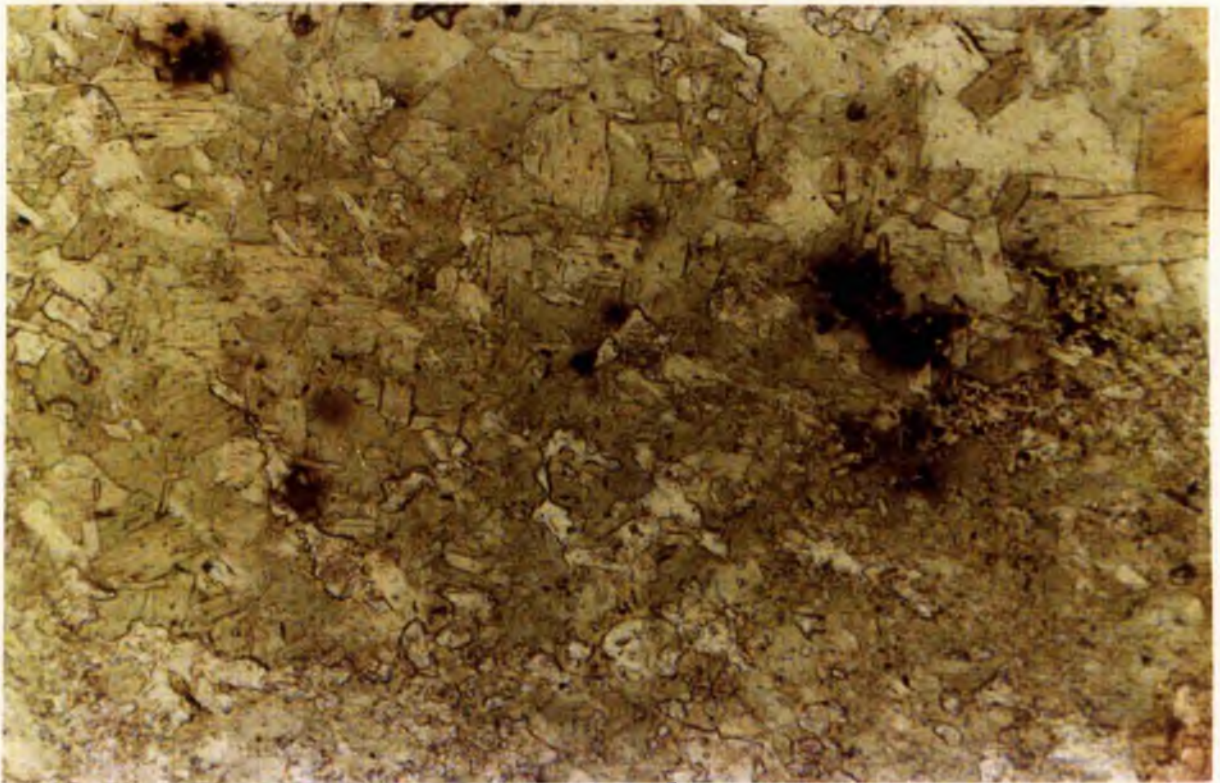


Plate 9.46            Small laths of pale green mica have developed from the fine-grained sericite in SS10/7. PPL x50

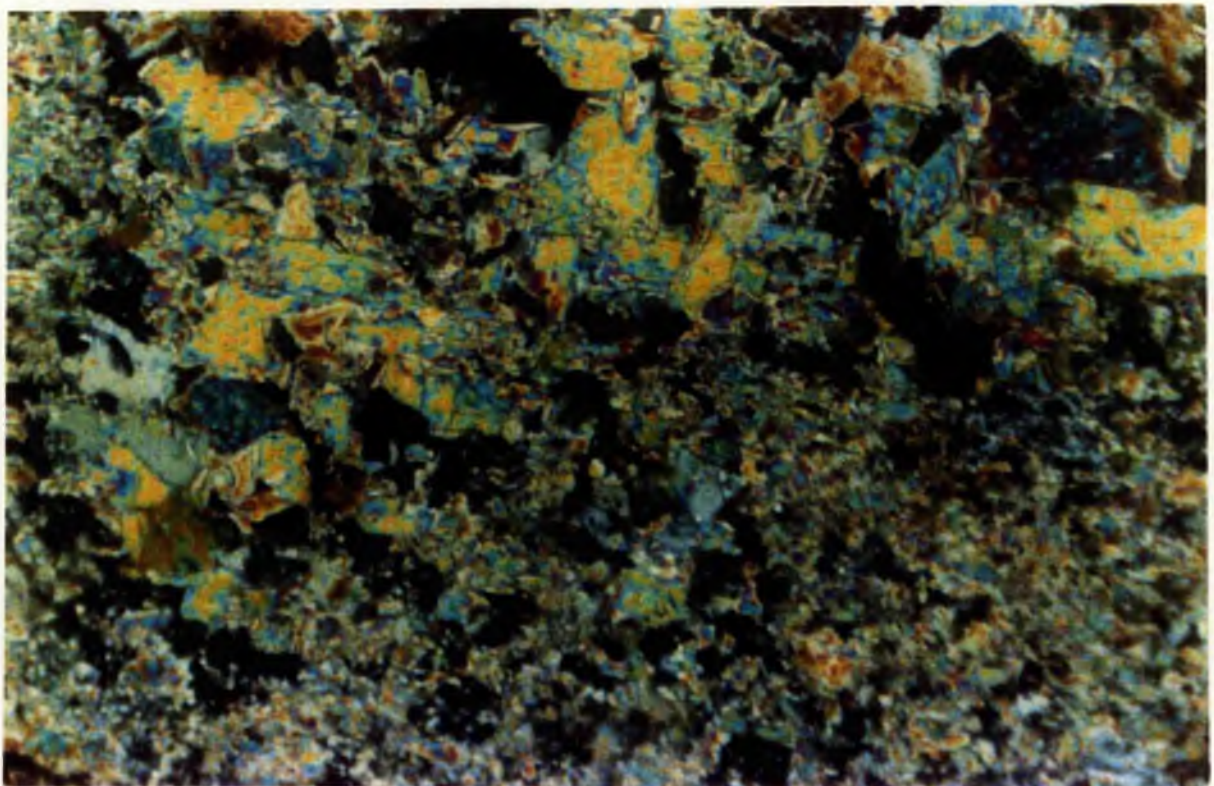


Plate 9.47            View as above under crossed polars.

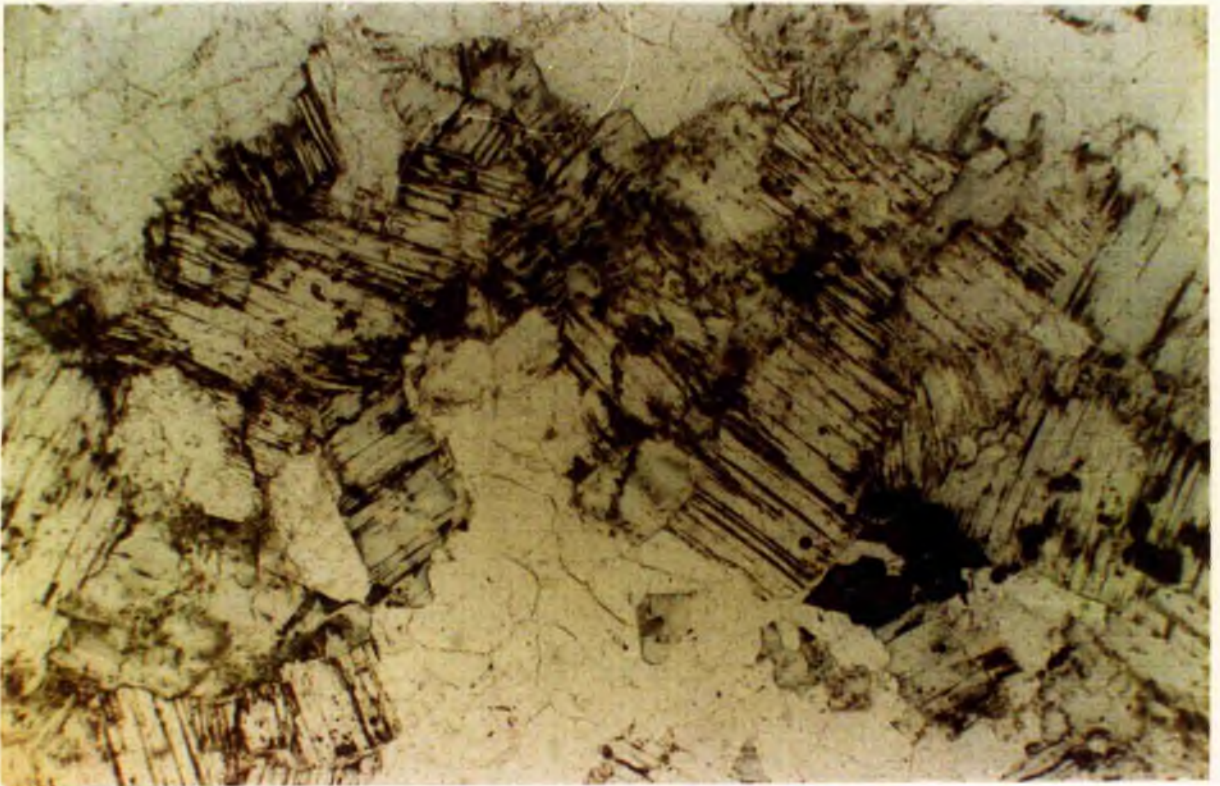


Plate 9.48

Photomicrograph showing large colourless zinnwaldite in SS8/3 with cleavage planes emphasised by chlorite. Accompanying quartz forms a mosaic of strained and unstrained crystals. Accessory cassiterite is strongly coloured. PPL x125

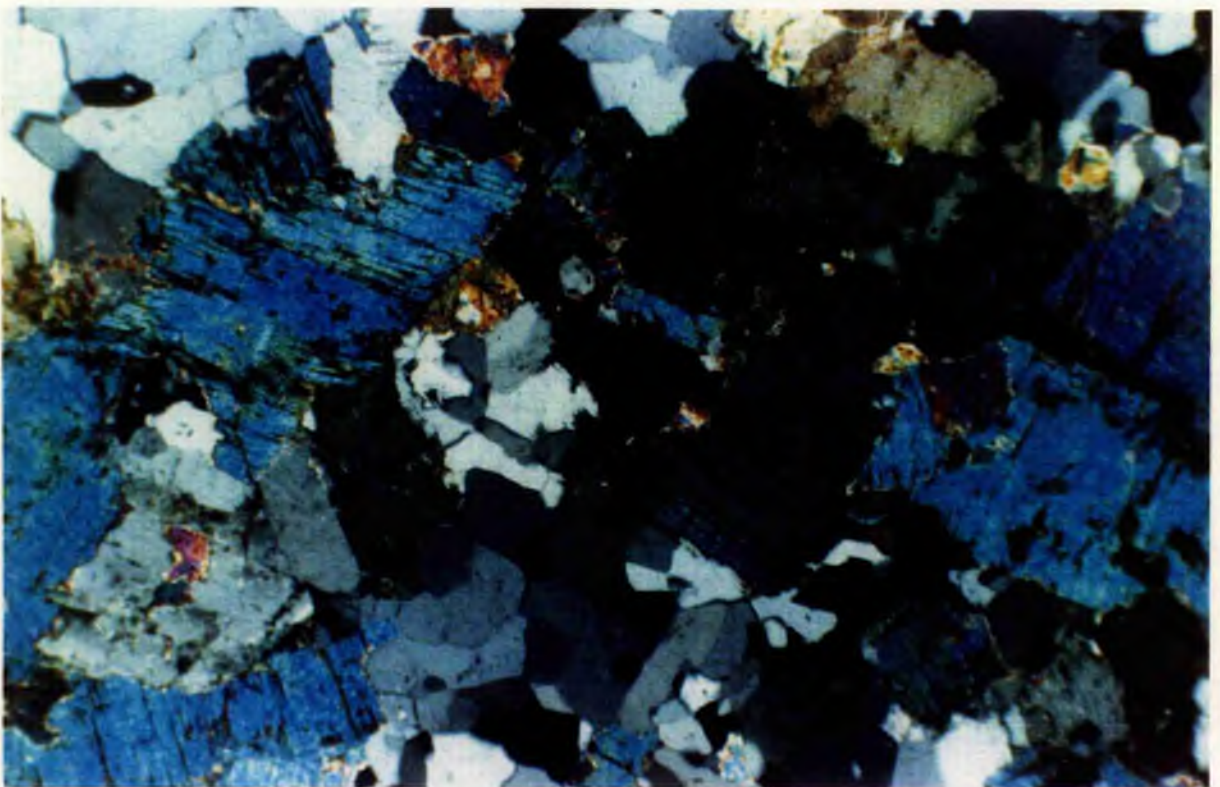


Plate 9.49

The same view as above in XPL.

Table 9.10 Acid metasomatism of perthite biotite granite - Stages 4 and 5

	Stage 4								
	SS6/1	SS7/1	SS8/3	SS10/2	SS11/5	SS20	SS23/6	SS27/7	SS47/3a
Quartz	58.1	70.8	48.5	24.4	47.1	60.3	66.7	39.7	59.6
Perthite							0.8	0.6	
Biotite	19.1	19.5	50.1	54.7	48.2		31.8	54.8	33.9
Chlorite						1.8			
Sericite						24.3			
Topaz	0.1			20.0	4.4	0.8		4.6	5.4
Fluorite	0.1	0.1	0.1		0.1		0.2	0.1	0.7
Sphalerite	22.1	5.1				10.3			0.1
Cassiterite	0.1	4.5	0.8		0.1	0.3	0.2	0.2	
Chalcopyrite				0.6		2.1			
Haematite	0.3		0.3				0.2		
Zircon	0.1		0.2	0.3		0.1	0.1		0.2
Monazite									0.1
Genthelvite					0.1				

	Stage 4 cont.			Stage 5	
	SS47/4	SS92	SS95	SS96	SS109C
Quartz	22.3	61.4	42.8	67.4	64.4
Perthite			0.4		
Biotite	57.0	23.4	40.4	29.3	0.9
Chlorite				0.2	1.2
Sericite					
Topaz	15.5	14.6	14.8	1.0	28.7
Fluorite	4.5	0.1	0.4	0.2	0.2
Sphalerite		0.2			2.2
Cassiterite	0.5	0.2		0.1	2.2
Chalcopyrite					
Haematite			1.2	1.8	0.2
Zircon	0.1	0.1			
Monazite	0.1				
Genthelvite					

crystals up to 1mm in size which are full of inclusions of mica.

In summary then, there was a coarsening of texture with this process and a change in the mica composition. Initially the mica was fine-grained sericitic and pale green; gradually the mica coarsened in texture into individual Li-Fe biotite flakes with a colour varying from honey to pale olive green. Ultimately, large books of colourless mica developed. As the process became increasingly acid there was an increase in modal quartz and a transition to stage 5.

## Stage 5 -Silexite formation

There was a gradual increase in quartz as the acid metasomatism became more silicic, resulting in the formation of a quartz-topaz rich rock in apical portions of the Rishi granite immediately beneath the roof in the Dutsen Rishi area. Topaz was generated by the breakdown of mica developed in earlier stages of alteration and is accompanied by accessory wolframite, fluorite, cassiterite, sulphides and beryl. This quartz-topaz-cassiterite assemblage has been termed a silexite by analogy with the work of the Australians particularly Plimer and Kleeman (1985).

SS109C which in hand specimen is very light in colour typifies this assemblage. It consists of quartz, up to 2mm in size, which has sutured margins and strain extinction, accompanied by a little fine-grained sericite with chlorite. The topaz occurs as abundant clusters which are up to 3mm in size (Plates 9.50 and 9.51). These clusters are composed of extremely fine-grained individual granules. Both sphalerite and cassiterite are abundant, each forming more than 2 modal percent (Table 9.10). The cassiterite is small in size (<0.75mm), deep yellow-brown in thin section, anhedral and sieve-like in form. The sphalerite is even smaller in grain size and forms scattered anhedral crystals which are extremely dark in colour to almost opaque. Galena and chalcopyrite also occur in small amounts.

## Selected sample localities

At some localities, samples record only one stage or process of alteration. At many localities however, more than one process or stage of alteration has been preserved. An example of several of these changes of acid metasomatism occurring at one locality can be monitored by samples from localities 106, 108 and 109. At each of these localities zoned veins occur. All three localities are close together and occur in the roof facies of the Rishi biotite granite immediately to the north of Dutsen Rishi.

### Locality SS109

Locality 109 is in the roof facies of the biotite granite immediately to the north of Dutsen Rishi. A zoned vein, 1m wide and trending 260° shows a transition from a marginal quartz-chlorite assemblage to a central cassiterite-rich silexite.

The dark grey, fine-grained hand specimen of SS109A consists of a quartz-chlorite assemblage. The quartz crystals are anhedral, clustered, composite, up to 3mm in size and slightly strained. The chlorite forms spongy clusters up to 7mm across. Deep orange-brown anhedral sphalerite, up to several mm in size, is accompanied by chalcopyrite as a common accessory. This is a typical stage 2 acid assemblage and grades into SS109B, which is paler grey in colour and contains topaz as granules in the groundmass in addition to the quartz-chlorite assemblage. The quartz is finer grained than in SS109A. Deep orange-brown sphalerite up to 2mm in size, is very abundant, often with a spongy texture. Traces of sericite suggest that this sample represents a transition towards the Stage 3 alteration process.

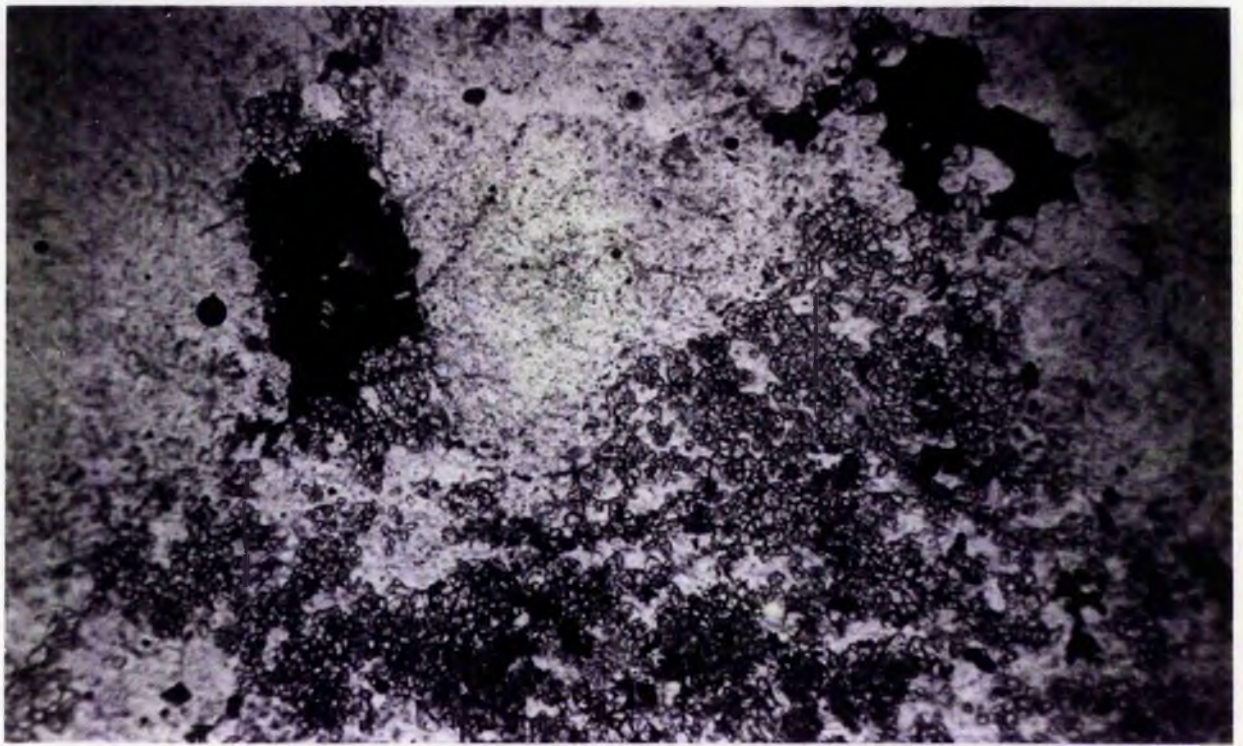


Plate 9.50      Photomicrograph of SS109C showing clustered granules of topaz accompanied by granular quartz, traces of sericite and anhedral sphalerite which appears opaque in this picture. x50

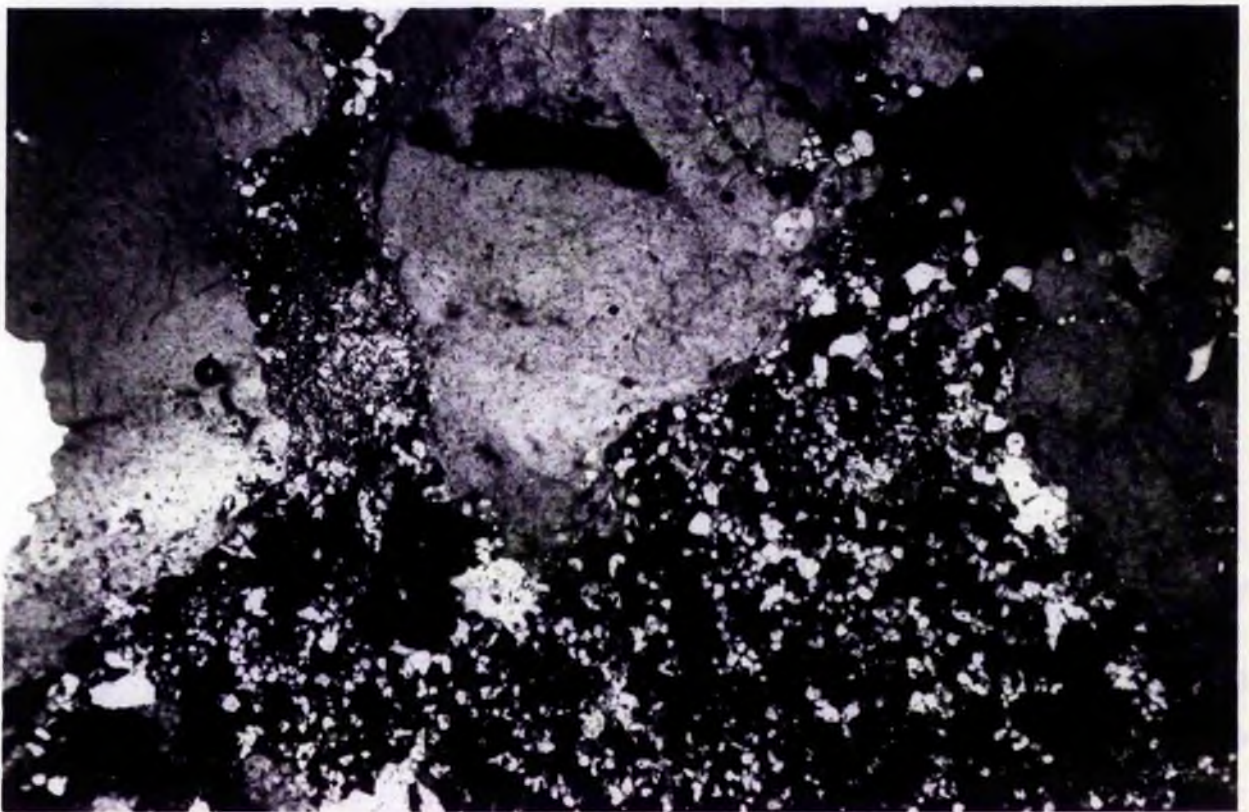


Plate 9.51      Similar view to above, under crossed polars.

The silixite, SS109C, represents a late-stage acid metasomatism and the zoned vein therefore records several of the acid alteration stages which grade into each other. The zoning shows that the acid metasomatism has been arrested at an earlier stage at the margins than at the centre where alteration processes have continued to more advanced stages. This is not always the case as example SS106 shows.

#### Locality 106

Near locality 109, across a valley from Dutsen Rishi, a massive mineralised vein trends  $214^{\circ}$  and cuts a marginal microgranite facies of the Rishi biotite granite. The vein which is 1.8m wide, is zoned (Fig 9.5). Certain zones are exceptionally cassiterite or sphalerite rich. The marginal zones of the vein are quartz rich (46%) with a decrease towards the centre to less than 10 modal percent (Fig 9.5).

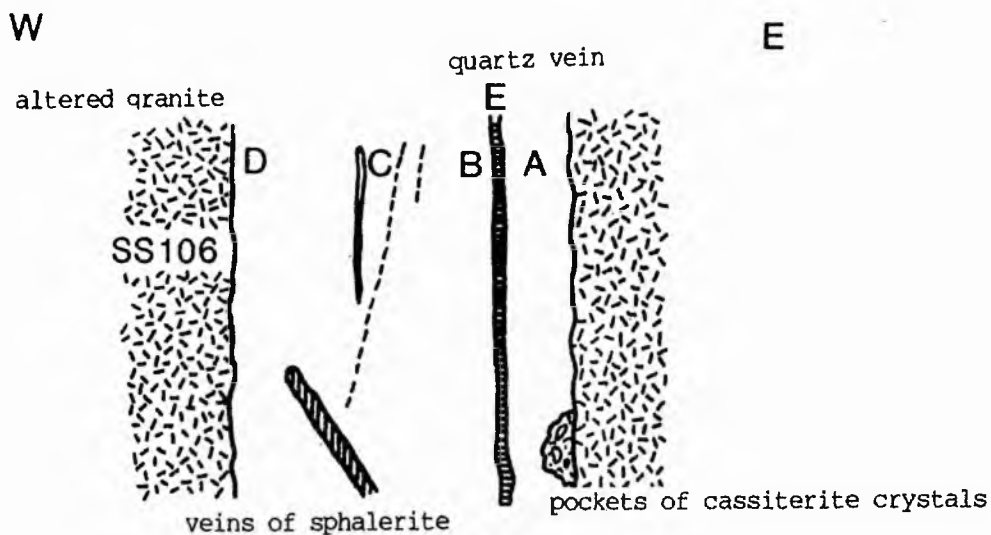
The microgranite, SS106, is pale grey with occasional feldspar phenocrysts up to 6mm in size. It shows reddening adjacent to the vein - a feature not common in the Saiya Shokobo Complex. Microcline-filledmiarolitic cavities also occur in the microgranite. In thin section the microgranite contains perthitic feldspars, 0.3mm in size, evenly distributed and often showing myrmekitic or granophyric intergrowths with quartz. This is typical of marginal fine-grained facies. The occasional feldspar phenocrysts are turbid reddened microcline. The quartz crystals are generally 0.3mm in size and unstrained although rare larger grains, occur in clusters which are also unstrained. The quartz contains abundant gas- and fluid-rich inclusions. The discrete ragged mica flakes, which are up to 0.4mm across, have been almost completely chloritised. They contain zircons surrounded by dark pleochroic haloes and may also enclose anhedral fluorite.

In thin section SS106A, which comes from close to the eastern margin of the pervasive vein, shows a mineralogical gradation. On the marginal side of the sample there is an abundant mosaic of strain-free amoeboid quartz with crystals commonly less than 0.5mm across and only rare phenocrysts up to 5mm in size. The quartz crystals are outlined by spongy aggregates of dark green chlorite. This zone therefore shows the acid metasomatism of a biotite perthite granite which has reached the stage 2 level described earlier, where all the granite perthite has been altered to chlorite (Plate 9.52). The inward zone of the same sample shows a discrete mosaic of strain-free quartz with crystals commonly less than 0.5mm in size. The quartz crystals are now surrounded by a fine-grained mesh of sericite corresponding to the stage 3 assemblage discussed above and chlorite is completely absent (Plate 9.53). Between the quartz-chlorite assemblage and the quartz-sericite assemblage there is a sharp but sinuous demarcation. Accessory cassiterite, sphalerite, topaz, and minor fluorite occur within both these zones.

In SS106B, there is a greater range in the size of the quartz grains than in SS106A, but the main difference is that vestiges of mottled perthite remain and both sericite and chlorite occur together. Sericite is dominant (Fig 9.6). There is no cassiterite but it is rich in deep-yellow, anhedral and skeletal sphalerite which also forms veinlets cross-cutting the micas (Plate 9.54). This zone represents stages 1-3 in the alteration sequence.

SS106C is darker in colour and finer-grained than SS106, 106A or 106B due to

Fig 9.5 Cross-section of locality 106 showing location of the samples



SS106 - chlorite perthite microgranite

SS106A - gradation from a quartz-chlorite assemblage  
to a quartz-sericite assemblage

SS106B - quartz-chlorite assemblage

SS106C - quartz-chlorite-sericite assemblage

	SS106	SS106A	SS106B	SS106C
quartz	26.7	46.3	32.8	9.4
perthite	67.3		19.1	24.8
albite	0.1		0.3	
sericite	0.3	12.6	38.1	21.5
chlorite	5.3	39.5	1.8	42.8
topaz		0.3		
fluorite	0.1	0.1	1.0	1.0
sphalerite	0.1	1.0	6.8	0.1
opaques		0.1		
zircon	0.1		0.1	0.1
monazite		0.1		0.3

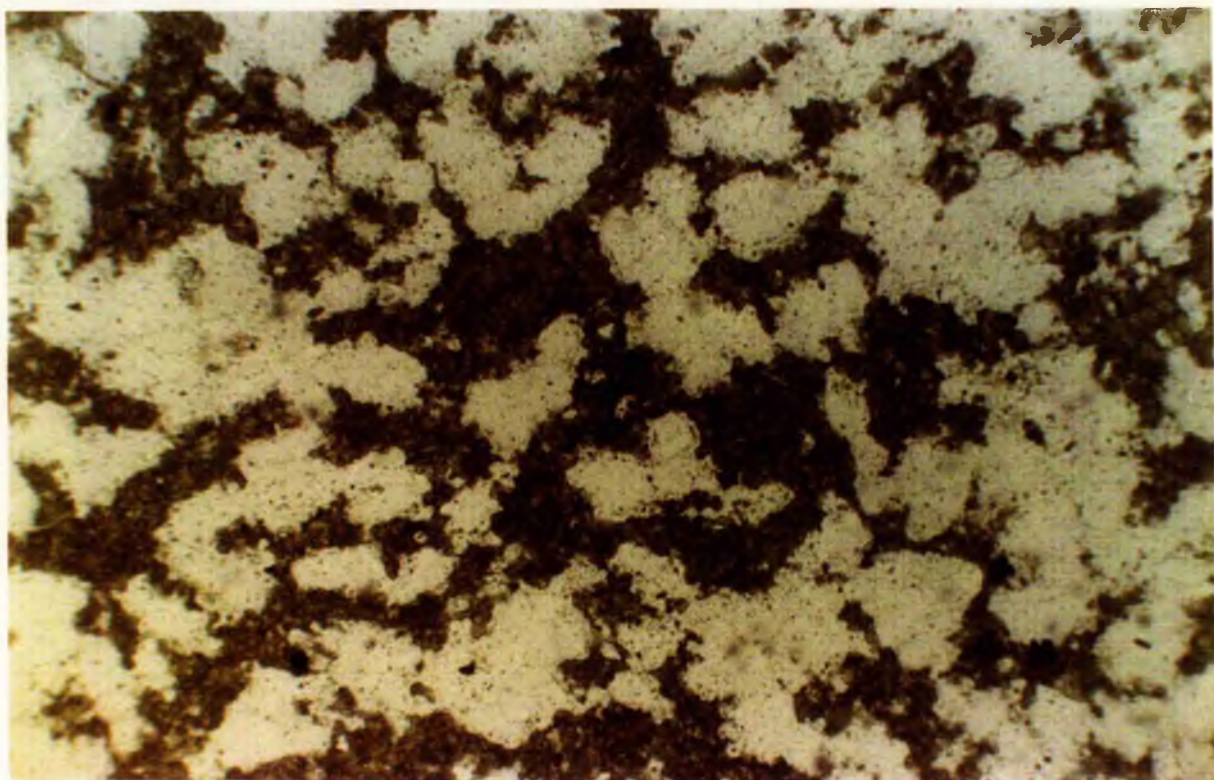


Plate 9.52

Photomicrograph of SS106A showing a quartz-chlorite assemblage of minerals. The spongy chicken-wire textured chlorite encloses strain-free quartz which is commonly less than 0.5mm in size. PPL x125

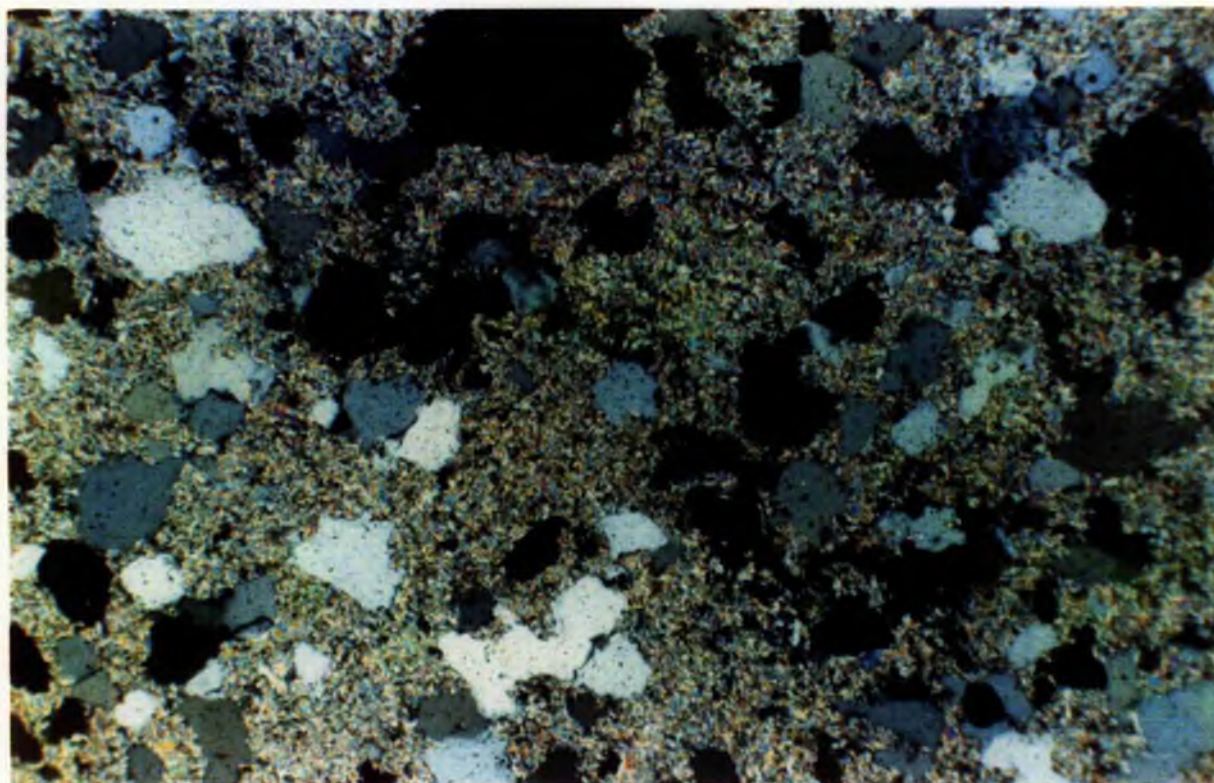


Plate 9.53

A different part of the same sample - SS106A consists of a quartz-sericite assemblage of minerals. The quartz crystals are now surrounded by a fine-grained mesh of sericite which has replaced the chlorite of the Plate above. XPL x125

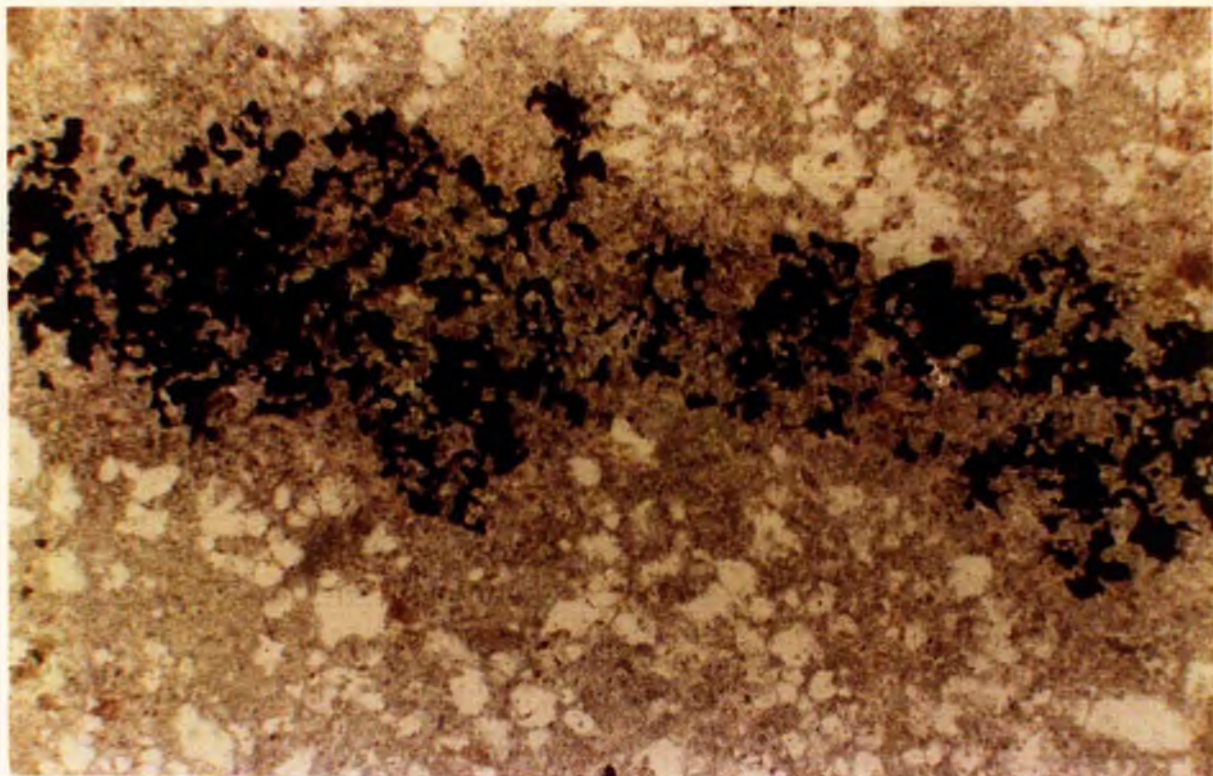


Plate 9.54

In this photomicrograph of SS106B, a 2mm-wide vein of sphalerite is cutting a quartz-chlorite mineral assemblage which also contains vestiges of mottled perthite. PPL x25

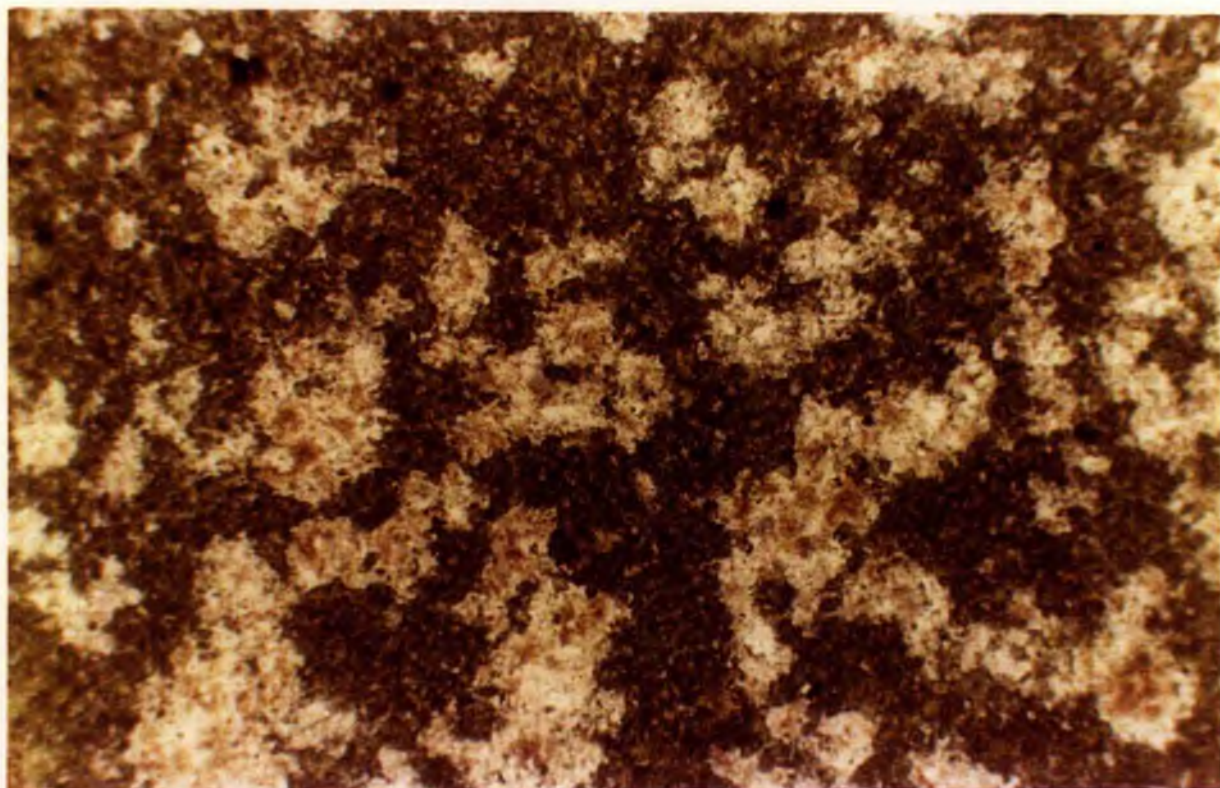


Plate 9.55

Spongy khaki-coloured chlorite has replaced perthite, vestiges of which remain as pinky brown patches in SS106C. PPL x50

the decrease in modal quartz and the increase in modal chlorite (Fig 9.6). In thin section the chlorite is seen replacing original mottled feldspar although turbid areas of microclinised perthite remain (Plate 9.55). Pale grey coloured mica forms narrow overgrowth rims on an earlier pale green phase. Fluorite, dark orange sphalerite, zircon and monazite occur as accessories.

SS106D which occurs on the western margin of the vein consists of a quartz chlorite assemblage similar to the marginal side of 106A, and is equivalent to a stage 2 alteration assemblage.

The late-stage quartz veins, eg. SS106E, are variable in thickness, have a honeycomb texture and contain masses of cassiterite 2.5 to 5cm across, stringers of cassiterite and irregular patches of sphalerite.

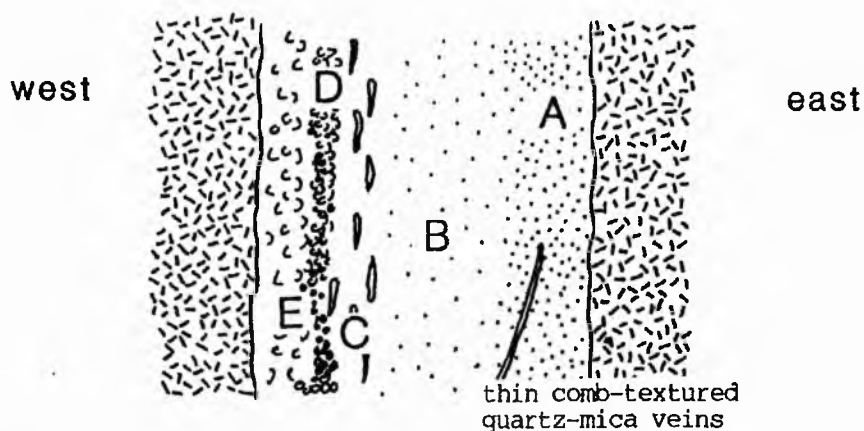
There is obviously a crude zonation in ore mineralogy with cassiterite being richest marginally and sphalerite richer towards the centre of the vein. Since 106B shows less complete alteration than 106A, it must be concluded that the ascending hydrothermal fluids did not affect the host rock uniformly. The controls of ore deposition were obviously changing within the channel in response to fluctuating conditions of temperature, pressure or fluid-rock reaction during migration of the fluid through the channelway. It seems probable that within the wallrock adjoining the channelway, transfer of chemical components was chiefly by diffusion so that chemical gradients will have been different around different minerals in the altering rock. The most important changes taking place probably related to  $H^+/OH$  balance. Hydrogen metasomatism has obviously been important as witnessed both by the chloritisation of the biotite and by the sericitisation of the mica (Meyer and Hemley 1967). The level of  $H^+$  metasomatism could only be maintained in an ore deposit if the temperature is increasing upwards or if oxidation, owing to mixing with oxygenated ground water produces more highly ionised sulphuric acid from less ionised  $H_2S$ . As both factors may be involved, local variations in the effect of the hydrogen metasomatism are bound to occur and may possibly explain why chloritisation has been more complete at the margins.

Meyer and Hemley (1967) show that there is a close correlation between hydrogen metasomatism and high sulphur fugacity in the sulphide assemblage and that strong hydrogen metasomatism only exists when the S:O fugacity ratio is relatively high, not merely when the oxygen fugacity is high. Therefore, changing content of total sulphur in the hydrothermal fluid is probably responsible for variations within this mineral assemblage. High sulphur ratios also favour the stability of chalcopyrite as opposed to pyrite (Sales and Meyer, 1948). However, the variation in the accessory ore assemblage strongly suggests that rapid changes in pressure and temperature dominated over slower, nearly steady state reactions.

#### Locality SS108

This locality lies in the contact zone of the Rishi biotite granite and basement granite. Four samples were taken from different parts of the 1m wide vein, the cross-section of which is shown in Fig 9.6. There is a gradation from a dark grey, fine-grained quartz-mica assemblage on the east side of the vein (SS108a), through a pale grey mica-quartz-topaz assemblage (SS108b) to facies in which quartz is dominant and mica occurs in decreasing modal proportions on the west side. Unlike the other veins described here therefore it has an

Fig 9.6 Cross-section of locality 108 showing assymetry of the vein



- SS108A - dark grey, fine-grained quartz-mica assemblage
- SS108B - pale grey, fine-grained mica-quartz-topaz assemblage
- SS108C - reddish, streaky, quartz-mica assemblage
- SS108D - reddened quartz with mica and haematite
- SS108E - honeycomb-textured quartz stained by haematite

	SS108A	SS108B	SS108C	SS108D
quartz	67.4	42.8	81.3	74.3
feldspar		0.4	0.1	
biotite	29.3	40.4	16.4	20.2
chlorite	0.2			0.4
topaz	1.0	14.8		
fluorite	0.2	0.4	0.2	0.3
cassiterite	0.8		0.4	1.0
haematite	1.8		1.6	2.6
siderite				0.3
other ores		1.2		
zircon				0.4
monazite				0.5

asymmetrical zonation.

In SS108a, the quartz forms a fine-grained mosaic of anhedral, sometimes slightly-strained crystals which may sometimes be outlined and emphasised by mica growth. The quartz is also very turbid due to finely divided mica disseminated throughout. The mica forms dark brown spongy aggregates up to 0.3mm in size composed of fine-grained granules less than 0.1mm in size. Individual flakes of similar small dimensions dusted throughout the quartz, impart the dark coloration to the whole rock. Accessory topaz, fluorite and cassiterite account for less than 2% of the modal percentage of the sample. A small amount of opaque minerals, listed as haematite, develop from the alteration of the mica.

In SS108b, the texture and characteristics of the quartz and mica are similar to those of 108a. The difference in colour however, is due to the development of topaz which accounts for 15% of the sample. It occurs as small anhedral crystals <0.2mm in size, as clusters and granular masses of small crystals, which are distributed evenly throughout the thin section.

SS108c consists of more than 80% quartz crystals which are much coarser textured than previous samples and may be more than 1cm in size. These show strained extinction and are very turbid due to the abundance of liquid-rich fluid inclusions rather than mica flakes. The mica is a light greenish brown in colour and shows cleavage traces emphasised by haematite. The micas which are individually less than 0.3mm in size are irregularly distributed throughout the rocks as clusters and streaks, this distribution gives a streaky appearance to the hand specimen. The quartz in hand specimen is rather pink-stained due to the development of haematite. Accessory fluorite and haematite are accompanied by a small percentage of cassiterite which occurs as subhedral deeply-coloured, zoned crystals which occur within the mica clusters.

In SS108d, the quartz is also coarse-textured and turbid but it is the characteristics of the mica that distinguish this sample as a separate mineral assemblage. There is a variation from the dark brown fine-grained mosaics already described, through to bright blue-green flakes associated with cassiterite crystals which are coarser textured than in other samples. These are pleochroic to colourless and occasionally show pale green patches of chloritisation. The cassiterite forms deeply-coloured, twinned and zoned crystals up to 0.4mm in size. Siderite, haematite or limonite, zircon and monazite occur as accessories.

Finally SS108e is of a honeycomb-textured quartz vein in which the cavities are coated with haematite generated from the breakdown of mica. The rock is almost entirely quartz and is therefore related to late-stage alteration processes which follow on from acid metasomatism and are covered in the next section.

#### Disseminated acid metasomatism

In many circumstances in the roof zone of the biotite granite, the development of a progression of stages of alteration within a vein-like structure, doesn't occur. Instead all the processes may be noted, but they are disseminated throughout the apical region of the biotite granite in an irregular manner. In practise it is possible to find a patch of quartz-topaz within a slightly

chloritised assemblage which may have localised development of sericite but in which the original perthite of the granite may still largely be unaltered. In addition, rather unusual mineral assemblages may be generated in the apical portions which are rich in genthelvite, topaz or sometimes ore minerals.

An example of this type of disseminated alteration occurs at locality 80. Sample SS80 comes from the roof zone near the southern margin of the Rishi biotite granite. In the sample, original perthite with traces of lamellar texture occurs but commonly there has been the development of a patch texture developing into a film texture. In addition, there has been the localised development of turbid microcline (Plate 9.56 and 9.57). The perthite accounts for 64% of the volume and is in the same proportions as an unaltered granite. Mica accounts for 30% of the remaining volume (Table 9.11). This is generally in the form of clusters of pale green sericite. Within the sericite clusters however, and also occasionally in solitary flakes, coarser laths of pale green lithium mica, up to 0.15mm across, have developed. Such sericite development and growth of new coarser mica, usually characterises an alteration assemblage described as stage 4 earlier. However, in such an assemblage all feldspar is normally destroyed. Also in this assemblage, there is no chloritisation of the feldspar. Instead topaz may be generated, or sericite formed, from perthite alteration. This mineral assemblage which includes genthelvite and topaz indicates very high HF activity which would account for the extremely low percentage of quartz in the sample (Table 9.11).

Table 9.11 Modal analysis of sample SS80 with disseminated metasomatism

Quartz	1.1
Perthite	63.7
Albite	0.3
Biotite	7.3
Chlorite	0.2
Sericite	22.4
Topaz	2.6
Genthelvite	2.4

#### Summary of the process of acid metasomatism

It is obvious that the effect of the acid metasomatism and the resulting mineral assemblage depended on the initial mineral assemblage of the rock that was being hydrothermally altered (Table 9.12). Acid metasomatism resulted in variations in texture and coloration, and different essential and accessory minerals were generated at different stages. In addition to variations in mineral assemblages, the mica compositions generated during acid metasomatism also depended on the original material that was being metasomatised. Such variations are discussed in Chapter 10.

Late stage silicification during acid metasomatism differs from the later silica metasomatism. Here at the late acid stage, the relative increase in silica was due to destruction of other minerals - mainly mica - which were removed leaving a honeycomb textured quartz. In contrast, the process of silicification which followed was due to the addition of silica, sometimes into vugs created by the mica destruction just described.

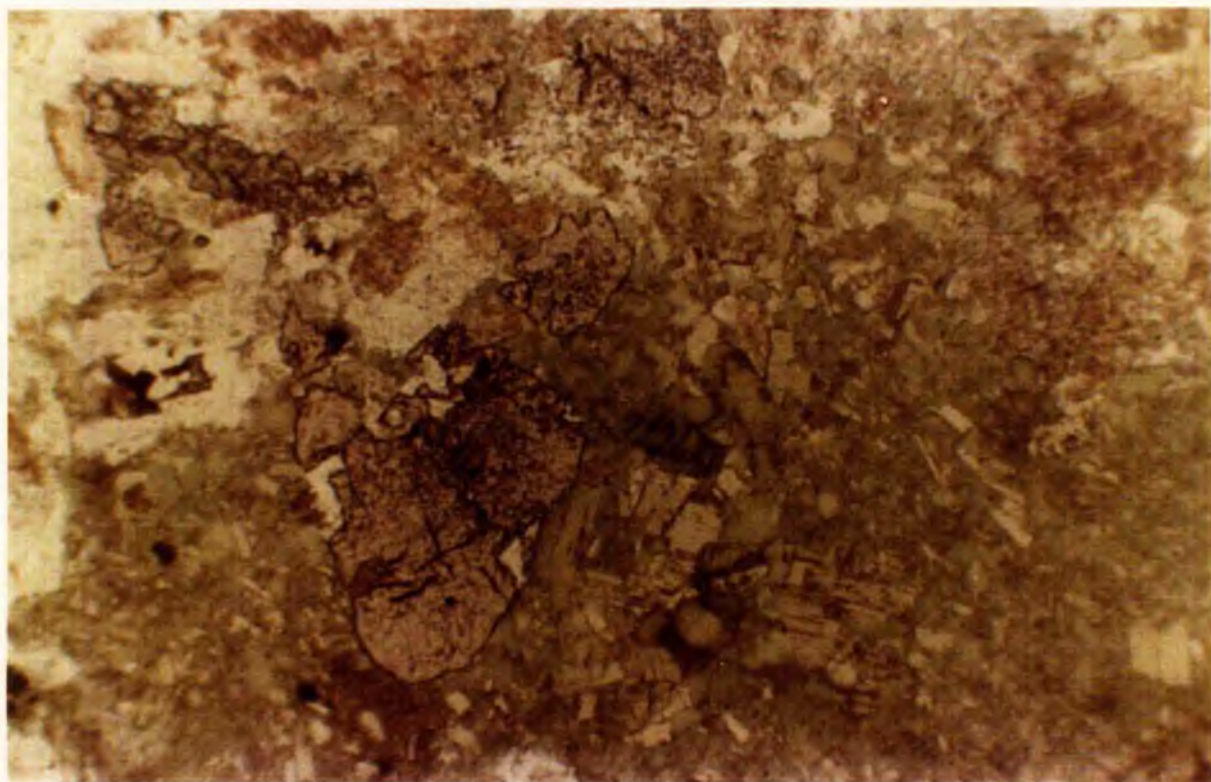


Plate 9.56

In this field of view mottled pinky brown microcline has been almost entirely replaced by pale green sericite which has partially coarsened in texture to give small euhedral crystals (centre). The view is dominated by pale pink genthelvite which has the appearance of garnet. SS80, PPL x50

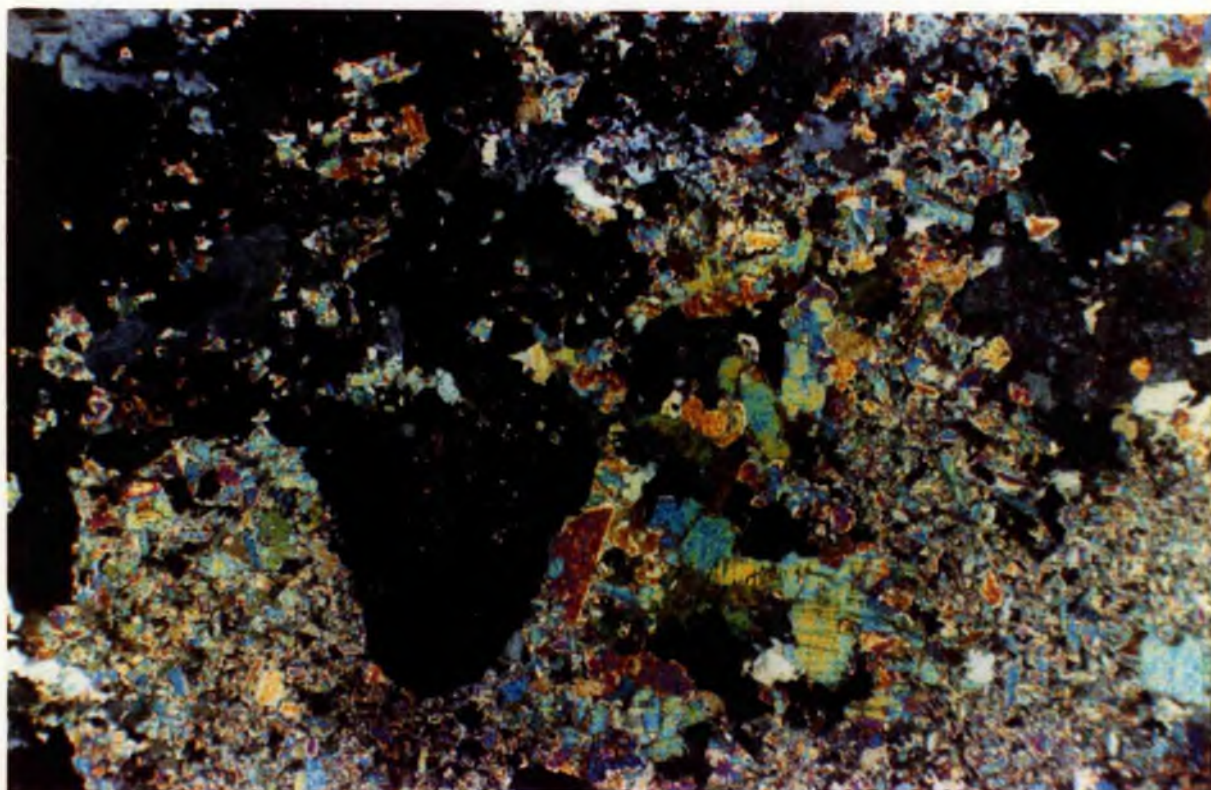


Plate 9.57

The same photomicrograph as above under crossed polars shows that the core of the genthelvite is full of inclusions of mica and other minerals while the margins are inclusion-free.

Table 9.12 The mineral assemblages generated during acid metasomatism of different rock types

Initial rock type	Major minerals	Accessory minerals	Colour	Texture
Basement trend la	chlorite zinnwaldite fluorite	quartz sericite, zircon epidote, monazite sphalerite chalcopyrite allanite	dark grey	coarse
Basement trend lb	quartz perthite chlorite biotite	sericite, zircon cassiterite monazite	pale	fine-grained
Volcanic rocks	quartz perthite biotite	chlorite, limonite haematite cassiterite sphalerite	pink to bluey-grey	altered groundmass
albitised facies	quartz albite/perthite sericite	chlorite topaz, fluorite sphalerite zircon, monazite cryolite, columbite thorite	white to pale greenish	fine-grained
microclinised facies	quartz siderophyllite microcline	cassiterite zircon haematite	pink to green or black	medium-grained

## Silica metasomatism

Silica metasomatism was the last major phase of alteration and ore deposition. During sodic and potash alteration processes, particularly during microcline formation, silica was released. During acid metasomatism, perthitic or microcline feldspar replacement by biotite mica resulted in the development of granular quartz.

Like potash and hydrogen ion metasomatism, the resulting silica metasomatism may have been pervasive or vein-controlled. Quartz may have been pervasively deposited into vugs in the cupola created by the earlier potash or hydrogen ion metasomatism, or it may have replaced all earlier formed minerals. Even more common are small quartz fissure-filling veins which are found throughout the biotite granite.

Several samples and analyses from Rishi show the effects of silicification (SS6, SS9/1, SS65/1, SS97, SS98, SS99 and SS117/5 - see Fig 9.7 for localities). In most samples, the rock consists of quartz with varying amounts of mica. Only rare traces of perthite or microcline remain.

Samples SS97 and SS99 come from a zoned vein close to the summit of Dutsen Rishi (Fig 9.7). In SS97, the quartz forms an anhedral mosaic comprising more than 80% of the modal volume (Table 9.13). The individual quartz crystals are commonly 2-3mm in size and occasionally more than 1cm across. These are commonly unstrained and turbid. Unlike many turbid quartzes described earlier, the turbidity is not so much due to fluid inclusions, as to finely comminuted and disseminated fragments of mica and possibly other minerals. The bulk of the mica occurs in clusters composed of stubby laths occasionally accompanied by granules. These are usually 0.2mm in size or less. There is a variation from almost colourless, through honey to a pale tan colour. Cleavages are emphasised by opaques and the cleavage traces are often bent. Haematite and limonite, derived from mica breakdown, line cracks, outline mica laths, infill cavities and locally stains quartz. Accessory cassiterite, up to 2mm in size is subhedral in form. It is deeply coloured with dark brown patches irregularly distributed through the crystal. Deep coloured zircons occur within mica clusters which are surrounded by pleochroic halos. Colourless fluorite occasionally occurs within the mica clusters also. Sample SS99, which comes from the same zoned vein as SS97 has many features in common. However, the mica is more regularly distributed through the rock. It has also been more extensively haematized, although vestiges of green mica occur in addition to the honey coloured variety. Accessory cassiterite is common. It is deeply coloured, skeletal in habit and distributed throughout the quartz suggesting that it was being deposited during silica metasomatism. Similarly dark coloured zircon also occurs within the quartz.

Samples SS117 and SS117/5 come from the roof of the biotite granite in the south west (Fig 9.7). These samples differ from the Dutsen Rishi material in the size and distribution of the mica and in the nature of accessory minerals. The quartz is turbid - more abundant than in the Dutsen Rishi samples (Table 9.13) - sometimes slightly strained, commonly 2-3mm and occasionally up to 1cm in size. The mica forms well developed laths up to 5mm across, which have a slight tendency towards a sieve-like texture. Clusters, up to 5mm across also occur and these are composed of stubby laths of mica. In both habits the mica is commonly

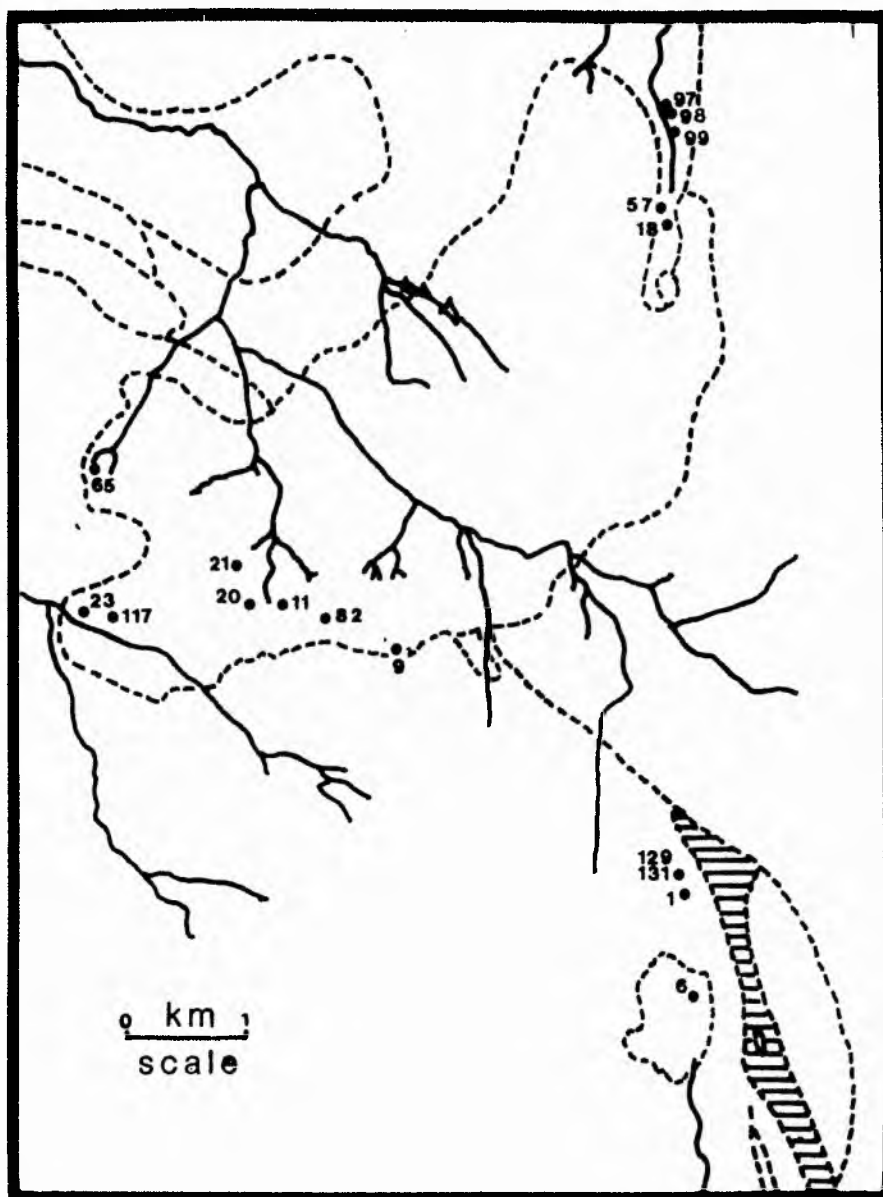


Fig 9.7 Sample localities of silica metasomatised facies and late-stage alteration

a blue green colour. Occasionally, the mica encloses recognisable inclusions of feldspar which may be albite or microcline. Haematite development within these micas was less than in the two samples described above, although the cleavages are often emphasised and may also be bent, sometimes spectacularly so. Colourless fluorite is commonly enclosed within mica, along with TiO<sub>2</sub> minerals, monazite and fluorite. Large anhedral cassiterite which occurs within both mica and quartz crystals may be accompanied by traces of chalcopyrite. Genthelvite has also been noted in these samples which were collected close to a genthelvite-bearing pegmatite.

Unlike the Tibchi and Ririwai complexes, there are few samples that indicate that a major sulphide deposition of ores was deposited at the silicification stage. Sample SS6 however, is rich in sphalerite with only a trace of cassiterite. In other samples eg SS9/1, cassiterite occurs without sphalerite. It is dark in colour, strongly zoned and may enclose zircon which is surrounded by pronounced pleochroic haloes.

Table 9.13 Silica metasomatism

	SS6	SS9/1	SS65/1	SS97	SS99	SS117/5
Quartz	74.3	91.4	88.8	81.5	74.3	88.5
Perthite		3.8	0.2	0.1		0.1
Albite		0.8				
Biotite	6.2	2.2	8.3	16.4	20.2	10.0
Chlorite	1.8	0.3	2.5		0.4	
Topaz						0.1
Fluorite	0.3	0.1		0.2	0.3	0.1
Sphalerite	16.1					
Cassiterite	0.4	1.2		0.2	1.0	0.1
Other ores	0.8	0.1	0.2	1.6	2.6	0.4
Zircon	0.1				0.4	0.6
Siderite					0.3	
Monazite					0.5	
Genthelvite						0.1
Clay minerals		0.1				

## LATE STAGE ALTERATION

### Introduction

In the first part of this thesis late stage argillic and zeolitic processes of alteration were described. Although both of these processes can be recognised in the Rishi area, their importance, both in terms of volumetric extent and ore deposition are not important. However, the late-stage mineralogical changes that have taken place are far more complex than described earlier. Because of the complexity of the alteration changes, plus the isolated nature of the sample localities (Fig 9.7), it was not possible to categorise all the mineralogical changes into a chronological sequence.

## Zeolitic alteration

Zeolite development was restricted to infillings in miarolitic cavities particularly those developed in microcline. Since the recorded zeolite is always associated with microcline it is believed to have grown at the expense of the feldspar. The zeolite which is almost certainly natrolite, usually occurs as white or colourless radiate sheaves or laths. It may be accompanied by quartz, chlorite or a honey-coloured nearly-isotropic clay mineral (?nontronite). Epidote which occurs in small traces in several samples may be contemporaneous in formation.

By analogy with the work of Savage et al (1985), coupled with the knowledge that zeolites are common in hot spring environments (White 1955), it seems likely that this type of alteration was a very late-stage process induced by meteoric water alteration.

## Chloritic alteration

Chloritic alteration was described earlier as part of the acid metasomatic process. However, there was clearly a second stage of chloritic alteration. At this later stage, chlorite may have been associated with zeolite formation, with carbonate development, silica deposition and low temperature ore formation. Chlorite veins can be seen cross-cutting minerals formed during earlier alteration processes and sheaves of chlorite can be found in cavities in ore minerals such as sphalerite.

The late-stage chlorite is very pale green to colourless, and nearly always shows low birefringence rather than anomalous interference colours. In SS57/3 chlorite development appears to have coincided with jarosite and alunite formation.

## Carbonate alteration

This late-stage alteration process was characterised by the development of siderite at the expense of mica. In several samples from the Dawa Mining camp area, siderite developed along mica cleavages and was itself largely altered to haematite or limonite. Samples SS1 and SS129 are very similar. They are characterised by around 30% quartz with 50% blue-green mica in large plates up to 4mm across (Table 9.14). The mica cleavages, which are sometimes curved and bent are emphasised by siderite development and sometimes accompanied by traces of fluorite. There is abundant fluorite in SS114. The siderite forms a colourless high relief mineral with rhombohedral cleavage which may form more than 6% of the rock (Table 9.14). The siderite is characterised by a marginal alteration which resulted in cherry red haematite or dark opaque iron oxide development (Plate 9.58). Where this occurs along mica cleavages the opaques serve to emphasise the cleavage traces of the mica further. Sometimes larger anhedral patches of siderite occur, unrelated to the mica cleavages, but again they show the same alteration features (Plate 9.59). Cassiterite, sphalerite and molybdenite are variously abundant and accessory minerals include zircon, monazite, fluorite and sphene. The texture of SS131 which is extremely micaceous, is unusual. Much of the mica is very pale green to colourless and

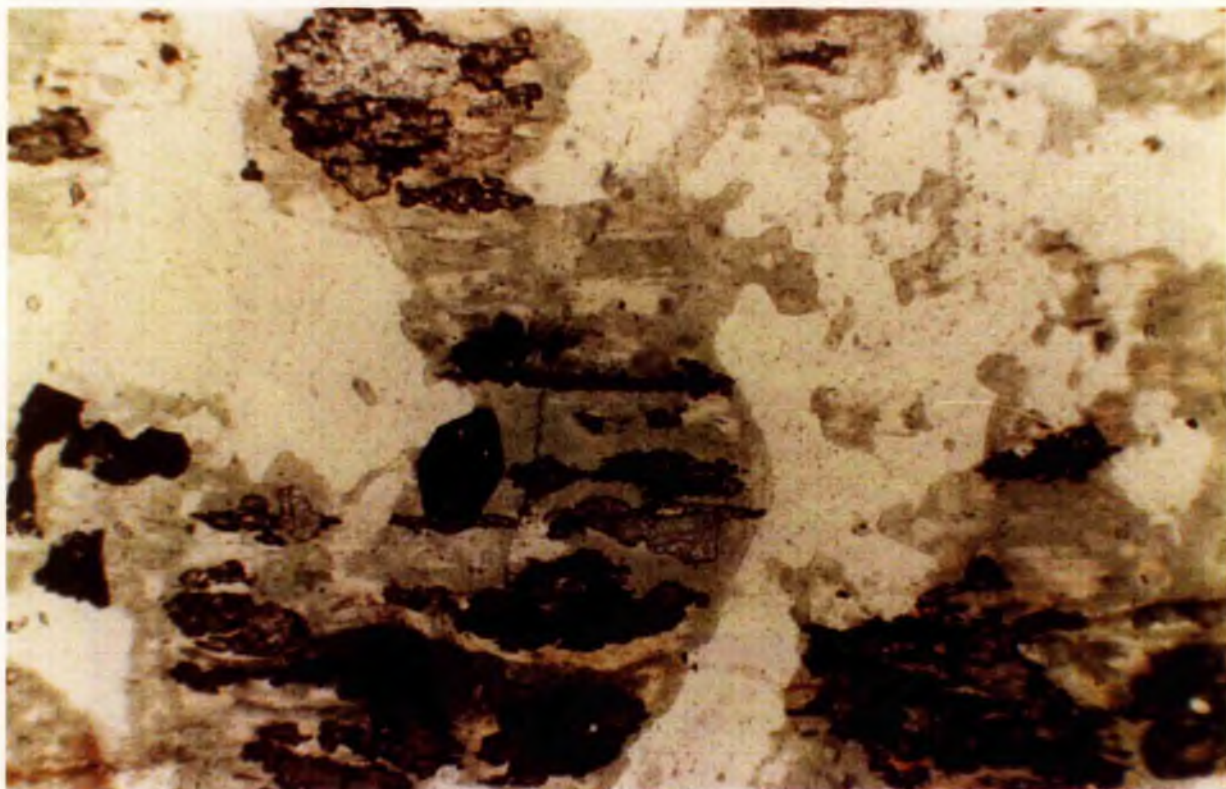


Plate 9.58

Photomicrograph of SS1 showing the development of siderite along the cleavages of the blue-green coloured mica. The siderite has partially altered to haematite which emphasises the cleavage traces further. A small euhedral crystal of molybdenite (opaque) occurs near the centre of the field of view. PPL x50

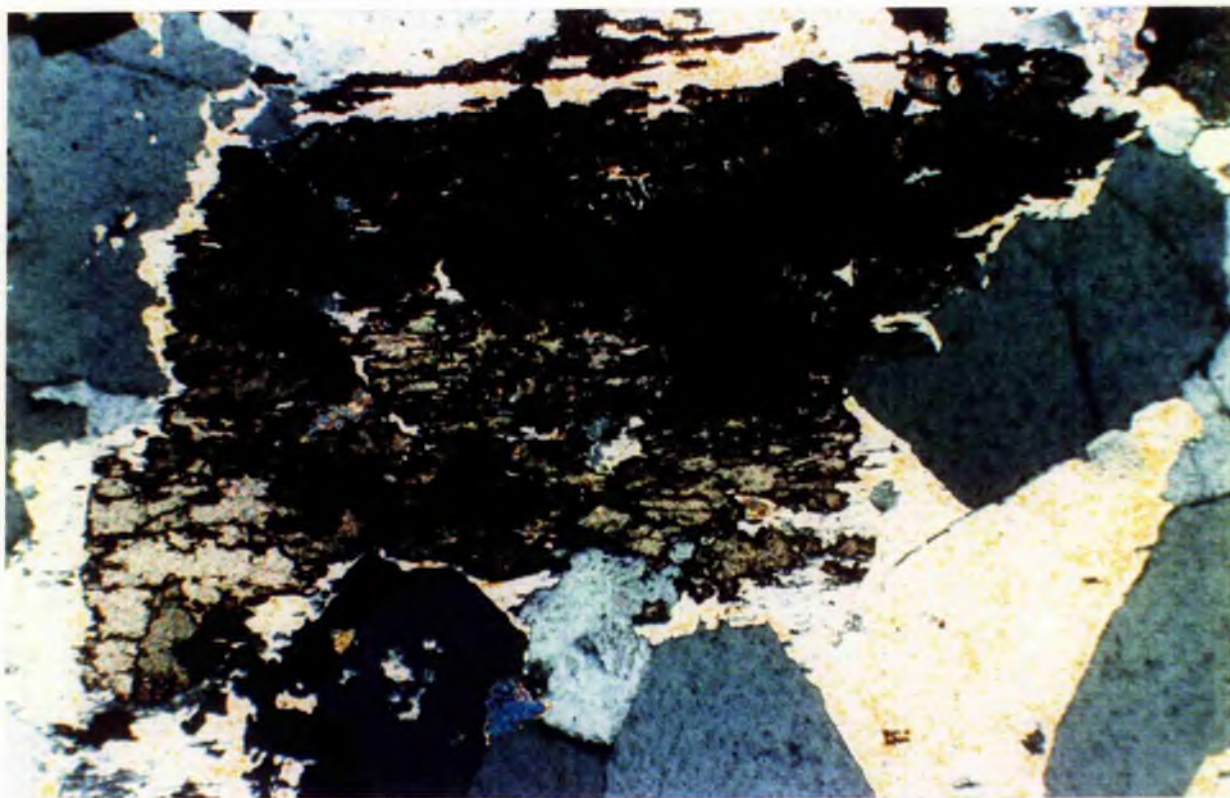


Plate 9.59

Large anhedral patch of siderite in cross-polarised light showing the extensive alteration to haematite. SS1, x50

forms large flakes up to 4mm across in which the cleavages are emphasised by iron oxides developed from almost complete siderite breakdown. In addition to the large mica flakes, there are small euhedral crystals, no more than 0.1-0.2mm across which are interstitial to the main mica flakes (Plates 9.60 and 9.61). These are often perfect crystals cut across the optic axis. It seems that there are two generations of mica growth, an early development as the result of feldspar breakdown, followed by the growth of small interstitial plates due perhaps to a sudden volatile loss. This phenomenon may partially explain the curved cleavage traces of the mica plates.

Table 9.14 Modal analyses of samples which have undergone late-stage alteration

	SS1	SS129	SS131	SS11/2
Quartz	32.4	27.3	1.3	32.1
Perthite				13.4
Biotite	49.4	53.5	78.0	20.4
Chlorite/sericite	0.6	0.7	0.9	29.4
Fluorite	0.7	3.4		3.2
Sphalerite	2.4	2.1		0.2
Cassiterite	0.7	1.6	0.7	0.5
Sphene		0.1		
Molybdenite	0.4	2.3		
Haematite/limonite	7.1	2.4	18.0	0.3
Zircon	0.3	0.1		
Siderite	6.0	6.4	1.1	
Monazite		0.1		
Apatite				0.1

During acid metasomatism, mica must have grown in a acid environment of low pH. At the late stage of carbonate development, there must have been availability of CO<sub>2</sub> which would have led to an increase in pH as temperature fell. Such changes in fluid composition coupled with a decrease in temperature clearly de-stabilised the mica and led to the formation of siderite. The only other area where siderite development occurred on this scale is in the Igo area of the Afu complex. The Igo locality is also believed to be near the roof of the biotite granite and so it may be that the development of a carbonate alteration phase reflects a process that developed where fluid remained for a long period within the system.

#### Argillic alteration

Argillic alteration was a late stage process, characterised by the formation of kaolinite generated from feldspar breakdown at low temperatures. The degree of argillic alteration in the Rishi area was limited and very patchy. Clay minerals may have developed interstitial to quartz in pale green coloured massive quartz veins, or clays may have infilledmiarolitic cavities or cavities in pegmatitic pods, or have coated crystals and infilled intra-crystal voids in

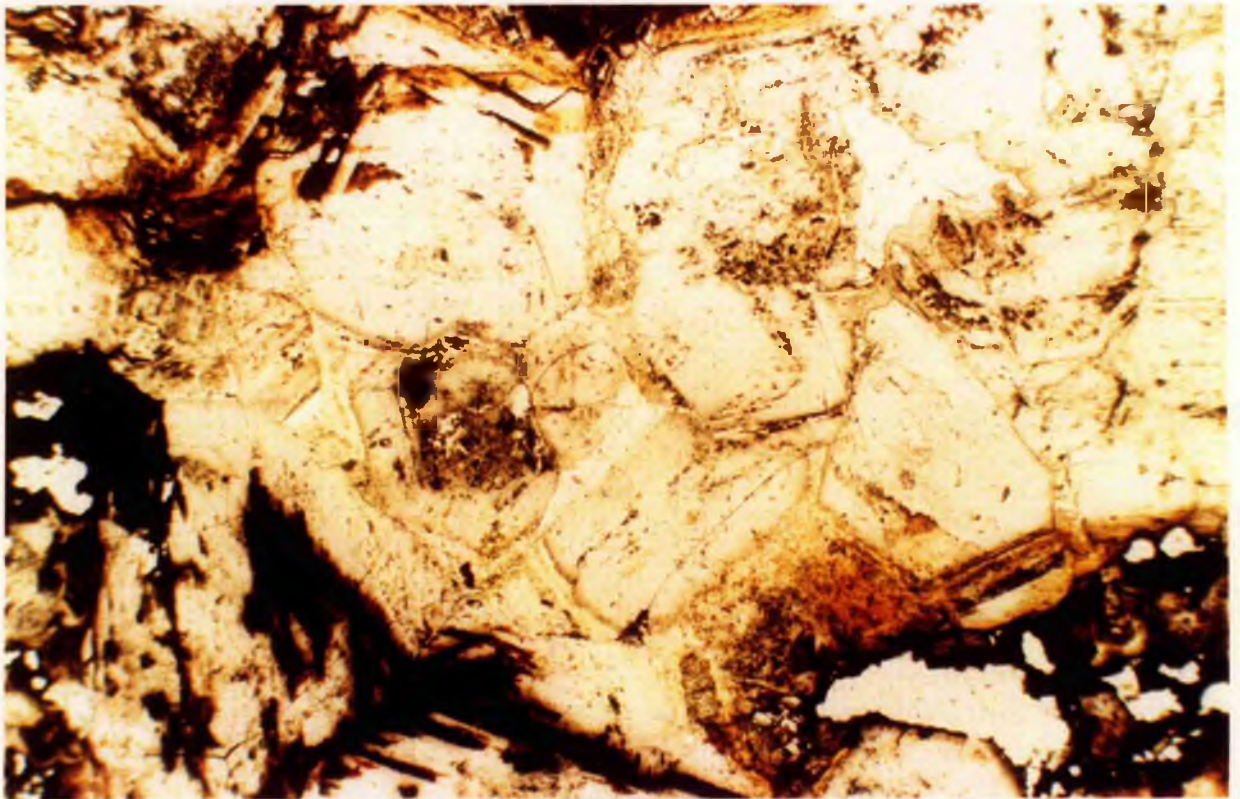


Plate 9.60

Small euhedral mica crystals less than 0.3mm in size developed in small cavities between large colourless mica books which are up to 4mm across. SS131, PPL x125

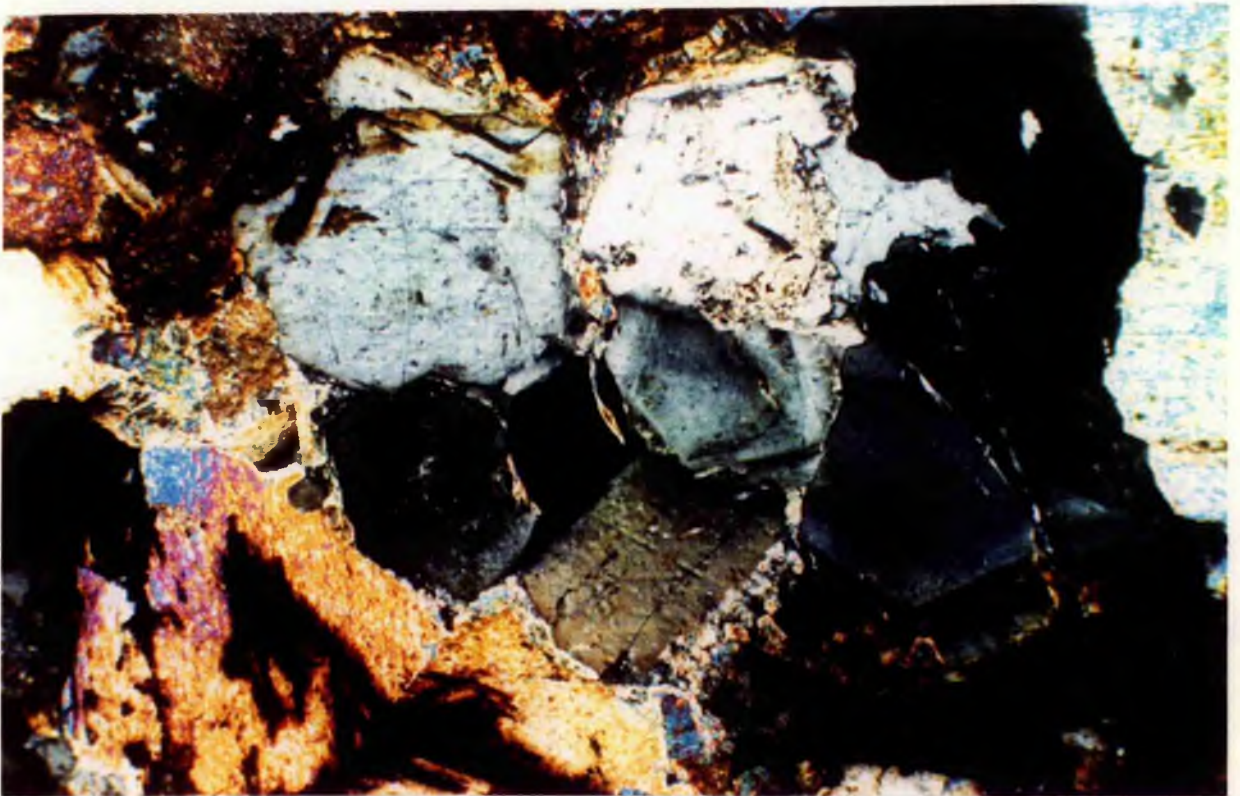


Plate 9.61

Same view as above under crossed polars.

veins. Several samples which have been silicified show traces of clay mineral development from vestiges of remaining perthite. These are nearly always kaolinite and show the characteristic hexagonal plates in SEM photographs (E.K.Walton pers. comm). However, SS20 is an apple-green coloured vein which contains quartz and a clay mineral which proved to be illite on microprobe analysis. The formation of this vein may have resulted from the passage of meteoric water along a zone of weakness exploited by the vein.

#### Late-stage processes

All these late-stage processes described, may be more or less coincident in time and space and the different products may have resulted from changes in the temperature and compositional profile of the late-stage fluids. In fact, some of the late-stage effects such as zeolite formation and clay mineral development are almost limited to miarolitic cavities. This perhaps indicates that these low temperature assemblages developed only in small pockets where trapped droplets of fluid could not escape but remained and equilibrated within the host rock.

At a late stage in the sequence of alteration processes, the build up in fluid pressure may have resulted in brecciation of some of the earlier formed mineral assemblages e.g. SS11/2, SS20/1 and SS82, where the brecciated vein material has been cemented by amethyst. Sample SS11/2 (Plate 9.62), from the southwestern part of the biotite granite, is a mineralised breccia which formed after acid metasomatism and formation of fluorite which occurs as angular fragments, sometimes purple-coloured and up to 2mm in size. The breccia consists of angular fragments of quartz, feldspar, chlorite and fluorite, set in a fine-grained, somewhat banded matrix composed of small quartz grains, finely comminuted microclinised feldspar, chlorite and quartz (Plate 9.63). Sericite alteration of the feldspar resulted in the formation of aggregates of fine-grained white mica, but there was also the development within these aggregates of larger laths. Tabular, colourless mica laths have also grown in vugs created by brecciation. There are also thin late-stage cross-cutting quartz stringers that contain deep red, strongly-zoned cassiterite and sphalerite which appears to have grown after brecciation.

Late-stage chlorite has grown in sheaves, filling cavities created by brecciation. Amethyst also occurs in miarolitic cavities (eg. SS 11/3, SS18/9, SS18/10) associated with adularia, indicating its late-stage origins of the assemblage.

#### Secondary ore mineral formation

It seems likely that secondary ore minerals formed at this late stage. The most noticeable area for such alteration occurs where the basement has been mineralised to the north of Dutsen Rishi. A description of these alteration products is given later in the Chapter.

Supergene weathering of the ores still continues. In the last visit to the area nearly all mining activity had ceased, pits had been abandoned for more than a year and all fresh sulphide ores had a superficial coating of secondary minerals. There was a coating of smithsonite on sphalerite; chalcantite, malachite and azurite have developed from chalcopyrite, and pyrolusite is being produced by the breakdown of Mn rich wolframite or other ores. Several of these alteration products can be seen in sample SS33/4.



Plate 9.62

Brecciated vein which consists of angular fragments of quartz, feldspar, chlorite and fluorite set in a fine-grained somewhat banded matrix of quartz, finely comminuted microcline, and chlorite.

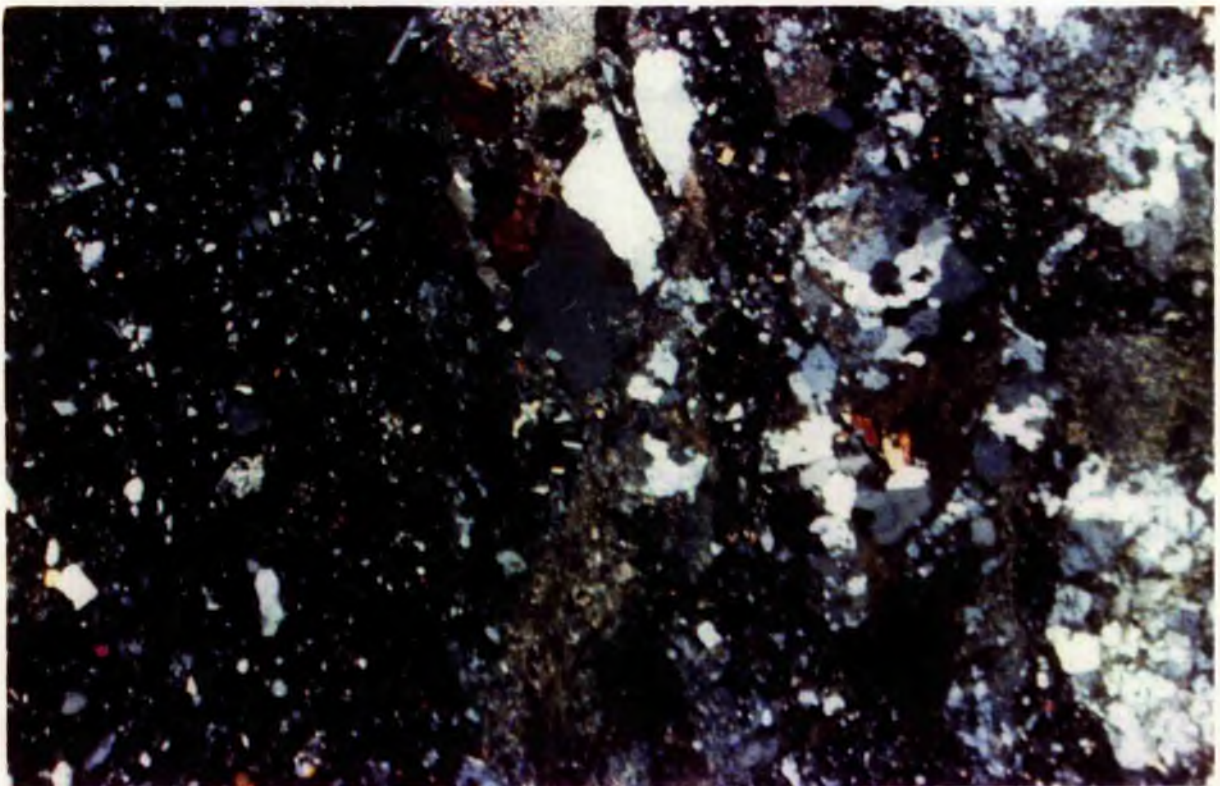


Plate 9.63

Photomicrograph of part of the vein above in cross-polarised light. SS11/2 x50

In many other tin provinces worldwide, there was extensive late-stage alteration, notably clay mineral development. The fact that these late-stage alteration processes are very minor in Nigeria suggests that the province must be different in some way to other areas where extensive late-stage alteration occurred. It is possible that meteoric water circulation was limited because fracturing and fissuring of the volcanic pile did not take place to any great extent which inhibited water permeation. The type of country rock, which is relatively impermeable basement, must also have played an important role on the control of meteoric-hydrothermal convection systems.

#### Summary of the hydrothermal alteration processes

From the preceding descriptions it is obvious that the processes of hydrothermal alteration are complex and depend not only on the temperature and composition of the fluid, but also on the initial rock type and to a certain extent on how long the fluids were retained. The different mineral assemblages indicate that alteration took place within an  $\text{Na}_2\text{O}-\text{K}_2\text{O}-\text{SiO}_2-\text{H}_2\text{O}-\text{F}$  system which produced albitisation then microclinisation of feldspars during sodic and potassic alteration, and ultimately a destruction of the feldspars during acid metasomatism. Late-stage processes include silicification as the dominant event.

The sodic effect appears to have been largely overprinted and masked in the Saiya Shokobo Complex. Both sodic and potash metasomatism affected the perthitic feldspars, first by a coarsening of the domains within the perthite and then by the development of albite or microcline. The disseminated process of potash metasomatism (microclinisation) appears to have been a more important process in the Saiya Shokobo complex than in other complexes so far studied.

The process of acid metasomatism may have followed sodic and potassic metasomatism. This process was responsible for the development of chlorite and/or Fe-Li micas by the destabilisation of feldspars. However, in many areas acid metasomatism was the first and only process of hydrothermal alteration. Obviously the residual fluids at these particular localities were initially very acid and were responsible for disseminated greisenisation in the roof zone without prior sodic or potassic alteration.

The mineral assemblages developed during these successive processes of alteration do not equate directly with those developed in porphyry copper deposits:-

Albitisation, chloritic alteration, zeolitic alteration and carbonate formation are all special types of propylitic alteration in the porphyry copper setting according to Meyer and Hemley (1967). However, the processes are not directly comparable as there was only a trace of epidote with the albitised assemblage in Nigeria whereas it is a common accessory in albitised rocks of porphyry copper deposits. Other accessory minerals described as common in the porphyry copper setting are rare to absent in Nigeria. Even the potash metasomatism is not directly comparable between the two provinces. In Nigeria, mica was chloritised as microcline developed, whereas for the porphyry copper deposits, it appears that new mica growth was concomitant with potash feldspar development.

Chlorite formation at the expense of biotite was the result of weak hydrogen ion metasomatism and is thus equivalent to propylitic alteration in porphyry copper deposits.

Quartz mica greisen development is similar to sericitic or phyllic alteration in porphyry copper deposits and the quartz-topaz greisen (silexite) to advanced argillic (Rose and Burt 1979). The difference between the two provinces is the larger amount of fluorine present in the anorogenic setting.

Several important points emerge from this detailed petrographic study:-

(i) for the first time in the Nigerian province the complexity of the alteration processes has been monitored. New mineral assemblages such as a microclinised albite-rich rock have been recognised.

(ii) the tremendous range of textural variations even within the comparative small size of the Rishi biotite granite had not been previously appreciated or explained.

(iii) disseminated metasomatism and mineralisation can occur at any stage

(iv) the process of acid metasomatism may have followed sodic or potash metasomatism. However, it may also have been the first (and only) process of hydrothermal alteration.

(iii) the microclinites of the Saiya Shokobo complex are not reddened as in the Ririwai complex and have been mistaken for albitites in field mapping.

(iv) for the first time potash metasomatism of volcanics and basement host have been recognised.

In order to understand more about the fluid-rock reactions and to understand how the change from one process to another occurs, it is necessary to study the PVTX conditions of the fluid. Before considering the fluid characteristics however, the bulk rock chemistry of the rock samples already described has been examined in order to learn something about element mobilities during different alteration processes. Most major and trace elements of low ionic potential, together with many elemental and isotopic ratios are known to be sensitive to hydrothermal alteration reactions. A study of elemental behaviour during different alteration stages must be the first step to an understanding of the fluid characteristics responsible for alteration.

## GEOCHEMISTRY OF THE ALTERATION PROCESSES

### Introduction

It is clear from the mineralogical variations just described, that the different mineralogical facies must show a range of both major and trace element chemistry. For the major elements there is a wide variation in Si, Al, K, Na, Fe and to a lesser extent in Ti, Mg, Mn and Ca. Many major element studies on

granites, including this thesis, have made use of the diagram of bivariate oxide percentage against percent of silica of Harker (1909), or oxide percentage Larsen index (Larsen 1938), or oxide percentage differentiation index (Thornton and Tuttle 1960). However, there are a number of inadequacies in the use of oxide percentage bivariate diagrams to show petrogenetic trends and these have been discussed by Chayes (1964), Pearce (1969) and Batchelor and Bowden (1985) among others. At least during granite differentiation to highly fractionated compositions there is usually a systematic positive or negative correlation of both major oxides against silica and these diagrams have certain merits. This is not the case however during hydrothermal alteration. An alternative approach using cationic/molecular values has been used. This method, which is found in French classification schemes and is also described in Batchelor and Bowden (1985), expresses whole-rock chemistry as cationic parameters in terms of mineralogical components. These components can be varied according to rock type or alteration process being studied.

#### GEOCHEMICAL TECHNIQUES

In contrast to the data in Part 1, all the major and much of the geochemical trace data have been measured by XRF techniques, details of which are given in Appendix 2. International reference standards have also been analysed as unknowns and are compared with recommended values to give an estimate of experimental accuracy and precision. The elements Be, Li, Sn, Mo and F were analysed by atomic absorption, whilst W was analysed by a colorimetric method (see Appendix 3). The detection limits for these trace elements are given in Appendices 2 & 3. The complete summary of techniques utilised is given as a flow chart in Appendix 4.

The R1-R2 factors refer to the de la Roche et al (1980) multicationic parameters:

$$R1 = 4Si - 11(Na+K) - 2(Fe+Ti)$$

$$R2 = 6Ca + 2Mg + Al$$

For the hydrothermally altered rocks the Q and F parameters of de la Roche (1964) have been calculated since these discriminate better between sodic and potassic metasomatic processes:

$$Q = 1/3Si - (K+Na+2/3Ca)$$

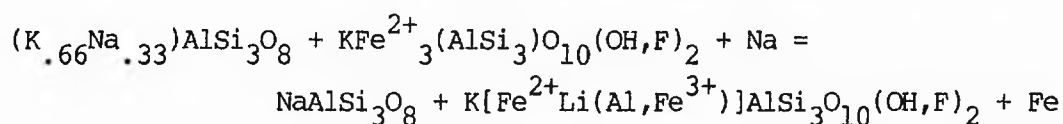
$$F = K - (Na+Ca)$$

The programme used to calculate these values on a BBC microcomputer is given in Appendix 5.

During hydrothermal alteration, density changes can often lead to apparent variations in elemental concentrations. In discussing geochemical changes during alteration no account has been taken of these density changes since there may be as much variation in density between samples of the same process as between samples of different processes. This may be due to textural variations but is more linked to the abundance of ore minerals and the type of ore mineral in question. Slight apparent differences in elemental variations may therefore not be strictly valid. Since many of the chemical variations however show changes in concentrations over several orders of magnitude, it seems reasonable to discuss such changes without recourse to density comparisons.

## Sodic metasomatism

Sodic metasomatism was either a weak process at Rishi, or else the effects were overprinted by later processes. It is clear from Table 9.15 that it is not possible to identify a sample that has suffered sodic metasomatism from whole rock chemistry alone. This is partly because later processes may have removed Na from the sample but also because even where the sodic process can be recognised in thin section studies, the potash content of the rock may exceed the soda content as in SS48/1 (Table 9.15). In this particular case, since petrographic studies show that there has been Na for K replacement in the original perthite to produce albite, it seems that the potassium released during feldspar alteration, was not lost from the system, but was all consumed in the formation of honey-coloured zinnwaldite perhaps according to the following equation:-



perthite + annite + Na = albite + zinnwaldite + Fe

The geochemical data, obtained from seven analyses (Table 9.15), indicates that during sodic metasomatism there was a loss of Fe as the original annitic mica was destroyed, an increase in Al and an overall decrease in silica, although this was only slight and does not compare with the silica reduction during albite formation as in some complexes.

Norm calculations in Table 9.15, show that there was a slight increase in **ab** in these samples when compared with the average for the original rock type and a concomitant small decrease in **q**. However, on the Q-Ab-Or plot, (Fig 9.8), the shift of plotting positions for these samples towards the Q-Ab join is almost imperceptible.

The plotting positions of sodic metasomatised facies of the biotite granite on the Q-F plot fall slightly to the left of the normal field for biotite granite (shown as field 3 in Fig 9.9) indicating that the process of sodic metasomatism was weak or largely overprinted. Two analyses plot rather differently - one is more silica enriched and the other more potash enriched. In the case of the former (SS189), weak acid metasomatism has been overprinted on the sodic effect and in the case of SS48/1 there has been a potassic imprint which reached a maximum in other parts of the same rock sample (SS48/1a).

In addition to these major element changes, the fluid contained important concentrations of trace elements. The most interesting increase was in Ba which increased from an average of <5ppm for the biotite granites to an average of 50ppm in the sodic metasomatised roof facies and with individual samples reaching 110ppm. Such Ba values normally characterise basement granitoids. An equally interesting feature was the lack of appreciable increase in Hf in the soda metasomatised facies of Rishi, because in all other complexes there was a marked increase in Hf at this stage. Since increase in Hf was also usually associated with increased Zr - as Hf is accommodated within the zircon structure

Table 9.15 Sodic metasomatised facies of the Rishi area

	SS42/2	SS44/2	SS48/1	SS55/8	SS69	SS189	SS190
SiO <sub>2</sub>	76.94	76.90	75.31	78.40	76.79	76.72	77.60
TiO <sub>2</sub>	0.09	0.02	0.04	0.05	0.04	0.08	0.06
Al <sub>2</sub> O <sub>3</sub>	12.84	12.81	13.32	12.40	12.62	12.21	12.71
Fe <sub>2</sub> O <sub>3</sub>	1.16	1.20	0.90	1.26	1.24	1.71	1.56
MnO	0.01	0.02	0.02	0.02	0.14	0.02	0.03
MgO	0.01	0.10	0.02	0.00	0.00	0.07	0.03
CaO	0.65	0.59	0.06	0.23	0.37	0.11	0.08
Na <sub>2</sub> O	4.16	3.94	3.93	4.40	4.20	3.07	4.15
K <sub>2</sub> O	3.83	3.91	5.71	4.24	4.16	4.53	4.07
P <sub>2</sub> O <sub>5</sub>	0.00	0.00	0.02	0.00	0.01	0.00	0.02
H <sub>2</sub> O			0.42				
Total	99.69	99.49	99.75	101.00	99.57	98.52	100.31
R1	2719	2777	2261	2634	2528	2915	2700
R2	322	319	269	268	288	255	259
Q	203	209	169	200	189	229	209
F	-65	-55	-7	-56	-63	-5	-49
Ba		85	28	0	0	110	46
Be							10
Ce		127	27	119	92	470	86
Cr		0	0	0	0	15	0
Cu		4	16	20	15	19	28
F			1900	2600	2300		2300
Hf		8	9	7	5	15	14
La		74	17	73	60	783	57
Li		49	253	194			410
Mo			<14	<14			<14
Nb		147	395	139	152	381	330
Ni		4	9	9	11	9	9
Pb		76	29	16	18	56	66
Rb		447	1188	796	647	1003	1028
Sn			42	40			432
Sr		25	8	0	4	2	3
Th		56	126	60	61	121	127
V		4	1	4	2	0	1
Y		164	14	127	124	144	57
Zn		119	113	161	179	1984	346
Zr		203	202	162	154	465	384
Zr/Hf		25	22	23	31	31	27
Ce/Y		0.77	1.93	0.94	0.74	3.26	1.51
quartz	36.70	37.62	30.52	36.11	34.24	41.20	37.73
ortho	22.63	23.10	33.74	25.05	24.28	26.76	24.05
albite	35.13	33.32	33.24	37.21	37.72	25.96	35.10
anorth	3.22	2.93	0.17	1.14	1.77	0.55	0.27
corund	0.67	1.03	0.62	0.16	0.25	2.06	1.38

Fig. 9.8 Q-Ab-Or plot of sodic and potassic metasomatised Rishi samples (data from Tables 9.15 & 9.16)

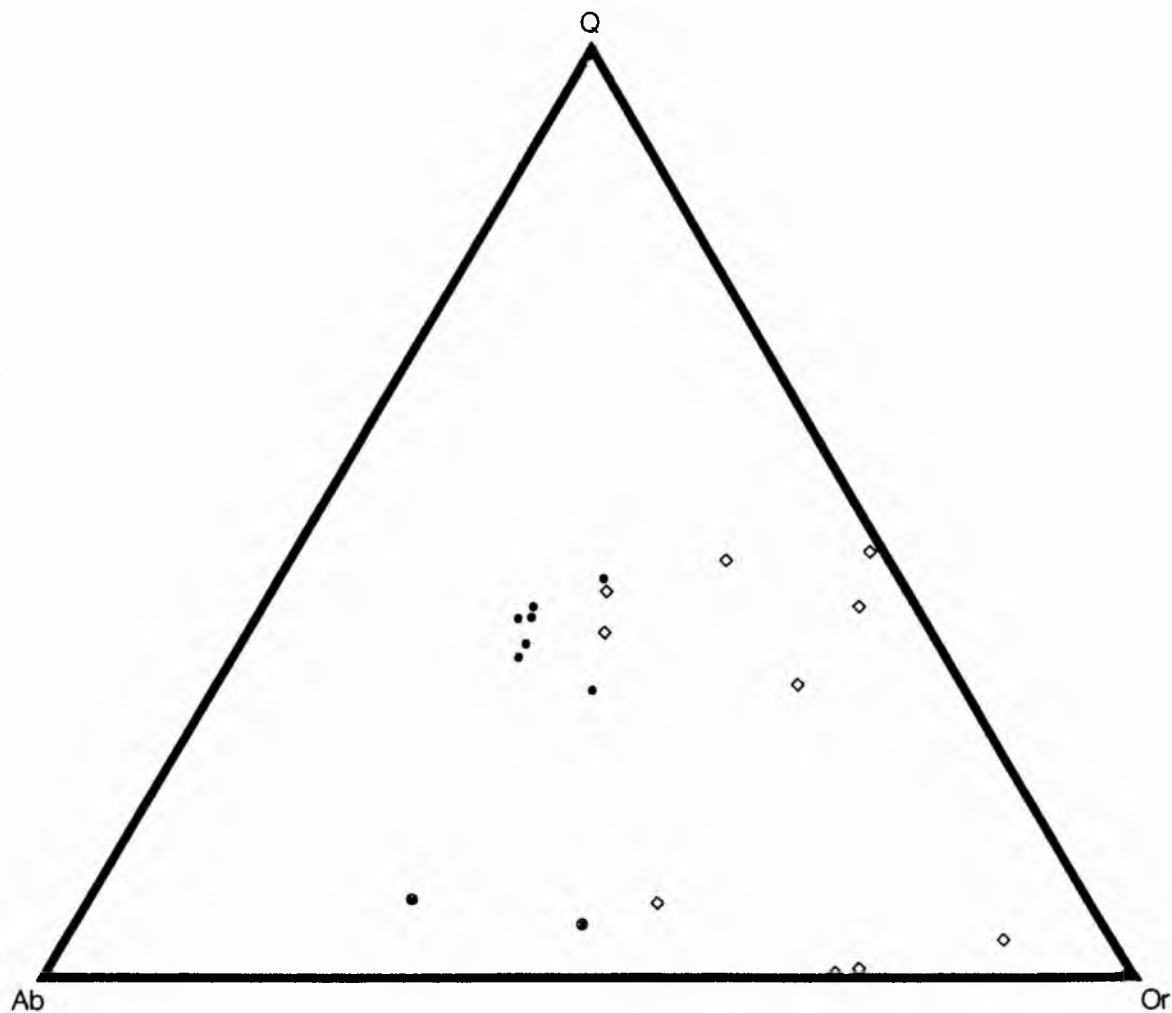


Fig 9.9 QF plot of sodic metasomatised samples for the Rishi biotite granite.

open circle = altered granite  
 cross within a circle = altered basement  
 star = altered granite porphyry

Field 1 = basement monzogranite  
 Field 2 = volcanics  
 Field 3 = biotite granite

fields defined from data in Chapter 8.

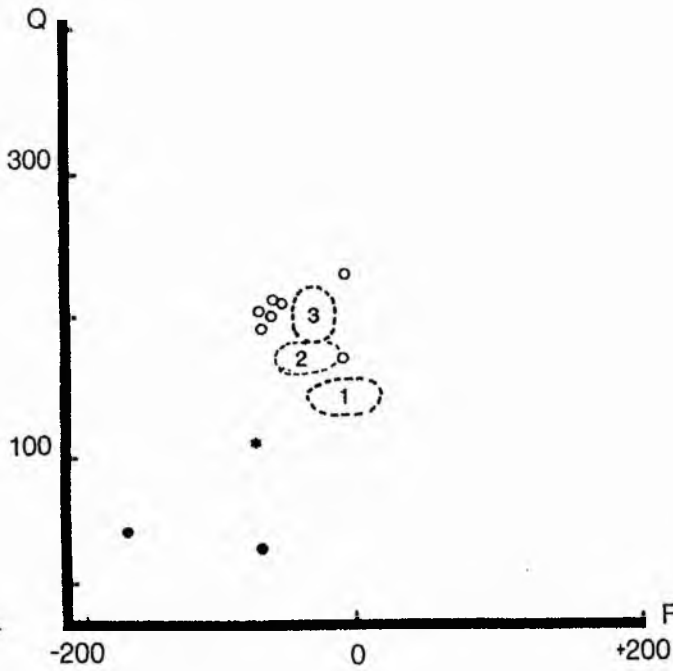
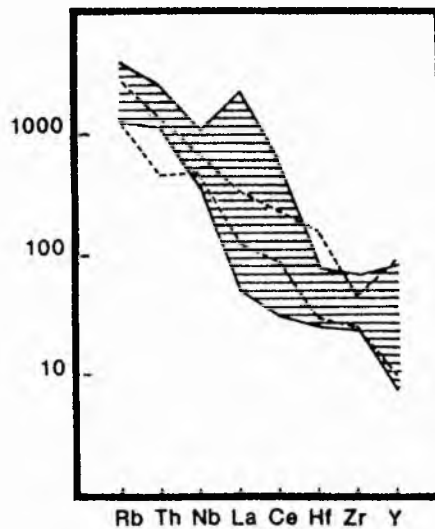


Fig 9.10 Chondrite-normalised trace element data for sodic metasomatised rocks (shaded field) compared with biotite granite (field defined by dashed lines)



- it is difficult to explain this lack of increase in Hf when there was a slight overall increase in Zr. However, the increase in Zr in Rishi samples, was not as dramatic as in sodic facies of some other complexes and where the increase in Zr was greatest in Rishi samples (SS189 and SS190) the increase in Hf was also the highest.

Most sodic metasomatised granites in Nigeria show increases in Rb, Th and Nb and the Rishi area is no exception. There was an increase in Rb from an average around 600ppm to around 850ppm; Th increased from an average of ~50ppm to 75ppm; and Nb increased from an average 200ppm for the biotite granites to an average of 250ppm in the soda metasomatised facies. The highest Nb value was found in SS48/1, which was also noted to contain columbite in thin section. Most sodic metasomatised facies in Nigeria have increased levels of Li. Although SS190 is lithium enriched, there was no systematic increase in all samples. This applies also to La and Ce and the chondrite-normalised plot (Fig 9.10) shows that both La and Ce may be enhanced, depleted, or remain the same as in the biotite granites. However, although there appears to be no systematic variation, further petrographic studies have shown that SS189 and SS190 which give the high La and Ce peaks are volcanic rocks that have been metasomatised to granite. Therefore, the high La and Ce peaks are "inherited" from the volcanic pile.

Other sodic metasomatised granites in Nigeria show increases in Zn and particularly Sn (Kinnaird et al 1985) but this does not seem to have been the case in Rishi and in fact most Zn values were decreased.

In other similar metasomatised areas, there was an increase in uranium and REE's and whilst no data exists for the Rishi area certain statements can be made. Uraninite crystals have been identified in an albite pegmatite from Ladini (SS117/6) and traces of autunite have been found on some specimens (SS115 and SS116) so it is assumed that there was also an increase of uranium here in the Saiya Shokobo complex. An increase in Ce and La in several of the soda metasomatised samples also indicates that there was a localised increase in rare earths. Again there is a correlation between high La and Ce with high Zr, suggesting that the rare earth elements are only retained where zircon formation occurred.

In addition to sodic metasomatism of biotite granite and the volcanic pile, it also seems apparent from further petrographic studies, modal data and cationic plots that sodic metasomatism of the basement has occurred. Thus samples SS17/3 and SS17/5 for example may have originally been very albite rich, although later acid metasomatism has masked the albite abundance.

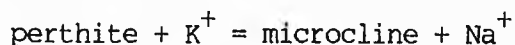
In summary, the combination of geochemical and petrographic studies has emphasised that in addition to sodic metasomatism of the Rishi biotite granite, both the volcanic pile and basement country rock have been albitised. This fact had not initially been appreciated on petrographic studies alone.

#### Potassic metasomatism

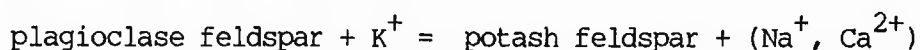
There was a dramatic increase in K content of the potash metasomatised facies and lesser changes in many of the other major elements together with a wide variation in trace elements. However, the subtle variations in the geochemistry of this process are dependent on whether it was the country rock, the volcanic

pile or the Rishi biotite granite that was being affected, and the extent of the earlier sodic metasomatism upon the various rock types. Thus table 9.16 groups the potash metasomatised rocks according to the rock type being affected. Whilst three of these samples are described as metasomatised albitised facies, there is the possibility as described earlier, that the unaltered albite laths in these rocks may have grown from the Na released during perthite alteration. However, since SS48, collected close to SS48/1a, is clearly an albitised rock it does seem likely that the potash process was superimposed on sodic metasomatism and that this grouping in Table 9.16 is valid.

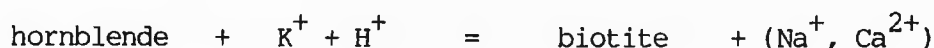
The increase in K during potash metasomatism resulted from the growth of new microcline and concomitant loss of Na and Ca from the breakdown of perthite in the volcanic rocks and biotite granite:-



In the basement there may also have been potash metasomatism of an original plagioclase feldspar.



As acidity increased any original hornblende will also have been affected and altered to biotite:-



Although these equations suggest loss of Ca, the Ca content of some of the samples was increased, regardless of the initial rock type. This was probably due to fluorite growth although the overall fluorine content of these rocks tends to be lower than in sodic metasomatised samples. There was a decrease in silica which, as the process of potash metasomatism became intense, resulted in desilication and silica levels as low as 57.73% in honeycomb-textured microclinites (SS20/3 in Table 9.16). Alumina was also increased, particularly in the facies that had already been albitised and in the potash metasomatised basement. This alumina increase reflected the growth of new mica at the same time as microcline development, and iron was depleted since the new mica was Li-Al rich.

Norm calculations in Table 9.16, show that there is a dramatic increase in normative Or balanced by a decrease in Ab and Q. In the Q-Ab-Or plot of Fig 9.8, the salic compositions plot away from the central field of biotite granite towards the Q-Or join, or towards the Q pole, and are represented by open diamonds.

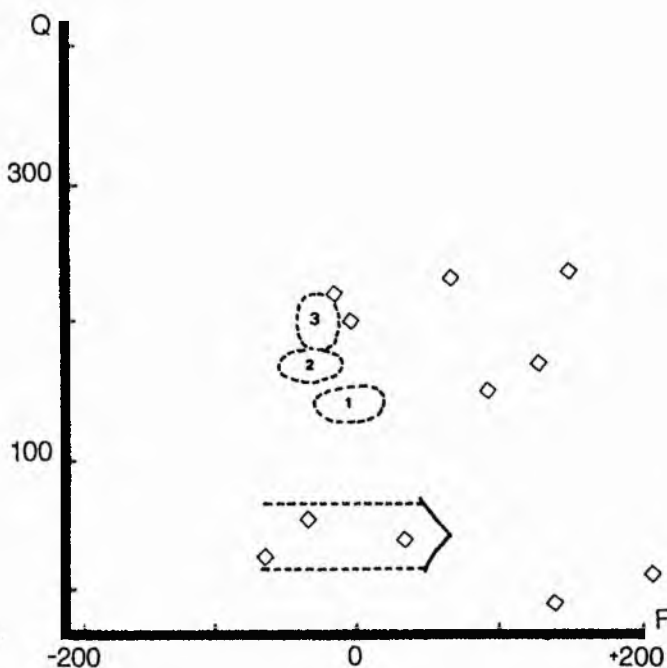
For rocks that have undergone potash metasomatism there is a wider spread of plotting positions on the Q-F cationic diagram (Fig 9.11):-

(i) Where microclinisation was extreme and desilication occurred then the compositions trend towards the microcline pole.

Table 9.16 Potash metasomatised rocks of the Rishi area

	albitised		48/1a	perthite granite			SS20/3	basemt	volc	pegs	
	SS23/9	23/12		SS8/1	SS106	12/13		SS17/3	SS86	SS9/11	SS70
SiO <sub>2</sub>	65.05	66.04	68.02	60.42	74.95	74.84	57.73	61.48	77.73	76.69	73.74
TiO <sub>2</sub>	0.00	0.00	0.00	0.01	0.07	0.08	0.08	0.99	0.05	0.04	0.00
Al <sub>2</sub> O <sub>3</sub>	18.80	18.50	17.77	17.68	12.10	12.25	13.12	18.09	12.47	12.33	14.23
Fe <sub>2</sub> O <sub>3</sub>	0.36	0.52	0.80	0.86	3.26	3.84	17.86	3.60	1.03	1.74	0.70
MnO	0.00	0.02	0.00	0.02	0.05	0.06	0.21	0.05	0.01	0.22	0.06
MgO	0.02	0.00	0.03	0.29	0.11	0.00	0.00	2.07	0.05	0.00	0.08
CaO	0.41	0.38	0.17	0.13	0.58	0.57	1.50	2.87	0.37	0.25	0.12
Na <sub>2</sub> O	3.28	1.17	4.53	2.67	1.51	0.20	0.45	4.42	3.45	3.29	1.66
K <sub>2</sub> O	11.90	14.36	8.70	11.40	5.96	7.72	6.40	6.16	5.40	4.45	8.71
P <sub>2</sub> O <sub>5</sub>	0.00	0.01	0.01	0.02	0.04	0.01	0.15	0.39	0.00	0.01	0.00
F <sub>2</sub> O	0.22	0.19	0.19	0.10						0.38	
F=O	-0.09	-0.08	-0.08	-0.04						-0.16	
Total	99.95	101.11	100.14	93.56	98.63	99.57	97.50	100.12	100.56	99.24	99.30
R1	378	614	868	390	2978	3010	1739	970	2661	2853	2268
R2	413	404	368	375	305	301	418	765	287	269	296
Q	-3	19	44	5	233	238	152	33	200	221	169
F	140	260	36	154	67	147	95	-63	-3	-16	129
Ba	0	8	57	0	0	117	0	3467	0	0	13
Be	20	71		3						24	
Ce	44	40	51	35	97	115	187	134	78	110	116
Cr	0	0	0	0	0	0	0	0	0	0	0
Cu	7	18	13	14	33	13	10	12	0	7	18
F	2200	1900	1900	1000						3800	
Hf	8	8	9	13	11	4	4	7	24	9	2
La	20	19	18	0	104	51	69	59	42	62	34
Li	6	4		109						249	
Mo	<14	<14	<14	<14						16	
Nb	56	45	169	224	141	147	226	16	221	190	58
Ni	11	57	13	10	14	16	86	12	71	1	56
Pb	522	84	35	5201	457	154	203	34	21	110	302
Rb	1514	1579	1745	1262	706	937	2563	456	994	816	1115
Sn	4860	135		62400						324	
Sr	23	11	21	212	22	13	23	319	4	1	1
Th	8	16	105	12	46	60	79	10	62	67	32
V	7	5	5	10	4	6	0	105	6	5	10
Y	97	62	28	79	124	143	160	26	138	121	77
Zn	73	342	78	2120	2683	855	826	86	386	263	399
Zr	290	249	196	200	202	195	183	357	305	163	30
Zr/Hf	36	31	22	15	18	49	46	51	13	18	15
Ce/Y	0.45	0.65	1.82	0.44	0.78	0.80	1.17	5.15	0.57	0.91	1.51
quartz	0.00	3.51	8.02	0.63	42.08	42.95	27.84	4.16	36.15	40.03	30.39
ortho	70.31	84.84	51.40	67.35	35.21	45.61	37.81	36.39	31.90	26.29	51.46
albite	27.03	9.90	38.31	22.58	12.77	1.69	3.81	37.38	29.18	27.83	14.04
anorth	1.44	1.82	0.78	0.51	2.62	2.76	6.46	11.34	1.84	1.17	0.60
nephel	0.38										
corund		0.37	0.62	0.76	2.21	2.55	3.09		0.28	1.67	1.86
wollas	0.19										
di kwo	0.06										
di ken	0.05										
hy ken			0.07	0.72	0.27			5.15	0.12		0.20
magnet		0.07		0.04			0.45			0.60	0.20
haemat	0.36	0.47	0.80	0.83	3.26	3.84	17.55	3.60	1.03	1.32	0.56
ilmen				0.02	0.11	0.13	0.15	0.11	0.02	0.08	
rutile					0.01	0.01		0.83	0.04		
titan								0.25			
apatit		0.02	0.02	0.05	0.09	0.02	0.36	0.92		0.02	
TDI	97.34	98.25	97.73	90.56	90.06	90.25	69.46	77.94	97.23	94.15	95.89

Fig 9.11 QF plot of potash  
metasomatised samples for the Rishi  
biotite granite. For explanation see  
text



(ii) Where potash metasomatism resulted in a K for Na exchange only, with no removal of silica, compositions plot towards the microcline-quartz join.

(iii) Three samples have compositions that plot in a slightly different field from those described above - one of which is SS48/1a. It has already been stated that 48/1a is a sample that has had a potash metasomatism superimposed on a sodic effect. It appears therefore that the Q-F plot is capable of distinguishing samples which have suffered both processes of cation metasomatism. If this is the case then sample SS173, the highly altered sample from the quartz feldspar porphyry feeder dyke, has also undergone both processes.

There was a decrease in abundance of some trace elements when compared with the average for the initial rock type (Fig 9.12) and particularly when compared with sodic metasomatism (Fig 9.10). Thus Nb values which increased from an average of 200ppm for Rishi biotite granite to 250ppm in sodic facies decreased to an overall mean of 136ppm for all the potash altered rocks in Table 9.16. Thorium and La decreased in abundance compared with sodic facies but are comparable with values in similar previously unaltered samples. As an example Th values in the Rishi biotite granite average ~50ppm whereas in sodic facies this level increases to an average of 75ppm; in the potash metasomatised granite the average of four samples is back to 50 and even in the potash altered albite-rich rocks (SS23/9, SS23/12 and SS48/1a in Table 9.16), the average is <50ppm.

Certain trace element values however were enhanced reflecting the increased potash content. Thus Rb and Sr concentrations rose, sometimes dramatically so. For example, for Rb, the increase was from an average of 664 ppm for 15 samples of the Rishi biotite granite to an average of 1367 ppm for the four samples of potash-rich metasomatised granite and an average of 1244 ppm for all the eleven

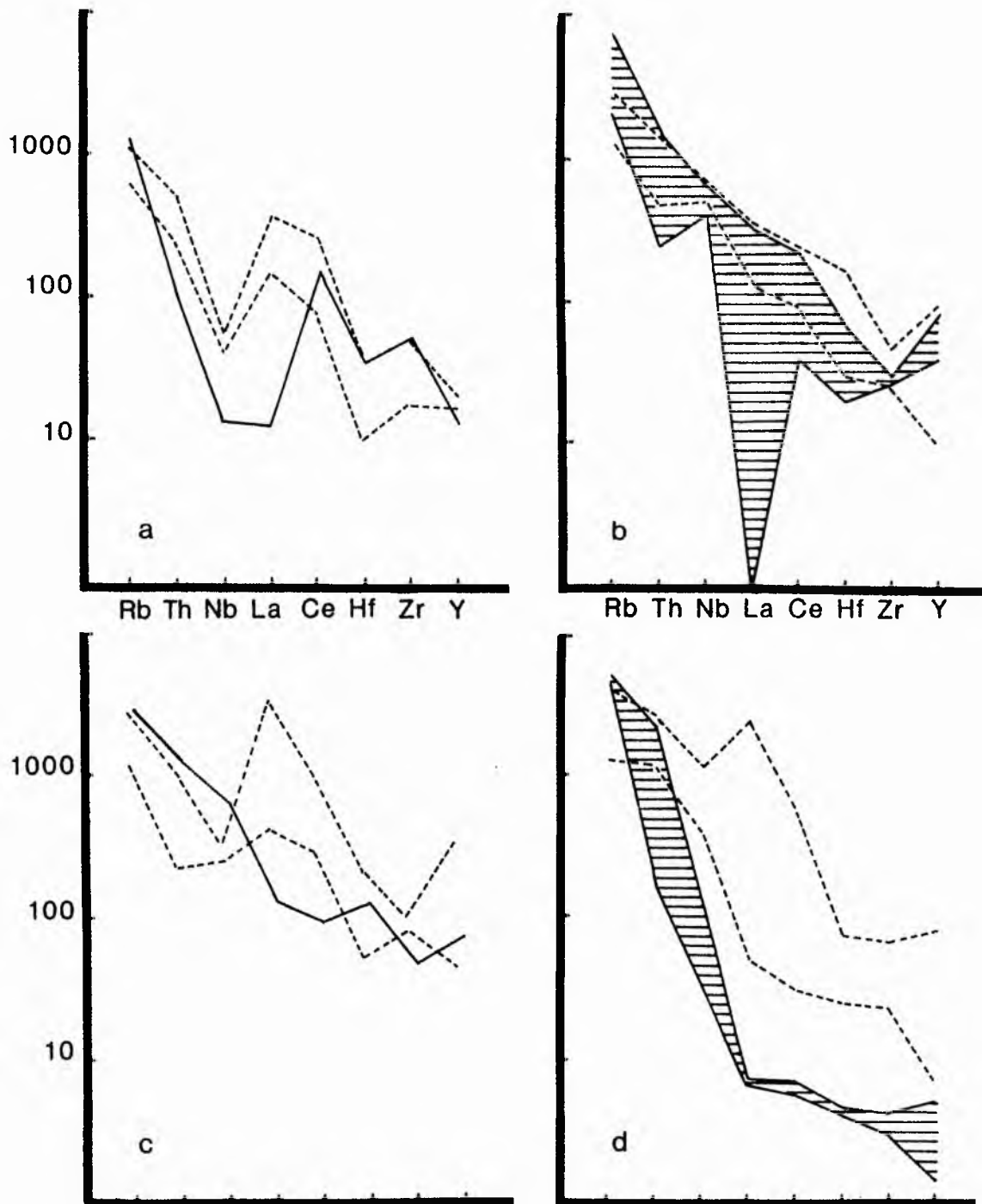


Fig 9.12 Chondrite-normalised trace element data of potash metasomatised rocks (shown as solid lines) compared with:  
 (a) basement monzogranites of Rishi  
 (b) Rishi biotite perthite granite  
 (c) quartz feldspar porphyritic ignimbrite  
 (d) biotite granite that had been sodic metasomatised  
 all shown as dotted fields within each diagram

(Chemical data for potash metasomatised samples from Table 9.16)

samples in Table 9.16. Similarly for Sr the increase was from an average of 5 ppm for 15 samples of the biotite granite to 68 ppm for the four most potash-enriched samples (Table 9.16) and an average of 59 ppm for the eleven potash metasomatised samples overall. More surprisingly there was a noticeable increase in Ni at this stage whatever the initial rock type, for example the average in 15 samples of biotite granite is 13 but in the potash metasomatised granite samples it is 32 ppm and overall for the potash facies it is also 32 ppm. It is not clear which mineral lattice is the host for this nickel.

Elements like Ba show a wide range in values with the highest content in the altered basement facies as expected. However, as with other facies there was no consistent variation so that potash metasomatised albitised facies contain between 0 and 57 ppm Ba and potash altered perthite granites contain between 0 and 117 ppm Ba. The Ba is almost certainly within the feldspar lattice although there is no correlation between feldspar abundance and Ba enrichment however, and the possibility remains that small quantities of barytes in the groundmass may have been missed.

The five samples that have been analysed for Mo, indicate that there was no major increase at this stage. An increase had been expected since molybdenite formed during the potash process in other complexes, notably Ririwai. There was however an overall increase in Pb, particularly in sample SS8/1 which must almost certainly contain traces of galena. This is unexpected as earlier studies did not indicate that Pb was introduced during potash metasomatism. Cr was totally removed at this stage, irrespective of the initial rock type and Cu levels remained low.

There was an increase in Sn at this stage, particularly in SS8/1 and enhanced levels of Zn although there was less overall than in the sodic metasomatised facies. This pattern of trace element variation has also been noted in other parts of the province.

Chondrite-normalised trace element assemblages are compared with the original rock types that have been metasomatised in Fig 9.12. The overall distribution of trace element abundance was dependent on the original rock type and the four graphs emphasise the different trace element assemblages. In the graphs (a), (b) and (c), the chondrite-normalised plot for the potash metasomatised rocks shows a similar - but depleted - pattern compared with the original rock. However, where potash metasomatism has overprinted sodic metasomatism the depletion in the trace element spectrum is most pronounced (Fig 9.12d).

## Acid metasomatism

### Introduction

Acid or "hydrogen ion" metasomatism was a widespread effect that may have been a disseminated process or may have occurred along distinct zones. As the name implies the hydrothermal alteration resulted from fluids that were progressively more acid in nature due to the gradual build up in  $H^+$  in the evolving fluid. Since the process may have affected all rock types it is hard to make any generalised statements relating to the chemistry of this process since there is

a wide variation in major, trace and ore element concentrations. These variations are reflected in the wide range of modal concentrations of the accessory minerals. Clearly such variations will be partly controlled by the chemical composition of the host rock that is being affected and partly by the extent of the earlier processes that have enhanced or depleted selected elemental concentrations. The geochemical trends therefore are grouped into several categories eg. acid metasomatised basement, altered volcanics etc. (Tables 9.17 - 9.22) and are discussed separately. However, there are often wide chemical variations within one group as well as between the various categories.

#### Altered basement

As described in the petrology section, two different mineralogical assemblages have been recognised:-

#### Ore-rich assemblage (Trend 1a)

All these samples come from the basement to the north of Dutsen Rishi and are close to the contact with the underlying biotite granite. The contact zone is richly mineralised and pits dug for the extraction of the ore, often expose the biotite granite roof. The rocks are coarse textured, mineralogically very variable and richly mineralised. They tend to be quartz poor when compared with the unaltered hornblende biotite basement monzogranite and this is reflected in both the modal and chemical analyses. The lower the silica content, the greater the ore enrichment. Chemically, as well as being low in silica these rocks contain negligible soda, due to feldspar alteration (Table 9.17). There was a considerable enrichment in iron, both due to the development of ore minerals and the growth of Li-Fe micas. There is also a high Ca content which reflects a large modal percentage of fluorite. It is envisaged that some of this calcium was liberated by breakdown of plagioclase in the monzogranite and that it combined with the fluorine in the fluids evolved from the biotite granite. The potash content is moderate due to the abundance of mica and microclinised feldspar.

It is in the modal analysis that the clue to the variable trace element chemistry lies. The combination of high Ce and  $P_2O_5$  particularly in SS93 reflects the abundance of monazite. However, the absence of Ce in SS57/4 which contains allanite, is surprising. The high La, Hf, Y and Th recorded for SS93 are probably in the monazite which forms both large tabular crystals and a meshwork of rosettes.

There was an increase in F in the three samples that were analysed. In addition to the formation of fluorite, some of the fluorine was almost certainly incorporated in the new mica. Such mica growth was also responsible for increased Li and is probably also host to other elements such as Cr, where there is an unusually high level.

High Cd in SS93 reflects the presence of greenockite (CdS) as a discrete phase in the accessory assemblage whilst high Be is due to traces of beryl.

Rb, since it followed K, was concentrated in both mica and feldspar. There is a varying proportion of these in the altered basement from zero feldspar to nearly 50% and from less than 10% mica to more than 50%. Rb fluctuations

Table 9.17 Acid metasomatised porphyritic older granite facies of the Rishi area

	Trend la						Trend lb	
	SS57/4	SS57/14	SS57/15	SS93	SS94	SS102	SS17/2	SS17/5
SiO <sub>2</sub>	71.54	70.86	52.25	47.80	62.06	65.00	70.66	55.41
TiO <sub>2</sub>	0.55	0.57	0.57	1.78	0.58	0.10	0.20	1.62
Al <sub>2</sub> O <sub>3</sub>	9.71	13.77	20.96	10.43	6.71	14.48	14.30	17.39
Fe <sub>2</sub> O <sub>3</sub>	11.85	4.20	9.92	22.04	12.90	5.58	2.37	7.21
MnO	0.24	0.05	0.09	0.25	0.12	0.06	0.02	0.11
MgO	0.39	0.42	0.46	0.40	0.34	0.41	1.46	3.46
CaO	0.60	0.78	1.37	10.00	0.96	1.67	1.23	4.54
Na <sub>2</sub> O	0.21	2.65	0.53	0.23	0.26	0.17	2.95	4.45
K <sub>2</sub> O	4.03	5.99	2.87	1.96	2.58	2.04	6.27	3.03
P <sub>2</sub> O <sub>5</sub>	0.45	0.18	0.33	3.33	0.08	0.01	0.04	0.63
H <sub>2</sub> O						1.60		
F <sup>-</sup>				2.80		1.93		0.90
F=O				-1.18		-0.81		-0.38
Total	99.57	99.47	89.35	99.84	86.59	92.24	99.50	98.37
R1	3436	2258	2357	2046	3099	3648	2128	1180
R2	274	374	581	1294	251	483	485	999
Q	297	171	195	97	269	292	149	45
F	68	28	19	-144	29	8	16	-160
Ba	237	772	92	432	0	0	1879	478
Be				11				65
Cd				150				
Ce	0	323	415	7938	89	70	67	262
Cr	0	0	0	0	0	0	0	97
Cu	251	78	1901		14666	70	25	0
F				28000		19300		9000
Hf	4	7	10	160	40	12	2	6
La	3	205	284	4326	80	39	51	101
Li				800		665		73
Mo				<14		<14		<14
Nb	129	32	36	200	31	4	15	26
Ni	80	17	16		52		8	24
Pb	4179	76	3723		128	15500	54	83
Rb	1934	383	1012	635	947	525	397	496
Sn				8100		850		108
Sr	180	110	211	666	23	47	245	342
Th	3	30	70	1916	114	45	13	42
V	42	23	18	0	29	9	18	164
W						<4		
Y	71	51	17	330	153	48	34	56
Zn	11292	1033	16999		42019	16800	270	883
Zr	270	410	290	1473	153	100	121	358
Zr/Hf	68	59	29	9	4	8	61	60
Ce/Y	0.00	6.33	24.41	24.05	0.58	1.46	1.97	4.68
quartz	46.7	42.8		0.9	2.9		33.8	8.4
perthite							26.4	54.0
microcl	0.1	29.9						
albite		18.0						3.4
clay min					6.6			
sericite							0.1	
biotite	6.7	0.2		39.5	30.8		23.3	29.6
chlorite	9.4	7.2		16.9	8.8		15.6	
fluorite	6.7	0.1		20.1	2.6			
sphaler	26.3			2.3	17.2			
cassit	0.1			2.5	0.3			0.6
chalcopy	1.2			7.9	28.8			
haematit	0.4	0.9		0.7	0.8		0.3	2.6
zircon	0.2	0.7		0.4	0.2		0.3	0.2
monazite	0.3			7.9	0.9			
sphene		0.1						
allanite	1.6			0.9				
apatite		0.1			0.2			1.2

however, do not directly correlate with K content. The chondrite-normalised plot of selected trace elements (Fig 9.13a) emphasises a wide range of values for most of the trace elements, particularly Ce, Th and La.

The basement signature of these rocks can only be partially recognised by the high Ba, La, Sr, Zr levels and low Nb levels. Thus although most of the samples are characterised by high Ba levels, there are two with zero Ba. There is no feldspar remaining in several of the samples with high Ba levels, which suggests that the barium must lie within the lattice of another mineral. The most obvious alternative would be biotite, but again there is no obvious correlation for all samples between biotite abundance and Ba concentration.

The ore elements Zn, Sn, Cu and Pb are locally very variable. All samples contain sphalerite, cassiterite, chalcopyrite and galena to some extent. However, the lack of direct correlation between element abundance in the chemical analysis and ore percent in the mode is a function of inhomogeneity in the samples.

#### Ore-poor assemblage (Trend 1b)

These are pale-coloured, fine-grained and micaceous samples which were originally basement, and which are believed to have suffered sodic metasomatism prior to acid alteration.

As with the samples of Group 1a there may have been a decrease in silica as a result of acid metasomatism, although there is a variation in most of the major elements. The two samples analysed are richer in MgO and Na<sub>2</sub>O but may also be more enriched in K than the ore-rich group.

The chondrite-normalised plot of selected trace elements (Fig 9.13b) is almost identical to that for unaltered basement and shows a much narrower range of variation than for samples in Group 1a.

There was no deposition of ore minerals and as a result the trace element concentrations are markedly depleted in Zn, Sn, Pb and Cu compared with Group 1a. The accessory mineral assemblage is limited to zircon, monazite and occasional cassiterite. However, the basement signature of high Ba, La, Sr, Zr together with low Nb levels can still be recognised.

In Part I of this thesis, using the Q-F multicationic plot, 4 different "trends" were recognised for acid metasomatism which could be correlated with known structural environments and known sequences of alteration: Trend 1 involved acid metasomatism of basement rocks.

The detailed petrography of this thesis however, shows that whilst Fig. 4.4 (page 76) is valid, it is an oversimplification. For example the earlier work only recognised one alteration trend for the basement rocks. In Fig 9.14 however, which shows the plotting position of the unaltered basement and hydrothermal variants, it is obvious that there are two trends for the basement on this diagram:-

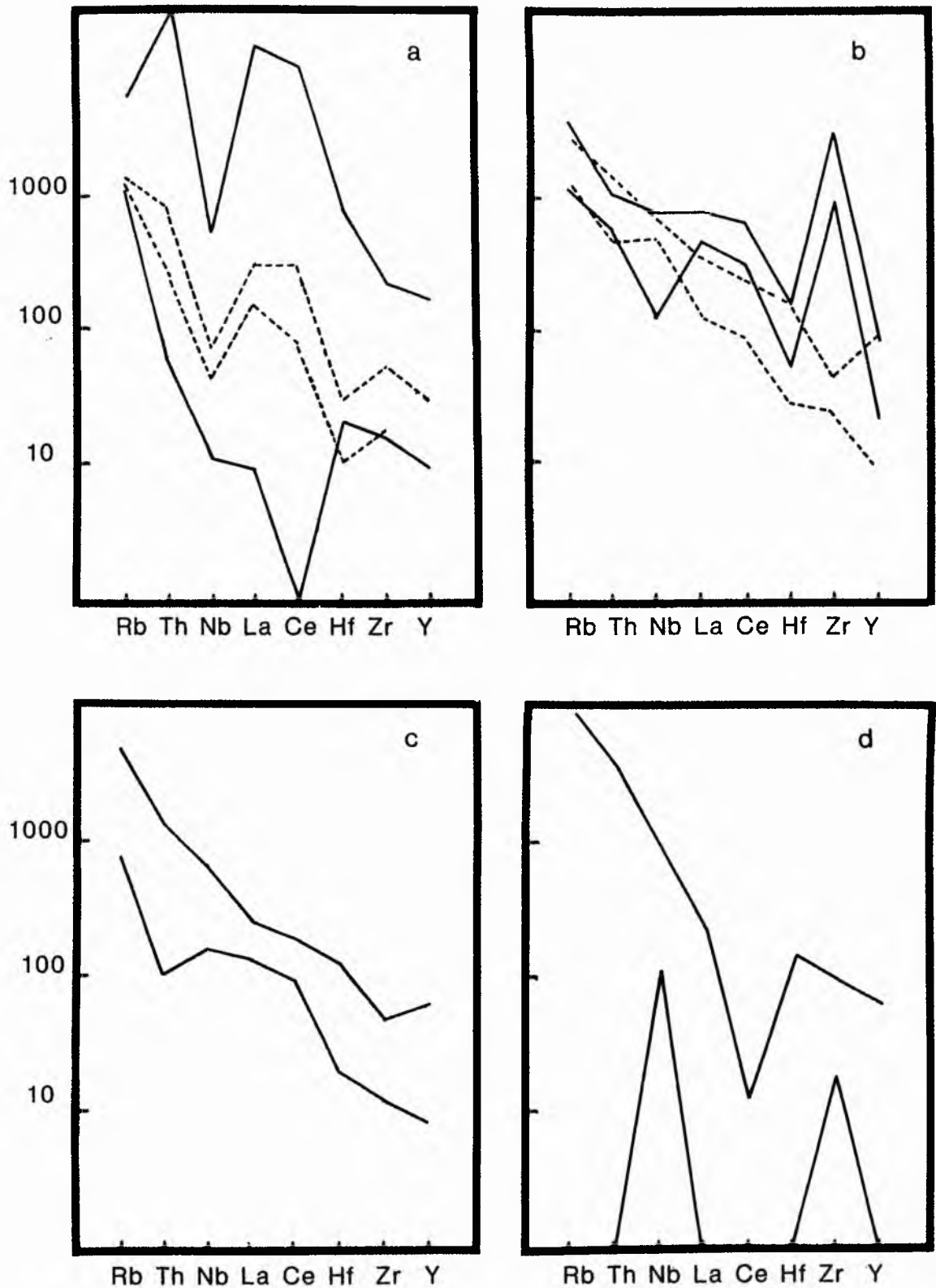
(i) the trend towards the albite pole

Fig 9.13 Chondrite-normalised trace element data for acid metasomatised rocks

- (a) basement monzogranites of Rishi
- (b) porphyritic volcanic rocks
- (c) sodic metasomatised granite
- (d) potash metasomatised granite

The dotted zone in (a) and (b) shows the range of elements for the equivalent unaltered rock type.

(Chemical data for acid metasomatised samples from Table 9.17)



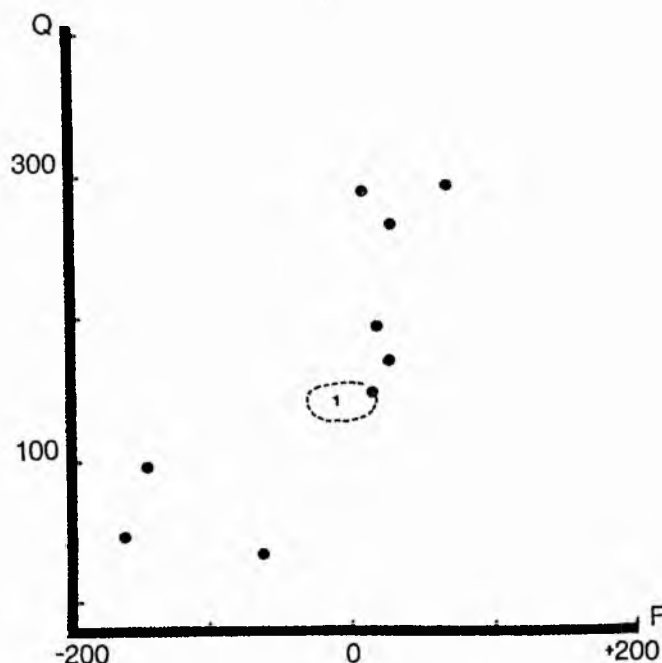
(ii) the trend towards the quartz pole

-In Part I of this thesis, the first trend was noted, but erroneously attributed solely to fluorite development on the assumption that the calcium had come from the basement. However, the trend towards the albite pole actually resulted from sodic metasomatism in some samples. Also the calcium enrichment cannot be solely attributed to the composition of the basement and thus this trend of cation metasomatism therefore should more correctly be regarded as Na + Ca metasomatism or/and fluorite development. Acid metasomatism may have overprinted the effect of sodic metasomatism so that the original abundance of albite is not distinguishable and has been masked by sericite development.

-The second trend of acid metasomatism of the basement with compositions plotting towards the Q pole has not been noted hitherto. It results from acid metasomatism of the basement hornblende granite that had either not been metasomatised or else affected by potash metasomatism.

Although two separate types of altered basement have been recognised in the petrographic section and also from trace element geochemistry, these two trends on the Q-F plot do not exactly coincide with the separate categories of Group 1a and Group 1b described in the earlier sections. Thus sample SS93 which resulted from acid metasomatism and is extremely ore enriched (Group 1a), plots with the samples that represent acid metasomatism superimposed on slight sodic metasomatism (Group 1b). The plotting position towards the albite pole has been determined by the high Ca content of the sample which has 20% fluorite.

Fig 9.14 QF plot of acid metasomatised samples of the basement monzogranite, relative to the field for unaltered monzogranite of the Rishi area. For explanation see text



## Volcanic rocks

Most, if not all the samples from the volcanic pile, together with both the samples of the feeder dyke, show some degree of alteration. In most cases the quartz remains as embayed phenocrysts and the feldspar shows varying degrees of alteration. Silica percentage in the altered volcanics remains very much the same as in lesser altered facies (Table 9.18) because the quartz phenocrysts of the volcanic rocks remain identifiable. It is in the groundmass that fluid reactions are observed; with increasing groundmass coarsening and mica development (SS150 and SS164) potash and iron values were enhanced and alumina values decreased due to mica growth and feldspar destruction. There was a sharp decrease in soda content as feldspar was destroyed. The high CaO content of SS173, the feeder dyke is rather unusual: since there is no fluorite it must occur in part in feldspar or may largely be accounted for by the abundant apatite in the sample.

Acid metasomatism of the volcanic pile has led to compositions which plot on the Q-F diagram well away from the general field of volcanic rocks shown in Fig 9.15. Samples which plot close to the general field for the volcanic rocks show only slight acid metasomatism which resulted in groundmass coarsening. In the more altered samples of SS164 and SS150 where there has been abundant biotite development in the groundmass the compositional trend is towards the microcline-quartz join.

Fig 9.15 QF plot of acid metasomatised samples of the quartz feldspar porphyritic ignimbrite (v) and feeder dyke (f) relative to the field for unaltered volcanics of the Rishi area. For explanation see text

(Chemical data for acid metasomatised samples from Table 9.18)

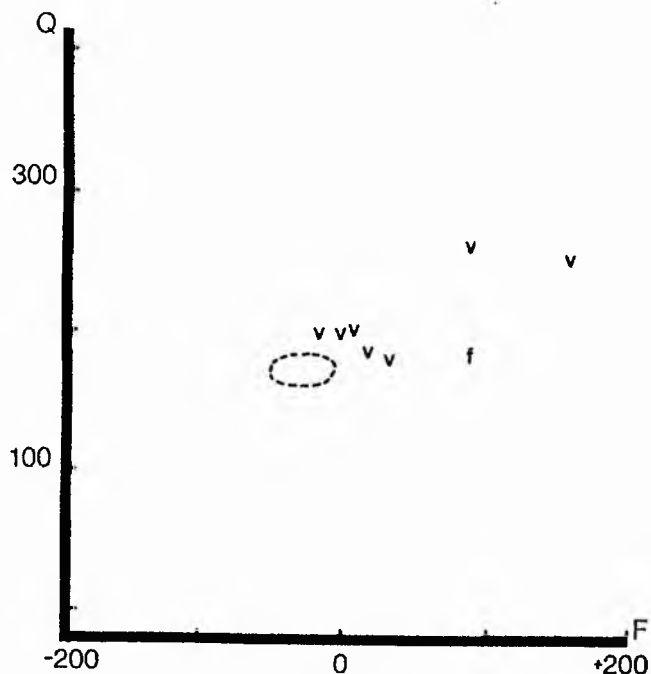


Table 9.18 Acid metasomatised volcanic rocks of the Rishi area

	volcanic pile			volcanic feeder	
	SS84	SS150	SS164	SS173	SS175
SiO <sub>2</sub>	74.75	75.93	75.49	62.73	74.94
TiO <sub>2</sub>	0.20	0.19	0.19	0.93	0.23
Al <sub>2</sub> O <sub>3</sub>	12.62	10.11	11.09	18.53	12.87
Fe <sub>2</sub> O <sub>3</sub>	2.66	5.82	4.34	3.32	0.80
MnO	0.03	0.03	0.06	0.05	0.02
MgO	0.09	0.09	0.04	1.66	0.02
CaO	0.42	0.31	0.12	2.94	0.85
Na <sub>2</sub> O	3.10	0.96	0.09	3.69	1.86
K <sub>2</sub> O	5.84	5.92	7.66	6.30	7.65
P <sub>2</sub> O <sub>5</sub>	0.01	0.02	0.05	0.37	0.04
F <sub>2</sub> O		0.26	0.53	0.39	
F=O		0.11	0.22	0.16	
Total	99.72	99.53	99.44	100.75	99.28
R1	2440	3181	3091	1288	2516
R2	297	236	232	760	344
Q	185	260	251	60	183
F	16	89	158	-38	87
Ba	0	0	12	1853	21
Be		8	306	14	
Ce	256	522	376	120	360
Cr	0	0	0	16	4
Cu	80	27	29	6	11
F		2600	5300	3900	
Hf	10	30	12	6	13
La	148	257	204	52	296
Li		84	912	36	
Mo		45	<14	33	
Nb	113	261	43	10	86
Ni	97	4	10	13	9
Pb	32	102	14	21	423
Rb	855	406	1299	453	606
Sn		27	67	27	
Sr	7	26	6	337	38
Th	52	28	43	11	21
V	0	0	2	102	0
Y	88	156	44	27	95
Zn	446	235	1676	162	1001
Zr	637	2009	672	341	668
Zr/Hf	64	67	56	57	51
Ce/Y	2.91	3.35	8.55	4.44	3.79
quartz		63.0	49.0	68.7	
feldspar		0.8	29.7	5.0	
biotite		34.2	18.6	3.0	
chlorite		1.2	0.7	0.8	
fluorite			0.1	0.8	
columbite			0.1		
other ores		0.6	1.7	20.8	
zircon				0.1	
monazite		0.2	0.1	0.1	
apatite				0.1	

When the trace element behaviour is compared with unaltered facies of the volcanic rocks, no clear pattern of element variation emerges from Table 9.18. Whereas there was an increase in elements like F and Ce, most elemental concentrations lie within the range for the volcanic pile as a whole and elements like Rb, Y and Nb may show an increase or a decrease.

In the most altered rocks (SS150 and SS164) the Zr/Hf ratio shows a moderate increase, due both to slight increases in Zr and slight decreases in Hf. The chondrite-normalised plot of selected trace elements (Fig 9.13b) contrasts with that of the "unaltered" volcanic rocks, most notably in the lack of La peak and the appearance of the Zr peak. No zircon appears in the modal analysis but it is almost certainly present as minute crystals within the small mica granules.

In comparing "altered" facies with "unaltered" facies of the volcanic rocks however, it is hard to escape the impression that there has been hydrothermal alteration of all the volcanic pile to a greater or lesser extent which would account for high levels of certain elements such as Zn in facies considered unaltered. Since both the feeder dykes have been altered it is not possible to discuss chemical changes that have taken place during hydrothermal metasomatism compared with unaltered samples of the same feeder dyke. When compared with 20 samples of feeder dykes in other Nigerian complexes however, most elemental concentrations lie more or less within the range as a whole. There was perhaps a tendency to slight depletion of many trace elements particularly Nb.

#### Acid metasomatised albite-rich facies

The intensity of the earlier sodic metasomatism was important in determining the relative concentrations of major and trace elements during acid metasomatism.

During sodic metasomatism there was an increase in Na, coupled with a decrease in Fe - as the original annitic mica was destroyed - and an overall decrease in silica. Potassium was not lost from the system after albitisation of the feldspars but was incorporated in zinnwaldite development.

The acid metasomatic process which was superimposed on sodic metasomatism continued the decrease in silica content more especially so in mica-rich samples. Potash levels however, remained much the same as in the albitised facies. Soda levels, whilst reduced by acid metasomatism, nevertheless remained the highest of any acid metasomatised rock and thus reflected the earlier process. In several cases the soda occurs in cryolite as well as in vestiges of albite.

Four samples in which acid metasomatism was superimposed on a sodic assemblage of minerals are plotted on the Q-F multicationic diagram as shown in Fig 9.16. Only one SS117/6 plots within the appropriate trend given in Fig 4.4. This is not surprising in view of the weak sodic metasomatism that occurred at Rishi. Other complexes discussed later, substantiate the trend II of Fig 4.4.

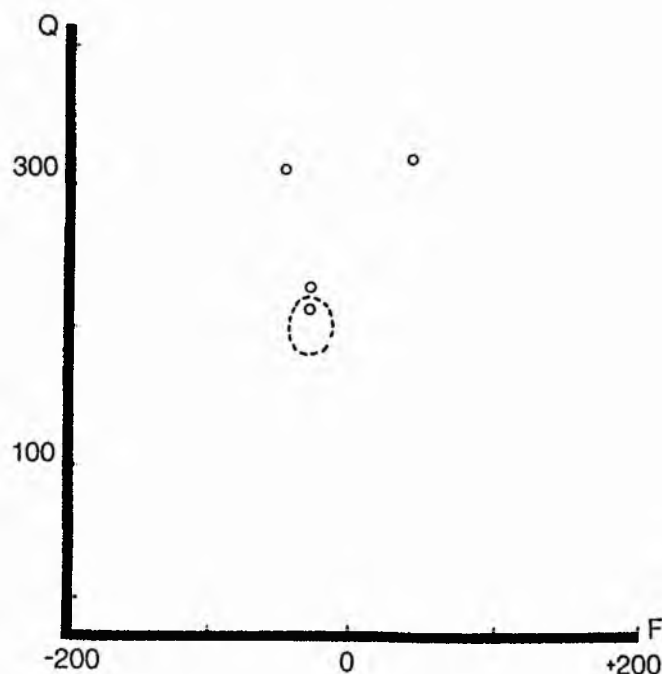
The trace element assemblage was often dramatically enhanced during sodic metasomatism, notably in elements like Nb and Rb. Elevated levels of Rb were further enhanced in some samples during acid metasomatism although there is no direct correlation between high Rb and K concentration. In contrast, in acid

Table 9.19. Acid metasomatised albite-rich facies of the Rishi area

	SS9/4	SS20/1	SS77	SS117/6
SiO <sub>2</sub>	75.85	58.51	77.06	63.87
TiO <sub>2</sub>	0.02	0.00	0.06	0.09
Al <sub>2</sub> O <sub>3</sub>	9.25	17.21	11.86	11.98
Fe <sub>2</sub> O <sub>3</sub>	8.29	3.24	1.82	16.42
MnO	0.10	0.03	0.02	0.00
MgO	0.25	0.20	0.02	0.24
CaO	0.17	0.24	0.33	0.37
Na <sub>2</sub> O	0.77	1.79	3.60	1.12
K <sub>2</sub> O	3.49	1.75	4.49	3.34
P <sub>2</sub> O <sub>5</sub>	0.00	0.03	0.01	0.00
H <sub>2</sub> O	1.00			
F <sup>-</sup>	0.93		0.35	
F=O	0.39		0.15	
Total	99.73	83.00	99.47	97.43
R1	3753	2770	2756	3441
R2	212	373	269	287
Q	319	226	212	313
F	46	-25	-27	-43
Ba	0	0	0	0
Be			8	
Ce	124	80	124	168
Cr	0	0	0	0
Cu	118	6631	11	15
F	9300		3500	
Hf	4	25	6	20
La	55	42	77	83
Li	2146		250	
Mo	<14		<14	
Nb	133	55	214	126
Ni	<10	16	8	21
Pb	33	876	46	1285
Rb	1558	271	802	1668
Sn	60		81	
Sr	4	5	4	38
Th	49	5	65	64
V	5	0	0	1
Y	75	16	121	84
Zn	793	51782	361	158
Zr	91	82	197	320
Zr/Hf	23	3	33	16
Ce/Y	1.65	5.00	1.02	2.00
quartz	57.3	40.4	54.0	
microcl/perth	8.4	3.3	3.7	
albite	4.2	0.3	4.1	
biotit/seric	28.4	37.8	33.6	
chlorite	0.3	5.2	0.7	
topaz	0.3	0.2	0.1	
fluorite	0.7	0.5	0.2	
sphalerite		10.7	0.5	
chalcopryrite		1.2		
haematite	0.1	0.2	0.2	
zircon	0.1	0.1	0.2	
monazite	0.1	0.1	0.1	
cryolite			2.5	
columbite	0.1			
thorite			0.1	

Fig 9.16 QF plot of acid metasomatised albite-rich samples relative to the field of biotite granite

(Chemical data from Table 9.19)



metasomatised facies there was a decrease in Nb; there was also an overall decrease in Th, Y and Zr (Fig 9.13c). However the increase in Ba noted during sodic metasomatism was not continued during the acid process and Ba was removed completely. In the acid metasomatised samples Ce, Hf, La, Ni, Sn and Mo levels remained the same as in the albitised facies, Cr levels continued to be consistently low; F and Li increased due to higher modal proportions of mica; Cu, Pb and Zn were notably increased due to the development of ore minerals.

#### Acid metasomatised microcline-rich facies

Again the intensity of the earlier potash metasomatism was important in determining the geochemistry of the elements during this process.

During the earlier potash metasomatism, there was a marked increase in K and Al, and a decrease in Na, Ca and Fe. There was also a decrease in silica concentration to as low as 57% SiO<sub>2</sub>, when potash metasomatism was intense. This silica depletion that was initiated in the earlier stage, was further depleted during acid metasomatism, the depletion was to 35% in an almost monomineralic mica rock (SS44/1). Soda and CaO concentrations were also further depleted whilst there was also a reduction in K content. There was a tendency for Al to decrease during acid metasomatism, except in samples where the earlier potash process was extreme and high levels of Al were introduced at the potash stage. There was an overall increase in iron content during acid metasomatism, due to the formation of lithium-iron micas.

The plotting position of these four samples on the Q-F multicationic diagram (Fig 9.17), is dependent on the intensity of the earlier process so that where microclinite formation was followed by acid metasomatism the plotting position

Table 9.20. Acid metasomatised microcline-rich facies of the Rishi area

	SS8/3	SS44/1	SS54/2	SS117/5a
SiO <sub>2</sub>	62.91	35.39	72.51	54.20
TiO <sub>2</sub>	0.00	0.33	0.06	0.10
Al <sub>2</sub> O <sub>3</sub>	13.77	19.90	12.58	9.70
Fe <sub>2</sub> O <sub>3</sub>	13.05	31.95	5.43	27.30
MnO	0.31	0.26	0.05	0.31
MgO	0.07	1.12	0.10	0.02
CaO	0.00	0.30	0.03	0.12
Na <sub>2</sub> O	0.00	0.72	1.18	0.11
K <sub>2</sub> O	5.62	9.47	7.60	5.85
P <sub>2</sub> O <sub>5</sub>	0.02	0.02	0.00	0.00
H <sub>2</sub> O	1.76			
F	0.10	3.08		1.30
F=O	0.04	1.29		0.55
Total	97.57	101.25	99.54	98.46

R1	2548	-920	2495	1516
R2	274	478	255	204
Q	229	-31	202	171
F	119	172	123	119

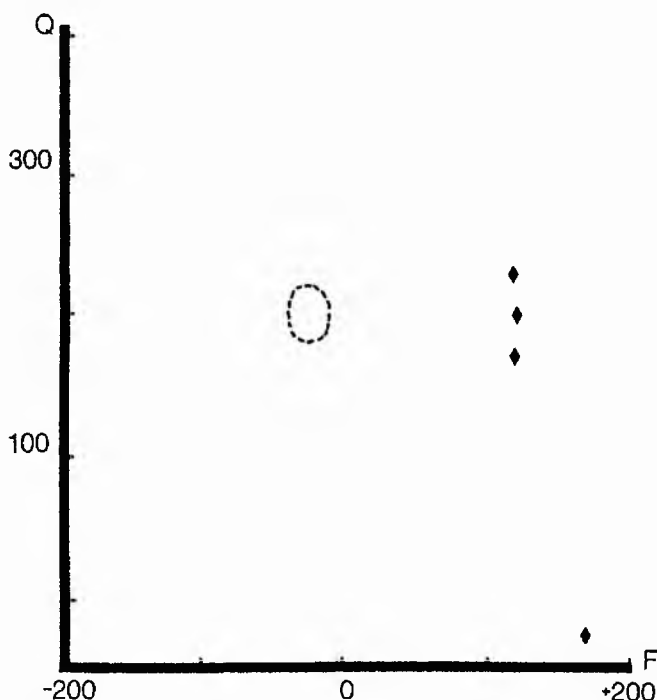
Ba	0	92	46	0
Be		3		6
Ce	11	0	112	130
Cr	10	0	0	0
Cu	23	0	19	
F	1000	30800		13000
Hf	20	0	4	29
La	0	0	72	71
Li	4543	1748		2160
Mo	<14	<14		39
Nb	38	252	188	296
Ni	0	0	53	
Pb	245	22	34	2059
Rb	2647	2802	1642	3309
S	400			
Sn	1220	27		6900
Sr	2	19	1	70
Th	0	25	78	173
V	3	0	4	0
Y	0	18	40	122
Zn	1059	1726	438	
Zr	622	132	198	550
Zr/Hf	31	*	50	19
Ce/Y	*	0.00	2.80	1.07

\* Hf or Y = 0

quartz	0.8			35.9
feldspar				0.3
biotite	98.0			61.2
chlorite	0.1			
fluorite	0.1			0.2
cassiterite	-0.1			1.2
haematite	0.5			0.5
zircon	0.3			0.6
monazite	0.1			0.1

Fig 9.17 QF plot of acid metasomatised microcline-rich samples, relative to the field of biotite granite

(Chemical data from Table 9.20)



lies close to the mica pole. Where desilication did not occur during potash metasomatism, the subsequent acid assemblage composition plots towards the microcline-quartz join.

During potash metasomatism there was a decrease of some trace element concentrations when compared with the average for biotite granites and particularly when compared with sodic metasomatism. Thus Nb, Th and La showed a decrease compared with the sodic facies. During acid metasomatism however, there is no obvious trend compared with the potash process:-

	potash mean	acid range	mean
Nb	136	38-296	196
Th	50	0-173	69
La	43	0- 72	36

and values for all three elements may show enrichment or impoverishment. Such contrasts are emphasised by a comparison of values for SS44/1 and SS117/5a where the mineralogy is identical and only the modal proportions of quartz and mica differ. Ideally, highest trace element concentrations would be expected in the more micaceous sample, SS44/1, rather than in the more quartz-rich sample, SS117/5a, but this is not the case.

There is a similar wide variation in Ba content with concentrations from 0-92 ppm. In the potash facies, Ba was tentatively ascribed to occurrence in the feldspar lattice although it was noted that there was no correlation between feldspar abundance and Ba enrichment. In the acid metasomatised samples however,

The equations on the ensuing pages are not necessarily balanced. They are approximate equations essentially for disequilibrium reactions.

the highest Ba concentration is in the monomineralic mica rock so the Ba must be within the mica lattice.

There was an increase in F during acid metasomatism and this must also be located within the mica structure since fluorite and topaz occurrence is negligible in these samples.

Despite the overall decrease in K compared with the earlier potash metasomatised facies, there was a marked increase in Rb but an overall decrease in Sr except in SS117/5a. During potash metasomatism, there was an increase in Rb from an average of 664 ppm in the biotite granites to an average of 1367 ppm in the K metasomatised facies. This was elevated to an average of 2600 ppm during this stage of acid metasomatism.

During the process of acid metasomatism there was an overall decrease in Y with a wide range of values from 0-122ppm and a wide variation in Ce from 0-130 ppm with sample SS117/5a having highest enrichment of both elements. The chondrite-normalised plot of selected trace elements (Fig 9.13d) substantiates the wide variability in Th, Hf, La and Ce in addition to Y.

As regards the ore minerals there are comparisons and contrast with the potash facies. Cu remains low, Pb and Sn appear less enriched, whilst there was a slight increase in Zn and possibly Mo.

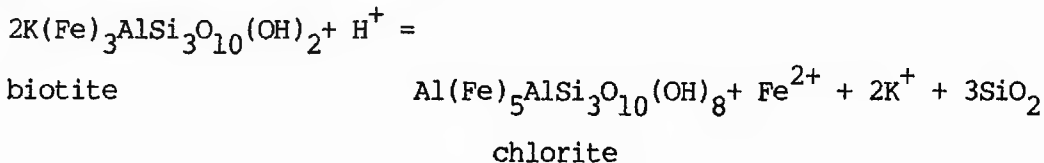
Therefore, although some chemical trends can be established there are some elements that show increases or decreases compared with the earlier potash metasomatism and these elements may exhibit wide ranging concentrations.

#### Biotite perthite granite

During acid metasomatism of the Rishi biotite granite there were a series of stages that have been recognised depending on the percentage of feldspar, chlorite, sericite, biotite and topaz that are present in the mineral assemblage.

During the first stage of alteration there was a progressive chloritisation of the mica and also of the perthite, according to the equations:-

chloritisation of biotite: Eq. 1



chloritisation of microcline/perthite Eq. 2

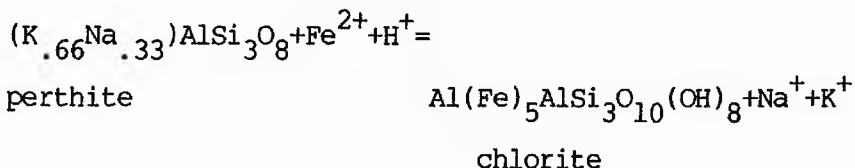
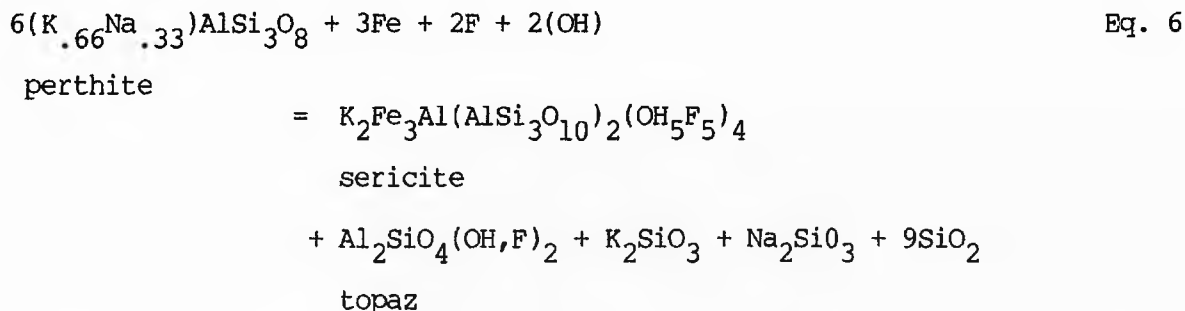




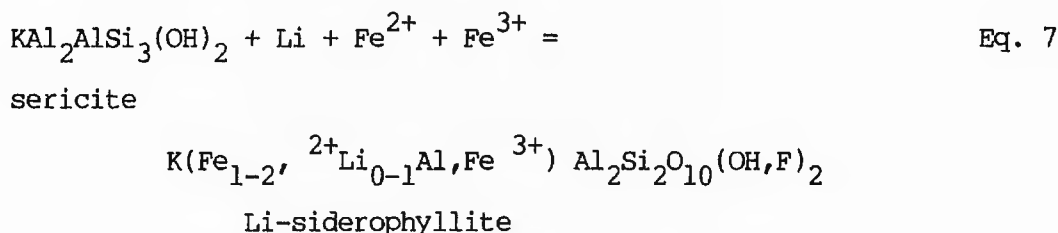
Table 9.21. Acid metasomatised Rishi biotite perthite granite

	average Rishi bg	Stage 1 SS12/3	SS12/4	Stage 2 SS16/6	SS18/1	SS35/2	SS109A	Stage 2-3 SS106A	SS109B
SiO <sub>2</sub>	76.85	76.31	74.36	54.11	84.70	75.13	66.20	73.50	58.50
TiO <sub>2</sub>	0.05	0.01	0.00	0.07	0.09	0.05	0.10	0.10	0.10
Al <sub>2</sub> O <sub>3</sub>	12.40	12.93	10.23	18.96	4.04	8.02	14.27	8.50	13.47
Fe <sub>2</sub> O <sub>3</sub>	1.56	1.61	0.83	13.95	7.54	6.87	7.48	6.29	2.61
MnO	0.03	0.18	0.08	0.15	0.06	0.15	0.08	0.09	0.03
MgO	0.08	0.24	0.25	0.04	0.01	0.11	0.39	0.04	0.23
CaO	0.39	0.57	0.61	0.51	0.45	0.33	1.25	0.78	1.22
Na <sub>2</sub> O	3.69	3.65	0.00	0.51	0.12	0.00	0.17	0.33	0.17
K <sub>2</sub> O	4.71	4.96	3.09	1.49	0.70	3.20	2.09	2.95	0.67
P <sub>2</sub> O <sub>5</sub>	0.01	0.01	0.03	0.03	0.03	0.00	0.01	0.01	0.01
H <sub>2</sub> O	0.36				1.20		1.07	2.41	0.88
F	0.36	0.31	0.56		0.14		1.60	0.43	1.80
F=O	0.15	0.13	0.24		0.06		0.67	0.18	0.76
Total	100.43	100.65	89.80	89.82	99.02	93.86	94.04	95.25	78.93
R1		2568	4207	2721	5241	4080	3668	3927	3609
R2		278	278	429	128	198	433	252	406
Q		232	339	246	445	344	302	325	290
F		89	55	6	3	62	17	38	-13
Ba	7	0	0	0	0	6	14	0	0
Be			5				7	5	6
Ce	124	132		190	156	187	86	79	73
Cr	3	0	0	1	0	0			
Cu	10	5	39	662	1194	36	84	36	122
F	3560	3100	5600		1400		16000	4300	18000
Hf	11	8	5	7	13	5	9	11	22
La	71	76		56	55	89	49	39	41
Li	136	28	500		1438		512	251	591
Mo	<14	17	44		<14		<14	<14	<14
Nb	200	174	134	61	168	116	6	77	2
Ni	13	4	0	2	6	36			
Pb	46	150	3396	2101	139	6261	20000	10900	41000
Rb	664	479	676	568	375	683	426	647	84
S					13700				
Sn	70	67	7540		330		840	1620	190
Sr	5	3	48	6	12	221	54	6	97
Th	47	29	38	51	41	39	49	36	25
V	3	4	3	6	5	0	10	0	3
W						<4	<4	8	
Y	133	150	131	74	129	66	27	131	11
Zn	327	367	1944	28523	16800	3822	13500	17300	21600
Zr	225	188	143	148	326	147	122	126	61
Zr/Hf	20	24	29	21	25	29	14	11	3
Ce/Y	0.93	0.88		2.57	1.21	2.83	3.19	0.60	6.64
quartz		29.0			71.0			46.3	
perth		64.4							
albite		1.9							
biotite		0.6							
sericite							12.6		
chlorite	3.8			27.8			39.5		
topaz					0.1			0.3	
fluorite	0.3			0.1			0.1		
sphaler					0.8			1.0	
chalcopy				0.1					
haematit							0.1		
monazite							0.1		
beryl					0.1				

destabilisation of any remaining perthite to sericite and topaz according to the reaction of Nockolds and Richey (1939), assuming no alumina was added or removed:



The alteration assemblage consists of quartz-chlorite-sericite and stage 4 was reached when sericite dominated over chlorite. The analytical data for eight samples representing stage 4 of acid alteration is given in Table 9.22. At this stage silica was decreased (except in SS20/4), alumina may have increased or decreased, iron increased dramatically (except in SS20/4), whilst potash levels remained similar to earlier stages. During stage 4, abundant topaz developed as chlorite disappeared from the assemblage. Ultimately large discrete flakes of a trioctahedral Li or Li-Fe mica developed from the sericite, and the modal percentage of topaz decreased as the new mica developed indicating that the fluoroaluminosilicate was taken into the mica lattice. A possible equation for siderophyllite development from sericite could be:-



For the trace elements, many elemental abundances such as those of Ba, Ce, Cr and Hf did not change in concentration as acid metasomatism continued. Elements such as Zr and La show quite a variation (Fig 9.18b). Li and Rb increased, whilst Nb and Y decreased in abundance. The ore minerals were still at elevated concentrations although Pb values are lower than in the samples which showed less acid metasomatism (Stage 1-2).

During stage 5, topazification of mica (Li-siderophyllite) resulted in the release of silica in the reverse of equation 7:-

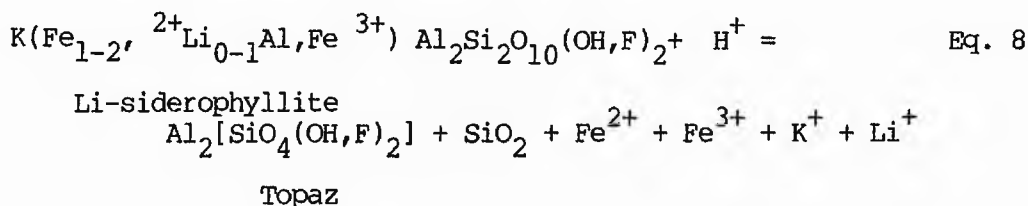


Table 9.22. Acid metasomatised Rishi biotite perthite granite

	Stage 4							Stage 5		Dissem
	SS11/8	SS20/4	SS23/6	SS81	SS95	SS96	SS106B	SS106C	SS109C	
SiO <sub>2</sub>	61.28	76.46	67.70	57.16	71.63	42.46	61.26	63.87	65.10	55.32
TiO <sub>2</sub>	0.12	0.00	0.21	0.08	0.35	0.23	0.04	0.09	0.10	0.07
Al <sub>2</sub> O <sub>3</sub>	12.21	10.91	7.67	13.88	12.14	30.52	12.11	11.98	16.41	18.48
Fe <sub>2</sub> O <sub>3</sub>	15.05	1.87	16.46	19.11	7.44	6.47	5.38	16.42	0.67	12.42
MnO	0.22	0.02	0.30	0.21	0.06	0.16	0.07	0.24	0.01	0.15
MgO	0.04	0.42	0.01	0.15	0.69	0.56	0.18	0.37	0.06	0.42
CaO	0.34	0.18	0.34	0.12	0.60	0.12	0.79	1.12	2.09	0.20
Na <sub>2</sub> O	0.17	0.76	0.14	0.12	0.00	0.18	1.87	0.00	0.17	3.64
K <sub>2</sub> O	4.74	1.11	4.32	6.10	2.14	2.20	5.27	3.34	0.19	7.02
P <sub>2</sub> O <sub>5</sub>	0.02	0.00	0.00	0.03	0.09	0.01	0.01	0.00	0.25	0.00
H <sub>2</sub> O	0.58		1.12				3.60		0.35	
F <sup>-</sup>	0.12		0.16				0.57	0.73	2.40	0.93
F=O	0.05		0.07				0.24	0.31	1.01	0.39
Total	94.84	91.73	98.36	96.96	95.14	82.91	90.91	97.85	86.79	98.26
R1	2568	4514	3030	1857	4739	2081	2047	3058	4210	438
R2	278	254	187	293	337	639	331	373	549	404
Q	232	373	275	182	400	181	158	270	326	38
F	89	-4	81	124	35	39	37	51	-39	28
Ba	14	0	17	12	4	336	0	31	0	108
Be								5	2	632
Ce	162	92	156	120	46	28	60	129	169	197
Cr	7	0	4	0	0	0	0	0	0	0
Cu	46	5686	0	463	403	510	3105	15	104	125
F	1200		1600				5700	7300	24000	9300
Hf	3	27	4	3	11	10	18	6	13	1
La	57	38	61	53	67	41	226	81	98	85
Li	2844		1854					362	186	1363
Mo	<14		<14				<14	<14	<14	<14
Nb	228	61	164	161	37	29	16	119	10	204
Ni	6	28	4	165	28	33	14	2		93
Pb	1530	2060	334	609	212	65	1435	584	7127	460
Rb	1985	332	1925	2724	825	1108	497	881	24	2196
S										
Sn	8060		100				216	3510	19400	2227
Sr	64	3	0	23	33	39	4	35	436	29
Th	311	0	128	51	137	36	0	30	140	63
V	5	0	9	0	38	30	0	7	3	0
W							<4			
Y	55	13	98	84	25	22	57	127	2	173
Zn	1946	51393	1175	5326	598	1067	49442	1787	8200	1932
Zr	140	63	223	167	155	158	96	222	90	191
Zr/Hf	47	2	56	56	14	16	5	37	7	191
Ce/Y	2.95	7.08	1.59	1.43	1.84	1.27	1.05	1.02	84.50	1.14
quartz		60.3	66.7		42.8	67.4	32.8	9.4	64.4	
perthite		0.8		0.4		19.1	24.8			
albite							0.3			
biotite			31.8		40.4	29.3			0.9	
sericite 24.3						38.1	21.5			
chlorite 1.8					0.2	1.8	42.8	1.2		
topaz		0.8			14.8	1.0			28.8	
fluorite			0.2		0.4	0.2	1.0	1.0	0.2	
sphalerite		10.3					6.8	0.1	2.2	
cassiterite		0.3	0.2			0.1			2.2	
chalcopyr		2.1								
haematite			0.2		1.2	1.8			0.2	
zircon		0.1	0.1				0.1	0.1		
monazite								0.3		

At this latest stage of acid metasomatism, the ore elements were less abundant, with the exception of Sn (Table 9.22). This stage was characterised by high alumina and fluorine levels due to abundance of topaz. No explanation at this stage is offered for the unusually high Sr content of SS109C. The chondrite-normalised plot of selected trace elements (Fig 9.18b) confirms the wide range of concentrations particularly in Rb, Th and Y during the later stages of acid metasomatism.

On the Q-F multicationic diagram (Fig 9.19), acid metasomatism of a perthite granite resulted in compositions which plot towards the silica pole. If there has been a trace of an earlier potash metasomatism there may be a slight displacement towards the microcline pole. Nevertheless, the plotting positions of these rocks occupy a distinctive field. There does not seem to be any clear distinction however, between early stages of alteration i.e. the Stages 1-3 and the later stages 4-5. This is due to the wide variations in major element chemistry at each stage with varying proportions of quartz and chlorite/sericite.

Fig 9.19 QF plot of acid metasomatised biotite perthite granite relative to the field of "unaltered" biotite granite

(Chemical data from Tables 9.21 & 9.22)

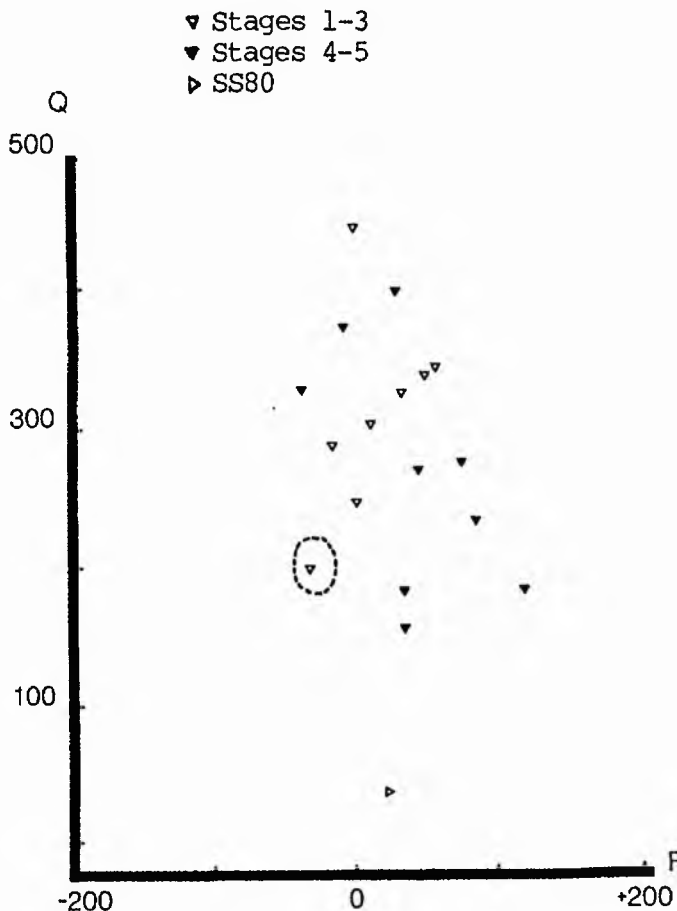
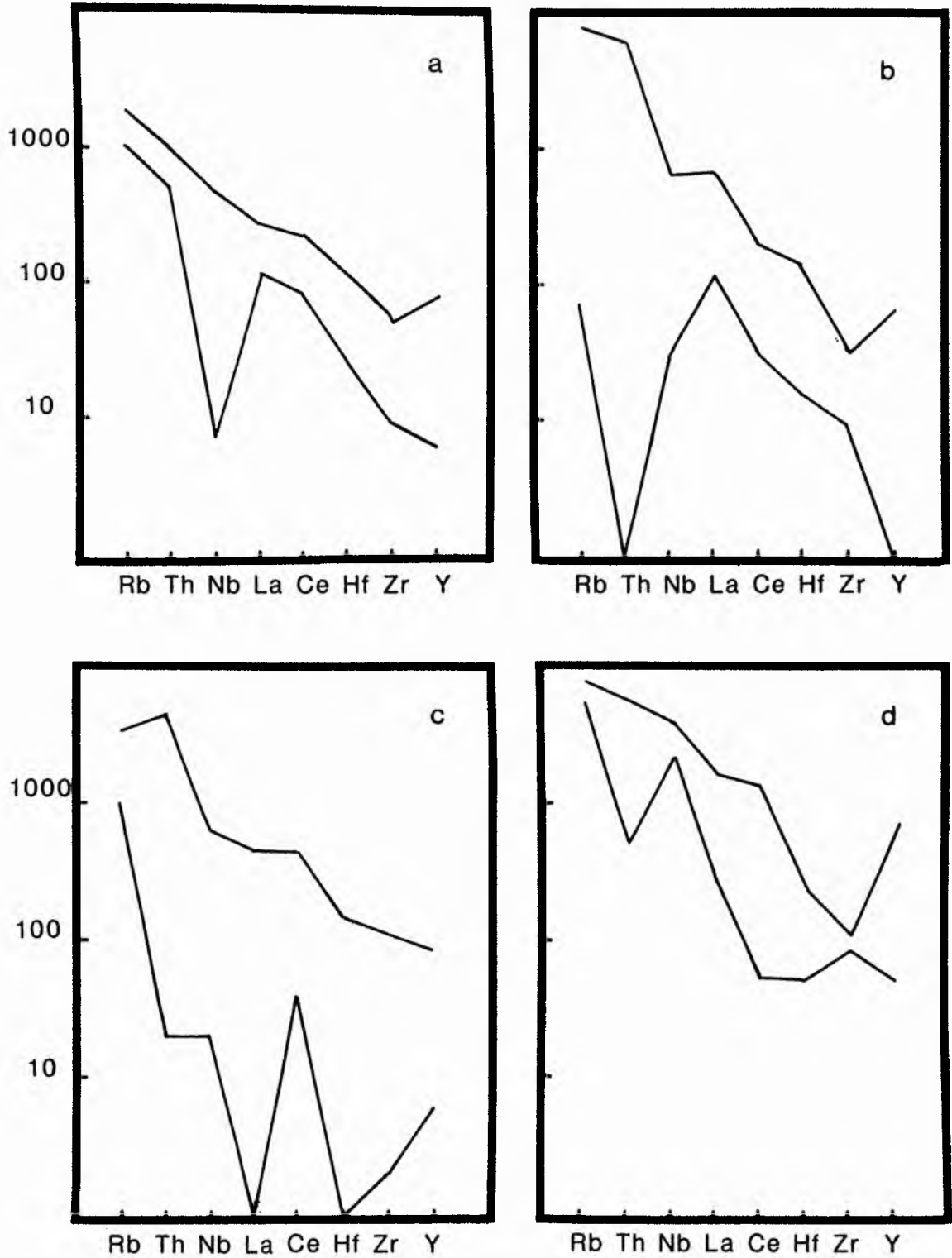


Fig 9.18 Chondrite-normalised trace element patterns for:

- (a) acid metasomatised biotite perthite granite, Stages 1-3
- (b) acid metasomatised biotite perthite granite, Stages 4-5
- (c) silica metasomatised samples
- (d) late-stage alteration processes.

Details are discussed in the text.



For SS80 which represents a disseminated acid metasomatism, all the various stages of alteration are recorded within the biotite granite. There was a decrease in silica content balanced by an increase in alumina, iron and potash, whilst soda content remained much as in an unaltered biotite granite due to the fact that not all feldspar was destroyed. In the Q-F multicationic plot (Fig 9.19), the displacement towards the mica-albite join suggests that there may have been both sodic and potassic metasomatism prior to the acid alteration. For SS80 (Table 9.22), the trace element concentrations of Ce, Cr, Hf, La, Nb, Rb, Th, Y and Zr in the acid metasomatised sample are similar to the biotite granite whereas increased F, Li and Rb values are characteristic of acid metasomatism. Higher niobium levels probably represent the earlier imprint of sodic metasomatism. Very high Be content is due to the abundance of genthelvite in the cupola of the granite pluton. Such high Be concentrations are only found in the top 30 metres of the cupola zone. The reason for the high Ba content is not known.

## Discussion

In Part 1 of this thesis, in addition to rocks that had undergone sodic or potassic metasomatism there were four different "trends" recognised for acid metasomatism which could be correlated with known structural environments and known sequences of alteration (Fig 4.4, page 76). These different trends were shown on a Q-F plot.

Trend 1 involved acid metasomatism of basement with a trend towards the albite pole.

Trend 11 defined a process of acid metasomatism overprinting a sodic effect

Trend 11 was defined as vein-controlled acid metasomatism

Trend 1V was considered as pervasive acid metasomatism.

The detailed petrography of this chapter confirms that these trends exist at Rishi. In addition however, this work has shown that there are several mineralogical assemblages that were not previously recognised and that whilst Fig 4.4 is valid, it is an oversimplification.

During acid metasomatism there was a wide variation in major and trace element chemistry and an attempt has been made to correlate the chemistry of a particular process against that of the original rock. However, the mineralogy is so inhomogeneous that it leads to inconsistencies such that a thin section which contains allanite but no Ce appears in the analysis. Normally, bulk samples overcome such problems of geochemical analyses but the very nature of these localised and sometimes small patches of alteration means that it is frequently impossible to produce bulk powders. Despite these problems it has been possible to make a number of correlations and conclusions. The following processes have been recognised:-

(i) acid metasomatism of basement granitoids

(ii) acid metasomatism of the volcanic feeder dyke and volcanic pile

(iii) acid metasomatism overprinted on albitised rocks

(iv) acid metasomatism overprinted on microclinised rocks

(v) acid metasomatism of biotite perthite granite in various stages to produce a series of different mineralogical assemblages with progressive metasomatism.

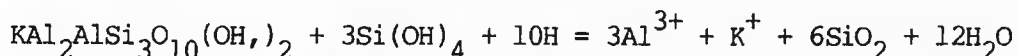
A further possibility exists of the acid metasomatism overprinting a previous Na + K alteration and if the acid metasomatic process was overprinted on these two previous processes then this might explain why some trace element abundances are extreme (unusually low or high).

It is important to note that the trend toward the quartz pole on the Q-F diagram during acid metasomatism is not due to silicification. Because the Q-F plot is a multicationic diagram, the overall trend towards the Q pole is due to an overall decrease in the (K+Na+2/3Ca) expression which determines the position on the y-axis. The trend is therefore due to the reduction in alkali elements at this stage rather than to an increase in silica although some samples do show a trend towards silicification in the later stages of acid metasomatism.

#### Silica metasomatism

The increase in quartz during the late-stage silicification process followed on from acid metasomatism and lead to the obvious increase in silica. Thus as equations 1,5 and 6 indicate there was a release of silica during the chloritisation of biotite, during sericitisation of perthite and as a result of the topazification of mica. Silicification is often favoured by high pH as in the equation for silicification of sericite by Meyer and Hemley (1967):-

Eq. 9



although a high aqueous silica activity is of course implicit. This increase in silica was coupled with a decrease in all the other major elements. However, there wasn't the marked decrease in all the trace elements during silicification that had been noted in earlier publications on other complexes.

On the Q-F multicationic plot (Fig 9.20), silica metasomatism resulted in compositions which plot close to the Q pole. This trend towards the Q pole continued the trend developed during acid metasomatism as alkali elements were removed by acid-enriched fluids. The increased silica concentrations were balanced by further alkali element reductions, most notably in soda (Table 9.23). In fact the Na<sub>2</sub>O content is negligible and was almost completely removed since there is no vestige of feldspar remaining in these samples. TiO<sub>2</sub>, MnO, MgO and P<sub>2</sub>O<sub>5</sub> concentrations did not change from biotite granite values and CaO content was only slightly decreased. K<sub>2</sub>O and Al<sub>2</sub>O<sub>3</sub> values are proportionately decreased and are dependent on the abundance of mica. Fe<sub>2</sub>O<sub>3</sub> values reflect the development of haematite both along mica cleavages where mica occurs, or as a coating on quartz grains to give a reddened coloration. On the Q-F multicationic diagram the analyses inevitably plot towards the quartz pole, overlapping the field of the latest phases of acid metasomatism.

To a certain extent trace element abundance also reflects mica percentage

Table 9.23 Silica metasomatised samples of the Rishi area

	SS97	SS98	SS99	SS117	SS117/5
SiO <sub>2</sub>	91.70	80.15	92.78	85.60	90.90
TiO <sub>2</sub>	0.08	0.05	0.43	0.10	0.10
Al <sub>2</sub> O <sub>3</sub>	3.54	7.17	2.92	2.77	1.20
Fe <sub>2</sub> O <sub>3</sub>	3.15	8.11	2.92	6.39	3.40
MnO	0.05	0.08	0.03	0.10	0.00
MgO	0.08	0.43	0.24	0.01	0.05
CaO	0.16	0.12	0.16	0.30	0.02
Na <sub>2</sub> O	0.00	0.00	0.00	0.23	0.24
K <sub>2</sub> O	1.36	2.94	0.94	1.51	0.15
P <sub>2</sub> O <sub>5</sub>	0.00	0.01	0.06	0.01	0.81
H <sub>2</sub> O				0.51	
F <sub>2</sub>				0.70	
F=O				0.29	
Total	100.12	99.06	100.48	97.94	96.87
R1	5706	4444	5873	5101	5843
R2	91	175	86	87	28
Q	477	380	492	431	493
F	26	60	17	19	-5
Ba	17	96	29	0	0
Be				15	2
Ce	124	35	383	113	143
Cr	0	0	0		
Cu	84	149	394	13	
F				7000	
Hf	0	0	29	14	13
La	0	51	145	55	73
Li				723	353
Mo				<14	
Nb	29	7	43	214	131
Ni	15	13	11		
Pb	240	119	111	1764	415
Rb	515	1241	388	811	522
Sn				6150	1100
Sr	13	5	24	56	16
Th	222	1	152	145	150
V	7	5	11	0	0
W				40	
Y	19	12	31	164	151
Zn	284	404	255	1000	
Zr	170	13	734	262	266
Zr/Hf	*	*	25	19	20
Ce/Y	6.53	2.92	12.35	0.69	0.95
*Hf value = below detection					
quartz	81.5		74.3		88.5
perthite	0.1				0.1
biotite	16.4		20.2		10.0
chlorite			0.4		
topaz					0.1
fluorite	0.2		0.3		0.1
cassiterite	0.2		1.0		0.1
haematite	1.6		2.6		0.4
zircon			0.4		0.6
siderite			0.3		
monazite			0.5		
genthelvite					0.1

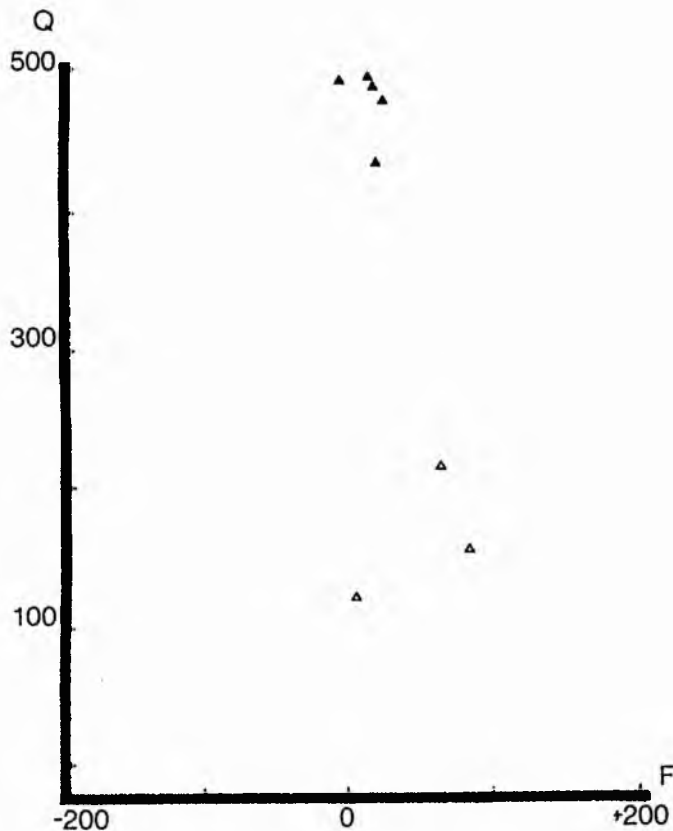


Fig 9.20 QF plot of silica and late-stage altered samples

(Chemical data from Tables 9.23 & 9.24)

▲ silica metasomatism  
 △ late-stage alteration

so that Li and Rb variation and perhaps increased Cr can be ascribed to mica abundance. The chondrite-normalised plot of selected trace elements (Fig 9.18c) shows how the concentrations of elements like Ce and Hf may be quite high. As in all earlier stages, high Ce and La contents coincide with monazite abundance, high Be with the occurrence of genthelvite, high F levels with fluorite occurrence and mica abundance, and the Zr variations with percentage of zircon. The Hf concentrations vary directly with Zr abundance.

Sn levels remained high in the two samples analysed. However, Zn, Cu, Mo and Pb levels (with the exception of SS117) were lower than in the acid metasomatism stage. This is surprising because Ixer (in Kinnaird et al., 1985) found that at Ririwai, during the silicification phase the major sulphide ores were deposited. The one W value is considerably above background levels which is consistent with the sporadic occurrence of ferberite in some of the quartz veins.

#### Late-stage alteration

Only one of the late-stage processes of alteration has been analysed and this is the carbonate phase. This is characterised by siderite development which obviously involved an addition of Fe and CO<sub>2</sub> to the system. FeO concentrations reached a maximum 25% in SS31. A possible equation for siderite after mica may be:-

Eq. 10

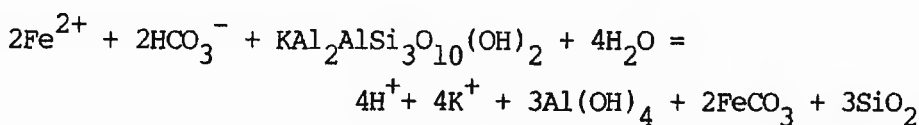


Table 9.24. Late-stage alteration (carbonate alteration) of samples from the Rishi area

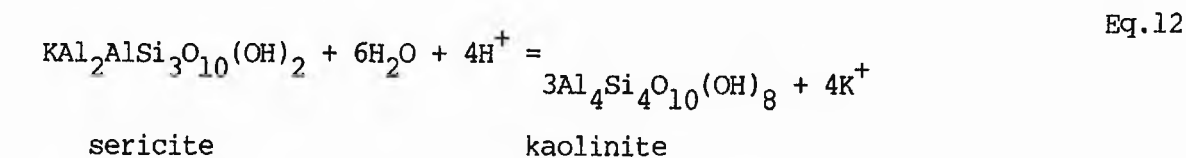
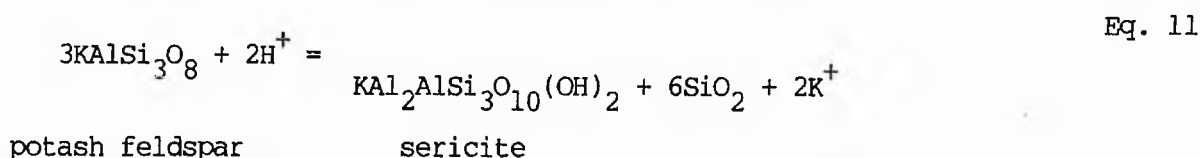
	SS1	SS129	SS131
SiO <sub>2</sub>	59.80	52.30	47.90
TiO <sub>2</sub>	0.11	0.10	0.10
Al <sub>2</sub> O <sub>3</sub>	10.07	9.70	10.91
Fe <sub>2</sub> O <sub>3</sub>	16.47	21.10	25.07
MnO	0.19	0.00	0.27
MgO	0.01	0.23	0.04
CaO	0.64	0.02	0.29
Na <sub>2</sub> O	0.49	2.57	0.20
K <sub>2</sub> O	4.40	4.08	4.74
P <sub>2</sub> O <sub>5</sub>	0.02	0.10	0.01
H <sub>2</sub> O	1.60		2.53
F <sup>-</sup>	0.08		0.32
F=O	0.03		0.14
Total	93.86	90.20	92.24
R1	2364	1085	1380
R2	267	204	247
Q	215	120	155
F	66	3	89
Ba	0	5	33
Be		10	12
Ce	315	1208	49
Cr	0		
Cu	7		
F	800		3200
Hf	11	29	49
La	99	540	
Li	2900	2376	1786
Mo	940		<14
Nb	860	1184	1403
Ni	6		
Pb	495	181	141
Rb	2287	2047	2871
Sn	4290	400	330
Sr	35	144	2
Th	27	301	62
V	0	0	0
Y	174	1605	109
Zn	6636		6500
Zr	702	611	774
Zr/Hf	64	21	16
Ce/Y	1.81	0.75	0.45
quartz	32.4	27.3	1.3
biot/sericite	0.6	0.7	0.9
chlorite	0.6	0.7	0.9
fluorite	0.7	3.4	
sphalerite	2.4	2.1	
cassiterite	0.7	1.6	0.7
sphene		0.1	
molybdenite	0.4	2.3	
Haem/limonite	7.1	2.4	18.0
zircon	0.3	0.1	
siderite	6.0	6.4	1.1
monazite		0.1	

It is notable that there was a dramatic increase in many trace elements at this late alteration stage (Table 9.24). The chondrite-normalised plot of selected trace elements in Fig 9.18d, emphasises the high levels of Rb, Nb and Zr in particular. In addition Be and Li are high together with Sn, Zn and Pb. Cu, in the one sample analysed is very low and Mo may be high which is consistent with the occurrence of molybdenite in SS1 and SS129.

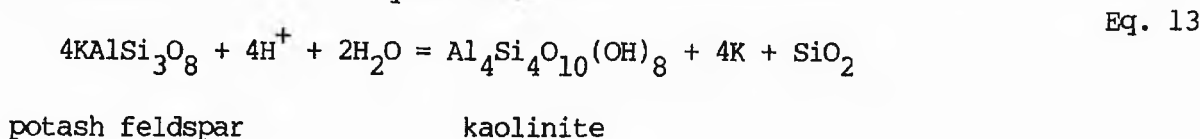
The late-stage increase in Fe could have been an important control on the late chlorite formation. Chlorite may have resulted from weak acid metasomatism in the earlier stages and in the late-stage alteration developed due to Fe metasomatism. In the first case, chlorite developed at the expense of biotite, in the latter case chlorite was generated as a result of feldspar instability in Fe-rich fluids. The chlorite development during greisenisation was clearly as a result of acid metasomatism but the late-stage chlorite may be concomitant with the carbonate process in which large quantities of Fe were obviously exchanged to the rock from the fluid.

As the development of zeolitic minerals was very limited it is not possible to discuss the chemistry of the process in the same terms as the other alteration assemblages. Nevertheless, the existence of a zeolite facies indicates low temperature fluids with low sulphur fugacities. This is consistent with secondary haematite formation developed at the expense of micas and ore minerals.

The kaolinisation of feldspar which developed to a minor degree in many places can be considered as an extreme acid metasomatism according to the equations:-

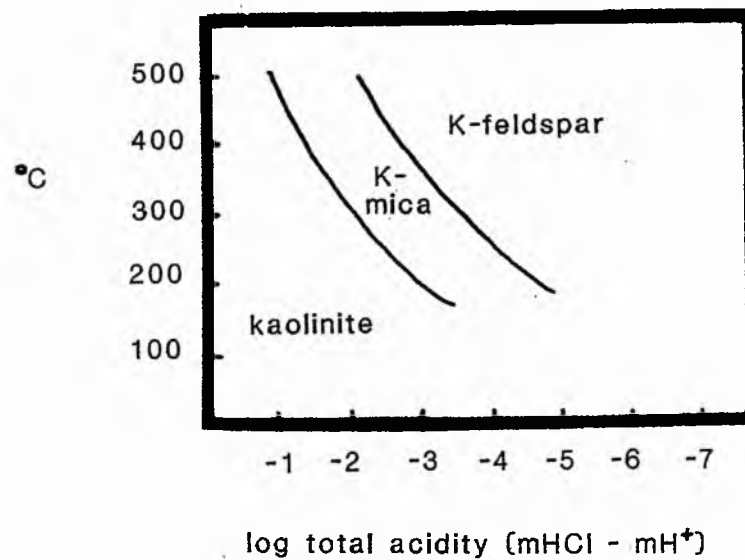


or kaolinite may have been produced directly from potash feldspar by a combination of the two equations:-



Such kaolinisation of feldspars occurred as the temperature of the fluid fell and in response to changing  $\text{K}^+/\text{H}^+$  concentration in the fluid (Fig. 9.21). In plotting the major element analyses on the Q-F multicationic diagram it is interesting that they fall in the field of potash metasomatism. This late-stage increase in potash may have resulted from the silicification of minerals like

Fig. 9.21 Stability fields of K-feldspar, K-mica and kaolinite  
(after Meyer and Hemley, 1967)



sericite etc. in which there was a release of  $K^+$  to the fluid. There was also a trend of late-stage processes towards the sodic field. It is possible that this is due to the intrusion of another granite pluton at depth.

## MINOR AND TRACE ELEMENT VARIATIONS AS INDICATORS OF HYDROTHERMAL ALTERATION

### Introduction

In Chapter 4, a number of trace element patterns were used to examine the processes of alteration for the Nigerian province as a whole. In this section, detailed data for one complex has been examined to see if the models devised for data from samples collected in widely separated complexes is valid. It is not possible to compare all these trace element patterns since strontium isotopic data, uranium values and rare earth data are not available for the Saiya Shokobo complex. Nevertheless, if the ideas derived from Nigerian data as a whole are validated by the detailed study of one complex then further credibility is given to the interpretation of uranium and strontium data, even though only generalised data exists. Also this detailed study of one complex has made it clear that other element pairs and trace element patterns can be used to monitor hydrothermal processes.

### K/Rb

Rubidium is enriched in many of the Nigerian anorogenic granites. Since Rb behaves as an incompatible element with  $K_2O < 0.1$  and is therefore concentrated in the fluid phase, it would seem likely that a granite such as the Rishi biotite granite which has been extensively modified by rock-fluid interaction should be particularly enriched in Rb. This in fact is the case. Rb values within the Rishi biotite granite, which average 602ppm (13 samples), are consistently higher than the average for Nigerian biotite granites as a whole, which is 464ppm (68 samples), indicating that fluid reactions must have been important even in the apparently unaltered biotite granite. There is a variation in the K/Rb ratio for Rishi biotite granite samples from  $>45$  in SS35 to  $<20$  in SS85/1.

During the hydrothermal alteration processes both Rb and K values were modified resulting in widely varying K/Rb ratios. Thus Rb values range from 24 to 6900 ppm and  $K_2O$  values vary from 0.15 to 11.90%. During sodic metasomatism Rb increased from the average of 602 ppm for the biotite granite to a maximum of 1188 ppm. Since K values decreased however, as Na replaced K in perthites, the K/Rb ratio decreased also and varied from 36 in SS44/2 to 16 in SS190. During potash metasomatism, values of  $K_2O$  rose to a maximum of 14.36% and Rb values were enriched to a maximum of 2563 ppm, with a range in the K/Rb ratio between  $>65$  in SS17/2 and  $<9$  in SS57/4. Perhaps surprisingly, the Rb values were at a maximum during acid metasomatism although Rb values varied depending on the rock type undergoing the acid metasomatism. Thus basement and volcanic rocks do not show enhanced Rb values, whereas in acid metasomatised albite-rich rocks Rb values increased significantly, reaching a maximum in acid metasomatised microcline-rich rocks. Because these rocks are rich in mica, the K content is also high and the K/Rb ratio is very variable as Table 9.25 shows:-

Table 9.25 K/Rb variations in acid metasomatised Rishi samples

	K/Rb highest	K/Rb lowest
Table 9.18	60.52 in SS150	24.48 in SS164
Table 9.19	26.80 in SS20/1	8.31 in SS117/6
Table 9.20	19.21 in SS54/2	7.34 in SS117/5a
Table 9.21	42.98 in SS12/3	7.75 in SS18/1
Table 9.22	44.01 in SS106B	8.24 in SS96

Bowden and van Breemen (1972) and more recently Bowden and Turner (1974), suggested that Nigerian granites containing high Rb up to 1500 ppm and low K/Rb ratios down to 35, have undergone substantial recrystallisation in the subsolidus during albitisation. This trend of K/Rb ratios to low values in Nigerian granites was believed to represent a degree of post magmatic adjustment to mineralising albite-rich fluids (Bowden and Kinnaird 1984c). Clearly, for the Rishi samples where extensive hydrothermal modifications have occurred there are a wide range of K/Rb ratios to very low levels. These K/Rb ratios do monitor hydrothermal effects since there is a significant reduction in the ratio with continued hydrothermal modification. Thus samples that have suffered acid metasomatism have the lowest K:Rb ratios. There is no clearly defined range of Rb values or K/Rb ratios for each of the individual processes.

#### Rb/Sr

In Part 1 of this thesis from a compilation of chemical data for the Nigerian anorogenic province as a whole, it was found that the Rb/Sr ratio increased from 200 in the hornblende granites and porphyries, through 300 for peralkaline granites to 400 for the biotite granites. For hydrothermally altered rocks the ratios were found to increase even further reaching a maximum of >850 in potash metasomatised rocks. For the Rishi area, the pattern that emerges is rather different. For the biotite granite the Rb/Sr value varies between 267 and 29 with a mean of 133 (Table 8.7) and is even lower in the volcanic rocks, since they contain slightly higher strontium (Table 8.6). During hydrothermal metasomatism, the ratios are widely varying but they are consistently lower than the province for a whole. This is because of the elevated levels of Sr in many of the Rishi samples. For example in the potash metasomatised samples of Table 9.16 where there is a range in the ratios from 1.5 to 1115 with an average of 245, the strontium values vary from 1 to 212.

In Part I, it was envisaged that a more detailed study of the Rb/Sr behaviour of one complex might indicate which of the different processes of hydrothermal alteration had occurred. Unfortunately, this has not proved the case and the

only conclusion that can be reached is that the hydrothermal alteration did modify the Rb/Sr values but not in a systematic manner.

Ce/Y: monitors of REE behaviour

Cerium reflects light rare earth behaviour and Y can be considered as a heavy rare earth. In the absence of a complete spectrum of rare earth element data therefore, the behaviour of these two elements can be used as indicators of rare earth element mobility.

However, during hydrothermal alteration  $Ce^{3+}$  will oxidise to  $Ce^{4+}$  and as such becomes more mobile (Masuda and Nagasawa 1975). This loss will therefore cause the ratio to fall and may affect petrogenetic interpretations based on its use as a LREE. To monitor this Ce loss the La/Ce ratio can be used. For the Nigerian granites as a whole this La/Ce ratio ranged from 0.27 to 1.31 compared with a global average for acid igneous rocks of 0.7 (Wedepohl 1970). Even within one granite type - the riebeckite biotite granite, the range was from 0.27 to 1.27, but these granites were from different complexes. For the Rishi biotite granite the La/Ce ratio is restricted to the range 0.50 to 0.62 and approximates more closely to the global average. It therefore seems reasonable to discuss Ce behaviour relative to Y for hydrothermal processes which have affected this granite.

There may have been an increase or decrease in Ce during sodic metasomatism since there is the range of Ce from 27-470 ppm compared with an average of 124 ppm for the Rishi biotite granite. For Y there was a tendency to decrease from an average of 133 ppm in the biotite granite to a mean of 105 ppm in the sodic facies. Although there was a tendency to an increase in the Ce/Y ratio, since concentration is so variable it is an over simplification to state that HREE are being depleted at this stage. However, during potash metasomatism there was a notable depletion in both Ce and Y for facies that had already undergone sodic metasomatism, but not in the facies where potash metasomatism was the first alteration process. So for these rocks the Ce/Y ratio is low but the ratio may be high in potash altered perthite granites.

The chemistry of the initial rock type was important in controlling geochemical enrichments or depletions during acid metasomatism. In addition the effect of an earlier sodic process or potash alteration led to extreme variations. Where acid metasomatism affected the basement, Ce values ranged from 0 to 7938 ppm in sample SS 94 which has 10% monazite, and Y values may range from 17 to 330 ppm with the highest concentrations also in SS94. In acid metasomatised volcanic rocks the Ce values are high (120-522 ppm) with a mean of 327 ppm. This is a reflection of the higher Ce in volcanic rocks where the mean for 10 is 329 ppm. The lowest Ce and Y values are for the feeder dyke SS173. Y values range from 27 -156 ppm with the highest values in SS150 which shows the greatest degree of alteration and in which the only volcanic nature of the rock is the embayed phenocrysts. Ce/Y ratios vary from 2.91 to 8.55.

For acid-altered albite-rich rocks, the Ce range is from 80-168 ppm with a mean of 124 which is identical to that of the biotite granite and within the range of Na altered rocks; Y is from 16-121 and with a mean of 74. Ce/Y ratios are from 1.02 to 5.

In contrast, where acid metasomatism has overprinted potash metasomatism, the Ce range is from zero in the monomineralic mica-rock (SS44/1) to 130 ppm in the quartz-mica assemblage of SS117/5a. This is a reflection of the two extreme processes since Ce was depleted during microcline formation and when the acid process was superimposed all Ce was entirely stripped out. For Y, there is a slightly wider range of values from 0-122 ppm with the highest Y content - like the highest Ce enrichment - also in SS117/5a although this sample does not appear to have more monazite than other samples.

During pervasive acid metasomatism of an unaltered biotite granite, the Ce range was from 28-187 ppm with a mean of 107 ppm compared with the average for an unaltered biotite granite of 124 ppm. During later stages of this process, there was a tendency for Ce to decrease. For Y, the decrease was more emphasised with the result that the Ce/Y ratio increased although not in a steady manner.

During silica metasomatism, Ce values were maintained but Y values varied from 12-164 ppm to give Ce/Y ratios from 0.69 to 12.35. During the late-stage processes of alteration Ce and Y values tended to increase, sometimes dramatically so, with Ce up to 1208 and Y up to 1605 in SS129. Some of this must have been incorporated within the fluorite lattice.

In a study of rare earth element mobility during alteration in S.W. England, Alderton et al (1980), found that trivalent REE were removed from the system during K-silicate alteration, Eu was lost during sericitic alteration, all REE were lost during tourmalinisation and light REE were lost during chloritic and argillic alteration. Unfortunately, no clear pattern has emerged from the study of Ce/Y ratios in Rishi rocks. The problem is as much a function of the modal variability of accessory monazite and zircon or other phases, which host the rare earths rather than being no consistent variation within each process. In Fig. 9.22, the Ce/Y ratio has been plotted against silica abundance. The Rishi biotite granite, the basement monzogranite and the volcanics define fairly clear but separate fields on this diagram. The wide spread of the other sample data emphasises the range in Ce/Y ratios that developed during hydrothermal modifications by rock fluid interaction.

In other words, differing elements may have been mobile at different stages of alteration but it is difficult to prove for the Rishi rocks due to the extreme mineralogical variability of many of the samples.

#### Zr/Hf

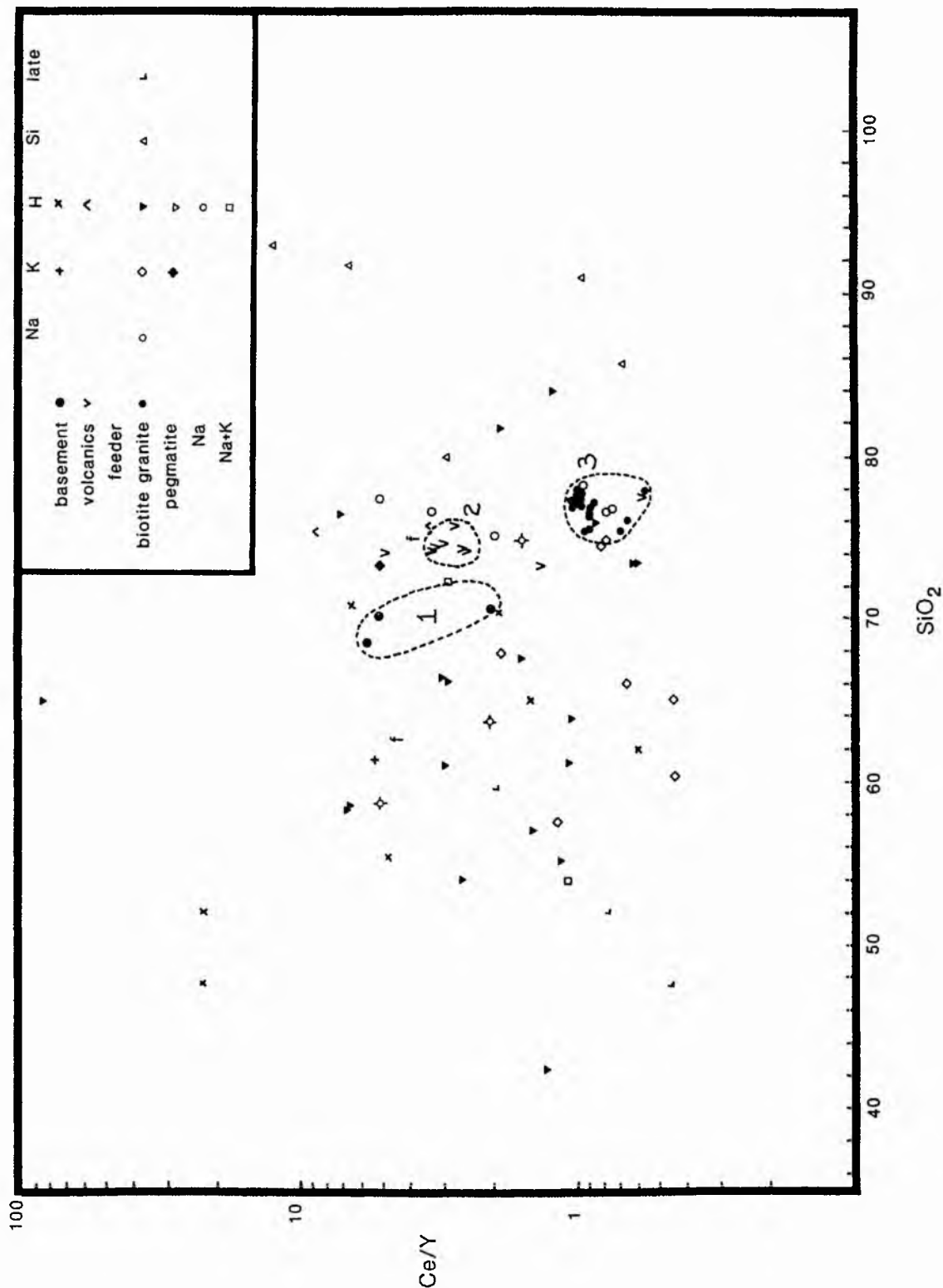
The average crustal values for Zr/Hf is approximately 50 (Wedepohl 1969). In the Nigerian province - as discussed in part 1 - the most unevolved rock, the Kila Warji syenite, together with the monzonites approximate to this value. All other rock types show a considerable range of ratios.

For the Rishi rocks, the Zr/Hf ratio of the basement monzogranite varies from 46-51 which is close to the worldwide average. For the volcanics the ratio is between 16 and 64 and for the Rishi biotite granite the range is between 13 and 37 which is within the range for Nigerian biotite granites as a whole.

The sodic metasomatised facies, irrespective of the rock type that is being altered has a narrow range of ratios with Zr/Hf of 22-31, potash rocks show a

Fig 9.22 Ce/Y versus silica diagram to show changing element ratios during hydrothermal alteration

- Field 1 basement monzogranite
- Field 2 volcanic rocks
- Field 3 "unaltered" biotite granite



range of 13-51. As with other elemental variations, the Zr/Hf ratios are most variable for samples that have suffered acid metasomatism and silicification as Table 9.26 shows:-

Table 9.26 Zr/Hf variations in acid metasomatised Rishi samples

Acid + basement monzogranite	4- 68
Acid + volcanics	51- 67
Acid + Na	3- 33
Acid + K	19- 2
Acid biotite granite (Stages 1-3)	3- 29
" " " (Stages 4-5)	2-191
Silicification	19- 2
Late-stage	16- 64

Such deviation of Zr/Hf ratios from average crustal values together with widely fluctuating ratios, is ascribed to differential mobilities of Zr and Hf during hydrothermal alteration. In Part 1, on the information available, it was thought that there was a decreasing Zr/Hf ratio with increasing hydrothermal alteration. This is perhaps an oversimplification for the Rishi rocks. During sodic and potassic metasomatism the statement is valid. However during acid metasomatism and subsequent alteration processes, Zr/Hf values are very variable, and thus widely varying ratios appear to characterise the most altered facies.

#### Li

Lithium levels are high in most Nigerian anorogenic granites. The range for biotite granites throughout the Province in Part 1 was found to be from 1 to 558 ppm with an average of 210. The Li content was found to increase in sodic and potassic metasomatised samples reaching a maximum of 6000 ppm in some acid metasomatised samples. As Table 9.27 shows the Rishi biotite granite is similar to other biotite granites throughout the province with a range from 19 to 269 ppm and a mean of 136 ppm. For sodic metasomatised samples the maximum value is greater than for the province as a whole although for potassic samples values are lower. However, in the acid metasomatised samples the Li enrichment is extreme reaching 4543ppm in an acid metasomatised microcline. Lithium levels are high in all acid metasomatised samples irrespective of whether the original rock type was basement monzogranite (73-800ppm), Rishi biotite granite (28-2844ppm), volcanic rocks (36-912ppm), albite-rich samples (250-2146ppm) or microcline-rich rocks (1748-4543ppm).

In many parts of the world lithium has been used as a pathfinder element for tin deposits. For the Rishi area, the enrichment in lithium is more dramatic than in most other Nigerian complexes and is clearly a good indicator of the enhanced tin levels. However, there is no direct correlation between

lithium enrichment and tin enhancement. The elevated lithium levels are at an extreme in samples that have been modified by intense hydrothermal rock-fluid interaction. High lithium content therefore in these granites appears to be a reflection of the extent of subsolidus reactions and hydrothermal modifications.

Table 9.27 Comparison of lithium values in Rishi samples with those in the Nigerian province as a whole.

	Nigerian Province	Rishi
biotite granite range	1-558	19-269
biotite granite mean	210	136
sodic metasomatism	max 363	49-410
sodic metasomatism mean		226
potash metasomatism range	260-4270	4-249
potash metasomatism mean	1160	92
acid metasomatism max	6000	4543
silica metasomatism		353-723
late-stage metasomatism		1786-2900

#### CHAPTER SUMMARY

The effect of the hydrothermal processes that have occurred during the emplacement of the Rishi biotite granite have proved to be very complex and have been oversimplified in past literature.

The biotite granite itself has been shown to have been modified by fluid reactions with the growth of subsolidus mica and coarsening of the domains within perthites. Elemental monitors such as Zr/Hf and Ce/Y ratios support the conclusion that even within the apparently "unaltered" biotite granite there has been a certain degree of rock-fluid interaction. Further fluid reaction resulted in a sequence of hydrothermal alteration processes.

These different processes of alteration occurred in different parts of the pluton due to varying structural controls. Several different styles of alteration are well exemplified in the Rishi biotite granite particularly pervasive metasomatism. Unlike other studied complexes however, this pervasive process is potassic in Rishi not sodic as in the Ririwai, Afu and Jos Bukuru complexes.

In addition to the Rishi biotite granite, the host rocks which surround and overlie the biotite granite pluton have also been affected. Thus the Pan-African basement monzogranite country rock which surrounds the Rishi biotite granite and the volcanic pile which overlies it, have also been hydrothermally altered by volatiles escaping from the biotite granite cupola. In the basement this alteration is at a maximum close to the contact. In the volcanic pile the degree of alteration does not directly correlate with distance from the

contact. There appear to be distinct zones of modification and reaction as indicated by groundmass coarsening.

A sequence of alteration processes can also be recognised in the basement and volcanic rocks although the mineralogical assemblages related to each process are not always as clearly defined in the basement or volcanic pile as they are in the biotite granite.

Each process has a different geochemical signature although the original rock type had a fundamental control on the final elemental abundances. Nevertheless each process can be recognised by several criteria:-

The first stages of sodic metasomatism resulted in coarsening domains within perthites. With continued rock-fluid reaction and mineralogical modification, there was an increase in modal albite accompanied by the growth of zinnwaldite mica and the development of an accessory mineral assemblage of zircon, thorite, cryolite, columbite, monazite and uraninite. Geochemically sodic metasomatism was characterised by an increase in Na and Al and a decrease in Si and Fe together with an increase in most trace elements when compared with the average for the biotite granite. The sodic effect was overprinted in the biotite granite by later potassic and acid metasomatism. The "wave" of sodic metasomatism clearly extended outwards into the basement and upwards into the volcanic pile.

Potash metasomatism was characterised by textural changes within perthites, by the increase in modal microcline, the growth of chlorite and the development of an accessory mineral assemblage which nearly always included some cassiterite and sphalerite accompanied by fluorite, monazite and zircon. As with the biotite granite, potash metasomatism of both the basement and volcanic rocks can be recognised by the microclinisation of the feldspar phenocrysts. Geochemically the process was characterised by K for Na exchange, a decrease in silica when the process became intense, and increased alumina concentrations. There was a decrease in the abundance of most trace elements concentrations, although the ore elements Sn and Zn were increased and both Rb and Sr levels rose with K enrichment.

Acid metasomatism of both biotite granite and surrounding rock types, was characterised by the destruction of feldspar, the growth of chlorite, sericite and trioctahedral mica and the development of a wide range of accessory minerals including cassiterite, chalcopyrite and sphalerite. Acid metasomatism of the basement monzogranite resulted in the development of the widest range of accessory minerals with a recorded assemblage which includes sphalerite, cassiterite, chalcopyrite, fluorite, zircon, monazite, allanite, sphene, apatite, jarosite, natrolite, and nontronite. For the acid metasomatised volcanic rocks and samples of biotite granite that were initially albite-rich, the accessory assemblage also includes cryolite and columbite reflecting the effect of an earlier phase of sodic metasomatism. Where acid metasomatism was not preceded by earlier phases of metasomatic alteration in the biotite granite, a sequence of stages in the mineralogical modification of the granite can be recognised. Initially, the feldspar and original mica of the granite were chloritised so that a quartz-chlorite assemblage was produced. Gradual sericitisation of the chlorite produced a quartz-chlorite-sericite assemblage and eventually a quartz-sericite or quartz-siderophyllite rock. In some localities a silixite (a quartz-topaz assemblage) was produced at a late-stage with the replacement of mica by topaz.

The geochemical characteristics of acid metasomatism were in part controlled by the rock type undergoing alteration and in part dictated by the extent of the modifications created by earlier process of hydrothermal alteration. The intensity of the acid metasomatism process itself also clearly had an effect on the final geochemical distribution of the elements. For the major elements, whilst the process was generally characterised by increasing Fe and an almost complete loss of Na (except in the volcanic rocks), the silica and alumina concentrations may have increased or decreased during the process of acid metasomatism and the potash levels remained high. Trace element concentrations were very varied and also reflect the extent of earlier hydrothermal imprints, the intensity of the acid process and the chemistry of the original rock. However, Li, Rb, Sn, Zn and F levels were consistently high and often reached extreme concentrations during this process.

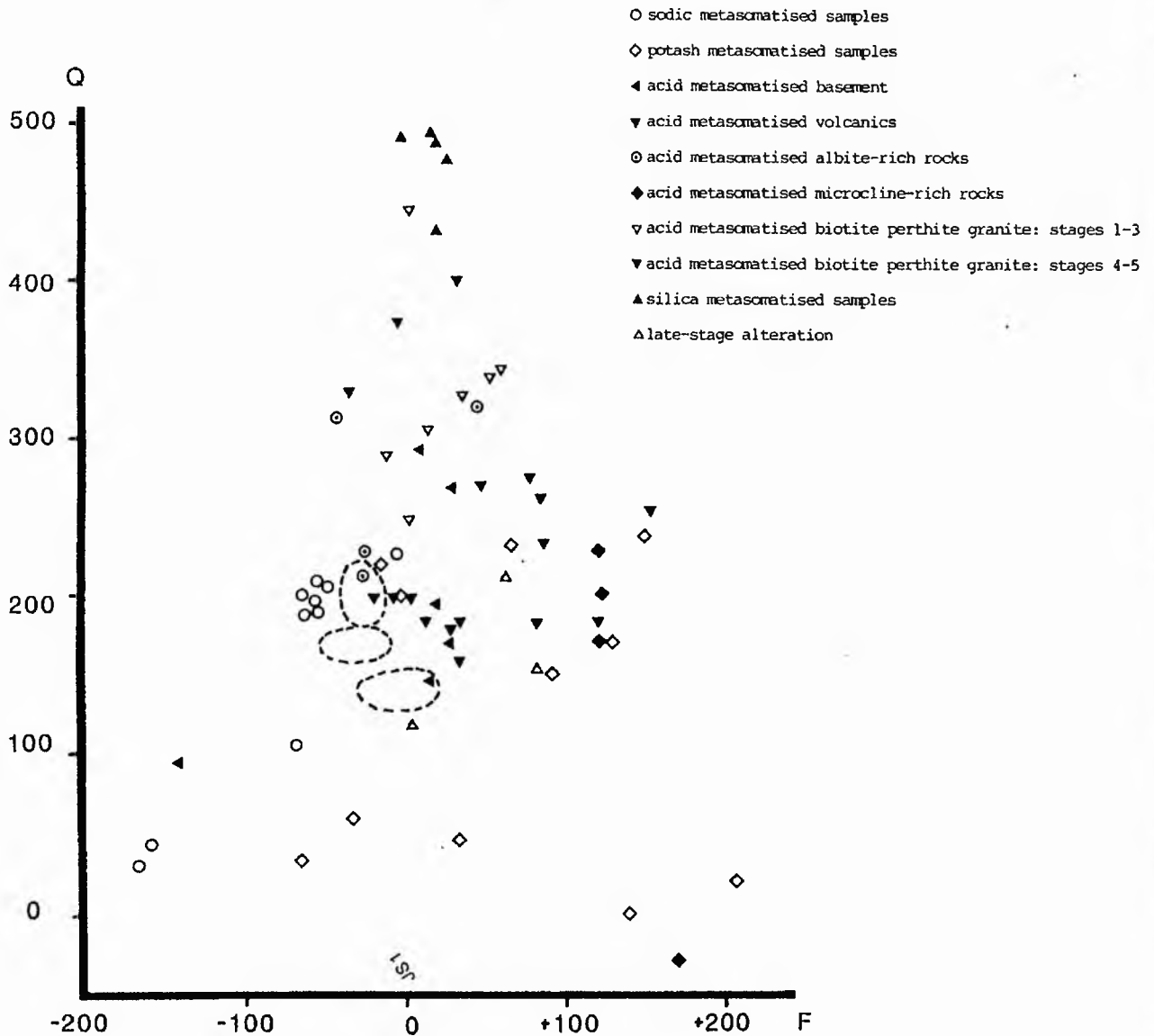
Silica metasomatism resulted in increased  $\text{SiO}_2$  and Fe, the gradual silicification of all earlier formed minerals and the deposition of an accessory assemblage which included wolframite, haematite, sphalerite and cassiterite together with fluorite, monazite, zircon, genthelvite and other minor minerals. In contrast to other complexes this was not a major sulphide deposition stage at Rishi.

During late-stage alteration iron enrichment continued, with the formation of a second generation of chlorite and siderite development together with localised clay mineral or zeolite growth. Characteristic accessory minerals include molybdenite and haematite. Secondary ores minerals must also have been generated at this stage. As the development of zeolitic minerals was very limited it is not possible to discuss the chemistry of the process in the same terms as the previous alteration assemblages.

It is important to re-iterate that whilst all these process can be recognised it is by no means easy, and where several processes have affected the same sample - which is not unusual - it can be difficult to assign a sample to a particular category of alteration.

The major element variations that occurred with each hydrothermal process can be plotted on multicationic diagrams to define "trends" or fields of alteration (Fig 9.23). The concept in Part I of several different trends on the Q-F plot has been found to be valid if rather oversimplified. However the work of this chapter has shown that it is the alteration process that is the most important, not the rock type, in defining the "trend" or field that the whole-rock chemistry determines on the Q-F diagrams. Thus for sodic metasomatism, which can usually be recognised on the Q-F plot by compositional trends plotting towards the albite pole, the effect is most obvious in altered basement samples (Fig 9.23). For potash metasomatism the trend was towards the Q-Or join, with a trend towards the microcline pole when intense potash metasomatism resulted in desilication. During acid metasomatism several different trends on the Q-F plot have been established (Fig 9.23). These correspond to similar trends established in Part I for samples from the Province as a whole. However, Trend II as defined in part 1 (acid metasomatism of soda-rich rocks - see Fig 4.4, page 76), is only weakly apparent in the Rishi area. The Q-F diagrams emphasise the importance of the potassic process at Rishi that has not been so apparent in other studied complexes and have also established two trends for acid metasomatised basement. Disseminated acid metasomatism (Fig 9.23) established

Fig 9.23 Summary Q-F plot for the Rishi samples showing trends of sodic, potash, acid, silica and late-stage metasomatism



trends towards the q pole which were continued during silica metasomatism. The final trend related to late-stage processes was to compositions which plot in the potassic field. Such a late-stage trend has not hitherto been observed from other samples.

## Discussion

The mineralogical and geochemical effects of sodic metasomatism within the Rishi biotite granite have largely been masked and overprinted by a later process, or combination of processes of hydrothermal alteration. However, there must have been a "wave" of sodic metasomatism which extended outwards into the basement and upwards into the volcanic pile. Such sodic metasomatism of the volcanic pile was responsible for the development of peralkaline pyriboles throughout much of the volcanic pile. However, close to the contact with the biotite granite, most of the mineralogical and changes that have been monitored at the base of the pile, are clearly attributable to potassic metasomatism. These effects "overprinted" the changes induced during sodic metasomatism. Remnants of the sodic event remain however, as evidenced by the peralkaline minerals in samples taken close to the biotite granite contact near Ladini. Further, there are elevated levels of Nb, in most of the volcanic rocks which are attributed to the effects of the sodic wave of alteration. The wave of sodic metasomatism which affected the volcanics was also responsible for modifications within the basement monzogranite. The albite that was developed was almost totally destroyed during later acid metasomatism.

It would appear that the potash metasomatism process that followed the sodic process did not extend as far into the volcanic pile as the sodic process. Selected horizons have been microclinised but the strongest effect within the volcanic pile occurs close to the contact with the biotite granite roof. At this level, there has been a remarkable "granitisation" of the volcanic pile e.g. SS86. Porphyritic or equigranular medium-grained granite was produced at the base of the volcanic pile by hydrothermal alteration. The first stage in the process would have been the alteration of the groundmass to a quartz-mica assemblage to produce the porphyritic texture, with increasing growth of the phases in the groundmass the medium-grained texture would have been produced. The clue to such volcanic origins for granite samples of this type comes from the high La content and occurrence of residual embayed quartz phenocrysts. It is tempting to wonder how many other granites in other complexes may be granitised volcanics, particularly those that have been mapped as sheet-like intrusions.

There was an enrichment of certain trace elements in most of the alteration processes and notably in the volatile elements. The Rishi biotite granite contains low Ba and Sr which is consistent with a high volatile-rich magma, since both elements are unable to be incorporated in volatile-rich magmas and residual fluids (Groves and McCarthy 1978). Because the magma was fluorine enriched the intrusion temperature is deduced as very low for a granite magma with relatively slow cooling probably within a closed system.

## Conclusion

The variation in major chemical data together with trace elemental assemblages and elemental ratios support the petrological interpretation of extensive and progressive hydrothermal alteration. Subsolidus re-equilibration has been an important process within the Rishi biotite granite and surrounding rock types.

Each process of alteration that had been noted in other complexes has also occurred at Rishi to a greater or lesser extent. Each hydrothermal process that

modified the original mineralogy of the granite and its surrounding rock types is characterised by local textural and colour variations, by structural changes in the alkali feldspar, by the growth of new micas, by changing compositions of the opaque minerals, by the assemblage of ore and accessory minerals and by whole rock geochemical variations. It is apparent that whatever may have been the initial character of some of the rocks described, much of it has been lost through post-magmatic processes.

## CHAPTER 10

### MINERAL AND FLUID CHEMISTRY

#### Introduction

In the previous Chapter it was stated that the sequence of subsolidus hydrothermal alteration processes that modified the original mineralogy of the granites can be recognised in several ways. This includes the growth of new micas, changing compositions of the opaque minerals, and a changing assemblage of accessory minerals for each stage of the alteration processes.

The different processes of sodic, potassic, acid and silica metasomatism must have been initiated both by changes in the chemistry of hydrothermal fluid and by changes in pressure and temperature of the fluid as it continued to exchange with the host rock. In the first part of this Chapter, the mineralogy and mineral chemistry of the sheet silicates and sulphide-bearing phases are examined to show how the mineral compositions responded to changes in fluid composition. In addition a paragenetic sequence is presented for the changing assemblage of ore minerals associated with the successive processes of hydrothermal alteration.

In the second part of the Chapter, attempts are made to monitor the changing PVTX conditions of the fluid with which the different sheet silicates and ore assemblages were in equilibrium. The ultimate aim was to determine the changes in the physical and chemical characteristics of the fluid responsible for the successive alteration stages.

#### MINERAL CHEMISTRY

##### Analytical techniques

The analytical data of this chapter has largely been gained from the use of a Jeol JXA733 electron probe microanalyser. The probe utilises 3 wavelength dispersive spectrometers and quantitative data is obtained by reference to analysed standards, mainly of pure metals. Several correction factors have to be applied to this data and these, together with more detailed descriptions of the probe appear in Appendix 6.

#### SHEET SILICATES

##### Introduction

The main mineralogical expression of peraluminous character in the anorogenic granites of Nigeria is the development of a trioctahedral lithium-iron or more rarely a lithium-aluminium mica together with topaz and sericite. The micas show abrupt compositional changes linked to periods of disseminated or vein controlled mineralisation. During hydrothermal alteration the sheet silicate composition changed in response to the changing fluid conditions so that late magmatic annite was destroyed and subsequently there was the formation of chlorite, the generation of sericite and eventually the growth of a new

trioctahedral Li-Fe mica from chlorite or sericite. In their very high Fe/Mg ratios, these trioctahedral micas and chlorites strongly reflect the original bulk composition of the granites. In some localities there was a late-stage development of illite, kaolinite or montmorillonite generated from either feldspar or sheet silicate minerals.

#### Classification of the Li-Fe trioctahedral micas

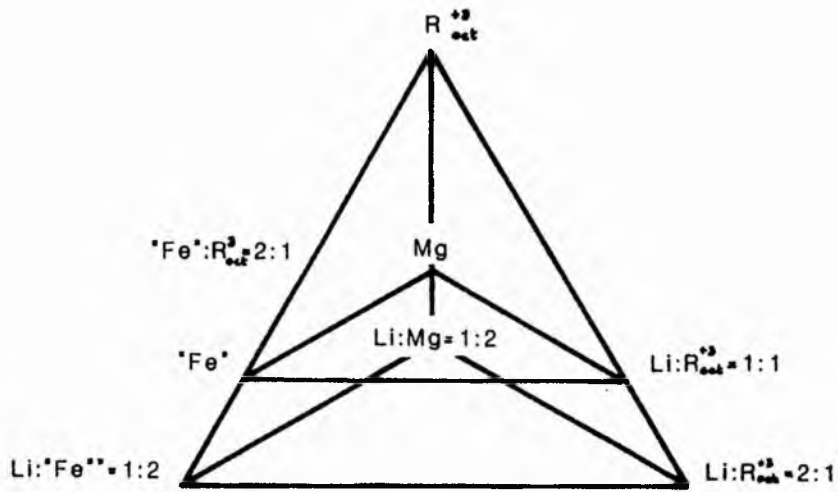
The chemistry of trioctahedral micas is very variable and this variation is linked to the filling of the various cationic sites in the lattice. Table 10.1 gives the idealised formulae for some trioctahedral mica end member varieties although few natural micas have the exact composition specified by these theoretical or idealised formulae.

Table 10.1 End-member compositions of the Li-Fe trioctahedral micas

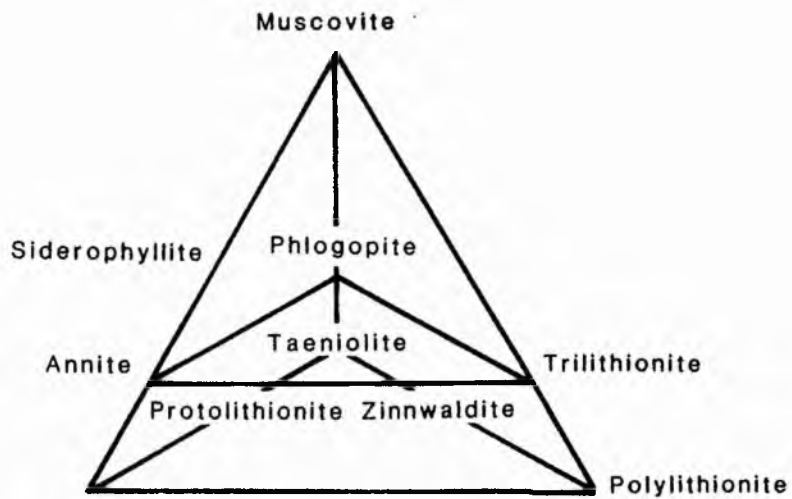
	x=2	y=6			z=8	
		Fe <sup>2+</sup>	Li	Al, Fe <sup>3+</sup>	Al	Si
annite	K <sub>2</sub>	6	0	0	2	6
ferri-annite	K <sub>2</sub>	6	0	0	Fe2	6
siderophyllite	K <sub>2</sub>	4	0	2	4	4
lithian siderophyllite	K <sub>2</sub>	3-4	1-0	2	3-4	4-5
protolithionite*	K <sub>2</sub>	4	1	1	4	4
zinnwaldite	K <sub>2</sub>	1-3	1-3	2	1-3	5-7
ferroan- polyolithionite	K <sub>2</sub>	0-1	3-4	2	1-0	7-8
trilithionite	K <sub>2</sub>	0	3	3	2	6
polyolithionite	K <sub>2</sub>	0	4	2		8
lepidolite*	K <sub>2</sub>	0	2.5	3	2-3	5-6

\* The terms protolithionite and lepidolite appear to have been discontinued in recent literature

Assigning a name to any particular mica within the Li-Fe assemblage is difficult and there is no generally accepted method. Such Li-Fe micas have been analysed by Rieder (1970) for the Erzgebirge tin province and he constructed a triangular diagram to assist in the naming of mica compositions (Fig 10.1). The diagram was modified by Bowden and Kinnaird to a simple bivariate plot for the study of Nigerian micas which are Mg-poor (Fig 10.2). The two axes were defined as follows:-



A pyramid for plotting atomic octahedral compositions of Li-Fe-Mg-Al micas



Nomenclature of end member compositions

Fig 10.1

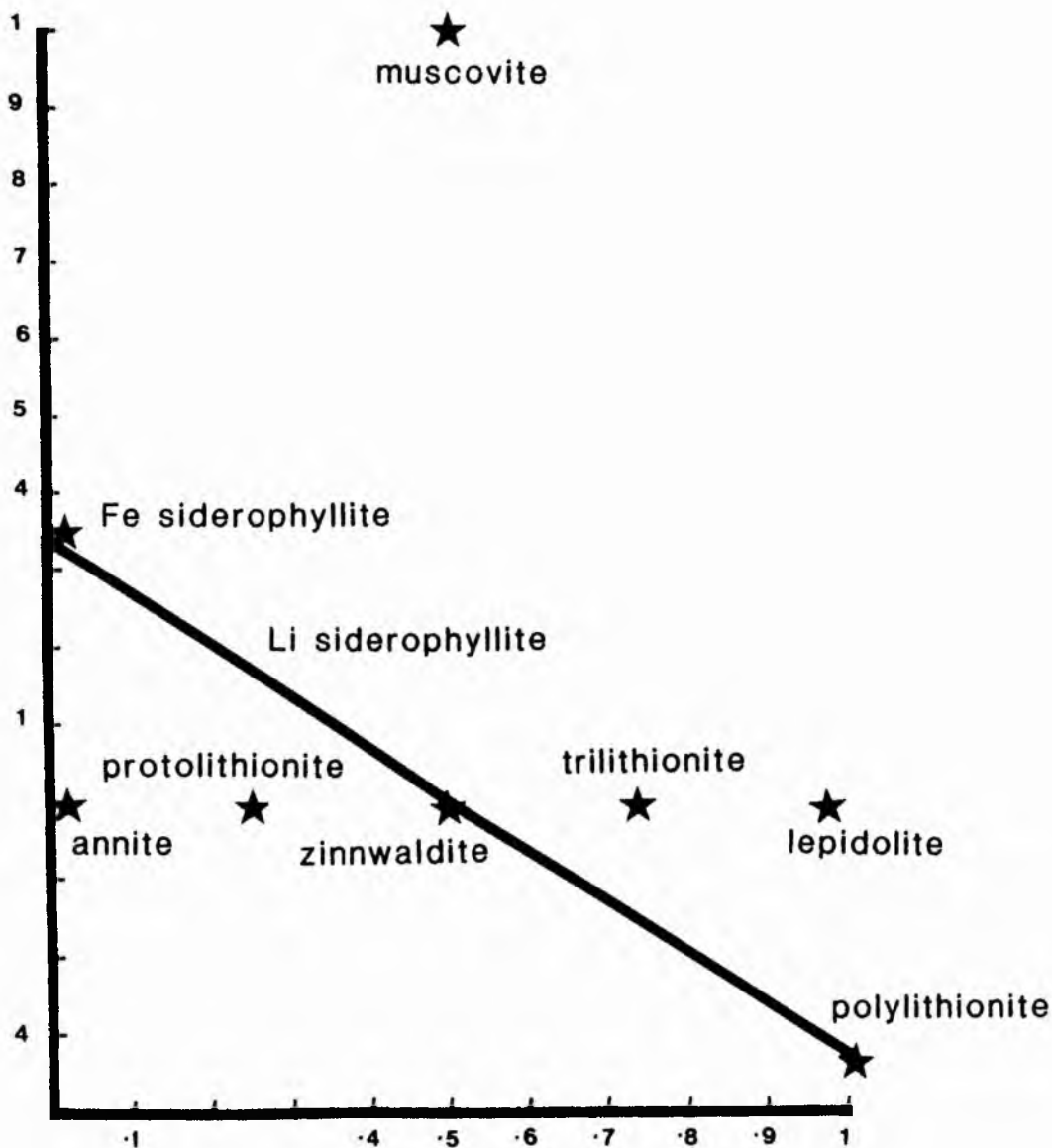


Fig 10.2 Modified Rieder diagram for trioctahedral micas (from Bowden and Kinnaird 1984a)

$$x = \frac{2Li}{2Li + Fe}$$

$$y = \frac{R^{3+} \text{ exc}}{\text{sum oct}}$$

where LR is Li or  $R^{3+}$  oct whichever is smaller;

Fe is  $Fe^{2+} + Mn^{2+}$  and

$R^{3+}$  is the sum of the octahedral cations.

The bivariate diagram was utilised to interpret mica compositions within the Nigerian Province and the plot proved that there was a correspondance between the mica composition and type of hydrothermal alteration.

The potential of such a diagram is limited unfortunately because it is not possible to consider microprobe data on the Rieder diagram or the Bowden and Kinnaird modification. This is because one of the three parameters in the Rieder diagram - the X axis in the Bowden and Kinnaird plot - is effectively defined by the amount of Li and Li cannot be analysed on the microprobe. The difficulty of presenting probe or XRF data is further compounded by the lack of  $Fe^{3+}$  values. Finger (1972) has produced a method for recalculating  $FeO(t)$  to give  $Fe_2O_3 + FeO$ . In addition, Hughes and Hussey (1976) suggest that it is possible to divide the total iron as  $Fe_2O_3$  by five and to apportion one-fifth to  $Fe^{3+}$  and four-fifths to  $Fe^{2+}$ . However, it is not feasible even to make an estimation for  $Fe^{3+}$  to  $Fe^{2+}$  ratios if one considers the immense variation in  $Fe^{3+}:Fe^{2+}$  ratios from XRF and wet chemical analyses (Table 10.2 to 10.5). As an example, the micas from SS117/5 and SS44/1 contain almost identical amounts of  $FeO$  - 28.10 and 28.01% respectively - yet their  $Fe_2O_3$  contents are 2.48 and 0.59 respectively. Further, SS117 with 25.30%  $FeO$  contains 7.29%  $Fe_2O_3$ .

The most up-to-date work on the micas is the Mineralogical Society of America Volume on Micas, edited by Bailey (1984). Within the volume, a vector presentation of Li mica compositions has been drawn up by Cerny and Burt. This a complex polyhedron with five vectors dependent upon the structural proportions of Fe, Si, Al and Li. There are two major drawbacks to this system. Firstly it again requires Li in the analyses to name the mica. Secondly, only end member compositions are plotted as single points so that when a composition falls between points it is not obvious from the diagram how the mica should be named.

Since examination of mica compositions for the Nigerian Province clearly showed variations in Si, Al, K,  $Fe^{3+}$ ,  $Fe^{2+}$ , Li and F contents with lesser variations in Ti, Mg and other cations, depending on hydrothermal alteration effects, it was necessary to try to diagrammatically represent such variations. It was also necessary to give a name to each species. Various methods were attempted, plotting element against element variations in bivariate or triangular diagrams. Eventually, it became obvious that as variations in cationic abundances involved so many elements, a multi-cationic method was required which did not include Li or Fe (other than as total  $FeO$ ) and the data was plotted on an R1-R2 plot shown in Fig 10.3. The R1-R2 plot was devised originally for whole rock variations with the parameter values chosen to represent a fractionating magma. However, in plotting:-

$$R1 = 4Si - 11(Na+K) - 2(Fe+Ti) \text{ against}$$

$$R2 = 6Ca + 2Mg + Al$$

many of the above cations are incorporated. For elements like Li which aren't included in the multicationic parameters, there is a tendency for their concentrations to vary with selected major elements which are included. Thus

Table 10.2 Chemical compositions and structural formulae for micas from hastingsite and biotite granites

Table no	Mica from enclave in Gaisvat biotite granite		Micas from "hastingsite" biotite granites					Micas from biotite granites					Afu biotite granite	Kerko biotite granite			
	1	2	3	4	5	6	7	8	9	10	11	12			13	14	15
Sample no	GU 13	L 953	L 1622	PB 45	PB 51	PB 67	AF 70	AF 71/1	-	X 568	JB 2 <sup>6</sup>	B 47	SS 34	SS 38	SS 48	AF 49 <sup>7</sup>	AF 39
SiO <sub>2</sub>	39.97 <sup>1</sup>	35.14	30.72	33.10	35.94	35.36	34.72	36.46 <sup>1</sup>	37.58	37.38	35.4	36.48 <sup>3</sup>	36.90 <sup>1</sup>	37.6	40.12 <sup>1</sup>	36.7	32.86 <sup>2</sup>
TiO <sub>2</sub>	1.72 <sup>1</sup>	2.87	3.04	2.96	3.33	3.04	4.01 <sup>1</sup>	3.92 <sup>1</sup>	1.42	1.84	2.83	1.50	1.83 <sup>1</sup>	3.18	0.90 <sup>1</sup>	3.12	3.44
Al <sub>2</sub> O <sub>3</sub>	18.31 <sup>1</sup>	6.44	11.54	9.77	11.71	10.90	12.31	12.05 <sup>1</sup>	15.43	11.89	13.20	18.97	12.27 <sup>1</sup>	13.41	18.80 <sup>1</sup>	11.77	11.18
Fe <sub>2</sub> O <sub>3</sub>	-	4.40	11.62	12.19	5.00	3.76	2.14	1.72 <sup>1</sup>	4.69	4.38	1.28	0.62	2.18 <sup>1</sup>	2.16	1.84 <sup>1</sup>	7.75	2.62
FeO	20.79	34.92	26.49	24.48	23.91	31.38	28.08	25.54	25.00	28.65	29.90	28.80	30.11	28.26	20.45	21.19	33.47
MnO	0.38 <sup>1</sup>	0.53	0.64	0.40	0.50	0.65	0.45 <sup>1</sup>	0.46 <sup>1</sup>	0.20	0.41	0.39	0.57	0.49 <sup>1</sup>	0.39	0.27 <sup>1</sup>	0.27	0.46
MgO	3.68 <sup>1</sup>	0.43	0.15	1.95	6.35	1.06	4.26 <sup>1</sup>	5.24 <sup>1</sup>	0.32	0.22	2.39	0.38	0.07 <sup>1</sup>	0.06	0.48 <sup>1</sup>	8.06	0.83
CaO	0.15 <sup>1</sup>	0.97	1.70	2.37	1.65	nd	0.56 <sup>1</sup>	0.53 <sup>1</sup>	1.15	0.16	0.51	0.44	0.06 <sup>1</sup>	0.14	0.07 <sup>1</sup>	0.62	0.14
ZnO	0.29	nd	nd	nd	nd	nd	0.10	0.08	nd	nd	nd	0.16	0.39	0.44	0.32	0.06	0.20
Li <sub>2</sub> O	1.01	nd	nd	nd	nd	nd	0.18	0.22	nd	0.77	0.21	0.73	0.72	0.79	1.48	0.19	0.24
Na <sub>2</sub> O	0.25 <sup>1</sup>	0.74	0.44	0.41	0.42	0.97	0.49 <sup>1</sup>	0.20 <sup>1</sup>	1.67	0.39	0.29	0.11	0.33 <sup>1</sup>	0.26	0.32	0.34	0.11
K <sub>2</sub> O	9.55 <sup>1</sup>	8.92	4.35	5.43	6.95	9.04	8.30 <sup>1</sup>	8.37 <sup>1</sup>	7.34	8.78	7.22	8.50	8.88	7.93	8.94	7.38	8.00
Rb <sub>2</sub> O	0.60	nd	nd	nd	nd	nd	0.10	0.11	nd	nd	nd	0.44	0.58	0.56	1.15	0.04	0.20
P <sub>2</sub> O <sub>5</sub>	0.02 <sup>1</sup>	0.03	0.06	-	-	-	0.32 <sup>1</sup>	0.30 <sup>1</sup>	tr	nd	0.08	0.01	0.01 <sup>1</sup>	0.05	0.02 <sup>1</sup>	0.05	0.05
H <sub>2</sub> O <sup>+</sup>	1.06	3.12	8.27	5.55	4.15	3.74	1.55	2.21	nd	1.84	2.22	1.15	1.57	1.83	1.15	1.08	2.68
H <sub>2</sub> O <sup>-</sup>	0.14	0.06	0.27	1.94	0.03	nd	0.12	0.15	0.52	0.67	0.18	0.16	0.10	0.11	0.12	0.12	0.09
F	4.00	2.47	nd	nd	nd	nd	1.78	1.48	2.01	4.36	1.95	4.11 <sup>5</sup>	2.77	3.57	3.93	1.19	0.31
Sub-total	101.92	101.04	99.29	100.55	99.94	99.90	99.47	99.04	97.60 <sup>8</sup>	101.94 <sup>9</sup>	98.05	103.13	99.26	100.74	100.36	99.93	96.88
Less O=F,Cl	1.68	1.04	-	-	-	-	0.75	0.62	0.91	1.86	0.82	1.73	1.17	1.50	1.66	0.50	0.13
Total	100.24	100.00	99.29	100.55	99.94	99.90	98.72	98.42	96.69	100.08	97.23	101.40	98.09	99.24	98.70	99.43	96.75
R1	-285	-1160	-232	-275	-254	-1146	-737	-451	-661	-654	-368	-451	-673	-421	-168	-263	-803
R2	558	251	416	542	721	266	513	553	441	261	432	438	251	281	400	697	275
Li	4715	nd	nd	nd	nd	nd	858	1025	nd	3577 <sup>10</sup>	975	3401	3363	3669	6899	882	1115
Cu	7	nd	nd	nd	nd	nd	19	9	nd	nd	nd	8	22	10	16	23	15
Zn	2300	nd	nd	nd	nd	nd	768	650	nd	nd	nd	1253	3110	3555	2545	450	1630
Rb	5470	nd	nd	nd	nd	nd	890	1005	nd	nd	nd	4020	5340	5140	10540	360	1820
Sr	20	nd	nd	nd	nd	nd	20	20	nd	nd	nd	50	20	60	20	20	20
Structural formula	3	3	2	2	2	2	3	3	2	3	3	3	3	3	3	3	3
Z Si	6.116	5.899	5.305	5.525	5.659	5.810	5.776	5.929	5.950	6.030	5.860	5.736	6.151	6.059	6.226	5.905	5.688
Al <sup>[4]</sup>	1.884	1.274	2.349	1.922	2.173	2.111	2.224	2.071	2.050	1.970	2.140	2.264	1.849	1.941	1.774	2.095	2.281
Fe <sup>3+</sup>	-	0.556	0.346	0.553	0.168	0.079	-	-	-	-	-	-	-	-	-	-	0.031
ZZ	8.00	8.00 <sup>11</sup>	8.00	8.00	8.00	8.00	8.00	8.00	8.00	8.00	8.00	8.00	8.00	8.00	8.00	8.00	8.00
Y Al <sup>[6]</sup>	1.417	-	-	-	-	-	0.189	0.238	0.829	0.291	0.436	1.251	0.561	0.554	1.665	0.136	-
Ti	0.198	0.092	0.395	0.372	0.394	0.376	0.502	0.479	0.169	0.223	0.352	0.177	0.229	0.385	0.105	0.377	0.448
Fe <sup>3+</sup>	-	-	1.164	0.978	0.424	0.386	0.268	0.210	0.559	0.532	0.159	0.073	0.273	0.262	0.215	0.938	0.310
Mg	0.839	0.108	0.039	0.485	0.490	0.260	1.056	1.270	0.076	0.053	0.590	0.089	0.017	0.014	0.111	1.933	0.214
Li	0.622	-	-	-	-	-	0.120	0.144	-	0.500	0.140	0.462	0.483	0.512	0.924	0.123	0.167
Zn	0.033	-	-	-	-	-	0.012	0.010	-	-	-	0.019	0.048	0.052	0.037	0.007	0.026
Fe <sup>2+</sup>	2.660	4.903	3.826	3.417	3.148	4.312	3.906	3.473	3.310	3.861	4.139	3.787	4.197	3.808	2.654	2.851	4.545
Mn	0.049	0.075	0.094	0.057	0.067	0.090	0.063	0.063	0.027	0.056	0.055	0.076	0.069	0.053	0.035	0.037	0.067
Y	5.82	5.18	5.52	5.31	5.52	5.42	6.12	5.89	4.97	5.52	5.93	5.88	5.64	5.75	6.40	6.08	6.08
X Ca	0.021	0.168	0.301	0.424	0.278	-	0.032	0.030	0.195	0.010	0.074	0.072	0.009	0.014	0.008	0.097	0.015
Na	0.074	0.241	0.147	0.133	0.128	0.309	0.158	0.063	0.513	0.122	0.093	0.034	0.107	0.081	0.096	0.106	0.037
K	1.864	1.910	0.958	1.156	1.396	1.895	1.761	1.736	1.482	1.807	1.525	1.705	1.888	1.630	1.770	1.515	1.766
Rb	0.059	-	-	-	-	-	0.011	0.011	-	-	-	0.044	0.062	0.058	0.115	0.004	0.022
OX	2.02	2.32	1.41	1.71	1.80	2.20	1.96	1.84	2.19	1.94	1.69	1.86	2.07	1.78	1.99	1.72	1.84
OH OH	1.082	3.494	9.526	6.179	4.359	4.099	1.720	2.397	-	1.980	2.451	1.206	1.746	1.967	1.190	1.159	3.094
F	1.936	1.311	-	-	-	-	0.936	0.761	1.006	2.225	1.021	2.004	1.460	1.819	1.929	0.606	0.170
OH-group	3.02	4.80	9.53	6.18	4.36	4.10	2.66	3.16	1.08 <sup>12</sup>	4.23 <sup>13</sup>	3.47	3.25	3.21	3.79	3.12	1.76	3.26
+ve Charge	44.983	43.195	44.000	44.000	44.000	44.000	45.344	44.842	44.000	43.780	44.528	44.750	44.794	44.214	44.881	46.235	44.736

<sup>1</sup>X.R.F. determination. <sup>2</sup>Combined gravimetric and A.A. determination. <sup>3</sup>Colorimetric determination. <sup>4</sup>Fluorine determination using fusion method of decomposition. <sup>5</sup>Includes 35 ppm Be. <sup>6</sup>Includes 6 ppm Be. <sup>7</sup>Includes 0.27% Cl. <sup>8</sup>Includes 0.09% Cl, 0.03% S, 0.08% CO<sub>2</sub>. <sup>9</sup>Converted from percentage. <sup>10</sup>Includes Ti=0.271. <sup>11</sup>Includes Cl=0.072. <sup>12</sup>Includes Cl=0.025.

Table 10.3 Chemical compositions and structural formulae for micas from biotite and zinnwaldite granites of the Nigerian anorogenic province.

Sample no	Kana biotite		Rafin Gabas biotite		Awalande biotite		Odesi albite zinnwaldite granite, group 1		Odesi albite zinnwaldite zinnwaldite granite, group 3		Odesi albite zinnwaldite granite, group 4		Undifferentiated granites from the Afu complex				
	18	19	20	21	22	23	24	25	26	27	28	29	30	31	32	33	34
AF 90	AF 28 <sup>6</sup>	AF 22/77	AF 25/78	AF 24/72	AF 100/1	AF 62	AF 101/1	AF 102	AF 60	AF 124	AF 59/3	AF 40 <sup>8</sup>	AF 59/4	AF 98	AF 52 <sup>1</sup>	AF 77	
SiO <sub>2</sub>	34.10 <sup>5</sup>	35.11 <sup>2</sup>	35.7	34.98 <sup>2</sup>	35.08 <sup>2</sup>	36.28 <sup>2</sup>	38.32 <sup>2</sup>	37.19 <sup>4</sup>	36.55 <sup>3</sup>	38.44 <sup>4</sup>	40.36 <sup>2</sup>	40.85	43.55 <sup>2</sup>	34.85 <sup>1</sup>	34.50 <sup>8</sup>	34.17 <sup>3</sup>	
TiO <sub>2</sub>	2.79	1.75	1.62	1.19	1.10	1.36	1.52 <sup>1</sup>	1.43 <sup>4</sup>	1.04	1.30 <sup>4</sup>	0.53	0.25 <sup>4</sup>	0.10	0.53	2.60 <sup>1</sup>	1.98	
Al <sub>2</sub> O <sub>3</sub>	15.76	16.13	17.81	18.42	17.88	14.51	12.49 <sup>4</sup>	13.88 <sup>4</sup>	11.38	13.73 <sup>4</sup>	15.99	18.20 <sup>4</sup>	17.39	21.21	16.19 <sup>1</sup>	17.38	
FeO <sub>3</sub>	10.13	9.53	2.60	5.59	4.44	1.40	4.83 <sup>4</sup>	2.83 <sup>4</sup>	4.65	1.09 <sup>4</sup>	3.13	4.88 <sup>4</sup>	4.92	7.73	7.34	1.68	
FeO	24.40	24.32	29.70	27.32	26.69	31.70	31.03	28.91	30.90	26.60	19.91	16.39	13.10	13.60	24.59	29.80	
MnO	0.54	0.56	0.46	0.40	0.19	0.66	0.53 <sup>1</sup>	0.54 <sup>1</sup>	0.63	0.63	0.52	0.55 <sup>1</sup>	0.45	0.58	0.44 <sup>1</sup>	0.54	
MgO	0.84	0.82	0.25	0.07	0.09	0.16	0.02 <sup>1</sup>	0.05 <sup>1</sup>	0.08	0.34	0.04	0.04 <sup>1</sup>	0.24	1.97 <sup>1</sup>	0.20	0.28	
CaO	0.25	0.08	0.12	0.11	0.08	0.24	0.24	0.09 <sup>1</sup>	0.46	1.47	0.17	0.09 <sup>1</sup>	0.32	0.38	0.29 <sup>1</sup>	0.21	
ZnO	0.44	0.19	0.16	0.35	0.17	0.73	0.92 <sup>1</sup>	0.89 <sup>1</sup>	1.16	1.31	1.82	1.67	1.67	0.16	0.21	0.36	
Li <sub>2</sub> O	0.14	0.37	0.27	0.16	0.32	0.09	0.23 <sup>1</sup>	0.31 <sup>1</sup>	0.14	0.14	0.40	0.38	3.45	0.28	0.65	0.88	
Na <sub>2</sub> O	8.21	8.51	8.38	8.69	8.77	8.16	8.82 <sup>1</sup>	8.51 <sup>1</sup>	8.54	8.75	9.01	8.74 <sup>1</sup>	9.03	11.06	8.74	9.08	
K <sub>2</sub> O	0.01	0.05	0.01	0.05	0.05	0.37	0.44	0.01 <sup>1</sup>	0.37	0.71	0.93	1.04	1.04	0.21	0.20	0.46	
Pr <sub>2</sub> O <sub>5</sub>	2.37	1.01	2.15	1.28	1.33	1.21	1.30	1.17	1.01	1.01	1.01	1.01	0.05	0.01	0.05	0.01	
H <sub>2</sub> O <sup>+</sup>	0.09	0.08	0.15	0.09	0.17	0.16	0.10	0.13	0.12	0.13	0.16	0.13	0.20	0.70	2.97	1.43	
F	1.42	2.43	2.06	2.59	2.82	3.31 <sup>5</sup>	3.58 <sup>5</sup>	3.58 <sup>5</sup>	4.48 <sup>5</sup>	4.85 <sup>5</sup>	5.50 <sup>5</sup>	5.99 <sup>5</sup>	4.42 <sup>5</sup>	6.57 <sup>5</sup>	1.20	2.82	
Sub-total	101.95	100.64	102.24	101.98	100.35	100.89	99.84	100.77	102.20	99.92	102.18	101.29	98.79	103.49	99.02	101.67	
Less O=F,Cl	0.60	1.02	0.87	1.09	1.19	1.39	1.58	1.51	1.88	2.04	2.32	2.52	1.86	2.77	0.50	1.19	
Total	101.35	99.62	101.37	100.89	99.16	99.50	98.26	99.26	100.32	97.88	99.86	98.73	96.93	100.72	98.52	100.48	
RI	-700	-736	-608	-688	-708	-467	-500	-533	-618	-376	-205	-98	-88	-865	-406	-721	
RZ	375	341	374	377	364	318	253	281	334	363	334	365	354	469	445	395	
L1	2044	789	2415	2554	2787	3401	4185	4407	5373	6110	10000	11779	16000	18100	1326	3019	
Ca	25	31	27	18	23	11	11	10	25	8	10	30	9	30	20	22	
Zn	1800	1555	1325	1240	1290	3809	1860	7930	3857	11800	14600	3710	4580	13400	1270	1710	
Rb	2170	2120	2760	3110	3400	4020	4460	1730	5240	6500	8480	9480	7320	11700	1900	2740	
Sr	30	350	20	20	20	30	30	10	30	30	410	20	20	50	20	50	
Structural formula	3	3	3	3	3	3	3	3	3	3	3	3	3	3	3	3	
Z	5.431	5.739	5.665	5.621	5.708	5.968	6.309	6.068	5.995	6.238	6.185	6.230	6.677	5.173	5.632	5.510	
Al <sup>(IV)</sup>	2.569	2.261	2.335	2.379	2.292	2.032	1.691	1.932	2.003	1.762	1.815	1.770	1.323	2.827	2.368	2.456	
Fe <sup>2+</sup>	8.00	8.00	8.00	8.00	8.00	8.00	8.00	8.00	8.00	8.00	8.00	8.00	8.00	8.00	8.00	8.00	
Al <sup>(VI)</sup>	0.389	0.647	0.986	1.109	1.137	0.781	0.732	0.747	0.128	0.604	0.073	0.507	1.819	0.005	0.716	0.867	
Tl	0.334	0.215	0.193	0.144	0.135	0.168	0.188	0.175	0.037	0.061	0.061	0.028	0.012	0.081	0.321	0.242	
Fe <sup>3+</sup>	1.214	1.172	0.330	0.676	0.944	0.173	0.347	0.574	0.574	0.133	0.361	0.560	0.548	0.982	0.231	0.802	
Mg	0.199	0.078	0.054	0.017	0.022	0.039	0.005	0.012	0.020	0.082	0.129	0.009	0.002	0.035	0.471	0.048	
L1	0.282	0.112	0.352	0.355	0.355	0.485	0.596	0.623	0.765	0.855	1.325	1.552	2.127	2.469	0.182	0.418	
Zn	0.026	0.025	0.019	0.018	0.020	0.057	0.029	0.119	0.058	0.176	0.176	0.352	0.495	1.389	0.019	0.023	
Fe <sup>2+</sup>	3.250	3.297	3.942	3.671	3.632	4.361	4.272	3.945	4.238	3.610	2.552	2.080	1.498	1.743	3.441	3.041	
Mn	0.073	0.078	0.062	0.054	0.054	0.092	0.074	0.075	0.088	0.087	0.057	0.058	0.071	0.075	0.060	0.074	
X	5.77	5.82	5.91	6.04	5.94	6.15	5.90	6.04	6.07	5.65	5.65	6.33	6.33	6.42	5.65	5.80	
Ca	0.037	0.004	0.018	0.009	0.004	0.040	0.010	0.007	0.042	0.123	0.026	0.008	0.010	0.028	0.028	0.090	
N	0.043	0.117	0.083	0.050	0.101	0.029	0.080	0.098	0.045	0.044	0.119	0.130	0.166	0.053	0.062	0.041	
K	1.668	1.774	1.774	1.774	1.820	1.712	1.852	1.771	1.791	1.708	1.719	1.726	1.766	2.163	1.781	1.879	
Rb	0.025	0.024	0.031	0.035	0.039	0.047	0.052	0.020	0.060	0.074	0.092	0.102	0.079	0.126	0.031	0.048	
PX	1.77	1.92	1.83	1.88	1.96	1.85	1.99	1.90	1.94	1.95	2.00	1.97	2.02	1.87	1.90	2.06	
OH	2.518	1.301	2.276	1.372	1.444	1.328	1.428	1.273	1.313	1.299	1.384	0.610	0.205	0.716	3.148	1.699	
F	0.715	1.256	1.034	1.316	1.451	1.722	1.953	1.847	2.324	2.489	2.668	2.143	3.183	3.183	1.624	1.396	
TOH-group	3.23	2.36	3.31	2.69	2.90	3.05	3.38	3.12	3.64	3.79	4.25	3.50	2.35	3.50	3.76	2.95	
+ve Charge	44.767	45.642	44.650	45.312	45.105	44.950	44.620	44.879	44.363	44.212	43.750	44.500	45.652	44.099	44.239	45.052	44.905

1 X.R.F. determination. 2 Gravimetric and A.A. determination. 3 Colorimetric determination. 4 Gravimetric determination. 5 Fluorine determination using fusion method of decomposition. 6 Includes 14 ppm Be. 7 Includes 6 ppm Be. 8 Includes 4 ppm Be. 9 Includes 57 ppm Be. 10 Includes 3 ppm Be. 11 Includes 1.81% insoluble residue. 12 Includes 0.47% insoluble residue.

Table 10.4 Chemical composition and structural formulae for micas from biotite granites and pegmatites of the Niger/Nigeria anorogenic province

Micas from biotite granites													Micas from pegmatites				
Tarraroudji biotite granite													Rayfield Gona biotite granite	Sahon South biotite granite	Gida zinnwaldite granite	Quissat biotite granite	
Table no	35	36	37	38	39	40	41	42	43	44	45	46	47	48	49	50	51
Sample no	2444	2505	2510	2518	2536	2501	2528	2531	2540	TA 3	TA 11/2	TA 23	JRU125	JRU64K	AF 117	AF 59/1 <sup>6</sup>	GU30
SiO <sub>2</sub>	34.90	37.40	35.60	36.04	37.56	33.84	32.20	32.80	31.35	35.43 <sup>2</sup>	37.56 <sup>2</sup>	37.37 <sup>2</sup>	41.11	43.8	39.13 <sup>3</sup>	42.7	42.0
TiO <sub>2</sub>	3.50	2.00	1.20	2.20	1.60	1.80	2.20	2.10	2.00	1.15	1.38	1.32	0.30	0.10	0.47	0.61	0.16
Al <sub>2</sub> O <sub>3</sub>	9.75	13.92	13.34	13.60	16.50	17.70	15.02	15.80	14.65	19.69	18.83	18.99	16.59	20.82	16.03	19.79	21.40
Fe <sub>2</sub> O <sub>3</sub>	14.74	5.42	13.12	7.80	7.08	12.40	18.45	17.55	19.60	1.04	-	2.58	2.00	-	-	-	0.24
FeO	22.20	24.34	19.44	24.84	23.51	18.27	16.97	17.78	18.36	26.15	25.52	23.25	22.61	15.82	27.04	15.52	18.30
MnO	0.52	0.50	0.50	0.50	0.50	0.55	0.70	0.56	0.45	0.71	0.69	0.59	0.67	0.86	0.46	0.39	0.52
MgO	0.05	0.40	0.95	0.76	0.74	0.95	1.38	1.51	0.80	0.23	0.25	0.29	0.13	0.01	0.01	0.01	0.07
CaO	1.50	1.72	2.14	0.26	0.04	1.74	0.24	0.44	0.58	0.12	0.08	0.08	nd	0.07	0.05	0.07	0.10
ZnO	nd	0.16	0.24	0.22	nd	0.31	1.53	0.23	0.31								
Li <sub>2</sub> O	nd	0.64	0.94	0.99	1.85	2.71 <sup>3,4,7</sup>	1.50 <sup>1,8,9</sup>	3.14 <sup>2,3</sup>	1.48 <sup>3,0,7</sup>								
Na <sub>2</sub> O	0.65	0.65	0.60	0.45	0.52	0.80	0.65	0.50	0.50	0.35	0.52	0.40	0.16	0.21	0.35	0.31	0.23
K <sub>2</sub> O	6.40	7.90	8.15	7.40	8.30	7.50	7.60	5.80	7.30	8.69	9.13	9.39	9.92	8.64	8.93	8.83	9.17
Rb <sub>2</sub> O	nd	0.35	0.37	0.44	nd	0.80	0.79	1.52	0.66								
P <sub>2</sub> O <sub>5</sub>	0.01	0.01	0.01	0.01	0.01	0.01	0.04	0.01	0.11	0.01	0.01	0.01	nd	0.01	0.01	0.05	0.05
H <sub>2</sub> O <sup>+</sup>	5.20	5.33	5.01	5.32	4.55	4.43	4.20	4.68	3.84	2.35	1.78	1.60	1.12	2.35	1.43	1.02	1.31
H <sub>2</sub> O <sup>-</sup>	0.92	0.32	0.14	0.64	0.15	0.22	0.42	0.67	0.60	0.15	0.22	0.18	0.29	0.15	0.24	0.11	0.13
F	nd	3.10	3.90	3.30	4.00	4.40 <sup>5</sup>	7.44 <sup>5</sup>	2.83									
Subtotal	100.34	99.91	100.20	99.82	101.06	100.21	100.07	100.20	100.14	100.32	101.42	101.00	102.74	100.66	102.37	101.74	98.96
Less O,F,Cl	-	-	-	-	-	-	-	-	-	1.30	1.64	1.39	2.31	1.68	1.85	3.13	1.19
Total	100.34	99.91	100.20	99.82	101.06	100.21	100.07	100.20	100.14	99.02	99.78	99.61	99.95	98.98	100.52	98.61	97.77
R1	-490	-449	-646	-431	-494	-780	-852	-336	-847	-578	-562	-592	-324	580	262.9	223	53
R2	354	477	538	332	365	581	389	432	389	410	390	395	332	416	414	396	433
Li	nd	2989	4391	4586	nd	12600	6986	14600	6874								
Cu	nd	35	10	10	nd	16	8	8	8								
Zn	nd	1253	1970	1770	nd	2470	12300	1880	2460								
Rb	nd	3250	3380	3990	nd	7290	7215	13900	6020								
Sr	nd	10	10	10	nd	20	10	20	20								
Structural formula	2	2	2	2	2	2	2	2	2	3	3	3	3	3	3	3	3
Si <sup>[4]</sup>	5.716	5.988	5.694	5.831	5.831	5.308	5.148	5.201	5.061	5.607	5.874	5.866	6.302	6.394	6.157	6.298	6.438
Al <sup>[4]</sup>	1.882	2.012	2.306	2.169	2.169	2.692	2.830	2.799	2.787	2.393	2.126	2.134	1.698	1.606	1.843	1.702	1.562
Fe	0.402	-	-	-	-	0.022	0.152	-	-	-	-	-	-	-	-	-	-
ΣZ	8.00	8.00	8.00	8.00	8.00	8.00	8.00	8.00	8.00	8.00	8.00	8.00	8.00	8.00	8.00	8.00	8.00
Al <sup>[6]</sup>	-	0.615	0.208	0.424	0.850	0.581	0.154	0.280	1.344	1.280	1.344	1.380	1.300	1.976	1.130	1.739	2.304
Ti	0.431	0.241	0.144	0.268	0.187	0.212	0.264	0.250	0.243	0.137	0.162	0.156	0.035	0.011	0.056	0.068	0.018
Fe <sup>+</sup>	1.415	0.653	1.579	0.950	0.827	1.464	2.197	2.094	2.229	0.124	-	0.305	0.231	-	0.056	0.068	0.018
Mg	0.012	0.095	0.226	0.183	0.171	0.222	0.329	0.357	0.192	0.054	0.058	0.068	0.030	0.002	0.002	0.002	0.016
Li	-	-	-	-	-	-	-	-	-	0.407	0.591	0.625	1.141	1.591	0.949	1.863	2.100
Zn	-	-	-	-	-	-	-	-	-	0.019	0.028	0.026	-	0.033	0.178	0.025	0.035
Fe <sup>+</sup>	3.041	3.259	2.600	3.361	3.052	2.397	2.269	2.358	2.479	3.461	3.337	3.052	2.899	1.931	3.558	1.914	2.346
Mn	0.072	0.068	0.068	0.069	0.066	0.073	0.095	0.075	0.062	0.095	0.091	0.078	0.087	0.106	0.061	0.049	0.068
Y	4.97	4.93	4.83	5.25	5.15	4.95	5.15	5.29	5.20	5.58	5.61	5.69	5.72	5.65	5.93	5.66	5.73
X	Ca	0.261	0.293	0.365	0.043	0.005	0.290	0.033	0.073	0.078	0.018	0.011	-	0.009	0.006	0.002	0.007
Na	0.206	0.202	0.186	0.141	0.157	0.243	0.201	0.154	0.156	0.107	0.158	0.122	0.048	0.059	0.107	0.089	0.068
K	1.337	1.613	1.663	1.527	1.644	1.501	1.550	1.173	1.503	1.754	1.821	1.880	1.940	1.609	1.792	1.661	1.793
Rb	-	-	-	-	-	-	-	-	-	0.036	0.037	0.044	-	0.075	0.080	0.144	0.065
ΣX	1.80	2.11	2.21	1.71	1.80	2.04	1.78	1.40	1.74	1.92	2.03	2.06	1.99	1.75	1.99	1.90	1.93
OH OH	5.681	5.692	5.345	5.741	4.712	4.635	4.479	4.950	4.135	2.481	1.857	1.675	1.145	2.268	1.501	1.003	1.339
F	-	-	-	-	-	-	-	-	-	1.552	1.929	1.638	2.662	1.847	2.190	3.47	1.372
ECM-group	5.69	5.69	5.34	5.74	4.71	4.64	4.48	4.95	4.14	4.03	3.79	3.31	3.81	4.14	3.69	4.47	2.71
+ve Charge	44.000	44.000	44.000	44.000	44.000	44.000	44.000	44.000	44.000	43.967	44.214	44.686	44.195	43.865	44.309	43.526	45.289

<sup>2</sup>Combined gravimetric and A.A. determination. <sup>3</sup>Colorimetric determination. <sup>5</sup>Fluorine determination using fusion method of decomposition. <sup>6</sup>Includes 28 ppm Be.

Table 10.5

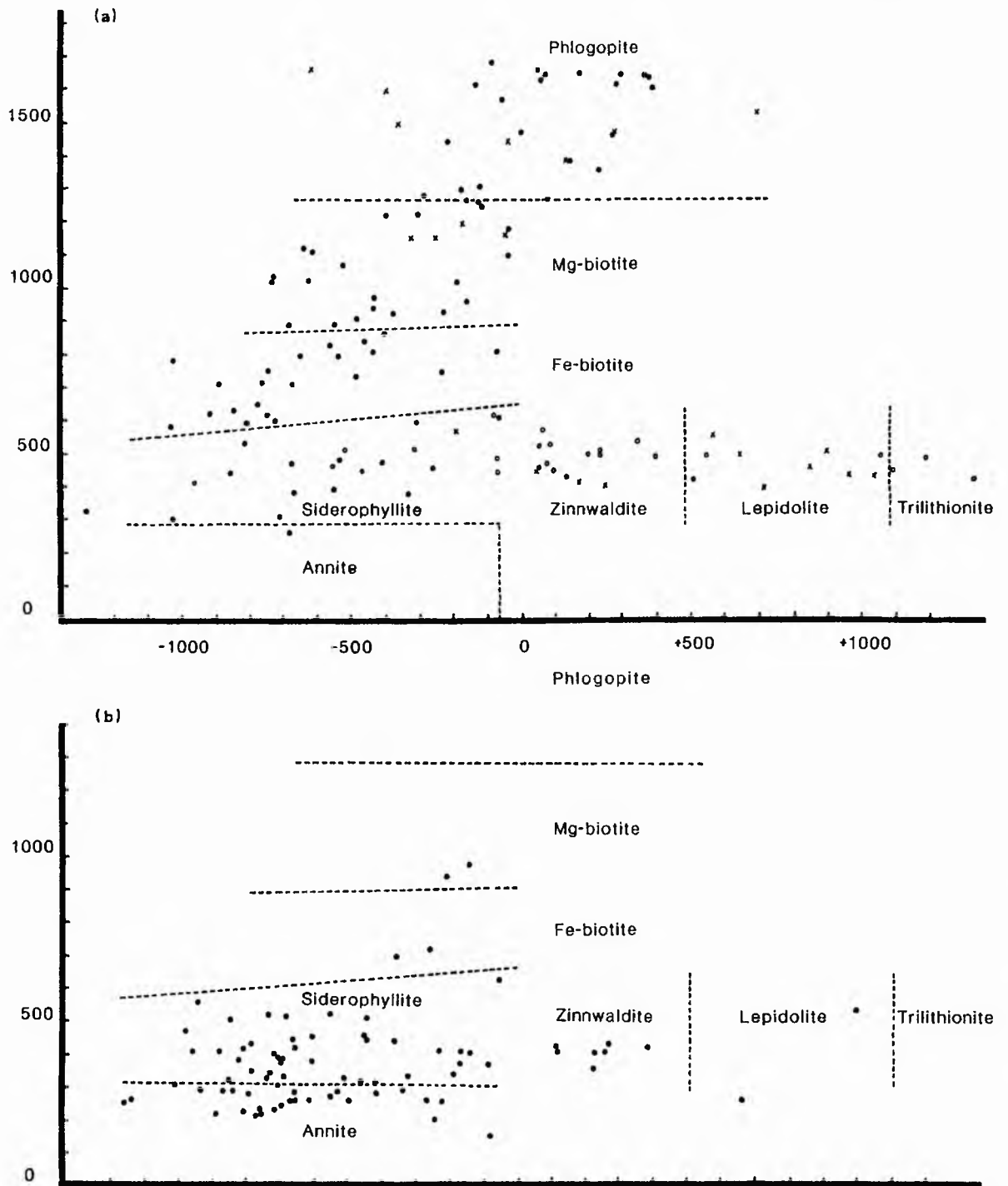
Chemical composition and structural formulae for micas from hydrothermal veins in the Niger/Nigeria anorogenic Province.

## Micas from hydrothermal veins

	Ririwai biotite granite	Rafin Gabas biotite granite			Agwalande biotite granite		Tarraouadji biotite granite
Table no	52	63	64	65	66	67	68
Sample no	X.700	Af 23/1 <sup>9</sup>	Af 22/3 <sup>10</sup>	Af 22/12 <sup>11</sup>	Af 106	GT	TA 4/5
SiO <sub>2</sub>	42.24	34.47 <sup>4</sup>	32.40 <sup>2</sup>	37.0	51.49 <sup>4</sup>	39.00	37.45 <sup>1</sup>
TiO <sub>2</sub>	0.16	0.10 <sup>4</sup>	0.10	0.25	0.06 <sup>4</sup>	0.01	0.09 <sup>1</sup>
Al <sub>2</sub> O <sub>3</sub>	19.62	16.89 <sup>4</sup>	14.34	15.23	27.16 <sup>4</sup>	20.20	22.14 <sup>4</sup>
Fe <sub>2</sub> O <sub>3</sub>	2.02	2.32 <sup>4</sup>	4.17	3.45	0.18 <sup>4</sup>	2.45	3.07 <sup>1</sup>
FeO	18.64	30.72	31.17	30.56	-	21.80	19.94
MnO	0.30	0.28	0.24	0.21	0.31	0.68	0.61 <sup>1</sup>
MgO	0.08	0.75	0.29	0.39	0.01	0.56	0.08 <sup>1</sup>
CaO	0.11	0.12	0.07	0.07	0.04	tr	0.04 <sup>1</sup>
ZnO	nd	0.09	0.16	0.15	0.04	nd	0.27
Li <sub>2</sub> O	1.90	0.45	0.48	0.50	4.56	nd	1.54
Na <sub>2</sub> O	0.14	0.18	0.21	0.23	0.48	0.27	0.38 <sup>1</sup>
K <sub>2</sub> O	8.84	8.67	8.41	8.39	9.66	9.22	9.33 <sup>1</sup>
Rb <sub>2</sub> O	nd	0.32	0.34	0.33	0.96	nd	0.52
P <sub>2</sub> O <sub>5</sub>	nd	0.01	0.01	0.01	0.10	0.16	0.01 <sup>1</sup>
H <sub>2</sub> O <sup>+</sup>	2.35	2.10	2.23	2.60	2.30	1.06	0.81 <sup>1</sup>
H <sub>2</sub> O <sup>-</sup>	0.48	0.10	0.17	0.16	0.10	nd	0.09
F	5.02	2.44	3.71	3.74	2.43	3.75	4.00
Subtotal	102.01 <sup>12</sup>	100.01	98.50	103.27	99.88	99.16	100.37
Less O=F,Cl	2.12	1.03	1.56	1.58	1.02	1.58	1.68
Total	99.89	98.98	97.13 <sup>13</sup>	101.69	98.86	97.58	98.69
	124	-710	-856	-521	995	-321	-455
	401	381	303	326	538	424	442
Li	nd	2090	2230	2322	21200	nd	7143
Cu	nd	59	1496	148	8	nd	8
Zn	nd	695	1290	1200	294	nd	2180
Rb	nd	2920	3150	5010	8800	nd	4760
Sr	nd	20	20	40	50	nd	20
Structural formula	3	3	3	3	3	3	3
% Si	6.212	5.652	5.482	5.806	6.895	6.190	5.844
% Al <sup>[4]</sup> <sub>3+</sub>	1.788	2.348	2.518	2.194	1.105	1.810	2.156
% Fe <sup>3+</sup>	-	-	-	-	-	-	-
ΣZ	8.00	8.00	8.00	8.00	8.00	8.00	8.00
Y Al <sup>[6]</sup>	1.613	0.916	0.342	0.622	3.181	1.969	1.916
Ti	0.020	0.012	0.013	0.029	0.006	0.001	0.011
Fe <sup>3+</sup>	0.224	0.286	0.531	0.407	0.018	0.293	0.361
Mg	0.018	0.183	0.073	0.091	0.002	0.048	0.019
Li	1.124	0.297	0.327	0.316	2.456	-	0.967
Zn	-	0.011	0.020	0.017	0.004	-	0.031
Fe <sup>2+</sup>	2.293	4.212	4.411	4.010	-	2.894	2.602
Mn	0.037	0.039	0.032	0.028	0.035	0.091	0.081
ΣY	5.33	5.96	5.75	5.52	5.70	5.30	5.99
X Ca	0.017	0.019	0.011	0.010	0.002	-	0.005
Na	0.040	0.057	0.069	0.070	0.125	0.083	0.115
K	1.658	1.813	1.815	1.679	1.650	1.867	1.857
Rb	-	0.034	0.037	0.033	0.083	-	0.052
ΣX	1.72	1.92	1.93	1.79	1.86	1.95	2.03
OH OH	2.305	2.297	2.517	2.721	2.054	1.122	0.843
F	2.335	1.265	1.985	1.856	1.029	1.882	1.974
EOH-group	4.64 <sup>15</sup>	3.56	4.50	4.58	3.08	3.00	2.82
+ve Charge	43.355	44.438	43.498	43.423	44.917	44.995	45.183

<sup>1</sup>X.R.F. determination. <sup>2</sup>Combined gravimetric and A.A. determination.  
<sup>3</sup>Colorimetric determination. <sup>4</sup>Gravimetric determination. <sup>5</sup>Fluorine  
determination using fusion method of decomposition. <sup>6</sup>Includes 6 ppm Be.  
10 ppm Cr, 6 ppm Cd. <sup>7</sup>Includes 19 ppm Be, 30 ppm Cr, 30 ppm Cd. <sup>8</sup>Includes 39 ppm  
Be. <sup>9</sup>Includes 6 ppm Be. <sup>10</sup>Includes 180 ppm Be. <sup>11</sup>Includes 8 ppm Be. <sup>12</sup>Includes  
0.02% Cl, 0.02% S, 0.05% CO<sub>2</sub>. <sup>13</sup>Includes 0.19% CuO. <sup>14</sup>Converted from percentage.  
<sup>15</sup>Includes Cl = 0.005.

Fig 10.3 R1-R2 plot of Li-, Fe-, Li-Fe and Mg-rich micas (a) worldwide (b) Nigerian anorogenic province



(a) data mainly from Foster (1960), Deer, Howie and Zussman (1965) and Rieder (1970)

(b) data from Abernety (unpubl.), Bennett (1981), Kinnaid (1977) and this work

high levels of Li correspond with high Al and high Si content, and variations in these elements will therefore tend to highlight variations in Li.

Whether it is valid to use a diagram constructed for a fractionating magma system could be argued. There is no doubt however, that this diagram is very useful. It has the advantage that probe data can be plotted on it since it does not require F or Li in the analysis. In addition because values of  $Fe^{3+}$  are generally small and the molecular weight of  $Fe_2O_3$  is high, the plotting position of any particular mica composition is little affected by utilising total iron as FeO. Initially, the purpose of calculating mica compositions in terms of R1-R2 parameters was to rationalise the colour changes as a function of multi-cationic variations. However it became obvious that the more important use of the diagram was that it could be used to assign a name to an individual mica. The R1-R2 plot appears therefore to be the first satisfactory diagram for typing a trioctahedral mica from major element data alone and therefore has important implications for mineralogical and petrological study.

In order to test the use of this multicationic approach outlined above, named trioctahedral micas from the literature were plotted on the R1-R2 diagram (Fig 10.3a). All the different trioctahedral micas occupied different parts of the plot and fields for annite, siderophyllite, zinnwaldite, lepidolite, trilithionite and phlogopite could be readily defined. In addition it was also possible to subdivide the true biotites (i.e. trioctahedral micas with Mg and Fe) into Mg biotites (those where  $Mg > Fe$ ) and Fe biotites (those where  $Fe > Mg$ ).

The names assigned to each mica in Fig 10.3a and in the following sections appear to fulfil the requirements of end-member compositions of Foster (1960), Deer, Howie and Zussman (1965), Rieder (1970) and Czerny and Burt (1984).

### Trioctahedral micas in the Niger-Nigeria Province

Analytical data for the micas separates from the Niger-Nigerian Province is given in Tables 10.2 to 10.5, together with the R1-R2 values and structural formulae. As the tables show, there are eight important cations in the octahedral Y sites, Al,  $Fe^{2+}$ ,  $Fe^{3+}$ , Li,  $Mn^{2+}$ , Mg, Ti, and Zn, with other substitutions occasionally by  $Cr^{3+}$ , Ba and Sr. Of the octahedral occupancy, the variation in  $Fe^{2+}$ , Li, Al and  $Fe^{3+}$  are important in the naming of the mica. For an ideal trioctahedral mica, cationic octahedral site-occupancy should be equal to six. For the analysed micas this idealised site filling value is rarely achieved and the calculated values usually lie between five and six. The sum of the cations in the tetrahedral Z sites is eight and site occupancy is by silicon, aluminium and sometimes iron. The interlayer X site is dominated by K with small amounts of Na, Rb and Ca. The cell contains twenty oxygens plus fluorine and/or hydroxyl groups which accounts for four cations. The analysed micas, closely approach the ideal electrical neutrality with 44 negative and positive charges per cell.

The data of Bowden and Kinnaird (1984a) suggested that the alteration processes in the Nigerian anorogenic granites can be monitored by the micas whose compositions lie within the annite -siderophyllite -zinnwaldite-lepidolite spectrum. To test this statement, one hundred chemical analyses for micas from the Nigerian Province were plotted on the R1-R2 plot (Fig 10.3b) The micas were from granite porphyry, quartz syenite, alkali feldspar biotite granite, biotite

syenogranite and hydrothermally altered rocks. Only four fell outside the annite - siderophyllite - zinnwaldite - lepidolite fields. The two Mg-biotites and one of the Fe-biotites were analysed by Bennett (1981). They occur in the Amdulayi alkali feldspar syenite of the Shira complex in association with occasional ilmenite grains in the outer part of a zoned pseudomorph in which the centre is filled by richterite. The remaining Fe-biotite is from the Fier hastingsite biotite granite of the Sara Fier Complex (analysis in MacLeod et al 1971).

Using unpublished data of Abernethy, Bowden and Kinnaird (1984a) utilised a modified Rieder (1970) diagram to establish two compositional trends for the Nigerian micas (Fig 10.4). These were related to the different hydrothermal alteration processes of sodic, potash and acid metasomatism. Micas growing during sodic metasomatism ranged from the original annite where metasomatism was not intense (Fig 10.4), through zinnwaldite to lepidolite where metasomatic sodic alteration was most intense. In contrast, micas growing during potassic metasomatism ranged from annite to ferrous-siderophyllite and during acid metasomatism this trend was continued through lithian siderophyllite towards zinnwaldite (Fig 10.4). Therefore, whilst micas of zinnwaldite composition occur in both sodic and acid metasomatised rocks, the process of development of such similar micas in the two contrasting settings appeared from this diagram not to be the same. Also when viewed in thin section, the micas do not look the same even though they are compositionally similar.

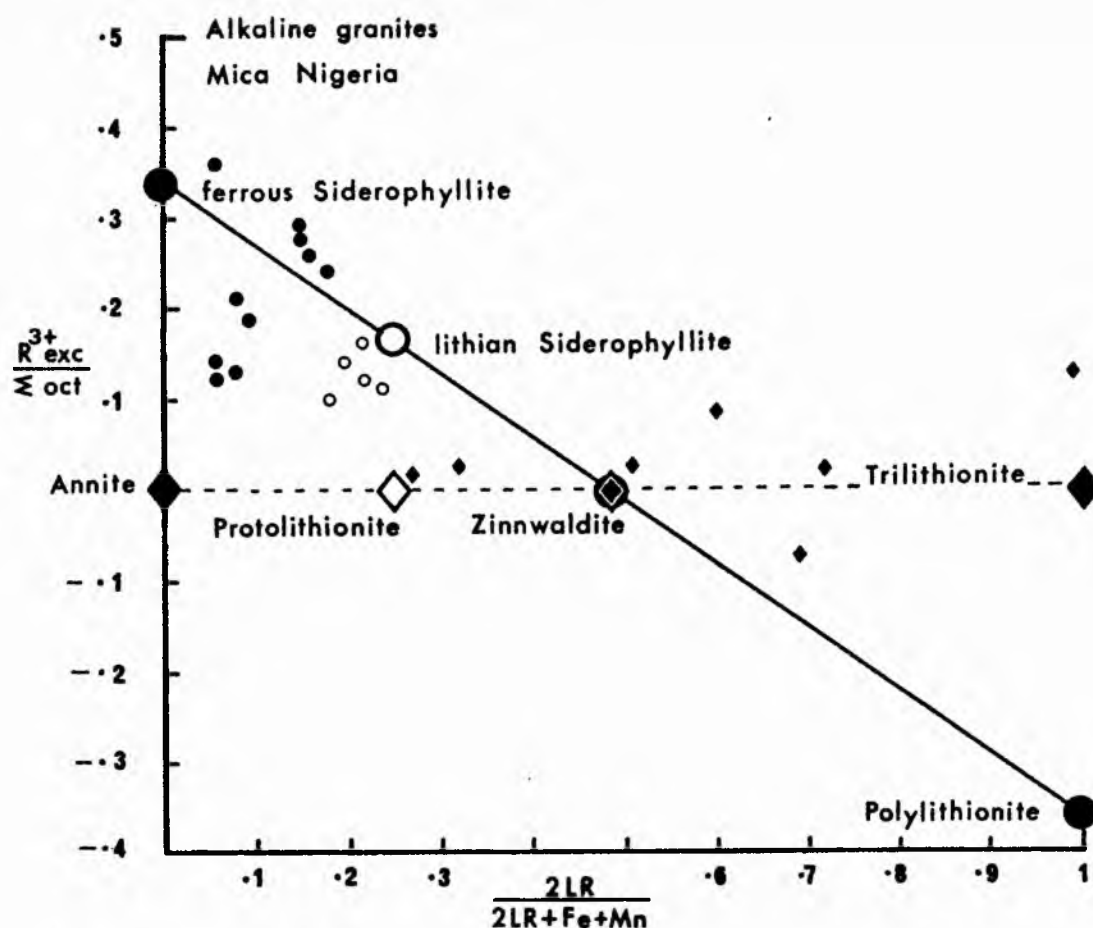
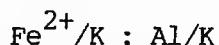
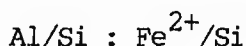
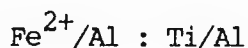
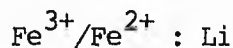
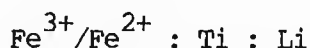
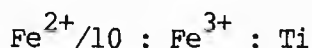


Fig 10.4 Compositional variations in trioctahedral micas, from the Afu complex, Nigeria. Mica compositions determined by C. A. ABERNETHY and R. A. BATCHELOR.  $R^{3+} exc = \sum Al^{3+} + Fe^{3+} - Li$ ;  $LR = \sum Al^{3+} + Fe^{3+}$  or  $Li$  whichever is the smaller quantity.  $\Sigma oct$  is sum of octahedral cations in the structural formula. Micas growing during sodic metasomatism (albitization indicated by closed diamonds). Micas growing during potassic metasomatism (microclinization) indicated by closed circles. Micas growing during acid metasomatism (greisenization) indicated by open circles. Plotting parameters adapted from RIEDER (1970).

The coloration of a mica is not always a reliable guide to its composition. However iron-rich micas are dark in colour and the most iron-enriched, which is assumed to be the most primitive mica, occurs in coarse grained biotite granite and varies from chestnut to greeny black in colour. These micas are also titanium rich micas and the Ti:Fe ratio is clearly responsible for variations in colour. With decreasing iron content the colour of the mica ranges through tan and khaki to grass green, blue green and pale steel blue to beige or colourless when iron-poor and lithium-enriched. The colour of lepidolite from the Afu Complex is pale purple.

In an attempt to monitor the elements responsible for colour variation, a number of graphical plots have been considered. The difficulty is, that varying proportions of Li, Al, Fe<sup>2+</sup>, Fe<sup>3+</sup>, Mg, Li and Ti undoubtedly affected the mica colour and in conventional variation diagrams it is not possible to include all the cations. Several simple chemical comparative diagrams were utilised and from a combination of these it was anticipated that it would be possible to monitor the chemical causes of colour variations. The following comparative plots were constructed:-



In the plot of  $\text{Fe}^{2+}/10 : \text{Fe}^{3+} : \text{Ti}$  (Fig 10.5a) the compositions were well spaced throughout the diagram. The dark coloured, tan, chestnut and black micas plot close to the centre of the diagram with the Ti varieties showing the greatest Ti enrichment whilst deep blue green contains low Ti. In the pale green micas Fe<sup>3+</sup> is high, whilst in colourless samples either Fe<sup>2+</sup> or Fe<sup>3+</sup> is low, or both. However, the plot failed to discriminate between micas of certain colours, for example between dark blue green, dark grass green and black maximum absorption colours.

A distinction between these colours was more successful on a triangular diagram of  $\text{Fe}^{3+}/\text{Fe}^{2+}$  against Ti and Li (Fig 10.5b). The colourless micas plotted close to the Li pole and the chestnut and black micas plotted close to the Ti pole. Khaki and honey coloured micas plotted towards the Ti=Li position. However, in this diagram it was difficult to separate micas which were blue green from those which were deep green because these colour variations are almost certainly due to changing Fe<sup>3+</sup>:Fe<sup>2+</sup> ratios, which cannot be discriminated on this plot.

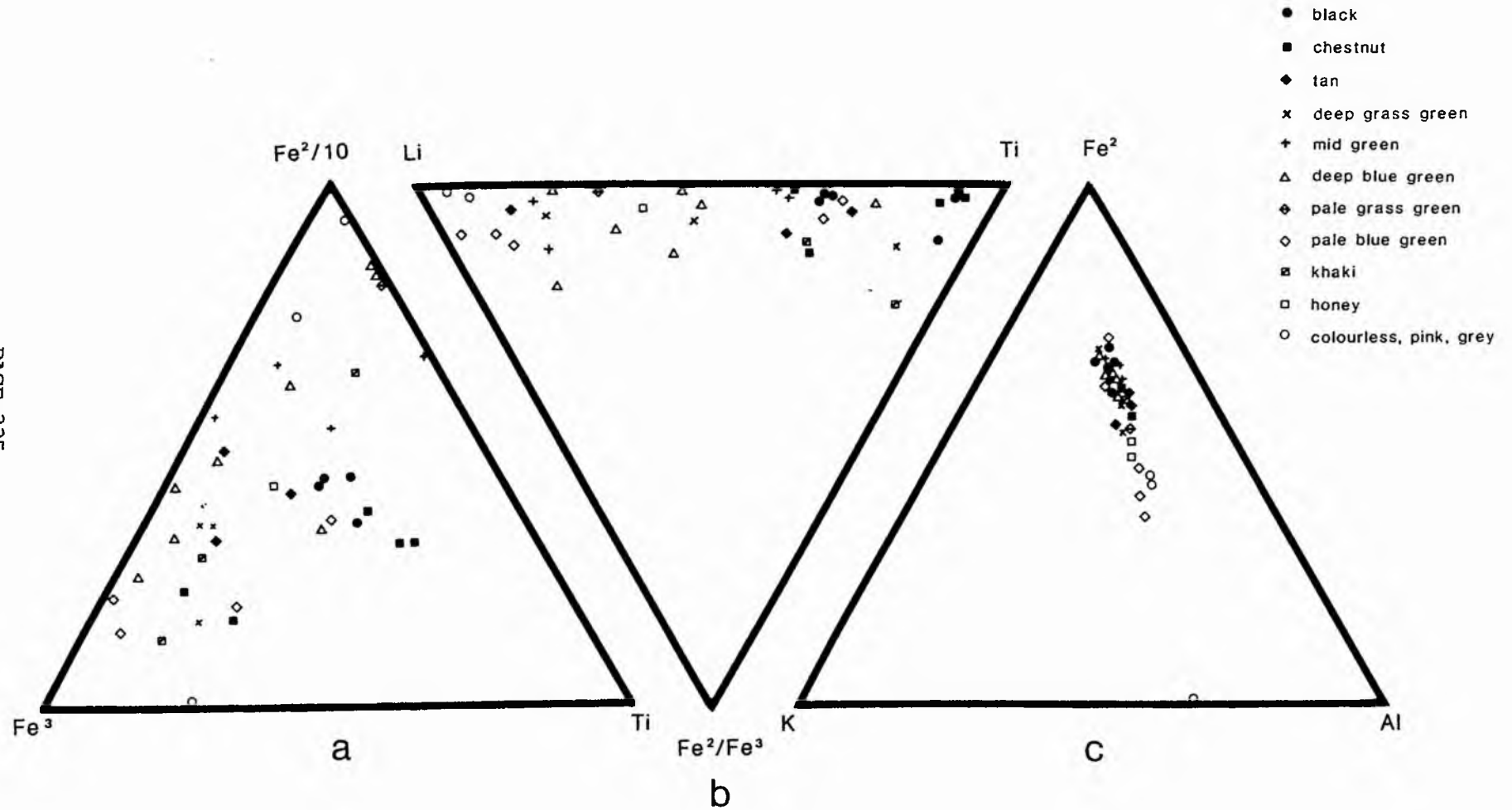


Fig 10.5 Selected compositional plots for the micas showing colour variations as a function of elemental variations

In the  $Fe^{2+} : K : Al$  diagram (Fig 10.5c), colourless and pale-coloured micas plot towards the Al pole with honey and khaki colours intermediate (  $Al:Fe = 1$  approx) while darker colours plot towards the  $Fe^{2+}$  pole. However, there was no distinction between dark blue and dark green for example, or between chestnut, tan and black. In other diagrams such as the plot of molecular percentage of  $Al/K : Fe^{2+}/K$  (Fig 10.6) there seemed to be no consistent colour variation with plotting position other than for the palest and colourless varieties.

In none of the diagrams chosen was there an absolute clear pattern - in other words there always seemed to be one or more analyses that plotted in a spurious position from that anticipated from its colour. For bulk mica analyses by XRF and AA, it seems almost certain that minerals interleaved with the mica may be responsible for this difficulty in attributing colour to chemical composition. It has been noted that fluorite, ilmenite, haematite, molybdenite, siderite and other minerals are interleaved along the mica cleavage and therefore a high iron or titanium content in a bulk mica analysis could have resulted from these included minerals rather than occurring within the mica lattice. This would explain why several of the blue-green micas plot within the annite field, since they nearly always have haematite along the cleavage and commonly ilmenite too.

On the multi-cationic R1-R2 plot (Fig 10.7), there are generalised variations in colour with changing composition. Thus micas with high negative values of R1 (>500) are deeply coloured. With increasing R1 values due to increasing silica and K and decreasing Fe and Ti there is a decrease in the intensity of coloration through blues and greens to colourless. With increasing R2 values where R1 values are between -400 and -1000 there is an overall change in coloration with chestnut coloured micas showing enrichment in Mg (Fig 10.7).

No absolute statements can be made therefore on colour variations. However, generalised conclusions can be made:-

- (1) colourless micas are low in Fe and Ti, but rich in Si, Al, and Li.
- (2) pale blue green is chemically similar to the colourless with high Si, Al and Li, low  $Fe^{2+}$  and sometimes significant  $Fe^{3+}$
- (3) deep blue green mica is low in Ti and Al but with variable  $Fe^{2+} : Fe^{3+}$  and high Li.
- (4) chestnut colours are due to high Ti and / or high Mg
- (5) black coloration is due to high  $Fe^{2+}$ ,  $Fe^{3+}$ , Ti and Mg

There appears to be no systematic relationship between K, Mn or F content and colour variation.

Fig. 10.6 Molecular proportions of Al/K against Fe<sup>2+</sup>/K

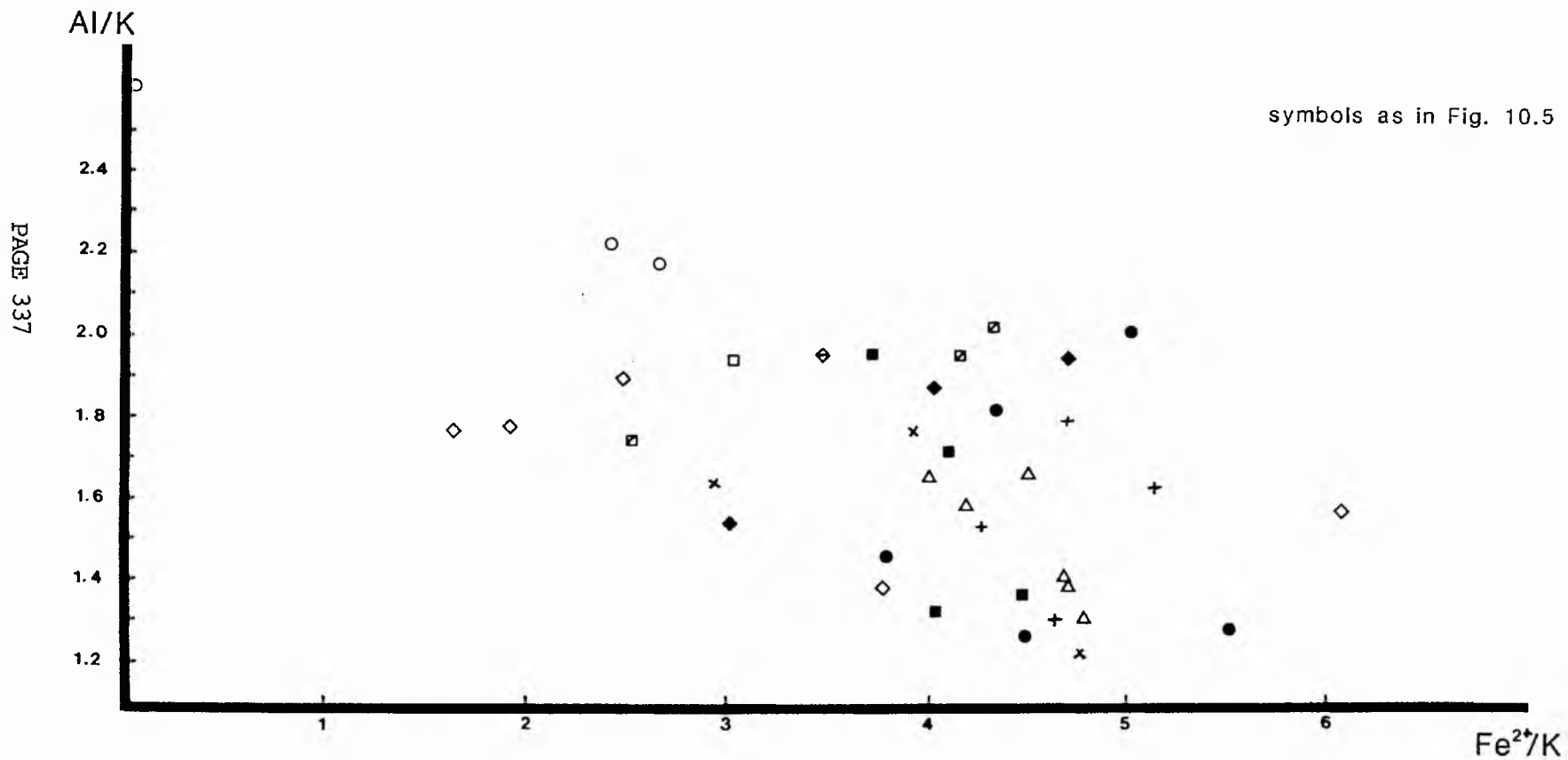
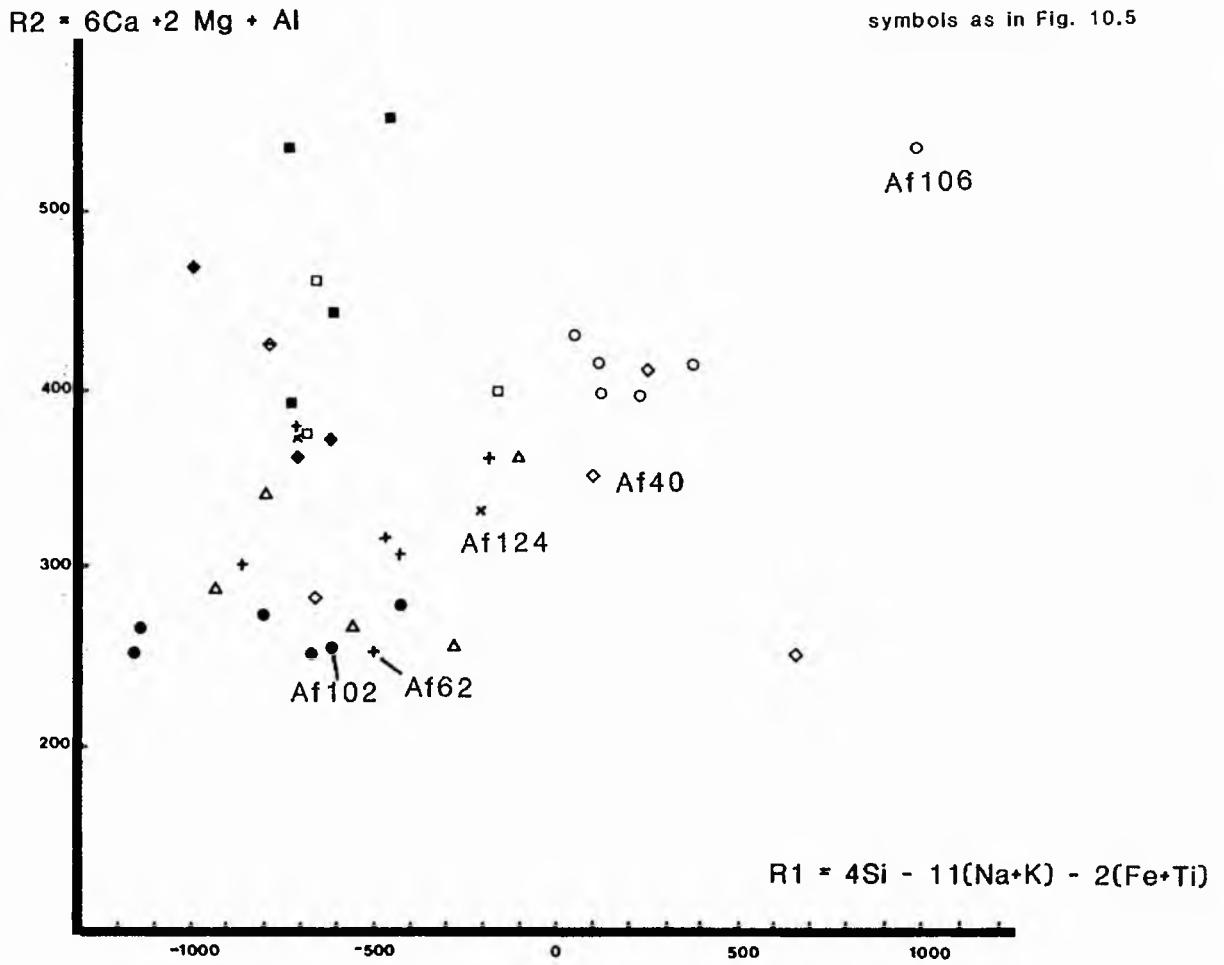


Fig. 10.7 R1-R2 compositional plot showing colour variations in selected Nigerian micas



## Trioctahedral micas in the Saiya Shokobo Complex

### Introduction

In order to understand more about varying mica compositions during hydrothermal alteration, a number of analyses were made on micas from the volcanic rocks, the biotite granite and different alteration assemblages in the Saiya Shokobo Complex. Within this complex the compositional range of the trioctahedral mica is similar to that for the province as a whole. Also the complete colour variations from black to chestnut through blue and honey to colourless can be observed in this one complex and have provided an ideal testing ground for earlier hypotheses.

### Optical characteristics of micas from the volcanic pile and biotite granite

The mica of the porphyritic ignimbritic pile occurs as groundmass clusters, commonly 2mm in size but ranging up to 4mm across, or as isolated granules in the groundmass. More rarely skeletal flakes developed and like the clusters are associated with accessory zircon, fluorite and apatite. In colour the mica varies from almost colourless through shades of khaki and greeny brown to tan and is pleochroic to straw yellow.

Within the biotite granite, the mica varies according to the facies:-

- In the coarse-grained facies, (SS41/1a, SS43, SS58/1, SS63/2 & SS64/1) and the medium-grained facies, the biotite shows the same features of colour variation and texture. The biotite occurs as ragged, skeletal or sieve-textured flakes or occasional aggregates up to 5mm in diameter, scattered irregularly through the rock. It varies from bluish green through khaki to deep bluey or brownish green or almost black and is pleochroic from pale green to yellow brown or khaki. In some medium- and all fine-grained granite facies the biotite is lighter in colour, often a pale bluey green and may be pleochroic from light brown to colourless, or be pale grey. Pleochroic haloes surrounding monazite, zircon and occasional allanite are particularly noticeable in these paler varieties. Fluorite often occurs, usually as rounded or subhedral masses within or around the mica and sometimes along the micas cleavage traces. In light-coloured biotite, it is not uncommon to find haematite and rutile in minute rods associated with the fluorite along cleavage traces. In SS63/2 the cleavage traces are bent and heavily accentuated by opaques and limonitic streaks. In SS43 which is a coarse-grained granite the mica formed ragged plates associated with fluorite, allanite and zircon. Occasionally the mica can be seen breaking down to secondary ilmenite, haematite and rutile assemblages. These opaque phases define the cleavage planes.

- In the granophyres, (SS23/13 and SS24/2), mica ranges from skeletal and sieve-textured to discrete ragged plates or clusters, often chloritised and associated with opaques and fluorite. It varies in colour from grass green to very deep greeny-brown maximum absorption colours and is pleochroic to straw yellow or pale green.

- In the porphyritic facies, the biotite varies from grass green through deep green to black in colour with little variation in any one section. It is nearly

always skeletal in texture, with occasional discrete well-formed flakes or felted aggregates (SS42/1). The skeletons have often enveloped rounded quartz and sometimes rounded or euhedral fluorite and more rarely zircon and monazite. There is no chloritisation and the cleavages, although distinct, are not characterised by extensive haematite development. Sample SS53 differs a little from the other four samples. There are colour variations within individual micas ranging from tan to deep green. Cleavages are emphasised by haematite development and occasional chloritisation.

- Biotite microgranite is commonly developed at the contact with the volcanics. In SS49/2B the mica is variable in colour from pale tan to deep chestnut - often within one sample - but the general tendency is towards a deep green colour in this facies.

#### Chemical composition of micas from the volcanic pile and biotite granite

The immense colour variation in the micas even within one granite facies such as a coarse-grained granite suggests that there is a wide range in the chemical composition of the Rishi micas. Thirteen micas were analysed by bulk XRF/AA techniques and 66 microprobe analyses were made as traverses across micas in polished sections of seven samples. The mica in SS48 was analysed using both techniques as a check against different analytical methods giving different results.

Chemical data on the mica concentrates which were analysed by XRF and AA techniques is given in Table 10.6 and the microprobe data is given in Tables 10.7 to 10.12. In determining the structural formula from probe data, the structure was based on 23 oxygens where fluorine data existed, and on 22 oxygens where there was no fluorine analysis. For the XRF/AA data the structural formula is based on 24 oxygens.

Table 10.6 shows that the same eight cations are important in the octahedral Y sites of the Rishi micas as in all the Nigerian biotites; with Al, Ti, Fe<sup>2+</sup>, Fe<sup>3+</sup>, Li, Mn<sup>2+</sup>, Mg, and Zn, and rarer substitution occasionally by Ba and Sr. The idealised cationic octahedral site-occupancy which should be six, was rarely achieved and the calculated values usually lie between 5.5 and 6.0. The sum of the cations in the tetrahedral Z sites is eight and site occupancy is always by silicon and aluminium for Rishi micas. The interlayer X site is dominated by K with small amounts of Na and Rb with traces occasionally of Ca.

Compositionally, the tan coloured biotite of the ignimbritic pile is the most iron and titanium enriched within the whole complex and contains up to 35% FeO in SS67 with up to 2.8% TiO<sub>2</sub> (Table 10.7). It plots within the annite field in Fig 10.8. The development of this mica in the devitrified groundmass of the volcanic pile suggests that the mica was late magmatic to subsolidus in origin and that it represents the most primitive or "least evolved" composition in the Saiya Shokobo complex. There is no mica in the quartz feldspar porphyry feeder dyke to the ignimbritic pile, further supporting the suggestion that the mica in the ignimbritic pile was of subsolidus origin.

In the petrography section it was stated that the most pristine granite samples were SS41/1a and SS58/1, since they contained a lamellar perthite.

Table 10.6 Mica compositional variations in Rishi samples. Bulk analyses by Atomic Absorption and XRF techniques

	SS34	SS38	SS48	SS8/3	SS27/4	SS44/1	117/5A	SS23	SS23/4	SS23/6	SS63/1	SS117	SS117/5	
SiO <sub>2</sub>	36.90	36.70	40.12	41.36	37.09	33.75	39.20	36.40	33.15	37.69	35.46	36.10	45.50	
TiO <sub>2</sub>	1.83	3.18	0.90	0.16	0.54	0.97	2.58	0.60	0.53	0.36	0.61	3.07	2.47	
Al <sub>2</sub> O <sub>3</sub>	12.27	13.41	18.80	20.88	20.59	18.79	12.24	12.54	13.13	15.11	16.63	13.26	10.42	
Fe <sub>2</sub> O <sub>3</sub>	2.18	2.16	1.84	0.42	<0.01	0.59	2.98	1.34	5.82	2.79	<0.01	7.29	2.48	
FeO	30.11	28.26	20.45	17.86	25.46	28.01	29.00	31.20	30.60	27.99	31.30	25.30	28.10	
MnO	0.49	0.39	0.27	0.44	0.42	0.26	0.43	0.61	0.58	0.54	0.48	0.51	0.40	
MgO	0.07	0.06	0.48	0.03	0.06	1.08	0.03	0.07	0.13	0.05	0.04	0.05	0.13	
CaO	0.06	0.14	0.07	0.07	0.19	0.38	0.15	0.12	0.24	0.08	0.15	0.20	0.40	
Na <sub>2</sub> O	0.33	0.26	0.32	0.14	0.73	0.23	0.10	0.14	0.09	0.06	0.32	0.11	0.10	
K <sub>2</sub> O	8.88	7.93	8.94	8.86	9.73	8.57	8.15	8.62	8.98	8.80	9.19	8.82	6.09	
P <sub>2</sub> O <sub>5</sub>	<0.01	<0.05	0.02	<0.05	<0.01	<0.05	<0.01	<0.01	<0.01	0.10	<0.01	<0.01	<0.01	
H <sub>2</sub> O <sup>+</sup>	1.57	1.83	1.15	1.58	1.37	2.03	2.28	0.83	1.98	2.33	2.46	2.64		
H <sub>2</sub> O <sup>-</sup>	0.10	0.11	0.12	0.14	0.17	0.17	1.61	0.20	0.07	0.07	0.20	1.40	1.56	
Li <sub>2</sub> O	0.22	0.79	1.49	1.79	1.23	0.44	1.40	1.34	0.71	0.77	0.74	2.73	1.96	
F	2.77	3.57	3.93	2.62	4.30	3.17		3.28	3.80	2.52	2.80			
F=O	1.16	1.49	1.65	1.10	1.81	1.33		1.38	1.60	1.06	1.18			
Total	96.63	97.35	97.25	95.30	100.09	97.16	100.16	95.92	98.22	98.20	99.22	101.49	99.62	
R1	-673	-421	-168	122	-785	-655	-275	-557	-933	-426	-786	-660	665	
R2	251	281	400	418	427	462	257	262	289	307	344	284	254	
Ba									45+15					
Be							6	39				16	19	
Cd							6					10	30	
Cr							10					20	30	
Cu	22	<10	16	16	175	16		25	8	7	10+10			
Rb	5340	5140	10540	6480	5045	3530		4840	4760	7290	5460			
Sr	<20	<60	<20	<20	<10	<20		<40	<50	<20	<10			
Zn	3110	3555	2545	1280	2097	1865	1660	4015	4234	2470	2820	2510	3140	
Structural formulae														
Si (4)	6.151	6.059	6.226	6.567	5.773	5.723	6.217	6.258	5.532	6.069	5.726	5.728	6.846	
Al (4)	1.849	1.941	1.774	1.433	2.227	2.277	1.783	1.742	2.468	1.931	2.274	2.272	1.154	
Z	8.000	8.000	8.000	8.000	8.000	8.000	8.000	8.00	8.000	8.000	8.000	8.000	8.000	
Al (6)	0.561	0.554	1.665	2.274	1.550	1.214	0.505	0.799	0.114	0.936	0.892	0.208	0.694	
Ti	0.229	0.385	0.105	0.018	0.063	0.115	0.308	0.078	0.067	0.044	0.074	0.366	0.279	
Fe <sup>3+</sup>	0.273	0.262	0.215	0.048	0.070	0.070	0.356	0.173	0.731	0.338	0.870	0.281	0.281	
Mg	0.017	0.014	0.111	0.007	0.014	0.254	0.007	0.018	0.032	0.005	0.010	0.012	0.029	
Li	0.483	0.512	0.924	1.084	0.764	0.292	0.415	0.429	0.477	0.499	0.474	0.810	0.551	
Zn	0.048	0.052	0.037	0.018	0.030	0.027		0.063	0.065	0.030	0.042			
Fe <sup>2+</sup>	4.197	3.808	2.654	2.250	3.314	3.693	3.847	4.486	4.270	3.769	4.227	3.357	3.536	
Mn	0.069	0.053	0.035	0.056	0.055	0.035	0.058	0.089	0.082	0.074	0.066	0.069	0.051	
Y	5.88	5.64	5.75	5.75	5.79	5.70	5.50	6.13	5.84	5.69	5.78	5.69	5.42	
Ca	0.009	0.014	0.008	0.002	0.030	0.054	0.025	0.022	0.041		0.024	0.034	0.064	
Na	0.107	0.081	0.096	0.041	0.220	0.070	0.031	0.047	0.029	0.019	0.100	0.034	0.029	
K	1.888	1.630	1.770	1.702	1.932	1.723	1.649	1.890	1.911	1.808	1.893	1.785	1.169	
Rb	0.062	0.058	0.115	0.069	0.055	0.040		0.059	0.056	0.068	0.062			
X	2.070	1.780	1.99	1.81	2.24	1.89	1.70	2.02	2.04	1.90	2.08	1.85	1.26	
OH	1.746	1.967	1.190	1.587	1.350	2.135		0.952	2.204	2.503	2.607			
F	1.460	1.819	1.929	1.248	2.117	1.581		1.783	2.011	1.283	1.430			
OH	3.21	3.79	3.12	2.84	3.47	3.72		2.74	4.22	3.79	4.04			
+ve	44.794	44.214	44.881	45.164	44.534	44.285	44.000	45.265	43.785	44.214	43.963	44.000	44.000	
Sample                      Rock type                      Colour														
SS34	porphyritic biotite granite							deep green to black						
SS38	porphyritic biotite granite							deep green to black						
SS48	albitised biotite granite							honey						
SS8/3	acid altered K-rocks (micatites)							pale grey to colourless						
SS27/4	acid altered K-rocks (micatites)							pale grass green						
SS44/1	acid altered K-rocks (micatites)							khaki						
SS117/5a	acid altered K-rocks (micatites)							deep blue green						
SS23	acid altered perthite granite (Stage 3-4)							deep blue green						
SS23/4	acid altered perthite granite (Stage 3-4)							deep blue green						
SS23/6	acid altered perthite granite (Stage 3-4)							deep blue to grass green						
SS63/1	acid altered perthite granite (Stage 3-4)							deep blue to grass green						
SS117	silicification							pale blue green						
SS117/5	silicification							pale blue green						

Table 10.7 Microprobe analyses of Biotite in  
SS67 and SS85b quartz feldspar  
porphyritic ignimbrite

	SS67 58	SS67 62	SS85b 19	SS85b 43
SiO <sub>2</sub>	35.63	35.64	34.20	39.67
TiO <sub>2</sub>	2.60	2.84	n.a	n.a
Al <sub>2</sub> O <sub>3</sub>	13.93	13.78	12.79	14.56
FeO	34.01	34.89	27.67	29.84
CaO	0.02	0.01	n.a	n.a
Na <sub>2</sub> O	0.01	0.32	0.27	0.16
K <sub>2</sub> O	9.20	8.85	6.97	9.29
ZnO	0.38	0.45	n.a	n.a
Total	95.78	96.78	81.90	93.52
R1	-792	-850	-217	-416
R2	275	271	250	286
Q	2	-1	33	17
F	195	177	139	192
Si <sub>4</sub>	5.830	5.786	6.336	6.402
Al <sub>4</sub>	2.170	2.214	1.664	1.598
Al <sub>6</sub>	0.514	0.426	1.130	1.174
Ti	0.330	0.352	0.000	0.000
Fe(t)	4.664	4.752	4.290	4.026
Zn	0.044	0.044	0.000	0.000
Na	0.000	0.110	0.088	0.044
K	1.914	1.826	1.650	1.914

Table 10.8. Compositional variations in biotite from SS43 coarse-grained biotite granite. Microprobe analyses

	1	3	4	5	6	7	13	14	15	7	1	2	3	4	5	6	12
SiO <sub>2</sub>	36.99	37.79	37.38	36.58	37.84	37.07	37.80	38.42	38.49	38.36	41.27	37.82	37.22	38.12	37.45	37.88	39.08
TiO <sub>2</sub>	1.56	1.41	1.19	1.13	1.05	1.12	1.27	1.20	1.41	1.74	1.60	1.58	1.48	1.67	1.84	1.81	0.65
Al <sub>2</sub> O <sub>3</sub>	13.15	13.54	12.34	12.48	12.57	12.69	12.70	12.50	12.43	12.71	13.88	12.99	12.89	12.56	12.17	12.29	13.54
FeO	31.77	31.88	32.94	34.05	31.93	32.90	33.99	33.39	32.93	33.08	28.38	33.56	33.71	33.66	34.56	33.75	32.23
MnO	0.39	0.31	0.46	0.51	0.51	0.43	0.62	0.57	0.54	0.37	0.26	0.38	0.46	0.57	0.58	0.55	0.45
MgO	0.00	0.00	0.01	0.00	0.01	0.00	0.01	0.03	0.01	0.02	0.04	0.01	0.00	0.00	0.01	0.00	0.17
CaO	0.01	0.01	0.01	0.02	0.00	0.00	0.00	0.00	0.01	0.03	0.07	0.00	0.00	0.00	0.00	0.02	0.00
Na <sub>2</sub> O	0.20	0.14	0.22	0.22	0.14	0.12	0.17	0.17	0.22	0.15	0.15	0.20	0.19	0.10	0.17	0.17	0.26
K <sub>2</sub> O	11.05	11.05	10.97	10.96	10.94	10.97	8.40	8.36	8.23	8.61	7.64	8.40	8.26	9.12	8.81	8.72	8.18
P <sub>2</sub> O <sub>5</sub>	0.00	0.00	0.00	0.00	0.00	0.02	0.01	0.01	0.00	0.06	0.00	0.00	0.00	0.03	0.00	0.01	0.00
NiO	0.04	0.04	0.01	0.00	0.00	0.00	0.00	0.01	0.02	0.00	0.04	0.01	0.00	0.01	0.00	0.00	0.00
Cr <sub>2</sub> O <sub>3</sub>	0.00	0.00	0.00	0.00	0.02	0.00	0.00	0.01	0.01	0.00	0.00	0.03	0.03	0.01	0.00	0.01	0.02
SrO	0.00	0.00	0.08	0.06	0.05	0.05	0.09	0.11	0.10	0.12	0.05	0.09	0.07	0.12	0.06	0.14	0.13
BaO	0.00	0.00	0.01	0.00	0.00	0.04	0.00	0.00	0.00	0.00	0.01	0.01	0.00	0.04	0.02	0.00	0.00
Total	95.16	96.17	95.62	96.01	95.06	95.41	95.06	94.78	94.30	95.25	93.39	95.08	94.31	96.01	95.67	95.35	94.56
R1	-1113	-1038	-1099	-1179	-1001	-1081	-484	-415	-390	-475	80	-489	-494	-607	-633	-560	-315
R2	259	267	244	247	247	249	250	247	245	254	282	255	253	246	239	243	267
Q	-36	-30	-33	-37	-27	-31	26	30	32	25	61	25	25	15	15	19	35
F	228	230	226	225	228	229	173	172	167	177	156	172	169	190	182	179	165
Si <sub>4</sub>	6.094	6.116	6.160	6.050	6.226	6.116	6.182	6.270	6.292	6.160	6.556	6.160	6.138	6.182	6.138	6.182	6.314
Al <sup>6</sup>	1.906	1.884	1.840	1.950	1.774	1.884	1.818	1.730	1.708	1.840	1.444	1.840	1.862	1.818	1.862	1.818	1.686
Ti	0.646	0.712	0.558	0.492	0.668	0.580	0.624	0.568	0.690	0.580	1.152	0.646	0.646	0.580	0.492	0.558	0.888
Fe	0.198	0.176	0.154	0.132	0.132	0.132	0.154	0.154	0.176	0.220	0.198	0.198	0.176	0.198	0.220	0.220	0.088
Mn	4.378	4.312	4.532	4.708	4.400	4.532	4.642	4.554	4.510	4.488	3.762	4.576	4.642	4.554	4.730	4.598	4.356
Mg	0.044	0.044	0.066	0.066	0.066	0.066	0.132	0.132	0.066	0.044	0.044	0.044	0.066	0.088	0.088	0.000	0.066
Mg	0.000	0.000	0.000	0.000	0.000	0.000	0.000	0.000	0.000	0.000	0.000	0.000	0.000	0.000	0.000	0.000	0.000
Sr	0.000	0.000	0.000	0.000	0.000	0.000	0.000	0.000	0.000	0.220	0.000	0.000	0.000	0.022	0.000	0.022	0.022
Ca	0.000	0.000	0.000	0.000	0.000	0.000	0.000	0.000	0.000	0.000	0.022	0.000	0.000	0.000	0.000	0.000	0.000
Na	0.066	0.044	0.066	0.066	0.044	0.044	0.044	0.044	0.066	0.044	0.044	0.066	0.066	0.022	0.044	0.044	0.088
K	2.310	2.288	2.310	2.310	2.288	2.310	1.760	1.738	1.716	1.782	1.540	1.738	1.540	1.892	1.848	1.826	1.694

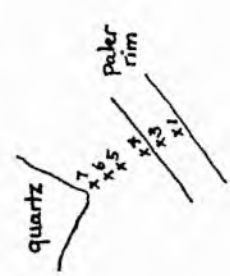
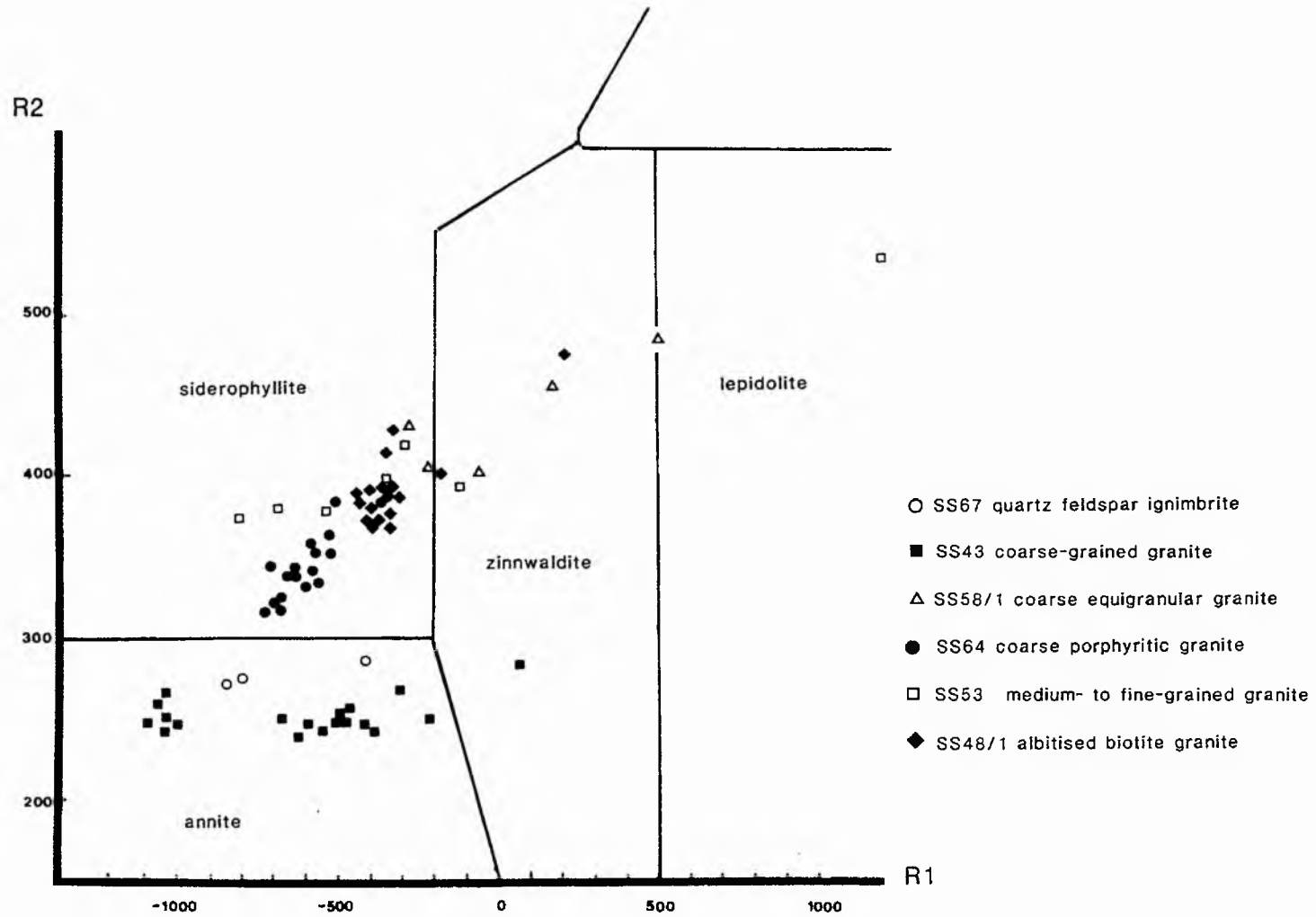
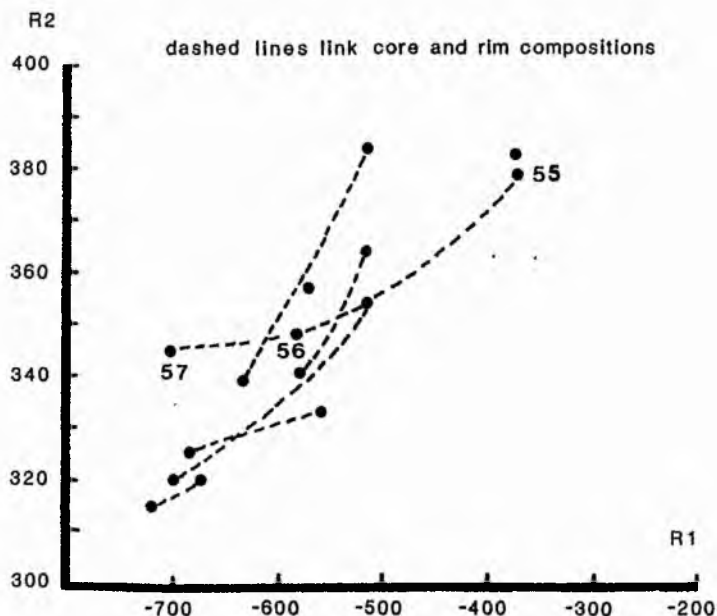


Fig.10.8 R1-R2 Compositional plot of micas from the Rishi biotite granite (microprobe analyses)



However, in terms of mica composition, the closest to the primitive mica composition described above is in the coarse-grained granite SS34. The mica is optically and chemically similar to that in the volcanic pile with compositions which plot within the annite field. However when analyses were made on traverses across individual crystals, compositional variations were observed between a crystal core and the crystal margin. These compositional variations from core to rim, when plotted on the R1-R2 diagram define a trend, parallel to the R1 axis, towards the zinnwaldite field (Fig 10.8). In one traverse six analyses were made, two of the paler rim and four of the darker centre. The two analyses in the paler rim show an increase in alumina and potash, a decrease in iron and Mn but surprisingly an increase in Ti. Clearly, the rims show chemical compositions which must have re-equilibrated with a fluid at subsolidus temperatures.

Fig 10.9. R1-R2 compositional variations within the mica from SS64 coarse porphyritic granite. Numbers refer to analytical points given in Table 10.9



Such chemical re-equilibration is emphasised by analyses of micas within the coarse-grained granite SS64 (Table 10.9). In this case the mica formed ragged flakes which are often skeletal and containing rounded fluorite, zircon or monazite with the development of opaques along the cleavages. Locally the mica can be seen developing at the expense of the perthite. In colour the mica is pale tan or pale greeny brown and is pleochroic to straw yellow. Compositionally it plots not within the annite field but within the siderophyllite field of the R1-R2 diagram (Fig 10.8). Again there are chemical variations from core to rim with compositions defining a trend at 45° to the R1 axis towards the zinnwaldite field. This is shown particularly in spot 13/8 of the sample where analyses 55-57 (Table 10.9) traverse a colour-zoned flake. Analysis 57 is in a greeny brown zone, 56 is in a pale greeny brown zone and analysis 55 is in a pale yellow brown zone. The compositional trend defined by these three analyses is shown on Fig 10.9. The decrease in coloration is linked with a decrease in iron and titanium (and also in magnesium) and an increase in potash, alumina and silica. The most deeply coloured mica analysed in the sample was at spot 64 - this was a dark brown stripe in an otherwise tan coloured mica and proved to be the most iron-enriched sample of the rock with 32.34% FeO. Most of the other analysed micas contain less than 30% FeO with the pale zone of analysis 55 containing less than 23% FeO. This decrease in colour intensity with decrease in iron content is a common phenomenon, however more surprisingly, there seems to be no correlation between coloration and Ti content.

For micas from SS58/1 (Table 10.10), which is also a coarse-grained granite with an equigranular texture, the compositional trend is continued from the siderophyllite field into the zinnwaldite compositional field and towards lepidolite (Fig 10.8). Optically the mica varies from blue green to almost colourless and forms ragged, skeletal and sieve-textured flakes up to 6mm in size. Four analyses have been made on one such flake - two towards the centre of the flake, and two towards the rim. In both cases the analyses at the core of the mica gives a siderophyllite composition whilst those at the rim give a zinnwaldite composition. Analysis 15 in Table 10.10 is of a pale-coloured trioctahedral mica developed at the margin of a chlorite. Compositionally this mica analysis plots on the zinnwaldite-lepidolite boundary of the R1-R2 diagram.

The mica in SS53 (Table 10.11), which is a medium- to fine-grained biotite granite, shows a wide range in chemical composition. Seven analyses from five separate micas gave compositions which plot from the siderophyllite field through zinnwaldite to the lepidolite field. In thin section the colour variation is from remnant patches of tan coloration within deep green mica, to rare colourless biotite.

## Discussion

It is obvious that the micas in the four biotite granites examined must have been re-equilibrating with the hydrothermal fluid and have been modified from an original annitic composition. The most primitive mica occurs in the coarse-grained granite whilst the most evolved occurs in the medium- to fine-grained facies. However, the inescapable conclusion is that ALL the biotite granite has been modified, since even in coarse-grained facies with primitive mica compositions the chemical evidence proves that the mica rims have been

Table 10.9. Compositional variations in biotite from SS64/1 - porphyritic granite

	39	40	41	42	43	46	47	48	50	55	56	57	63	64	65	66	67
SiO <sub>2</sub>	37.74	37.66	38.38	38.11	38.42	39.50	37.80	38.28	38.42	40.58	39.03	37.76	37.04	37.11	37.23	38.69	38.74
TiO <sub>2</sub>	1.48	2.18	2.51	1.78	1.30	1.14	1.50	1.29	1.13	0.76	0.83	1.05	1.94	1.92	2.08	0.84	1.04
Al <sub>2</sub> O <sub>3</sub>	16.11	15.77	15.87	16.54	16.72	17.20	16.47	16.53	17.05	18.95	17.39	16.81	15.29	15.55	15.67	17.32	17.05
FeO	30.83	31.79	30.73	29.83	29.00	27.53	29.18	29.60	28.38	22.92	27.72	29.56	31.19	32.34	30.52	27.75	29.21
MnO	0.38	0.39	0.34	0.44	0.39	0.46	0.44	0.49	0.45	0.34	0.42	0.35	0.52	0.42	0.50	0.40	0.40
MgO	0.24	0.27	0.34	0.29	0.29	0.33	0.35	0.28	0.28	0.22	0.24	0.31	0.30	0.26	0.25	0.32	0.31
CaO	0.05	0.02	0.04	0.00	0.00	0.10	0.00	0.00	0.00	0.00	0.00	0.00	0.00	0.00	0.00	0.01	0.02
Na <sub>2</sub> O	0.23	0.23	0.22	0.23	0.12	0.19	0.09	0.19	0.12	0.16	0.13	0.27	0.17	0.06	0.02	0.17	0.10
K <sub>2</sub> O	8.95	9.28	9.23	9.57	9.88	9.80	9.47	9.66	9.46	10.11	10.01	9.74	9.48	9.35	9.67	9.83	9.52
Cl <sub>2</sub> O <sub>3</sub>	0.00	0.05	0.03	0.01	0.00	0.00	0.00	0.00	0.00	0.00	0.06	0.00	0.05	0.00	0.04	0.02	0.00
Total	96.01	97.64	97.69	96.80	96.12	96.25	95.30	96.32	95.29	94.04	95.83	95.85	95.98	97.01	95.98	95.35	96.39
R1	-555	-682	-597	-655	-632	-522	-577	-632	-513	-374	-578	-706	-725	-683	-689	-574	-519
R2	333	325	332	339	342	364	340	338	384	383	353	345	315	318	320	357	352
Q	1	4	9	1	-1	4	6	1	8	5	0	-6	-1	5	1	0	9
F	182	189	188	196	206	200	198	199	197	209	208	198	196	197	205	203	199
Si <sub>4</sub>	5.984	5.918	5.984	5.984	6.050	6.138	6.006	6.028	6.072	6.270	6.116	5.984	5.940	5.896	5.940	6.094	6.072
Al <sub>4</sub>	2.016	2.082	2.016	2.016	1.950	1.862	1.994	1.720	1.928	1.730	1.884	2.106	2.060	2.104	2.060	1.906	1.928
Al <sub>6</sub>	0.998	0.884	0.888	1.042	1.152	1.284	1.086	1.360	1.240	1.724	1.328	1.040	0.822	0.800	0.888	1.306	1.218
Ti	0.176	0.264	0.286	0.220	0.154	0.132	0.176	0.154	0.132	0.088	0.088	0.132	0.242	0.220	0.242	0.110	0.132
Fe	4.092	4.180	4.004	3.916	3.828	3.146	3.872	3.894	3.740	2.970	3.630	3.916	4.180	4.290	4.070	3.652	3.828
Mn	0.044	0.044	0.044	0.066	0.044	0.066	0.066	0.066	0.066	0.044	0.066	0.044	0.066	0.066	0.066	0.044	0.044
Mg	0.066	0.066	0.088	0.066	0.066	0.066	0.088	0.066	0.066	0.044	0.066	0.066	0.066	0.066	0.066	0.066	0.066
Cr	0.000	0.000	0.000	0.000	0.000	0.000	0.000	0.000	0.000	0.000	0.000	0.000	0.000	0.000	0.000	0.000	0.000
Ca	0.000	0.000	0.000	0.000	0.000	0.022	0.000	0.000	0.000	0.000	0.000	0.000	0.000	0.000	0.000	0.000	0.000
Na	0.066	0.066	0.066	0.066	0.044	0.066	0.022	0.066	0.044	0.044	0.044	0.088	0.044	0.022	0.000	0.044	0.022
K	1.804	1.870	1.826	1.914	1.980	1.936	1.914	1.936	1.914	2.002	2.002	1.980	1.936	1.892	1.958	1.980	1.892

PAGE 347

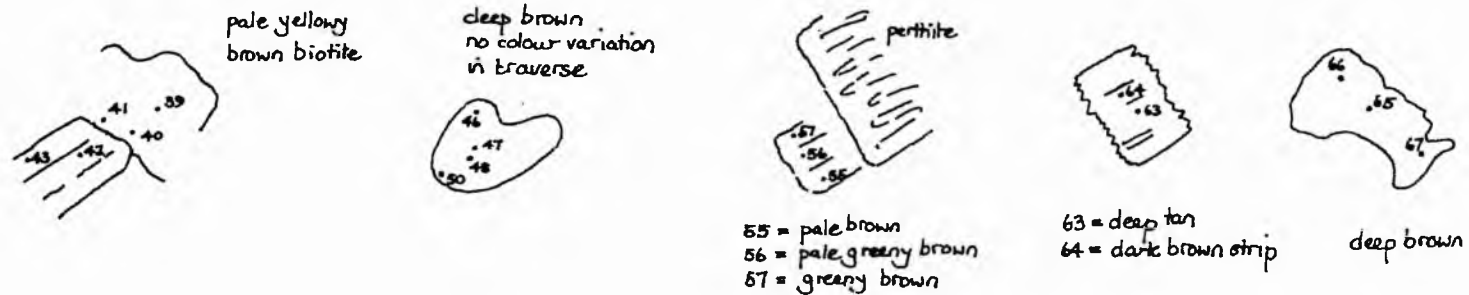


Table 10.10 Compositional variations in biotite from SS58/1 equigranular coarse-grained granite

	7	8	9	11	15
SiO <sub>2</sub>	41.76	41.85	42.28	44.33	47.48
TiO <sub>2</sub>	0.00	0.01	0.06	0.28	0.07
Al <sub>2</sub> O <sub>3</sub>	21.60	21.78	20.60	20.84	24.52
FeO	19.47	20.19	19.96	18.39	13.17
MnO	0.54	0.58	0.50	0.48	0.20
MgO	0.00	0.00	0.00	0.00	0.07
CaO	0.00	0.03	0.00	0.00	0.00
Na <sub>2</sub> O	0.06	0.33	0.15	0.25	0.10
K <sub>2</sub> O	8.83	10.18	10.35	10.29	9.65
Cr <sub>2</sub> O <sub>3</sub>	0.00	0.04	0.00	0.05	0.05
Total	92.26	94.99	93.90	94.91	95.31
R1	154	-271	-213	-60	503
R2	424	430	404	409	484
Q	42	5	10	19	55
F	186	205	215	210	202
Si <sup>4</sup>	6.380	6.292	6.424	6.556	6.688
Al <sup>4</sup>	1.620	1.708	1.576	1.444	1.312
Al <sup>6</sup>	2.274	2.142	2.120	2.186	2.758
Ti	0.000	0.000	0.000	0.022	0.000
Fe	2.486	2.530	2.530	2.266	1.562
Mn	0.066	0.066	0.066	0.066	0.022
Mg	0.000	0.000	0.000	0.000	0.022
Ca	0.000	0.000	0.000	0.000	0.000
Na	0.022	0.088	0.044	0.066	0.022
K	1.716	1.958	2.532	1.936	1.738

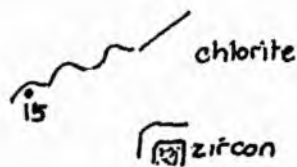


Table 10.11 Compositional variations in biotite from SS53 medium- to fine-grained biotite granite

	6	10	12	13	48	51	56
SiO <sub>2</sub>	37.84	44.21	37.89	38.61	36.10	39.35	36.10
TiO <sub>2</sub>	1.04	0.30	1.22	1.01	1.20	0.84	1.29
Al <sub>2</sub> O <sub>3</sub>	18.78	27.01	19.27	19.79	19.32	20.68	19.01
FeO	25.62	9.19	28.55	26.65	26.87	23.54	29.13
MnO	0.00	0.00	0.00	0.00	0.00	0.00	0.00
MgO	0.00	0.00	0.00	0.00	0.00	0.00	0.00
CaO	0.22	0.04	0.00	0.04	0.00	0.12	0.00
Na <sub>2</sub> O	0.20	0.04	0.17	0.16	0.14	0.24	0.10
K <sub>2</sub> O	7.80	5.40	9.30	8.96	9.67	9.19	9.93
ZnO	0.19	0.03	0.19	0.38	0.33	0.37	0.23
Total	91.69	86.22	96.59	95.60	93.63	94.33	95.79
R1	-113	1404	-535	-346	-683	-288	-795
R2	392	534	378	392	379	418	373
Q	35	129	7	18	-10	14	-14
F	155	113	192	184	201	185	208
Si <sup>4</sup>	6.050	6.578	5.874	5.984		6.072	5.720
Al <sup>4</sup>	1.950	1.422	2.153	2.016		1.928	2.280
Al <sup>6</sup>	1.592	3.308	1.367	1.592		1.834	1.284
Ti	0.132	0.044	0.132	0.110		0.088	0.154
Fe	3.432	1.144	3.696	3.454		3.036	3.872
Mn	0.000	0.000	0.000	0.000		0.000	0.000
Mg	0.000	0.000	0.000	0.000		0.000	0.000
Zn	0.022	0.000	0.022	0.088		0.044	0.022
Ca	0.044	0.000	0.000	0.000		0.022	0.000
Na	0.066	0.000	0.044	0.044		0.066	0.022
K	1.584	1.034	1.848	1.760		1.804	2.002

6 = brown

10 = uniformly yellow

12 = mottled medium brown

13 = yellowy

48 = dark stripe in brown mica

51 = yellowy brown

56 = greeny brown zone along cleavage

compositionally modified. A similar conclusion was reached in Chapter 9 on the basis of textural, mineralogical and whole rock geochemical evidence.

In addition a compositional plot of all the analyses of the micas from the four biotite granites shows two distinctive trends: one from annite directly to zinnwaldite, as shown by SS43; the other from annite through siderophyllite to zinnwaldite as shown by SS64 etc. These compositional trends of the micas within the biotite granite are identical to those discussed by Bowden and Kinnaird (1984a) based on the modified Rieder diagram for hydrothermally altered rocks. In this earlier work the trend from annite directly to zinnwaldite was related to sodic metasomatism whilst the trend from annite through siderophyllite to zinnwaldite was related to potash followed by acid metasomatism. This hypothesis will be tested in the next section.

The conclusion must be that the micas in the Rishi granite have responded to chemical changes in the hydrothermal fluid and were modified continually by fluids that were successively responsible for sodic, potassic, acid and silica metasomatism. It is therefore not surprising that the granite micas exhibit the same wide diversity of optical and compositional variation as to be found in any of the altered facies. The examination of mica compositional variations in the different alteration assemblages may define a range of compositions for each process.

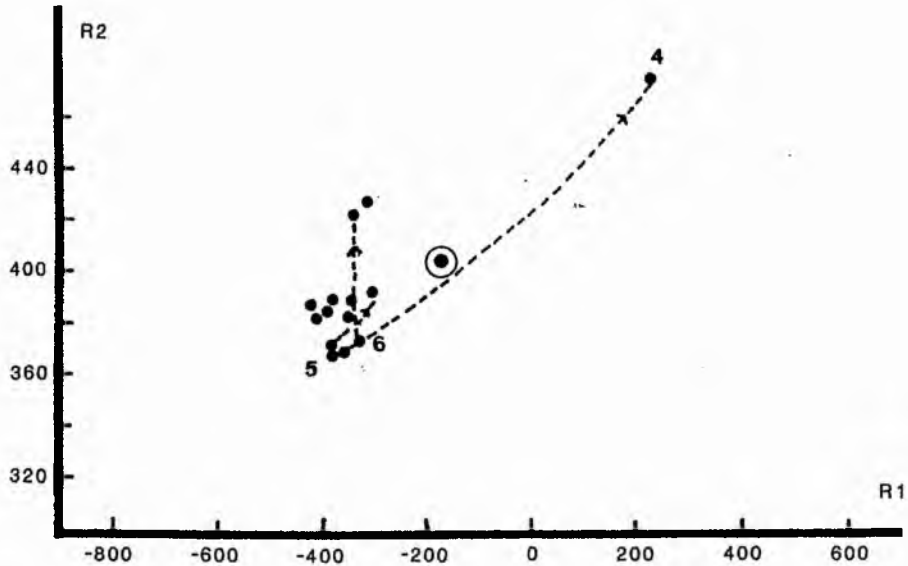
#### Micas from the alteration assemblages

In SS48 (Table 10.2) where sodic metasomatism has left its imprint the biotite formed honey-coloured lenticular sieve-textured laths which enclose rounded quartz, albite and fluorite. In other sodic facies of the Rishi granite, it is very pale grey or beige to tan in colour. Commonly the tan coloured core is rimmed by paler or colourless biotite and compositionally varies from 18% total iron (as FeO) for a pale rim to 25.7% FeO for a tan coloured core. In all cases the paler rims had lower Fe content and there was a systematic decrease in iron content with decreasing colour. This decrease in iron is balanced by an increase in alumina. When compared with the most primitive mica of the biotite granite iron content of these micas is significantly lower, potash content is less, while silica values are approximately the same. There was an increase in alumina and a marked increase in fluorine content of biotites in the albitised facies, averaging 5% and reaching a maximum of 6.6% although there was no relationship between colour and fluorine content.

What is most important is that the mica composition of a sodic metasomatised facies is distinct from that of a primitive mica. Moreover, although there are compositional variations from core to rim, the core compositions are not those of the primitive mica. In other words, the mica which grew during sodic metasomatism was "new" and all the pre-existing mica was destroyed since the "new" mica was not moulded onto any pre-existing mica.

For this sample SS48, both microprobe analyses (Table 10.12) and an XRF analysis (Table 10.6) on a mica separate were obtained. R1-R2 parameters were calculated on both types of analyses and their plotting positions compared in Fig 10.10.

Fig 10.10. R1-R2 compositional variations within the mica from SS48 albite biotite granite. Numbers refer to analytical points given in Table 10.12. Sample point in circle is the bulk analysis of Table 10.6



Analytical data obtained for SS48 using two different techniques were plotted on Fig 10.10. The bulk sample analysed by XRF and AA is shown as a point within a circle on Fig 10.10. Its plotting position is intermediate in composition between samples from core and rim as analysed by microprobe. This means that the bulk analysis is giving an overall composition which is what would be expected. The similarity of plotting positions for both complete analyses and partial analyses by probe, vindicated the chosen R1-R2 method of classification.

During potassic metasomatism original mica was chloritised and new biotite was generated. In SS8/1a skeletal lenticular mica which has the form of the zinnwaldite generated during sodic metasomatism has been chloritised. Within this chlorite, small flakes of a new, second generation of colourless zinnwaldite mica have generated from the chlorite in a process which appears to be zinnwaldite to chlorite to zinnwaldite. In other samples new mica generated during potassic metasomatism may be pale green in colour and zinnwaldite also developed from the breakdown of microcline feldspar as the process of alteration became more acid.

Table 10.12 Compositional variations in biotite from SS48 albitised granite

	4	5	6	7	11	12	13	14	68	69	70	71	72	73	74	75
SiO <sub>2</sub>	41.11	38.08	38.18	39.48	36.96	37.56	37.64	38.55	38.80	39.40	39.45	39.02	39.12	38.84	39.18	42.89
TiO <sub>2</sub>	0.54	0.88	0.97	0.71	0.94	0.90	0.96	1.03	1.04	1.00	1.06	1.06	0.91	0.97	0.82	0.96
Al <sub>2</sub> O <sub>3</sub>	22.84	17.77	17.90	20.08	17.66	17.78	17.92	18.98	18.64	18.76	18.79	18.38	18.57	18.62	18.74	20.62
FeO	18.46	24.77	24.97	22.90	24.82	25.10	25.74	23.71	24.66	24.95	23.79	24.93	23.96	24.00	24.26	25.08
MnO	0.18	0.29	0.17	0.38	0.23	0.32	0.13	0.27	0.34	0.31	0.20	0.23	0.32	0.32	0.24	0.26
MgO	0.41	0.39	0.44	0.42	0.39	0.46	0.41	0.36	0.35	0.36	0.42	0.41	0.39	0.35	0.40	0.48
CaO	0.06	0.00	0.01	0.00	0.01	0.00	0.00	0.02	0.00	0.01	0.00	0.01	0.00	0.02	0.01	0.00
Na <sub>2</sub> O	0.19	0.42	0.18	0.31	0.28	0.41	0.27	0.16	0.31	0.41	0.35	0.33	0.35	0.35	0.40	0.28
K <sub>2</sub> O	8.19	8.81	8.97	9.45	8.57	8.57	8.81	9.25	9.18	9.06	9.41	9.32	9.17	8.93	9.07	10.06
F <sub>2</sub> O	4.13	5.28	4.35	6.10	4.42	4.23	6.59	4.20	0.00	0.00	0.00	0.00	0.00	0.00	0.00	0.00
=O	1.74	2.22	1.83	2.57	1.86	1.78	2.78	1.77	0.00	0.00	0.00	0.00	0.00	0.00	0.00	0.00
ZnO	0.27	0.35	0.35	0.55	0.26	0.46	0.39	0.34	0.00	0.00	0.00	0.00	0.00	0.00	0.00	0.00
SnO <sub>2</sub>	0.03	0.07	0.12	0.06	0.00	0.00	0.00	0.00	0.00	0.00	0.00	0.00	0.00	0.00	0.00	0.00
Cr <sub>2</sub> O <sub>3</sub>	0.00	0.00	0.00	0.00	0.00	0.00	0.00	0.00	0.03	0.01	0.01	0.06	0.06	0.01	0.09	0.00
Total	94.67	94.89	94.78	97.87	92.68	94.01	96.08	95.06	93.35	94.27	93.48	93.75	92.85	92.41	93.22	100.63
R1	229	-383	-337	-344	-332	-368	-388	-337	-384	-425	-385	-417	-351	-317	-350	-316
R2	475	368	374	415	367	372	372	392	383	387	389	382	384	385	388	428
Q	47	11	15	8	14	13	13	12	10	7	7	8	11	14	12	15
F	167	173	184	191	173	169	178	191	185	178	188	187	183	178	180	205
Si <sup>4</sup>	5.980	6.808	6.739	6.831	6.693	6.670	6.854	6.693	6.116	6.138	6.160	6.138	6.160	6.138	6.160	6.204
Al <sup>6</sup>	2.020	1.192	1.261	1.169	1.307	1.330	1.146	1.307	1.884	1.862	1.840	1.862	1.840	1.862	1.840	1.796
Al <sup>6</sup>	2.442	2.557	3.465	2.925	2.465	2.396	2.695	2.580	1.570	1.570	1.614	1.548	1.614	1.898	1.636	1.724
Ti	0.069	0.115	0.138	0.092	0.138	0.115	0.138	0.138	0.132	0.110	0.132	0.132	0.132	0.132	0.088	0.110
Fe(t)	2.553	3.703	3.680	3.312	3.749	3.726	3.910	3.450	3.256	3.256	3.102	3.278	3.168	3.168	3.190	3.036
Mn	0.023	0.046	0.023	0.046	0.046	0.046	0.023	0.046	0.044	0.044	0.022	0.022	0.044	0.044	0.022	0.022
Mg	0.092	0.092	0.115	0.115	0.115	0.115	0.115	0.092	0.088	0.088	0.088	0.088	0.088	0.088	0.088	0.110
Zn	0.023	0.046	0.046	0.069	0.046	0.069	0.046	0.046	0.000	0.000	0.000	0.000	0.000	0.000	0.000	0.000
Cr	0.000	0.000	0.000	0.000	0.000	0.000	0.000	0.000	0.000	0.000	0.000	0.000	0.000	0.000	0.000	0.000
Ca	0.000	0.000	0.000	0.000	0.000	0.000	0.000	0.000	0.000	0.000	0.000	0.000	0.000	0.000	0.000	0.000
Na	0.069	0.138	0.069	0.092	0.092	0.138	0.092	0.046	0.088	0.132	0.132	0.132	0.110	0.110	0.132	0.088
K	1.725	2.001	2.024	2.093	1.978	2.369	2.047	2.047	1.848	1.804	1.870	1.870	1.848	1.804	1.826	1.848
F	2.162	2.990	2.415	3.335	2.530	2.369	3.795	2.300								

The mica generated from acid metasomatism of microcline-rich facies is very variable in optical characteristics ranging from deep blue green (SS117/5a) and grass green (SS27/4) through khaki (SS44/1) and pale grey to colourless (SS8/3). Compositionally they range from siderophyllite to zinnwaldite when pale in colour.

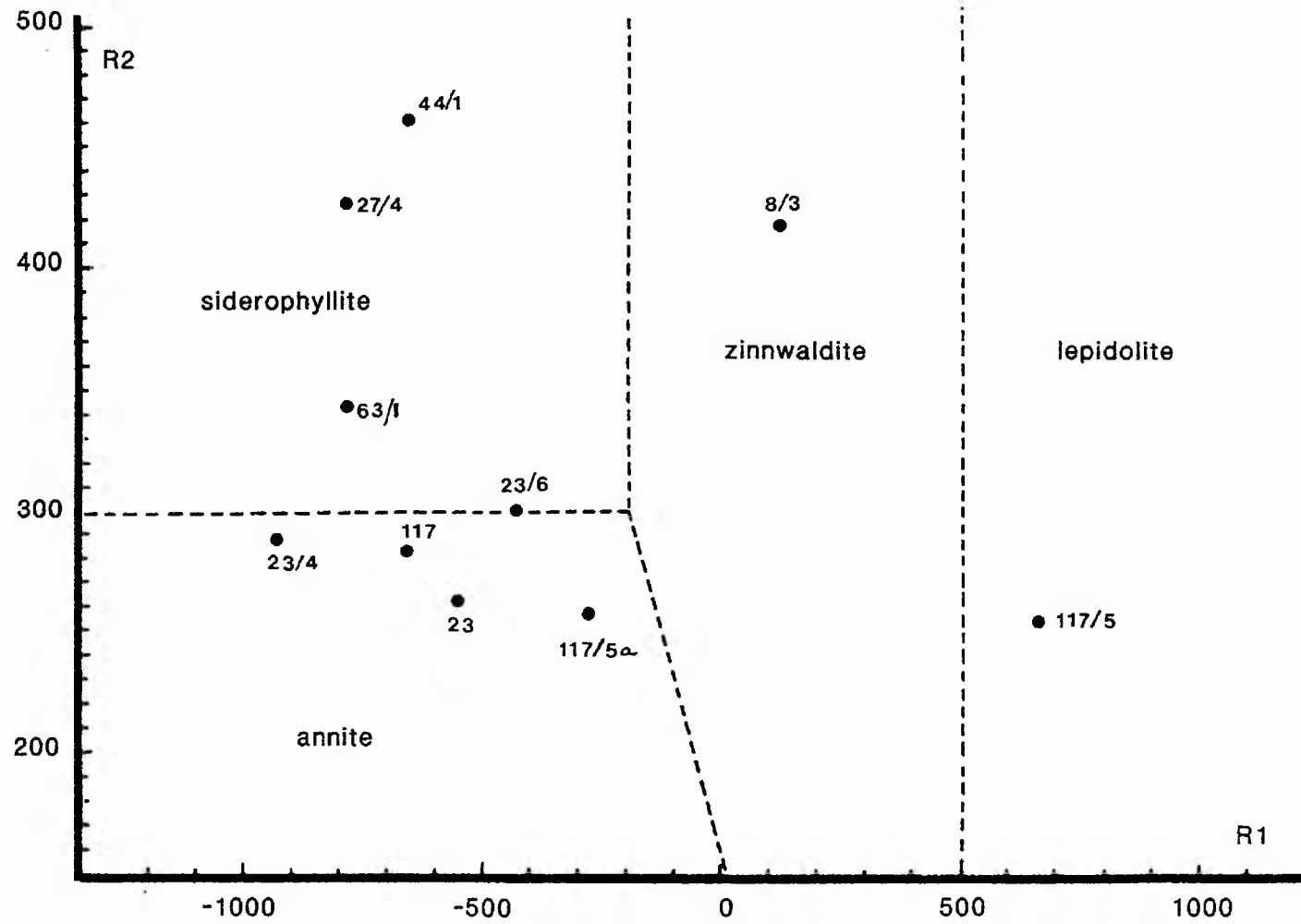
Where acid metasomatism was the only major process, the new trioctahedral mica generated from chlorite during acid metasomatism of a perthite granite is always a deep blue green in colour and compositionally falls within the siderophyllite field. Despite the fact that the mica in silica metasomatised facies is a paler bluey-green than in acid altered facies there is little compositional difference and all analyses fall within the siderophyllite field although these late micas are alumina-poor and silica enriched compared with earlier phases of mica. They also reflect the build up in volatile components in the late-stage fluids as they are the most  $\text{Li}_2\text{O}$  and  $\text{H}_2\text{O}$  enriched micas within the province.

Although there is only limited chemical data available for the range of micas generated during acid, silica and late-stage metasomatism, it appears that the compositional trends on the R1-R2 plot (Fig 10.11) are the reverse of those developed during sodic and potash metasomatism. During the early stages of alkali metasomatism there was a trend from original annite compositions through siderophyllite to zinnwaldite and even lepidolite in some samples. During acid and silica metasomatism the new mica generated plots in the range lepidolite and zinnwaldite through siderophyllite to annite. Although no compositional data is available for micas generated during late-stage alteration, it would seem reasonable to expect that they would be annitic in composition since the fluids were known to have been iron-enriched (Chapter 9).

Such a range in mica compositions means that it is not possible to relate mica composition to process of alteration directly without other mineralogical or chemical information. It does however mean that the micas were extremely sensitive indicators of the chemical changes in the fluid during their evolution and modification by rock-fluid interaction.

Whilst it is not possible to relate mica of a particular composition to one process directly, this study has shown that the coloration of the mica is in the first approximation, an indicator of its composition. Annitic micas are tan through deep chestnut brown to almost black; siderophyllites are deep grass green or deep aquamarine blue to pale shades of green and steel blue whilst zinnwaldites are pale grey, honey or colourless. The major departures from this scheme are for those micas which have been analysed by the bulk technique and for which traces of ilmenite, haematite, siderite, fluorite and other minerals, interleaved along the cleavage have given spurious results.

Fig 10.11 R1-R2 plot of bulk chemical analyses of micas from hydrothermally altered rocks



## Comparisons with other complexes within the Nigerian anorogenic province

Most complexes show a restricted range of mica chemical compositions similar to those from the Saiya Shokobo complex. For the Afu Complex however, where sodic metasomatism was intense there is a trend for mica compositions (as noted above) which can be plotted on the multicationic diagram (Fig 10.7). The micas Af102, Af62, Af124, Af40 and Af106 define this trend. Between the two end members of this trend, from Af102 to Af106 there is an increase in Si, K, Al and Li, a decrease in  $Fe^{2+}$  and Ti with no systematic variation in F and  $Fe^{3+}$ , although in the case of the latter, there is an overall decrease. For F there is an increase and then a gradual decrease. There is a progression in colour variation from deep greeny black in Af102, through mid greeny brown to pale blue-green (Af40) to palest pink in Af106 which is lepidolite

In the Saiya Shokobo Complex, the range of micas rather surprisingly appears to be identical to those of the Afu complex. Since the evidence of sodic metasomatism has largely been overprinted by later processes, the effects of albitisation do not appear to have been as dramatic in the Rishi area as they were in the Afu complex. However, the mica compositions would indicate that sodic metasomatism did affect the Rishi biotite granite. Such evidence combines with the occurrence of cryolite and columbite in some samples, together with textural and chemical modifications of the perthites in both the volcanic pile and basement. These were discussed in Chapter 9.

The available data from the Rishi area also appears to substantiate the existence of two separate trends from annite:

- (i) directly from annite through zinnwaldite to lepidolite:
- (ii) from annite through siderophyllite to zinnwaldite and lepidolite.

Whilst trend (i) can be related to sodic metasomatism in the Afu complex and trend (ii) can be related to potassic and acid metasomatism at Afu, the trends are not directly comparable with those developed in Rishi micas. However, for the Rishi area, no albite-rich rocks comparable to those at Afu have so far been located and mica compositions related to an intensive albitisation process are therefore not available. More microprobe data is required on other micas to contribute further to this fascinating range of mica compositions and to establish the relationship of the compositional trends to successive hydrothermal processes.

## Discussion

The mica which is most enriched in iron occurs within the volcanic pile above Dawa Mining camp. This mica must have grown from a fluid that existed before significant feldspar breakdown began since feldspar phenocrysts remain intact in the porphyritic ignimbrite. This mica is not truly magmatic but can be regarded as the "starting point" against which later compositional trends can be compared.

The biotite granites also contain similar iron-rich micas to the volcanic pile. However, microprobe analyses show that there may be zonations within the mica in which there are distinct compositional differences between core and rim. What is most important is that these compositional trends can be observed within all the granite facies as well as in the obviously hydrothermal altered zones. Thus for example, within the coarse-grained biotite granite, there is a compositional and colour variation of the mica, that records later stages of fluid reaction similar to those observed in various hydrothermal assemblages.

The interpretation must surely be that the mica which grew from a fluid in the volcanic pile developed at an earlier stage than those in the biotite granite at depth. The reactions that began in the volcanic pile must have continued for longer at subvolcanic depths within the granite. Since the granite cupola is a shallow outward dipping feature it must be concluded that within the granite the fluid was retained and could re-equilibrate to lower temperatures through changing compositions. This is reflected in the mica compositions which show varieties of texture, colour and composition within one rock sample.

The primitive trioctahedral mica found in the volcanic rocks and in some biotite granite samples is annitic with >4 cations of iron per 22 oxygens. In contrast to Foster's claim that such micas are extremely rare, these iron rich micas are not uncommon. Other extremely iron-rich micas occur in the Zigau porphyry and the Eldewo alkali feldspar biotite granite of the Shira Complex (Bennett 1981) with up to 40% FeO and >5 Fe<sup>2+</sup> cations in the octahedral Z site. Similar iron-rich micas are recorded in other granites from high level anorogenic complexes elsewhere in the world including those of the Pikes Peak batholith (Barker et al 1975), the Mourne Mountains (Brown 1956) and the Finnish rapakivi granites (Simonen and Vormaa 1969).

As far as natural iron-rich biotite is concerned, according to Rutherford (1973), if the iron-rich biotite is a magmatic phase then the rock must have crystallised at a p<sub>H<sub>2</sub>O</sub> greater than 2kb. Clearly for the annite of the Rishi volcanic pile this would seem unreasonable. The effects of Na and Al on the stability of iron biotites are such that it is apparently impossible for other than an aluminium-rich Fe-biotite to crystallise from syenitic magma. Considering the experimental and field data it seems unreasonable to believe that the annite in the volcanic pile is other than hydrothermal in origin.

With continued hydrothermal alteration there is a change from an iron biotite to a Li-Fe-Al biotite. The experimental data of Rutherford (1973) has shown that the Al content of a biotite is a function of f<sub>O<sub>2</sub></sub>, T and p<sub>H<sub>2</sub>O</sub> during biotite crystallisation. The experimental data of Rutherford (1973) shows that the substitution of aluminium for divalent iron plus silicon ( $2Al^{3+} = Fe^{2+} + Si^{4+}$ ) results in a considerable increase in the iron biotite stability field and are also more sensitive to f<sub>O<sub>2</sub></sub> and/or temperature variations than are alumina-rich biotites.

The stability of annite is lower in quartz bearing systems than those in which quartz is absent, and is sensitive to changes in f<sub>O<sub>2</sub></sub> and p<sub>H<sub>2</sub>O</sub> as well as temperature (Eugster and Wones, 1962). The maximum thermal stability of annite co-existing with quartz was found to be approximately 700°C at an f<sub>O<sub>2</sub></sub> defined by the QFM buffer, and the stability field widens considerably from this point with decreasing temperature and f<sub>O<sub>2</sub></sub>. An iron enrichment trend is probably established by a decrease in f<sub>O<sub>2</sub></sub> in a water undersaturated magma. The synthetic Li-Fe micas

have an extensive stability field below 550°C and together with the mode of occurrence of all these micas, formation below such a temperature would appear likely.

### Summary

There is a systematic relationship between the optical and chemical properties of the micas. The mica in the volcanic rocks is annitic whilst the granitic mica compositions range from annite to lepidolite and show the same optical and chemical properties of micas in successively hydrothermally altered rocks. Mica compositions of hydrothermally altered rocks however, are very variable, even within one stage of hydrothermal alteration.

During sodic metasomatism original annitic mica was destroyed and replaced by compositions within the zinnwaldite field. During potassic metasomatism, there was a change from annitic to zinnwaldite compositions also but with a different trend on the R1-R2 plot with compositions in the range annite-through siderophyllite to zinnwaldite and lepidolite. During later stages of metasomatism, there was a reverse in the compositional trends with a range from lepidolite and zinnwaldite back to siderophyllite and ultimately annite.

On the Rieder plot, the majority of the Saiya Shokobo micas for which wet chemical data was available plotted in a field which lies along the siderophyllite-zinnwaldite tie-line. This field was defined as the field of pervasive potash metasomatism by Bowden and Kinnaird (1984a). The previous chapter has emphasised how important a process of potash metasomatism was in the Saiya Shokobo Complex which therefore appears to support this original statements. Further, it was encouraging that when these micas were transferred to the multicationic diagram they also plotted within the siderophyllite to zinnwaldite field. With these diagrams and earlier interpretations as a basis it was possible to examine the micas in the different alteration assemblages. The multicationic diagram also offered a systematic basis on which to account for the dramatic variations in mica coloration which are not satisfactorily accounted for in the Rieder plot.

In conclusion, it is clear that the micas that formed at each alteration stage were in equilibrium with the evolving fluids. At each stage the mica was destroyed or replaced by a new mica with a composition compatible with that of the co-existing fluid.

## CHLORITE

### Introduction

Twenty one chlorites were analysed by microprobe from several different biotite granite and altered assemblages.

### Optical and physical properties

The chlorites vary in colour from pale yellow, pale green and pale brown through shades of khaki and deep brown or green to almost black. Most commonly though they are deep green in colour. The palest coloured chlorites have the lowest iron content and the lowest refractive indices. With increasing iron and decreasing silica content the refractive index increased.

### Chemistry and structure

The chemistry and structure of the mineral group is described in relation to a chlorite with chemical composition  $Mg_6Si_8O_{20}(OH)_4 + Mg_6(OH)_{12}$  which has an equal number of talc and brucite layers. However, the analysed chlorites contain negligible MgO and are exceptionally iron-rich (Table 10.13). They appear to be the most iron-enriched chlorites recorded. However, since these chlorites are derived from annitic micas which are the most iron-enriched biotites known, this is not surprising.

The tetrahedral sites are occupied by Si and Al with proportions varying between  $Si_{5.3}$  and  $6.7$  and  $Al_{0.9}$  and  $2.6$ . The octahedral sites in both the "talc" and "brucite" layer are filled by Fe and Al together with lesser amounts of Mn, Ti, Na, K, Mg and Ca in many samples. The total octahedral site occupancy varies between 11.54 and 12.10 except for sample 29 which is only 10.78.

According to Deer, Howie and Zussman, Volume 3 on Sheet Silicates (1965), the variations in chlorite chemistry can be classified in a number of ways, but the accepted method appears to be that of Hey (1954) in which the  $Fe^{3+}$ ,  $Fe^{2+}$ , Mg and Si content is taken into account (Fig 10.12). Although the analyses of the chlorites are by microprobe and the ratio of  $Fe^{3+}$  to  $Fe^{2+}$  is not known, the classification can still be used because of the extreme iron enrichment of these Nigerian chlorites. With such a high iron content the ratio of  $Fe^{2+}$  to  $(Fe^{2+}+Mg)$  is close to unity. With one exception the number of silicons varies between 5.348 and 6.2 and the octahedral site occupancy by  $Fe^{2+}$  varies between 7.868 and 9.352. Thus these chlorites fall in the daphnite field of Fig 10.11. The chlorite at spot 29 in SS58/1, mentioned above, which contains 6.792 silicons and only 6.132  $Fe^{2+}$  together with a significant potassium content appears to be a mixture of chlorite and illite.

With continued hydrothermal alteration, new zinwaldite or siderophyllite mica was generated from this chlorite. During its formation the iron was released and often formed haematite rods etc. along the cleavage of the new trioctahedral mica.

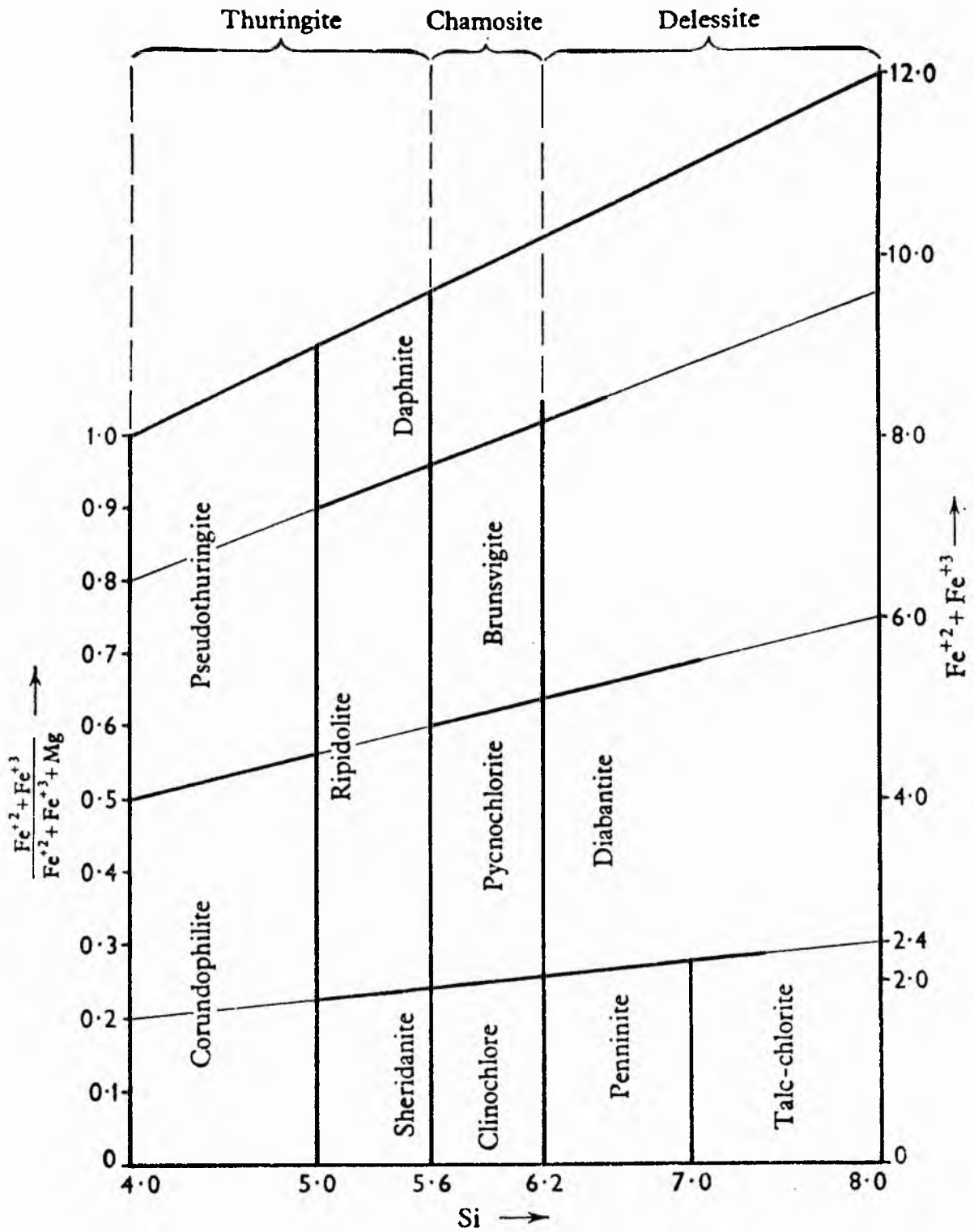


Fig 10.12 Nomenclatures for chlorites after Hey (1954).

Table 10.13 Microprobe data on compositional variations in chlorites.

## CHLORITE - SS58/1

	19	1	13	14	18	19	21	22	23	24	25
SiO <sub>2</sub>	23.39	24.95	23.23	24.43	24.47	23.30	23.10	23.27	23.21	23.45	22.82
TiO <sub>2</sub>	0.04	0.16	0.03	0.04	0.10	0.05	0.22	0.04	0.04	0.00	0.00
Al <sub>2</sub> O <sub>3</sub>	18.84	18.41	19.38	19.44	18.97	19.61	18.65	18.64	19.11	19.36	18.84
FeO	44.20	45.74	46.99	46.00	48.05	48.43	46.79	48.07	48.27	47.29	47.72
MnO	0.57	0.21	0.44	0.32	0.23	0.04	0.58	0.55	0.55	0.54	0.66
MgO	0.04	0.01	0.03	0.01	0.00	0.03	0.03	0.03	0.06	0.03	0.06
CaO	0.00	0.00	0.02	0.04	0.00	0.03	0.01	0.02	0.03	0.02	0.03
Na <sub>2</sub> O	0.02	0.00	0.00	0.18	0.02	0.00	0.23	0.15	0.12	0.09	0.08
K <sub>2</sub> O	0.03	0.24	0.03	0.11	0.33	0.00	0.00	0.01	0.02	0.01	0.03
P <sub>2</sub> O <sub>5</sub>	0.09										
NiO	0.03										
Cr <sub>2</sub> O <sub>3</sub>	0.01	0.01	0.05	0.00	0.02	0.00	0.04	0.03	0.05	0.00	0.00
SrO	0.00										
BaO	0.05										
Total	87.31	89.73	90.20	90.57	92.19	91.49	89.64	90.81	91.46	90.79	90.24
Si	5.544	5.768	5.404	5.600	5.572	5.348	5.404	5.404	5.348	5.404	5.348
Al	2.456	2.232	2.596	2.400	2.428	2.652	2.596	2.596	2.652	2.596	2.652
Σ oct	8.000	8.000	8.000	8.000	8.000	8.000	8.000	8.000	8.000	8.000	8.000
Al	2.808	2.780	2.696	2.836	2.640	2.668	2.556	2.500	2.556	2.668	2.556
Fe	8.764	8.820	9.128	8.820	9.128	9.296	9.184	9.352	9.296	9.128	9.352
Mn	0.112	0.028	0.084	0.056	0.056			0.112	0.112	0.112	0.140
Mg									0.028		0.028
Ti		0.028			0.028		0.028				
Na				0.084			0.112	0.056	0.056	0.028	0.028
K		0.084		0.028	0.084						
P	0.028										
Σ tet	11.71	11.74	11.91	11.82	11.94	11.96	11.88	12.02	12.05	11.94	12.10

## CHLORITE in SS58/1 and SS106/4

	28	29	30	31	32	33	34	35	36	5
SiO <sub>2</sub>	26.59	33.06	24.22	23.81	24.40	22.55	23.62	23.68	23.35	26.17
TiO <sub>2</sub>	0.04	0.08	0.06	0.09	0.11	0.22	0.05	0.08	0.06	0.08
Al <sub>2</sub> O <sub>3</sub>	18.46	19.69	19.12	18.29	19.33	18.51	20.10	18.49	19.38	21.52
FeO	41.01	34.70	43.30	47.72	45.08	44.04	46.80	46.57	47.26	35.29
MnO	0.86	0.49	0.44	0.69	0.41	0.57	0.73	0.65	0.70	0.54
MgO	0.04	0.05	0.07	0.04	0.06	0.06	0.03	0.08	0.04	0.07
CaO	0.07	0.01	0.10	0.06	0.03	0.13	0.03	0.05	0.05	0.05
Na <sub>2</sub> O	0.20	0.14	0.50	0.05	0.48	0.45	0.06	0.20	0.10	0.04
K <sub>2</sub> O	0.89	2.89	0.55	0.01	0.20	0.14	0.10	0.06	0.06	0.05
F <sub>2</sub> O										0.12
ZnO										0.05
SnO <sub>2</sub>										0.56
Cr <sub>2</sub> O <sub>3</sub>	0.05	0.00	0.00	0.00	0.01	0.00	0.00	0.00	0.08	0.03
Total	88.21	91.11	88.36	90.76	90.11	86.67	91.52	89.86	91.08	84.47
Si	6.104	6.792	5.656	5.516	5.600	5.432	5.376	5.516	5.376	
Al	1.896	1.208	2.344	2.484	2.400	2.568	2.624	2.484	2.624	
oct	8.000	8.000	8.000	8.000	8.000	8.000	8.000	8.000	8.000	
Al	3.116	3.692	2.920	2.500	2.836	2.696	2.780	2.585	2.640	
Fe	7.868	6.132	8.456	9.268	8.652	8.876	8.932	9.072	9.100	
Mn	0.168	0.084	0.084	0.140	0.084	0.112	0.140	0.140	0.140	
Mg	0.028	0.028	0.028	0.028	0.028	0.028		0.028	0.028	
Ti				0.028	0.028	0.028				
Ca	0.028		0.028			0.028				
Na	0.084	0.056	0.224	0.028	0.224	0.224	0.028	0.084	0.056	
K	0.252	0.784	0.168		0.056	0.028	0.028	0.028	0.028	
tet	11.54	10.78	11.91	11.99	11.91	12.02	11.91	11.96	11.99	

OTHER SHEET SILICATES

Introduction

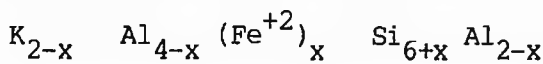
During acid hydrothermal alteration there was often the development of "sericite" at the expense of feldspar or chlorite. Such a term has been used to define a fine-grained colourless to pale green sheet silicate without regard to whether the mineral is a trioctahedral or dioctahedral mica or even a clay mineral such as illite. In most samples, the sericite is extremely fine-grained but in sample SS20 the sericite varies in habit from fine mottled 'sericitic' flakes to sheaf-like in form and in colour from pale yellowy green to colourless. Several analyses were made on the different forms and different coloured examples and the data is presented in Table 10.15. From the analytical data it was difficult to decide whether the mineral is a late-stage ferroan disordered muscovite or whether it is crystalline iron-rich illite or phengite. The distinction between such mineral can essentially only be made in conjunction with an XRD study of the structure which has not been undertaken. However, Deer Howie and Zussman in Volume 3 of the Sheet silicates (1965), have shown that it is possible to distinguish between the illite group and muscovite from structural formulae calculated on the basis of 20 oxygens (Table 10.14).

=====  
 Table 10.14. Principal variations in illite compositions  
 with reference to muscovite  
 =====

	X	Y <sup>6</sup>	Z <sup>4</sup>
Muscovite	K <sub>2</sub>	Al <sub>4</sub>	Si <sub>6</sub> Al <sub>2</sub>
Illite	K <sub>2-x</sub>	Al <sub>4</sub>	Si <sub>6+x</sub> Al <sub>2-x</sub>
Phengite	K <sub>2</sub>	Al <sub>4-x</sub> (Mg, Fe <sup>2+</sup> ) <sub>x</sub>	Si <sub>6+x</sub> Al <sub>2-x</sub>

=====  
 Data from Deer, Howie and Zussman, Volume 3, Sheet Silicates 1965.

Utilising such a calculation, the data in Table 10.15. shows that for the analysed samples in SS20, there is a deficiency in the filling of the x site by K+Na+Ca and the occupancy by Al of the y site is considerably less than 4. In addition, there is excess silica in the z site and the formula based on 20 oxygens is therefore:



This formula appears to approximate more closely to phengite than muscovite although it is not clear from Deer Howie and Zussman, how ferroan muscovite can

be distinguished from phengite. It seems likely that the mineral in question is showing mixed features of various illite minerals.

The analytical data was therefore recalculated on the basis of 23 oxygens as illite contains 24 O,OH,F per unit cell and fluorine was included in the probe analyses. The data is given in Table 10.15.

Table 10.15 Microprobe data on the composition of "illite" in SS20

	1	3	5	6	7	8
SiO <sub>2</sub>	40.34	47.89	49.27	46.51	46.35	47.05
TiO <sub>2</sub>	0.04	0.06	0.01	0.01	0.05	0.01
Al <sub>2</sub> O <sub>3</sub>	27.83	29.74	32.22	28.54	28.80	27.14
FeO	5.31	5.52	4.28	4.29	5.82	6.81
MnO	0.07	0.06	0.05	0.08	0.04	0.13
MgO	0.00	0.00	0.00	0.00	0.06	0.02
CaO	0.10	0.09	0.04	0.06	0.00	0.04
Na <sub>2</sub> O	0.11	0.05	0.04	0.04	0.04	0.00
K <sub>2</sub> O	8.72	9.52	10.31	9.40	9.11	9.86
F <sup>2</sup>	1.52	2.22	0.85	0.60	2.28	1.05
=O	0.64	0.93	0.36	0.25	0.96	0.44
ZnO	1.27	0.12	0.11	0.09	0.34	0.11
SnO <sub>2</sub>	0.05	0.05	0.12	0.09	0.47	0.41
Total	84.72	94.37	96.94	89.45	92.42	92.19
Si	6.461	6.861	6.775	6.934	7.038	7.084
Al	1.539	1.139	1.225	1.066	0.962	0.916
	8.000	8.000	8.000	8.000	8.000	8.000
Al	3.714	3.805	3.994	3.945	4.558	3.891
Fe	0.711	0.652	0.493	0.535	0.736	0.851
Mn	0.010	0.007	0.006	0.010	0.000	0.023
MgO	0.000	0.000	0.000	0.000	0.023	0.000
Ti	0.005	0.006	0.001	0.000	0.000	0.000
Ca	0.018	0.013	0.006	0.010	0.000	0.000
Na	0.034	0.015	0.010	0.010	0.023	0.000
K	1.783	1.715	1.809	1.788	1.771	1.886
Zn	0.150	0.012	0.012	0.010	0.023	0.023
Sn	0.000	0.000	0.000	0.000	0.023	0.023
F	0.769	0.990	0.371	0.285	1.104	0.506

## Discussion

Perez (1985), in a study of hydrothermal alteration of the Taghouaji Complex of Niger, found similar late-stage sheet silicates with almost identical composition to those in the Saiya Shokobo complex. He described them as either intergrown with-, or forming a rim around, zoned biotites or as replacements after feldspar in altered granite, greisens or quartz veins. However, on chemical evidence alone he chose to call these sheet silicates, ferroan muscovite. Utilising the method of Deer Howie and Zussman (1965) described above, the Taghouaji sheet silicates also show a deficiency in the filling of the *x* site with an excess silica in the *z* site together with a *y* site occupancy by Al of considerably less than 4. They seem to correspond better with ferroan illite than ferroan muscovite although the question cannot be satisfactorily determined without structural studies of the sheet silicate state.

Therefore in the absence of structural data, the use of the term sericite to include fine-grained trioctahedral, dioctahedral micas and mixed-layer aggregates is a useful descriptive terminology.

## ORE PARAGENESIS

### Introduction

The first aim of this study of the ore minerals has been to determine at what stage the different ore minerals have been introduced relative to the hydrothermal processes that have been described.

However, the main purpose of a study of the ore minerals was to determine any significance chemical variations in major and trace elements from different periods of mineralisation. Such a study could lead to conclusions related to temperature of formation, partitioning of elements between minerals and ultimately to conclusions on the physico-chemical nature of the ore-forming fluid itself. Sphalerite is one of the best minerals to use in this type of study, due to its abundance, widespread occurrence in several different hydrothermal phases and because of its varied major and trace element chemistry.

The ore paragenesis has been determined both by a study of thin sections and a more limited study of polished ores. Where identification of sulphide phases proved difficult they were identified by probe analyses. This section has also had the benefit of help from Dr. Rob Ixer of Aston University, who first drew the author's attention to the gold occurrence at Dawa.

Studies of polished ore samples show that early formed minerals are enclosed by later phases, and therefore help to distinguish the paragenetic sequence. Textural and geochemical evidence discussed later, indicates that as in the Ririwai Complex (Ixer et al 1987), each hydrothermal alteration process essentially dissolved or replaced earlier phases and then re-precipitated them with compositions compatible with the evolving fluid. Early formed minerals like thorite are consistently enclosed by later phases.

The sequence of ore deposition established by Ixer (in Kinnaird et al 1985a) for the Ririwai Complex is similar to that at Rishi. The biotite granite contains, thorite, monazite, allanite, zircon, columbite, cassiterite, sphalerite and chalcopyrite; the basement contains chalcopyrite, sphalerite, cassiterite, monazite and other ores, whilst even the volcanics contain occasional cassiterite and allanite.

The descriptive section which follows attempts to put the ore minerals into a generalised paragenetic sequence. However, several minerals form more than one phase: zircon occurs in several generations, sphalerite has at least two phases of crystallisation, cassiterite occurs at several of the alteration stages, and different habits of chalcopyrite indicate at least two periods of formation. Nevertheless, it has been possible to make a generalised paragenetic sequence (Fig 10.13).

#### Ore Petrology

Zircon is common as euhedral equant crystals up to 0.5mm in size which occur within the biotite granite and at all stages of alteration. In the biotite granite it may occur along mica cleavages, or form discrete crystals which are turbid, colourless and strongly compositionally zoned as shown by the birefringence (Plate 10.1). It occurs in association with thorite. During sodic metasomatism, the zircon that formed was very dark in colour, often metamict and clearly rich in uranium, thorium or hafnium. Zircons which developed in later processes of alteration are less strongly coloured, rarely metamict and may or may not be zoned.

Thorite, which is less common than zircon, occurs as small elongate or equant crystals either within mica which also contains zircon, or sometimes possibly forming metamict rims to the zircon. Thorite formed early in the paragenetic sequence during sodic metasomatism but has also been recognised in acid altered basement (SS93) and acid altered microcline-rich rocks, suggesting that like zircon it formed at several stages of alteration.

Cryolite is not widely reported from the anorogenic province. It is known to be abundant in the Odegi biotite granite of the Afu Complex but had only otherwise been reported as an abundant accessory in the arfvedsonite albite granites. MacLeod et al (1971), state that cryolite distribution has been investigated in the Kaffo granite of the Ririwai Complex where localised values of over 3% have been recorded. In the Saiya Shokobo Complex, it occurs in sodic metasomatised rocks or acid metasomatised facies that had previously undergone sodic metasomatism. It forms skeletal anhedral crystals up to 0.3mm in size (Plate 9.32 and 9.33), distinctive because of their low birefringence and negative RI, which form up to 2.5% of the modal percentage of a rock (SS77).

Fig 10.13 Paragenetic Sequence of Ores

	sodic	potash	acid	silica	late
zircon				-----	
thorite		-----	-----	-----	
cryolite					
uraninite	-----				
ilmenite	-----	-----	-----	-----	
TiO <sub>2</sub> minerals			-----		
columbite		-----			
haematite				-----	-----
monazite				-----	-----
cassiterite	-----	-----	-----	-----	-----
molybdenite		-----	-----	-----	-----
wolframite			-----	-----	-----
genthelvite	-----	-----	-----	-----	-----
Bi-minerals			-----		
sphalerite	-----	-----	-----	-----	-----
stannite					
pyrite		-----	-----	-----	-----
chalcopyrite			-----	-----	-----
galena		-----	-----	-----	-----
greenockite			-----		
siderite			-----	-----	-----
gold				-----	-----
chalcocite				-----	-----
covellite				-----	-----
malachite					-----
pyrolusite					-----
jarosite					-----
smithsonite					-----
cerussite					-----
limonite				-----	-----
goethite				-----	-----

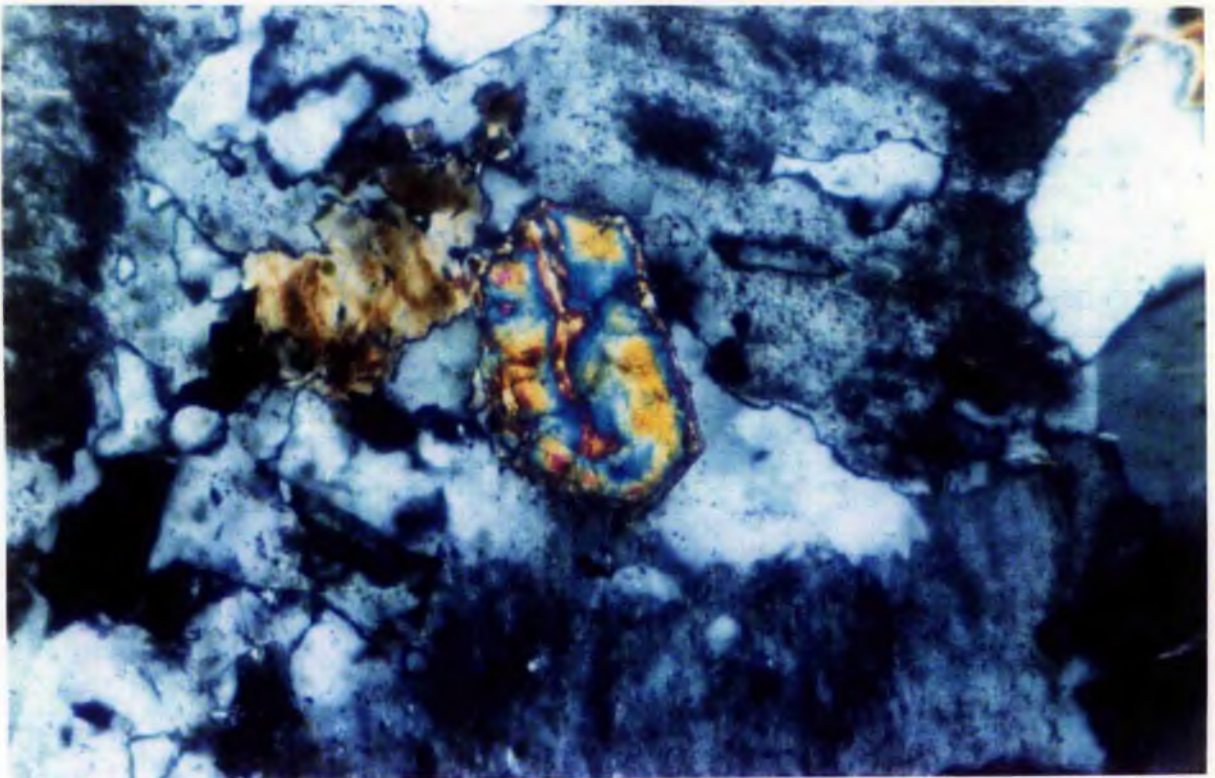


Plate 10.1

Photomicrograph of a zoned zircon in zinnwaldite albite granite. SS64/1, XPL x125

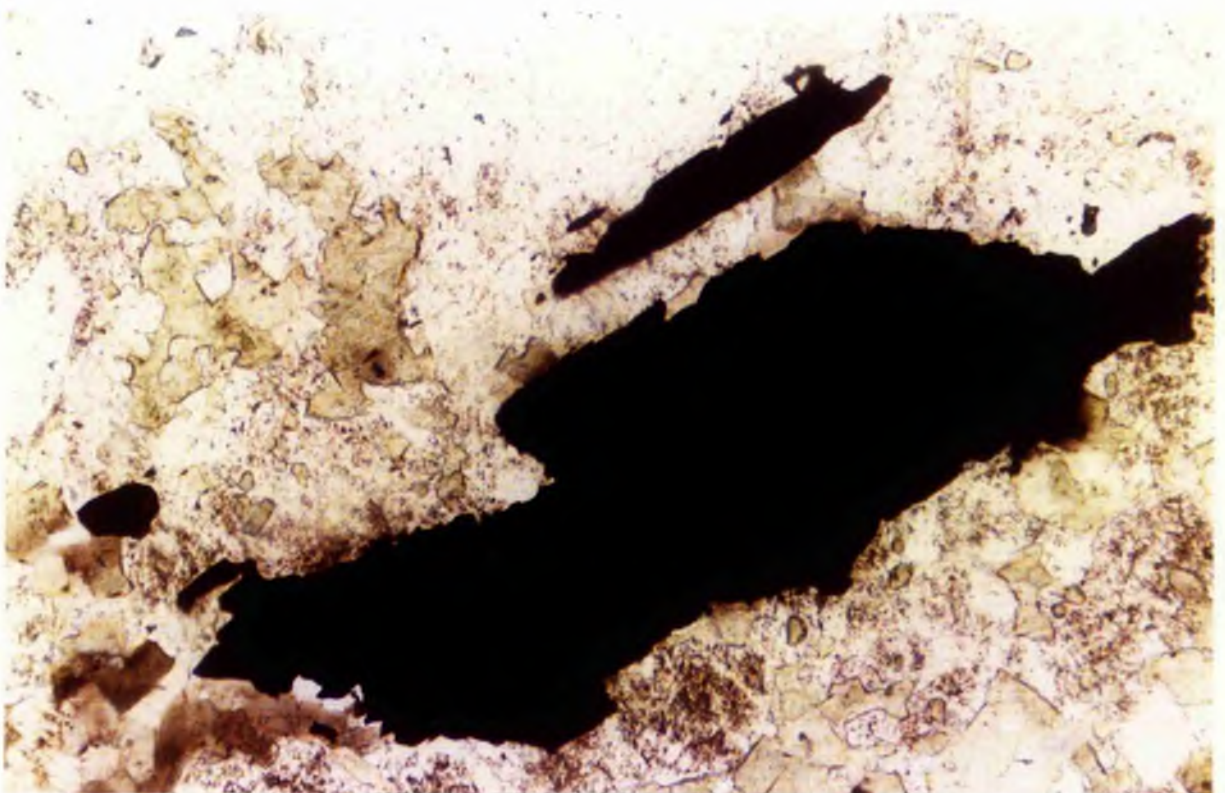


Plate 10.2

Thin section photograph in plane polarised light showing ragged columbite (bottom) and a lath of ilmenite in SS9/4. x125

Uraninite occurs as small discrete clusters of black crystals on a genthelvite pegmatite (SS117/3) and on SS117 and SS116. Autunite has been noted on several hand specimens, indicating that although uraninite development was not abundant, small amounts of uraninite must have had a widespread distribution. It is generally associated with minerals of the sodic assemblage of alteration and on rather thin evidence coupled with analogy with studies on the Ririwai complex, it is therefore grouped with the sodic minerals.

Ilmenite is more abundant than in the Ririwai Complex and in addition to occurring with columbite is associated with  $TiO_2$  minerals. Both ilmenite and  $TiO_2$  minerals occur within micas and form laths commonly parallel to the cleavage of the mica. The ilmenite may have been haematized and the development of red haematite emphasises the cleavages of the mica further especially in SS63/1.

Columbite is not a common accessory and is limited to facies where the imprint of sodic metasomatism remains. It occurs in only three thin sections (SS164, 48/1a, 9/4) where it forms opaque, ragged skeletal prismatic laths (Plate 10.2), up to 1mm in length, which may be occasionally reddish and translucent at the edges. These prismatic crystals may be aligned along mica cleavages or occur within albite in the albitized facies. They are associated with ilmenite which has largely been haematized. The columbite crystals are less abundant than at Ririwai. However, there is more ilmenite.

Haematite is ubiquitous and commonly forms the most abundant opaque phase. It occurs intergrown with, or as an alteration product of columbite, ilmenite and  $TiO_2$  minerals in the sodic assemblage of ores and is generated at all later hydrothermal alteration stages. It may occur as minute acicular crystals less than 0.01mm in microcline and it is common along cleavage planes in micas of the acid alteration assemblage, where it developed from ilmenite breakdown etc. Haematite was particularly common, though never abundant in the silica and late-stage alteration stages where it formed from wolframite, siderite and sulphide alteration. This late-stage haematite often forms a thin coating on other minerals and gives a pink coloration to quartz veins.

Allanite is a rare mineral and only occurs in altered basement monzogranite (SS57/14 and SS93) where it is moderately abundant (up to 1%). It forms dark brown, skeletal prismatic crystals up to 1mm in length. These are accompanied by, and intimately associated with, monazite which appears to be replacing the allanite (Plate 9.24).

Monazite is a common accessory, especially in the mineralized basement. It may occur as a mesh of acicular crystals up to 0.5mm in length, as rosettes of radiating aggregates and as prismatic crystals up to 4mm by 1mm in size (Plate 10.3). It is associated with sphalerite and chalcopyrite in SS93 where it may occur enclosed in fluorite or mica. It is surrounded by pronounced pleochroic haloes in biotite, indicating that like the monazite at Ririwai described by Ixer et al (1987), it is also a U/Th bearing phase. It encloses zircon and haematite.

Cassiterite varies in colour in hand specimen according to source, ranging from dark brown to black and occasionally crystals may show an adamantine lustre



Plate 10.3

Large prismatic monazite crystal 4mm long by 1mm in size. Smaller crystals of monazite form a meshwork in the biotite, and are surrounded by distinctive pleochroic haloes. Accessory sphalerite (dark red) and fluorite are also common. PPL x15

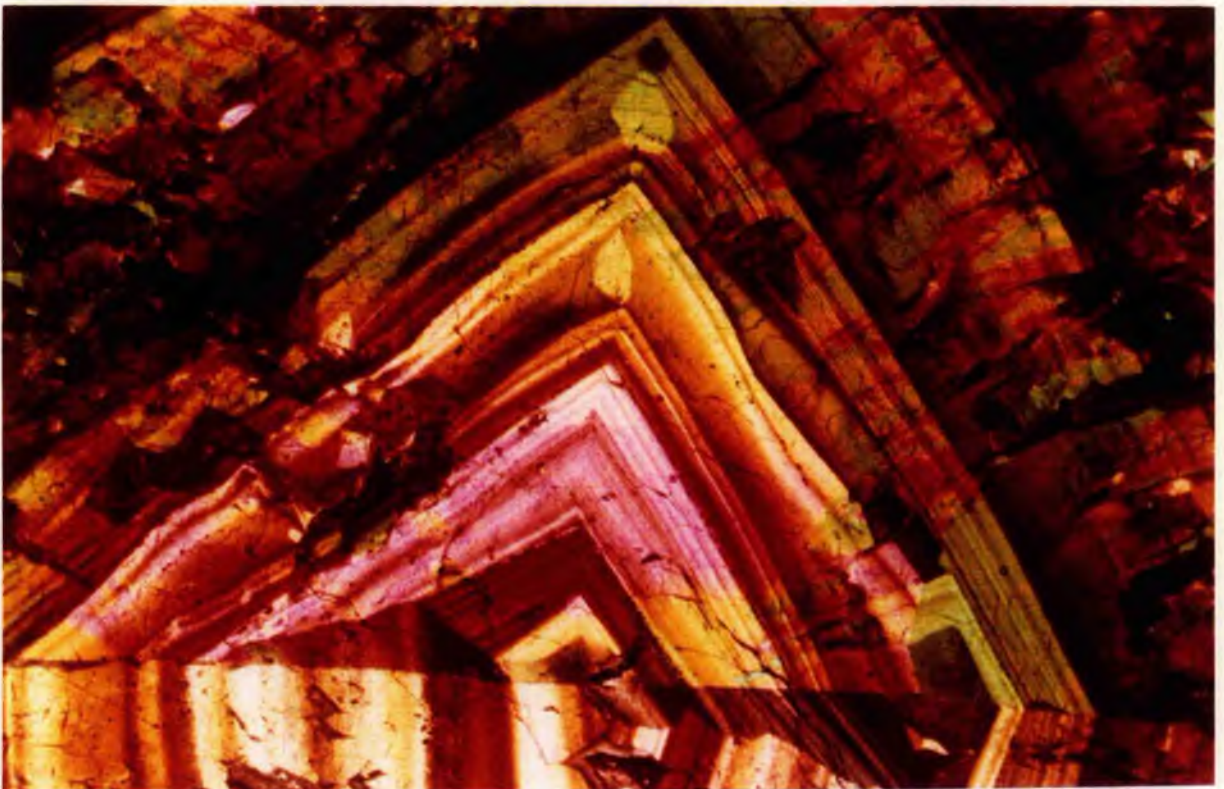


Plate 10.4

Zoned cassiterite in SS113 from near Dawa mining camp. XPL x15

but more commonly it displays a submetallic lustre, or it may be brown and hackly in late-stage alteration assemblages. In thin section or polished ore the cassiterite is commonly zoned and often spectacularly so (Plate 10.4).

Polished and thin sections of cassiterite show different characteristics in different hydrothermal assemblages. Sections of early formed cassiterite disseminated within granite or hydrothermal vein wallrocks are small and euhedral in thin section. In polished section these cassiterites are zoned and simply twinned crystals that contain few inclusions, possibly of columbite or  $TiO_2$  minerals (by analogy with the Ririwai material described in Kinnaird et al 1985a) The cassiterite associated with potassic and acid metasomatism was often larger in grain size, up to 0.5cm, strongly zoned and often deeper in colour, strongly pleochroic, and sometimes highly birefringent (SS8/1a, 8/lb, 12/2, 23/9, 63/1 and SS94). Although there was no consistent pattern to the zoning, either chemically or in colour, there does tend to have been a change from darker coloured at the core to paler margins. Inclusions of monazite, zircon and thorite are common. Wolframite or sphalerite may also be closely associated with the cassiterite crystals. In polished section this cassiterite is a darker grey in colour than the earlier phase. It is sometimes intergrown with the sulphides, particularly sphalerite, which may be enclosed in cassiterite rims.

Table 10.16 Microprobe analyses of compositional variations within a zoned cassiterite.

SS106/4

	brown 1	brown 4	colourless 3	colourless 2
$SiO_2$	0.26	0.43	0.31	0.10
$TiO_2$	0.04	0.08	0.23	0.13
$Al_2O_3$	0.00	0.00	0.00	0.02
$Fe_2O_3$	0.22	0.08	0.11	0.23
$MnO$	0.00	0.00	0.00	0.05
$MgO$	0.10	0.11	0.14	0.12
$CaO$	0.23	0.21	0.21	0.30
$Na_2O$	0.33	0.00	0.24	0.20
$K_2O$	0.05	0.00	0.00	0.03
$F^2$	0.00	0.00	0.00	0.89
$F=O$	0.00	0.00	0.00	0.38
$ZnO$	0.00	0.00	0.12	0.10
$SnO_2$	99.53	99.27	100.14	100.93

During acid metasomatism of a perthite granite, in the early stages of alteration the cassiterite that developed was small, deeply coloured and simply twinned (SS12/2a). In later stages of acid alteration, cassiterite crystals were coarser <0.3cm, sometimes anhedral and deep reddish or dark brown in colour and

strongly pleochroic in thin section. (SS6/1, 7/1, 8/3, 11/5, 27/7 and SS47/4). In SS109C - the silixite - the cassiterite is yellow-brown in thin section and sieve-like in texture. During silica metasomatism, the cassiterite was coarsest in texture and is up to 1cm in size. It is dark in colour, twinned, strongly pleochroic and strongly zoned (SS9/1, 97 and SS99). Cassiterite that developed from late-stage alteration, is smaller and <0.3mm in size. It is pale brown, yellowish, or colourless in thin section and in polished section the coarse crystals are an even darker grey than the earlier phases of cassiterite.

Cassiterite nearly always contains inclusions of thorite together with inclusions of monazite, zircon and other minerals occasionally which enables its position in the paragenetic sequence to be established.

Microprobe analyses (Table 10.16), show traces of  $\text{SiO}_2$ ,  $\text{TiO}_2$ ,  $\text{FeO}$ ,  $\text{MgO}$ ,  $\text{CaO}$ ,  $\text{Na}_2\text{O}$ ,  $\text{K}_2\text{O}$  together with Nb and Zn. However, the microprobe standard used was not pure and analytical data was quantitatively unsatisfactory.

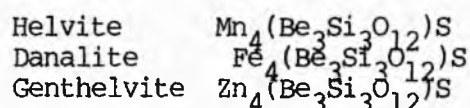
Molybdenite occurs as an accessory in several samples from Dawa as equant flakes up to 5mm in diameter (SS1, SS12/2, SS12/4, SS12/8, SS114 and SS129), where locally it may form up to 1% of the rock. It also occurs as curved laths occasionally along bent cleavages in the large mica crystals. It is easily recognisable in hand specimen by its metallic silver sheen and hardness of 1 and in polished section by its white colour and high reflectance.

Wolframite occurs in more than one generation. An early phase forms along the cleavages of micas formed during acid metasomatism. The more dominant a later phase of wolframite formation resulted in the growth of skeletal lath-like crystals up to 4mm in length in quartz veins in the basement and also in aggregates of smaller prismatic crystals. It is iron-rich ferberite in composition.

Genthelvite, although not an ore mineral as such, is a beryllium zinc and sulphur bearing phase which has been included for study here since its occurrence and local abundance have important implications for interpretation of fluid compositions and particularly sulphur fugacity. It is the most abundant beryllium mineral in the Nigerian ring complexes and is found in a number of other complexes, (Ririwai, Jere Sanga, Jarawa and Jos Bukuru) in addition to the occurrence in the Saiya Shokobo complex. It formed either as a mineral in pegmatitic pods and veins or as disseminations in biotite granite roof facies. Genthelvite occurs only within the biotite granite contact zones less than 30m from the contact (Kinnaird 1977). Most occurrences therefore, are situated in the northern part of the province where granitic members of the ring complexes are exposed at or near their upper contacts (These are shown by a solid diamond and Be symbol on the 1:50,000 scale map). Southwards, where the volcanic cover and roof zones have been eroded, beryllium mineralisation is less conspicuous. Genthelvite has been recorded up to 18cm in size, but it is commonly less than 2mm in size and in the Saiya Shokobo is up to 3cm in size in SS117/3. Genthelvite is widespread but not abundant in many samples from the Dawa and Ladini areas (eg. SS1/5, SS11/5, SS24/2, and SS117/3) and forms up to 2.5% of SS80 which is a biotite perthite granite roof sample that has been extensively altered by acid metasomatism.

Genthelvite is red in colour and resembles almandine garnet from which it can be distinguished in hand specimen by its inferior hardness and the smell of H<sub>2</sub>S when scratched. In thin section it is greyish or very pale pink and isotropic. It may occur as euhedral crystals which are characterised by triangular forms in thin section. The mineral is frequently traversed by numerous cracks which serve to distinguish it from other isotropic minerals. More commonly however, the genthelvite occurs as anhedral sometimes sieve-textured crystals which clearly formed late. It encloses a variety of other minerals commonly mica, but also albite, cassiterite, columbite, zircon, fluorite and quartz. Quite commonly the genthelvite has a core which is very sieve-textured which poikilitically encloses an abundance of inclusions and an outer rim which is more continuous with less inclusions of other minerals. This growth feature perhaps suggesting more than one phase of formation (Plate 9.56 & 9.57).

Genthelvite is a cubic mineral and is one of an isomorphous series in which the three end members are:-



The structure of the helvite group of minerals is of a framework silicate, similar to sodalite. The framework of genthelvite is formed by the linkage of SiO<sub>4</sub> and BeO<sub>4</sub> tetrahedra in approximately equal numbers, each corner oxygen being shared by two tetrahedra. Cubo-octahedral units are formed bounded by six rings of four tetrahedra parallel to 100 and eight rings of six tetrahedra parallel to 111: the six-membered rings define a set of channels which intersect to form large cavities. The cavities are occupied by sulphide ions which are tetrahedrally co-ordinated by Zn (Fe, Mn) ions.

Chemically, the analysed sample from locality SS117 differs in the molecular proportions of FeO and ZnO from the genthelvite of the Rayfield area of the Jos-Bukuru complex analysed by von Knorring and Dyson (1959).

The sample from locality 117 Ladini, therefore is genthelvite in composition but with sufficient iron to be transitional towards danalite. Danalite has actually been recorded by Taylor (1959) in the Dawa area. However, samples collected from this area by the author have all proved to have zinc predominant and therefore to be genthelvite. In a province however, where so many minerals are iron enriched it seems quite feasible to expect danalite. The danalite described by Taylor is similar in optical and physical properties to the genthelvite described here. No detailed chemical analysis was given but X-ray data "showed Fe as the major constituent with subordinate zinc, minor manganese, a trace of chromium and BeO of 13.0%." Taylor quotes a density of 3.44 which is towards the upper limit for danalite.

It is interesting to speculate whether there is a change in the Zn:Fe ratio in genthelvite from different alteration assemblages. Just as sphalerite varies in composition so may there be a variation from danalite to genthelvite. It is even possible that the Zn:Fe is temperature sensitive and could be used as a geothermometer although insufficient data exists to test the hypothesis.

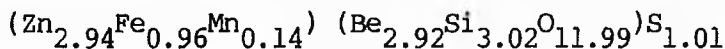
Table 10.17. Compositional variations of genthelvite

	Harwell	SS117(Ladini)
SiO <sub>2</sub>	30.70	31.5
TiO <sub>2</sub>	n.d.	<0.1
Al <sub>2</sub> O <sub>3</sub>	0.18	n.d.
FeO	11.73	23.70
MnO	1.72	3.10
Na <sub>2</sub> O	tr.	0.15
K <sub>2</sub> O	n.d.	<0.07
BeO	12.39	12.20
ZnO	40.56	25.50
MgO	tr.	<0.04
CaO	tr.	0.08
S	5.50	5.00
	102.78	101.00
O=S	2.74	2.49
Total	100.04	98.51

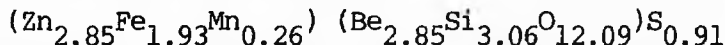
Structural formulae:

Si	0.511	0.524
Fe	0.163	0.330
Mn	0.024	0.044
Be	0.495	0.488
Zn	0.498	0.313
S	0.172	0.156

Harwell, Jos Bukuru complex (von Knorring and Dyson, 1959):-



Ladini, Saiya Shokobo complex:-



Native bismuth, accompanied by mosaics of bismuthinite crystals, are associated with chalcopyrite. Occasionally, acicular crystals of bismuthinite are enclosed in galena, indicating the lateness of the galena formation.

Sphalerite is the most abundant ore mineral of the Saiya Shokobo Complex and can be found in masses up to 30cm across in the Dutsen Rishi area. It occurs in the Rishi biotite granite and it may occur in disseminated or vein-controlled mineralised assemblages, to a greater or lesser degree, associated with all the hydrothermal phases of alteration. In massive form it varies in colour from reddish brown to almost black in hand specimen and in thin section it ranges from blood red through orange to yellow and almost colourless. This coloration, is largely attributed to iron content. However, although the amount of iron that can be accommodated in the sphalerite structure increases with increasing

temperature, such that the iron content of the sphalerite can be used as a geothermometer, this does not seem feasible for sphalerites from the Nigerian Province. Firstly, because the Province is very iron rich, so that all minerals are iron end-members or iron enriched, and secondly, because in most occurrences where the amount of co-existing pyrrhotite is extremely small and the fluids are constantly changing, it would be extremely difficult to establish equilibrium conditions between sphalerite, pyrite and pyrrhotite. Also Ramdohr (1969) has found that a high sulphur pressure in the fluids from which crystallisation has taken place results in transparent iron poor sphalerites, regardless of temperature.

For the Rishi rocks, the colour of the sphalerite is variable even within one thin section, eg SS94, suggesting the existence of more than one generation and in polished ore blocks several generations of sphalerite clearly co-exist. An early inclusion-free generation consists of a uniformly grey phase showing citrone-yellow internal reflections. The later generation of sphalerite is a darker grey with dark orange internal reflections and full of inclusions of chalcopyrite and stannite. This phase of sphalerite may be associated with, and sometimes replaced by, galena. In addition to forming a discrete ore mineral, sphalerite is also common as an exsolved phase within chalcopyrite. The sphalerite itself contains abundant exsolved blebs of chalcopyrite, whilst massive chalcopyrite in SS102, is rimmed by sphalerite. In SS20/2 however, sphalerite itself is rimmed by chalcopyrite. There are also stannite rims to both sphalerite and chalcopyrite, indicating that stannite formed late in the sequence.

Sphalerite was sparse in abundance until  $K^+$  alteration where it is moderately abundant in microcline-rich facies as ochre-coloured sieve-textured, anhedral crystals which exsolve chalcopyrite. During acid metasomatism there was a variation in coloration. In acid metasomatised basement, the colour ranges from ochre to blood red, whereas in acid metasomatised  $Na^+$  or  $K^+$  assemblages it is commonly a deep orange or orangy yellow. There is also a systematic colour variation developed during progressive stages of acid metasomatism of a perthite granite. In stages 1 and 2 of the alteration the sphalerite that formed was blood red in colour (SS15a, 15b, 16/1, 16/2, 16/6, 18/6, and 64/2). During stages 3 and 4 it became a deep orangy yellow colour (SS12/6, 12/7, 12/8, 12/9, 33/4, - 7/1, 20 and 47/3a). During silica and late stage metasomatism, the coloration is in shades of yellow (SS6, 1, 129, 20).

The sphalerite is commonly anhedral and nearly always sieve-textured. It encloses quartz, sericite, chlorite, Li-mica or fluorite, according to the stage at which it developed.

One hundred and thirty-six microprobe analyses were made of sphalerite from five samples. Comparative analyses were made on sphalerite formed during acid metasomatism of different initial assemblages. This included analysis of small discrete grains of sphalerite, traverses across anhedral masses, and spot analyses of inclusions of sphalerite within other minerals such as chalcopyrite and galena. It also included different coloured sphalerites; red in SS102, orangy yellow in 20/1, 20 and 6/1 and deep yellow in SS18.

The five rocks studied were:-

- SS20/1 - which had undergone sodic then acid metasomatism
- SS102 - which is an acid metasomatised basement granite
- SS18 - which is an acid metasomatised perthite granite
- SS6/1 - which is also an acid metasomatised perthite granite
- SS20 - which is a late-stage quartz-illite vein

Four zoned sphalerites were analysed from sample SS20/1. In addition an average for the 25 points analysed in the same slide are given in Table 10.18a.

In SS102, a traverse across a large sphalerite crystal, 0.7cm across was undertaken. Seventeen analyses were made; analysis 1 in Table 10.18b represents one rim, whilst analyses 6,7,8,9 and 10 are across the core and analysis 16 is the other margin of the sphalerite crystal. In the same sample a number of small discrete grains and blebs exsolved from chalcopyrite were also made for comparison.

In SS18, 7 analyses from 4 discrete grains showing exsolution of other mineral phases were compared with 2 analyses from separate grains which did not show exsolution phenomena (Table 10.19a).

In SS6/1, 17 analyses were made on 15 small discrete crystals and the results given in Table 10.19b.

Finally, in Table 10.19c sphalerites from the late-stage quartz-illite vein SS20 were analysed and the mean of 7 analyses from 4 crystals is given.

In all the alteration types, the sphalerite is moderately iron rich with varying traces of Cu, Pb, Mn, Sn and Ni. There seems little difference in chemistry of sphalerites whether they are small grains or large crystals. However, in SS102 the small discrete deep orange-coloured crystals of sphalerite had a lower iron concentration than the accompanying large deep blood-red mass which was analysed. Sphalerite exsolution blebs within chalcopyrite however, not surprisingly show a higher copper content, together with a higher Fe percentage, than discrete grains. Analyses from grain centres compared with rim compositions together with analytical traverses across large grains show that there is always a sharp decrease in Fe% at the margins and a concomitant increase in Zn. The variation is always seen irrespective of grain size. There may also be a slight decrease in Cu.

The sphalerite that formed early in the hydrothermal alteration sequence is darkest in colour. This contains the highest iron content with mol% of 13% FeS in SS102. Clearly there was a trend towards a paler colour due to a decrease in iron content in the sphalerite that formed during later stages of alteration and this undoubtedly represents a decrease in temperature. The most iron-poor sphalerite with 6.68 mol% FeS, is in SS6/1, which formed during the latest stage of acid metasomatism of a biotite perthite granite. However, sphalerite from SS20 contains a higher mol% FeS than 6/1 even though it occurs in a late-stage alteration assemblage and would be expected to have a lower iron concentration. It has an average 9.5 mol% FeS compared with an average of 6.7% in 6/1. This must be a reflection of the iron-enrichment of the late-stage fluids which was noted in the geochemistry section and therefore emphasises the unreliability of the iron content of these sphalerites as a geothermometer.

In summary therefore, there was a decrease in iron from core to rim in

Table 10.18 Microprobe analyses of sphalerite in SS20/1 and SS102

## (a) Sphalerite in SS20/1

	mean	range	
Zn	62.60	61.18-65.40	
Fe	4.13	1.57- 5.30	
Cu	0.34	0.04- 2.37	
Pb	0.20	0.00- 0.28	25 analyses from 9 grains
Mn	0.02	0.01- 0.02	
Sn		0.00- 0.06	
Ni	0.02	0.01- 0.05	
S	32.86	32.50-33.28	
Total	100.17		

	Fe %		Cu %		Zn %		no.of anal
core	rim	core	rim	core	rim		
5.30	3.88	0.05	0.11	61.99	62.56	4	
5.22	3.68			61.70	63.38	3	
5.13	3.40	0.09	0.17	61.74	63.35	2	
4.94	2.32	0.10	0.26	61.97	64.89	2	

## (b) SS102 Traverse through a large sphalerite - 1cm across

	1	2	3	4	5	6	7	8
Zn	60.86	60.62	60.67	59.92	58.92	58.90	60.31	60.00
Fe	6.11	6.11	6.59	6.78	7.37	7.37	6.82	7.21
Cu	0.28	0.35	0.48	0.39	0.52	0.64	0.37	0.37
Pb		1.28	1.20	1.23	1.29	1.39		
Mn	0.16	0.08	0.07	0.08	0.10	0.07	0.01	0.01
Ni		0.11	0.06	0.09	0.08	0.10	0.03	0.03
S	33.09	32.97	32.83	32.94	33.24	33.23	33.30	33.09
Total	100.50	101.52	101.90	101.43	101.52	101.70	100.84	100.71

	9	10	11	12	13	14	15	16
Zn	59.38	60.50	60.86	60.10	60.59	60.60	60.55	61.06
Fe	7.51	6.92	6.70	6.99	5.68	6.36	6.48	5.73
Cu	0.53	0.42	0.26	0.54	0.40	0.29	0.65	0.35
Pb					0.17	0.16	0.17	
Mn	0.03		0.01	0.01	0.01	0.02	0.01	0.02
Sn	0.02							
Ni	0.03	0.02	0.02	0.04	0.02	0.02		0.02
S	33.18	33.16	33.11	33.24	33.00	32.98	32.96	33.36
Total	100.65	100.02	100.96	100.92	99.87	100.43	100.82	100.54

Average comp<sup>n</sup> of small grains

	mean	range
Zn	61.74	61.42 - 62.20
Fe	5.48	5.43 - 5.55
Cu	0.14	0.08 - 0.20
Pb	0.01	0.00 - 0.04
Mn	0.03	0.01 - 0.04
Sn		
Ni		
S	33.04	32.94 - 33.18
Total	100.44	

Average comp<sup>n</sup> of large grains

	mean	range
Zn	60.30	59.38 - 61.06
Fe	6.72	5.68 - 7.51
Cu	0.40	0.26 - 0.65
Pb	0.04	0.00 - 0.17
Mn	0.02	0.01 - 0.04
Sn		0.00 - 0.02
Ni	0.02	0.00 - 0.04
S	33.10	32.90 - 33.36
Total	100.60	

5 analyses from 4 grains

Mol % FeS = 9.81

4 analyses from 4 grains

Average comp<sup>n</sup> exsolving from chalcopyrite

	mean	range
Zn	58.34	55.37 - 61.46
Fe	7.00	5.83 - 8.06
Cu	2.04	0.22 - 3.57
Pb	0.14	0.00 - 0.19
Mn	0.01	0.00 - 0.02
Sn		0.00 - 0.01
Ni	0.01	0.00 - 0.02
S	32.99	32.87 - 33.16
Total	100.53	

av. 6 analyses

mol % FeS = 12.53

Table 10.19 Microprobe analyses of sphalerite in SS18, SS6/1 and SS20

(a) SS18 Average sphalerite compositions in small discrete grains

	with exsolution		without exsolution
	mean	range	
Zn	62.03	61.18 - 62.62	62.34
Fe	5.29	4.84 - 5.82	5.80
Cu	0.11	0.04 - 0.23	0.09
Pb	0.31	0.00 - 0.59	
Mn	0.02	0.00 - 0.05	
Sn		0.00 - 0.02	0.01
Ni	0.01	0.00 - 0.04	
S	32.34	31.46 - 32.83	31.95
Total	100.11		100.19

7 analyses from 4 grains

2 analyses from 2 grains

(b) SS6/1 Average sphalerite compositions in small discrete grains

	mean	range
Zn	63.10	62.09 - 64.31
Fe	3.73	3.14 - 4.29
Cu	0.10	0.08 - 0.15
Pb	0.08	0.00 - 0.23
Mn	0.02	0.00 - 0.04
Sn		0.00 - 0.03
Ni	0.01	0.00 - 0.03
S	33.02	32.36 - 33.74
Total	100.06	

17 analyses from 15 grains

Mol % FeS = 6.68

(c) SS20 Average sphalerite compositions in small discrete grains

	mean	range
Zn	62.03	61.02 - 62.78
Fe	5.30	4.91 - 5.69
Cu	0.17	0.10 - 0.25
Mn	0.04	0.04
Sn		0.00 - 0.01
S	32.89	32.70 - 33.03
Total	100.43	

7 analyses from 4 grains

mol % FeS = 9.49%

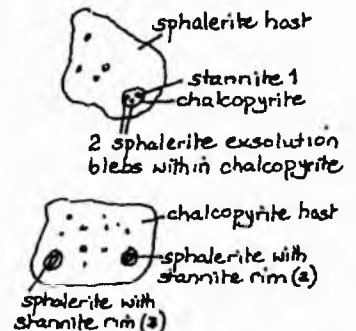
individual crystals and a decrease in iron with time, reflecting decreasing temperature with time. At the latest stage of alteration however, the sphalerites show elevated iron concentrations due to their growth from iron-enriched fluids.

Stannite is quite common within other sulphide phases and occurs as inclusions within both sphalerite and chalcopyrite. There is however, always an intimate mixture of all three and stannite is always associated with chalcopyrite. In SS102, where sphalerite is the host, the stannite occurs in exsolved chalcopyrite blebs which contain inclusions of stannite and sphalerite <5 microns in size. Also in SS102, where chalcopyrite is the host, the stannite forms a pale grey rim, a few microns wide, surrounding sphalerite and replacing it (see sketch in Table 10.20).

Compositionally, from the three analyses obtained, there appears to be a difference in stannite composition according to host, thus when it occurs in chalcopyrite rather than in sphalerite, there is an increased Sn and Cu content and when it occurs in sphalerite there is an increased zinc content to make the analysed sample a zincian stannite:-

Table 10.20 Microprobe analyses of stannite compositions

	1	2	3	Cumming 1931
Sn	24.64	27.60	27.82	26.65
Cu	26.33	27.68	27.77	31.56
Fe	11.86	11.70	11.63	3.65
Zn	7.97	4.31	3.94	7.72
Ni	0.04			
S	30.08	29.25	29.24	29.75
Total	100.92	100.54	100.40	99.34
Stannite formula	$Cu_2FeSnS_4$			
Zincian stannite	$Cu_2(Zn,Fe)SnS_4$			



This means that compositional variations in the stannite inclusions are controlled by the composition of the host mineral rather than by changes in the chemistry of the fluid.

Pyrite is not a common mineral in the Saiya Shokobo Complex. Where it occurs (eg, in the central zone of SS6/1) it is found in association with sphalerite and cassiterite. It may however, also occur as fine-grained intergrowths in chalcopyrite or as rarer pyrite cubes as in SS 6/1. One of these has been analysed and three analyses across the cube are shown in Table 10.21. Analysis 1 is from the centre of the cube and the other two represent diagonal corners.

Table 10.21 Compositional variations across pyrite from SS6/1

	1	2	3	mean
Fe	46.83	46.87	46.85	46.85
S	53.16	53.12	52.71	53.00
Total	99.99	99.99	99.56	99.85



Table 10.22 Compositional variations of chalcopyrite in SS102 and SS20/1

## SS102

	traverse						
	core						rim
	1	2	3	4	5	6	7
Cu	34.51	34.04	34.17	34.15	31.03	34.10	34.05
Fe	30.29	30.59	30.54	30.62	30.57	30.49	30.14
Zn	0.00	0.01	0.40	0.01	0.06	0.06	0.15
Sn	0.18	0.15	0.20	0.17	0.12	0.43	0.40
Ni	0.00	0.00	0.00	0.00	0.01	0.00	0.00
S	34.52	34.55	34.70	34.99	35.08	35.09	34.54
Total	99.50	99.34	100.01	99.94	96.87	100.17	99.28

## Exsolved blebs within large sphalerite

	1	2	3	4	5
Cu	34.36	34.30	34.36	34.50	34.21
Fe	30.68	30.26	30.27	30.41	30.66
Zn	0.02	0.01	0.00	0.19	0.33
Sn	0.14	0.28	0.44	0.03	0.00
S	34.43	34.29	34.48	34.55	34.51
Total	99.63	99.14	99.55	99.68	99.71

## Small discrete grains

	1	2	3	4	5
Cu	34.34	34.43	34.84	34.26	34.58
Fe	30.46	30.64	30.47	30.67	30.70
Zn	0.05	0.00	0.00	0.21	0.00
Sn	0.00	0.05	0.04	0.04	0.04
S	34.04	34.42	34.18	33.91	33.90
Total	99.83	99.54	99.53	99.09	99.22

## SS20

	1	2	3	4	5	6	7	8	9
Cu	34.76	34.58	34.69	34.70	34.75	34.62	34.08	34.35	34.39
Fe	30.35	30.45	30.58	30.57	30.57	30.76	30.58	30.64	30.50
Zn	0.00	0.00	0.40	0.00	0.00	0.00	0.12	0.00	0.00
Mn	0.23	0.03	0.03	0.03	0.03	0.00	0.00	0.00	0.00
Pb	0.00	0.00	0.00	0.00	0.00	0.75	0.75	0.75	0.75
Sn	0.20	0.00	0.17	0.07	0.09	0.19	0.07	0.02	0.02
S	34.58	34.53	34.20	34.44	34.21	34.27	34.32	34.38	34.20
Total	99.72	99.59	100.07	99.81	99.65	100.59	99.92	100.14	99.86

1,2,4,5 discrete grains  
 3 exsolved bleb from sphalerite  
 6,7,8,9 exsolved blebs in galena

## SS20/1

	traverse			
	core			rim
	1	2	3	4
Cu	34.51	34.52	34.83	33.96
Fe	30.71	30.51	30.92	30.38
Zn	0.04	0.03	0.10	0.86
Sn	0.02	0.02	0.05	0.04
Ni	0.02	0.02	0.00	0.01
S	34.46	34.80	34.54	34.66
Total	99.80	99.94	100.48	99.95

## Exsolved blebs within large sphalerite

	1	2	3	4	5	6
Cu	34.47	34.40	34.00	33.72	34.05	34.37
Fe	30.74	30.50	29.96	30.17	29.81	30.41
Zn	0.09	0.45	1.33	1.72	1.64	0.57
Pb	0.04	0.04	0.04	0.04	0.00	0.00
Sn	0.08	0.08	0.06	0.06	0.00	0.00
Ni	0.00	0.00	0.00	0.00	0.02	0.00
S	34.47	34.44	34.58	34.61	34.66	34.56
Total	99.89	99.81	99.97	100.32	100.18	99.91

Chalcopyrite is a more common sulphide in the Saiya Shokobo complex than in many other mineralised areas. It appears to form more than one generation and occurs exsolved along cleavage traces in sphalerite, as rims around sphalerite and as discrete masses up to 5cm across.

The major phase of chalcopyrite formation was associated with  $H^+$  metasomatism. It occurs in mica rich zones and is associated with sphalerite and cassiterite. At this acid stage of hydrothermal alteration in some areas chalcopyrite may have been more abundant than sphalerite. The greatest concentration is in the acid metasomatised basement granite north of Dutsen Rishi, where it reached a modal volume of nearly 29% in SS94. Unlike the Ririwai Complex, where the chalcopyrite was associated with silica metasomatism, in the Saiya Shokobo Complex, copper was not enriched during silica metasomatism and was at very low levels during late-stage alteration.

Sphalerite, chalcopyrite and stannite belong to the same structural group and hence their mutual compatibility and development of complex exsolution textures as in SS102. In this and other samples, chalcopyrite which has exsolved from sphalerite, may itself be exsolving sphalerite or stannite. The same feature has been noted for sphalerite.

Forty seven microprobe analyses of chalcopyrite were made on polished sections from four samples. Of these analyses 15 were made on blebs exsolved from other minerals, 21 on discrete grains and 11 on two separate traverses. The traverse showed that there was no systematic elemental variation from core to rim, although there may have been a patchy enrichment in tin, particularly towards the margin (Table 10.22). There was also no obvious systematic variation in chemistry with different chalcopyrite habit.

There was also no difference in chemical composition according to the stage in the alteration processes at which the chalcopyrite formed. Similarly, there is no variation in chemistry of the chalcopyrite whether it occurred as exsolved blebs within sphalerite, or whether it formed as discrete grains or masses. There is a standard composition of 34-35% Cu, 30-31% Fe and 34-35% S. The enclosed phases in sphalerite show increased Zn content in the marginal zone which grades into the sphalerite host.

The conclusion is that the chalcopyrite analysed forms a mineral of "standard" composition with little obvious chemical variation at different hydrothermal stages of alteration.

Galena, which is less abundant at Rishi than in several other mineralised complexes, particularly Ririwai, was late in the paragenetic sequence. It occurs as anhedral inclusions within chalcopyrite which it appears to replace and as small discrete crystals in SS20. Ten analyses were obtained from two separate samples (SS20 and SS18). One of these comes from the north of Dutsen Rishi and one from the southern margin of the biotite granite. Both contain traces of Zn, Fe, Cu and Sn. Since there are inclusions of stannite, chalcopyrite and sphalerite, these elements are probably related to such mineral phases. The analyses show significant variations only in zinc content (Table 10.23)

Table 10.23 Compositional variations in galena in SS18 and SS20.

	SS18-1	2	3	4	SS20-1	2	3	4	5	6
Pb	81.74	81.74	80.20	81.32	82.97	83.67	83.64	81.99	83.60	83.05
Zn	0.88	3.64	2.64	1.61						0.60
Cu	0.49	0.23	0.38	0.38	0.06	0.06	0.79	0.06	0.06	0.06
Fe	0.27	0.27	0.32	0.20			0.34			
Sn	0.06	0.02	0.02	0.03	0.03	0.03			0.03	0.03
Mn					0.02	0.03		0.04	0.04	0.02
S	11.75	12.09	11.93	12.08	11.96	11.92	12.06	12.02	11.97	12.15
Total	95.19	97.99	95.49	95.62	95.04	95.71	96.84*	94.11	95.70	95.91

Analyses SS18-3 & 4, SS20-3 are phases within chalcopyrite; the remaining seven analyses are of isolated discrete grains.

\* includes 0.1% Ni

Greenockite has been identified in the mineralised basement sample, SS94. It was identified on an SEM scan of a thin section and shown to occur as discrete grains and not as a coating on sphalerite. It is associated with sphalerite, chalcopyrite, fluorite and cassiterite.

Siderite developed during late-stage alteration. In hand specimen it is a reddish brown in colour and in thin section it is pale pink to colourless when fresh but is frequently altered to haematite and/or limonite. It commonly occurs along mica cleavages where it is accompanied by fluorite. Sometimes larger anhedral patches of rhombohedral siderite occur, unrelated to mica cleavages but again they are heavily altered to iron oxides.

As is common in Nigeria, there was very little supergene alteration at Rishi. There is no secondary enrichment of ore minerals and any supergene alteration is limited to surface coatings on exposed mineralised faces. All the major sulphides are altered along fractures, cleavage or grain boundaries. Thus covellite, chalcocite, malachite and azurite developed from chalcopyrite alteration; zinkosite, goslarite and smithsonite from sphalerite alteration; cerussite undoubtedly develops from galena alteration although it has not actually been noted; haematite, which varies from botryoidal masses to earthy coatings may have developed from the breakdown of ore minerals such as chalcopyrite, sphalerite and wolframite, whilst limonite and jarosite forms yellowy coatings to a number of unworked and long abandoned pits; and lastly dendritic pyrolusite formed from the breakdown of Mn-bearing minerals.

Contribution towards a knowledge of fluid characteristics from mineral compositional data.

The development of a sequence of ore minerals indicates that there must have been a change in the nature of the fluid with time. This change in fluid characteristics has often been ascribed mainly to falling temperature. However, the detailed petrographic studies of this thesis enable several statements to be made and hypotheses to be considered:

(i) The mutual growth characteristics of both sphalerite and cassiterite in some samples leads to speculation on the nature of a fluid that can at the same time deposit an oxide and a sulphide phase. If sulphur ions were available then an explanation must be sought as to why cassiterite and not stannite was formed. The answer may lie in the nature of the fluid and its behaviour. If the fluid was boiling it seems likely that the tin could have partitioned to the vapour phase and zinc to the residual liquid phase.

(ii) The reduction in silica content at various stages of alteration, the formation of abundant fluorite or topaz, together with the growth of fluorine-rich micas indicates that the fluids must have been HF rich.

(iii) The build up in Be in the cupola zone of the Rishi granite indicates a high HF activity in the fluids (Burt 1975, 1977). It seems likely that there was a decrease in pH of the fluid with time. Removal of Na and K from the fluid during the earlier processes of alteration would naturally have lead towards pH of greater acidity. However, several other reactions that have been observed must reinforce this increase in acidity; for example the deposition of cassiterite and other oxides early in the paragenetic sequence which removed  $O_2$  from the fluid must indirectly have increased the hydrogen ion concentration of the fluid.

(iv) Several minerals which were deposited at more than one alteration stage, have different chemical compositions at each stage. In the case of the micas, there is evidence of stage zoning. In other words there is no recognisable "early" composition at the core with successive compositional variations grading outwards to form zones. (this doesn't mean that there is no zonation at all.) This would suggest that the early formed micas were dissolved and reprecipitated with compositions compatible with the evolved fluid.

(v) There was obviously an enrichment of iron in the late-stage fluids as evidenced by late Fe-rich sphalerite growth, annite development, siderite formation and haematite alteration.

Having studied the chemical and mineralogical changes that have occurred during hydrothermal alteration and deduced as much as possible about the nature of the fluid that caused such alteration, it now seems relevant to discuss the characteristics of the fluid itself. This is possible by a study of the fluid that was trapped in inclusions and forms the basis of the next section of the chapter.

## FLUID CHARACTERISTICS

### Introduction to fluid inclusion studies

A common assumption in fluid inclusion studies is that late fluids have the lowest densities. However, Swanenberg (1980), has described situations where higher density fluid inclusions formed later than lower density fluid inclusions. It is therefore necessary in a study of hydrothermal ore deposits to clarify the sequence of hydrothermal phenomena prior to an inclusion study. Based on the preceding petrological study and mineralogical data a programme of fluid inclusion microthermometry was initiated.

According to Burt (1981), the alteration assemblages in greisen and fluorine-rich porphyry ore deposits can be modelled by a consideration of the system  $K_2O-Al_2O_3-SiO_2-H_2O-F_2O_{-1}$ . Equilibria in this system have been depicted on quartz and fluid-saturated chemical potential vector diagrams whose axes are governed by the potential activity of

$\mu_{HF}$  (acidity - where  $\mu_{HF} = \mu_{HCl} + \mu_{FCl-1}$ ) and

$\mu_{KF}$  (salinity where  $\mu_{KF} = \mu_{NaCl} + \mu_{KNa-1} + \mu_{FCl-1}$ )

where  $\mu$  is the chemical potential. Advantages of this approach are that it reflects the importance of the anion F, which unlike Cl is incorporated into the lattice of the greisen minerals (mainly topaz, mica and fluorite) and that mineral stabilities can be correlated with ore-forming processes. According to Burt, the most important of these processes is probably vapour phase separation from an aqueous brine or magma (first or second boiling). Burt states that fluid inclusion studies have shown that boiling has occurred in all porphyry and many (but not all) greisen deposits. He believes that vapour phase separation from a magma must similarly be responsible for the formation of greisen-like mineral assemblages in gem pockets and miarolitic cavities in more deeply seated pegmatites and granites.

The aim of this fluid inclusion study was to test the conclusions of Burt and to see if stages of hydrothermal alteration could be attributed to boiling fluids.

From the information gained in inclusion studies it has become apparent that there were two different fluids, one associated with the volcanic rocks which originated from depth and one which was retained within the biotite granites to shallow levels within the crust. The discovery of relatively dense  $CO_2$ -rich inclusions in the phenocrysts of quartz in the ignimbrites, places a depth constraint on the source of magma generation, prior to eruption. It also has serious implications on the modelling of the emplacement mechanism of the subvolcanic-volcanic assemblages.

### Techniques of study

More than one hundred sections were examined for fluid inclusion characteristics. The abundance, size and type of fluid inclusions were recorded

and on the basis of this data, samples were selected for microthermometric studies. This preliminary thin-section study suggested that fluid inclusions were moderately abundant in quartz and feldspar phenocrysts of the volcanic pile and feeder dyke, in quartz and feldspar of the biotite granite and in quartz and sometimes fluorite or topaz - where they occurred - in hydrothermal variants of the major rock types. By noting the relative proportions of the different phases within the inclusions, crude estimates were made of composition, density and approximate homogenisation temperature of the individual inclusions. Because of the abundance of fluid inclusions in quartz and because quartz is often the most common mineral, it is inevitable that much of the following information is derived from quartz alone.

Recognition of primary inclusions ranged between difficult to impossible since many of the criteria for recognition of primary inclusions did not apply (Roedder 1984). Melt inclusions in the ignimbritic pile are regarded as primary. Isolated inclusions were usually interpreted as being primary unless modified by later observations and if not primary, were then considered as having formed earlier than clusters or trails of inclusions. Inclusions lying along healed fractures, recognised under the microscope by slightly varying the plane of focus, were regarded as secondary. Where possible, clustered inclusions and obvious secondary inclusions were avoided in thermometric studies.

Because of the difficulty of making a paragenetic classification into primary and secondary inclusions, a classification scheme based on the differing proportions of solids, liquid and vapour at room temperature was used. Such a scheme is easier to apply because subjectivity is kept to a minimum. Utilising the scheme of Weisbrod (1981), the different types of inclusions were divided into the Types L, S, V, C and M that were described in Chapter 5.

Besides the determination of the shape and size of the inclusions and the estimation of their content with a normal petrological microscope, the main part of the fluid inclusion study involved the microthermometric measurement of phase transition temperatures that occur in inclusions. These measurements were made on a Linkam TH600 stage - which is described in Appendix 6 - utilising wafers of sample which were polished on both sides.

During routine measurements the following phenomena were recorded:-

- Tf : the temperature at which the inclusion froze during supercooling.
- Te : the temperature of initial melting of an inclusion from frozen - this is the eutectic melting temperature for the system and indicates the nature of the dissolved cations.
- Tm : the melting temperature of the last solid that had been crystallised on fast freezing i.e. melting of last ice crystal, melting of hydrates or clathrates.
- Ts : end of dissolution of solid phases at high temperature.
- Th : temperature of total homogenisation of the different phases within an inclusion. Such homogenisation may be by the expansion of the vapour bubble so that homogenisation is to the vapour phase (V), by expansion of the liquid phase (L) or by fading of the meniscus between the two phases, at or near, a critical temperature. This is known as critical homogenisation.

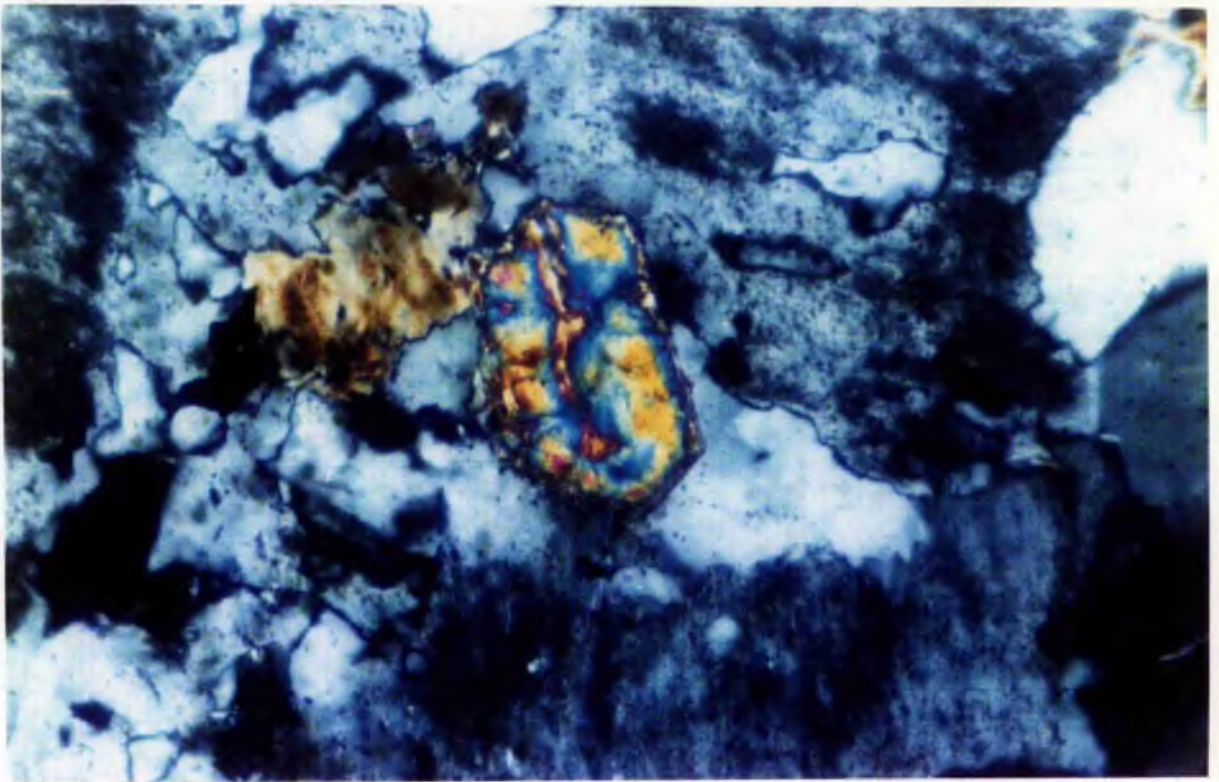


Plate 10.1

Photomicrograph of a zoned zircon in zinnwaldite albite granite. SS64/1, XPL x125

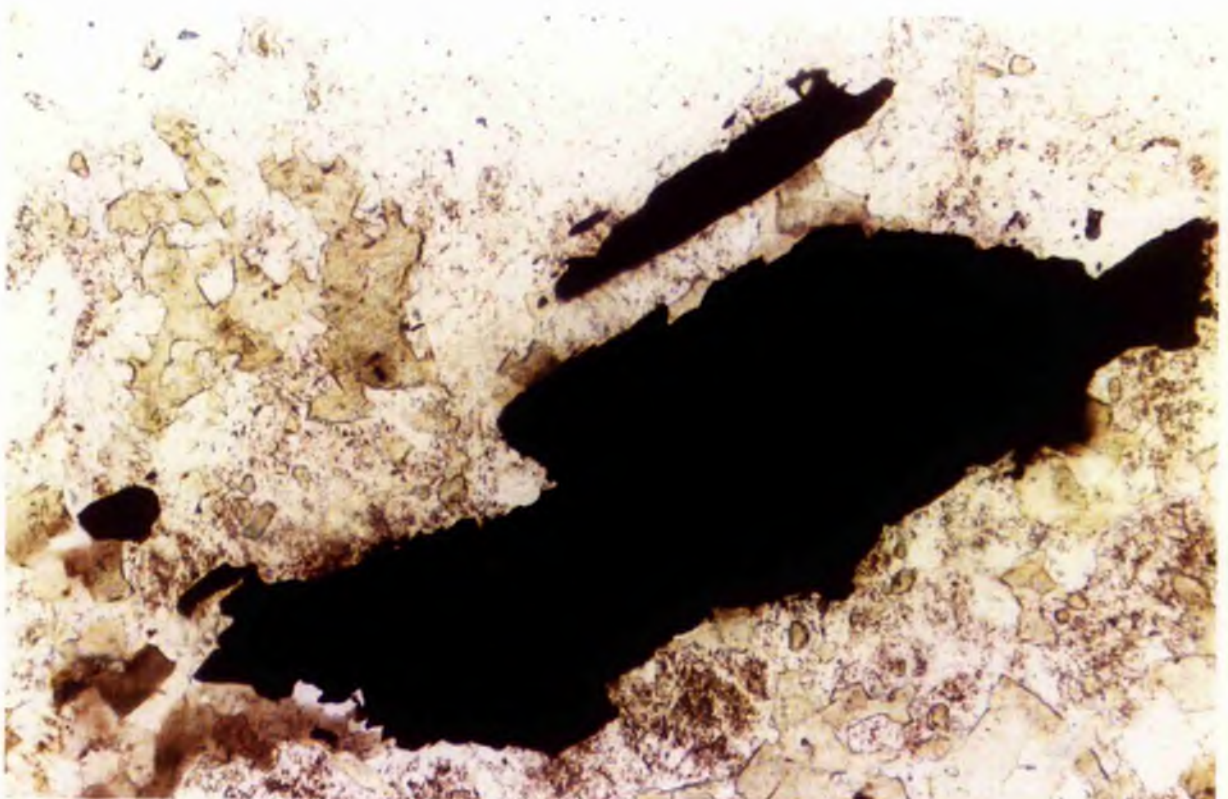


Plate 10.2

Thin section photograph in plane polarised light showing ragged columbite (bottom) and a lath of ilmenite in SS9/4. x125

The most difficult inclusions to analyse are those which fall in the NaCl-H<sub>2</sub>O-CO<sub>2</sub> system because they develop at least five phases on freezing (aqueous liquid, ice, gas hydrates, solid CO<sub>2</sub>, CO<sub>2</sub>-rich liquid and CO<sub>2</sub>-rich vapour. Up to 6 different measurements of phase transitions are theoretically possible:-

- (i) final temperature of solid CO<sub>2</sub> melting ( $T_{mCO_2}$ ).
- (ii) first melting temperature of the aqueous phase ( $T_e$ )
- (iii) the last melting temperature of the aqueous phase ( $T_m$ ).
- (iv) dissociation temperature of clathrate ( $T_{mclath}$ ),
- (v) partial homogenisation of the CO<sub>2</sub> phases ( $T_{hCO_2}$ ) and
- (vi) the total homogenisation of the system ( $T_{htot}$ ).

From this data concentration values for NaCl, CO<sub>2</sub> and CH<sub>4</sub> may be obtained. CO<sub>2</sub> and CH<sub>4</sub> data are expressed in vol% rather than as mole fractions and salinity is expressed in wt % NaCl equivalent. Salinities in H<sub>2</sub>O-NaCl-CO<sub>2</sub> systems can only be estimated from the depression of freezing point of ice, ( $T_{fice}$ ). This is because on cooling the presence of CO<sub>2</sub> results in clathrate formation, which removes water from the aqueous phase thus increasing the salinity of the residual solution. The temperature of final clathrate melting is a function of the salinity of the aqueous phase and can be used as a precise alternative. In practice this proved an unsatisfactory technique either because of the difficulty of observing clathrate melting, or because the clathrate was not in equilibrium with CO<sub>2</sub> liquid and vapour, and in the absence of either phase the temperature of clathrate melting is no longer solely a function of salinity. The fact that the melting point of the clathrate sometimes occurred at temperatures greater than 10°C indicates the presence of other gases in addition to CO<sub>2</sub> within the inclusions. The salinities for CO<sub>2</sub>-bearing inclusions are often therefore, only an approximation.

## Thermometric studies

### Introduction

In Part I of this thesis, from data acquired on samples collected throughout the province, little information was obtained on the nature of the magmatic fluid. In an attempt to monitor the characteristics of the early fluid exsolved from the granitic melt in the Rishi complex, several samples of the volcanic rocks were examined. Samples from the biotite granite were contrasted with hydrothermal variants to provide an insight into subsolidus behaviour at shallow depth.

In the Rishi samples, all types of inclusions - L,V,C,M and S were identified. Melt inclusions (Type M) are abundant in fractured and embayed quartz crystals of the volcanic pile and are rare in quartz of the biotite perthite granite. CO<sub>2</sub>-bearing inclusions (Type C) are abundant in the volcanic pile, occasionally common in a few altered cupola samples and absent in most hydrothermal assemblages. Type S inclusions which contain a high density saline fluid with solid daughter phases, occur in the volcanic pile and in many of the hydrothermal assemblages. Type L, liquid-rich inclusions are ubiquitous and occur as secondary inclusions in the volcanic rocks and the biotite granite and as primary and secondary inclusions in all the hydrothermally altered rocks. Type V-, vapour-rich inclusions, occur in all the assemblages produced in the early stages of hydrothermal alteration. They decrease in abundance in samples from later stages and are much less common in silica metasomatised rocks.

## Fluid inclusions in the Rishi volcanic pile

In the quartz feldspar porphyry of the ignimbrite pile, fluid inclusions are found in both perthitic feldspar and quartz phenocrysts.

The fluid inclusions in many perthitic feldspar phenocrysts are extremely abundant and the sheer abundance of inclusions makes it hard to distinguish the particular type of inclusion, although the presence of saline inclusions has been noted. In a study of inclusions in ejected blocks from Ascension Island, Roedder and Coombs (1967) found that whereas there were abundant melt inclusions in the quartz phenocrysts, the fluid inclusions within the feldspar were only dense saline fluids.

The abundance of fluid inclusions within the feldspar phenocrysts of the ignimbritic pile indicates that a potential existed for exchange between the feldspar host and the inter-crystalline fluid of its saline inclusions during cooling. Such exchange according to Orville (1962, 1963) can be very fast, as it can occur by simple diffusion without any revision of the Al-Si network of the framework. Orville's data indicates that alkali exchange over distances of many microns is possible in 12 hours at 600°C (1962). As with the material from Ascension Island, the feldspars in the volcanic pile at Rishi contain so many saline inclusions that most of the feldspar lattice is within a few microns of a saline inclusion. According to Roedder and Coombs (1967) this saline fluid containing both K and Na, provides a small alkali 'ion' reservoir for exchange during cooling and exsolution, and also provides a hydrous fluid through which the later reconstructive formations such as changes in the structural state might be facilitated. The rates of both Na-K ordering (perthitic exsolution) and Al-Si ordering might thus be expected to be considerably higher in such inclusion-rich feldspars.

Since inclusions in the glassy feldspar phenocrysts of the Rishi volcanic pile were much less abundant than in perthitic feldspars, it seems possible that the inclusions in the perthitic feldspars may not have been trapped during early crystallisation in the magma chamber.

The inclusions in the quartz phenocrysts are either ovate or irregular in shape or sometimes in the form of negative bipyramidal crystals and may be of types S, C, M or V. They vary in size up to 40 microns. The following data has been obtained on inclusions in quartz phenocrysts:

The M-type (melt) inclusions contain a brownish de-vitrified glass together with a small vapour bubble or bubbles. These inclusions were originally silicate melt and represent trapped droplets of granitic magma. The temperature of trapping of the melt inclusions in the volcanic pile is above that measurable on the Linkam TH600 stage. However, Th has been determined for phenocrysts of various silicic lavas elsewhere which are analogous to these Rishi volcanic rocks. Anorthoclase from quartz-free lavas of Pantelleria yielded homogenisation temperatures in the range 970-1020°C (Benhamou and Clocchiati 1976), whereas inclusions in quartz and anorthoclase of quartz-bearing lavas showed minimum Th of 750-800°C.

Co-existing with the melt inclusions in quartz phenocrysts of the Rishi volcanic rocks are type S inclusions which are up to 20 microns in size. These

are dense saline inclusions which contain several daughter solids. Relatively large cubes of a daughter mineral have been recognised in many inclusions together with one or more birefringent phases which are usually too small to identify. In SS116 there is also a solid which forms a bundle of birefringent needles. The cubic daughter mineral has been identified as halite due to its shape, isotropic nature and its RI which is close to that of quartz. The concentration of NaCl in the original fluid was estimated from approximate calculations of the apparent volume of the various phases. They range from over 50 up to 70 wt per cent NaCl corresponding to a saturated liquid in the pure system NaCl-H<sub>2</sub>O at 300°C (Keevil 1942). The density of these inclusions may be as high as 1.4 gm/cm<sup>3</sup>. Many of the smaller inclusions which do not show daughter phases are regarded as metastable S-type inclusions which are too small for daughter phases to have nucleated. The vapour bubble in some Type S inclusions has a small amount of CO<sub>2</sub> which forms a border to the H<sub>2</sub>O vapour bubble and becomes more distinct on cooling. The amount of CO<sub>2</sub> is around 4 vol%.

Occasionally type V inclusions occur in which there is low density aqueous fluid as vapour. Assuming these inclusions are of pure water, the density of filling (0.5 gm/cm<sup>3</sup>) requires that trapping occurred above 364°C and 210 bars. Any salts in solution would raise these minimum temperatures. It is assumed that these gas-rich inclusions represent the vapour phase from simple boiling of the dense saline fluid phase. Such boiling may have resulted from pressure loss during eruption.

More commonly the gas rich inclusions are type C inclusions which contain an aqueous fluid and very large vapour bubble of CO<sub>2</sub> which separates into two phases on cooling below 20°C. Rarely were pure CO<sub>2</sub> inclusions observed. For sample SS161, homogenisation of the two CO<sub>2</sub> phases is to the vapour phase in the temperature range 27.4 to 31.1°C corresponding to a density close to critical density for CO<sub>2</sub> of 0.468 gm/cm<sup>3</sup>. Occasionally however, homogenisation temperatures were as high as 33.5°C suggesting the presence of other gaseous phases such as H<sub>2</sub>S. On freezing the triple point of CO<sub>2</sub> was depressed to -56.80°C suggesting the presence of ~2.0% CH<sub>4</sub>.

For CO<sub>2</sub> inclusions close to the critical density of 0.468 gm/cm<sup>3</sup>, assuming no excess pressure, it means that the confining pressure at the time of entrapment must have been >2 kbars. This indicates that the quartz phenocrysts must have grown from a silicate magma within a magma chamber which was at a depth of ~6 km or greater.

It is possible to estimate the bulk density of the fluid and the overall CO<sub>2</sub> content of H<sub>2</sub>O-CO<sub>2</sub> inclusions by using the following measurements of observations (Shepherd et al 1985):

- (i) partial homogenisation of the CO<sub>2</sub> phase (this defines  $\rho_{CO_2}$ )
- (ii) volume proportions of CO<sub>2</sub>-rich and H<sub>2</sub>O rich phases (visual estimation)
- (iii) salt content of the of the aqueous phase

(i) ThCO<sub>2</sub> (L+V → V) = 27-31°C = 0.37 to 0.468 gm/cm<sup>3</sup>.

(ii) CO<sub>2</sub> phase occupies 60% by volume

H<sub>2</sub>O phase occupies 40% by volume

(iii) Taking the density of the fluid phase as  $1.2 \text{ gm/cm}^3$  from data above and assuming that the solubility of  $\text{CO}_2$  in the  $\text{H}_2\text{O}$  phase and  $\text{H}_2\text{O}$  in the  $\text{CO}_2$  phase is negligible at room temperature then the bulk density of the  $\text{CO}_2\text{-H}_2\text{O}$  fluid is given by:-

$$\frac{(0.6 \times 0.4)}{\text{vol} \times \rho} + \frac{(0.4 \times 1.2)}{\text{vol} \times \rho} = 0.72 \text{ g/cm}^3$$

wt%  $\text{CO}_2$  is given by  $0.24/0.72 = 33 \text{ wt}\% \text{ CO}_2$

The fluid from sample SS161 was also analysed chemically on a fluid extraction system linked to a gas chromatograph. The result indicated that the bulk composition of the fluid is:

85% water,  
11%  $\text{CO}_2$ ,  
2% unidentified non-condensibles  
with a  $\text{H}_2\text{O}:\text{CO}_2$  ratio of 7.6:1.

For details of the fluid  
extraction train see  
Appendix 8.

Thus the calculated wt%  $\text{CO}_2$  in the fluid from observations on type C inclusions was clearly too high. However, this calculation assumes that the fluid was homogeneous on trapping and it seems unlikely that this was the case. Data by Bowers and Helgeson (1983), suggest that with such saline fluids there is an increase in the immiscibility field between  $\text{H}_2\text{O}$  and  $\text{CO}_2$  such that the possibility of trapping immiscible liquids in the system  $\text{H}_2\text{O-NaCl-CO}_2$  is extremely likely. Moreover, immiscibility in fluid systems is quite a common phenomenon (Roedder and Coombs 1967; Weisbrod, 1981). In fact Roedder (1984), states that in some environments, most inclusions are formed from heterogeneous systems of two or more fluids. From the observations and calculations therefore it is concluded that fluid trapped in the volcanic rocks at Rishi was of a heterogeneous nature. Since all the inclusions described are believed to be primary, the occurrence of such a primary heterogeneous assemblage implies the coexistence of a silicate magma and a dense saline brine. This saline fluid must itself have become immiscible probably through boiling due to pressure release to give a  $\text{CO}_2$ -rich vapour phase in addition to the dense saline brine. The amount of NaCl in the system would have affected the degree of immiscibility of  $\text{CO}_2$  and water (Bowers and Helgeson 1983).

#### Summary of the thermometric data for the volcanic rocks

The inclusions within the quartz phenocrysts of the volcanic pile indicate that the phenocrysts crystallised from a silicate melt in a magma chamber at a depth of approximately 6km, assuming normal lithostatic pressure. The inclusions are believed to represent the late-magmatic fluid which was a dense saline brine with a density of at least  $1.2 \text{ g/cm}^3$  co-existing with the silicate melt. Eruption of the silicate magma to the surface resulted in rapid loss of pressure which led to the unmixing of  $\text{CO}_2$  from the magma possibly at a depth of around 2km, aiding ignimbritic eruption and also fracturing some of the phenocrysts. Modern magma chambers at similar depths are known to periodically de-gas (G.C. Brown pers. comm) and eruption may have been triggered by build up in volatile pressures.

It has always been assumed that the magma chambers of the anorogenic complexes

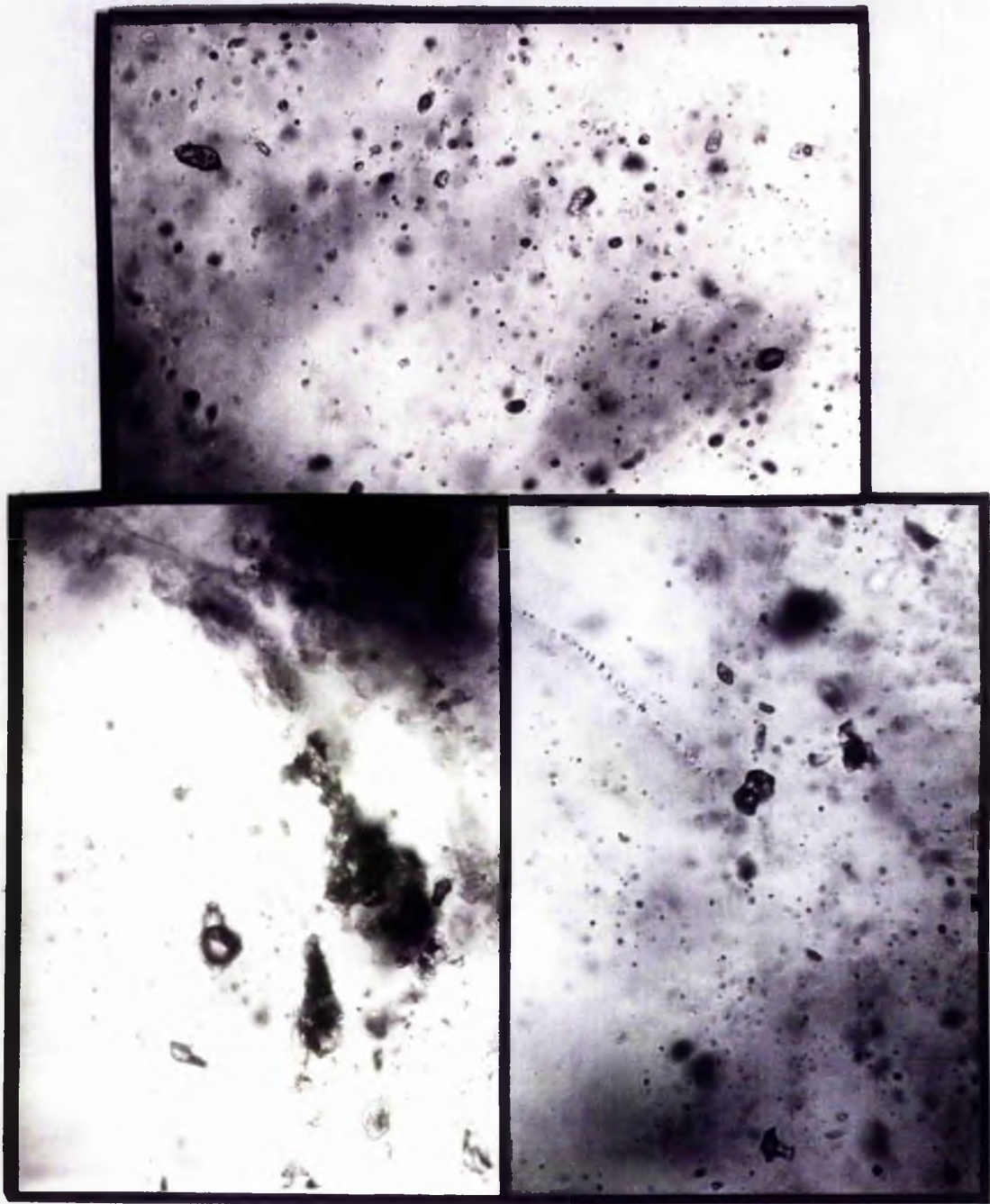


Plate 10.5 Composite of photomicrographs showing the range of fluid inclusions in quartz phenocrysts from SS161. The largest inclusion (centre bottom left) which is of CO<sub>2</sub> is approximately 20 microns in size.

in Nigeria that fed the volcanic piles, and from which the granite plutons were derived, were located at depths of around 5-8 kms in the crust. Fluid inclusion observations from the volcanic pile of the Rishi area have provided the first direct evidence to confirm these assumptions.

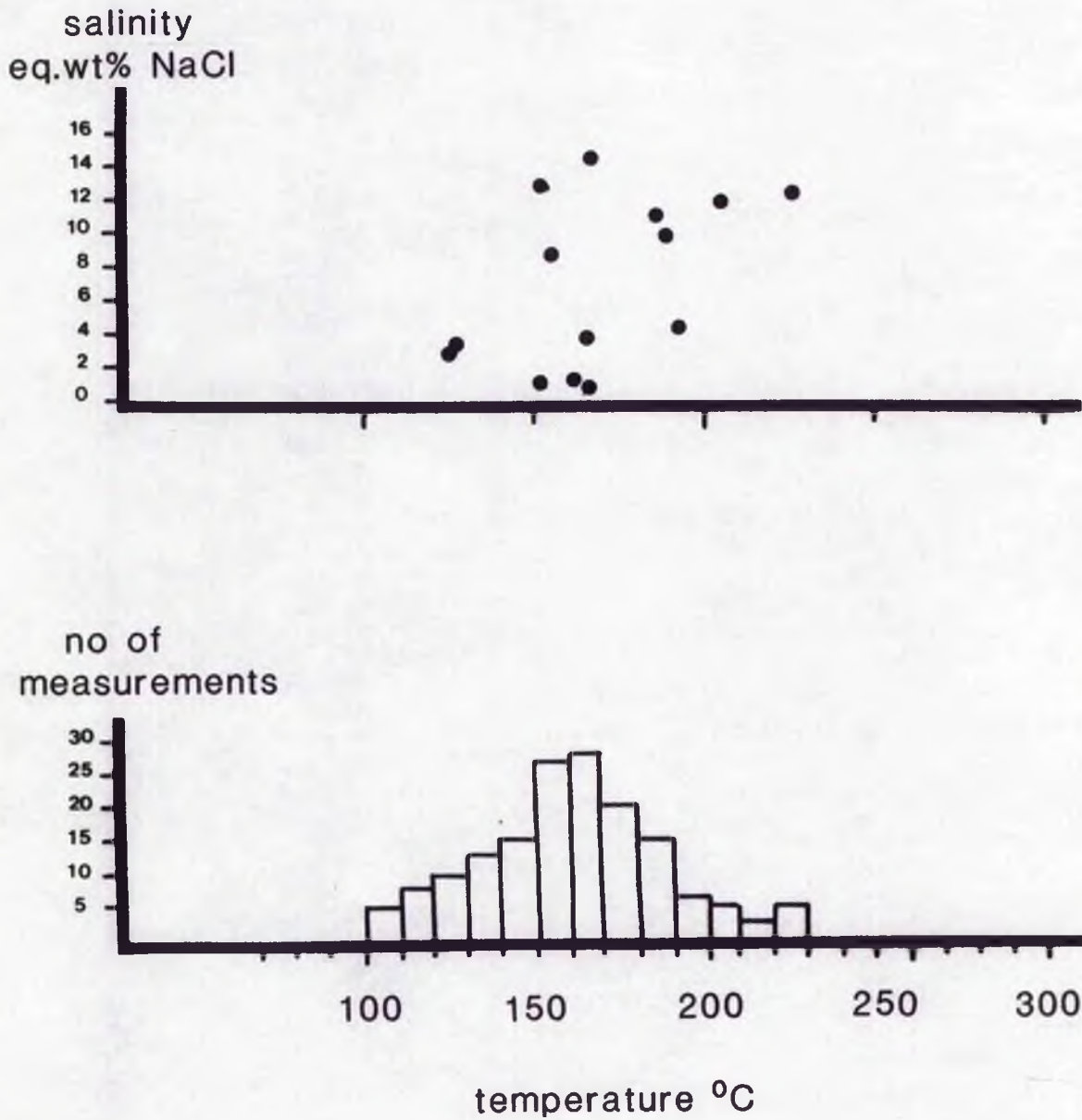
#### Fluid inclusions in the biotite granite

The fluids trapped in granitic quartz can either represent the earliest fluids evolved from the cooling magma or later fluids developed during hydrothermal alteration. Both types of fluid may have been trapped in the biotite granite in apparently unaltered samples. Under high power magnification, almost all the quartz crystals of the biotite granite are cross-cut by networks of healed fractures, often in several generations. This observation together with the distribution of the various types of inclusions, clearly indicate a long and more or less continuous history of fluid circulation, healing of fissures and trapping of fluid.

Twenty thin sections were studied for their fluid inclusion abundance and SS34, a porphyritic biotite granite was selected for thermometric studies. In SS34 the most fundamental observation is that there are no melt inclusions in the biotite granite and all the homogenisation data gives low temperatures for fluid entrapment. The other major observation is that on freezing the gas bubble collapses in the temperature range  $-37$  to  $-58^{\circ}\text{C}$ , and reappears on warming to  $+0.8^{\circ}\text{C}$ . indicating that the fluid is aqueous and dilute. On warming, ice can exist metastably in this vapour-free situation to above  $0^{\circ}\text{C}$  (Roedder, 1967 quotes to at least  $6.5^{\circ}\text{C}$ ). In this vapour-free situation the melting temperature of the last ice-crystal which varied from  $-10.8$  up to  $+1^{\circ}\text{C}$  can only be an approximation of the salinity under such metastable conditions. The maximum salinity corresponding to this data is 14.5 eq wt% NaCl. Obviously a determination of salt content from ice melting temperatures in these cases will be erroneous. However, in general, the lower the temperature of the freezing of an inclusion, the more the dissolved salt it contains so that the freezing temperature of the inclusion can be used with caution as a guide to fluid salinity.

The main homogenisation temperature range was from  $150$ - $230^{\circ}\text{C}$  with a mean of  $166^{\circ}\text{C}$  (Fig 10.14). Such low temperatures were also obtained from silica metasomatised rocks and were not expected in the "unaltered" biotite granite. According to Roedder (1984), rocks of granitic composition that crystallised near the surface and hence crystallised rather quickly, may contain melt inclusions. In contrast granites that crystallised more slowly at depth normally reveal no glass inclusions which Roedder (p387), suggests results from the fact that textures of minerals in granites are mainly a product of their subsolidus recrystallisation. Further he states that granites formed under relatively shallow conditions have not recrystallised but have either trapped silicate melts, which have homogenisation temperatures in the range  $900$ - $1100^{\circ}\text{C}$ , or hydrosaline melts yielding large cubes of NaCl, liquid and vapour at room temperature. The observations made on the granitic rocks from Rishi show exactly the opposite. In the petrographic section of Chapter 9, recrystallisation of quartz has been shown to have occurred at a late-stage in many parts of the Rishi cupola. Such a process would account for the overall lack of melt inclusions in the granitic quartz. Furthermore, inclusions with homogenisation

Fig 10.14 Th-salinity plot and Th histogram showing frequency distribution of homogenisation temperatures for two phase aqueous inclusions in quartz from SS43 biotite perthite granite



temperatures in excess of 400°C are uncommon and hydrosaline inclusions are very rare.

### Summary

The biotite granites contain type L and V inclusions and only rarely are type M, S or C observed. Trapping temperatures were less than 230°C and the fluids were less than 14.5 eq wt% NaCl with a density in the range from 1.06 to 1g/cm<sup>3</sup>. This corresponds to a minimum vapour pressure of 64 bars. The inescapable conclusion of this data is that the biotite granites themselves are the result of substantial hydrothermal modification. A similar conclusion was reached in Chapter 8 on the basis of petrographic and chemical data.

### Hydrothermal alteration assemblages

If, as the data above indicates, the biotite granite has re-equilibrated with hydrothermal fluids to low temperatures and pressures, some explanation must be sought to interpret the differences between biotite granite and mineralised alteration assemblages. Such a discussion is only possible after the fluid characteristics of the hydrothermal assemblages have been considered.

In the hydrothermally altered rocks there may be a wide range in fluid characteristics in terms of inclusion type, composition, density variations and homogenisation temperatures. As far as possible, the samples selected for study recorded the mineralogical assemblage of the appropriate alteration process with the minimum of overprinting by successive processes. However, as the petrographic descriptions of Chapter 9 made clear, there has inevitably been some overprinting of one process on another.

### Zinnwaldite albite granite

Fluid inclusion studies were undertaken on samples SS48 and SS44/2b which have a saccharoidal texture related to alteration. Mineralogically these samples are characterised by abundant laths of albite and lenticular sieve-textured zinnwaldite mica (Plates 9.9 and 9.10).

The inclusion population in the quartz crystals is very varied. Types M, C, S, V and L occur, with a wide variation in filling ratio of the different inclusions indicating a broad range in fluid density. Only types L, V and C were common. The melt inclusions tended to be rather small.

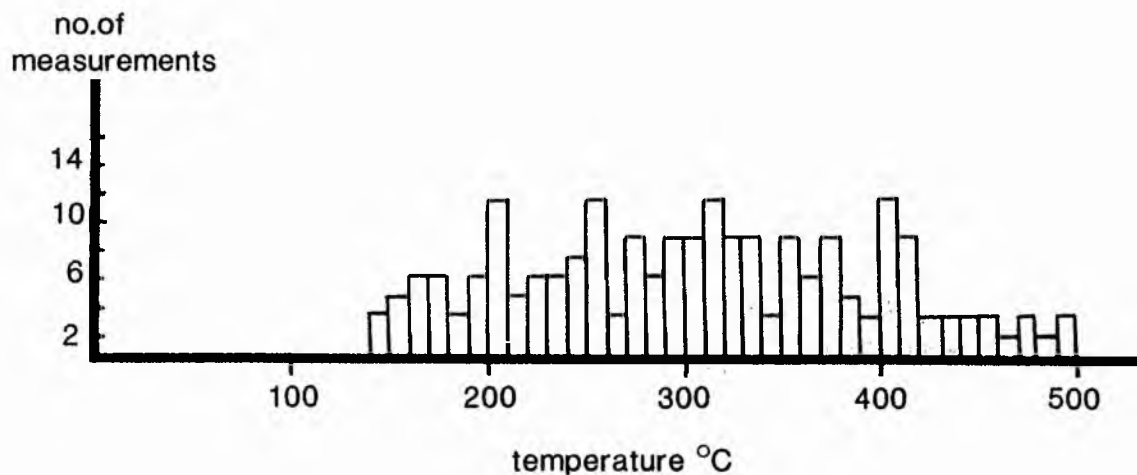
The Type S inclusions contain varying phase ratios, which give calculated salinities up to 45 wt% NaCl. Dissolution temperatures for the halite daughter crystals gave an unrealistic range of temperatures suggesting that the fluids were either trapped over a wide temperature interval, or that the inclusions contain a fluid that was inhomogeneous when trapped due to boiling. The latter explanation is preferred.

The type V inclusions often have negative crystal form and range in size up to 15 microns. Because of the form of the inclusions precise homogenisation temperatures were not measurable.

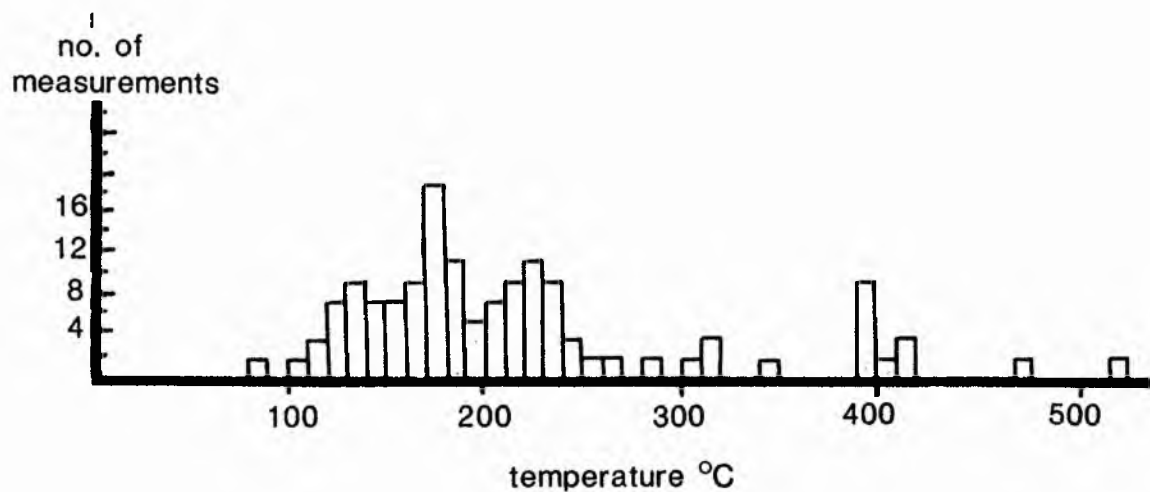
The Type C inclusions, which account for less than 10% of the population as a

Fig 10.15 Th histograms showing frequency distribution of homogenisation temperatures for two phase aqueous inclusions in quartz

### Zinnwaldite albite granite



### Microcline pegmatites



whole, are characterised by a large volume of  $\text{CO}_2$  between 50 and 70%. Homogenisation of the two phases of  $\text{CO}_2$  was to the vapour state with total homogenisation of the  $\text{H}_2\text{O}$  and  $\text{CO}_2$  to the vapour state (disappearance of the  $\text{H}_2\text{O}$  phase if decrepitation did not occur), giving a low density for these inclusions. Using the method of Shepherd et al (1985) described earlier the  $\text{CO}_2$  content of the fluid as a whole was calculated to be less than 23 wt %. However, the actual content was probably much less than this, where homogenisation measurements were possible, the total homogenisation temperatures of  $\text{CO}_2$  and  $\text{H}_2\text{O}$  in the type C inclusions fell in the range from 400-500°C.

The bulk of the data in Fig 10.15a was obtained from type L inclusions. Salinity for the higher temperature inclusions (>350°C) was around 15-18 wt% NaCl but for lower temperatures of homogenisation there was a great variation in salinity. Such a wide range in homogenisation temperatures as shown in Fig 10.15a with no defined peak is difficult to interpret and will be discussed later. However, during sodic metasomatism it appears that an important unmixing took place between 400 and 500°C, probably in response to a sudden loss of pressure which could have resulted from fracturing of the volcanic pile or the rise of the granite magma to high levels in the crust. At this early stage in fluid evolution there was a loss of  $\text{CO}_2$  although the volumetric percentage of  $\text{CO}_2$  in inclusions is always moderate. Such  $\text{CO}_2$  unmixing in response to pressure loss could have been also have been encouraged by the high salinity of the fluids.  $\text{CO}_2$  was important in the early fluids with effervescence early in the mineralisation sequence when up to 23%  $\text{CO}_2$  was present in the fluid. From the data of Haas (1971), the vapour pressure in NaCl-saturated brine inclusions homogenising at 400°C - assuming a lithostatic overburden of 2.70 g/cm<sup>3</sup> - is a minimum of 300 bars with a minimum depth of formation of 1150 metres.

#### Microcline pegmatites

Two hydrothermal pegmatite samples, showing equilibrium crystallisation, were chosen to study the nature of the fluids responsible for potash metasomatism: SS9/11 an amazonite pegmatite and SS4/3 a pink microcline pegmatite.

Sample SS4/3, is of a pegmatite that consists largely of microcline feldspar and quartz which, from the texture, seemed likely to be minerals co-existing in equilibrium. Only fluid inclusions in the quartz were studied. Type V and type L inclusions are dominant. The type V inclusions are of a low density 0.02-0.26 g/cm<sup>3</sup> aqueous fluid which co-existed with type L-rich inclusions which had a density range of 0.78-0.964 g/cm<sup>3</sup>.

There is a wide range in homogenisation temperatures with a few inclusions giving homogenisation temperatures between 400 and 527°C. The bulk of the homogenisation temperatures fall within the range 140-220°C (Fig 10.15b). Salinity in all the inclusions is low. The lowest melting temperature of the last ice crystal was -9.8 (corresponding to 14 eq.wt % NaCl. The main salinity range is from 5-9 eq wt % NaCl. For many inclusions however, the vapour bubble collapsed on supercooling below -40°C and only reappeared as the last ice crystal melted at around -4 to 3°C. Although this phenomena indicates that the fluids were very dilute, the temperature of melting of the last ice crystal cannot be used to indicate the precise salinity because of the metastable conditions within the inclusion.

The fluid has a low volume % of  $\text{CO}_2$ . On cooling the inclusions below -47°C a

double bubble of CO<sub>2</sub> appeared in some inclusions which homogenised at -20°C. This indicates a very low vapour pressure of CO<sub>2</sub> and therefore a low confining pressure at the time of trapping.

Sample SS9-11 is of quartz crystals from an amazonite pegmatite. It contained abundant inclusions, many of which were highly irregular in shape. As with sample SS 4/3 Types L and V inclusions are dominant. However, a few Type S inclusions also occur in this sample. Before thermometric experiments, many of the inclusions in the sample appeared to be monophasic liquid. However after repeated freezing and heating runs many of these nucleated a vapour bubble. Homogenisation temperatures of both Types L and V inclusions were in the range 130 to 420°C. The homogenisation temperatures of the vapour-rich inclusions could be measured accurately in the very irregularly shaped inclusions and were in the range 230-400°C perhaps suggesting that boiling of the fluid ceased below 230°C.

### Summary

For the samples that have been described which are representative of early sodic and potash metasomatic processes, there is a wide range of inclusion size, composition, density, and salinity reflected in the occurrence of type L, type S and type V inclusions with Type C inclusions and occasionally Type M, in quartz crystals of the albite-bearing rocks.

For the zinnwaldite albite samples, there is a wide range of homogenisation temperatures with no clearly defined peak on the histogram (Fig 10. 15a). The albite-bearing rocks however, are characterised by an important CO<sub>2</sub> component in the fluid.

Within both the hydrothermal microcline-bearing pegmatites discussed, whilst there was a wide range of fluid characteristics, the dominant inclusion type is of low salinity, low temperature inclusions that were presumed to be secondary. Homogenisation temperatures were generally within the range 130 -240°C. The homogenisation temperatures in the range from 400 to 420°C may be closer to the true temperature of the potash metasomatism.

### Greisenised samples from the roof zone

The homogenisation temperatures for previous samples have proved much lower than anticipated. In an attempt to monitor the successive changes from the high temperature, dense saline late-magmatic fluids of the volcanic pile to low temperature, low salinity fluids of late-stage alteration therefore, samples of pervasive acid metasomatism were chosen for study.

The zoned vein SS109 which is situated high in the roof zone near Dutsen Rishi was selected as an example of acid metasomatism affecting the biotite perthite granite. Petrographic details of samples from the different zones are given in Chapter 9.

### SS109A quartz-chlorite assemblage

In SS109A, which is a quartz-chlorite rock containing sphalerite and chalcopyrite

there is a mixture of Types L, V, C and S inclusions with transitions between the different groups.

The type S inclusions are characterised by two daughter minerals and in one of the inclusions the melting temperature of these solids was 220°C and 363°C, well above the homogenisation temperature of 206°C of the vapour to liquid in the inclusion. In another case, only one solid was visible due to the small size of the inclusion and the melting temperature was 216°C and in a similar inclusion the solid melted at 344°C. Most solids however had not dissolved at temperatures in excess of 370°C and where decrepitation had not occurred were still present at 420°C, indicating a salinity equivalent of >47 wt% NaCl. Calculations of salinity from volume percentage of NaCl indicated a salinity of greater than 51 wt% NaCl but this only approximates to the situation as it does not take into account the second daughter mineral. Density of these fluids at the time of trapping was at least 1.272 gm/cm<sup>3</sup>. A further observation on daughter salts occurred occasionally when at temperatures in excess of 350°C, two solids appeared in the fluid of a previously homogeneous vapour-rich inclusion. Although small, one phase appeared to have a rhombohedral form and high birefringence and was assumed to be either a carbonate or perhaps an iron chloride; the other was prismatic in shape with low birefringence and may be anhydrite (CaSO<sub>4</sub>.2H<sub>2</sub>O). Taking the inclusion where the homogenisation of vapour + liquid to vapour occurred at 206°C and the dissolution of the halite occurred at 363°C then the vapour pressure was around 100 bars at the time of trapping.

The type L inclusions, are filled with a dense saline fluid with a small vapour bubble that contains a low volume of CO<sub>2</sub>. Some of these, inclusions develop hydrohalite on freezing indicating from the NaCl-H<sub>2</sub>O phase diagram a salinity equivalent to 23.3 - 26.3 wt % NaCl. In other type L inclusions, coarse ice crystals develop which finally melt in the temperature range -20.5 to -9.2°C which corresponds to a fluid salinity of 23 to 13 eq.wt.% NaCl. The first melting temperature of these inclusions when frozen ranged between -33°C and -27°C. Homogenisation of these inclusions was to the liquid phase at temperatures generally in the range 190°C to 350°C with the higher temperatures of homogenisation corresponding to the higher salinity inclusions (Fig 10.16a). Density of the fluid in these inclusions varied from 0.98 to 1.15 gm/cm<sup>3</sup>. A phenomenon observed on several occasions was of apparent homogenisation to the liquid phase at temperatures between 149°C and 279°C and later the sudden reappearance of a large vapour bubble with almost instant homogenisation into the vapour phase between 319°C and 334°C. These inclusions are assumed to contain a fluid close to the critical density and are therefore transitional to type V, the vapour-rich inclusions.

Type V inclusions occur in which the vapour bubble exceeds 70% of the volume of the inclusion. The inclusions are often up to 40 microns in size and irregular in shape which has enabled precise homogenisation temperatures to be measured in the range 330-360°C. Measurement of the salinity proved extremely difficult and accounts for the few points shown on Fig 10.16a.

Type C inclusions which may also be up to 40 microns in size contain CO<sub>2</sub> the two phases of which, only become apparent on cooling. Homogenisation of the CO<sub>2</sub> phases to the liquid state, for most inclusions took place between +15 and +16°C corresponding to a fluid density of 0.84 gm/cm<sup>3</sup>.

On supercooling, the CO<sub>2</sub> in these inclusions melts from frozen at temperatures

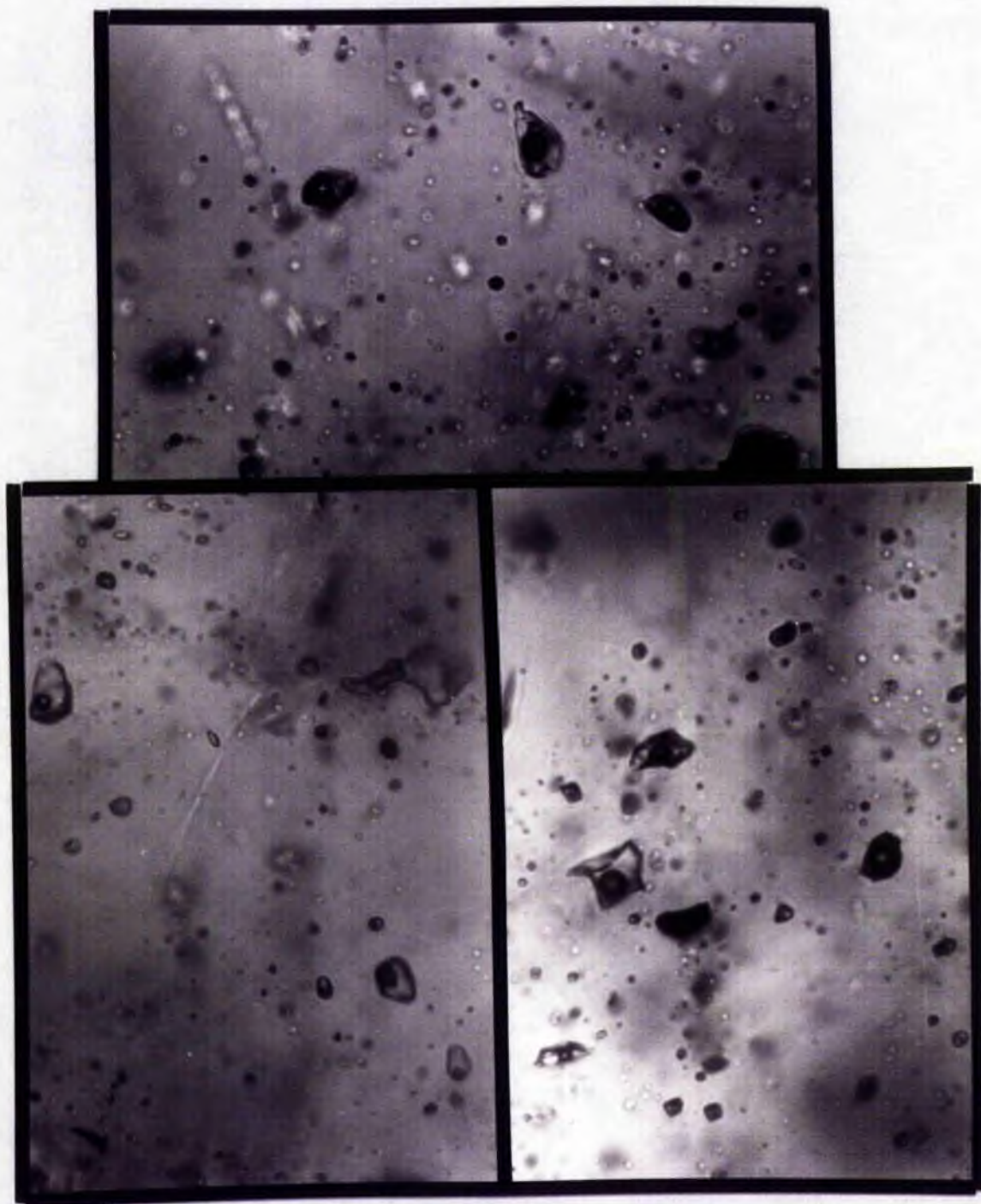
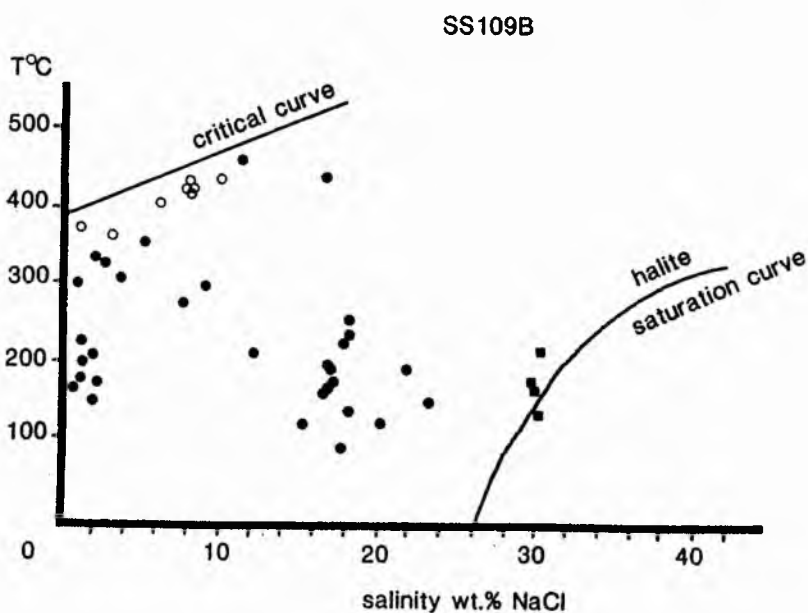
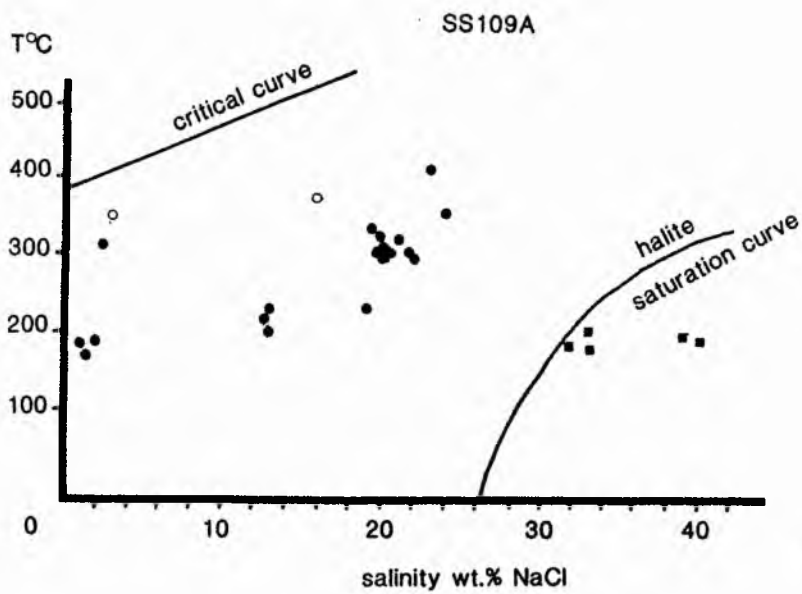


Plate 10.6 Composite of photomicrographs showing the range of fluid inclusions in quartz from SS109. The largest inclusion is 16 microns across. Top plate shows the daughter-rich inclusions in SS109A. Below left - two phase inclusions in SS109B. Below right gas-rich and liquid-rich inclusions in SS109C

Fig 10.16 Th-salinity plot for inclusions in quartz from SS109A and SS109B. Open circles represent two phase aqueous inclusions which homogenise to the vapour state, solid circles are those which homogenise into the liquid state. Squares are halite-bearing inclusions: those to the left of the halite saturation curve  $T_h > T_{sNaCl}$  (temperature of halite dissolution); those to the right  $T_{sNaCl} > T_h$  and those close to or on the curve  $T_{sNaCl} = T_h$ .



between  $-56.6$  and  $-57$ . The addition of  $\text{CH}_4$  lowers the triple point of  $\text{CO}_2$ . However, the temperature of the final melting of the  $\text{CO}_2$  ice does not uniquely define the bulk composition of the fluid, because  $\text{CH}_4$  is strongly partitioned into the vapour bubble and the measured melting temperature relates only to the  $\text{CH}_4$  depleted liquid phase. The true  $\text{CH}_4$  content is derived from the data of Heyen et al (1982). Their interpretive graph uses the final melting temperature of solid  $\text{CO}_2$  together with the temperature for  $\text{CO}_2$  liquid-vapour homogenisation. Assuming that the effects of  $\text{N}_2$  and other gases on the triple point of  $\text{CO}_2$  are small compared to that of  $\text{CH}_4$ , then these values would indicate concentrations of from 0 to 2.8%  $\text{CH}_4$  relative to  $\text{CO}_2$  (after Heyen et al 1982). However, other common gases in addition to  $\text{CH}_4$  are known to depress the triple point of  $\text{CO}_2$  below  $56.6^\circ$  and the addition of  $\text{H}_2\text{S}$  would also have this effect. One homogenisation temperature for the two phases of  $\text{CO}_2$  above the critical temperature of  $31.1^\circ\text{C}$  for  $\text{CO}_2$ - $\text{CH}_4$  systems, suggests that at least in some inclusions there is a small proportion of  $\text{H}_2\text{S}$  since the critical temperature for  $\text{CO}_2$ - $\text{H}_2\text{S}$  is  $+100.4$  (i.e. the maximum homogenisation temperature for a mixed  $\text{CO}_2$ - $\text{H}_2\text{S}$  fluid). Without a chemical analysis of the volatile components the identification of this additional gas phase cannot be made for sure. However, since sphalerite and chalcopyrite occur in the mineral assemblage it would seem reasonable to suggest that  $\text{H}_2\text{S}$  is present whilst not discounting the possibility of traces of methane or/and nitrogen.

In addition to the above inclusions, there is a fifth type of inclusion which contain low density fluids co-existing with high density brine. These are interpreted as representing condensates from a boiling fluid.

There is a continuum of inclusion types in SS109A, such that a gradation exists between different 'types' of inclusions. Inclusions have been identified in which the large vapour bubble of  $\text{CO}_2$  is accompanied by two daughter crystals similar to those described in type S inclusions. These both decreased in size on heating and were still both present although much reduced in size at  $420^\circ\text{C}$  on decrepitation of the inclusion. Homogenisation of the liquid to gas phase occurred at  $380^\circ\text{C}$ .

#### SS109B quartz-chlorite-sericite-topaz assemblage

Fluid inclusions in the quartz crystals are a combination of Types L, V and S.

Type S inclusions in contrast to those in sample SS109A contained only one solid which was much smaller in size than similar daughter minerals in SS109A. These solids dissolved in the range  $300$ - $332^\circ\text{C}$  indicating a fluid salinity of around 37-40 eq.wt % NaCl with a fluid density of less than  $1.2\text{g/cm}^3$ .

The Type L inclusions are abundant and up to 30 microns in size. On freezing hydrohalite developed in several inclusions indicating a salinity equivalent between 23.3 and 26.3 wt% NaCl. Where ice crystals developed the last melting temperatures were within the range  $-12$  to  $-21^\circ\text{C}$  corresponding to a salinity of 16-23 eq wt% NaCl. Homogenisation temperatures ranged from  $140^\circ\text{C}$  to  $470^\circ\text{C}$ .

Low density vapour-rich inclusions (Type V) were sometimes up to 50 microns in size. Homogenisation temperatures were in the range  $406$  to  $437^\circ\text{C}$ .

Many planes of secondary inclusions contain a uniform ratio of phases. There

are major variations in the fluid density between individual planes that were presumably trapped at different times. Simple variations in the confining pressure could account for these differences.

#### SS109C quartz-topaz assemblage

SS109C forms the central part of the zoned vein and is a chalcopyrite-, galena-bearing silicite. The inclusions are smaller and not as abundant as in SS109A and SS109B and are dominated by Type L inclusions with some type V and only rarely Type S inclusions. The fluids are dilute with salinities less than 5 eq. wt% NaCl and homogenisation temperatures from 200 - 356°C (Fig 10.17). Fluid density varied from 0.6 to 0.904 g/cm<sup>3</sup>.

Salinity is clearly lower than in samples 109A or 109B. Also no CO<sub>2</sub> was observed in any of the inclusions during cooling experiments. This was verified by a chemical analysis of the extracted fluid which showed that compositionally it contained insufficient CO<sub>2</sub> to be detectable during freezing experiments:

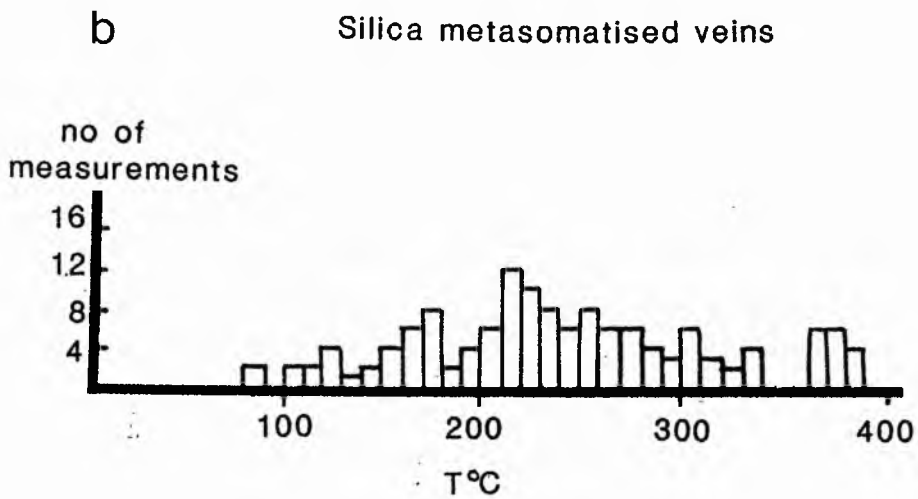
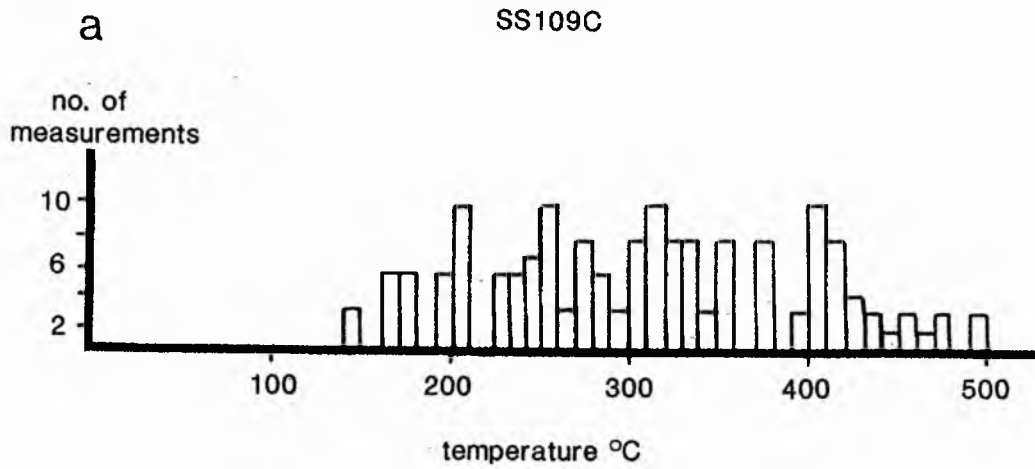
H <sub>2</sub> O:	97.6%
CO <sub>2</sub> :	1.7%
non-condensibles:	0.7%
H <sub>2</sub> O:CO <sub>2</sub> :	57

#### Interpretation of data for SS109

Within samples from vein SS109 there is a co-existence of liquid-rich, solid-rich and gas-rich inclusions. Fig 10.17 shows a broad spread of data points between the halite saturation curve and the critical curve. Such an association of inclusions could be interpreted either as a mixing between a low salinity/high temperature fluid and a high salinity slightly cooler fluid or the boiling of a moderately dilute fluid. Since SS109 is a vein in biotite granite which is only a few metres below the volcanic pile, either situation would be possible. From the information available there is no way of differentiating between the two although a boiling model is favoured even though it cannot be demonstrated conclusively that the vapour-rich fluids and liquid-rich inclusions have the same homogenisation temperature range.

For SS109A it is envisaged that the bulk fluid was around 22 eq wt% NaCl salinity at a temperature 300-320°C with a density of around 1.2 g/cm<sup>3</sup>. As the fluid boiled the salinity of the fluid would have gradually increased as the temperature of the fluid cooled. With continued boiling the fluid salinity gradually exceeded 26 wt% NaCl (NaCl saturation at 20°C, giving rise to halite-bearing inclusions at room temperature. At 200°C, the fluid was saturated in respect of NaCl and halite precipitation occurred. As a result of boiling, vapour bubbles were trapped together with halite-bearing inclusions. The apparent compositional gap between 24 and 29 eq. wt % NaCl is considered to be a result of halite metastability. The high homogenisation temperatures of the Type V inclusions are attributed to small amounts of fluid adhering to the vapour bubble when it was trapped. Some inclusions have homogenisation temperatures above 320°C suggesting that they are trapped non-homogeneous fluids rather than vestiges of an earlier higher temperature fluid. The low salinity liquid-rich inclusions in the sample are interpreted as a trapped condensate from the

Fig 10.17 Th histograms showing frequency distribution of homogenisation temperatures for two phase aqueous inclusions in quartz



boiling fluid.

The amount of confining pressure at the time of fluid trapping can be assessed in several ways. From the tables of Haas (1971) for a fluid of ~22 wt% NaCl that was boiling at 320°C the depth of formation was around 1000m with a pressure of around 95 bars if the confining pressure was hydrostatic. A similar confining pressure was determined by using temperature-density diagrams for NaCl solutions (Walther p126 in Shepherd et al 1985) indicates that the vapour pressure in some inclusions was between 100 and 150 bars. A different confining pressure was obtained independently from binary H<sub>2</sub>O-CO<sub>2</sub> diagrams (from Walther p.138 in Shepherd et al 1985) suggesting that the pressure was in excess of 300 bars. However, the latter method assumes homogeneous trapping of the fluid which has not occurred.

For SS109B, the inclusion data could be interpreted in two ways:

(i) that the initial fluid was at a temperature of >400°C and a salinity of <6 wt% eq. NaCl and that progressive boiling with decreasing temperature resulted in the trapping of more saline inclusions.

(ii) that the initial fluid was within the temperature range ~240-260°C and had a salinity around 18 eq.wt% NaCl. Boiling of the fluid due to repeated pressure release led to the trapping of vapour-rich inclusions together with saline inclusions which were saturated with respect to NaCl at temperatures around 200°C. Low salinity inclusions trapped at similar temperatures are considered to be trapped condensate.

The second is the preferred alternative and the high homogenisation temperatures of the Type V inclusions are attributed to small amounts of fluid adhering to the vapour bubble when it was trapped. If the fluid of 18 eq. wt% NaCl did boil at around 250°C then the minimum depth of formation was 400m at a pressure of 40 bars.

For SS109C, the fluids were more dilute than in the other samples although homogenisation temperatures cover a wide range 200-356°C. The vapour pressure for these dilute inclusions indicate that the confining pressure must have been very low and suggests that at this late-stage of acid metasomatism the vein was connected to the surface.

Greisenised samples from the basement

Several samples of acid metasomatised basement were studied, SS57/4, SS93 and SS18/1. They all contained only low saline Type L inclusions which all showed similar ranges of homogenisation temperatures, fluid salinity and fluid density:-

SS93(2A) is a chlorite rich vein resulting from acid metasomatism of the basement to the north of Dutsen Rishi. The sample is exceptionally rich in ores, particularly sphalerite. Inclusions were examined in fluorite from the vein because it is very quartz-poor. The sample is believed to have been derived from fluids that were not dissimilar from those that caused the acid metasomatism at locality SS109C, and in the sample studied the inclusions appear to be dominated by type L inclusions filled with a low salinity fluid. Homogenisation

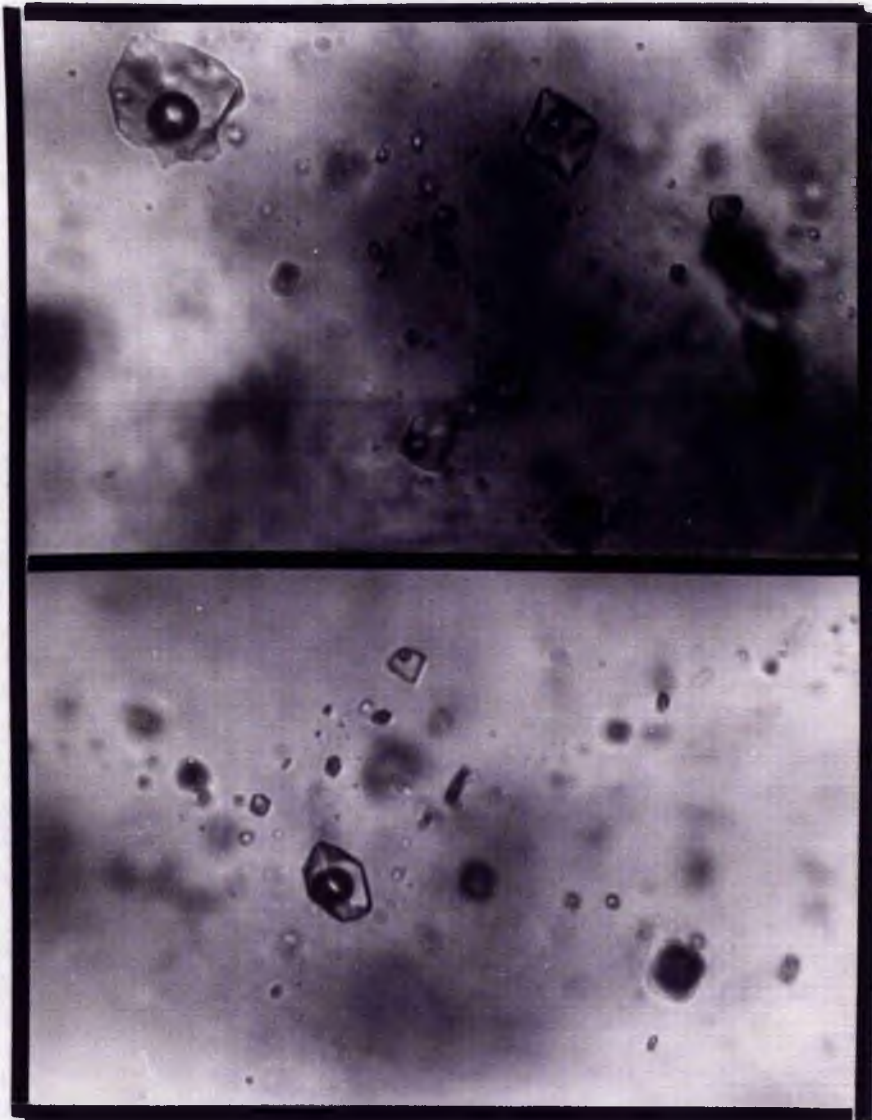


Plate 10.7 Dilute two-phase Type L inclusions in quartz from SS93 which is acid metasomatised basement. The size of the largest inclusion is 20 microns.

temperatures were within the range 255-312°C. Fluid salinity was less than 5.2 eq wt% NaCl for all the inclusions with the lower temperature inclusions giving low salinities to <1 eq wt% NaCl with a fluid density around 0.94 g/cm<sup>3</sup>.

#### Summary

The initial fluids that caused greisenisation of the roof facies of the biotite perthite granite appear to have been moderately saline >20 eq wt% NaCl at temperatures >300°C with a density of around 1.2 g/cm<sup>3</sup>. It is envisaged that there was frequent boiling in the temperature range 250-140°C due to repeated pressure release so that a mixed assemblage of inclusions was trapped. Some inclusions were type S or type V but the majority were of type L. In the late stages of acid metasomatism the fluids were dilute with salinity equivalent of <6 wt% NaCl.

Fluids that moved out from the granite and altered the basement monzogranite in the endocontact zone were rapidly cooled and diluted so that homogenisation temperatures were in the range 255-312°C with a salinity of less than 5 eq. wt% NaCl.

#### Silicified mineralised veins (Fig 10.17b)

Sample SS10/8 is a silicified mineralised vein rich in sphalerite and chalcopyrite. During freezing experiments for most inclusions the bubble collapsed on fast freezing and only reappeared at temperatures in the range +1.4 to + 8.5°C. Under such conditions of metastability, ice melting temperatures give erroneous salinity equivalents. However, bubble collapse on freezing which is due to the expansion of ice crystals is typical of very low salinity inclusions. For inclusions where T<sub>m</sub> could be measured there was a range between -3.2°C and -10.9°C corresponding to a salinity of 5.2 to 14 eq. wt% NaCl. It has a wide range of homogenisation temperatures from 140-360°C. However, there appeared to be no direct correlation between higher temperature and higher salinity data.

Sample SS117/5 has undergone silica metasomatism. It contains only type L inclusions with a very small vapour bubble. They vary in size up to 30 microns in the samples studied. Freezing experiments show that the first melting temperature is around -34°C with final ice crystal melting between -3.5°C and -0.3°C corresponding to a salinity of 5.5 to <1 eq.wt% NaCl. The total homogenisation was to the liquid state with T<sub>h</sub> range of 204 - 299°C. Fluid density at the time of trapping was a maximum of 0.92 gm/cm<sup>3</sup>. No CO<sub>2</sub> was observed during freezing experiments and a chemical analysis of the fluid showed that the amount of CO<sub>2</sub> in the inclusion is below the limit detectable by microthermometric techniques and has the following bulk composition:

H <sub>2</sub> O:	97.0%
CO <sub>2</sub> :	1.9%
non-condensibles:	1.1%
H <sub>2</sub> O:CO <sub>2</sub> :	51

SS8/2 is a sample from a quartz lined vug in a porphyritic biotite granite facies, which is interpreted as having formed as a result of silica mobilisation. The inclusions are dominantly type L with a small vapour bubble although monophase liquid-rich inclusions, indicative of trapping temperatures

below 70°C also occur. The inclusions are very large and may exceed 100 microns in size. The fluids at the time of trapping were very dilute <4.5 eq wt% NaCl and temperatures of homogenisation of the vapour-bearing Type L inclusions ranged up to 196°C. Density of the fluids at the time of trapping was between 0.77 and 0.98 gm/cm<sup>3</sup>. No boiling phenomena are observed in fluid inclusions of minerals from the silica metasomatism stage, but it is assumed that pressures remained low. As pressure-corrections for non-boiling fluids at such low pressures are small, the formation temperatures can be considered equal to the homogenisation temperatures.

Several inclusions exhibited metastable behaviour. Initially they appeared monophasic liquid inclusions but after successive heating and freezing runs a vapour bubble nucleated. After homogenisation to the liquid state, these vapour bubbles failed to re-nucleate unless drastically supercooled. However, they re-homogenised at similar temperatures on each successive heating run indicating that they had not leaked during experimentation.

Sample SS18/8 is of a silica-rich vein with mica, fluorite, sphalerite and cassiterite. The characteristics of the fluid are similar to those described for SS117/5 and a chemical analysis of the fluid also showed similar concentrations of H<sub>2</sub>O, CO<sub>2</sub> and non-condensibles;

		repeat
H <sub>2</sub> O:	97.1%	97.4
CO <sub>2</sub> :	1.4%	1.4%
non-condensibles:	1.4%	1.1%
H <sub>2</sub> O:CO <sub>2</sub> :	69	69

The maximum depth of mineralisation during silica metasomatism can be estimated from the data of Haas (1971). For the inclusions with the highest homogenisation temperatures and highest salinity (299°C and <4.5 eq. wt% NaCl) a depth of 1000m is obtained. It is assumed that many of the inclusions which have lower vapour pressures indicate that the veins were in open communication with the surface.

#### Late-stage alteration

The late-stage fluids which caused siderite formation must obviously been CO<sub>2</sub>-rich although no inclusions have been studied in these assemblages. Gold mineralisation is often associated with CO<sub>2</sub>-rich fluids and it is assumed that the gold mineralisation noted by Ixer (pers comm) in Dawa samples is related to this late-stage alteration.

#### Variations in fluid inclusion populations in the hydrothermal alteration assemblages

The samples of zinnwaldite albite granite SS48 and SS48/1 which contain a wide range of inclusion types, have homogenisation temperatures ranging from <200-500°C and which also contained CO<sub>2</sub> are in the first instance hard to explain. However, in the petrographic descriptions of Chapter 9, it was noted that there had been microcline development in this zinnwaldite albite-rich rock suggesting that later processes of alteration may have slightly overprinted the mineralogical assemblage of the sodic process of metasomatism. If more than one

stage of alteration had occurred then the wide spread of homogenisation temperatures could relate to more than one process of subsolidus re-equilibration of the minerals with the hydrothermal fluid.

For the samples of microcline pegmatite, the homogenisations within the range 130-240°C were lower than expected. However, mineralogically there is evidence that the process of microcline formation and the growth of new mica may be closely linked and in sample SS4/3 the microcline-rich pocket has a border of siderophyllite-rich greisen. Such a phenomenon supports the concept of a boiling fluid with microcline developed from the trapped fluid and the greisen rim formed from pneumatolitic alteration.

The fluid inclusion populations of the three sets of samples SS109A, -B and -C suggest that there was more than one period of boiling which has given rise to a wide range of homogenisation temperatures in the fluid inclusion populations.

The combined effects of boiling together with metamorphic overprinting of one process on another reinforced the wide spread of inclusion characteristics observed in many samples and will be discussed in more detail in the next section.

## Interpretation of the data and discussion of fluid behaviour

### Introduction

Fluid inclusion studies indicate that there were two sets of fluids:

- (i) the fluid that came up from approximately 6km depth; and
- (ii) the fluid retained in the magma pulse that followed behind the volcanic eruption.

(i) the fluid that came from >6km depth was trapped as inclusions within quartz phenocrysts of the ignimbritic pile. Inclusion studies indicate that at this depth, silicate melt co-existed with a dense saline brine which later separated into two immiscible phases, one a low density CO<sub>2</sub> phase, the other a dense saline aqueous fluid.

(ii) the fluid retained in the magma chamber at the depth of 6km must have had a rather different composition. The behaviour of this fluid within the granitic liquid at any given point will have been dependent on localised conditions of T-V-P-X and also on the relative proportions of rock-water ratios. The concentration of trace elements into the residual fluid cannot satisfactorily be explained by crystal fractionation for these anorogenic granites and a different explanation is necessary. A mechanism that appears to explain the data is a modified Soret effect, described in Roedder (1984). This process is a combination of convection and Soret diffusion in a thermal gradient and a gravitational field, and does not require the presence of a separate vapour phase (Shaw 1974), although partitioning will occur if a vapour-phase developed. In this process, the progressive enrichment of the upper part of a magma chamber in water, and other changes in melt structure, resulted in a redistribution of the elements on a large scale.

The structure of a silicate melt is a function of P-V-T-X bulk composition. It

consists essentially of an infinite network of linked  $\text{SiO}_4$  tetrahedra in which some of the bridging bonds Si-O-Si are replaced by non-bridging bonds. Addition of free oxygens to the system has the effect of modifying the silicate network. Depending on the number of non-bridging oxygens per silicon atom 1, 2 or 4 (Mysen et al 1980), the melt will be broken down to a series of sheets, chains or monomers. The most significant influence on melt structure and liquidus phase relationships is the presence of  $\text{H}_2\text{O}$ , F and  $\text{CO}_2$ . Disruption of the strong Si-O-Si bonds through reaction with water results in a reduction in silicate polymerisation and a decrease in magma viscosity. However, the high levels of fluorine in these granites must have increased the viscosity to enable the magmas to rise to high levels in the crust. The incorporation of hydroxyl, carbonate and fluoride complexes is likely to have had significant effects upon network ordering and trace element partitioning in the cooling pluton.

As the granite magma rose to higher levels in the crust the fluid would have re-equilibrated with the magma and would have been modified in composition. Such modifications were achieved in several ways. During time, the fluid pressure decreased both because of migration to shallower depths in the crust and because of expansion within fractures. At the same time there would have been a fall in temperature because of exchange of heat with the wallrock or possibly by mixing with cooler groundwaters.

In some cases the confining pressure was reduced sufficiently for the remaining fluid within the granite pluton to have boiled. Certainly the fluids that caused the acid metasomatism and ore deposition at locality SS109 boiled at temperatures around  $300-200^\circ\text{C}$ . The data from this locality has enabled an interpretation of results obtained from the albite-bearing and microcline-rich samples where it was suggested that the combined effects of boiling and metasomatic overprinting resulted in the wide spread of homogenisation temperatures observed for the fluid inclusion populations especially in the albite-rich sample.

Two different possibilities existed therefore:

(i) that the fluids re-equilibrated and were retained within the granite pluton until final solidification and did not boil;

(ii) that the fluids boiled at several stages during the ascent of the granite pluton.

(i) Fluid evolution without boiling:

Where the fluids were retained to low temperatures without boiling, fluid evolution was governed by several functions. Burt (1981) suggests that early increase in acidity and decreases in salinity may be due to (1) temperature decrease which caused oxidation and ionisation (2) abrupt pressure and density changes caused by vertical throttling of fluids through constricted openings and (3) dilution of magmatic water by meteoric water. By far the most important of these factors was the simple cooling process. However, the subsolidus equilibration that takes place in response to this fluid is also governed by the chemistry of the fluid too. Experimental work by Orville (1963), with feldspars and alkali chloride solutions, suggested that fluids become successively enriched in Na as the temperature falls whatever the composition of the crust.

Na-rich fluids can be in equilibrium with K-rich rocks and a late stage Na-rich fluid will cause the formation of K-rich feldspars. At 350°C, fluids are extremely rich in Na. Also he suggested that if temperature is kept constant and anions change then the feldspar composition will change such that if carbonate is flushed through the rock K feldspar will form without a change in temperature of the fluid.

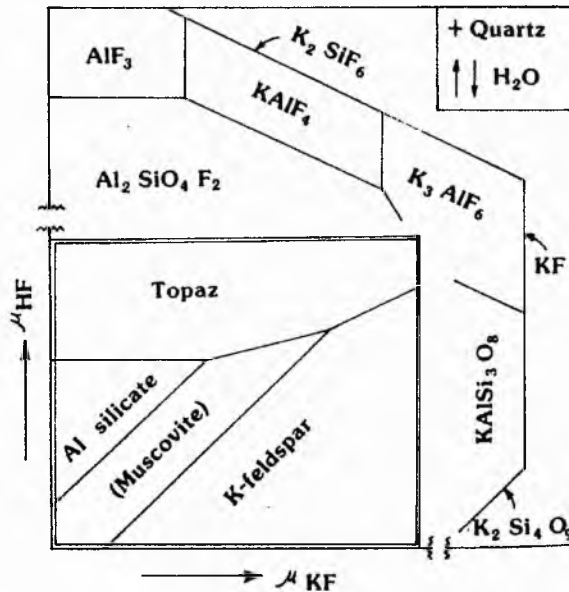
As the fluid cooled according to Burt (1981) the activity potential of HF would have increased and he concluded that acid metasomatism can occur in the absence of boiling, either due to high temperature vapour phase separation or due to cooling and decompression of moderate temperature, moderate salinity aqueous fluids at depth. However, whilst this may result in the dissemination of ore minerals, boiling of the fluid would appear to be a pre-requisite for the formation of ore deposits of any significance.

(ii) Fluid evolution in which boiling occurred:

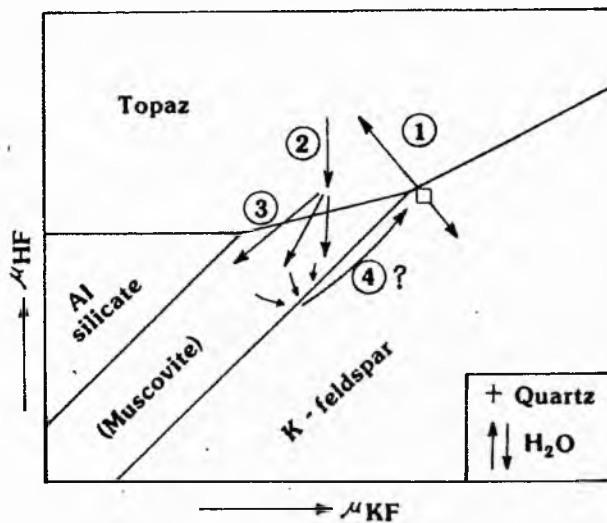
At subvolcanic levels, there is abundant evidence that some granitic magmas became saturated in volatiles. Explosive volcanism and ash extrusion, miarolitic cavities and brecciated intrusions indicate a high potential energy. All the evidence at Rishi points to periods of repeated boiling. Fluid inclusion studies published in the available literature have shown that such boiling has occurred in all porphyry copper and molybdenum deposits and many (but not all) mineralised greisen deposits in the world.

The histogram for SS48 and SS44/2b (Fig 10.15a) - the albite zinnwaldite granites - show a symmetrical array of Th values for dominantly liquid and vapour inclusions in the sodic metasomatised samples. Such an array could be linked to boiling of a fluid at around >350°C which changed both the characteristics of the fluid and led to the saccharoidal textured rock and the formation of columbite, cryolite etc. During boiling CO<sub>2</sub> partitioned to the vapour phase together with HCl, HF etc. Such unmixing of CO<sub>2</sub> could have partly been in response to pressure loss but would also have been encouraged by the high salinity of the fluids. By analogy with the data of Orville described above, this change in the anions in the fluid would have led to the development of K feldspar. In addition, during boiling there is an increase in acidity and decrease in salinity in the vapour phase and an increase in salinity and decrease in acidity in the residual fluid phase. This results in a sharp separation in chemical properties of the fluid and co-existing vapour, which can result in the formation of potassic alteration to K feldspar below as a result of fluid interaction and the development of greisenisation with topaz above. The fluid modified the granite mineralogy to produce microclinised perthites, chloritised mica and new microcline where fluid was retained. Thus in Fig 10.18 from Burt (1981) the fluid would have followed the path 1a and the vapour would have followed the path 1b. On cooling and neutralisation by reaction with wallrock, the vapour phase would have decreased in acidity and moved into the mica field, along trend 2 and any dilution by meteoric water would continue the trend (trend 3) into the mica field. If there were no acidity increase due to boiling, merely a salinity decrease, then the K feldspar would alter directly to mica. This type of alteration is observed in the acid alteration of a biotite perthite granite described on pages 239-258. It is also particularly well seen in SS80, where disseminated acid metasomatism has resulted in the sericitisation of feldspar, and the formation of genthelvite (pages 258 & 259).

Fig 10.18 Vector diagrams from Burt (1981) showing the effects of varying chemical potentials related to increasing acidity and salinity in the presence of quartz and an aqueous phase in the system  $K_2O-Al_2O_3-SiO_2-H_2O-F_2O_{-1}$ .



(a) Schematic  $\mu_{HF}-\mu_{KF}$  diagram for the system  $K_2O-Al_2O_3-SiO_2-H_2O-F_2O_{-1}$  at fixed  $P, T, \mu_{SiO_2}$ , and  $\mu_{H_2O}$ . Phase relations among  $K_2Si_4O_9$ , K-feldspar, topaz, and the fumarolic halides outside the central double-walled box are hypothetical.



(b) Enlargement of the boxed area from Figure a. The numbered arrows indicate the possible evolution of greisenizing fluids in a porphyry deposit due to (1) boiling, (2) neutralization and cooling, (3) dilution, and (4) recycling (if it occurs). Several of these processes may occur simultaneously. Muscovite is probably unstable at initial magmatic temperatures (as indicated by the parentheses).

As suggested by Burt (1981), HF fugacity must have been high during acid metasomatism. There are a number of mineralogical assemblages which apparently indicate this:-

(i) Phenakite has been recorded in several localities in the Rishi biotite granite which is an indicator of relatively high HF fugacity causing the breakdown of beryl to topaz plus phenakite and quartz (Burt 1975).

(ii) The rare assemblage genthelvite-topaz (found in SS80) is stable only at low  $H_2S$  and very high HF fugacities and with increasing  $H_2S$  fugacity becomes a sphalerite-topaz assemblage (Burt 1977)

(iii) The development of topaz from feldspar, according to the acidity-salinity diagrams of Burt (1981), involves an increase in HF activity, in other words involves an increase in pH.

The conclusions therefore must be that the biotite granites ARE the result of hydrothermal processes but the principal difference is that for the unmineralised plutons elsewhere in Nigeria the self-generated fluids did not boil and therefore no greisenisation occurred. The granitic plutons must have risen to different levels in the crust in different complexes. At Rishi in the Saiya Shokobo complex where the granite reached extremely high levels in the crust and intruded its own volcanic pile the fluids boiled. In other complexes where the confining pressure remained greater because the plutons rose to less shallow depths then boiling did not occur.

In simplistic terms it is suggested that sodic metasomatism preceeded boiling. As the fluids boiled and cooled and lost  $CO_2$ , the condensate was responsible for potash metasomatism and the vapour phase caused acid metasomatism (greisenisation) with later, cooler fluids responsible for silica metasomatism and late stage alteration.

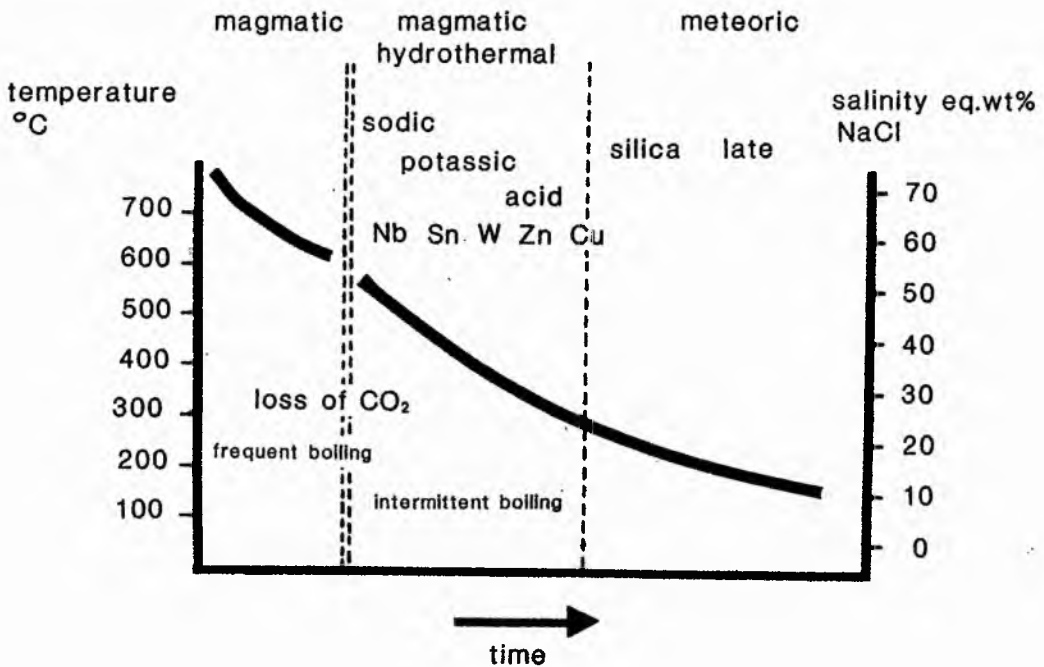
## Conclusions

Field studies, petrographic observations and fluid inclusion studies indicate that the hydrothermal evolution of the fluid results from a discontinuous sequence of specific events, each related to stages of fluid-rock interaction, percolation through micro-fractures, active fluid circulation and healing of fissures. However, although the evolution is discontinuous due to boiling and gas effervescence, the thermodynamic properties of the fluid can be essentially described by a continuous evolution. A summary schematic diagram of fluid inclusion data for the Rishi hydrothermal system is shown in Fig 10.19. This indicates the high temperature and high initial salinity of the fluids.

The evidence cited above indicates that the earliest fluids which were trapped within the volcanic pile were very saline in excess of 50 eq wt% NaCl and possibly as high as 70 eq wt% NaCl. The early fluids were trapped at temperatures probably in excess of 750°C at a depth of at least 6km and contained >10 wt %  $CO_2$ . The quartz phenocrysts originated from a depth of around 6km and were therefore interpreted as having formed in a magma chamber at this depth. This is the first time a depth constraint has been determined for the

anorogenic granites.

Fig 10.19 Summary diagram of fluid inclusion data for the Rishi hydrothermal system illustrating the very high initial temperature and salinity of the fluids



The residual fluids within the Rishi granite intrusion ranged from hydrosaline, with a density as high as  $1.2 \text{ g/cm}^3$  to low density steam at a density of  $\ll 1 \text{ g/cm}^3$ . The quartz in most biotite granites must have recrystallised to low temperatures and most inclusions in the granites are of low salinity fluids with a density close to  $1 \text{ g/cm}^3$ .

Sodic, potash or acid metasomatism may largely overlap in terms of temperature and salinity of the fluids. Thus if the potash process is first, with no earlier sodic event, then it takes place at high temperatures which is evidenced by cross-hatched twinning of microcline in SS20/2. If acid metasomatism is essentially the first process to operate then it too may begin at high temperatures. This process begins if the fluid is already very HF-rich.

The acid (greisenisation) process largely overlaps the temperature range for the potash process. The difference must have been in the decrease of the K/H ratio as HF activity increased. The transition from microcline to greisen in samples such as SS20/2 and 20/3 results from fluid boiling such that the vapour

was very acid enriched and caused an acid assemblage to generate whereas the fluid left behind was enriched in K which resulted in microcline formation. On rare occasions this fluid permeated the acid assemblage and veins of microcline cross-cut mica-rich assemblages as in SS23 (Plate 9.34). In quartz of these mica-rich assemblages, the inclusions are always gas-rich. Repeated boiling occurred during acid metasomatism particularly in the early stages, causing local trapping of inhomogeneous fluids such that vapour-rich, fluid-rich and saline droplets were trapped simultaneously.

During late-stage acid metasomatism there was a build up in silica content. This was not true silica metasomatism because no silica was added to the system. Instead it is envisaged that increased HF activity dissolved mica to produce honeycomb textured quartz-rich rocks. As fluid temperatures fell below 300°C there was an increase in pH, the silica-saturated fluids deposited silica in the honeycombs and vugs created during earlier processes. In effect the same acid fluid which had destroyed the mica then re-deposited the silica in suitable conditions of pH and temperature.

Subsequently, lower temperature (<300°C) dilute (<14 wt % NaCl) and very low temperature (<70°C) dilute (<10 wt. % NaCl) fluids entered the vein systems but not the granite as a whole.

The existence of a late-stage zeolite facies indicates low temperature fluids with low sulphur fugacities. This is consistent with secondary haematite formation developed at the expense of wolframite and other ores. Zeolites also indicate relatively high pH or high alkali ion/H<sup>+</sup> values (Meyer and Hemley 1967).

Pressures during much of the hydrothermal alteration remained less than 100 bars corresponding to depths less than 1200m below the ground water table at the time. Fluids forming vein minerals were of relatively low salinity, NaCl dominated brines that were well below their critical temperature.

This observation of wide fluid variation has also been noted by Roedder (p400 1984) who comments that such fluids may have very different isotopic values and K/Na ratios than those present in the parent magma. If these fluids are given off by the intrusive body at a pressure greater than the local hydrostatic pressure, they will mix with, and flush out, any pre-existing fluid. As such fluids leave their source, the pressure drop may result in a new stage of immiscibility (boiling and effervescence of gases or condensation of a liquid phase from lower density fluids) but as such low density fluids contact cooler country rocks, they may eventually recondense. As a result of such processes, inclusions of early magmatic fluid may have an extremely wide range in salinity and density, without any mixing with meteoric waters. Konnerup-Madsen (1979a) found salinities ranging from 2 to 60 wt% NaCl in inclusions from deep-seated granitic intrusions which he suggested were trapped during final solidification at 5-6kbar and 700-800°C. Highly saline fluids have been ascribed to boiling by many workers. However, boiling will not increase the salinity by more than a few wt. percent NaCl and heat to sustain such continued boiling within a small pocket of fluid can be hard to explain.

The thermometric data presented here is in general agreement with that of Part 1 of this thesis for the generalised range of processes. However at Rishi the temperatures are slightly lower (or the pressure slightly higher) than those

determined from other complexes.

A great deal has been learnt about the fluid reactions and nature of the fluid from experimental data but much more requires to be done to obtain a clearer picture of the fluid evolution. In particular more analytical data is required in order to quantify changing Na/K+ concentrations in the fluid and the increasing acidity of the fluid in particular. Perhaps the most exciting discovery of this work was the recognition of two different fluids and the most important aspect concerns the constraints that the inclusion data imposes of the depth of origin of the plutons. The interpretation of some of the data could be consistent with the influx of meteoric water into a more saline hydrothermal fluid. The question on the origin of the fluids and the possible role of meteoric water in hydrothermal ore deposition of the anorogenic province forms the basis of Chapter 12.

#### SUMMARY OF PART 11 AND COMPARISONS WITHIN NIGERIA

The Saiya Shokobo complex forms a distinctive hill mass which covers an area of approximately 250km<sup>2</sup>. The main structural feature of the complex is the elliptical fracture 17km in diameter which has largely determined the outline of the central massif of the Saiya Shokobo Hills and has controlled the emplacement of several of the intrusions of the complex. The complex is dominated by volcanic rocks which are confined within this elliptical fracture. During the latest stage of magmatic activity, the emplacement of a granite pluton moved beyond the confines of the main fracture and was intruded eccentrically to the north east of the main part of the complex. Thus the biotite granite intruded both its own volcanic pile and the basement hornblende biotite monzogranite.

The volcanic rocks are composed of crystal-rich ignimbrites with fractured and embayed quartz phenocrysts. The main feeder dyke, which occupies an early ring fracture, is also porphyritic. However, the phenocrysts are typically in synneusis-type aggregates and are modally less abundant. High in the volcanic pile arfvedsonite with minor amounts of aegirine developed in the groundmass of the ignimbrite. In samples collected close to the granite roof, the matrix consists of quartz and alkali feldspar with the development of sieve-textured brown biotite and with no amphibole.

The Rishi biotite granite was the final intrusive phase, emplaced to a high level within the Saiya Shokobo complex. The main granite mass covers an area of 13km<sup>2</sup> with small windows of granite exposed in the volcanics to the south. The main granite is commonly coarse- to medium-grained and cream or pink in colour when fresh. However there is a wide range of subtle coloration and grain size ranging from coarse- to fine-grained, and from equigranular to porphyritic and granophyric. The essential minerals are perthitic feldspar surrounded by clusters of glassy quartz crystals and ragged discrete flakes of biotite irregularly distributed throughout the granite. Accessory minerals include zircon, fluorite, and rutile which are widely distributed with columbite, cassiterite, sphalerite and other minerals locally.

Such textural and mineralogical variations are interpreted to be the result of

rock-fluid subsolidus re-equilibration. In addition to the mineralogical and textural variations in the Rishi biotite granite, a sequence of alteration assemblages has been recognised which are indicative of continued fluid mobility at successively lower temperatures: small patches of saccharoidal white feldspar and lenticular zinnwaldite; local development of microcline; chloritisation of feldspar or biotite, greisen formation, silicification and late-stage alteration processes.

These hydrothermal modifications have been concentrated in the roof and marginal zones of the pluton and along ring dykes where hydrothermal fluids utilised vertical pathways of escape.

The processes of hydrothermal alteration are complex. They depend not only on the temperature and composition of the fluid, but also on the initial rock type that was being affected, the extent of earlier rock-fluid reaction and on how long the fluids were retained. The different mineral assemblages indicate that alteration took place within an  $\text{Na}_2\text{O}-\text{K}_2\text{O}-\text{SiO}_2-\text{H}_2\text{O}-\text{F}$  system which produced albitisation, then microclinisation of the feldspars during sodic and potassic alteration, and ultimately a destruction of the feldspars during acid metasomatism. This was followed by lower temperature silicification and late-stage alteration processes.

In addition to the alteration of the Rishi pluton itself, the host rocks which surround and overlie the pluton have also been affected. Thus the Pan-African basement monzogranite country rock which surrounds the Rishi biotite granite and the volcanic pile which overlies it have also been hydrothermally altered by volatiles escaping from the biotite granite cupola. For the first time, a sequence of alteration processes can also be recognised for the basement and to a more limited extent for the volcanic pile although the effects are not always as clearly defined in the basement or volcanic pile as they are for the biotite granite. Geochemically the basement monzogranites, the volcanic rocks and the Rishi biotite granite are distinctive in terms of their trace element assemblage such that each can be distinguished even when there has been intense hydrothermal alteration. Thus the basement monzogranite has higher Ba, V, Sr, Zr and Ce, slightly higher La with lower Nb, Y, Zn and Rb than the Rishi biotite granite. The volcanics can be distinguished by their enhancement of Ce, La, Zn and Zr contents compared with <sup>other</sup> rocks types.

Each of the hydrothermal alteration processes has a distinctive geochemical signature although the original rock type exerted a control on the final element abundances. However, the major element variations that occurred have been plotted on multicationic diagrams to define trends or fields of alteration and these have shown that it is the process that is more important in defining the trend, rather than the initial rock type. Thus the controlling factor is the physico-chemical nature of the hydrothermal fluid itself.

Each of the hydrothermal alteration process was characterised by a different assemblage of ore minerals. Columbite was introduced during sodic metasomatism, cassiterite and wolframite were associated with potassic metasomatism whilst cassiterite, wolframite, sphalerite and chalcopyrite were the main ores of the greisenisation process. The development of a sequence of ore deposition indicates that this was related to changing physico-chemical conditions in the fluid mainly due to falling temperature.

The PVTX nature of the fluids which were responsible for hydrothermal alteration have been monitored by a study of fluid inclusion characteristics in selected samples. The earliest fluids that were trapped in the quartz phenocrysts of the volcanic pile indicate that the fluids that separated from the silicate melt at a depth of around 6km, were highly saline, probably at temperatures in excess of 750°C. Frequent boiling and loss of CO<sub>2</sub> occurred in these early stages. Loss of CO<sub>2</sub> appears to have been important for the deposition of columbite during sodic metasomatism. As the fluids cooled and lost CO<sub>2</sub>, the condensate was responsible for potash metasomatism and the vapour phase caused acid metasomatism with later, cooler fluids responsible for silica and late-stage alteration.

The importance of boiling in the formation of the ore deposits within the roof of the Rishi pluton must be emphasised.

The sequence of subsolidus hydrothermal processes that were described in Chapter 9 indicate that all the hydrothermal modifications that have been recognised in other anorogenic complexes in the Nigerian Province (discussed in Part 1) have also occurred at Rishi. There are however, subtle differences, not least the fact that the lower part of the ignimbritic pile at Rishi has undergone a potassic metasomatism whereas in other complexes the alteration of the volcanic pile is attributed solely to a sodic effect.

In Chapter 3 of this thesis, it was emphasised that although a series of alteration processes could be recognised within the anorogenic province as a whole, there was considerable variation from complex to complex in the subsolidus assemblages and sequential changes related to the different processes of alteration. In most complexes only one or two stages were developed to any degree.

A comparison of the Q-F plots of six complexes (Fig 10.20 and 10.21) shows at a glance that no two of the complexes display an identical pattern of alteration. The Q-F plot for Rishi (Fig 10.21c) differs from all the other complexes because of the dominant potassic metasomatic process that preceded the acid metasomatism. The major point about potash metasomatism at Rishi is that it can be a disseminated process. In other complexes, most notably Afu, Ririwai, Dutsen Wai and Jos Bukuru, the disseminated process of alteration is sodic metasomatism with concomitant deposition of columbite etc. Whilst in the Ririwai complex a disseminated process of both acid and silica metasomatism has been recognised (Kinnaird 1985).

Much has been written about the hydrothermal mineral assemblages in this chapter. However, even for the main mass of the Rishi biotite granite, the inescapable conclusion is that it too has been extensively modified by hydrothermal alteration. This is based on a number of observations that have been recorded in Part 11 of this thesis:

- (i) the diversity of textural variations from coarse-, medium- and fine-grained to porphyritic and granophyric within the small granite stock
- (ii) the irregular distribution of mineral phases, particularly mica
- (iii) the wide range in perthitic textures
- (iv) the deviation in Zr:Hf and Ce/Y ratios from average granite values

Fig 10.20 Summary Q-F cationic plots for hydrothermally altered samples from the Afu, Banke, Tibchi and Ririwai complexes. Symbols as in earlier Figures

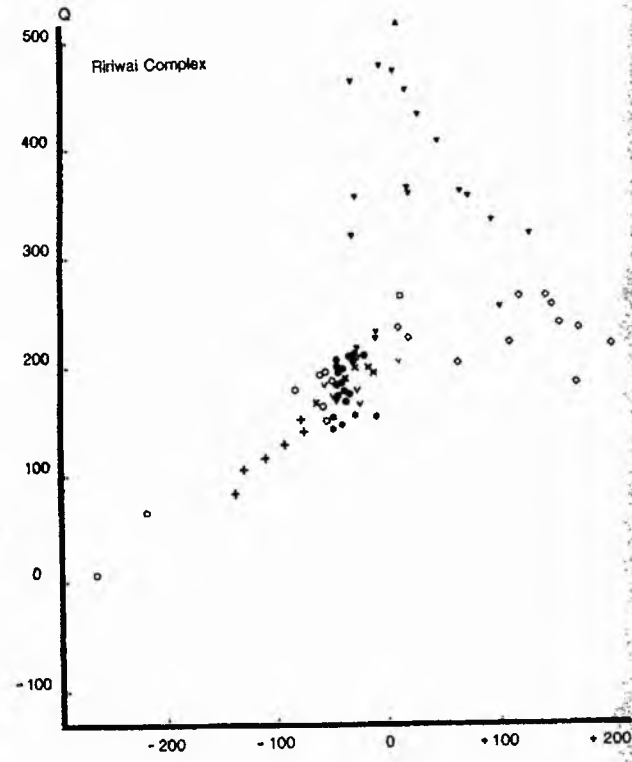
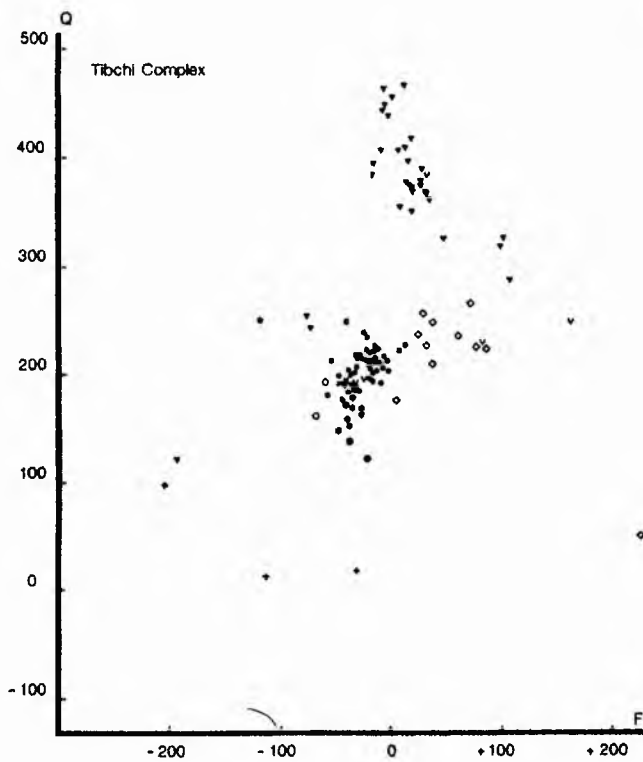
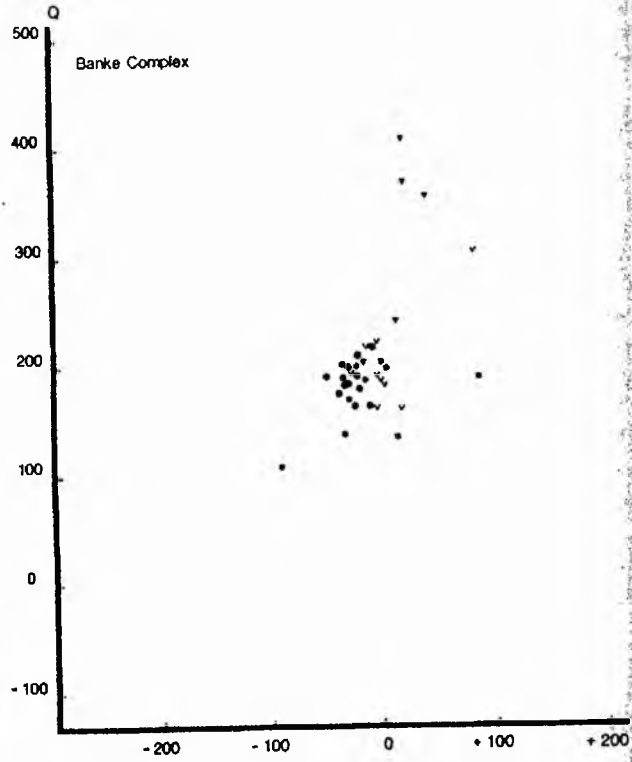
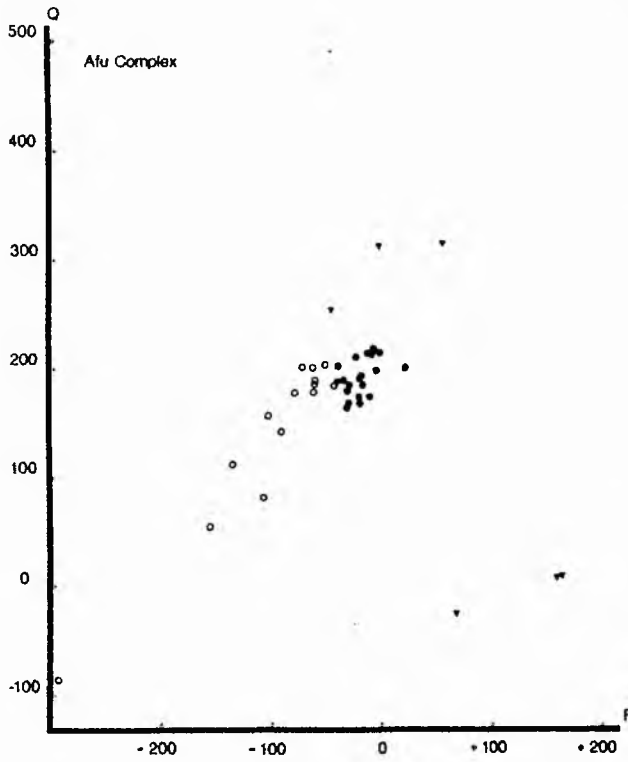
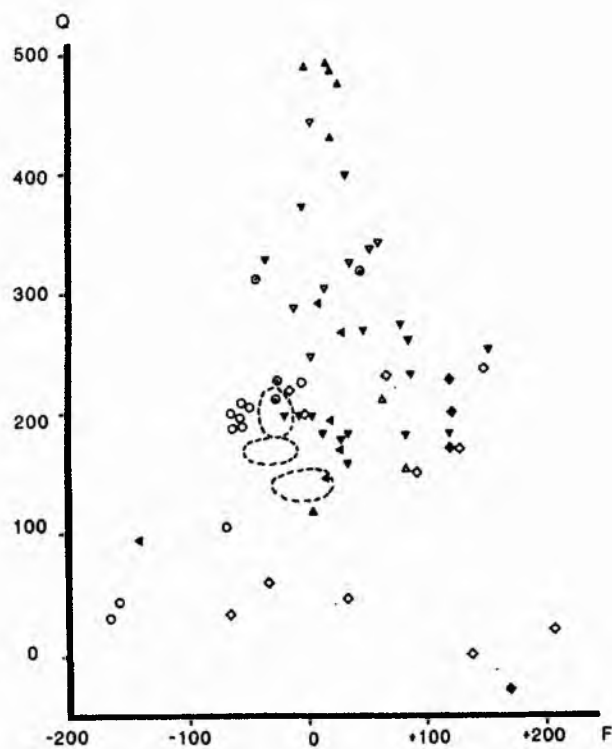
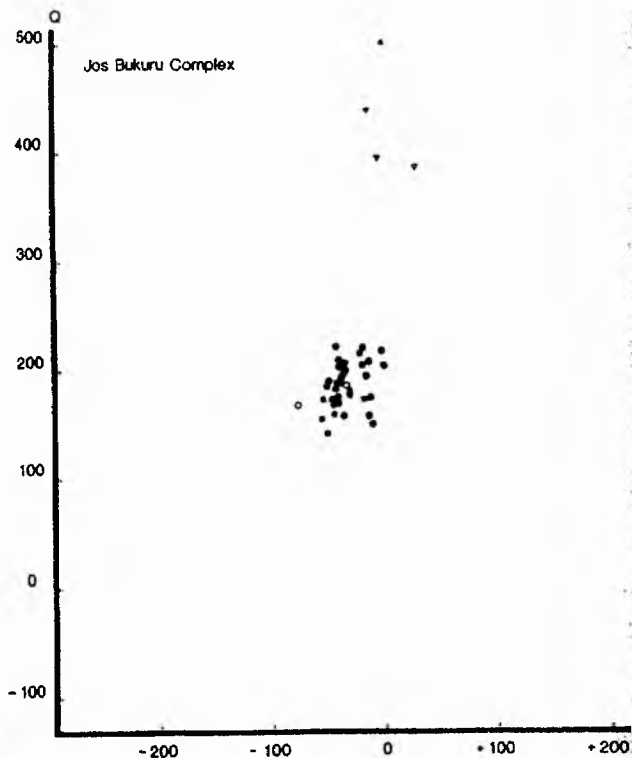
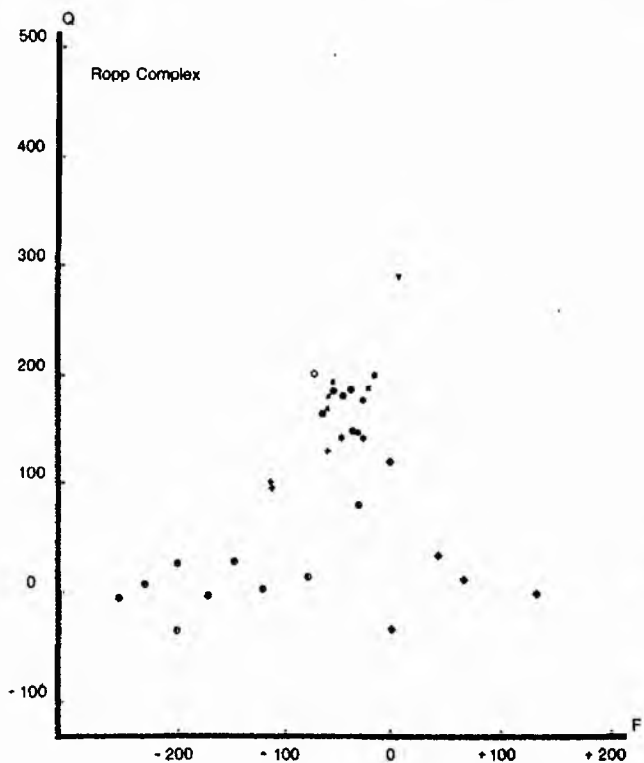


Fig 10.21 Summary Q-F cationic plots for hydrothermally altered samples from the Ropp, Jos Bukuru and Rishi complexes. Symbols as in earlier Figures



(v) the enrichment of certain trace elements, notably F, Li, Nb, Sn, and Zn when compared with other low Ca granites - such values are not compatible with simple fractionation models.

(vi) the extremely broad range of mica compositions in the granite showing as wide a diversity of compositional variations as any of the micas within hydrothermally altered rocks.

(vii) the lack of melt inclusions and the low homogenisation temperatures within the range 150-230°C also substantiates subsolidus re-equilibration to low temperatures.

Thus whatever may have been the initial character of the Rishi pluton, much of the evidence has been lost through postmagmatic processes.

## PART 3

### MINERALISATION - SOURCE OF FLUIDS AND ORE METALS

#### SYNOPSIS

In the earlier part of this thesis a series of hydrothermal alteration and mineralisation processes have been examined together with evidence in support of fluid modification of volcanic and granitic rocks. The nature and origin of the hydrothermal fluids has also been discussed. In this part of the thesis, the high heat production capacity of the anorogenic granites is presented (Chapter 11) and the ability of the ring complexes to create meteoric hydrothermal cells is considered. Such an investigation seeks to discover whether the lower temperature processes of hydrothermal alteration which occurred below approximately 300°C were influenced by meteoric water. It seems possible that the sequential process which began by reactions with magmatic water may have been succeeded by reactions with meteoric water in the later stages of alteration.

Detailed stable isotopic data, presented in Chapter 12, have been used to examine the source of the fluids and the ore metals and to consider the involvement of meteoric water. The final conclusion based on this data on the origin and evolution of hydrothermal fluids and sequence of mineralisation stages within the anorogenic province has important petrogenetic and economic implications.

## CHAPTER 11

### HEAT FLOW, HIGH HEAT PRODUCTION GRANITES AND RADIOELEMENT VARIATIONS

#### HEAT FLOW

##### Introduction

Heat flow is a transfer of thermal energy largely by conduction and convection. Heat flow is measured in  $\text{mWm}^{-2}$ . Within a continental region of up to 1500ma heat flow is derived from three components:-

- Almost 60% of the heat flow is a constant **deep** background heat which comes from the lower crust and underlying mantle
- Almost 40% comes from the slowly decaying **radiogenic component** of the upper crust.
- A small component is the more rapidly decaying **heat** of formation. This is heat supplied during the last episode of regional magmatism and/or metamorphism. For continental provinces older than 500ma this component is negligible and the effects of magmatism and/or metamorphism have completely dissipated after 1500ma.

Except for a few distinctive zones, continental heat flow is fairly constant at about  $55\text{mWm}^{-2}$ . Heat flow over continental shield areas however, is generally lower than over other continental provinces (Table 11.1), although the Indian shield and the central Australian shield have higher values due to the enriched heat production.

34+8	Canadian shield
36+8	Baltic shield
37+8	Ukrainian shield
39+8	west Australian shield
42+5	Brazilian shield
71+11	Indian shield
83+21	central Australian shield

Table 11.1 Heat flow values (in  $\text{mWm}^{-2}$ ) for Precambrian Shield areas (Brigaud et al 1985)

Since heat is flowing from the interior of the earth, the temperature increases with depth. This rate of temperature rise, or geothermal gradient, has been calculated from measurements in mines and drill holes. The average on continents is about  $35^{\circ}\text{C Km}^{-1}$ . However, this only applies to the top 10km at most. At greater depths the gradient must decrease to only a few degrees per kilometer in the lower crust and to less than one degree per kilometer at depths of a few hundred kilometers into the upper mantle.

## Heat flow within the West African shield

Results on 16 sites within the West African Shield (in Brigaud et al 1985), confirm the existence of a low heat flow over the West African craton ranging between 30 and 40  $\text{mWm}^{-2}$  and averaging 37  $\text{mWm}^{-2}$ . This value probably varies from place to place with local variations in surface heat production but is very close to those obtained in other Precambrian shields. This more recent work confirms the generalised heat-flow contouring of Africa (Gass et al 1978) which showed that heat flow variations in Nigeria are in the range 40-50  $\text{mWm}^{-2}$ . The site localities of Brigaud et al (1985) are shown on a Fig 11.1 which is a compilation of localities made by Ballard and Pollack (1985).

In addition to the Precambrian shield, Brigaud et al (1985) also measured heat flow in the anorogenic complex of Tadhak, 200km west of Tessalit in Mali (Fig 11.1). It is 260ma old and is composed of nepheline syenites, ijolites and carbonatites. Surface heat flow is 68  $\pm 10$   $\text{mWm}^{-2}$  at In Imanal. Because no heat production measurements were made at this site, it was not possible to determine whether this high value is due to radioactivity or to a reactivation of the basement.

At In Imanal the temperature gradient within the anorogenic ring complex was determined at 23  $^{\circ}\text{C Km}^{-1}$ , whereas the thermal gradient in the shield areas ranged between 10-12  $^{\circ}\text{C Km}^{-1}$ .

The apparent high heat flow within an anorogenic complex has important implications for mineralisation since in zones of high heat flow, hydrothermal fluid cells, once initiated, may be perpetuated. Although no detailed work on heat flow is available in Nigeria, it is interesting to consider the known empirical relationship between high surface heat flow and high heat production as a function of radioactivity in the crust:-

$$q^0 = q^* + A_0 D$$

where  $q^0$  = surface heat flow,  $q^*$  = probable heat flow from deep sources ie. background heat,  $A_0$  = the surface heat production and D is a function of the thickness of the radioactive layer (Brown, Plant and Lee 1979).

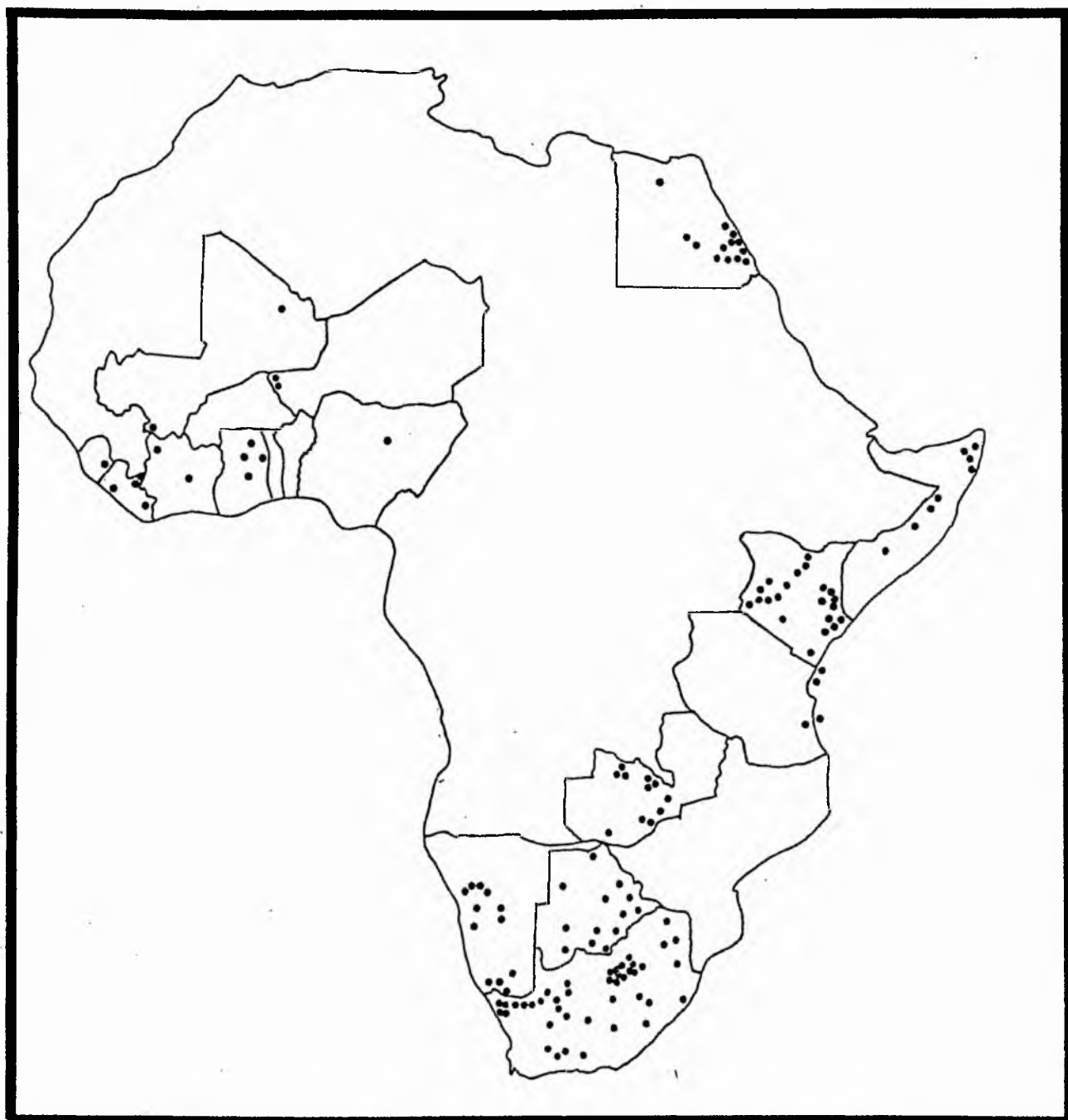
This means that if heat production can be calculated, an idea of the heat flow can be gained. Since no detailed heat flow data is available for the Nigerian granites, but radiogenic heat production can be calculated, this method can be applied.

## HEAT PRODUCTION

### Introduction

Since radioactive decay converts mass to energy all naturally radioactive isotopes generate heat to some extent. However, only significant contributions arise from the decay series of  $^{238}\text{U}$ ,  $^{235}\text{U}$ ,  $^{232}\text{Th}$  and  $^{40}\text{K}$ . During magmatic differentiation these elements are enriched in progressively more acidic phases. Thus these isotopes are concentrated high in the crust and decrease exponentially with depth since they do not easily substitute in the structure of

Fig 11.1 HEAT FLOW SITES IN AFRICA



compiled by Ballard and Pollack (1985)

the minerals stable in the lower crust or mantle. Shaw (1980), estimates that 23% of the K and 15% each of the U and Th, in the total crust plus mantle, are now in the continental crust, which is only 0.5% of the total mass of crust plus mantle. Consequently, radiogenic heat produced by these elements in the upper few kilometers of crust accounts for about 40% of the average heat flow on continents (Pollack and Chapman 1977). A small proportion of granitic (and syenitic) rocks contain above normal radioelement concentrations. Under a favourable combination of structural and hydrologic conditions the heat generating capacity of these 'hot' granites is significant with respect to low temperature mineralising processes. The association between mineralisation and anomalously radioactive granites is more than a matter of geochemical affinities. Depending upon its radioelement content, an anomalous granite has a heat generating capacity which may be many times greater than average granite. Although the amount of heat produced is small, it is produced over a long period of time with a half-life controlled by the decay of the parent nuclides. This fact can maintain the temperature of an anomalous granite above its surroundings for hundreds of millions of years, up to 100 times or more the cooling period of an 'average' intrusion (Darnley 1982).

Radioactive heat production is a thermal property of rocks independent of in situ temperature and pressure. The radiogenic heat produced can be calculated as Heat Production Units (HPU) and expressed in terms of thermal conductivity according to the data of Rybach (1976):-

$$A \text{ (HPU)} = 0.371\rho \times 0.41868 (0.718c_U + 0.193c_{Th} + 0.261c_K)$$

where  $\rho$  is the density of the rock; 0.41868 is the conversion factor from cal/cm<sup>3</sup> sec to cal/gramme year;  $c_U$  and  $c_{Th}$  are in weight ppm and  $c_K$  in weight per cent.

#### Heat production in the Nigerian Anorogenic Ring Complexes

Clearly, the Nigerian granites with their high potash values and enriched U and Th levels will have high heat production averages compared with many granites. Further, since it has been demonstrated that in rocks with nearly similar bulk chemistry, heat production is higher in the "wet" facies (containing mica or amphibole) than in the "dry" facies containing mainly pyroxene (Smithson and Heier 1971, Smithson and Decker 1973), it is not surprising that the alkaline biotite and arfvedsonite granites have higher heat production values than the ferroaugite-ferrohedenbergite granite porphyries, quartz porphyries and fayalite granites.

Geochemical, thermodynamic and empirical data (Rybach 1976) indicate that heat production decreases with depth and that within a granite body heat production decreases towards the centre. If this is the case then hydrothermal alteration and mineralisation would be anticipated to be at a maximum in the margins and roof zone of an intrusion which is exactly what happens in the younger granite province.

In Cornwall, Tammemagi and Wheildon (1977) have noted high heat flow associated with the granite batholith and normal values adjacent to it, whilst for southern Britain, Richardson and Oxburgh (1978) have shown that heat flow and heat productivity are linearly correlated. In areas such as Nigeria where

heat flow data are limited therefore, it is important to identify zones in which  $q^*$  is likely to be augmented by crustal heat sources. For Nigeria  $A_0$  can be calculated for a number of different rock types (Table 11.2).

The summary of results shows that parental syenite and volcanic feeder intrusions have a low heat production of <2HPU (Table 11.2). For the peralkaline syenites, granite porphyry and volcanic rocks, where there has been limited rock fluid interaction, heat production values rise to 5HPU.

Biotite granites and arfvedsonite granites show a range of 2.12 - 3.45 HPU comparable with similar granites worldwide. However, where there has been significant hydrothermal alteration, heat flow values rise considerably (Table 11.3). Granites which have suffered sodic metasomatism show the most marked increases. In the biotite alkali feldspar granites and arfvedsonite granites (samples N80,82,83) slight sodic metasomatism increased the HPU value to a maximum of 12.8 HPU for surface samples. Where the process has been intense the values increase still further. In the albitite of the L13 core from the Ririwai biotite granite there is a maximum of 25HPU at 411m. This zone has been interpreted as the roof of another biotite granite at depth. The highest heat producing values so far recorded are found for the arfvedsonite albite granite of the Kaffo valley in the Ririwai complex, where the range is from 28-59 HPU. Since geochemically high U values are only recorded in granites retaining their record of sodic metasomatism, it follows that granites where subsequent process have been overprinted upon the albitisation, heat production values will be decreased. Thus high heat production is not a characteristic feature of the Rishi biotite granite as the sodic metasomatism process was largely overprinted by later processes.

During potash metasomatism the HPU values decreased markedly whilst during  $H^+$  metasomatism they rose slightly, only to fall again presumably during the silicification process.

Comparison of borehole core samples through the Ririwai biotite granite (Table 11.3) and similar surface samples indicate that there are surface reductions of heat production. This is largely due to uranium leaching during hydrothermal alteration, since borehole Th values are similar to and do not exceed surface values, whereas borehole uranium values vary from 4 to 26 times recorded surface values. The lower uranium but similar thorium contents of the biotite granites from the surface compared to drill-hole L13, show that uranium has been remobilised from the surface granites and presumably lost by weathering.

Combined neutron activation and particle track analysis (MacKenzie et al 1984) confirm the relative fixation of Th and the relative mobility of uranium during periods of rock-fluid interaction (Kinnaird et al 1985b). The biotite granite is rich in uranium, with a thorium/uranium ratio 0.8 to 1.0 (Iyer et al 1987). Later hydrothermal fluids have altered earlier minerals and redistributed the elements from biotite and precipitated minor amounts of cassiterite, sulphides and coffinite.

During sodic metasomatism MacKenzie et al (1984) found that there is an enrichment in both U and Th and the Th/U ratio was significantly decreased from the average for the unaltered granite. In contrast Iyer et al (1987) found that both the bulk analyses and the Th/U ratio for the albitites are similar to those of the biotite granite of core L13. Both observations however may be valid,

Table 11.2 . Radioelement concentrations and heat productivities for volcanic rocks, ring dyke granite porphyries and syenites in the Nigerian Younger Granite Province.

Unit	Complex	Sample no	Rock type	U	Th	K <sub>2</sub> O	Th/U	HPU in $\mu\text{Wm}^{-3}$	
Volcanics	Ririwai	N85-69	volcanic feeder	0.18	17	5.42	21.3	1.74	
	Jos	L364	volcanic feeder	2.6	14	6.14	5.38	2.04	
	Buji	N2-69	crystal rich ignimbrite	2.8	17	5.61	6.07	2.25	
	Saiya Shokobo	Mb696	crystal poor comeditic ignimbrite	3.4	21	4.50	6.18	2.59	
	Buji	L939	ignimbrite	4.5	17	4.35	3.78	2.58	
	Kila	DT834	aegirine rhyolite	9.0	34	4.29	3.78	2.60	
	Buji	N1-69	crystal poor ignimbrite	4.0	20	4.72	5.00	2.68	
	Banke	B138	alkaline rhyolite lava	4.7	22	5.19	4.68	3.03	
	Buji	L814	crystal rich ignimbrite	5.9	20	4.53	3.38	3.14	
	Warji	DT837	crystal rich ignimbrite	6.4	24	3.61	3.75	3.46	
	Ririwai	N82-69	aegirine crystal tuff	7.3	37	4.51	5.07	4.63	
	Ririwai	N81-69	comeditic ignimbrite	8.9	40	4.09	4.49	5.19	
	Ring dykes	Zigau	ZG1	granite porphyry	3.7	12	5.13	3.24	2.10
		Ririwai	N96	granite porphyry	4.0	21	5.17	5.25	2.78
Ririwai		N116	fayalite granite porphyry	3.6	39	4.77	10.83	3.89	
Syenites	Kila Warji	KW6	plagioclase syenite	1.8	6.8	3.97	3.77	1.20	
	Dutse	DT25	alkali feldspar syenite	2.2	7.8	5.08	3.55	1.46	
	Shira	SH105	peralkaline quartz syenite	7.4	20	4.77	2.70	3.54	
	Shira	SH51	peralkaline syenite	8.1	30	5.31	3.70	4.43	

Tables 2 and 3 calculated according to Rybach (1976) using the following densities from Ajakaiye (1976b):-

volcanics 2.62, quartz and granite porphyries 2.61, fayalite granite porphyry 2.63, syenites 2.70, peralkaline granites 2.61, biotite granites (and hydrothermal variants) 2.60.

Source of data: Stavrakis (1975), Abaa (1976), Bowden *et al.*, (1981) Whitley (unpub. data), and Oosterom (pers. comm).

Table 11.3 Radioelement concentrations and heat productivities for peralkaline and biotite granites and hydrothermally altered variants in the Nigerian Younger Granite Province.

Unit	Complex	Sample No	Rock type	U	Th	K <sub>2</sub> O	Th/U	HPU in $\mu\text{Wm}^{-3}$
Peralkaline granites	Shira	SH5	arfvedsonite aegirine granite	3.9	12	4.79	3.10	2.12
	Dutse	D23	arfvedsonite aegirine granite	4.6	14	4.70	3.04	2.35
	Shira	SH90	aegirine microgranite dyke	7.0	5.5	4.01	0.79	2.44
	Ririwai	N83	arfvedsonite aegirine granite	14	51	4.97	3.64	7.23
	Ririwai	N80	" " "	10	120	5.18	12.00	10.85
	Ririwai	N82	arfvedsonite granite	17	124	4.56	7.29	12.80
Biotite granites	Amo	N25	biotite syenogranite	5.2	2.1	4.92	4.04	3.03
	Jos	N151	" "	5.4	22	5.56	4.07	3.20
	Jos	JB1149	" "	2	35	4.60*	17.50	3.25
	Amo	N28	" "	3.9	32	4.78	8.36	3.45
	Dutsen Wai	DW7	biotite alkali feldspar granite	7.5	23.7	4.33	3.16	3.75
	Ririwai	N77	" " " "	7.5	41	4.31	5.47	4.89
	Dutsen Wai	DW16	" " " "	10.0	33.1	4.74	3.31	5.01
	Ririwai	N91	" " " "	7.3	50	4.50	6.85	5.45
	Jos	JB1140	" " " "	11	35	4.52*	3.18	5.52
	Jos	JB1153	" " " "	11	35	5.13*	3.18	5.56
	Ririwai	N79	" " " "	10	47	4.50	4.70	5.92
	Ririwai	N92	" " " "	7.97	62.0	4.33	7.78	6.41
	Banke	B47	" " " "	12.4	48.5	4.89	3.91	6.64
	Shira	SH91	" " " "	13	47	4.64	3.62	6.67
	Jos	JB1152	" " " "	14	50	4.53	3.57	7.30
	Jos	JB1159	" " " "	17	45	4.43*	2.65	7.71
	Banke	B37	" " " "	20.6	36.1	4.86	1.75	7.83
	Ririwai	N75	" " " "	10	83	4.31	8.30	8.30
	Jos	JB1141	" " " "	21	55	4.39*	2.62	9.40
	Drill core L-13	Ririwai	L13-10 m depth	" " " "	30	25	4.62	0.83
		L13-115	" " " "	80	72	4.07	0.90	24.83
		L13-205	" " " "	53	51	5.01	0.96	16.85
		L13-310	" " " "	58	56	4.77	0.97	18.40
		L13-411	albitite	81	73	2.46	0.90	25.02
		L13-440	"	66	69	2.39	1.05	20.55
Albitised granites	Dutsen Wai	DW13	albite granite	39	88	4.93	2.26	16.30
	Saiya	SS12/3	biotite albite granite	77	64	4.69	0.83	23.56
	Shokobo							
	Dutsen Wai	DW11	arfvedsonite albite granite	96	44	4.97	0.46	27.70
	Ririwai	N87	" " "	60	190	4.56	3.17	27.75
	Ririwai	N88	" " "	105	100	4.55	0.95	32.82
	Afu	AF40	zinnwaldite granite	105	190	3.84*	1.81	38.76
	Ririwai	N89	arfvedsonite albite granite	105	225	4.38	2.14	41.09
	Ririwai	N86	" " "	145	350	3.79	2.41	59.29
	Potash metasomatism	Ririwai	R1-35	microcline wallrock	10.2	38.8	4.37	3.80
	Ririwai	R1-18	" "	12.8	41.7	6.15	3.25	6.07
H <sup>+</sup> metasomatism	Ririwai	R1-14	greisen + quartz vein	18.9	97.5	0.37	5.16	8.72
	Ropp	GAE539	pervasive greisen in basement	18	54	7.13	3.00	8.55
	Banke	B36	pervasive greisen zone	8.7	40.6	2.43	4.67	5.02
	Saiya	SS9/4	greisen	66	40	3.36	0.61	15.72

\* Whole rock analysis not available. K<sub>2</sub>O value has been averaged from 4 similar samples from same locality.

since the samples studied by MacKenzie et al were taken away from the mineralised lode area and the samples studied by Ixer came from a zone near the lode. The observations by Ixer et al may be a reflection of the fact that even the biotite granite of the core has been altered by hydrothermal processes. In fact Ixer states that the "presence of chloritised biotite, of columbite and ilmenite aligned along these altered mica cleavages, of altered zircon, trace amounts of cassiterite with sulphides together with fluid inclusion data, all suggest that the granite has suffered hydrothermal alteration."

During the ensuing potash metasomatism, the uranium introduced during sodic metasomatism was remobilised and the Th, therefore, preferentially concentrated resulting in an increased Th:U ratio. The presence of paragenetically late yttrium-coffinite suggests that uranium was also mobile during greisenisation. However, the presence of enhanced bulk rock thorium values together with the abundance of uranothorite (Ixer et al 1987) indicates that it too was mobile and crystallised during greisenisation.

Alpha-track distribution which represents the natural radioactivity from  $^{232}\text{Th}$  or  $^{238}\text{U}$  sites is concentrated in greisen zones (MacKenzie et al 1984). The major part of this alpha track activity can be related to enrichment in Th accompanied by Ce, HREE's, Sc and Cs. Some alpha tracks can be correlated with ore mineral distribution but Th is also enriched in zircon (up to 2%), xenotime (up to 5%) and monazite (up to 8%) as well as in thorite. In contrast, the sites of induced fission indicating the location of uranium, in a slice across the Ririwai lode (MacKenzie et al 1984), are concentrated in the potash metasomatised wallrock and are depleted in the greisen substantiating the removal of U during greisenisation. Uranium occurs in xenotime, monazite and columbite (up to 0.5%), thorite and zircon (up to 5%) as well as in rare uraninite and coffinite (Ixer et al 1985). Ixer et al (1987) however, note that the maximum uranium in core L13 is in the biotite granite.

In summary, it appears that uranium was concentrated early in the biotite granites where it formed discrete minerals. Some additional uranium may have been introduced during albitisation, but it was remobilised during microclinisation, lost by greisenisation and leached during surface weathering. In contrast, although thorium may also have been further supplemented during albitisation, its concentration was enhanced during greisenisation and it was not lost by low temperature surface weathering.

#### Geophysical characteristics of high heat production granites

Apart from their geochemical and mineralogical characteristics, uraniferous granites may also have distinctive geophysical expression. Strong negative Bouguer gravity anomalies have been identified as an important characteristic of known uraniferous granites in France (Moreau 1976), Canada (Darnley 1982) and the British Isles (Brown et al 1979). These intrusions exhibit negative Bouguer anomalies of the order of -40 mGal relative to their surroundings, suggesting that the relatively low density material of which they are formed extends to greater depths than is usual for most granite intrusions. The British granites that have high heat flow have large negative gravity anomalies, with Cairngorm -30 mgal, Weardale -37 and the Cornubian batholith -50 mgal (Brown et al 1979). Even greater negative anomalies occur in the Nigerian Province. Ajakaiye (1977), noted that the most prominent feature of the Bouguer gravity field is the major

low of -94 mgal centred on the Jos Bukuru Complex. Other complexes show negative anomalies between -25 and -85 mgal. Further, Ajakaiye has suggested from modelling of the gravity data that the granites of the Jos Bukuru complex extend to 12km, and to depths in excess of 5kms for some of the isolated complexes such as Banke and Ririwai.

Relationship between heat flow and heat generation. The possibilities for the development of long term hydrothermal circulation

Using the straight line graphical relationship:-

$$q = bA + q^*$$

where  $q$  = surface heat flow,  
 $A$  = heat generation ( $\text{mWm}^{-3}$ )  
 and  $b$  and  $q^*$  are constants,

- it can be estimated that surface heat flow within the Nigerian anorogenic granites may be of the order of  $80\text{mWm}^{-2}$  if an average figure of  $7\text{mWm}^{-3}$  for heat production is taken. Compared with the value of  $68\text{mWm}^{-2}$  determined for In Imanal by Brigaud et al (op cit),  $80\text{mWm}^{-2}$  seems reasonable. Since In Imanal is 290ma and the Nigerian complexes studied vary in age from 191-161m, the values for the Nigerian complexes would be expected to be higher.

Despite the volumes of granite, extending to depths of more than 5km in the crust, it is questionable how important the high heat production has been in the generation of hydrothermal circulation, since granites with the highest heat production tend to be thin and sheet-like and therefore make an insignificant contribution to  $q$  values. Clearly, the granite of L13 core (Fig 3.1) has a high heat production over 400m of depth. Verheijen and Ajakaiye however, only determined a heat flow value of  $38+2\text{mWm}^{-2}$  for the Ririwai complex. This seems very surprising both in view of the fact that extremely high heat production values have been calculated for Ririwai, and since much higher values have been calculated for an older (albeit compositionally different) anorogenic ring complex in Mali. Since highest heat production values found in samples analysed from Nigeria came from Ririwai, if the values of Verheijen and Ajakaiye are correct, it does seem doubtful that high heat production has been important in contributing in any way to the mineralisation.

However when compared with areas like Cornwall, where there has been extensive meteoric water involvement, the granites of Nigeria have much higher concentrations of uranium and thorium. Such uranium and thorium enrichment in the granites must have been capable of maintaining temperatures in a granite above its surroundings for some considerable time. It is hard therefore to assess the contribution that such radioactivity has made to the processes of mineralisation but impossible to discount its effect.

## CHAPTER 12

### ISOTOPIC CONSTRAINTS ON THE SOURCE OF THE MAGMA AND THE SOURCE OF THE FLUIDS

#### Introduction

Different researchers have conflicting opinions as to the source of the A-type granites, and the petrogenesis of the Nigerian intraplate alkaline magmatism is therefore of worldwide as well as regional significance. The Nigerian granites could have been derived from:

- (i) the mantle,
- (ii) 2,000 ma mid Proterozoic (Eburnean) cratonic granites and gneisses representative of the lower crust;
- (iii) late-Proterozoic Pan-African gneisses and granites representative of the upper crust

Stable isotopic studies coupled with analyses of radiogenic isotopes of Sr, Nd and Pb have considerably added to our understanding of the source of anorogenic alkaline magmas.

#### Rb/Sr

A detailed study of the Rb/Sr systematics of Nigerian granites was undertaken by van Breemen et al (1975) Suites of samples from six complexes were analysed to determine the ages and initial ratios of different units within each complex (Table 12.1). This work was supplemented by a further study on 11 complexes by Rahaman (1984) in which 40 Rb-Sr isotopic measurements were made on mineral and whole rock samples (Table 12.2). Most of the rocks analysed had high Rb/Sr ratios, resulting in high precision radiometric ages.

The most striking aspect for the Nigerian A-type granites is their extremely variable initial  $^{87}\text{Sr}/^{86}\text{Sr}$  ratios, ranging from  $0.752 \pm 0.021$  for the arfvedsonite albite granite of the Ririwai complex to values not significantly different from the mantle range of values in the most Sr-rich syenites of the Pankshin and Zaranda complexes (van Breemen et al 1975: Fig 12.1). Such extreme variability of ratios can be seen even within one complex in Nigeria. Thus in the Ririwai complex  $^{87}\text{Sr}/^{86}\text{Sr}$  ratios range from  $0.708 \pm 0.015$  for the granite porphyry and arfvedsonite granite to  $0.729 \pm 0.009$  for the biotite granite to  $0.752 \pm 0.021$  for the Kaffo Valley arfvedsonite albite granite. The relatively poor precision is a function of the increasingly high Rb content ( $>300\text{ppm}$  Rb, Table 12.2) and the low Sr contents ( $< 1\text{ppm}$ ). In some cases the error on the initial ratio was very large, resulting in uncertainties in the petrogenetic interpretation of the data. In order to improve the error, mineral separates from the same samples were re-analysed, by Dickin and Halliday (1987) to establish more accurate initial ratios (Table 12.3).

Clearly from the data in Tables 12.1-12.3 the different plutonic facies of the Ririwai complex exhibit markedly different initial strontium ratios (Fig 12.2), although they were probably intruded within a very brief time interval 167 ma

Fig 12.1 Strontium evolution plot showing the isochron ages and initial  $^{87}\text{Sr}/^{86}\text{Sr}$  ratios of the younger granites in relation to the mantle range and  $^{87}\text{Sr}/^{86}\text{Sr}$  growth lines of basement rock units (data from van Breemen et al 1975).

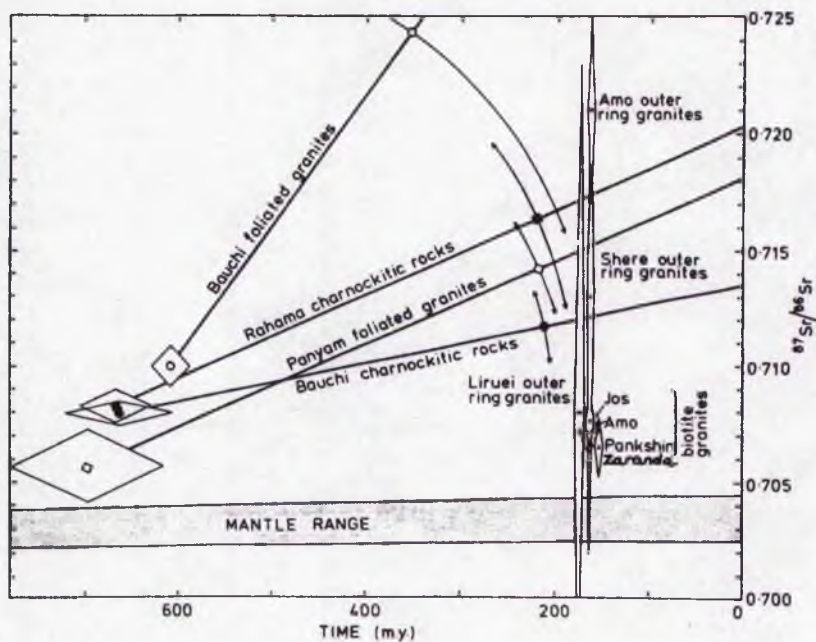


Fig 12.2 Initial strontium isotopic ratios for samples from the Ririwai complex: fg = fayalite granite; bg = bitoite granite; aag = arfvedsonite albite apogranite. Solid squares represent the average initial strontium isotopic ratio for each sample series. The thin vertical lines indicate the error of the initial values (after Bowden et al 1976)

Ririwai; Nigeria

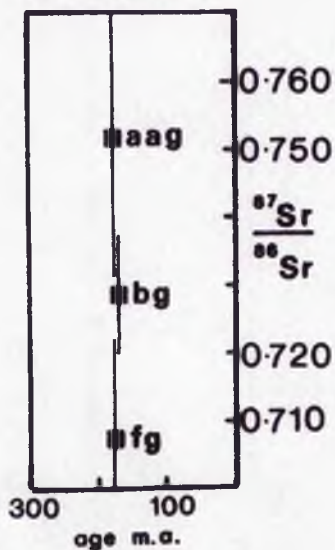


Table 12.1 Rb-Sr isotopic data from van Breemen et al (1975)

Sample	Rb (ppm)	Sr (ppm)	Rb/Sr weight ratio	<sup>87</sup> Rb/ <sup>86</sup> Sr atomic ratio	<sup>87</sup> Sr/ <sup>86</sup> Sr atomic ratio
<i>Shere Hills</i>					
arfvedsonite-fayalite granite					
362	211	21.2	9.93	28.89	0.77357
riebeckitic-arfvedsonite biotite granite					
360	227	9.46	24.0	70.30	0.86710
361	219	2.80	76.2	238.0	1.2537
riebeckitic-arfvedsonite granite					
355	166	3.01	55.4	166.2	1.1037
	168	2.99	56.1	168.4	1.1046
359	223	2.40	93.2	286.7	1.3694
364	296	2.38	120	376.7	1.6094
368	211	2.07	102	314.6	1.4318
366	244	1.67	146	466.6	1.7742
	241	1.67	144	458.6	1.7564
<i>Penakabin</i>					
coarse grained biotite granite and related rocks					
451	223	46.3	4.82	13.99	0.73963
450	236	35.8	6.60	19.18	0.74721
452	249	35.3	7.06	20.48	0.75002
454	253	30.6	8.27	24.06	0.76850
453	452	1.66	273	945.7	2.7594
syenite and related rocks					
470	556	532	0.106	0.3072	0.70644
467	106	52.7	2.02	5.849	0.75154
456	111	19.9	5.64	16.39	0.74357
<i>Zeevands</i>					
Syenite and related rocks					
790	31.6	527	0.060	0.1730	0.70535
385	73.0	90.7	0.806	2.331	0.71147
386	69.4	17.6	3.93	11.43	0.74699
390	77.3	10.7	7.20	20.95	0.76130
389	99.0	3.31	30.8	91.40	0.86912
K.feldspar	146	1.86	78.6	241.7	1.3496
391	81.1	2.39	33.9	100.7	0.96652
trechly-rhyolite					
387	102	3.55	28.9	85.55	0.93815
388	139	4.07	34.0	101.1	0.96989
<i>Loosd</i>					
arfvedsonite-fayalite granite porphyry					
433	126	13.1	9.62	28.02	0.77931
riebeckitic-arfvedsonite					
417	274	9.79	28.0	82.63	0.92775
420	414	8.26	50.1	160.0	1.0720
419	393	6.13	64.2	193.1	1.1753
421	411	4.81	85.5	262.8	1.3568
422	392	3.06	128.0	406.1	1.7014
albite-riebeckite granite					
427	1670	26.3	59.6	180.5	1.1679
426	1493	20.7	72.0	220.3	1.3003
425	1466	2.60	587	2869	7.8975
	1483	2.48	597	2941	7.9023
424	1341	2.13	629	3226	8.6394
423	1215	1.83	663	3677	8.5772
biotite granite (coarse, medium and fine textural variants)					
412	1007	23.3	43.3	129.2	1.0367
415	651	4.33	151	484.8	1.8761
429	764	3.93	194	647.9	2.2737
411	206	0.948	216	731.3	2.4465
431	916	3.43	266	938.8	2.9009
428	640	1.82	362	1335.5	3.9219
414	611	1.72	366	1347.5	3.9182
<i>Amo</i>					
riebeckitic-arfvedsonite biotite granite					
368	301	11.6	26.0	76.62	0.89660
	301	11.5	26.4	77.72	0.89847
366	254	9.67	26.4	77.74	0.90028
380	208	5.64	37.5	111.5	0.97621
378	181	2.96	61.3	185.0	1.1453
383	238	2.86	83.3	253.3	1.3070
379	240	1.99	142.0	454.2	1.7639
coarse grained biotite granite					
369	177	97.6	1.81	5.246	0.71920
370	165	62.9	2.62	7.594	0.72458
447	228	57.3	3.99	11.56	0.73411
<i>Jos</i>					
Coarse grained biotite granite (Jos phase) and medium grained biotite granite (Ngel phase?)					
473	294	51.0	5.77	16.77	0.74559
475	299	47.3	5.70	16.55	0.74681
478	238	34.2	6.95	20.30	0.75357
471	302	42.1	7.17	20.84	0.75656
	305	42.5	7.18	20.90	0.75588
477	297	14.8	17.4	50.79	0.82430
476	363	9.79	37.0	108.9	0.90753
474*	441	11.87	37.1	110.2	0.90985

Table 12.2 Rb-Sr isotopic data on anorogenic ring complexes from northern Nigeria, from Rahaman et al (1984)

Rb-Sr ISOTOPIC DATA				
Sample	Rb (ppm)	Sr (ppm)	<sup>87</sup> Rb/ <sup>86</sup> Sr Atomic ratio	<sup>87</sup> Sr/ <sup>86</sup> Sr Atomic ratio
<b>Daura-alkaline quartz syenite</b>				
DA WR	150	10.1	43.96	.90222
DA LF	213	5.83	110.9	1.1879
DA HF	32.6	3.97	23.98	.81156
<b>Matsena-arfvedsonite granite</b>				
MT WR	147	14.8	29.08	.81291
MT LF	270	5.58	147.5	1.2491
MT HF	191	22.3	24.93	.79894
<b>Dutse-aegirine, arfvedsonite, aenigmatite granite</b>				
DT WR	119	5.58	62.71	.90367
DT LF	208	3.69	172.1	1.2419
DT HF	38.52	4.21	26.73	.79777
<b>Shira-aegirine, arfvedsonite, aenigmatite granite</b>				
SH WR	144	44.2	9.475	.73178
SH LF	228	21.5	30.88	.78825
<b>Fagam-biotite granite</b>				
FG LF	545	3.76	472.2	1.9980
FG MF	180	3.12	175.4	1.1866
FG HF	32.6	1.00	96.59	.97594
<b>Ningi-riebeckite annite granite</b>				
NG TF	555	4.83	363.4	1.6581
NG HF	179	2.52	217.0	1.2772
<b>Tibchi-biotite granite</b>				
TB WR	472	9.09	156.0	1.0977
TB LF	674	6.57	319.9	1.4970
TB MF	171	6.43	78.28	.90717
TB HF	66.6	2.52	77.98	.90817
<b>Banke-biotite granite</b>				
BN WR	503	5.15	303.3	1.4620
BN LF	735	5.47	428.7	1.7607
BN MF	362	4.74	238.5	1.2959
BN HF	66.3	2.12	92.48	.93694
BN BI	3496	4.23	5624	14.576
<b>Dutsen Wai-biotite granite</b>				
DW WR	400	24.4	48.06	.84227
DW LF	463	9.92	139.7	1.0679
DW MF	205	9.66	62.49	.87719
DW HF	34.2	4.13	24.12	.78359
DW BI	3366	6.34	2468	6.9169
<b>Kudaru-biotite granite</b>				
KD WR	272	4.29	191.9	1.1828
KD LF	331	4.45	227.4	1.2627
KD HF	51.8	.993	156.4	1.0881
KD BI	1942	5.48	1942	5.4759
<b>Mada-biotite granite</b>				
MD WR	244	12.1	59.15	.83131
MD LF	367	18.1	59.33	.82985
MD HF	5.90	.923	18.56	.74663
MD BI	848	4.44	1608	4.1262

NOTE.—The following abbreviations have been used: WR, whole rock; BI, biotite; and for the feldspar separates LF, light fraction; MF, medium fraction; HF, heavy fraction and TF, total fraction. Other abbreviations relate to the names of the ring complexes indicated.

Table 12.3 Rb-Sr isotopic data on anorogenic ring complexes from northern Nigeria, from Dickin and Halliday (1987)

Sample No	Age Lithology	$\frac{87}{86}\text{Rb}$	$\frac{87}{86}\text{Rb}$	$\left(\frac{87}{86}\frac{\text{Sr}}{\text{Sr}}\right)_t$	2 $\sigma$	$t_{\text{Sr}}$
Ririwai complex						
417 - 422 WR	168) Riebeckite ) arfvedsonite granite			.7220	120	251
412 WR 414 WR	167) Biotite 167) granite	129.2 1348	1.04143 assume same initial ratio	.7345	70	429
427 R 426 A 426 P	166) Arfvedsonite- 166) albite 166) apogranite	13.27 30.57 5.62	.80456 .85756 .80674	.7732 .7854 .7935	40 80 20	978 1151 1267
Awo complex						
369 WR	162	5.25	.71902	.7069	5	37
Jos complex						
473 WR 474 WR	161) Biotite 161) granite	16.77 110.2	.74497 assume same initial ratio	.7066	10	33
Shere Hills complex						
362 R 361 R	161 Arfvedsonite- fayalite granite 161 Riebeckite- arfvedsonite-biotite granite (same unit as No 360)	21.57 172.0	.75942 1.10790	.7100 .7156	10 1.0	81 160
359 R	161 Riebeckite- arfvedsonite granite (same as unit No 355)	15.91	.75181	.7155	1	158
Pankshin complex						
451 470	151 Biotite granite 151 Syenite	13.99 0.31	.73614 .70544	.7062 .7048	13 2	27 7
Zaranda complex						
387 388	186) Trachy- 186) rhyolite	85.55 101.1	.93815 assume same initial ratio	.7150	100	152
790 385 389	186) 186) Syenite 186)	0.17 2.33 91.40	.70535 .71105 assume same initial ratio	.7049 .7049	1 1	9 9
Adrar Bous complex (Niger)						
61	470 Microgabbro		.77670	.7134	8	
Pan African Locality						
		$\frac{87}{86}\text{Rb}$	$\frac{87}{86}\text{Rb}$	$\frac{87}{86}\frac{\text{Sr}}{\text{Sr}_{107}}$		$^{107}\text{c}_{\text{Sr}}$
336 375 325 331 377 436 438	Panyam Bauchi " " " Rahama "			.7169 .7101 .7146 .7576 .7169 .7150 .7225		179 82 146 757 179 152 258
Eburnian (?) basement						
295 297 298 371 673 674	Malumfashi " " " " "	3.35 1.25 4.47 2.43 6.35 2.25	.8210 .7226 .7831 .7286 .7863 .7324			

ago.

Low initial ratios support a model of fractional crystallisation from mafic to intermediate sources and the general observation that low ratios characterise A-type granites that are associated with syenites and more mafic rocks, provide additional evidence for this model. However, using a fractionation model, high initial ratios such as those of the Ririwai complex cannot be explained without appealing to mixing or contamination of mantle and crustal material. If a lower crustal source is invoked, then isotopic variation may result from different source rocks and from the time lapse between production of the source and the generation of the A-type granites. Also it is possible that the metasomatic processes discussed in detail in the earlier part of this thesis have had a greater effect on changing initial  $^{87}\text{Sr}/^{86}\text{Sr}$  ratios in A-type granites relative to other granites (van Breemen et al 1975).

Clearly, for the Rb-Sr isotopic system, there is some mantle contribution to the granitoid complexes. Pb concentrations and Pb isotopic data may help to clarify the uncertainty of crustal/mantle sources.

Pb

Bowden and van Breemen (1972) discussed the isotopic composition of lead in some Nigerian Proterozoic, Palaeozoic and Mesozoic rocks and minerals and concluded that Jurassic granites with "old lead ages" cannot be assumed to have differentiated from upper mantle but have been derived by fusion of mineralised crustal rocks. Additional data by Tugarinov et al (1968) obtained on five samples from three complexes (Table 12.4), plotted on Fig 12.3 indicated that most of the lead values lie reasonably close to the 500 ma isochron, while grouping near two distinct growth lines. This indicated on the Holmes-Houterman model, that there was isotopic variations in the source region and possibly a crustal origin. Of particular interest are the two whole rock determinations from the Buji complex. Whilst the rhyolite rock-lead is radiogenically-deficient, the quartz porphyry containing hedenbergite and fayalite, from the same volcanic centre, is radiogenically enriched. Such variations within one centre led Bowden and van Breemen (1970) to suggest a model of progressive melting to account for the origin of the Nigerian anorogenic alkaline magmatism.

More recent data by Dickin and Halliday in Table 12.5 (1987), yield initial Pb isotopic compositions with a well-defined linear array on a Pb/Pb isochron diagram. The slope corresponds to an age of approximately  $1750 \pm 350$  ma. This lead was probably largely inherited from mid-Proterozoic (Eburnean) lower crust with subsequent contamination by Pan-African upper crust to varying degrees.

Pb concentrations are plotted against Rb/Sr ratios for representative samples of the Ririwai complex in Fig 12.4. Samples from the biotite granite and the riebeckite arfvedsonite granite define a trend which is consistent with crystal fractionation. In such a model Pb, Sr and Rb all act as compatible elements but Sr is partitioned much more strongly into crystallising feldspar than the other elements causing the Rb:Sr ratio to increase very rapidly as Pb concentrations fall away. In contrast, the arfvedsonite albite granite has a massive Pb content which can only be explained by hydrothermal contamination.

This model is supported by the Pb isotopic data (Fig 12.5) in which all the

Table 12.4

*Lead isotopic compositions from some Nigerian Mesozoic Rocks*

Complex	Rock Type	Mineral	Pb isotopic Composition		
			206 204	207 204	208 204
Ririwai	Albite-riebeckite granite	galena	18.14	1578	38.07
Ririwai	tin lode in biotite granite	galena	17.91	15.75	38.81
Buji	early vent rhyolite	(whole rock)	17.63	15.67	38.74
Buji	quartz-fayalite-hedenbergite porphyry	(whole rock)	21.69	15.95	38.64
Pankshin	hornblende-biotite granite	potash feldspar	18.36	15.96	39.63

Data taken from Tugarinov (1968) and Tugarinov *et al.* (1968).

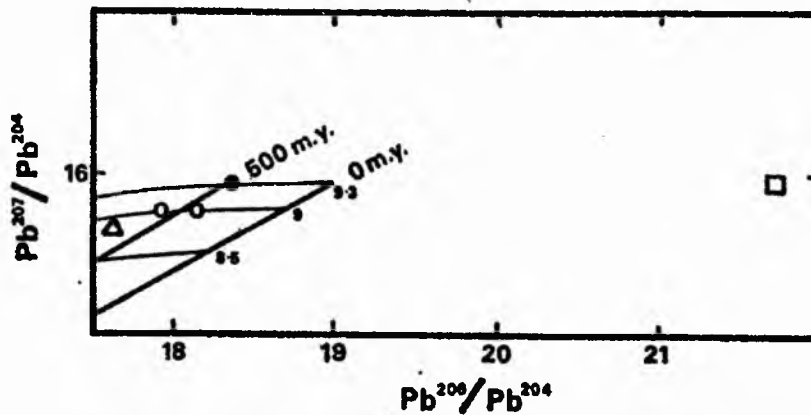


Fig 12.3

Plot of  $Pb^{206}/Pb^{204}$  versus  $Pb^{207}/Pb^{204}$  for whole rock, potash feldspar and galena from Mesozoic granites and volcanics of Northern Nigeria. Diagram shows pertinent growth lines and isochrons for a single-stage evolutionary model based on an 'age of the earth' of 4,550 million years and primordial lead of  $Pb^{206}/Pb^{204} = 9.56$  and  $Pb^{207}/Pb^{204} = 10.42$ . Open triangle-Buji rhyolite; open square-Buji quartz porphyry; open circles-ore leads from the Ririwai complex; closed circle. Pankshin younger granite.

Table 12.5 Lead isotopic data from Dickin and Halliday (1987)

	$\frac{^{206}\text{Pb}}{^{204}\text{Pb}}$	$\frac{^{207}\text{Pb}}{^{204}\text{Pb}}$	$\frac{^{208}\text{Pb}}{^{204}\text{Pb}}$	U ppm	Th ppm	Pb ppm	$\left(\frac{^{206}\text{Pb}}{^{204}\text{Pb}}\right)_t$	$\left(\frac{^{207}\text{Pb}}{^{204}\text{Pb}}\right)_t$	$\left(\frac{^{208}\text{Pb}}{^{204}\text{Pb}}\right)_t$
Ririwai complex									
417	18.238	15.582	39.438	9.8	102	43	17.85	15.56	38.11
422	18.341	15.599	39.314	12.3	63	40	17.81	15.57	38.41
412	18.702	15.618	39.666	19.7	102	42	17.88	15.58	38.28
414	18.900	15.645	39.982	8.3	46	17.3	18.06	15.60	38.46
424	18.291	15.537	38.769	78	230	274	17.65	15.51	38.27
427	17.842	15.611	38.685	198	376	465	17.84	15.61	38.69
Amo complex									
369	18.533	15.591	39.300	5.2	31	14.2	17.93	15.56	38.13
Jos complex									
473	18.378	15.567	39.273	10.8	48	24	17.63	15.56	38.13
474	18.193	15.572	39.227	12.9	53	33	17.55	15.54	38.45
Shere Hills complex									
362	18.201	15.562	39.156	7.8	32	21	17.61	15.53	38.36
360	18.017	15.559	38.929	8.8	40	49	17.72	15.54	38.50
355	17.830	15.555	38.574	6.9	7.8	74	17.68	15.55	38.52
Pankshin complex									
451	18.079	15.548	39.138	6.1	36	17.5	17.56	15.52	38.12
470	18.200	15.556	38.417	1.05	4*	7.8	18.00	15.55	38.17
Zaranda complex									
790	18.409	15.616	38.566	0.64	3*	21	18.35	15.61	38.48
387	18.214	15.670	39.116	6.8	16.5	16.3	18.42	15.63	38.49
388	18.692	15.665	39.274	2.57	10*	20	18.45	15.65	38.97
385	18.678	15.631	39.404	0.91	4*	4.4	18.29	15.61	38.84
389	18.959	15.648	39.497	2.14	11	6.1	18.29	15.62	38.38
Adrar Bous complex (Niger)									
60	17.755	15.456	37.682	.007	.03*	0.49	17.75	15.46	37.68
61	18.231	15.567	38.290	.029	.12*	0.43	18.23	15.57	38.28
Pan-African basement									
336	18.710	15.665	39.508	3.4	19.1	20.2	18.42	15.65	38.97
375	17.837	15.568	38.433	1.55	3.5	13.0	17.64	15.56	38.29
325	18.053	15.618	38.780	3.1	21	37	17.91	15.61	38.47
331	17.782	15.594	40.617	3.9	52	38	17.61	15.59	39.84
377	18.066	15.584	38.523	1.98	8.2	16.3	17.86	15.57	38.25
436	17.953	15.569	38.733	2.59	11.6	19.8	17.73	15.56	38.41
438	18.069	15.578	38.811	6.6	15.0	21	17.54	15.55	38.42
Eburnian basement									
295	19.402	15.510	38.073	2.13	8*	42	19.32	15.51	37.97
297	17.362	15.375	37.676	5.0	20*	34	17.12	15.36	37.36
298	19.530	15.830	39.446	1.28	5*	30	19.46	15.83	39.35
671	18.542	15.645	38.727	2.38	10*	40	18.44	15.64	38.59
673	19.768	15.789	38.533	1.27	5*	21	19.66	15.78	38.40
674	18.694	15.710	38.924	0.71	3*	20	18.63	15.71	38.84

\* Estimated concentration

t = age for Mesozoic granites, else 170 Myr

Average within run precision on Pb isotope ratios = 0.03 (2 $\sigma$ )Estimated absolute accuracy of Pb isotope ratios = 0.01, 0.007 and 0.02 (1 $\sigma$ ) for  $^{206}\text{Pb}/^{204}\text{Pb}$ ,  $^{207}\text{Pb}/^{204}\text{Pb}$  and  $^{208}\text{Pb}/^{204}\text{Pb}$  respectively

Fig 12.4 One model for the evolution of the principal units of the Ririwai complex. A = riebeckite arfvedsonite granite; B = arfvedsonite albite granite; C & D = extreme range of compositions in biotite granite

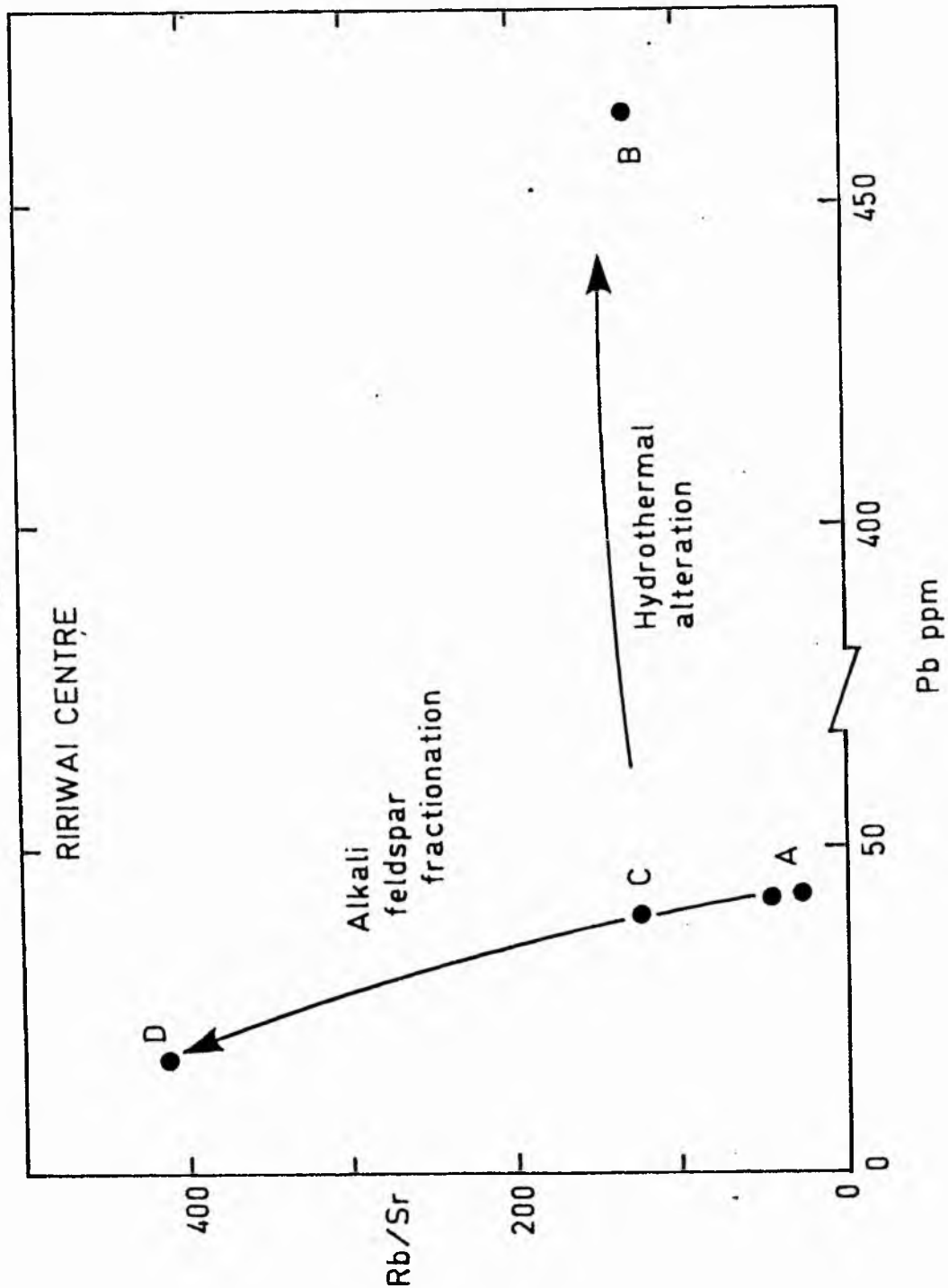
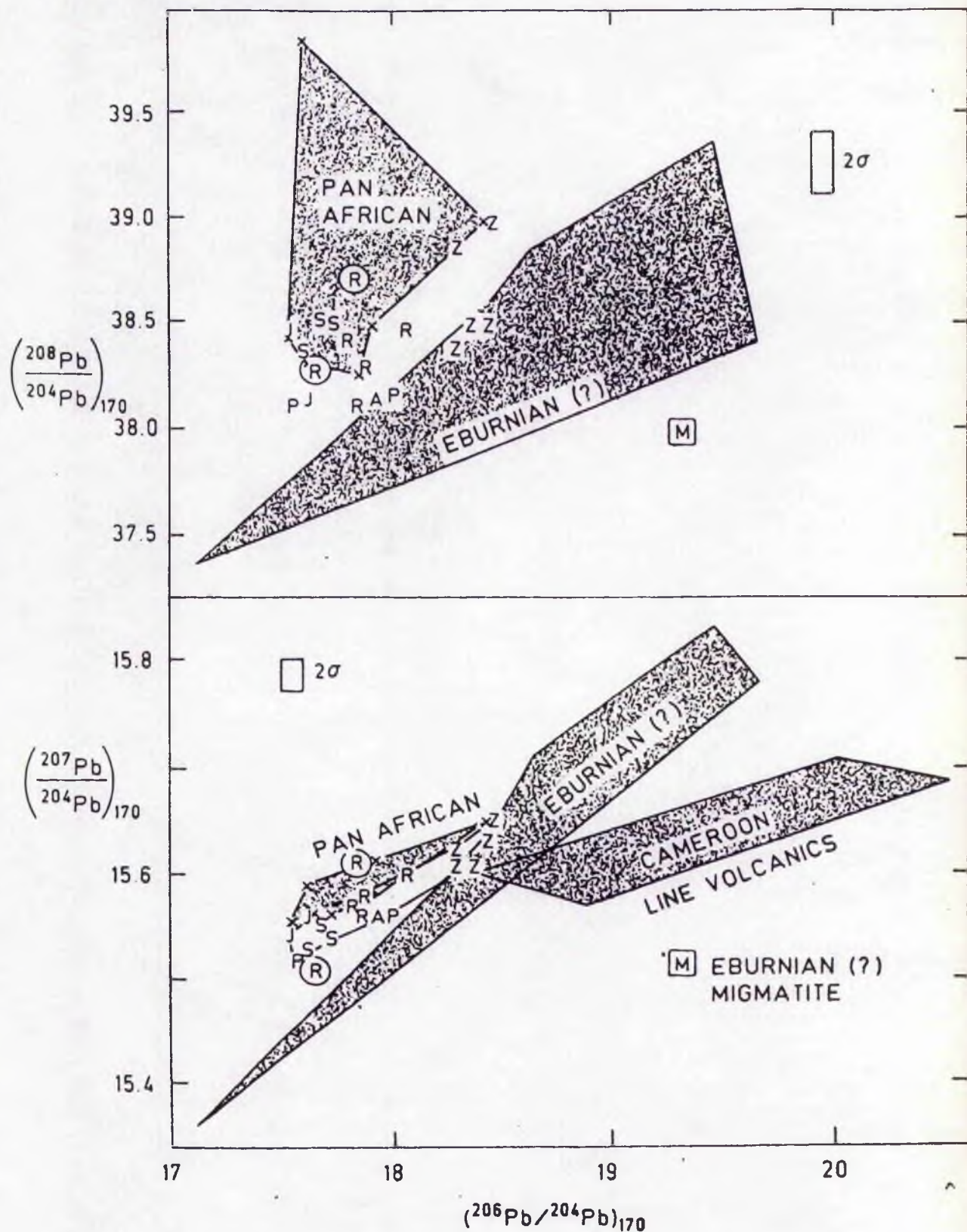


Fig 12.5 Initial Pb isotopic compositions of the anorogenic ring complexes and composition of representative possible source compositions at 170 ma (average age of magmatism). Letters are initials of complex name, encircled Ririwai samples - hydrothermally altered arfvedsonite albite granite.



Mesozoic granites, with the exception of the Ririwai arfvedsonite albite granite form a well-defined array on the  $^{207}\text{Pb}/^{204}\text{Pb}$  versus  $^{206}\text{Pb}/^{204}\text{Pb}$  isochron diagram. The altered samples of the apogranite plot well away from this array, suggesting that hydrothermal contamination has a rather erratic effect on Pb isotope compositions. The slope of the Pb/Pb isotope array for the remaining samples corresponds to an apparent age of  $1750 \pm 350$  ma (Dickin and Halliday 1987).

On Fig 12.5, Pb isotopic compositions of the Nigerian granite Pb array lies between the Pan-African and Eburnean crustal fields in both Fig 12.5a and Fig 12.5b. Coupled with the 1750 ma apparent age of the granites it suggests that the bulk of the Pb is derived from Proterozoic crust reworked in the Pan-African orogeny.

Therefore, the combined data from Tugarinov et al (1968) and Dickin and Halliday (1987) suggests that lead of upper and lower crustal ages has been involved in the alkaline magmatism. This does not preclude a mantle input but does suggest that fusion of crustal rocks has taken place.

#### Combined Nd/Sm and Sr data

In order to determine more about the contribution from each of the three possible sources mentioned in the introduction, Dickin and Halliday (1987) considered the evolution of  $^{87}\text{Sr}/^{86}\text{Sr}$  in each of the possible source materials and combined Nd/Sm studies to indicate possible source regions (Table 12.6):-

##### (i) Evidence for mantle signatures

The composition of the mantle beneath the Jos Plateau cannot be determined directly since the Mesozoic complexes are the only significant magmatic products of the Jos Plateau during the Phanerozoic. Dickin and Halliday (1987) therefore sampled mantle-derived basic magmas from Cameroon line volcanics and microgabbros from the Adrar Bous complex of Niger. The microgabbros had high initial ratios despite their basic composition indicating that they have been significantly contaminated by crustal material. The composition of the Cameroon Line volcanics (Halliday et al 1983) provided a much more satisfactory indication of the nature of the Nigerian sub-lithospheric mantle. These basalts from the continental sector display a wider range of isotopic compositions than those from the oceanic sector, which can be partly attributed to crustal contamination.

##### (ii) Evidence for mid-Proterozoic crustal signatures

The Benin-Nigeria Shield (Fig 1.1 page 5) lies within the southern prolongation of the Pan-African belt.

In southwest Nigeria the basement consists of charnockitic rocks of unknown age and a gneissic complex comprising banded gneisses, migmatites, quartzites schists, biotite and amphibole gneisses, amphibolites and marbles metamorphosed in the almandine-amphibolite facies. They are cut by foliated granites which have yielded Proterozoic ages (Rb-Sr WR isochrons of  $2270 \pm 30$  ma and  $2280 \pm 70$  ma and by porphyritic granites, subordinate quartz diorites and two mica granites which are considered to be Pan-African in age. The bulk of the metasedimentary rocks are probably of lower Proterozoic age but an age of 2750

ma indicates the presence of some remnant Archaean rocks. Rejuvenation during the Pan-African thermotectonic event produced biotite Rb-Sr and K-Ar ages around 500ma.

In a further effort to constrain the composition of the deep crust beneath the Jos Plateau a selection of metamorphic rocks were collected from the Zaria area of north central Nigeria. Rb-Sr isotopic studies have been undertaken by van Breemen et al (1977) on a small selection of samples from the Pan-African basement host of the Jos Plateau granite complexes. Recalculating the data to the new decay constants, these plutons range in age from  $596 \pm 23$  ma for foliated granites between Bauchi and Gogola River and  $654 \pm 128$  for monzodiorites and a hornblende biotite granite at Rahama to  $677 \pm 161$  ma for foliated granites at Panyam (Table 12.6). When Nd isotopic compositions are corrected using the Rb/Sr dates the initial  $^{143}\text{Nd}/^{144}\text{Nd}$  ratios, expressed in epsilon units (parts per ten thousand deviation from the bulk earth evolution line) are -1.6, -10.5 and -13.1 for the Panyam, Rahama and Bauchi samples respectively (Table 12.6). These very enriched source compositions are indicative of a large component of crustal basement in the Pan African granites and in fact the Rahama and Bauchi samples can be little more than remelted crust. When Nd model ages are calculated, they yield 810, 1590 and 1672 ma ages respectively for the three plutons. The last two ages are at the lower end of the 1600-2400 ma age range of the Eburnean orogeny which has been recognised in rocks from the Kaduna and Ibadan areas. Initial Sr isotope ratios of these granites (0.710 for Bauchi and 0.708 for Rahama, van Breemen et al 1977), are consistent with this interpretation of the Nd data, and indicate that the Pan-African crust was reworked from Eburnean basement, which may be present at depth over large areas (Dickin and Halliday (1987). Similar age data can be obtained from granulite facies xenoliths within the Cameroun line volcanics. These are believed by Dickin and Halliday (1987) to represent the crustal basement of the Jos Plateau. In general, it would appear that the Amo, Jos and Pankshin magmas may have been contaminated in the Eburnean (?) lower crust.

### (iii) Evidence for crustal signatures

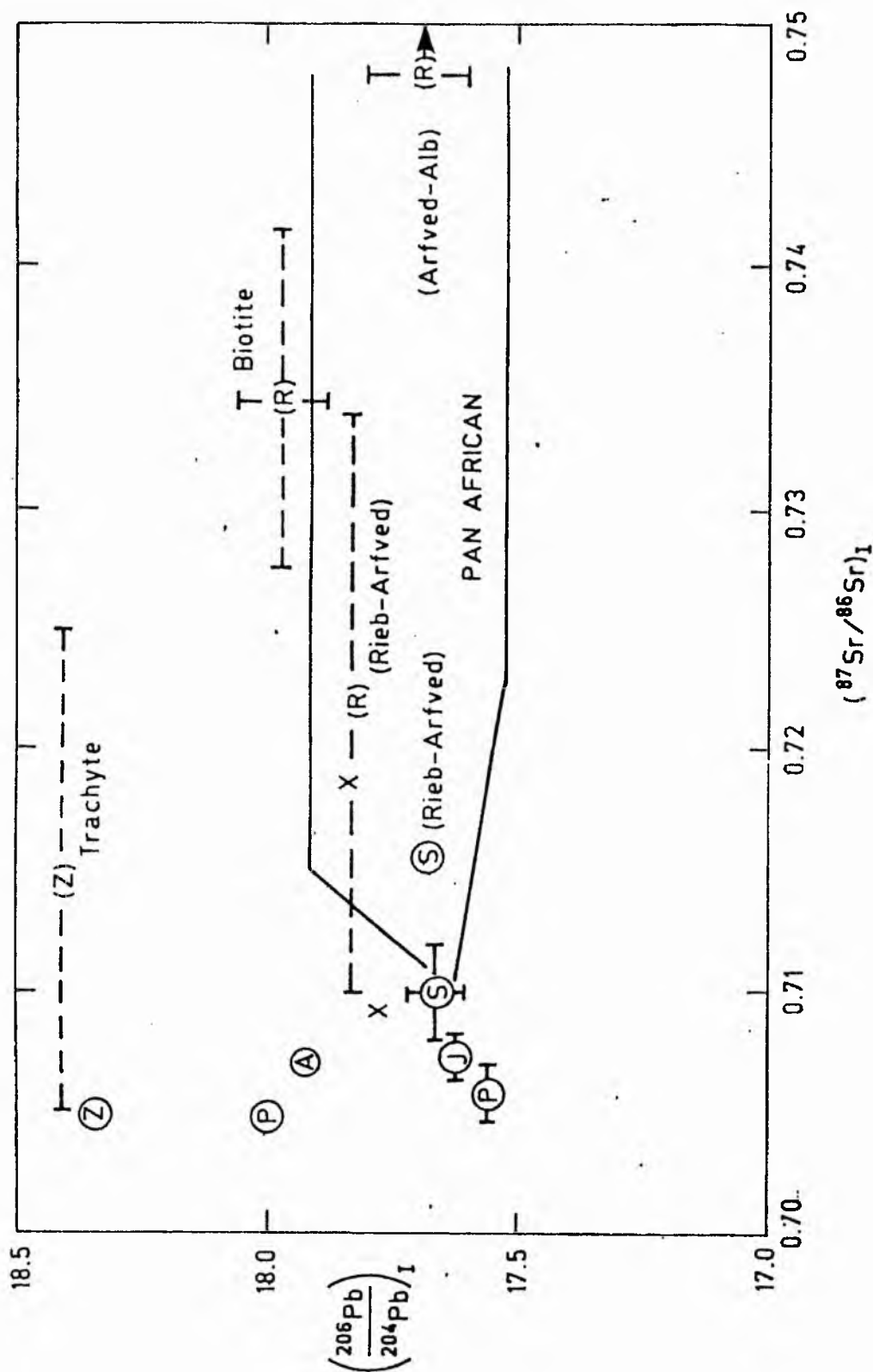
Precise identification of the crustal components in the Nigerian granites is difficult, not least because the Pan-African crust largely consists of reworked older basement. However, it would appear that the Shere Hills and Ririwai arfvedsonite granites (Table 12.6) contain a large fraction of a Pan-African component.

There appears to be a conflict with the Pb and the Sr and Nd isotopic data. However, Dickin and Halliday (1987) explain the different behaviour of the isotope systematics by the much higher Pb/Sr and Pb/Nd concentration ratios of crustal rocks relative to mantle-derived magmas. This is illustrated by the Pb versus Sr isotope diagram (Fig 12.6) in which the Nigerian anorogenic granites define a generally, inverse relationship between  $^{87}\text{Sr}/^{86}\text{Sr}$  and  $^{206}\text{Pb}/^{204}\text{Pb}$  which may be regarded as a mixing between mantle-derived magma with low  $^{87}\text{Sr}/^{86}\text{Sr}$  and radiogenic lead, and the high  $^{87}\text{Sr}/^{86}\text{Sr}$  and less radiogenic lead of the continental crust.

Table 12.6 Samarium-Neodymium isotopic compositions of the anorogenic ring complexes. Data from Dickin and Halliday (1987)

Sample Number	Locality	Lithology	(Ma)	Sm (ppm)	Nd (ppm)	$\frac{^{147}\text{Sm}}{^{144}\text{Nd}}$	$\frac{^{143}\text{Nd}/^{144}\text{Nd}}{+2 \text{ m}}$	$\left( \begin{array}{c} ^{143}\text{Nd} \\ ^{144}\text{Nd} \end{array} \right)$ (B.F.) t	$t_{\text{Nd}}$	$t_{\text{CHUR}}$ I.R.
438	Rahama	Pan African biotite-hornblende granite	654 (170)	9.896	54.85	.1091	.511726±19	.511605 (.512421)	-15.9	1590
385	Zaranda	Syenite	186±15	18.78	116.8	.09725	.512564±19	.512446 (.512400)	+0.9	
422	Ririwai	riebeckite arfvedsonite granite	167±5	35.32	112.9	.1891	.512434±20	.512229 (.512425)	-3.8	
451	Pankshin	biotite granite	151±4	68.97	338.2	.1233	.512361±43	.512240 (.512445)	-4.0	
295		Cournium migmatite	(170)	5.232	25.34	.1248	.511314±18	.511176 (.512421)	-24.3	2832
331	Bauchi	foliated granite	596 (170)	9.096	54.65	.1006	.511588±17	.511477 (.512421)	-18.4	1672 -13.1
417	Ririwai	riebeckite-arfvedsonite granite	167	18.48	82.36	.1357	.512436±25	.512288 (.512425)	-2.7	
360	Shere Hills	riebeckite arfvedsonite biotite granite	161±2	14.49	62.62	.1399	.512405±25	.512259 (.512432)	-3.4	
369	Amo	biotite granite	162±3	10.69	50.62	.1276	.512501±16	.512367 (.512431)	-1.3	
412	Ririwai	biotite granite	167±2	33.21	137.1	.1464	.512298±18	.512139 (.512425)	-5.6	
473	Jos	biotite	161±4	36.98	163.7	.1365	.512410±30	.512267 (.512432)	-3.2	
336	Panyam	foliated granite	677 (170)	6.148	36.38	.1022	.512101±16	.511996 (.512421)	-8.3	810 -1.56
t ± O	BULK EARTH	$\frac{^{143}\text{Nd}}{^{144}\text{Nd}}$				$\frac{^{147}\text{Sm}}{^{144}\text{Nd}}$	$\frac{^{144}\text{Nd}}{^{144}\text{Nd}} = 0.1966$			
		$\frac{^{87}\text{Sr}}{^{86}\text{Sr}}$				$\frac{^{87}\text{Rb}}{^{86}\text{Sr}}$	$= 0.0839$			

Fig 12.6 Initial Pb versus initial Sr isotopic compositions of Mesozoic ring complexes and field for Pan-African basement at 170 ma. Brackets represent ranges of Pb isotope compositions for individual units and estimated errors on initial Sr isotope compositions Data from Dickin and Halliday (1987)



## Stable isotope studies

### Introduction

Limited stable isotope data on the Nigerian province is available in the literature and this has been supplemented by new data for this thesis (with the help of Dr. Fallick of SURRC East Kilbride.) Because of the variety and complexity of magmatic processes the stable isotope studies are most helpful when combined with analyses of radiogenic isotopes. For this reason, four of the five whole-rock samples selected for study were originally analysed by van Breemen for Rb/Sr data and subsequently re-analysed by Dickin and Halliday for Sr, Nd and Pb data.

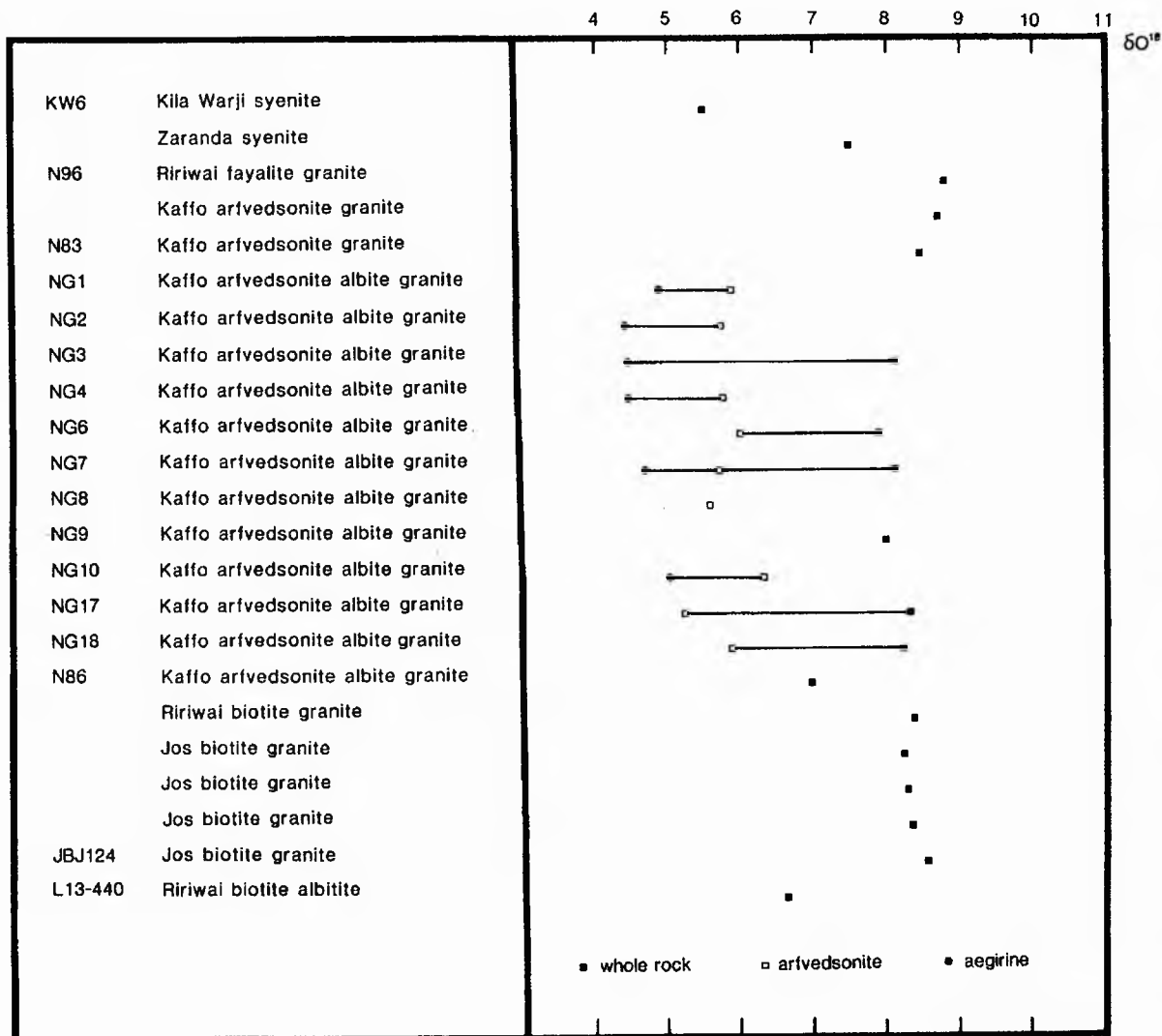
### Oxygen/Hydrogen

The Kila Warji fayalite syenite which is regarded as the least evolved rock in the Nigerian province has a  $\delta^{18}\text{O}$  value of 5.5 (Fig 12.7) This is a typical value for trachytes and syenites in anorogenic ring complexes and is within the normal basaltic range for mid-ocean ridge basalts. The Zaranda syenite gave a value of + 7.5 which is only slightly higher than MORB values which are typically + 5.5 to + 6.5. Whole-rock  $\delta^{18}\text{O}$  values increase from the syenites to the granites. Thus the value for the fayalite granite was  $\sim 8.8$ , whilst the peralkaline granites ranged from + 7.9 to 8.7 (Fig 12.7) and the biotite granites from + 8.2 to + 8.6. Arfvedsonite albite- and biotite albite facies gave whole rock  $\delta^{18}\text{O}$  values between + 6.54 and + 8.53‰. Arfvedsonite and arfvedsonite albite values have very similar values but very different  $\delta\text{D}$  values,  $-81 \pm 10$  compared with  $-124 \pm 5$ . Arfvedsonites from other arfvedsonite albite granites of the Jos Plateau are equally D-depleted (Sheppard and Bowden unpublished data). All arfvedsonites from the arfvedsonite albite granites have very low  $\text{H}_2\text{O}^+$  contents ( $\sim 0.4\%$ ) compared to those from arfvedsonite granites ( $\sim 1\%$ ). Whole rock fluorine contents are also very different. Biotites from the biotite granite have  $\delta\text{D} \sim 83 \pm 8$ .

Sheppard (1986) concluded on the basis of his data shown in Fig 12.7 and discussed above, that most granites were not modified by extensive meteoric hydrothermal alteration. Similarly the relatively few mineral-mineral O-isotope relationships (Borley et al 1976) suggest that many of the whole rock isotopic values could closely represent their magmatic values. Additional data by Kinnaird and Fallick is in agreement; the uniform  $\delta\text{O}^{18}$  values within a granite type and lack of D evidence for interaction with externally derived waters all suggest that the minerals are recording their original igneous values.

The D-depletion of the arfvedsonites, with values as low as -124 for the arfvedsonite of the albite granite, are often considered to be due to interaction with low  $\delta\text{D}$  meteoric waters (Taylor 1974, 1979; Sheppard 1977), extreme degassing processes (Nabalek et al 1983; Taylor et 1983) or involvement of extremely Fe-rich minerals (Suzuki and Epstein, 1976). Interaction with meteoric water with such low  $\delta\text{D}$  values can be ruled out on account of the latitude of Nigeria since the intrusion of the ring complexes. Latitudes have remained low so that  $\delta\text{D}$  values of meteoric water will always have been high. The effect of extreme iron enrichment does not account for such low values either since such low  $\delta\text{D}$  values are not found in very iron-enriched facies discussed later. Sheppard (1986) concluded therefore that the H- and O- isotopic

Fig 12.7 A compilation of  $\delta^{18}\text{O}$  analyses of mineral and whole rock samples from anorogenic complexes in northern Nigeria. Samples prefixed NG - from Borley et al (1976); un-numbered samples - from Sheppard and Bowden (in Sheppard 1986); remaining samples this work.



compositions might be reflecting the particular nature of the crustal source region and the magmatic processes which produced these granites. Sheppard suggests however, that mantle derived magmas are probably involved with the production of most anorogenic granites.

### Sulphur isotopes

There have been few sulphur isotope studies on primary sulphides in granites, yet such data have considerable potential in elucidating the petrogenesis in terms of granites derived either from igneous or metasedimentary protoliths (Laouar et al 1987). Sulphur isotope distributions have been studied in I- and S-type granites from key localities in Australia by Coleman (1979). Broad but distinctive ranges of  $\delta^{34}\text{S}$  were observed with  $\delta^{34}\text{S}$  values of -5 to 3.6‰ for I-types and 5 to 15‰  $\delta^{34}\text{S}$  for S types (Fig 12.8).

In this work classical A-type granites from Nigeria, and their sulphide minerals are currently being studied to compare the isotopic characteristics of their source regions with I- and S- types from Australia and Britain. For the Nigerian granites, several sulphide samples were selected for study from eight different and widely separated complexes. These sulphides which included sphalerite, chalcopyrite, galena and molybdenite ranged from ores that were disseminated throughout a granite to minerals that occurred in veins and lodes. Where possible pairs of co-existing sulphides were chosen as isotopic geothermometers. Since most of the sulphides were from veins they will be discussed in detail later, however as the results in Table 12.7 indicate all the Nigerian samples have  $\delta^{34}\text{S}$  values within a very restricted range of -1.44‰ to +1.75‰ which is identical with the mantle values derived from meteorites. In contrast to hydrogen, carbon and many other elements, sulphur in meteorites, which occurs most commonly as FeS (troilite) has a remarkably uniform composition of  $\delta^{34}\text{S} = 0.2 \pm 0.2\%$  (Thode et al 1961). Despite the fact that the mantle may have become locally heterogeneous during the last 2.5 billion years, Ohmoto (1986) believes that it is unlikely that the  $\delta^{34}\text{S}$  of the mantle rocks lies outside the range of -3 to +2‰. Continental and oceanic mantle xenoliths which have a wide range in their isotopic compositions of O, Sr and Nd have a very restricted range in  $\delta^{34}\text{S}$  values of -1.5 to +1.5 per mil.

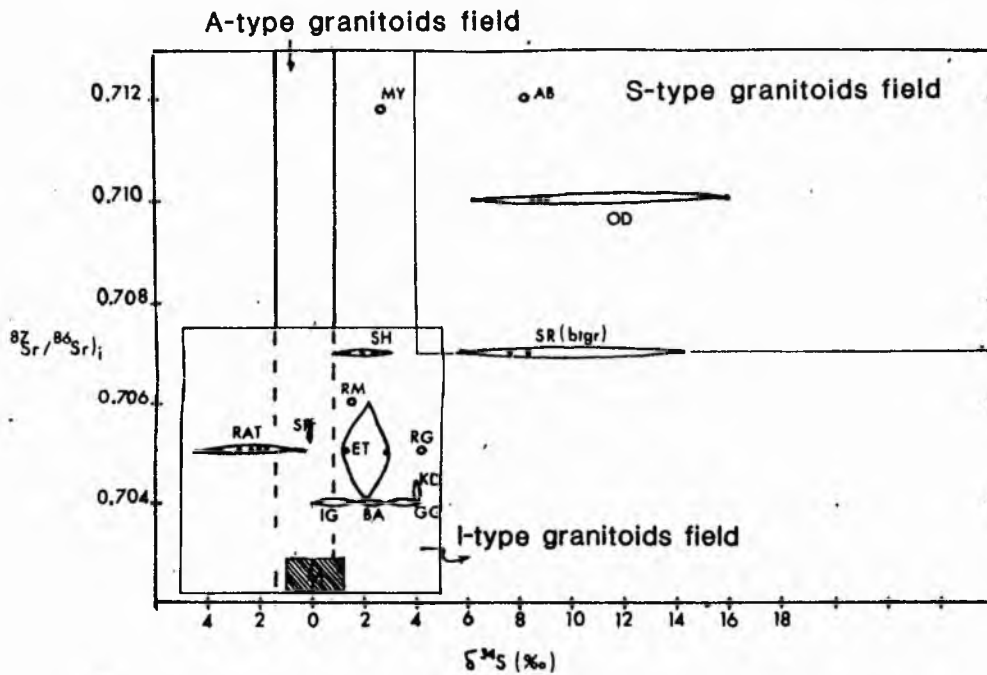
Thus in Figs 12.8a and 12.8b the anorogenic granites occupy distinctly different fields from S-type granites although they partially overlap with the field for I-type granites.

### Discussion on the source of the magma.

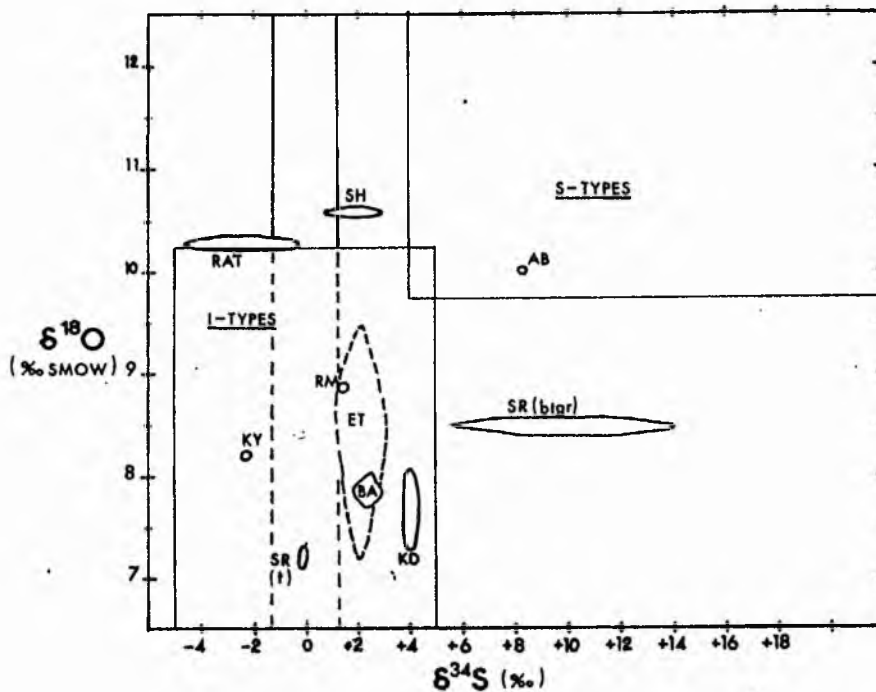
Combined Pb, Sr and Nd isotope data clearly indicate a multistage petrogenetic process with components from the mantle, mid Proterozoic (Eburnean?) lower crust and late Proterozoic (Pan African) upper crust (Dickin and Halliday 1987). The Zaranda complex has radiogenic initial Nd and Pb isotope compositions but unradiogenic Sr attributable to mantle derived differentiated magmas which have suffered limited crustal contamination. Other complexes trend towards less radiogenic Nd and Pb isotope ratios and more radiogenic Sr, indicative of an increasing contribution from the crust. In contrast, the Kaffo Valley arfvedsonite albite granite from the Ririwai complex contains isotope ratios of dominantly Pan African composition, suggesting considerable hydrothermal overprinting with fluids that have interacted with, or been derived from

Fig 12.8  $\delta^{34}\text{S}$  data for some British granitoids from Fallick et al unpublished data.

My=Moy; Ab=Aberdeen; OD=Oughterard; Sr(Btgr)=Strontian biotite granite; Sh=Shap; Rm=Ross of Mull; KY=Glen Kyllachy; Rat=Ratagain; Et=Etive; RG= Roundstone granite; KD=Kilmelford; BA=Ballachulish; IG=Inish; GG=Galway



(a)  $\delta^{34}\text{S}$  vs  $(^{87}\text{Sr}/^{86}\text{Sr})_i$  for some British Caledonian granitoids showing the range of isotopic composition for various possible source regions.



(b)  $\delta^{34}\text{S}$  vs  $\delta^{18}\text{O}$  for some British Caledonian granitoids showing the range of isotopic compositions for various possible source regions.

Pan-African crust (Dickin and Halliday 1987). This arfvedsonite albite granite has an initial Sr isotopic ratio of 0.792. However, such large scale disturbances of isotope ratios by hydrothermal processes does not appear to be widespread in the Nigerian alkaline ring complexes as a whole.

The oxygen and hydrogen isotopic data suggests that mantle derived magmas were probably involved with the production of most anorogenic granites. The generation of more  $^{18}\text{O}$ -rich magmas must involve crustal oxygen. Sheppard (1986) states that simple two end-member mixing between mantle-derived and crustal-derived magma is unlikely. Similarly, mixing that involved assimilation of country rocks by magma is not a simple two end-member process, implying that a multistage process was involved. Certainly the combined H, O and Sr data for the Kaffo valley arfvedsonite albite granite indicates that crustal rocks were involved in the genesis of the intrusion.

#### Conclusions on the source of the magma

In summary, the sulphur isotopic data indicates that the sulphur was derived from the mantle in all the ring complexes. The oxygen and hydrogen isotopic data suggests that whilst there was a mantle input to the magmatism, a multigenetic process must be envisaged. The Pb isotope compositions of Dickin and Halliday (1987), show that the lead of the ring complexes was probably largely inherited from the crust. The Nd and Sr isotopic ratios define a trend which is argued by Dickin and Halliday (1987) to reflect mixing between mantle-derived magmas and crustal melts in different proportions. The Pb isotope compositions do not correlate well with Nd or Sr, probably because the low Pb contents of mantle derived magmas allowed almost complete overprinting by crustal isotopic compositions.

In conclusion the recent isotopic evidence continues to support the hypothesis of van Breemen et al (1975) that the Nigerian intra-plate alkali magmatism is the result of mantle-derived magmas which have suffered a significant amount of contamination during their ascent through the ancient crustal basement.

## ORIGIN OF THE FLUIDS

### Introduction

The origin of fluids in hydrothermal systems has been actively debated in the past. The question has been partially resolved in recent years for many ore deposits, with the advent of stable isotopic studies. This is possible because the four major types of water - magmatic, metamorphic, seawater and meteoric water - have characteristic stable isotopic signatures. Applied to the analysis of isotopic data on hydrothermal minerals, fluid inclusions and waters from active geothermal systems, isotopic ratios indicate that waters of several origins are involved in ore deposition in the volcanic and subvolcanic intrusive environment (Sheppard 1977). For example, water of solely magmatic origin dominated main stage mineralisation of the Casapalca Ag-Pb-Zn-Cu deposits of Peru, whilst water solely of meteoric origin was responsible for the Cu-Zn-Mn deposits of Butte Montana. However, solutions of more than one origin were important in both porphyry copper and porphyry molybdenum deposits which have similarities in style, alteration processes and mineralisation with the Nigerian

tin province. In these porphyry deposits, the initial major ore transportation and alteration processes of K-feldspar and biotite alteration were magmatic-hydrothermal events that occurred between 700 and 500°C. These fluids were typically highly saline, Na-K-Ca-Cl rich brines, of more than 15 eq.wt% NaCl. The convecting meteoric hydrothermal system that developed in the surrounding country rocks with relatively low integrated water/rock ratios (less than 0.5 at.% oxygen) substantially collapsed as temperatures in the dying magmatic hydrothermal system fell below 350-200°C. These fluids generally had moderate to low salinities of less than 15 eq.wt% NaCl. Differences among these deposits are probably related in part to variations in the relative importance of the meteoric, hydrothermal and magmatic hydrothermal effects.

For the Nigerian province there has been no previous study of the fluids responsible for hydrothermal alteration. There are several possibilities for the origin of the fluids. The heat of the intrusions, plus the high heat producing capacity of these granites, could have been responsible for the creation of hydrothermal cells involving meteoric water as envisaged for north and southwest England by Moore (1982) and elsewhere. Alternatively it is possible that uranium introduction and associated mineralisation was a result solely of magmatic processes, with the hydrothermal fluid solely of magmatic origin. A further possibility exists of saline magmatic water mixing with dilute meteoric water which is consistent with some of the features observed in fluid inclusion studies.

Clearly, the petrological and radiogenic isotope data indicates that there has been a mantle input to the alkali granite system, with crustal contamination. The origin of the ore elements and hydrothermal fluids could likewise have had a contribution from both mantle and crustal sources.

#### Isotopic evidence

From the data in Chapter 10, the coexistence of low salinity inclusions with dense saline brines in the same samples, with wide variations in homogenisation temperatures was interpreted as a boiling phenomenon. However, mixing of a hot dense saline brine with cooler, dilute meteoric water would produce a similar range of inclusion types within a given population. From fluid inclusion studies alone it would be impossible to substantiate that such mixing was not the cause of the mixed inclusion populations although a boiling model was the preferred explanation in Chapter 10. The use of stable isotopes can help to resolve this problem.

#### Sulphur isotopes

Twelve different samples were selected for study from six widely spaced complexes. These samples included material from the Saiya Shokobo complex. Because detailed fluid inclusion studies in Chapter 10 indicated the existence of dense saline inclusions and low density fluids, it was anticipated that if any crustal sulphur was introduced by meteoric water during mineralisation then it should be recorded in the samples from the Rishi area of the Saiya Shokobo complex. These sulphides from the six complexes included sphalerite, chalcopyrite, galena and molybdenite from mineralised veins and lodes. Where possible co-existing pairs of sulphides were chosen as isotopic geothermometers. The samples chosen are listed in Table 12.7. All twelve samples gave  $\delta^{34}\text{S}$  values between - 1.44 and + 1.75

Table 12.7 Sulphur isotopes in co-existing sulphide assemblages

Complex	Sample no.	mineral	$\delta^{34}\text{S}_{\text{cdt}} (\%)$
Afu	AF23/	sp	-1.44
	AFJ2	cp	-0.55
Ririwai	J108	sp	+0.80
	R111	ga	-0.61
Saiya Shokobo	SS	sp	+0.72
	SS	cp	+0.17
	SS	sp	+0.07
Tibchi	TK02	ga	-0.01
	TK03	mo	+0.35
Kigom	KG5	ga	+1.48
	KG3	mo	+1.75
Jos Bukuru	JBj118A	ga	+0.48

sp = sphalerite  
ga = galena  
mo = molybdenite  
cp = chalcopyrite

The  $\delta^{34}\text{S}$  data indicates that the vein sulphur shows a narrow range of values which are within the limits discussed earlier that have been defined for the mantle. Therefore the sulphur in both the granites and mineralised veins is of mantle origin. It is perhaps not surprising that the sulphides in the veins show the same characteristics as those from the granite since the sulphides were disseminated throughout some granite plutons as a result of hydrothermal alteration. What is not clear at the moment is how long sulphur can retain its mantle memory. Also the very nature of hydrothermal alteration may mean that  $\delta^{34}\text{S}$  values have been modified by volatile loss.

Low oxygen fugacities in the mantle mean that sulphide is the stable form of sulphur. However, as magma rises through the crust, near-surface variations in oxygen fugacity will occur. As a result there may be either enrichment of  $^{34}\text{S}$  due to  $\text{H}_2\text{S}$  loss or relative depletion in  $^{34}\text{S}$  from loss of  $\text{SO}_2$ . If such modifications had occurred perhaps more variation would be expected from an orogenic centre to centre whereas a very restricted range of  $\delta^{34}\text{S}$  values have been obtained from the six widely spaced complexes.

Temperatures determined from co-existing mineral pairs

By choosing different pairs of sulphides from the same mineralised system it was possible to use the above data as a stable isotope geothermometer. The data, calculated by Fallick (Pers comm) is shown in Table 12.8, using the formula of Ohmoto and Rye (1979).

Table 12.8 Temperature calculations from sulphide pairs using the formula of Ohmoto and Rye (1979).

Sample	pair	-	T <sup>o</sup> C	Comment
Af23	sp-cp	-0.89		out of equilibrium
Saiya	sp-cp	-0.1		out of equilibrium
Shokobo	sp-cp	+0.55	253 <sup>o</sup>	
Tibchi	mo-ga	+0.26	830 <sup>o</sup>	
Ririwai	sp-ga	+1.41	443 <sup>o</sup>	
Kigom	mo-ga	+0.27	830 <sup>o</sup>	

The sphalerite-galena pair of the Ririwai lode indicate a temperature of formation of 443<sup>o</sup>C which is in good agreement with fluid inclusion geothermometry in which temperatures of 340-460<sup>o</sup>C were determined on various samples from the lode. A similar acceptable temperature of formation is given for samples from the Saiya Shokobo complex where 253<sup>o</sup> from the stable isotope geothermometer agrees well with the fluid inclusion temperature range of 240-260<sup>o</sup>C. For the sample from Afu the sphalerite and chalcopyrite were out of equilibrium. Such disequilibrium can actually be seen in hand specimen. An early stage of ore formation produced massive twinned sphalerite which was brecciated by explosive fluid activity. The sphalerite breccia has been recemented by fluorite and quartz with chalcopyrite.

The high temperatures provided by sulphur geothermometry for the samples from the Tibchi and Kigom complexes were surprising. Fluid inclusion geothermometry undertaken in St. Andrews by Turaki (pers. comm.) indicated similar fluid inclusion homogenisation temperatures to those of the Ririwai lode. It would appear therefore that molybdenite-galena are not a good mineral pair for geothermometry in the Nigerian anorogenic province possibly because in the paragenetic sequence of ore formation, there is more of a time interval between the formation of molybdenite and galena than for sphalerite and chalcopyrite or sphalerite and galena.

## Oxygen isotopic studies

A representative suite of samples of Nigerian rocks were chosen from three complexes; the Jos Bukuru, Ririwai and Saiya Shokobo complexes. It was necessary to do this to ensure that all types of mineralisation were covered both in peralkaline and biotite granites. The number of complexes sampled however, was kept to a minimum to ensure that it was possible to compare data obtained within each complex as well as between complexes. Mineral separates were obtained from each sample and  $\delta^{18}\text{O}$  values were determined for whole rock and co-existing minerals (microcline, quartz and mica). The results are shown in Table 12.9 and Fig 12.9.

### Albite-rich granites

Samples of both albitised peralkaline and albitised biotite granites were chosen for study. The Kaffo Valley arfvedsonite albite granite from the Ririwai complex was selected as the albitised peralkaline granite since Rb/Sr isotopic data was also available on the same material. The albitite from the L13 core through the Ririwai biotite granite was chosen for albitised biotite granite, together with the Rayfield Gona granite from the Jos Bukuru complex. The effects of albitisation varied from slight (in the Rayfield Gona granite) to intense in the other two samples. The data available on these three samples that have undergone sodic metasomatism has been supplemented by data also on the Kaffo Valley arfvedsonite albite granite by Borley et al (1976).

For the biotite granites  $\delta\text{O}^{18}$  for the albitite of L13 core (113-440) has a value of 6.64 compared the Ririwai biotite granite with a whole-rock value ~ 8.3. Such a decrease can be attributed to quartz removal during extreme albitisation and feldspar enrichment. For the Rayfield Gona granite of the Jos Bukuru complex where there is only a little variation in the modal proportion of the minerals between the "unaltered" and albitised portions, there is only a small variation in the whole rock value of the albitised granite of 8.53 compared with the Jos biotite granite which has a value ~8.3.

The arfvedsonite albite granite has a  $\delta\text{O}^{18}$  of + 8.2 compared with a similar values for the neighbouring arfvedsonite granite which has a value of + 8.7. The  $\delta\text{D}$  values are however very different at  $-81 \pm 10$  for the arfvedsonite granite compared with  $-124 \pm 5$  for the albitised arfvedsonite granite. Borley et al (1986) give whole rock  $\delta^{18}\text{O}$  value of  $+ 8.1 \pm 0.2\%$  for six samples (Fig 12.9) Variations in the  $\delta^{18}\text{O}$  values of + 5.3 to + 6.4% for the amphibole and + 4.4 to + 5.5 for the aegirine sets of analyses (Fig 12.9) are considered significant.

According to Borley et al (1976), variations in the  $\delta^{18}\text{O}$  values of the amphiboles and pyroxenes could be due to crystallisation from an initially heterogeneous magma, but the data also demonstrates the possibility of compositional adjustments of the minerals and subsolidus exchange of isotopes during albitisation. This latter interpretation is favoured here on the basis of the extensive hydrothermal modifications that have been the subject of this thesis. The oxygen isotope data also show that the  $\delta^{18}\text{O}$  values for the co-existing arfvedsonite and aegirines are low compared with those reported for other amphiboles and pyroxenes and that the Px-Am values are large, negative and constant. Borley et al (1976) suggested that the low  $\delta^{18}\text{O}$  values are related to special features of crystal chemistry of the alkali amphiboles and pyroxenes which are extremely F-rich and deficient in both Si and Al. Variations in the

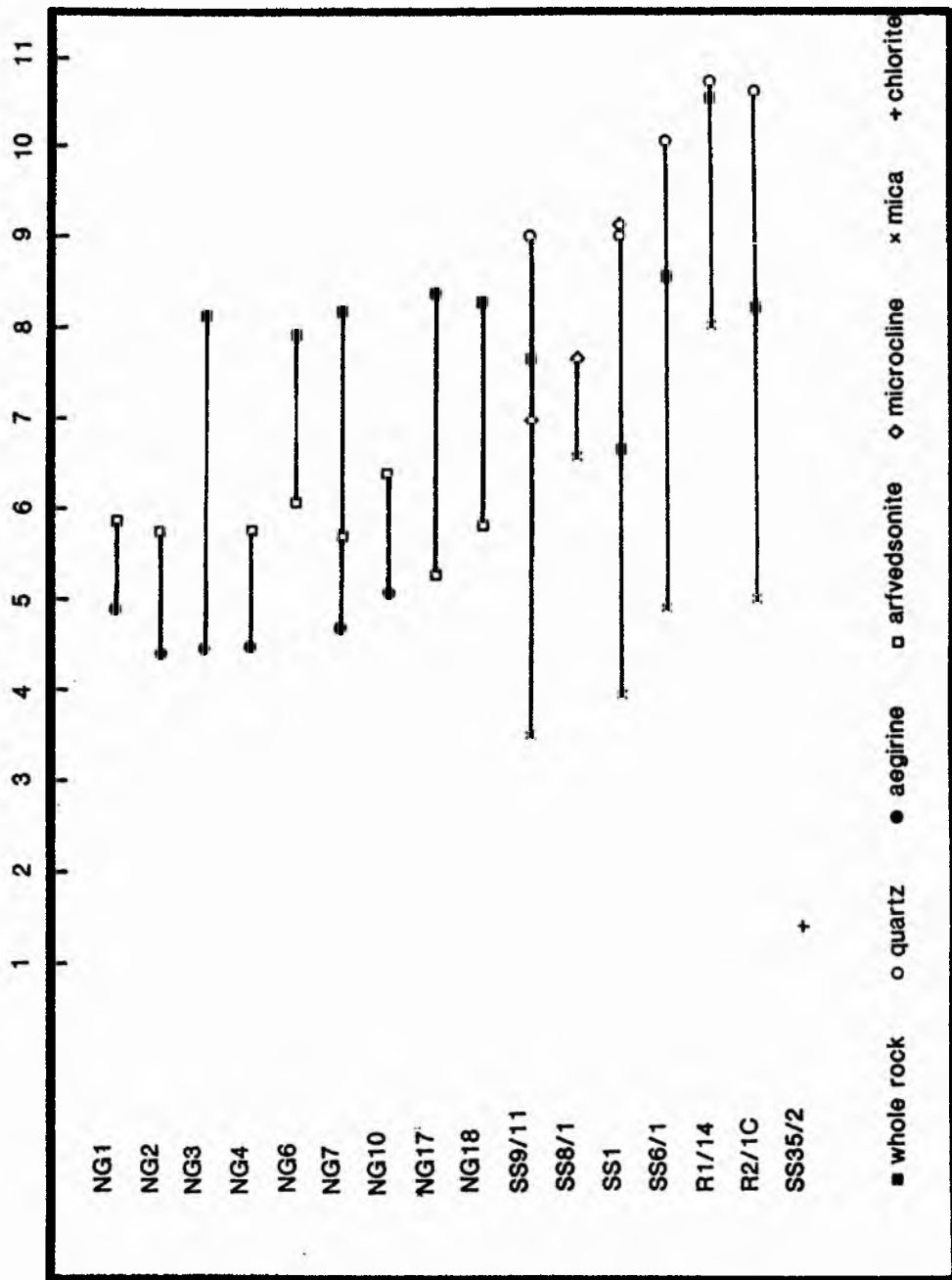


FIG 12.9 A compilation of  $\delta^{18}\text{O}$  analyses of mineral and whole rock data from hydrothermally altered samples

Samples NG1 to NG18 are of arfvedsonite albite granite from the Kaffo valley of the Ririwai Complex (from Borley et al 1976)

All other samples are described in the text

$\delta^{18}\text{O}$  values they suggest might be due to a "buffered" subsolidus exchange of isotopes during albitisation of the granite.

#### Microcline-rich rocks

Three samples containing microcline feldspar were selected for study; SS8/1 was a microclinised biotite perthite granite composed of siderophyllite mica and microcline, whilst SS9/11 is a microcline-quartz-mica pegmatite believed to have been formed during potash/acid metasomatism. In addition, SS1 is composed of a little microcline although it is dominated by mica, accompanied by quartz, siderite and molybdenite.

Table 12.9 Oxygen isotopic compositions of whole rock and mineral separates

Complex	Sample no.	Mineral	$\delta\text{D}\%$	$\delta^{18}\text{O}$
Saiya Shokobo	SS9/11	whole rock		7.62
		K feldspar		7.03
		quartz		9.02
		mica	-60	3.51
Saiya Shokobo	SS8/1	microcline		7.64
		mica		6.57
Saiya Shokobo	SS1	whole rock		6.66
		K feldspar		9.22
		quartz		9.03
		mica	-75	3.94
Saiya Shokobo	SS6/1	whole rock		8.54
		quartz		10.28
		mica	-59	4.91
Ririwai	R1/14	whole rock		9.99
		quartz		10.00
		mica	-48	8.10
Ririwai	R2/1C	whole rock		8.22
		quartz		10.70
		mica	-35	5.08

The whole-rock oxygen isotope data for these microcline-rich rocks shown in Table 12.9 and on Fig 12.9 varies between +6.6 (SS1) and +7.62% (SS9/11) values which are within the same range of the sodic metasomatised samples.

Variations in the  $\delta^{18}\text{O}$  values in both the mica and the microcline is quite wide:

mica 3.51 (SS9/11) to 6.57 (SS8/1)  
microcline 7.03 (SS9/11) to 9.22 (SS/1)

In fact for SS1, the quartz-K feldspar fractionation factor is reversed over that expected, and enrichment of K-feldspar would seem the most likely cause. In such a hydrothermal system rock-fluid isotopic equilibrium is almost certainly not attained since feldspar is known to equilibrate at a much faster rate than quartz which is slow to exchange with the fluid. Such a spread of values for these different minerals, as discussed above for the amphiboles and pyroxenes, is consistent with extensive hydrothermal modifications that occurred.

#### Acid metasomatism

Three samples were analysed for  $\delta^{18}\text{O}$  values. R1/14 and R2/1C are greisen samples from the Ririwai lode, the first from 30m depth the second from 60m depth. The mineralogy of both is dominated by quartz accompanied by siderophyllite or zinnwaldite mica together with a range of ore minerals principally cassiterite and sphalerite. Sample SS6/1 from the Saiya Shokobo complex is from greisen of similar mineralogy which is exceptionally rich in sphalerite (>10%). Whole rock  $\delta^{18}\text{O}$  values are not significantly different from other hydrothermally altered samples already described, except for R2/1C. However, as with the microcline-rich samples there is a wide variation in mica  $\delta^{18}\text{O}$  values from 4.91 to 8.10 although the quartz has a very limited range. This may be due to the fact that much of the quartz had recrystallised to a late stage within these acid assemblages.

#### Temperature determinations from co-existing mineral pairs

Using the isotopic fractionation data the temperature of formation of a mineral assemblage can be calculated from the oxygen isotope compositions of co-existing mineral pairs. The difference in  $\delta^{18}\text{O}$  between any pair of co-existing minerals is related to the temperature at which isotopic exchange took place between these minerals and the mineralising fluid. This is assuming that the water rock ratio was high in which case the isotopic composition would have remained the same and the isotopic composition of the minerals would have been temperature dependent. If the amount of fluid in contrast was small, the fluid would have rapidly been buffered by the rock and would have ceased to have an effect.

For some samples (Table 12.10) the temperatures obtained from this method are in the right order of magnitude for fluids in contact with granitic magmas. In addition, there seems good agreement between the oxygen isotopic data and the temperatures derived from homogenisation of fluid inclusions although stable isotopic temperatures seem to be consistently slightly higher than microthermometric data from fluid inclusions.

For some samples, it has been possible to determine temperatures from more than one pair of minerals within the same rock.

For SS 9/11 a quartz-microcline-mica pegmatite, there is reasonable agreement between the temperature of  $500^\circ$  from the quartz-biotite pair with the  $530^\circ$  obtained from the microcline-biotite pair (Table 12.10). The mineral pair quartz-microcline gave a lower temperature of  $420^\circ$  but this was in agreement with the temperature range from the fluid inclusion data.

Table 12.10  $\delta^{18}\text{O}$  geothermometry from co-existing mineral pairs

Sample	Mineral pair		Temp °C	Fluid inclusion Th °C
SS9/11	quartz-biotite	= 5.51	500	370-420
	k-spar-biotite	= 3.52	530	
	quartz-k-spar	= 1.99	420	
SS8/1	k-spar-biotite	= 1.07	1000	
SS1	quartz-biotite	= 5.09	530	
	k-spar-biotite	= 5.26	405	
	quartz-k-spar	= -0.19		
SS6/1	quartz-biotite	= 5.37	510	
R1/14	quartz-biotite	= 1.90	920	360-380
R2/1C	quartz-biotite	= 5.62	500	460

Another good comparison was obtained between fluid inclusion homogenisation temperatures and isotopic geothermometry for sample R2/1C. A temperature of 500 °C was calculated from the quartz-mica pair, which compares favourably with fluid inclusion data of 460 °C.

However the mineral pairs mica-microcline in SS8/1 and quartz-mica in R1/14 give spuriously high calculated temperatures indicating oxygen isotopic dis-equilibrium between the mineral pairs. Also, examination of mineral pairs shows that the quartz and feldspar of SS1 were clearly not in isotopic equilibrium (oxygen equilibrium). Where mineral pairs do not give reasonable temperatures there are several possible explanations:-

- (i) equilibrium conditions were not strictly met:
- (ii) either the minerals exchanged with the same fluid at different temperatures, or more likely, they exchanged with different fluid. Quartz is resistant to isotopic exchange at <350°C (unless it recrystallised at <350°C). K feldspar - O exchange = >+6 at < 350°C, therefore the minimum fluid composition = + 6 + + 9.22 = + 3.22
- (iii) several generations of quartz may occur in any one assemblage

(iv) Another source of uncertainty is the effect of fluid chemistry on mineral-water fractionation factors. Most investigators have assumed that the O or H isotopic fractionation factors between minerals and aqueous fluid are independent of solution chemistry. However Ohmoto (1986), quotes experimental data which suggests that a high salinity in the fluid may modify the fractionation factors by as much as 3%.

The isotope geothermometers therefore suggest that in some cases isotopic equilibrium between the minerals and the mineralising fluids appears to have been reached. However, in other samples this was obviously not the case.

#### Combined oxygen and hydrogen isotopic studies

The whole-rock oxygen isotope data for the albite-rich and microcline-rich rocks shown on Fig 12.9 varies between +6.6 and +7.62%. In contrast, the  $\delta D$  values of -60 to -75 for micas from the microcline-rich rocks are distinctly different from those of the sodic metasomatised rocks which a value of -124  $\pm$  5. The  $\delta D$  values of these microclinised-rocks are closely comparable both with the arfvedsonite granite values (-81%) and with the biotite granites (-85% ; both values for the Ririwai complex given in Sheppard 1986).

For the micas from the three greisen samples the  $\delta D$  values (Table 12.9) were within the range -35 to -59%. In addition a single value quoted for the Ririwai lode in Sheppard (1986) gave a value of -53. These are significantly higher than measured values for micas in the microcline pegmatites.

The isotopic compositions of the fluid in equilibrium with the various micas has been calculated using the method of Taylor (1974) and are presented in Tables 12.11 and 12.12.

Table 12.11 Mica-water hydrogen fluid compositions

Sample	Meas.	300°C	400°C	500°C	600°C
SS1	-75	-43	-47	-57	-60
SS6/1	-59	-27	-31	-41	-44
SS9/11	-60	-28	-32	-42	-45
R1/14	-48	-16	-20	-30	-33
R2/1C	-35	-3	-7	-17	-20

Table 12.12 Mica-water oxygen fluid compositions

Sample	Meas.	300°C	400°C	500°C	600°C
SS1	3.94	+0.94	+2.94	+4.44	+5.44
SS6/1	4.91	+1.91	+3.91	+5.51	+6.51
SS9/11	3.51	+0.51	+2.51	+4.01	+5.01
R1/14	8.10	+5.10	+7.10	+8.60	+9.60
R2/1C	5.08	+2.08	+4.08	+5.58	+6.58

In addition to the D/H data the total water content was measured on two micas:

R1/14 : 1.0 and 0.94 wt% H<sub>2</sub>O  
 SS6/1 : 1.45 wt% H<sub>2</sub>O

expressed as H<sub>2</sub>O+: wt% released above 120°C.

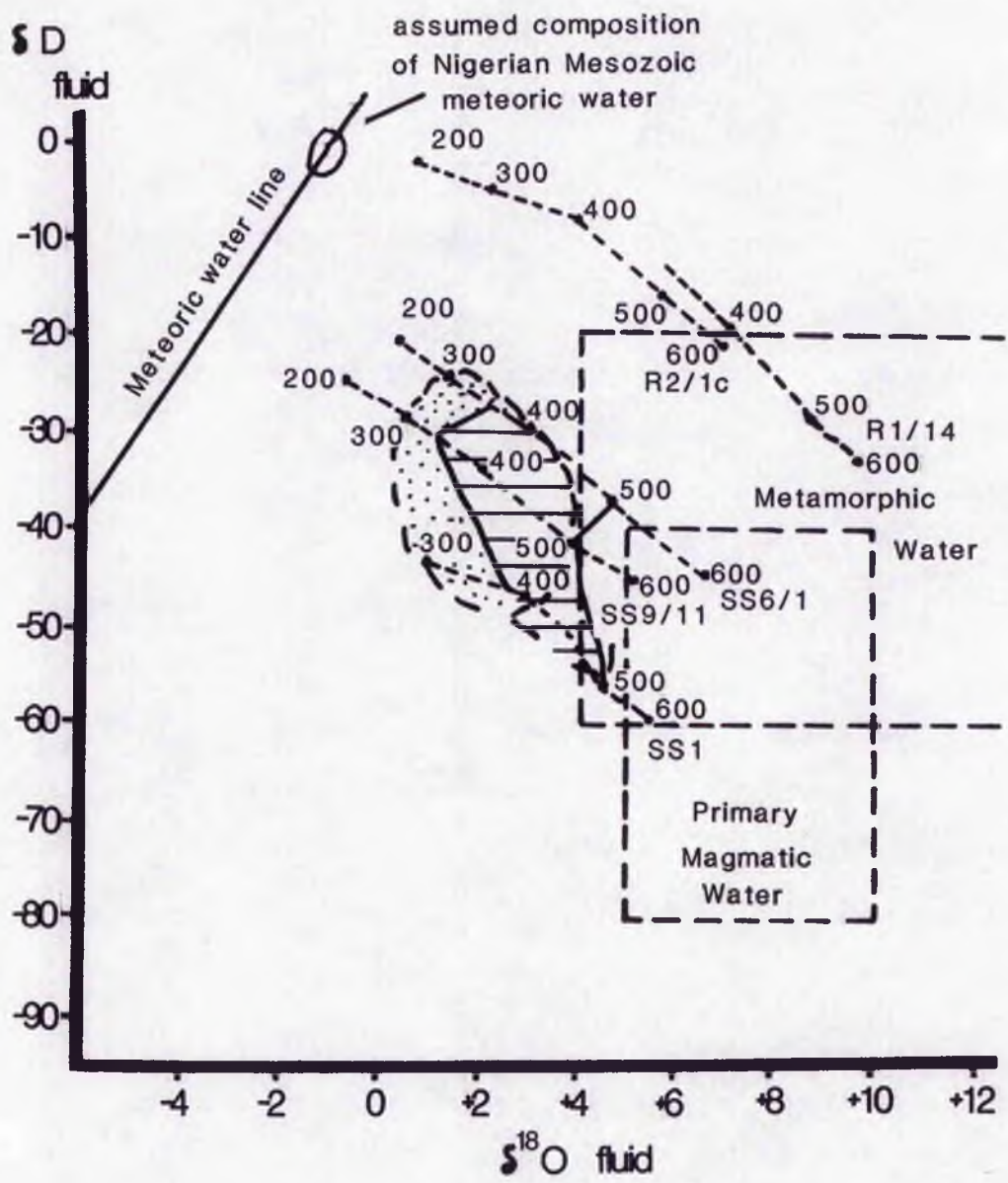
The calculated compositions for water in equilibrium with the micas shown in Tables 12.11 and 12.12 above has been plotted diagrammatically on Fig 12.10. The composition of the fluid in equilibrium with the greisen micas according to the isotopic geothermometers is shown as the shaded area and as a dotted field if homogenisation temperatures from fluid inclusions are used.

#### Discussion

Isotopically the  $\delta^{18}\text{O}$  of samples that have undergone albitisation are not very different from similar granites that have not been sodic metasomatised to any significant extent. The conclusion must be that the fluids which were responsible for sodic metasomatism did not differ much from the initial granite magma and that sodic metasomatism was probably initiated at the late-magmatic stage. Borley et al (1976) suggested a temperature of 750-700°C as the maximum temperature for the formation of the Kaffo Valley arfvedsonite albite granite with consolidation and albitisation occurring at temperatures down to 600°C. This is supported by fluid inclusion microthermometric data which would extend the lower limit.

The  $\delta\text{D}$  values of fluids associated with micas from hydrothermally altered rocks have been calculated according to the data of Taylor (1974) and were presented in Fig 12.10. This diagram could be interpreted in more than one way. Calculated  $\delta\text{D}$  values to as low as -7 for micas of the Ririwai lode appear to be consistent with a meteoric contribution to the fluids. Calculated values for the other micas suggest that the influence of meteoric water was significantly less. Calculated values for the fluid that could have been in equilibrium with the

Fig 12.10 Plot of  $\delta D$  versus  $\delta^{18}O$  for calculated isotopic compositions of the waters that would have been in equilibrium with the greisen micas. Shaded field is based on isotopic geothermometry, dotted field is based on fluid inclusion microthermometry.



biotite granites at late-magmatic temperatures is around 50 implying that for most of the micas the fluid was dominantly of magmatic origin. Fig 12.10 shows however that there is a trend away from the magmatic water compositions for the greisen micas.

- The simple explanation is that the fluid in equilibrium with the micas in the greisens was due to mixing between fluid of magmatic origin and meteoric water in equilibrium with the country rocks. However, only the micas from the Ririwai lode (sample R1/14 and R2/1C) plot directly towards the assumed meteoric water composition for Central Nigeria during the Mesozoic.

- An alternative explanation takes into account that since the fluids were repeatedly boiling that they were out of equilibrium with their host rocks. Since the fluids were boiling to temperatures as low as 300°C, this could have fractionated the isotopic compositions such that there would have been a relative increase in the lighter isotopes in the vapour phase. Both the vapour phase and the condensate would have had different isotopic characteristics. If each of these phases reacted with the host rock there would have been further isotopic exchange since both the vapour and condensate would have been out of equilibrium with the host rock and both would encourage isotopic exchange with the rocks they invaded. This has been shown to be a definite possibility from the experimental work of Cole and Ohmoto (1986).

From both the fluid inclusion homogenisation temperatures, and the isotopic geothermometers, it would seem that much of the hydrothermal alteration was high temperatures and took place at temperatures above 300°C. However, the homogenisation temperatures from fluid inclusions in granites indicates that hydrothermal alteration continued to temperatures of <200°C. This is closely comparable with data of Ferry (1985) who demonstrated a clear cut correlation between the degree of feldspar turbidity and  $\delta^{18}\text{O}$  in hydrothermally altered Skye granites. He showed that the temperature of alteration of these granites was about 350-450°C, based on various cation exchange geothermometers and phase equilibria, and that locally temperatures as low as 200°C were recorded. It must be stressed however, that in the case of the Skye granites, there was a significant proportion of meteoric water involved in the hydrothermal alteration whereas in the case of the Nigerian granites, meteoric water was only involved in late-stage alteration in veins close to the roof.

### Summary

In summary the foregoing data seems consistent with a fluid which was dominantly magmatic in origin; which derived its ore-forming constituents from the mantle (S + ?), and from the crust (Pb + ?). Near or at the level of final emplacement, the alkaline magma unmixed into two or three phases (silicate melt, saline to hypersaline fluid, CO<sub>2</sub> rich fluid). Meteoric water was only involved where substantial fracturing to the surface occurred as in the Ririwai complex. To date, no work has been undertaken on argillic alteration which may have been generated from late-stage magmatic hydrothermal fluids or from supergene weathering. The precise character of the hydrothermal fluids, their source and the effects on the evolution of the isotopic compositions of the systems must await more detailed studies. To resolve the problems more data is needed on micas of different compositions in systems where the fluids did not boil, to compare with further analyses of micas from greisens where the fluids have boiled.

## CHAPTER 13

### COMPARISONS WITH OTHER PROVINCES

#### Introduction

The Nigerian anorogenic Province has many comparisons with other Phanerozoic alkaline provinces in Africa. In particular, the similarities are most obvious for the oversaturated provinces of Sudan, Niger and elsewhere. However, despite some marked contrasts there are also comparisons to be made with undersaturated alkaline anorogenic magmatism, particularly with regard to the mineralisation of the carbonatite centres and surrounding fenitised country rocks.

Despite contrasting orogenic settings, the granites of Nigeria, Cornwall, Bolivia, S.E. Asia, Czechoslovakia and Australia are richly tin mineralised. Examination of the textural features related to such tin mineralisation suggests that the rocks have been subjected to widespread pervasive hydrothermal alteration.

In the comparative discussion which follows, the development of a hydrothermal fluid in provinces of contrasting petrology, and tin provinces of contrasting orogenic settings, is emphasised.

#### COMPARISON WITH OTHER ANOROGENIC PROVINCES

The Nigerian Province is one of many Phanerozoic anorogenic provinces on the African continent. The African Plate consists of various terranes of different Precambrian ages accreted during major orogenies. The Pan-African orogeny in late Proterozoic, played a major role in re-assembling old cratons and terranes to form the supercontinent Pangaea and its southern extremity, Gondwanaland. It was into this basement that the Phanerozoic plutonic complexes were emplaced. Since folding of any age later than Precambrian is rare in Africa and is restricted to the Atlas Mountains at the extreme north, the Cape fold belt at the southern tip of the continent and a belt on the extreme east of the Arabian peninsula, the Phanerozoic plutonism is anorogenic in nature and dominated by the formation of alkaline complexes which were often high level ring complexes (Fig.13.1).

Petrologically and geochemically the magmatism can be grouped into:-

- (i) oversaturated provinces (Nigeria, Cameroon, Sudan, Arabia);
- (ii) mixed silica saturated and undersaturated provinces (Nuanetsi, Namibia, Eastern and Western rift, Chilwa province) with strongly undersaturated provinces in Angola and Luderitz.

From the economic viewpoint both the alkaline granite complexes in the oversaturated complexes and the carbonatite centres in the undersaturated complexes are important. There are many mineralogical and geochemical parallels between such alkaline granite complexes and carbonatite centres, particularly

with the cause and effect of alkali metasomatism and especially with the abundance of rare-earth minerals, columbite, pyrochlore, zircon and complex Ti-Zr silicates and uranium/thorium abundance. In both undersaturated and oversaturated alkaline rocks a fluid phase developed during crystallisation and the resultant subsolidus reactions, geochemical variations and mineralisation depended on whether this fluid phase was retained or expelled.

#### Oversaturated complexes with granites and syenites

In Africa, dominantly oversaturated alkaline provinces like Nigeria have also been identified in Niger, Cameroon, Arabia, Sudan, Egypt and Ethiopia (Fig 13.1). These oversaturated complexes occur exclusively in Pan-African domains. As in Nigeria, in most of these oversaturated alkaline provinces the subvolcanic intrusions were overwhelmingly syenitic to granitic in composition with gabbroic rocks occupying about 5% of the total areal extent. Small proportions of basic rocks are found in Air (Niger), and to a limited extent in the Cameroon (Mboutou) where gabbros are associated with layered sequences.

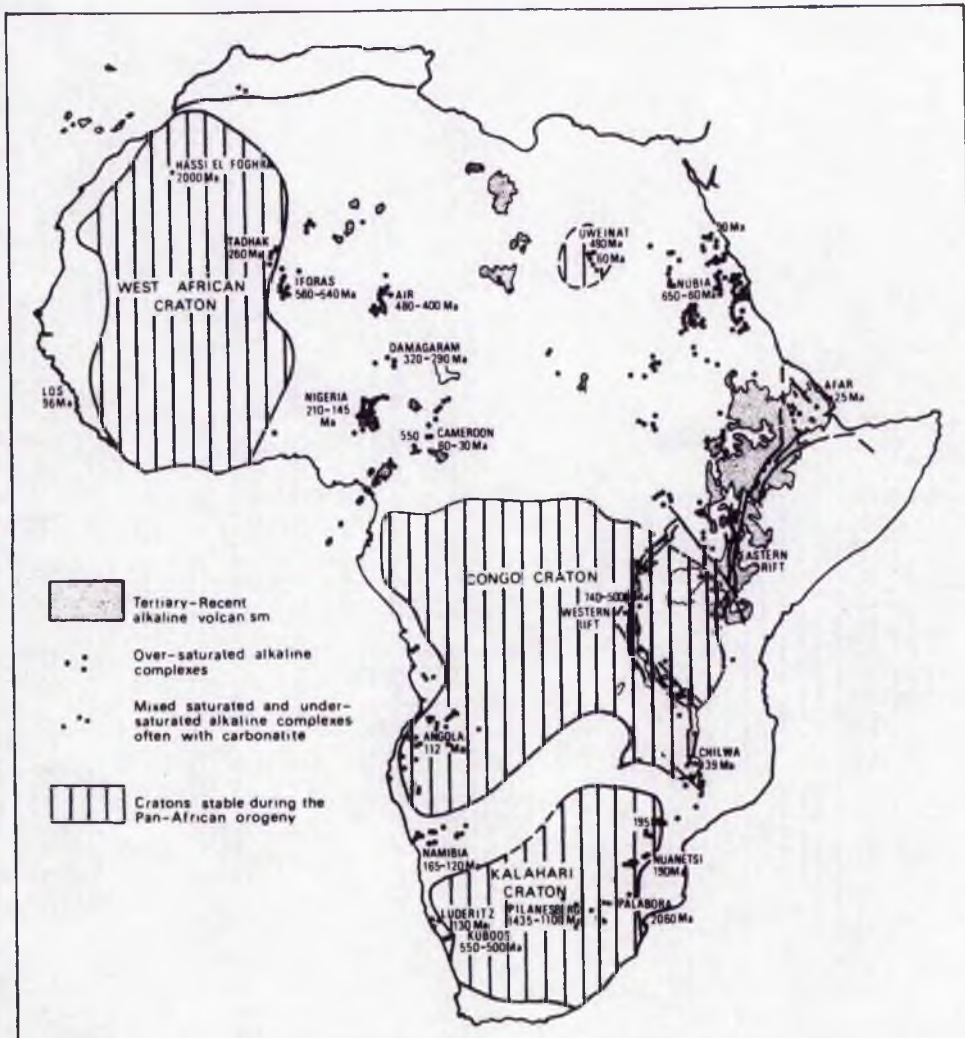
As in Nigeria, most of these oversaturated plutonic provinces are composed of chains of complexes often arranged concentrically as roots of volcanoes. In some instances the outer limits of the complexes are defined partly or completely by a ring dyke. Where the volcanic rocks have been preserved by downfaulting of the caldera the majority are dominantly rhyolitic and ignimbritic although some centres have preserved occasional successions of hawaiites, mugearites and trachytes confirming the dominantly alkaline trend from transitional ne-normative or hy-normative basalts. The subvolcanic assemblages include minor gabbros, monzogabbros, anorthosite, syenites, nordmarkites, fayalite hedenbergite granites, amphibole granites, albite rich- and albite-poor aegirine arfvedsonite granites, and biotite granites.

This anorogenic alkaline oversaturated plutonism occurred in three distinct periods; (i) end-Pan African e.g. Arabia and the Iforas province of Mali (ii) late Palaeozoic-Mesozoic e.g. Sudan, Niger and Nigeria (iii) Tertiary e.g. Cameroon.

In the Arabian Peninsula (Drysdall et al 1986) there was a substantial development of accreted terranes throughout the Late Proterozoic which can be modelled from their granite types and the basement into which they have been emplaced. Magmatism began 900-680ma ago with plutonic rocks of tonalitic and trondhjemitic affinities. In the period 680 and 660 ma ago there was a shift from arc magmatism to collision-related magmatism resulting in the formation of granodiorites and monzogranites up to 610 ma ago. The final phase of plutonism 610-510 ma resulted in the formation of widespread anorogenic peraluminous to peralkaline alkali-feldspar granites (Stoeser 1986) which have a number of features in common with the Nigerian anorogenic complexes.

A similar model can be applied to the formation of the Iforas Province in West Africa. The province is composed of nordmarkites, peralkaline and metaluminous granites and granite porphyries. Whole-rock Rb/Sr analyses have yielded Cambrian ages between 560 and 540 ma (Liegeois and Black 1983, 1984; Ba et al, 1985). Alkaline massifs of similar age have been recorded in northwest Hoggar and in southern Benin in the Pan-African belt close to the West African craton.

Fig 13.1 The distribution of the alkaline complexes in Africa  
(from Black et al 1985)



The Niger Province, has similar rock types to the Nigerian Province although the relative proportion changed with time from north to south. Thus peralkaline granites and quartz syenites predominate in the Air where they may be associated with anorthosites, leucogabbros and lenses of iron-titanium oxides often as layered, funnel-shaped intrusions (Black 1965, Black et al 1967, Husch and Moreau 1982, Leger 1985) whereas aluminous granites predominate in Nigeria. Even within Nigeria there is an overall change in lithological dominance from north to south with volcanics and peralkaline granites dominant in the north and biotite granites dominant in the south. The Niger-Nigeria Province ranges from lower Palaeozoic in Air (480-400 Ma) through Carboniferous in the Damagaram (320-290 Ma) to Mesozoic in Nigeria (215-140). During this period there was a southerly shift of centres of magmatic activity recording a period of practically continuous within-plate activity.

The Nubian Province, comprises over 130 alkaline complexes which are predominantly in Sudan but which extend into Egypt and Libya in the north and

into Ethiopia and Uganda in the southeast and south. The province includes alkali granites and syenites, rarer nepheline syenites and associated extrusive trachytes, rhyolites and ignimbrites (Vail 1985). As in the Niger-Nigeria province there was a petrological change with time. This was reflected in the degree of alkalinity and silica-saturation since the Palaeozoic complexes are generally oversaturated whereas undersaturated rocks and a carbonatite appeared in the Mesozoic (Black et al 1985). The Nubian Province comprises complexes which range in age from 650 to 25 ma, the most recent being in the Afar (Vail 1985). There were five peaks of plutonism within this period (Black et al 1985) and the time range was comparable with that of oversaturated alkaline magmatism in West Africa. However, there was no progressive change in age or distribution pattern of the episodic magmatism as in Niger-Nigeria, so that alkaline complexes of different ages occurred within the same region. The random distribution of ages of the complexes was a result of reactivation of the regions over various periods of time possibly related to the ultimate opening of the Red Sea rift system.

The Cameroon oversaturated province is dominated by a number of Tertiary alkaline granite ring complexes (Lasserre 1978) emplaced into end-Pan African basement, and orientated along the north-northeasterly Cameroon line. Some of these centres like Poli, Mayo Darle, are mineralised, while in others like Mboutou, and Goldes Velda (Jacquemin et al 1982) there are rock associations reminiscent of the Air gabbro-anorthosite-syenite association. However, in contrast to the Niger-Nigeria province there was no sequential age progression of the ring structures and there is an apparent random range in age between 60 and 30ma. The magmatism is related to north-northeasterly trending faults which are sinistral transcurrent faults which offset the Cretaceous basin and may continue eastwards into the Ngaoundere shear zone.

Some of the geochemical and petrological characteristics of these A-type granites have comparisons with other A-type provinces not only in Africa but throughout the world. They are all characteristically low in MgO and CaO and high in Na<sub>2</sub>O and K<sub>2</sub>O for given silica values. The most significant chemical feature is that slight differences in the ratio of Na+K to Al produced striking changes in the mineralogical composition of the suite of syenites and granites to give peralkaline, metaluminous and peraluminous variants. When the variation in the suite as a whole is considered, however, fractional removal of mineral phases only made a very limited contribution to the overall evolution of the magmas, and other factors must have been involved. A slight rise in Na<sub>2</sub>O occurred in some centres in Sudan (O'Halloran, 1985) from the metaluminous to alkali syenites, which can be attributed to concentrations of Na in the liquid as calcic pyroxene crystallised. The trend was limited and Na<sub>2</sub>O declined subsequently. The data for Na and K does not show the anticipated positive correlation against silica clearly, for either the peralkaline syenites or the granites. This is because subsequent hydrothermal alteration and fluid phase transfer has undoubtedly modified part of the original granite chemistry in other provinces as well as in Nigeria. These processes were responsible for an enrichment in LIL and HFS elements, particularly Nb, Sn, Hf, Zr & Ga, increases in Zn, Pb, and Y and low abundances of the transition metals V, Ni, Co and Cr. All the A-type granites are characterised by high concentrations of Sn, Be, Li, U, Zr, Nb, Th, K, Rb, Mo, Zn, F, W and by low K:Rb, Sr:Y and high Rb:Sr, and K:Ba ratios as a result of hydrothermal alteration. The trace element populations are particularly sensitive indicators of fluid reactions.

## The effect of late stage fluids

The mineralogical assemblages of many of these complexes was often the result of reactions with residual fluids. Fluids affected the late magmatic and particularly the subsolidus crystallisation history of a cooling subvolcanic pluton and to some extent the overlying volcanic pile. In the Nigerian province there were four periods of hydrothermal alteration that were important economically; sodic metasomatism (albitisation), potassic metasomatism (microclinisation), acid metasomatism (greisenisation) and silica metasomatism (silicification). Similar processes of alteration have been described in Niger (Perez 1985) Cameroon (Nguere and Norman 1985), Sudan (Almond 1967, 1977; el Samani 1985), Arabia (Jackson 1986) and Egypt (el Ramly et al 1971) although no detailed work on the sequence of alteration processes has been carried out in these provinces.

In Nigeria, on textural and field evidence the earliest process of alteration was sodic metasomatism. This alteration process occurred before jointing or faulting of the granites and therefore its effects are disseminated through a granite roof zone. The actual mineral assemblages resulting from sodic metasomatism depended on the intensity of rock-fluid interaction and on the initial mineralogy of the original rock-type. Sodic metasomatism occurred in both peralkaline and biotite granite cupolas and was economically important for the formation of the niobium-bearing ore minerals - pyrochlore and columbite - together with accessory minerals enriched in rare-earths, Th and U. Such mineralisation occurs in Saudi Arabia as well as Nigeria.

Potash metasomatism which followed sodic metasomatism in Nigeria, may also have been a disseminated process as shown in this thesis. More commonly it was restricted to localised alteration pods in the granite margins and immediately beneath the volcanic cover, or in wallrocks adjacent to major lodes. This process of alteration has not been described in detail for other provinces although the process may have occurred elsewhere but remain unrecognised. For example Almond (1967) describes feldspars that have been completely 'kaolinised' and then replaced marginally by zinnwaldite. Such kaolinisation may actually be microclinisation.

During acid metasomatism there was a progressive breakdown of 'granitic' minerals in response to changing  $K^+/H^+$  ratios in the fluid, resulting in a quartz-mica assemblage + chlorite + topaz + fluorite. This greisenisation process may have been locally pervasive within a granite roof zone as in Niger, Nigeria and Saudi Arabia or may have been concentrated along fissures and fractures in Niger, Nigeria, Cameroon, Sudan, Egypt and the Red Sea Hills. In Saudi Arabia the greisenisation process was responsible for the formation of wolframite (with scheelite) and molybdenite deposition (with powellite) together with pyrite, arsenopyrite, stannite, chalcopyrite, pyrrhotite, bismuthinite, galena, sphalerite, cassiterite, gold and argentite. In Sudan, the Saboloka complex has accessory cassiterite and wolframite, altering to haematite and manganese oxides with goethite, limonite, jarosite, molybdenite, scheelite, powellite, galena, fluorite and malachite.

The final major process of ore formation and hydrothermal alteration was silica metasomatism. Quartz may have been pervasively deposited into vugs in a cupola created by earlier alteration, or it may have replaced all earlier formed

minerals or commonly formed veinlets which are found in virtually all biotite alkali-feldspar granite masses. There was a major deposition of ores dominated by cassiterite, wolframite and sphalerite associated with quartz vein development, in the lodes of the Ririwai and Tibchi complexes of the Nigerian Province. In Saudi Arabia Jackson also records bastnaesite, zircon, uraninite and monazite associated with silicification at Jebel Hamra.

Argillic alteration, which involved the formation of clays (kaolinite and montmorillonite groups) at the expense of feldspar, is a late-stage process. It is apparent in only a few complexes in Nigeria although it is intense around some complexes in other provinces eg. Mayo Darle in Cameroon. Usually such argillic alteration is superimposed on an earlier alteration of the feldspars particularly following intense albitisation.

For Niger, the sequence of alteration stages for the Taghouaji complex is similar to that of Nigeria. Perez (1985) gives the succession as albitisation, greisenisation, then "muscovitisation", silicification and finally kaolinisation. In fact however, there is little difference between the greisenisation and "muscovitisation" except in the degree of mica readjustment to hydrothermal fluids. Although Perez states that a microclinisation process has not yet been identified, he does describe amazonite veins in the biotite granite. Since the microcline produced during hydrothermal alteration is difficult to recognise and does not have the characteristic tartan twinning it is possible that the process may have occurred, if not at Taghouaji, in some of the other Niger complexes.

In Sudan, Almond has described hydrothermal alteration and mineralisation in the Abu Dom area of the Sabaloka Complex. An early feldspar-phyric greisen - which may be equivalent to the potash metasomatism phase in West Africa, was followed and brecciated by a later greisenisation phase. This was succeeded by the emplacement and mineralisation of the stockwork quartz veins. The order of processes is similar to that in West Africa, although no albitisation process is described. Unlike many of the West African complexes however, the dominant ore mineral in the stockworks is wolframite and topaz is very scarce.

Hydrothermal alteration in the tin-mineralised Mayo Darle complex of the Cameroon line shows greisenisation, silicification, chloritisation and haematisation with zones of intense kaolinisation near the tin deposits.

#### The nature of the late-stage fluids

The PVTX nature of the fluids which were responsible for hydrothermal alteration has been monitored by a study of fluid inclusion characteristics in rocks of the Saiya Shokobo Complex in Nigeria. It has shown that at the magmatic stage the silicate melt, which was trapped as globules of silicate melt, co-existed with an immiscible saline fluid. The fluid phase itself separated into two immiscible phases possibly as a result of pressure release on eruption, and resulted in a CO<sub>2</sub>-rich gas phase and a saline fluid phase. The initial fluid was over 750°C with a salinity equivalent to >60wt % NaCl and a density as high as 1.4gm/cm<sup>3</sup>. The fluid inclusion population within the granites often do not contain melt inclusions suggesting that quartz has recrystallised at postmagmatic temperatures. The inclusions within the granites indicate a range of fluids trapped over a period when fluids cooled from >600 to <100°C.

During sodic metasomatism loss of  $\text{CO}_2$  appears to have been important for the deposition of uranium-enriched pyrochlore or thorite, and zircon which is also Hf-rich. Fluids were saline but ranged from high temperature to less than  $300^\circ\text{C}$ . Potash metasomatism covered a similar temperature range although much of the  $\text{CO}_2$  had been lost from the fluid at this stage. The process cannot have been entirely temperature dependent and the  $\text{Na}^+/\text{K}^+$  ratio in the fluid must have been largely responsible for determining which process operated. Pervasive acid metasomatism (greisenisation) resulted from fluids that were in the temperature range  $420\text{--}220^\circ\text{C}$  and which were subject to periodic boiling particularly in the temperature range  $270\text{--}380^\circ\text{C}$ . A minimum depth of 0.1km has been assessed for the pervasive acid metasomatism of the Ririwai and Saiya Shokobo complexes. Vein-controlled acid metasomatism generally took place in the temperature range  $270\text{--}380^\circ\text{C}$  from Na-Cl-F fluids that boiled as pressure was released in fissures and along incipient fractures. Major cassiterite deposition took place between  $300$  and  $380^\circ\text{C}$  in greisens often from fluids that were boiling. Silicification took place at less than  $300^\circ\text{C}$  with deposition down to less than  $70^\circ\text{C}$  from fluids that were gradually decreasing in salinity from  $\sim 10$  eq wt% NaCl to almost zero. Major sulphide deposition was in the range  $240\text{--}380^\circ\text{C}$ .

Broadly similar observations were made for Mayo Darle in Cameroon. Nguere and Norman (1985) suggest that there was a saline fluid phase in the granite during or soon after crystallisation with a salinity up to 60 eq wt% NaCl. Fluid inclusion studies on the quartz-tin veins indicate Na-Cl-F fluids at temperatures between  $200$  and  $600^\circ\text{C}$  and salinities up to 65 eq wt% NaCl which were subject to periodic boiling at temperatures above  $385^\circ\text{C}$ . Pressure fluctuations from hydrostatic to  $>$  lithostatic are indicated during mineralisation. The more extensive development of kaolinite around complexes like Mayo Darle may indicate more prolonged hydrothermal fluid circulation and the greater importance of meteoric water.

For the Jebel Eyob tungsten deposit of Sudan, el Samani (1985) has shown that the stockwork of greisen and quartz veins contain a generation of  $\text{H}_2\text{O}\text{--}\text{CO}_2$ -bearing inclusions that were trapped between  $320$  and  $340^\circ\text{C}$  at a pressure of less than 0.4kbar.

#### Mineralisation and economic aspects of the oversaturated ring complexes

As in Nigeria, over the continent of Africa as a whole, the major potential of the oversaturated complexes is for niobium, tin and tungsten mineralisation. However, apart from limited tin-tungsten mineralisation in central Sudan (Almond 1967, Vail 1978, 1979), Arabia (Jackson, 1986) and the Red Sea Hills (el Ramly et al 1971, Vail 1979) most cassiterite and wolframite production has been related to the Nigerian tin province.

The work of this thesis has shown that the mineralisation of a pluton generally occurs in the apical or marginal zones or in satellite dykes. Different styles of mineralisation tend to characterise different parts of a granite pluton (Kinnaird 1985, Jackson 1986). The styles of mineralisation which were compiled for this thesis have been widely recognised in other provinces:

- (i) pegmatitic pods in roof and marginal zones
- (ii) pervasive metasomatic disseminations in cupola zones

- (iii) stockworks and sheeted veins
- (iv) mineralised ring dykes
- (v) brecciated greisen deposits
- (vi) fissure-filling lodes
- (vii) late replacement bodies
- (viii) quartz rafts and veins
- (ix) late-stage veins of fluorite
- (x) alluvial deposits
- (xi) residual soils

No particular type of hydrothermal alteration is restricted to one particular style of mineralisation. Thus it is possible to have disseminated sodic, potassic, acid or silica metasomatism; altered ring dykes may show the effects of all the processes; pegmatitic pods may be generated at any hydrothermal alteration stage and fissure filling lodes show all types of hydrothermal alteration with earlier alteration assemblages overprinted by later ones.

#### Economic potential

The economic potential varies according to the style of mineralisation and the mineralogical association. Two distinctive mineralogical associations can be recognised in all the oversaturated provinces: a pyrochlore-columbite type with rare-earth enrichment and an oxide-sulphide assemblage with cassiterite, wolframite and sulphides.

(i) The pyrochlore/columbite association is related to sodic metasomatism of granite cupola zones. Usually such mineralisation occurs disseminated throughout a granite cupola although concentrations may occur in pegmatitic sheets and veins.

In Saudi Arabia, both pyrochlore and columbite occur together in late Pan-African alkaline anorogenic granites (610-510ma; Stoesser, 1986). Three different styles of Nb-Zr-REE mineralisation have been distinguished and summarised in Jackson (1986); disseminations in porphyritic alkali microgranite plutons and stocks such as Ghurayyah, Jabal Tawlah, and Umm al Birak; disseminations in layered aplite-pegmatite sheets in the apical or marginal zones of alkali granite porphyry plutons such as Jabal Sa'id (Habd ash Sharar pluton) and Sumr al Ishar (Habd ad Dayahin pluton); and disseminations in discordant felsic veins and pegmatites in Umm al Birak, Habd ad Dayahin, Babal Awja, Jabal Tuwalah and Jabal Kuara. The principal accessory minerals with the pyrochlore and columbite-tantalite are monazite, cassiterite, bastnaesite, synchesite, gargarinite, thorite and zircon. In addition accessory ixiolite and betafite have been recognised at Jabal Umm al Suqian (Bokhari et al 1986).

In Nigeria pyrochlore and columbite occur in different facies, pyrochlore characterises sodic metasomatised peralkaline granites whereas columbite occurs in zinnwaldite albite granites resulting from sodic metasomatism of biotite perthite granite. The pyrochlore-bearing granites occur in six localities in the Ririwai, Dutsen Wai, Shere, Buji, Ropp and Kigom Complexes. Pyrochlore is accompanied by Th-rich monazite, cloudy prisms of uranium-, thorium- and hafnium-enriched zircon, amblygonite, stellate clusters of astrophyllite, cryolite, thomsenolite, villiaumite and sometimes by narsarsukite and chevkinite. Columbite occurs in varying quantities in all complexes where fine-grained granites occur however, the highest primary enrichment occurs in localised parts of the Jos Bukuru complex and the Odegi area of the Afu complex. There is an associated substantial enrichment in heavy rare-earth elements and also uranium in the ores, particularly in the thorite, xenotime, monazite and zircon.

In Niger, a similar mineralogy to the albitised peralkaline granites of Nigeria has been noted by Perez (1985). Pyrochlore and columbite also occur separately in different facies, with pyrochlore in peralkaline granites and columbite in peraluminous granites. In the peralkaline granite, pyrochlore is accompanied by bastnaesite-synchesite, zircon, monazite, apatite, chevkinite, wiikite, Fe-, Ca- and REE-silicates, sphene rich in niobium and/or rare earths, oxy-fluorides of titanium and rare-earths and more rarely, fergusonite, fersmite, niobotitanates, xenotime, fluorite, and fluocerite in the Taghouaji complex. The reported uranium mineralisation at Bilet and Goundai (Moreau pers. comm) may belong to this mineral association. In the biotite granites disseminated columbite is accompanied by thorite, zircon, anatase, fluorite, fluocerite, topaz and more rarely by xenotime, monazite, ilmenite, haematite, magnetite, iron-titanium oxides, cheralite, wikiite, niobo-titanates and bastnaesite.

(ii) The oxide-sulphide assemblage of ores is related to potassic, acid and silica metasomatism and occurs in Niger, Cameroon, Sudan and Saudi Arabia as well as in Nigeria. It is a later mineral association than the previous rare-earth pyrochlore-columbite assemblage. In some provinces cassiterite is the dominant ore of this type, in others cassiterite is subordinate to wolframite. In some localities sulphides, such as sphalerite or galena, are the major ore mineral and this is especially the case in late-stage veins. The mineralisation type occurs in a wider style of deposits than the earlier type and whilst minerals of the association may be disseminated in granite cupola zones they may also occur in sheeted veins, stockworks, replacement bodies in brecciated deposits and late-stage veins.

In Niger cassiterite is disseminated in biotite granites at Tin Tajet, Chiriet, Agalak and Bagrezan. The most important mineralisation however, occurs in the El Meki, Guissat and Taghouadji complexes. In these complexes, in addition to disseminated cassiterite in the biotite granite, there are cassiterite-bearing greisens with wolframite, columbite, chalcopyrite and more rarely beryl, small veins of galena with or without a gangue mineral, veins of quartz with wolframite predominating and accompanied by cassiterite and chalcopyrite and late-stage veins of fluorite + barytes. Small veinlets carrying sphalerite and chalcopyrite occur in the volcanics. In the Taghouaji complex the greisens veins with cassiterite, also contain  $TiO_2$  minerals, zircon, columbite, sphalerite, pyrite and pyrrhotite; and the quartz veins contain cassiterite,

wolframite, pyrrhotite, fluorite, beryl, pyrite, sphalerite, molybdenite, arsenopyrite, galena and native bismuth. The late-stage barytes veins contain pods of fluorite, galena and beryl (Perez, 1985).

In Cameroon, the Mayo Darle complex of the Cameroon line consists of rhyolitic volcanics with clasts of benmoreite, granite porphyry, quartz-bearing syenite, biotite and riebeckite granites. All the mineralisation occurs in biotite granite and most occurs in conjugate fractures. Tin mineralisation occurs in a stockwork of veinlets 2.3km<sup>2</sup> in areal extent with grades of 0.3% Sn. There are vertical and horizontal lode veins with 2 to 20% SnO<sub>2</sub>, which occur near several highly silicified breccia pipes which themselves are barren. The greisen veins consist of quartz and zinnwaldite with accessory topaz and cassiterite.

In Sudan a wolframite- and cassiterite-bearing stockwork has been described from Abu Dom, in the Saboloka complex, 88km north of Khartoum (Almond 1966). The mineralised stockwork centres around a small lens-shaped mass of greisen 300m long, which lies on the contact of a porphyritic microgranite ring-dyke. Almond believes that the hydrothermal fluids have originated from a nearby mass of biotite-muscovite granite. The veins forming the stockwork are commonly less than 5cm wide and are composed largely of translucent white quartz with translucent to transparent quartz lining the numerous drusy cavities. These contain wolframite which has oxidised at the surface to form a mixture of manganese and iron oxides and cassiterite which is much sparser and more patchily distributed. These are accompanied by goethite, limonite, jarosite, powellite, galena, fluorite, molybdenite, scheelite, calcite and malachite in approximate order of abundance. The greisen lens in the centre of the stockwork is composed of quartz-zinnwaldite with sparse accessory magnetite, haematite, cassiterite, zircon and rare topaz. The greisen contains numerous miarolitic cavities, up to 10cm in diameter, lined with quartz and/or cassiterite.

In Saudi Arabia, in addition to the polymetallic rare-earth pyrochlore-columbite mineralisation in the alkali granites described above, vein or pegmatite deposits of fluorite are also commonly associated with alkali granites for example at Habd ad Dayahin, Jabal Habd ash Sharar, Jabal at Tuwalah and Umm al Birak. Galena-bearing veins also occur at Jabal Habd ad Dayahin and Jabal Habd ash Sharar. Elsewhere in Saudi Arabia there are polymetallic veins, stockworks and replacement bodies with deposits of Ag, As, Au, Be, Bi, Cu, F, Fe, Mo, Pb, Sn, Te, Th, U, W, Zn minerals. However these occur in Ca granites, granodiorites, tonalites and diorites which belong to the period from 900-610 ma.

In Nigeria, the cassiterite-sulphide assemblage of ores can be found in any of the styles of mineralisation listed above, although wolframite and sulphides do not survive in alluvial deposits. Thus cassiterite occurs as an accessory disseminated in many granites that have been affected by hydrothermal alteration throughout the Nigerian province. The values in a particular granite may vary from zero to over 400ppm SnO<sub>2</sub>. Disseminated cassiterite introduced during potassic and acid metasomatism is accompanied by monazite, zircon, cryolite, rutile, ilmenite, columbite, genthelvite or beryl, molybdenite, sphalerite and chalcopyrite. In addition to disseminated mineralisation, abundant cassiterite, varying from small to large anhedral or euhedral crystals, which may exceed 1cm in size, are found in mineralised ring dykes, veins, sheeted veins, replacement bodies, and stockworks throughout the Nigerian Province. In greisen veins the

accessory assemblage listed above is supplemented by stannite, pyrite, arsenopyrite, siderite, bismuth minerals, marcasite, galena, cubanite, pyrrhotite, powellite, greenockite and mackinawite. Silica metasomatism resulted in quartz veins with cassiterite, wolframite, sphalerite, native bismuth, bismuthinite, bismutite, haematite, chalcocite, covellite and tetrahedrite. Late fluorite-rich veins carry a mixed assemblage of the same oxide and sulphide ores dominated by cassiterite, wolframite, sphalerite and chalcopyrite. Supergene alteration of the primary ores has led to the secondary formation of smithsonite, cerussite and pyromorphite, bornite, azurite, malachite, chalcantinite, pyrolusite, haematite, limonite and jarosite.

In all these areas described however, the primary deposits are rarely exploited since primary enrichment is insufficient to be of more than local economic interest at the moment. It is the alluvial concentrations which have attracted exploitation. During the partial unroofing of mineralised granite cupolas due to uplift and erosion the ore minerals of both the two mineralogical associations described above are removed only to be redeposited in eluvial and alluvial deposits. The richest alluvial concentrations occur within the vicinity of granite cupolas that have only undergone shallow erosion. Alluvial deposits similar to those described in Part I of this thesis are not extensively developed in other provinces.

In Niger, alluvial cassiterite has been worked sporadically since 1948 at Taghouaji and El Meki. The tenor of alluvial tin in cassiterite-rich placer pockets has reached  $20 \text{ kg/m}^3$  but is generally less than  $3\text{--}4 \text{ kg/m}^3$ . Where small placer deposits do occur exploitation has been limited since they can only be worked on a seasonal basis due to lack of water for most of the year. More recently in 1963, cassiterite was discovered in the Agalak and Tainok complexes.

#### MIXED ALKALINE PROVINCES

In some provinces oversaturated complexes are accompanied by undersaturated alkaline complexes within the same province and within the same chronostratigraphic time span. The majority of the mixed saturated and undersaturated complexes in Africa are found south of the Sahara (Fig 13.1), either associated with magmatism along major lineaments activated during the fragmentation of Gondwanaland, or linked to the evolution of rifting in Eastern and Central Africa. Such mixed magmatism characterises Angola, Namibia, the Nuanetsi Province, the Eastern and Western Rift and the Chilwa Province.

In some provinces there is almost no oversaturated magmatism. Such undersaturated complexes associated with carbonatites (and kimberlites) of comparable age are confined to continental margin lineaments in south western Africa e.g. the Angolan Province and the Luderitz province of south west Africa and to a few locations in northern Africa, including the Tamdhak province on the edge of the West African craton and the Tamazert Province of Morocco.

Both the oversaturated and the undersaturated complexes in mixed provinces demonstrate similar structural features to the granitic anorogenic centres just described. Along the major rift zones all levels of erosion of undersaturated complexes can be studied from the alkalic volcanoes (e.g. Oldoinyo Lengai) to the partially eroded centres (eg Napak in Uganda) to the well exposed root zones at Chilwa Island and elsewhere in Malawi (Woolley and Garson 1970).

Carbonatite and undersaturated alkaline ring complexes in Africa belong to several periods of magmatism. The oldest Phanerozoic complexes were intruded in late Precambrian following Pan-African tectonism, controlled by major lineaments. During the early Phanerozoic and particularly following the Mesozoic continental fragmentation and separation of Africa from South America some of these lineaments were reactivated and new rift zones developed.

Along the continental margin of the western edge of Africa there are a series of northeast-southwest lineaments which may continue into oceanic transform systems (Sykes 1978). Marsh (1973) proposed that the southwest African and south American alkaline igneous provinces can be correlated with the initial break-up of Gondwanaland. This proposal was based on the fact that the lineaments lie on small circles centred on a Cretaceous pole of rotation which gave rise to the transform fault systems defined by Francheteau and Le Pichon (1972). An example of one of these lineament systems is the Namibian Province of Jurassic to Cretaceous age which spans a not dissimilar age range to the oversaturated complexes of Nigeria.

The Namibian Province (190-120 ma) comprises complexes aligned along a northeast trending lineament coinciding with the axis of the central zone of the Damaran orogenic belt of late Pan-African age. The separation of southern Africa from South America resulted in the reactivation of pre-existing northeast trending lineaments with the formation of incipient graben. These tectonic disturbances appear to be important not only for the emplacement of anorogenic complexes but also because they have provided active channels for metasomatic mineralising fluids (Pirajno and Jacob 1987). The ring complexes have been grouped by Prins (1978) into:

- (i) granitic types (Brandberg, Erongo, Gross and Klein Spitzkoppe)
- (ii) differentiated basic complexes (Cape Cross, Doros, Messum and Okonjeje)
- (iii) peralkaline complexes
- (iv) carbonatite complexes.

The oversaturated complexes occur towards the western coast in a zone characterised by abundant Pan-African granites, whilst the more undersaturated alkaline centres developed up to 100 km inland. Similar associations are also noted in the Angolan province and the Luderitz province but the proportions of oversaturated alkaline complexes is extremely limited. Nevertheless the majority of the igneous complexes near the Atlantic coast of southwestern Africa show age ranges consistent with the sequential opening of the south Atlantic. Thus the ring complex provinces of Angola, Namibia and Luderitz — all lie on narrow zones extending from the coast for several hundred kilometres inland. Their development, distribution and petrographic features differ from the complexes associated with rifting. The compositional variation is different for each lineament array in the proportion of oversaturated to undersaturated complexes, although kimberlites and carbonatites occur in each zone thus increasing the economic potential of the region. Similar associations are recorded along the major northwest-southeast lineaments in South America.

In contrast to the continental margin magmatism linked to transform systems, magmatism within the continental African plate is concentrated along zones of rifting. The orientation of these rift systems were themselves controlled by ancient structures within the Mozambique and Limpopo fold belts and lineaments within the craton. The alkaline magmatism predates the basaltic and related

lavas associated with the evolution of rift valleys from Cretaceous times onwards.

#### Mineralisation and Economic aspects of Oversaturated Ring Complexes in mixed provinces

Inevitably the granitic/syenitic complexes in mixed provinces show many of the features of the oversaturated provinces already described. The oversaturated complexes in mixed provinces tend to be small in size. Typical examples are Biega and Kahuzi, the only two oversaturated complexes in the western rift. They are adjacent complexes which lie to the southwest of Lake Kivu. Both complexes are small and consist of rhyolite and trachyte volcanics with subvolcanic granites and syenites.

In Namibia, the oversaturated complexes occur towards the western coast in a zone characterised by abundant Pan-African granites. The influence of the continental collision orogeny around 540-450 ma producing S-type granites with their attendant Sn-W mineralisation has provided a rich crustal source for rejuvenation during the fragmentation of Gondwanaland in the Mesozoic. Some of the mineralisation features recorded in Namibia by Piranjo and Jacob (1987) suggest that there has been reactivation along crustal lineaments generated during the opening of the South Atlantic. Not only has there been renewed fluid circulation within the S-type granites but there were new sources of mineralising fluids from the array of alkaline granite and carbonatite centres dated between 135 and 125 MA ago. An example of the multiplicity of mineralisation sequences has been recorded in the Brandberg region. Several processes of hydrothermal alteration have been described for this area, one of which is tourmalinisation of the metasedimentary country rocks surrounding the Brandberg massif. Such a process of alteration around the granitic margins has not been identified in other oversaturated anorogenic ring complexes in Niger, Nigeria, Cameroon, or Sudan. Tourmalinisation however is a common process in late-orogenic calc-alkaline leucogranites and it may be that part of the mineralisation in Namibia attributed to post-orogenic complexes is a reactivation phenomena in Cretaceous times.

In Namibia, both disseminated and vein-controlled mineralisation are found in granite and microgranitic complexes and also veins are found in the country rock beyond complexes and above what may be hidden cupola zones at depth. the following styles of mineralisation have been recognised:-

(i) pegmatitic pods and zoned or unzoned sheets with columbite-tantalite, beryl, pollucite, lepidolite, petalite, feldspars and micas and sometimes uranium in zoned pegmatites.

(ii) pervasive metasomatic disseminated mineralisation in cupola zones of cassiterite and rarely pyrochlore

(iii) sheeted veins and stockworks with wolframite and cassiterite

(iv) greisen veins and irregular replacement bodies with wolframite and cassiterite

(v) breccia pipes with cassiterite, topaz, beryl and tourmaline

(vi) quartz veins and stringers with cassiterite, wolframite, chalcopyrite, pyrite etc.

(vii) skarn mineralisation with cassiterite and Ag, where granite has intruded marbles

(viii) alluvial deposits of cassiterite, gold and other ores including around the Biega and Kahuzi complexes.

In the Brandberg massif von Knorring et al., (1985) records the occurrence of pyrochlore in a light grey, riebeckite-bearing granite. The uraniferous pyrochlore forms yellow, glassy grains associated with aegirine rosettes and riebeckite partly replaced by astrophyllite. There are also pegmatitic margins with larger amounts of pyrochlore, zircon, and additional monazite and fluorite.

The Sn, Sn-W and W deposits, can be geographically grouped into three major clusters or belts (Pirajno and Jacob 1987) and in almost all cases the mineralisation is associated with greisenisation and albitisation.

The mineralisation is characterised by a number of Sn-W, and Sn (+ minor Ag and base metals) hydrothermal deposits in quartz vein systems and Fe-rich replacement bodies. Sn-W and sulphide mineralisation is predominantly hosted in quartz veins forming a sheeted and anastomosing system. There were several phases of hydrothermal alteration and mineralisation. An early greisen stage with quartz + muscovite + cassiterite + wolframite, was followed by quartz and sericite + cassiterite, + fluorite; haematite + cassiterite + sulphides + graphite. An important feature at Brandberg West is the presence of a quartz-albitite plug which intruded the schist post-tectonically 2km northwest of the pit. The albitite has abundant carbonate-filledmiarolitic cavities indicating a high CO<sub>2</sub> activity similar to that observed in Nigerian albitised rocks.

- The central group comprises the northeast trending Strathmore-Uis belt located in a regional graben structure, and the east-west trending Neneis-Kohero belt, both containing Sn + Ta bearing syn to post-tectonic pegmatites. The Uis tin mine exploits some of the largest pegmatites in the belt which range in width up to 130m and in length up to 1500m. They are lenticular or sigmoidal in shape and consist of albite, microcline, quartz and muscovite with topaz, garnet, tourmaline, apatite, amblygonite, columbite, tantalite, lepidolite etc. The tin-bearing pegmatites show varying degrees of albitisation and greisenisation with late-stage chlorite and epidote alteration locally. Cassiterite is erratically distributed but abundant in the greisenised zones. These pegmatites are very similar to the pegmatites of central Nigeria.

-The southern group of the Erongo-Karibib area, includes a number of tungsten dominated greisens, and Sn + Ta + W in zoned pegmatites which intrude metasedimentary rocks. The pegmatites also contain Li, Be, Cs and Nb-Ta bearing minerals. The Spitzkoppe pegmatites contain topaz, beryl, aquamarine, amazonite, smoky quartz and fluorite and a zone of sulphides with arsenopyrite, covellite and chalcocite has also been recorded (Pirajno and Jacob 1987). The greisen deposits of this group are spatially and genetically related to the Erongo granite (Pirajno and Jacob 1987). The Kranzberg mine to the northeast of the Erongo complex was a major producer of tungsten metal until 1979 when it closed

due to falling metal prices. The mineralisation occurs in irregular greisen replacement bodies, veins and breccia pipes consisting of an assemblage of quartz, topaz, muscovite, fluorite, tourmaline, sericite, clay minerals and haematite. The ore minerals are dominated by ferberite with chalcopyrite, pyrite, arsenopyrite, native bismuth, molybdenite and scheelite as an alteration product of the wolframite. (Schlogl 1984). Three stages of hydrothermal alteration are described by Pirajno and Jacob (1987): an early phase of greisenisation followed by sericitisation with major mineralisation and by later pulses of haematite with wolframite deposition.

#### Mineralisation and Economic aspects of Undersaturated Ring Complexes in mixed provinces

Mineralisation associated with carbonatites has many features that are similar to the oversaturated alkaline granites especially with concentrations of niobium, rare earths and fluorine. However economic elements such as Li, Be, Y, Sn, Ta, and W are rare or virtually absent in calcic carbonatites, but are found in the associated syenites and fenites (Vartiainen and Woolley, 1976)

Both disseminated and vein-controlled mineralisation are found in many carbonatite centres. The hydrothermal alteration has not only affected the carbonatitic centres, as in the oversaturated complexes, but has also intensely altered the host rocks enclosing the complexes in some localities.

#### Summary comparisons between the oversaturated and undersaturated mineralisation:-

(i) similarities in processes of sodic and potassic metasomatism from fluids which must have been similar and which in many cases deposited the same spectrum of elements.

(ii) similarities in styles of mineralisation. In both oversaturated and undersaturated complexes there are: pegmatitic pods and lenses of alkali feldspar, with Nb minerals, uraninite, and thorite; disseminated mineralisation with Nb minerals, U-, Th- and REE-enriched minerals; stockworks, replacement veins and fissure-filling veins; vein controlled mineralisation; late-stage replacement bodies.

(iii) similarities of two distinct ore associations: apatite-magnetite-pyrochlore and rare-earth types in the carbonatites compared with a pyrochlore-columbite and an oxide-sulphide type in the granitic complexes.

(iv) similarities of mineral assemblages: in Table 13.1, both the magnetite-apatite and the rare-earth associations contain minerals that are generated during the sodic and potassic metasomatism in oversaturated complexes. There is a further correlation between late-stage mineral assemblages in carbonatites and acid metasomatised mineral assemblages in oversaturated centres. In simplistic terms there is a pyrochlore-columbite-RRE association and an oxide-sulphide assemblage in both groups.

Fig 13.1 Ore parageneses in carbonatites. There are two major periods of ore formation, an early magnetite-apatite type and a later type with rare-earths and strontianite. The late-stage mineralisation is volumetrically unimportant and economically insignificant.

magnetite-apatite type	Rare earth type	late-stage type
apatite magnetite pyrochlore fermite columbite pandaite luoshite zircon baddelyite aeschynite zircon	bastnaesite synchesite monazite strontianite goyazite barytes pyrite pyrrhotite sphalerite florencite fluorite tiO <sub>2</sub> minerals galena cordylite	barytes fluorite pyrolusite limonite pyrite chalcopryrite sphalerite

(v) similarity of ore paragenetic sequence from oxides to sulphides (albeit sulphides are much rarer in the undersaturated complexes than in oversaturated alkaline magmatism)

(vi) Elements which showed economic concentrations in the oversaturated spectrum such as Li, Be, Y, Sn, Ta and W are rare or virtually absent in calcic carbonatites, but are found in associated syenites and fenites (Vartiainen and Woolley 1976).

(vii) similarity of enrichments in F and Cl

(viii) economic importance of residual/alluvial deposits

(ix) possibly similar mantle source regions with varying extents of crustal contamination.

Summary contrasts between the oversaturated and undersaturated mineralisation:-

(i) the fundamental difference in bulk chemical compositions of the oversaturated and undersaturated complexes.

(ii) the lack in the carbonatite centres of an alteration process directly comparable with the acid metasomatism (greisenisation) of the granitic complexes.

(iii) enrichments in elements such as Ba and Sr in the undersaturated complexes in contrast to the oversaturated complexes where these elements are depleted.

(iv) the contrasting composition of the phosphates which are dominantly apatite in the undersaturated complexes and monazite/xenotime/amblygonite in the oversaturated provinces

(v) contrasting composition of pyrochlore; in the undersaturated rocks it is variable in composition and Ba-rich whilst in the oversaturated alkaline rocks pyrochlore has a relatively constant composition and is Ba-poor.

(vi) the lack of magnetite concentrations in oversaturated complexes

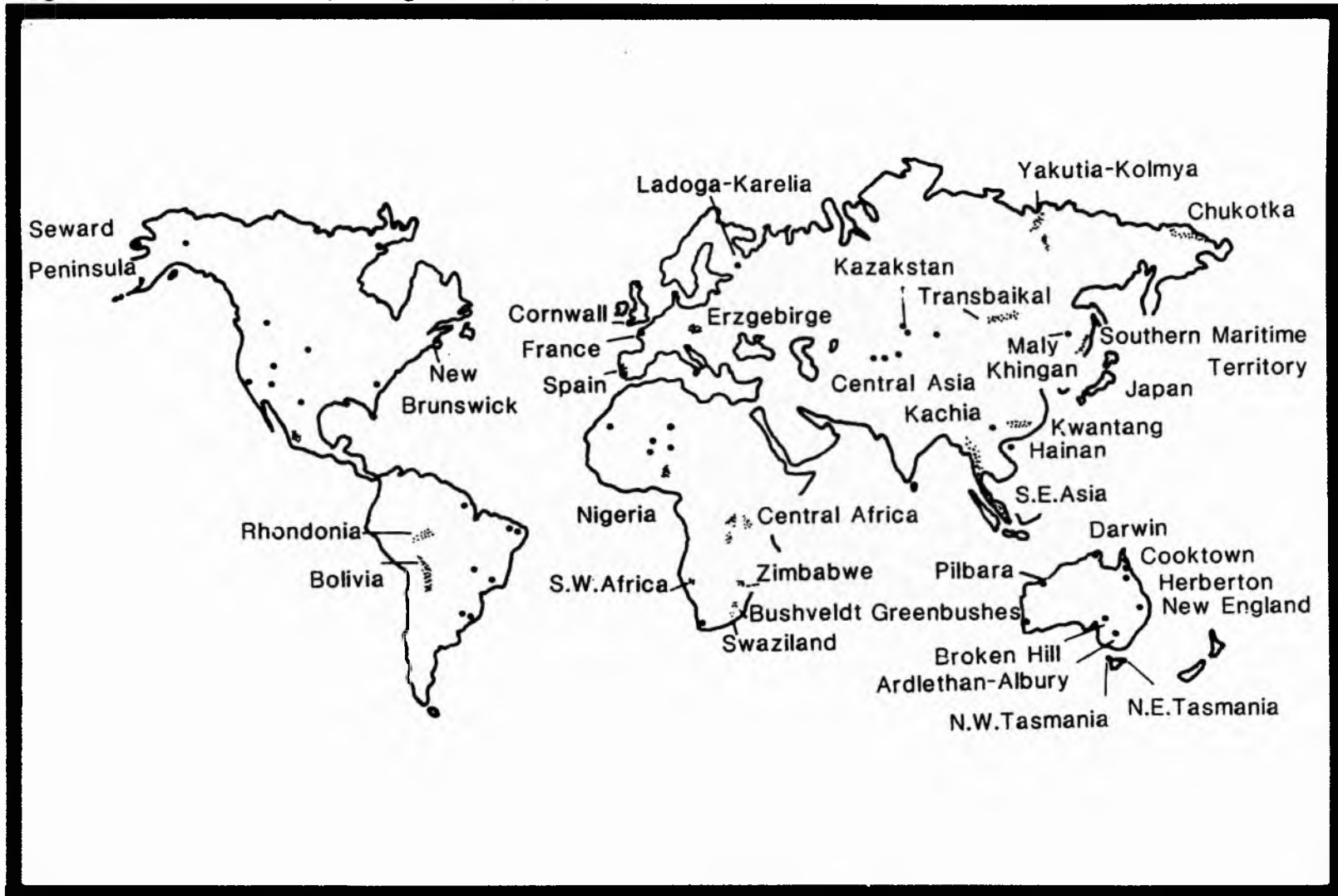
(vii) the paucity of sulphides in undersaturated complexes

Whilst there are obviously comparisons between Nigeria and many other A-type provinces in terms of styles of mineralisation, the occurrence of the same assemblages of ore minerals etc. related to similar sequences of hydrothermal alteration, there is nowhere in Africa that has so far been described, to suggest mineralisation to the same extent as in Nigeria. Such comparisons are much more common with tin provinces related to orogenic granites.

#### TIN PROVINCES COMPARED

There are 40-50 provinces that can be identified in the world (Fig 13.2) and

Fig 13.2 Location map of global tin provinces



only a small number of these are economically important. Excluding the Sino-Soviet block, tin production is dominated by five countries which account for 83% of world production. Malaysia produces approximately 40%, Bolivia 15%, Indonesia 12%, Thailand 11%, Australia 6%, Nigeria 1% and Zaire 1% with the remainder from a variety of small sources.

What is a striking fact is the fact that most tin mineralisation is post-Precambrian and confined to certain well-marked eras. Whilst tin concentrations occur ranging in age from Archaen to Tertiary 63% are associated with Mesozoic granites, 18% with Hercynian granites 7% with Caledonian granites and only 3% with Precambrian granites and pegmatites. In some of provinces tin of more than one age occurs. Thus in Nigeria tin can be found in Palaeozoic pegmatites cutting a polymetamorphic terrain and can be found in association with Mesozoic granites in ring complexes. In the Erzgebirge of East Germany, Lower Palaeozoic or Precambrian stratiform tin deposits, probably of volcanic exhalative origin occur together with deposits associated with Hercynian granites. Clearly it is possible that these granites represent anatectic material from the Lower Palaeozoic or Precambrian and that some of the stratiform tin was remobilised when the granitic magmas were formed by partial melting.

The big tin-tungsten provinces of the world appear to be associated with subduction zones, both ocean-continent (eg. the Andes) and continent-continent collision zones (eg Cornwall). According to Lameyre and Bowden, the different plate settings are characterised by granitoids of distinctive chemical characteristics which can be discriminated on the Streckeisen QAP diagram.

In addition to different plate settings for tin deposits they also occur related to granitoids that have been emplaced at different structural levels within the crust. Tin bearing rocks can be divided into :-

- (i) volcanic/subvolcanic - e.g. Mexico
- (ii) subvolcanic - e.g. Bolivia
- (iii) deep subvolcanic to high plutonic e.g. N.W. Tasmania, Herberton, New England, Cornwall.
- (iv) plutonic - N.E. Tasmania

Because even in plutonic intrusions there are often cusps of granite with subvolcanic characteristics, the Nigerian tin province has many features in common with granitoids of different depths of emplacement. In an attempt to highlight the comparisons and contrast between primary tin provinces, selected areas have been chosen from different plate settings and from different structural levels. The major features of these are described and then contrasted with the Nigeria Province.

- (i) Mexico - volcanic to subvolcanic

Lava flows, tuffs and volcanic breccias of andesites, rhyolites, dacites and latites are associated with minor intrusives dominated by sheets and dykes and rarer small plutons. Tin mineralisation occurs in small, fissure-filling veins and veinlets and occasional pipes within the volcanic sequence from fluids that were at temperatures of less than 150°C (Ypma and Simons 1969) and which also caused propylitic alteration.

(ii) Bolivia - subvolcanic

This tin province is related to a destructive plate margin between the South American and the Pacific Plate. The province contains the largest known reserves of tin outside southeast Asia. The Bolivian tinfield extends along the Andean ranges, east of the high plateau of the Altiplano, from northeast of Lake Titicaca to the Argentine border.

South of Oruro there is a tin-silver association spatially related to high level subvolcanic intrusions. At some of these volcanic centres, both the intrusives and the coeval volcanics are preserved, at others erosion has removed the volcanics completely leaving only the intrusives. This is the case at Llallagua, the world's largest tin mine working primary tin deposits. This mine is estimated to have produced over 500,000 tonnes of tin since the beginning of this century. The mine occurs in the Salvadora Stock which occupies a volcanic neck cutting the core of an anticline in Palaeozoic rocks. The stock is funnel-shaped and is made up of xenolithic and highly brecciated porphyry. The original porphyritic texture and rock composition have been almost totally overprinted by hydrothermal alteration. The ubiquitous brecciation is important because it has produced an increased permeability of the stock which has facilitated fluid movement and has given rise to a disseminated mineralisation. This dispersed mineralisation is of high enough grade to enable bulk whole-rock mining on the scale of a porphyry copper deposit. Hydrothermal alteration has produced a host rock consisting of quartz, tourmaline and sericite. There is a network of veins in and around the stock, with individual veins varying up to 1.8m width and averaging about 0.6m. The first stage of mineralisation involved the formation of quartz with bismuthinite and cassiterite. Wolframite and tourmaline also belong to this early stage. The oxide phase of mineralisation was followed by a sulphide phase principally of pyrrhotite and franckeite, the pyrrhotite being later replaced by pyrite, marcasite and siderite. Arsenopyrite, sphalerite, stannite and rare chalcopyrite were also formed (Evans 1980). Fluid inclusion work by Grant et al (1977) has shown that the pervasive alteration and vein growth, including cassiterite deposition, took place at temperatures from 400-350° dropping to 300°C and lower during sulphide deposition.

Recent isotopic work on Bolivian deposits suggests that the source region for the peraluminous magmas was upper amphibolite facies to lower granulite facies continental crust heated from a source in the mantle. It is therefore transitional from subduction related magmatism to intraplate. Lead isotopes indicate strong crustal affinities for host rocks and mineralisation with a mixture of Palaeozoic and Miocene ages.

(iii) Cornwall - deep subvolcanic to high plutonic

In contrast to the destructive ocean-continent plate margin, Cornwall represents a possible continent-continent collision zone. In a simplified model as envisaged by Mitchell and Garson (1976) there was continental collision with the concomitant folding of ocean sediments and associated thrusting with the Lizard representing a possible ophiolite complex. Each of the granites that is exposed at the surface is considered to link in with one major batholith at depth including the Scilly Isles.

Tin was mined in Cornwall probably as long as 2,000 years ago, and has been a

major world producer until last century. In addition, in past centuries Cornwall has also been a major producer of Cu thus emphasising that the same elements that occur both within the ocean-continent collision zone and in the intraplate setting of Nigeria occurred also in Cornwall. The earliest metalliferous mineralisation began with tin and tungsten mineralisation in and near granitic intrusions. This was followed by the formation of tin and copper in the main veins. Zinc and lead sulphides, Fe minerals (pyrite and siderite) and fluorite were introduced into earlier veins and cross courses. Later generations of mineralisation include Ag galena, barytes, U, Co Ni Sb minerals together with haematite.

The mineralisation occurs as:-

- (i) veins which are simple or complex fissure-filling systems up to 5m width. as typified by Cligga Head.
- (ii) replacement deposits known as carbonas, these are not common but do occur in the granite contacts, eg. Botallack area at the margins of the Land's End granite.
- (iii) pegmatites, developed at an early stage as small bodies in the granite roof zone.

Associated with these ore deposits is a wide range of alteration processes. K silicate alteration where it occurs at granite margins is an early alteration process which may be followed by albitisation in some areas eg. Geevor mine. This is followed by propylitic alteration around veins similar to that in Bolivia. Tourmalinisation was an important process in many areas.

A comprehensive field, petrographic, fluid inclusion, radiogenic and stable isotope study on part of the Land's End granite by Jackson et al (1982) has elucidated a great deal about the hydrothermal history of the pluton. The c. 290 ma high-level granites were derived from the anatexis of young pelitic-rich crustal rocks with high B, F, Sn, U etc. The main stage of mineralisation which was both temporally and spatially related to magmatism was responsible for a variety of metasomatic alteration, the emplacement of barren pegmatites, formation of Sn-Cu mineralised fissure systems and irregularly-shaped mineralised replacement deposits. The main ore-forming fluids were overwhelmingly meteoric in origin and dominantly of low to moderate salinity (10-20 eq. wt% NaCl) in the minimum temperature range 280-450°C with local fluctuations to more saline fluids.

The process of alteration in Cornwall that was so much more important than that in Bolivia, was argillic alteration which is found around some veins and as extensive pervasive areas in the roof zones of some granites, most notably in the western half of the St. Austell granite. The resulting china clay deposits were formed by Tertiary supergene fluids but some vein-controlled argillic alteration had a hydrothermal origin.

Apart from this more intense low temperature process than that of the porphyry tin deposits there are remarkable similarities of ore types and alteration processes. Yet the granites themselves are not identical nor do they plot in a similar field on the Streckeisen diagram.

Clearly, in all these three areas described from the highest level veins in

volcanic rocks of Mexico, to the mineralised plutons of Cornwall there are similarities with Nigeria. The major contrasts must be in the complete lack of any tourmalinisation process in Nigeria and the unimportance of argillic alteration. More detailed comparisons and contrasts form the basis of the final Chapter.

## CHAPTER 14

### SUMMARY AND CONCLUSIONS

#### SUMMARY

The Pan-African orogeny, regarded as a major event in the construction of Gondwanaland, played a dominant role in providing a variety of source materials for mineralisation, melting or assimilation as components of the Benin-Nigeria shield. Although the parent magmas of the oversaturated alkaline rocks which constitute the Nigerian province were initiated in the asthenosphere, it was the exploitation and reactivation of the Pan-African shear zones and transcurrent faults during the fragmentation of Gondwana that controlled the locations of Phanerozoic intra-plate magmatism in West Africa. The Nigerian province represents a region where progressive uplift was accompanied by periodic sequential development of ring complexes during the Mesozoic. Thus both the processes in the asthenosphere and the structure of the continental lithosphere exerted an important influence on the products of anorogenic magmatism.

The magmatic lineage comparable to other alkaline provinces can be established from preserved volcanic successions with associated andesites attributed to magma mixing. Whilst their magmatic derivation from mantle and crustal sources can be conclusively demonstrated, petrological and geochemical research has shown that some of the ring complexes demonstrate substantial evidence for postmagmatic metasomatism and mineralisation by magmatic hydrothermal fluids. Some of the alkaline ring complexes have become extensively mineralised in a wide spectra of ore minerals which bear some similarities to economic concentrations in undersaturated carbonatite complexes particularly with the abundance of sphalerite, rare-earth minerals, zircon and complex titanium silicates, uranium, thorium, columbite and pyrochlore. Superimposed upon this alkaline mineralisation is a more normal granitic assemblage of ore minerals, including cassiterite, wolframite, sphalerite, chalcopyrite and galena that are typical of other tin provinces in tectonic settings.

The early postmagmatic processes begin with an alkaline stage, which was represented by sodic metasomatism of perthite, growth of ordered albite, and other critical mineralogical and chemical changes. The dominant ore associated with the sodic metasomatism can be divided into two types of mineralisation: the columbite type is found in biotite apogranites; whilst the pyrochlore type can be found in peralkaline apogranites. The alkaline stage is followed by loss of Na, growth of intermediate microcline and can be termed microclinization or generally potash metasomatism. Except within the Saiya Shokobo Complex, the microclinization stage was more restricted in its development but it does have important ore associations. With changing conditions in the fluid, acid metasomatism became more widely pervasive, or was confined to pockets or fissures and fractures in the roof zones of biotite granite. Greisenisation can be found superimposed on various mineral assemblages. The mineralogical expression and the extent of greisen development depended on the intensity of albitisation and microclinisation and the timing of fracturing and fissuring in the roof zone. Important oxide ore associations are formed at this period. Since silica is released as a result of the earlier mineralogical changes, the final phase of alteration is a silicification process. A major sulphide ore deposition is related to this final silicification process.

Fluid reactions can be monitored and interpreted by the nature of the new subsolidus assemblages. The new silicate, oxide and sulphide minerals developed in response to rock-fluid interaction provide the criteria for assessing the ore-bearing potential of the Nigerian alkaline granitoids.

#### Styles of mineralisation

The styles of mineralisation in Nigeria are very variable and range from pervasive metasomatic disseminations or thin stringers, through stockworks and sheeted veins, to major lodes with altered wallrock. Such variability is characteristic of subvolcanic levels and has comparisons in all other A-type provinces and in other subvolcanic tin provinces such as Bolivia (Grant et al 1977) where the mineralogy is characterised by polymetallic sulphide rich ores.

#### Hydrothermal alteration processes

The processes of hydrothermal alteration established and the mineral assemblages that were generated within the Nigerian province have equivalents in all tectonic settings and at all structural levels. A summary of the metasomatic mineral assemblages associated with the late-stage rock-fluid reactions is given in Table 14.1.

There are, however, several significant differences. Firstly, there was no phase of boron metasomatism in any of the A-type provinces (with the exception of Namibia where reactivation occurred) and secondly, in none of the other major tin province was there a comparable sequence of alteration stages. In Nigeria, the sodic or albitisation process was the earliest, followed by potash metasomatism. This sequence is typical for A-type granites but in orogenic settings it is normal for potash metasomatism, to precede the sodic process.

#### Ore paragenesis

The early deposition of oxide ores first established at Ririwai (Kinnaird et al 1985), followed by later sulphide rich phases, has also been noted in Bolivia as well as in Cornwall (Moore 1982), Australia (Taylor 1974), Portugal (Plimer (1983), and Czechoslovakia (Baumann et al 1974). The anorogenic granites are distinguished by their early deposition of Nb ores enriched in REE, Zr and U. In no other province however, has the niobium mineralisation, been reported as of such importance.

A summary of the ore minerals found in the A-type provinces - particularly in Nigeria - is given in Table 14.2.

#### Fluid inclusion evidence

Comparison of fluid inclusion populations with other tin provinces shows that a number of similarities exist. For example, for the subvolcanic porphyry tin deposits of Choloroque, Bolivia, Grant et al (1977) have evidence for multistage boiling, with early (quartz tourmaline) alteration  $>500^{\circ}\text{C}$ , quartz cassiterite veins from  $250-300^{\circ}\text{C}$  and sulphide rich veins from  $100-300^{\circ}\text{C}$ . These fluids were also initially highly saline with salinity ranging from over 60 wt% in the early quartz tourmaline alteration to 10-20% for the sulphide veins. In contrast, the early fluids associated with the small, shallow, highly differentiated granitoids of Krupka and Cinovec in Czechoslovakia (Durisova et al 1979) are

TABLE 14.1 Summary table showing metasomatic mineral assemblages associated with hydrothermal alteration processes

Sodic		Potash	Acid	silica	late-stage
peralkaline	peraluminous				
albite	albite	microcline	quartz	quartz	kaolinite
ferrorichterite -	zinnwaldite-	chlorite	zinnwaldite-	siderite	montmorillonite
Li-arfvedsonite	lepidolite	annite-	siderophyllite-	haematite	epidote
aegirine	zircon	siderophyllite-	annite		chlorite
aenigmatite	cryolite	zinnwaldite	sericite		siderite
amblygonite	epidote	lepidolite	chlorite		
astrophyllite	chlorite		topaz		
chevkinite	siderite		zircon		
narsarsukite			fluorite		

Fig 14.2 Summary table showing ore minerals characteristic of mineralised anorogenic complexes

Sodic	Potash	acid	silica	late-stage
pyrochlore	cassiterite	cassiterite	cassiterite	smithsonite
columbite-tantalite	wolframite	wolframite	wolframite	goethite
cassiterite	zircon	sphalerite	sphalerite	limonite
zircon	columbite	molybdenite	TiO <sub>2</sub> minerals	jarosite
galena	monazite	monazite	bismuth	haematite
thorite	ilmenite	pyrite	bismuthinite	cerussite
xenotime	rutile	arsenopyrite	bismuthite	pyromorphite
ilmenite	molybdenite	genthelvite	haematite	bornite
magnetite	powellite	phenakite	chalcocite	azurite
cryolite	sphalerite	stannite	covellite	malachite
bastnaesite	stannite	chalcopyrite	galena	chalcanthite
synchesite	chalcopyrite	pyrrhotite	stannite	pyrolusite
genthelvite	arsenopyrite	bismuth	pyrite	
gargarinite	genthelvite	bismuthinite	marcasite	
apatite		galena	chalcopyrite	
chevkinite		siderite	cubanite	
wiikite		zircon	pyrrhotite	
uraninite		marcasite	mackinawite	
		greenockite	tetrahedrite	
		gold		
		argentite		
		rutile	bastnaesite	
			zircon	Jebel Hamra
			uraninite	Saudi
			monazite	

Table 14.3. Radioelement concentrations and heat productivities for Swedish U-rich granites, granites from Saudi Arabia.

SWEDEN <sup>1,2</sup>		SAUDI ARABIA <sup>3</sup>		BRITAIN								
		U	Th	K	Th/U	HPU in $\mu\text{Wm}^{-3}$	No of samples	U	Th	K	Th/U	HPU in $\mu\text{Wm}^{-3}$
Sweden	Torpa Granite	2.3	15.2	5.03	6.61	2.08	33	12.0	32.5	4.2	2.71	5.5
"	"	4.4	13.6	3.92	3.09	2.19	9	18.7	42.6	4.1	2.28	7.8
"	"	4.2	12.2	3.93	2.90	2.26	63	6.8	36.8	4.3	4.09	5.0
"	"	1.1	3.6	3.33	3.27	0.83	6	10.7	41.8	4.5	5.69	4.7
"	sheets	4.0	19.9	3.97	4.98	2.74	32	16.5	36.3	4.6	3.91	5.8
"	"	6.5	27.0	4.83	4.15	3.93	9	11.7	37.1	4.1	3.17	5.7
"	"	7.7	24.5	4.77	3.18	4.06	35	18.0	29.7	4.2	1.65	6.6
"	"	4.1	15.5	4.11	3.78	2.47	8	8.7	18.2	3.9	2.09	3.9
"	Revsund porphyry	6.2	13.4	4.09	2.16	2.86	14	10.5	17.9	4.1	1.70	4.2
"	"	10	36	4.50	3.60	5.40	1	12.9	12.3	4.3	0.95	4.6
"	"	9	18	4.3	2.00	3.20	1	9.7	38.1	4.2	3.94	5.6
"	"	18	19	4.5	1.06	6.26	1	10.2	28.3	4.0	2.77	4.49
"	"	11	12	4.1	1.09	3.98	1	11.3	19.1	4.3	1.69	4.68
"	"	15	8	4.1	0.53	4.72	1	16	40	3.36	2.50	7.30
"	"	12	42	4.5	3.50	6.32	1	3	2	3.24	0.67	1.23
"	"	22	47	4.2	2.14	9.16	1	4	4	3.23	1.00	1.63
"	"	13	50	4.8	3.85	7.14	1	14	39	2.61	2.79	6.63
"	"	19	71	5.9	3.74	10.19	1	3	14	4.23	4.67	2.17
"	"	13	55	5.5	4.23	7.55	1	3	21	3.79	7.00	2.62
"	"	16	77	6.0	4.81	9.85	1	3	19	3.78	6.33	2.48
"	"	15	55	4.8	3.67	7.99	1	7	20	4.23	2.86	3.63
"	"	8	42	4.6	5.25	5.31	1	12	24	3.56	2.00	5.15
"	"	27	80	5.0	2.96	12.75	1	49	117	4.32	2.39	21.39
"	"	19	90	5.0	4.74	11.40	1	1	3	1.34	3.00	0.60
"	"	18	58	5.1	3.22	8.98	1	3	1	0.64	0.33	0.91
"	"	15	47	4.6	3.13	7.42	1	9	20	4.30	2.22	4.21
"	"	5.1	21.8	4.13	4.27	3.16	1	3	26	4.30	12.00	2.62
"	"	5.5	25.9	4.03	4.71	5.53	1	3	25	4.13	8.33	2.93
"	"	5.6	26.8	4.10	4.79	3.62	1	6	23	4.35	4.00	4.20
"	"	5.4	24.0	4.04	4.44	3.38	1	4	22	4.08	3.83	3.57
"	"	5.8	25.2	4.08	4.34	3.56	1	7	22	3.93	5.50	2.96
"	"	5.6	25.7	4.25	4.59	3.56	1	4	22	3.92	6.71	5.50
"	"	4.7	25.1	4.28	5.34	3.30	1	7	53	3.26	7.57	5.86
"	"	5.3	26.9	4.31	5.08	3.57	1	6	27	3.80	4.50	3.82
"	"	5.0	19.7	3.43	3.98	2.93	1	5	24	3.92	6.00	3.10
"	"	5.2	19.8	3.49	3.81	2.99	1	2	18	4.43	3.40	2.92
"	"	6.0	22.3	3.51	3.72	3.36	1	4	18	4.53	9.00	2.22
"	"	5.6	20.1	3.41	3.59	3.10	1	4	20	4.81	5.00	2.90
"	"	5.5	20.1	3.49	3.65	3.08	1	1	9	4.77	15.00	1.77
"	"	5.3	19.8	3.45	3.74	3.01	1	8	31	3.80	3.87	4.62
"	"	4.7	19.6	3.10	4.17	2.81	1	5	11	4.12	2.20	2.47
"	"	5.3	20.2	3.35	3.81	3.03	1	1	1	3.53	0.20	1.71
"	"	5.3	20.0	4.40	3.77	3.11	1	2	2	3.64	2.00	0.75
"	"	1.3	7.4	2.6	5.69	1.07	1	104	625	2.59	6.01	71.23
"	"	3.2	19.7	3.4	6.16	2.95	1	88	160	2.63	1.82	34.41
"	"	6.5	13.8	3.4	2.12	2.90	1	363	590	1.58	1.63	136.14
"	"	3.3	15.9	3.8	4.81	2.25	1	827	827	3.86	-	>58.44
"	"	3.7	13.6	4.1	3.68	2.23	1	-	-	-	-	-
"	"	2.8	11.7	2.6	4.18	1.7	1	-	-	-	-	-
"	"	3.0	11.6	3.4	3.81	1.9	1	-	-	-	-	-
"	"	2.7	11.4	2.8	4.22	1.7	1	-	-	-	-	-
"	"	4.1	13.0	2.2	3.17	2.1	1	-	-	-	-	-
"	"	1.5	5.2	2.6	1.74	1.0	1	-	-	-	-	-
"	"	8.7	31.2	4.2	3.59	4.6	1	-	-	-	-	-
"	"	5.0	21.7	3.9	4.34	3.1	1	-	-	-	-	-
"	"	5.6	12.9	3.7	2.30	2.6	1	-	-	-	-	-
"	"	2.9	11.5	3.3	3.97	1.9	1	-	-	-	-	-
"	"	5.0	27.0	4.2	5.40	3.5	1	-	-	-	-	-
"	"	3.8	15.0	2.6	3.95	2.2	1	-	-	-	-	-

Source of data: <sup>1</sup>Constable and Hubbard 1982, <sup>2</sup>Wilson and Akerblom 1982, <sup>3</sup>Collins et al., 1982, <sup>4</sup>Stavrakis 1982, <sup>5</sup>Brown et al., 1982, <sup>6</sup>Webb and Brown 1984a, <sup>7</sup>Brown et al., 1979, <sup>8</sup>Webb and Brown 1984b, <sup>9</sup>Harris and Harriner 1980.

very dilute ~2-3 eq.wt% NaCl. However, like the early Nigerian fluids they are CO<sub>2</sub>-bearing, and would have circulated at temperatures above 390°C at rather low pressures. Durisova et al suggest that there was moderate CO<sub>2</sub> unmixing at 300-500°C which was responsible for greisenisation and cassiterite<sup>2</sup> deposition, generation of brines (~35 wt% NaCl) and formation (or at least recrystallisation) of topaz locally, due to a sudden drop of fluid pressure caused by the marked unmixing. Fluids at 100-300°C were responsible for sulphide-sulphate deposition. For Cornwall, Jackson et al (1977), found that early quartz-wolframite veins and greisens formed between 280 and 400°C and later sulphide veins from 240-320°C. These data are comparable with data for the Nigerian anorogenic province. In contrast with Nigeria however, evidence for fluid boiling is rare in Cornwall and CO<sub>2</sub> was found only in association with two tungsten veins

### Heat Production

In terms of heat production the Nigerian granites have few equals. Heat production values have been calculated for mineralised and non-mineralised British granites, for chemically similar granites of Saudi Arabia, for A-type granites of Australia and for uranium-rich granites of Sweden (Table 14.3). In Britain, the highest heat productivities have been found in the Cairngorm intrusion (Webb and Brown 1984, Brown pers comm). Plant et al (1980) noted that the Cairngorm intrusion was an evolved silica-rich biotite granite that could be distinguished from many other Caledonian granites by its enhanced levels of LIL elements coupled with HFS elements. Similar patterns of element enrichment have been noted for the Cornubian granites (Plant et al 1984) and in the Ghurayyah granite of the Midian Mountains of Saudi Arabia (Harris and Marriner 1980) which is markedly enriched in heat producing elements. However, despite petrological and geochemical similarities with Nigerian granites the Cairngorm granites do not have the extensive mineralisation found in the Nigerian province. Despite the high heat production of these granites they did not act as 'heat engines' and a large involvement of meteoric water in hydrothermal alteration and mineralisation is not envisaged for Nigeria.

Clearly when viewed in terms of intrusive form, styles of mineralisation, ore mineralogy, fluid inclusion studies and hydrothermal alteration, the ring complexes of Nigeria are similar to other tin provinces and other A-type complexes. However, the sequence of hydrothermal alteration processes, the fluid evolution, the importance of mineralisation combined with a high heat production makes this granitoid province unique.

### CONCLUSIONS

With the range of styles of mineralisation and ore deposition and the varied textures and mineralogical variations in alkaline granites being interpreted as a result of subsolidus reactions, certain established interpretations of petrogenesis must be questioned. Above all the role of fluids in cooling granite plutons cannot be ignored.

## SUGGESTIONS FOR FURTHER WORK

Just about every part of this study has aspects that could form the basis of further research.

In the past it has always been thought that it was only the biotite granites that underwent the sequence of hydrothermal alteration processes described in this thesis. It appeared that only sodic metasomatism affected the peralkaline granites. However, during this study it became apparent that the fluids emanating from the Rishi biotite granite modified the enclosing basement and volcanic pile in a number of different ways. It would seem likely that the peralkaline granites may also have a recognisable sequence of alteration processes and perhaps the hydrothermal alteration of peralkaline rocks could form the basis of a similar study to this thesis.

This thesis has shown that the Rishi biotite granite has been extensively affected by late-stage fluids even where mineralogical changes are not readily apparent. If such rock-fluid interaction has occurred extensively in other mineralised complexes then it is not surprising that the age of the mineralisation of the Ririwai lode is the same as that for the host biotite granite. Currently work is in progress to analyse fluids trapped in minerals. This new work aims not only to determine the nature and proportion of the trapped volatiles but will also ultimately undertake isotopic analysis of the trapped fluids too. It is hoped that these results will give more evidence not only on the age of the mineralisation relative to the granite but also by a study of the stable isotopes, on the source of the fluids.

Most of the granites used in fluid inclusion studies showed that the temperature of trapping of the inclusions ranged down to less than 200°C. Since the quartz porphyry ring dykes with their anhydrous mineralogy of fayalite and hedenbergite closely resemble the original granite magma, fluid inclusion studies should be undertaken on this rock type at the earliest opportunity. Much more systematic data from thermometric studies on fluid inclusions is required particularly to enable a number of useful diagrams to be constructed to display the data more effectively.

Research is planned to compare the fluids trapped as inclusions in the minerals of the Pan-African pegmatites with those trapped in the granites and their hydrothermal variants. The Pan-African pegmatites carry many of the same ore minerals as the anorogenic granites but differ in the presence of the abundant tourmaline that they contain. A preliminary study suggests that the pegmatite fluids were much richer in CO<sub>2</sub>. In addition, a comparison between the lead zinc mineralisation of the Benue Valley and the lead-zinc veins of the anorogenic granites is currently a joint project with Dr. S.O Akande of Ilorin University. This could be extended to a comparison of the ore minerals themselves.

The study of the mica mineral chemistry provided a fascinating insight into a subject which could be studied much more extensively. The use of R1-R2 diagrams to display mica major element variations could be modified by the use of other specially constructed multicationic diagrams and could form the basis of an entire study. Similarly the feldspar mineral chemistry was not studied in this thesis although the petrological variations described suggest that much work remains to be done.

Since the first recognition of A-type granites in 1979, the Nigerian province has provided much of the chemical data that has been used as a basis for comparison with I-type and S-type granites. It would also be interesting to extend this study into different A-type provinces in other parts of Africa to test the models defined for Nigeria.

## REFERENCES

- Abaa, S.I. 1976. Geochemistry and petrology of mineralisation at Ririwai, Gindi Akwati and Dutsen Wai in the Nigerian younger granite province. Unpubl. MSc, Ahmadu Bello University, Zaria Nigeria.
- Ajakaiye, D.E. 1968. A gravity interpretation of the Lireui younger granite ring complex of northern Nigeria. *Geol. Mag.* 105; 256-263
- Ajakaiye, D.E. 1977a. A gravity survey over the Nigerian younger granite province. In "Geology of Nigeria." Ed. C.A. Kogbe 207-224 Elizabethan Publishing Co. Lagos.
- Ajakaiye, D.E. 1977b. Densities of rocks in the Nigerian younger granite province. In "Geology of Nigeria." Ed. C.A. Kogbe 225-233. Elizabethan Publishing Co. Lagos.
- Ajakaiye, D.E., Hall, D.H. and Millar, T. 1983. Aeromagnetic anomalies across the Nigerian younger granite province. Abstract 14.09 IUGG XVIII p14.
- Akande, S.O., Horn, E.E. and Reutel, C. 1985. Textural, mineralogical and fluid inclusion studies of the lead-zinc fluorite veins in the Nigerian Benue trough: metallogenic relationships. In "Symposium on current research on fluid inclusions". Univ. Gottingen
- Alderton, D.H.M., Pearce, J.A. and Potts, 1980. Rare earth element mobility during granite alteration: evidence from southwest England. *Earth Planet. Sci. Lett.* 49; 149-165
- Almond, D.C. 1967. Discovery of tin-tungsten mineralization in northern Khartoum province, Sudan. *Geol. Mag.* 104; ppl-12.
- Almond, D.C. 1979. Younger granite complexes of Sudan. In 'Evolution and mineralization of the Arabian-Nubian Shield' Ed. A.M. al-Shanti. *Bull. Inst. Appl. Geol. King Abdulaziz University (Jiddah), Vol 1; 159-176.* Pergamon Press, Oxford.
- Aubert, G. 1969. Les cupoles granitiques de Montebbras et d'Echassieres (massif central Francais) et la genese de leurs mineralisations en etain, lithium, tungstene et beryllium. These Univ. Clermont, 345pp Clermont-Ferrand
- Ba, H., Black, R., Benziene, B., Diombana, B., Hascoet-Fender, J., Bonin, B., Fabre, J. and Liegeois, J-P. 1985. La provinces des complexes annulaire alcalins sursatures de l'Adrar des Iforas, Mali. *J.Afr. Earth Sci.* 3; 123-142
- Badejoko, T.A. and Imeokparia, E.G. 1979. Fluorine abundance in Jos-Bukuru younger granite complex of Nigeria with comments on petrogenesis. *J. Mining Geol.* 16; 1 1979 41-48. published by the Nigerian Mining and Geosciences Society
- Bailey, J.C., 1977. Fluorine in granitic rocks and melts: A review. *Chem. Geol.* 19; 1-42
- Bailey, S.W., 1984. 'Micas' Reviews in Mineralogy, vol. 13, Min. Soc. Amer. 584pp.

- Bain, A.D.N., 1934. The younger intrusive rocks of the Kudara Hills, Nigeria. *Q.Jl.Geol.Soc.Lond.* 90; 201-239
- Ballard III, S. and Pollack, H.N., 1985. Terrestrial heat flow in southern Africa. (Abst) 13th Coll. African Geology, University of St Andrews, 2.
- Barker, F., Wones, D.R., Sharp W.N. and Desborough, G.A. 1975. The Pikes Peak batholith, Colorado Front Range, and a model for the origin of the gabbro-anorthosite-syenite-potassic granite suite. *Prec. Res.* 2; 97-160
- Batchelor, R.A. 1983. Chemical analyses and normative compositions of various rock types from the Niger-Nigerian anorogenic province. Unpublished compilation, University of St. Andrews
- Batchelor, R.A. and Bowden, P. 1985. Petrogenetic interpretation of granitoid series using multicationic parameters. *Chem. Geol.* 48; 43-55
- Batchelor, R.A. and Kinnaird, J.A. 1984. Gahnite compositions compared. *Min. Mag.* 48; 425-429
- Baumann, L., Stenprok, M., Tischendorf, G. and Zoubek, V. 1974. Metallogeny of tin and tungsten in the Krusne Hory - Erzgebirge. Pre-symposium excursion guide, Mawam Symposium. Geological Survey Prague.
- Bayer, R. and Lesquer, A. 1978. Interpretation des anomalies gravimetriques de la bordure orientale du craton ouest-africain: geometrie d'une suture. *Bull. Soc. geol. Fr.*, 20; 863.
- Benhamou, G. and Clocchiatti, R. 1976. Glass inclusions in quartz and anorthoclase from Pantelleria peralkaline lavas: a thermometric study. *Bull. Soc. franc. Mineral. Cristallogr.*, 99, 111-116. (in french)
- Benkhelil, J. 1982 Benue Trough and Benue chain. *Geol. Mag.* 119; 155-168
- Bennett, J.N. 1981. The petrology and mineral chemistry of the Shira ring complex, northern Nigeria. Unpubl. PhD thesis, University of St. Andrews
- Bennett, J.N., Turner, D.C., Ike, E.C. and Bowden, P. 1984. The geology of some northern Nigerian anorogenic ring complexes. *Overseas Geol. & Miner. Resourc.* 61; 1-66 HMSO
- Black, R. 1965. Sur la signification petrogenetique de la decouverte d'anorthosites associees aux complexes annulaires sub-volcaniques du Niger. *C.R. Acaf. Sci.*, Paris, 260; 5829-5832
- Black, R. 1984. The Pan-African event in the geological framework of Africa. CIFEG Distinguished Lecture Series presented at the Technical University of Berlin, June 1984
- Black, R., Jajou, M. and Pellaton, C. 1967. Notice explicative de la carte geologique de l'Air a l'echelle 1/500 000. *Dir. Mines Geol. Niger.*
- Black, R., Caby, R., Mussine-Pouchkine, A., Bayer, R., Bertrand, J.M., Boullier, A.M., Fabre, J. and Lesquer, A. 1979. Evidence for late Precambrian plate tectonics in West Africa. *Nature, Lond.* 278; 223-227.

Black, R., Lameyre, J. and Bonin, B. 1985. The structural setting of alkaline complexes. *J. Afri. Earth Sci.*, 3; 5-16.

Bokhari, M.M., Jackson, N.J. and al Oweidi, K. 1986. Geology and mineralisation of the Jabal Umm Al Suqian albitized apogranite, southern Najd region, Kingdom of Saudi Arabia. In "Felsic plutonic rocks and associated mineralisation of the Kingdom of Saudi Arabia," Eds. A.R. Drysdall, C.R. Ramsay and D.B. Stoeser. *Sp. Vol. Journ. African Earth Sci. Vol 4*; 189-198

Bonin, B., Bowden, P. and Vialette, Y. 1979. Le comportement des elements Rb et Sr au cours des phases de mineralisation: l'exemple de Ririwai (Liruei) Nigeria. *C.R. Acad. Sci. Paris 289D*: 707-710

Borisenko, A.S. 1977. Study of the salt composition of solutions in gas-liquid inclusions in minerals by the cryometric method. *Soviet Geol. & Geophys.* 18, 11-19.

Borley, G.D. 1976. Ferromagnesian mineralogy and temperatures of formation of the younger granites of Nigeria. In "Geology of Nigeria." Ed. C.A. Kogbe 159-176 Elizabethan Publishing Co. Lagos

Borley, G.D., Beckinsale, R.D., Suddaby, P. and Durham, J.J. 1976. Variations in composition and  $O_{18}$  values within the Kaffo albite-riebeckite granite of the Ririwai complex, Younger Granites of Nigeria. *Chem. Geol.*, 18; 159-176, Amsterdam

Bowden, P. 1961. The geochemistry of some Nigerian igneous rocks. Unpubl. PhD thesis, Univ. Lond.

Bowden, P. 1985. The geochemistry and mineralization of alkaline ring complexes in Africa. *J. Afr. Earth Sci.* 3; 17-40

Bowden, P. and van Breemen, O. 1972. Isotopic and chemical studies on younger granites from northern Nigeria. In "African Geology." Eds. T. F. Dessauvagie and A.J. Whiteman. University of Ibadan Press, Ibadan, 1970.

Bowden, P. and Kinnaird, J.A. 1978. Younger granites of Nigeria - A zinc-rich tin province. *Trans. Inst. Min. Metall.* B78; 66-69

Bowden, P. and Kinnaird, J.A. 1984a. Geology and mineralization of the Nigerian Anorogenic Ring Complexes, with a geological map at the scale 1:500 000 *Geol. Jb.* B56; 3-65 Hannover

Bowden, P. and Kinnaird, J.A. 1984b. Petrological and geochemical criteria for the identification of (potential) ore bearing Nigerian granitoids. *Proc. 27 Int. Geol. Congress, Moscow 9*; 85-119 VNU Science Press, Utrecht, The Netherlands

Bowden, P. and Kinnaird, J.A. 1984c. The petrology and geochemistry of alkaline granites from Nigeria. *Phys. Earth Planet. Inter.*, 35; 199-211

Bowden, P. and Kinnaird, J.A. 1986. Magmatic and postmagmatic processes in the petrogenesis of evolved granites: anorogenic examples from Nigeria. 76 *Jahrestagung der Geologischen Vereinigung, Gissen*

Bowden, P. and Turner, D.C. 1974. Peralkaline and associated ring complexes in

- the Niger-Nigeria province, West Africa. In "The alkaline rocks" Ed. H. Sorensen. Wiley 330-351
- Bowden, P. and Whitley, J.E. 1974. Rare-earth patterns in peralkaline and associated granites. *Lithos* 7; 15-21
- Bowden, P., van Breemen, O. Hutchison, J. and Turner, D.C. 1976. Palaeozoic and Mesozoic age trends for some ring complexes in Niger and Nigeria. *Nature, Lond.* 259; 297-299
- Bowden, P., Bennett, J.N., Whitley, J.E. and Moyes, A.B. 1979. Rare earths in Nigerian Mesozoic granites and related rocks. In "Origin and distribution of the elements." Ed. L. H. Ahrens, 479-491 Pergamon Press
- Bowden, P., Bennett, J.N., Kinnaird, J.A., Whitley, J.E., Abaa, S.I., and Hadzigeorgiou-Stavrakis, P.K. 1981. Uranium in the Niger-Nigeria Younger granite province. *Mineral. Mag.* 44; 379-389
- Bowers, T.S. and Helgeson, H. C. 1983. Calculation of the thermodynamic and geochemical consequences of non-ideal mixing in the system  $H_2O-CO_2-NaCl$  on phase relations in geologic systems: equation of state for  $H_2O-CO_2-NaCl$  fluids at high pressures and temperatures. *Geochim. Cosmochim. Acta*, 47; 1247-1275.
- Breemen, O van, Hutchinson, J. and Bowden P. 1975. Age and origin of the Nigerian Mesozoic granites: A Rb-Sr isotopic study. *Contr. Mineral. Petrol.* 50; 157-172.
- Breemen, O. van, Pidgeon, R.T. and Bowden, P. 1977. Age and isotopic studies of some Pan-African granites and related rocks, north central Nigeria. *Precamb. Res.* 4; 307-319.
- Briden, J.C. 1967. Recurrent continental drift of Gondwanaland. *Nature* 215; 1334-1339.
- Brigaud, F. and Lucazeau F. 1985. Heat flow from the West African shield. *Geophy. Res. Lett. (AGU)*, 12; 549-552.
- Brown, G.C., Plant, J. and Lee, M.K. 1979. Geochemical and geophysical evidence on the geothermal potential of Caledonian granites in Britain. *Nature* 280; 129-131
- Brown, G.C., Webb, P.C., Lee, M.K., Wheildon, J. and Cassidy, J. 1982. Development of HDR reconnaissance in the United Kingdom. In "Proc. Int. Conf. on geothermal energy, Florence, Italy". 353-367 BHRA Fluid engineering, Cranfield, England
- Brown, P.E. 1956. The Mourne Mountains granites - a further study. *Geol. Mag.* 93; 72-84
- Burrus, R.C. 1981. Analysis of phase equilibria in C-O-H-S fluid inclusions. In "Short course in fluid inclusions: Applications to petrology." Eds. L.S. Hollister and M.L. Crawford 39-69. Mineral. Assoc. Canad. Short Course handbook, Calgary, Canada.
- Buchanan, M.S., MacLeod, W.N. and Turner, D.C. 1971. The geology of the Jos

Plateau. Bull. Geol. Surv. Nigeria 32; vol 2, 159pp

Burnham, C.W. 1979. Magmas and hydrothermal fluids. In "Geochemistry of hydrothermal ore deposits" Ed H.L. Barnes 71-136 John Wiley and Sons

Burt, D.M. 1971. Acidity-salinity diagrams-applications to greisen and porphyry deposits. Econ. Geol. 76; 832-843.

Burt, D.M. 1975. Beryllium mineral stabilities in the model system  $\text{CaO}-\text{BeO}-\text{SiO}_2-\text{P}_2\text{O}_5-\text{F}_2\text{O}_{-1}$  and the breakdown of beryl. Econ. Geol. 70; 1279-1292

Burt, D.M. 1976. Generation of high HF fugacities in miarolitic pegmatites and granites: the possible role of topaz. Geol. Soc. Amer., Abstracts with programs 8, (6) 798

Burt, D.M. 1977. Chalcophile-lithophile tendencies in the helvite group: genthelvite stability in the system  $\text{ZnO}-\text{BeO}-\text{Al}_2\text{O}_3-\text{SiO}_2-\text{SO}_{-1}-\text{F}_2\text{O}_{-1}$ . Amer. Geophys. Union, Trans. 58 (12); 1242

Burt, D.M. 1981. Acidity-salinity diagrams - Application to greisen and porphyry deposits. Econ. Geol. 76, 832-843

Burt, D.M. 1984. Relation of lithophile element mineralization to acid magmatism, Western USA. Proc. 27 Int. Geol. Congress, Moscow 9 27-39 VNU Science Press, Utrecht, The Netherlands

Butler, J.R., Bowden, P. and Smith, A.Z. 1962. K/Rb ratios in the evolution of the Younger Granites of northern Nigeria. Geochim. Cosmochim. Acta, 26; 89-100

Caby, R., Bertrand J.M.L. and Black, R. 1981. Pan-African closure and continental collision in the Hoggar-Iforas segment, central Sahara. In "Precambrian plate tectonics", Ed. A. Kroner, 407-431, Elsevier

Cerny, P. and Burt, D. M. 1984. Paragenesis, crystallochemical characteristics, and geochemical evolution of micas in granite pegmatites. Reviews in Mineralogy, Vol 13; 'Micas' edited by S.W. Bailey. Min. Soc. America, 257-297.

Chappell, B.W. and White A.J.R. 1974. Two contrasting granite types. Pacific Geology 8; 173-174 Melbourne

Charoy, B. 1979. Definition et importance des phenomenes deuteriques et des fluides associes dans les granites. Consequences metallogeniques. Mem. Sci. de la Terre, 37; 364pp

Chatterjee, A.K. 1980. Petrological and geochemical characteristics of some Nova Scotia granitoid rocks hosting Mo, Cu, Sn, W and U mineralisation. Int. Geol. Congr. Abstr. 26; no 3 p317 1980. 7-17th July Paris, France

Chayes, F. 1964. Variance-covariance relations in Harker diagrams of volcanic suites. J. Petrol. 5; 219-237

Coleman, M.L. 1979. Isotopic analysis of trace sulphur from some S- and I-type granites: heredity or environment? In "Origin of granite batholiths: geochemical evidence". Eds M.P. Atherton, J. Tarney. Shiva Publishing ltd., Orpington, Kent 129-133

Cole, D.R. and Ohmoto, H. 1986. Kinetics of isotopic exchange at elevated

temperatures and pressures. In "Stable isotopes in high temperature geological processes." Reviews in Mineralogy 12; 4-87

Collins, P.L.F. 1979. Gas hydrates in CO<sub>2</sub>-bearing fluid inclusions and the use of freezing data for estimation of salinity. Econ. Geol. 67; 365-392

Collins, W.J., Beams, S.D., White A.J.R. and Chappell, B.W. 1982. Nature and origin of A-type granites with particular reference to southeastern Australia. Contrib. Mineral. Petrol. 80; 189-200

Constable, J.L and Hubbard, F.H. 1982. U, Th and K distribution in a differentiated charnockite-granite intrusion and associated rocks from S.W. Sweden. In "Uranium 81." 39-45 Eds. P.R. Simpson, J.A. Plant and G.C. Brown

Crawford, M.L. 1981. Phase equilibria in aqueous fluid inclusions. In "Short course in fluid inclusions: Applications to petrology." Eds. L.S. Hollister and M.L. Crawford 39-69. Mineral. Assoc. Canad. Short Course handbook, Calgary, Canada.

Darnley, A.G., Smith, G.H., Chandler, T.R.D. and Dance, D.F. 1962. The age of the fergusonite from the Jos area, Northern Nigeria. Age Determ. Rep. No 10, Atomic Energy Div. Geol. Surv. G.B. 6pp

Darnley, A.G. 1982. 'Hot' granites: some general remarks. In "Uranium in granites". Ed. Y.T. Maurice Geol. Surv. Canada paper 81-23; 1-10

Debon, F. and le Fort, P. 1983. A chemical-mineralogical classification of common plutonic rocks and associations. Trans. R. Soc. Edinburgh (earth Sci.), 73 (for 1982): 135-149

Deer, W.A., Howie, R.A. and Zussman, J. 1966. Introduction to the rock forming minerals. Longmans, London, 528pp

Deer, W.A., Howie, R.A. and Zussman, J. 1965. Volume on sheet silicates. Longmans, London.

de la Roche, H. 1964. Sur l'expression graphique des relations entre la composition chimique et la composition mineralogique quantitative des roches cristallines - Presentation d'un diagramme destine a l'etude chimico-mineralogique des massifs granitiques et granodioritiques - Application aux Vosges cristallines. Sci. Terre, 9(3); 293-337

de la Roche, H., 1978. La chimie des roches presentee et interpretee d'apres la structure de leur facies mineral dans l'espace des variables chimiques: fonctions specifiques et diagrammes qui s'en deduisent; application aux roches ignees. Chem. Geol. 21: 63-87

de la Roche, H. and Leterrier, J. 1973. Transposition du tetraedre mineralogique de Yoder et Tilley dans un diagramme chimique de classification des roches basaltiques. C.R. Acad. Sci., Paris. Ser. D, 276; 3115-3118

de la Roche, H., Leterrier, J., Grand Claude, P and Marchal, M. 1980. A classification of volcanic and plutonic rocks using R1-R2 diagrams and major element analyses - its relationship with current nomenclature. Chem. Geol., 29; 183-210

- Dickin, A.P. and Halliday, A.N. 1987. A lead, strontium and neodymium isotope study of Nigerian Mesozoic ring complexes. Unpublished manuscript.
- Drysdall, A.R. and Douch, C.J. 1986. Nb-Th-Zr mineralization in microgranite-microsyenite at Jabal Tawlah, Midyan region, Kingdom of Saudi Arabia. In "Felsic plutonic rocks and associated mineralisation of the Kingdom of Saudi Arabia," Eds. A.R. Drysdall, C.R. Ramsay and D.B. Stoeser. Sp. Vol. Journ. African Earth Sci. 4; 275-288
- Durisova, J., Charoy, B. and Weisbrod, A. 1979. Fluid inclusion studies in minerals from tin and tungsten deposits in the Krusne Hory Mountains (Czechoslovakia). Bull. Mineral. 102; 665-675
- Eugster, H. and Wilson, G.A. 1985. Transport and deposition of ore-forming elements in the hydrothermal systems associated with granites. In "High heat production granites, hydrothermal circulation and ore genesis" Inst. Mining Metall. 87-98 London 593pp
- Eugster, H.P. and Wones, D.R. 1962. Stability relations of the ferruginous biotite, annite. J. Petrol. 3; 82-125
- Evans, A.M. 1980. An introduction to ore geology. Blackwell Scientific Publications. 231pp
- Falconer, J.D. 1911. The Geology and Geography of Northern Nigeria. MacMillan, London 295pp
- Falconer, J.D. and Raeburn, C. 1923. The Northern tinfields of Bauchi Province. Bull. geol. surv. Nigeria 9
- Farrington, J.L. 1952. A preliminary discussion of the Nigerian lead-zinc field. Econ. Geol. 47; 583-608
- Ferry, J.M. 1985. Hydrothermal alteration of Tertiary igneous rocks from the Isle of Skye, northwest Scotland. Part 11 granites; Contr.Min. Petrol. 91, 283-304
- Finger, L.W. 1972. The uncertainty in the calculated ferric iron content of a microprobe analysis. Carnegie Inst. Wash. Yearbk. 71; 600-603.
- Fitches, W.R., Ajibade, A.C., Egbuniwe, I.G. and Holt, R.W. 1983. Late Precambrian belts in Nigeria. Abstr. 12th Coll. Afr. Geol. Brussels.
- Ford, S.O. 1981. The economic mineral resources of the Benue Valley. EES 2; 154-163 Wiesbaden
- Foster, M. 1960. Interpretation of the composition of trioctahedral micas. U.S.Geol.Surv. Paper 354B; 1-49
- Fournier, R.O. 1976. Exchange of  $\text{Na}^+$  and  $\text{K}^+$  between water vapour and feldspar phases at high temperature and low vapour pressure. Geochim. et Cosmochim. Acta 40, 1553-1561
- Francheteau, J. and le Pichon, X. 1972. Marginal fractures zones as structural framework of continental margins in the south Atlantic ocean. Bull.Am.Ass. Petrol.Geol., 56; 991-1001

- Frantz, J.D., Popp, R.K. and Boctor, N.Z. 1981. Mineral-solution equilibria - V. Solubilities of rock forming minerals in supercritical fluids. *Geochim. et Cosmochim. Acta* 45; 69-77
- Gass, I.G., Chapman, D.S., Pollack, H.N. and Thorpe, R.S. 1978. Geological and geophysical parameters of mid-plate volcanism. *Phil. Trans. R. Soc. Lond. A* 288; 581-597
- Grant, J.N., Halls, C., Avila, W. and Avila, G. 1977. Igneous geology and the evolution of hydrothermal systems in some subvolcanic tin deposits of Bolivia. In "Volcanic processes in ore genesis." *Spec. Publ. 7 Geol. Soc. Lond.* 117-126
- Grant, N.K. 1969, The geochronology of Precambrian basement rocks from Ibadan, southwestern Nigeria. *Earth Planet. Sci. Letters*, 10; 29-38, Amsterdam
- Grant, N.K. 1971a. A compilation of radiometric ages from Nigeria. *Journ. Mining and Geol.*, 6; 37-54, Nigeria
- Grant, N.K. 1971b. South Atlantic, Benue trough and Gulf of Guinea triple junction. *Bull. Geol. Soc. Am.* 82; 2295-2298
- Grant, N.K. 1978. Structural distinction between a metasedimentary cover and an underlying basement in the 600ma old Panafrican domain of northwestern Nigeria, West Africa. *Bull. Geol. Soc. Am.* 89; 50-58
- Greenwood, R. 1948. Younger intrusive rocks of Plateau Province, Nigeria, compared with the alkalic rocks of New England. *Bull. Geol. Soc. Am.*, 62; 1151-1178
- Groves, D.L. and McCarthy, T.S. 1978. Fractional crystallisation and the origin of tin deposits in granitoids. *Mineral. Deposita*, 13; 11-26.
- Haag, H.L. 1943. Wolfram in Nigeria: with notes on cassiterite, wolfram and columbite. *Trans. Inst. Mining and Metall.* lii.
- Haas, J.L., 1971. The effect of salinity on the maximum thermal gradient of a hydrothermal system at hydrostatic pressure. *Econ. Geol.* 66; 940-946
- Halliday, A.N., Dickin, A.P. and G.E. Fitton, 1983. Nd-Sr-Pb isotopic evidence for the origins of the Cameroun Line volcanics and the nature of the mantle under West Africa and the eastern Atlantic, *Terra Cognita*, 3; 122-3
- o'Halloran, D. 1985. Ras ed Dom migrating ring complex: A-type granites and syenites from the Bayuda desert, Sudan. *J. Afr. Earth sci.* 3; 1/2 61-76
- Harker, A. 1909. The natural history of igneous rocks. Methuen, London 384pp.
- Harper, C.T., Sherrer, G., M<sup>C</sup>Curry, P. and Wright, J.B. 1973. K-Ar retention ages from the Pan-African of northern Nigeria. *Bull. Geol. Soc. Amer.* 84; 919-926 Colorado
- Harris, N.B.W. and Marriner, G.F. 1980. Geochemistry and petrogenesis of a peralkaline complex from the Midian Mountains, Saudi Arabia. *Lithos* 13; 325-336 Oslo

- Hemley, J.J. and Jones W.R. 1964. Chemical aspects of hydrothermal alteration with emphasis on hydrogen metasomatism. *Econ. Geol.* 59; 538-569
- Hey, M.H. 1954. Nomenclature of chlorites and oxidised chlorites, *Min. Mag.* 30; 277
- Heyen, G., Dubessy, J. and Ramboz, C. 1982. Modelling of phase equilibria in the system  $\text{CO}_2\text{-CH}_4\text{-C}_2\text{H}_6$  below 50° and 100 bar. Application to inclusion fluids. *Comp. Rend. acad. Sci. Paris*, 294, ser.11,261-264 (in French)
- Hughes, C.J. and Hussey E.M. 1976. M and Mg values in igneous rocks; proposed usage and a comment on currently employed  $\text{Fe}_2\text{O}_3$  corrections. *Geochim. Cosmochim. Acta* 40; 485-486
- Hurley, P.M., de Almeida, F.F.M., Melcher, G.C., Cordani, U.G., Rand, J.R., Kawashita, K., Vandomos, R., Pinson, W.H.J. and Fairbairn, H.W. 1966. Continental drift investigations - 14th ann. Prog. Rep. Massachusetts Inst. Technol. 3-16
- Husch, J. and Moreau, C. 1982. Geology and major element geochemistry of anorthositic rocks associated with Palaeozoic hypabyssal ring complexes, Air massif, Niger, West Africa. *J. Volcan. geotherm. Res.* 14; 14-66
- Ike, E.C. 1979. The structure, petrology and geochemistry of the Tibchi younger granite ring complex, Nigeria. Unpubl. PhD thesis Univ. St. Andrews
- Ike, E.C. 1983. The structural evolution of Tibchi ring complex - a case study for the Nigerian Younger Granite province. *J. geol. Soc.* 140; 781-788
- Ike, E.C., Bowden, P. and Martin R.F. 1984. Fayalite and clinopyroxene in the porphyries of the Tibchi Complex Nigeria. Postmagmatic initiation of a peralkaline trend. *Canad. Mineral.* 22; 401-409
- Ike, E.C., Bowden, P. and Martin R.F. 1985. Amphibole in the porphyries of the Tibchi anorogenic complex, Nigeria. Product of deuteritic adjustments. *Canad. Mineral.* 23; 447-456
- Imeokparia, E.G. 1982. Bedrock geochemistry as a guide to potential ore-bearing granites, Afu younger granite complex, central Nigeria. *Trans. Inst. Mining Metall.* 91; B123-129
- Imeokparia, E.G. 1984. Geochemistry of the granitic rocks from the Kwandonkaya complex, northern Nigeria. *Lithos* 17; 103-115
- Ishihara, S. 1977. The magnetite series and ilmenite series granitic rocks. *Min. Geol.* 27; 293-305
- Ixer, R.A., Ashworth, J.R. and Pointer, C. 1985. Mineralogical studies of the mineralization at Ririwai. In 13th Coll. African Geology, St. Andrews 10th-13th September 1985. Abstract Volume, Abstr.301
- Ixer, R.A., Ashworth, J.R. and Pointer, C. 1987. Accessory mineralogy of the Ririwai biotite granite, Nigeria, and its albitized and greisenized facies. In "African Geology Reviews" Eds. P. Bowden and J.A. Kinnaird. John Wiley and Sons (in press)
- Jackson, N.J. 1986. Mineralisation associated with felsic plutonic rocks in the

Arabian Shield. In "Felsic plutonic rocks and associated mineralisation of the Kingdom of Saudi Arabia," Eds A.R. Drysdall, C.R. Ramsay and D.B. Stoesser. Sp. Vol. J. Afr. Earth Sci. 4; 213-227

Jackson, N.J., Moore, J.M. and Rankin A.H. 1977. Fluid inclusions and mineralisation at Cligga Head Cornwall, England. J. Geol. Soc. Lond. 134 Part 3 343-349.

Jackson, N.J., Halliday, A.N., Sheppard, S.M.F. and Mitchell, J.G. 1982. Hydrothermal activity in the St. Just Mining District, Cornwall, England. In "Metallization associated with acid magmatism" Ed. A.M. Evans. pp 137-179 John Wiley and Sons 385pp

Jacobson, R.R.E. 1947. The Younger Granite complex of the Rirawai Hills, Nigeria. Unpubl. PhD thesis, University of London

Jacobson, R.R.E., MacLeod, W.N. and Black, R. 1958. Ring Complexes in the Younger Granite province of northern Nigeria. Mem. No.1 Geol. Soc. Lond. 72pp

Jacobson, R.R.E., Snelling, N.J. and Truswell, J.F. 1963. Age determinations in the geology of Nigeria with special reference to the Older and Younger granites. Overseas Geol. and Min. Resourc. 9; 168-182. London

Jacobson, R.R.E. and Webb, J.S. 1946. The pegmatites of central Nigeria. Bull. Geol. Surv. Nigeria 23

Jacquemin, H., Sheppard, S.M.F. and Vidal, P. 1982. Isotopic geochemistry (O, Sr, Pb) of the Golda Zuelde and Mboutou anorogenic complexes, North Cameroon: mantle origin and evidence of crustal contamination. Earth Planet. Sci. Lett. 61; 97-111

Jones, M.P. 1953. Preliminary investigation of the occurrence of columbite in the Afu Hills younger granite complex. Geol. Surv. Nigeria, Unpubl. Rep. No. 1114

Kayode, A.A. 1976. On the genesis of small and large feldspar porphyritic older granite in the Igbo Ora Complex, S.W. Nigeria. In "Geology of Nigeria". Ed C.A. Kogbe, Elizabethan Press. Lagos 75-84

Keevil, N.B. 1942. Vapour pressure of aqueous solutions at high temperatures. Am. Chem. Soc. J., 64; 841-850

Kelly, W.C. and Turneure, F.S. 1970. Mineralogy, paragenesis and geothermometry of the tin and tungsten depositis in the eastern Andes, Bolivia.. Econ. Geol., 65; 609-680

Kennedy, G.C. 1954. Pressure-volume-temperature relations in CO<sub>2</sub> at elevated temperatures and pressures. Am. J. Sci. 252; 225-241

Khaibullin, I.Kh., Novikov, B.Ye., Copeliovich, A.M. and Besedin, A.M (1980). Phase diagrams for steam solutions and calorific properties of two- and three-component systems: H<sub>2</sub>O-NaCl-, H<sub>2</sub>O-Na<sub>2</sub>SO<sub>4</sub>, and H<sub>2</sub>O-NaCl-Na<sub>2</sub>SO<sub>4</sub>. In "Water and steam" Eds J. Straub and K. Scheffler 641-647, Pergamon Press, New York.

Kinnaird, J.A. 1977. A geological investigation of some Nigerian Jurassic granites and their mineralisation. Unpubl. MSc thesis University of St. Andrews

- Kinnaird, J.A. 1979. Mineralisation associated with the Nigerian Mesozoic ring complexes. *Stud. Geol. Salamanca* 14; 189-220
- Kinnaird, J.A. 1981. Geology of the Nigerian anorogenic ring complexes, Map, Scale 1:500 000. John Bartholomew, Edinburgh
- Kinnaird, J.A. 1984. Contrasting styles of Sn-Nb-Ta-Zn mineralization in Nigeria. *J. Afr. Earth Sci.* 2; 185-222
- Kinnaird, J.A. 1985. Hydrothermal alteration and mineralization of the alkaline anorogenic ring complexes of Nigeria. *J. Afr. Earth Sci.* 3; No 1/2 229-251
- Kinnaird, J.A., Bowden, P., Ixer, R.A., Odling, N.W.A. 1985a. Mineralogy, geochemistry and mineralization of the Ririwai complex, northern Nigeria. *J. Afr. Earth Sci.* 3; No 1/2 185-222
- Kinnaird, J.A., Batchelor, R.A., Whitley, J.E. and MacKenzie, A.B. 1985b. Geochemistry, mineralization and hydrothermal alteration of the Nigerian High Heat Producing Granites. In "High Heat Production (HHP) Granites, Hydrothermal circulation and Ore Genesis." IMM London 169-195
- Klevtsov, P.V. and Lemlein, G.G. 1959. Pressure corrections for the homogenisation temperatures of aqueous NaCl solutions. *Dokl. Akad. Nauk. SSSR* 128; 1250-1253
- Knorring, von O. and Dyson, P. 1959. An occurrence of genthelvite in the younger granite province of northern Nigeria. *Am. Miner.*, 44; 1294-1298
- Knorring, von O., Horning, G., Concliffe, E. and Emmerman, R. 1985. Pyrochlore-bearing granitic rocks associated with the Brandberg intrusion in Namibia. In 13th Coll. African Geology, St. Andrews 10th-13th Spetember 1985. Abstract Volume, Abstr.281
- Kogbe, C.A. and Obialo, A.U. 1976. Statistics of Mineral Production in Nigeria (1946 to 1974) and the contribution of the mineral industry to the Nigerian economy. In "Geology of Nigeria." Ed. C.A. Kogbe 391-426 Elizabethan Publishing Co. Lagos.
- Kovalenko, N.I. 1976. The reactions between granite and aqueous hydrofluoric acid in relation to the origin of fluorine bearing granites. *Geokhimiya* 4; 503-515
- Lameyre, J. and Bowden, P. 1982. Plutonic rock type series: Discrimination of various granitoid series and related rocks. *J. Volc. and Geothermal Res.* 14, 169-186
- Laouar, R., Boyce, A.J. and Fallick, A.E. 1987. Sulphur isotope studies in Caledonian granites. *Abstr. Terra Cognita* 7; 405-406
- Larsen, Jr., E.S. 1938. Some new variation diagrams for groups of igneous rocks. *J. Geol.* 46; 505-520
- Lasserre, M. 1978. Mise au point sur les granitoids "ultimes" du Cameroun.

- Gisements, pétrologie et géochronologie. Bull. Bur. Rech. géol. minières 4; 143-159
- Le Bas, M.J. 1971. Peralkaline volcanism, crustal swelling and rifting. Nature 230, 85-87
- Leblanc, M. 1976. Proterozoic ocean crust at Bou Azzer (Morocco). Nature Lond. 261, 34-35
- Leger, J-M. 1985. Géologie et évolution magmatique du complexe plutonique d'Iskou (Air, Niger). J.Afr. Earth Sci. 3; 89-96
- Liegeois, J-P. and Black, R. 1983. Preliminary results on the geology and geochemistry of the late Pan-African composite batholith of western Iforas (Mali) Abstract 12th Colloquium Afr. géol. 62
- Liegeois, J-P. and Black, R. 1984. Petrographie et géochronologie Rb-Sr de la transition fini-panafricaine dans l'Adrar des Iforas (Mali): accretion crustale au Précambien supérieur. In "African Geology" Ed. J. Klerkx and J. Michot pp 115-146
- Lipman, P.W., Prostka, H.J. and Christiansen R.L. 1972. Cenozoic volcanism and plate tectonic evolution of the western United States. Part 1: Early and middle Cenozoic. Phil. Trans R. Soc. London 271A; 217-248
- Loiselle, M.C. and Wones, D.R. 1979. Characteristics and origin of anorogenic granites. Geol. Soc. Am. Abstr. 11; 468
- Luth, W.C. 1976. Granitic rocks. In "The evolution of the crystalline rocks". Eds. D.K. Bailey and R. Macdonald, 335-417. Academic Press, London
- McCurry, P. 1971. Pan-African orogeny in northern Nigeria. Bull. Geol. Soc. Am. 82; 3251-3262
- McCurry, P. 1973. Geology of the degree sheet 21, Zaria, Nigeria. Overseas Geol. Min. Resourc. 45 HMSO
- McCurry, P. 1976. The geology of the Precambrian to lower Palaeozoic rocks of Nigeria - A review. In "Geology of Nigeria." Ed. C.A. Kogbe, Elizabethan Press, Nigeria 15-40
- MacDonald, A.J. and Spooner, E.T.C. 1981. Calibration of a Linkam TH600 programmable heating-cooling stage for microthermometric examination of fluid inclusions. Econ. Geol. 76; 1248-1258
- Mackay, R.A., Greenwood, R. and Rockingham, J.E. 1952. The Geology of the Plateau Tinfields - Re-survey 1945-1948. Bull. Geol. Surv. Nigeria 19
- MacKenzie, A.B., Bowden, P. and Kinnaird, J.A. 1984. Combined neutron activation and particle track analysis of element distributions in a rock slice of mineralised granite. J. Radioanalytical Chem. 82; 341-352
- MacKenzie, W.S., Donaldson, C.H. and Guilford, C. 1982. Atlas of igneous rocks and their textures. Longman 148pp

- MacLeod, W.N. 1954. The geology of the Jos-Bukuru younger granite complex with particular reference to the distribution of columbite. *Rec. Geol. Surv. Nigeria*, pp7-34
- MacLeod, W.N., Turner, D.C. and Wright, E.P. 1971. The geology of the Jos Plateau. *Geol. Surv. Nigeria Bull.* 32; 120pp
- Manning, D.A.C. 1981. The effect of fluorine on liquidus phase relationships in the system Qz-Ab-Or with excess water at lkb. *Contr. Miner. Petrol.* 76, 206-215
- Manning, D.A.C. 1982. An experimental study of the effects of fluorine on the crystallisation of granitic melts. In "Metallization associated with acid magmatism." Ed. A.M.Evans 191-204 John Wiley and Sons.
- Manning, D.A.C. and Pichevant, M. 1984. Experimental studies of the role of fluorine and boron in the formation of late-stage granitic rocks and associated mineralisation. *Proc. 27 Int. Geol. Congress Moscow 9*, 353-372 VNU Science Press, Utrecht, The Netherlands
- Marsh, J.S. 1973. Relationships between transform directions and alkaline igneous rock lineaments in Africa and south America. *Earth Planet. Sci. Lett.* 18; 317-323
- Martin, R.F. and Bowden P. 1981. Peraluminous granites produced by rock-fluid interaction in the Ririwai nonorogenic ring complex, Nigeria; mineralogical evidence. *Canad. Min.* 19; 65-82 Toronto
- Masuda, A. and Nagasawa. S. 1975. Rocks with negative cerium anomalies dredged from the Shatsky Rise. *Geochem. J.*, 9; 227-233
- Matheis, G. and Caen-Vachette, M. 1983. Rb-Sr isotopic study of rare metal bearing and barren pegmatites in the Pan-African reactivation zone of Nigeria. *Jl. Afr. Geol.* 1; No 1 35-40
- McWilliams, M.O. 1981. Palaeomagnetism and Precambrian tectonic evolution of Gondwana. In "Precambrian plate tectonics" Ed. A. Kroner, 687-695, Academic Press, London
- Meyer, C. and Hemley, J.J. 1967. Wallrock alteration. In "Geochemistry of hydrothermal or deposits". Ed. H.L. Barnes. Holt Reinhart and Winston, New York. 166-235
- Mitchell, A.H.G. and Garson, M.S. 1976. Mineralization at plate boundaries. *Miner. Sci. Engng*, 8; 129-169
- Moore, J.M., 1982. Mineral zonation near the granite batholiths of southwest and northern England and some geothermal analogues. In "Metallization associated with acid magmatism." Ed. A.M. Evans 229-241 John Wiley and Sons
- Moreau, M. 1976. L'uranium et les granitoides: essai d'interpretation. In "Geology, Mining and Extractive Processing of Uranium". Ed. M.J. Jones. Inst. Minin. Metall. London, 83-102

- Mustart, D.A. 1972. Phase relations in the peralkaline portion of the system  $\text{Na}_2\text{O}-\text{Al}_2\text{O}_3-\text{SiO}_2-\text{H}_2\text{O}$ . Unpubl. PhD thesis, Stanford University, U.S.A.
- Mysen, B.O. and Virgo, D. 1980. Trace element partitioning and melt structure; an experimental study at latm pressure. *Geochim. Cosmochim. Acta* 44; 12, 1917-1930
- Nabelek, P.I., o'Neil, J.R. and Papike, J.J. 1983. Vapour phase exsolution as a controlling factor in hydrogen isotope variation in granitic rocks: The Notch Peak granitic stock, Utah. *Earth Planet. Sci. Lett.* 66; 137-150
- Nguere, F.R. and Norman, D.I. 1985. The Mayo Darle tin deposit, Cameroon. Abstract 302-303: 13th Colloquium of African Geology, St. Andrews Scotland September 1985. CIFEG publication occasionelle 1985/3. 397pp
- Norrish, K. and Hutton, J.T. 1969. An accurate x-ray spectrographic method for the analysis of a wide range of geological samples. *Geochim. Cosmochim. Acta* 33; 4, 431-453
- Ohmoto, H. 1986. Stable isotope geochemistry of ore deposits. In "Stable isotopes in high temperature geological processes" Eds. J.W. Valley, H.P. Taylor Jr., and J.R. O'Neil 491-556
- Ohmoto, H. and Rye, R.O. 1979. Isotopes of sulphur and carbon. In "Geochemistry of hydrothermal ore deposits", 2nd edition Ed. H.L. Barnes. J. Wiley and Sons, New York, 509-567
- Olade, M.A. 1980. Geochemical characteristics of tin-bearing and tin-barren granites, northern Nigeria. *Econ. Geol.* 75; 71-82
- Orville, P.M. 1962. Alkali metasomatism and feldspars. *Norsk geol. Tidsskr.* 42; 283-316
- Orville, P.M. 1963. Alkali ion exchange between vapour and feldspar phases. *Am.J.Sci.*, 261; 201-237
- Orville, P.M. 1972. Plagioclase cation exchange equilibria with aqueous chloride solution. Results at 700°C and 2000 bars in the presence of quartz. *Am.J.Sci.*, 272; 234-272
- Oversby, V.M. 1975. Lead isotope study of aplites from the Precambrian rocks near Ibadan southwestern Nigeria. *Earth Planet. Sci. Letters*, 27: 177-180 Amsterdam
- Oyawoye, M.O. and Hirst, D. 1964. Occurrence of a montmorillonite mineral in the Nigerian younger granites at Ropp, Plateau Province, northern Nigeria. *Clay Min. Bull.* 5; 427.
- Pearce, T.H. 1969. A contribution to the theory of variation diagrams. *Contrib. Mineral. Petrol.* 19; 142-157
- Pearce, J.A. and Gale, G.H. 1977. Identification of ore-deposition environment from trace element geochemistry of associated igneous host rocks. In "Volcanic processes in ore genesis" Spec. Publ. No. 7 Geol. Soc. Lond. 14-24

Perez, J-B. 1985. Nouvelles donnees sur le complexes granitique anorogenique de Taghouaji (Republique du Niger) influence des fluides au cours de la cristallisation. These de l'Universite de Nancy.

Piper, J.D.A. 1973. Geological interpretation of palaeomagnetic results from the African Precambrian. In "Implications of Continental drift to the earth sciences", Eds. D.H. Tarling and S.K. Runcorn 1: 19-32, Academic Press, London

Pirajno, F. and Jacob, R.E. 1987. Tin-tungsten mineralization in the Brandberg West-Goantagab area of the Damara orogen, Namibia. Abstr. 851-854 Geocongress, July 86, Johannesburg, South Africa.

Pitcher, W.S. 1982. Granite types and tectonic environment. In "Mountain building processes." Ed. K.J. Hsu 19-40 Academic Press, London

Plant, J., Brown, G.C., Simpson P.R. and Smith, R.T. 1980. Signatures of metalliferous granites in the Scottish Caledonides. Trans. Inst. Min. Metall. 89; B198-B210

Plant, J., Simpson, P.R., Green, P.M., Watson J.V. and Fowler, M.B. 1984. Metalliferous and mineralised Caledonian granites in relation to regional metamorphism and fracture systems in northern Scotland. A reply. Trans. Instn. Min. Metall. 93; B47-49

Plimer, I.R. 1983. The geology of tin and tungsten deposits. Inst. Mineral. Petrol. Leoben, Austria. Course Handbook 1-212

Plimer, I.R. and Kleeman, J. 1985. Mineralisation associated with the Mole granite, Australia. In "High heat production granites, hydrothermal circulation and ore genesis" Spec. Iss. Trans. Inst. Mining and Metall. 593pp

Pollack, H.N. and Chapman, D.S. 1977. On the regional variation of heat flow, geotherms and lithospheric thickness. Tectonophysics 38, 279-296

Prins, P. 1978. The geochemical evolution of the alkaline and carbonatite complexes of the Damaraland igneous province, South West Africa. Ann. Univ. Stellenbosch. Ser. Al. (geol) pp145-278

Raeburn, C., Bain, A.D.N. and Russ, W. 1927. The tinfields of Zaria and Kano Provinces. Bull. Geol. Surv. Nigeria 11; 69pp

Rahaman, M.A., Breemen, O.van, Bowden, P. and Bennett, J.N. 1984. Age migrations of anorogenic ring complexes in northern Nigeria. Jl. Geol. 1984 92 173-184

Randohr, P. 1969. The ore minerals and their intergrowths. Pergamon Press.

el Ramly, M.F., Budanov, V.I. and Hussein, A.A.A. 1971. The alkaline rocks of southeastern Egypt. Geol. Surv. Egypt. 53.

Raulais, M. 1946. La serie granitique ultime de l'Air au Niger et sa mineralisation stannifere. C.R.Acad. Sci. Fr., 325 1-194

Raulais, M. 1948. Sur la decouverte de wolfram dans le jeune granite a biotite de l'Air (Niger). C.R. Soc. Geol. Fr., 113-114

- Raulais, M. 1957. La mineralisation de Air (Terr. du Niger) et ses relations avec la tectoniques. C.R. Acad. Sci. Fr., 244 913-916
- Richardson S.W. and Oxburgh E.R. 1978. Heat flow, radiogenic heat production and crustal temperatures in England and Wales. J. Geol. Soc. London 135 323-337
- Rieder, M. 1970. Chemical composition and physical properties of lithium-iron micas from the Krushne Hory Mountains (Erzgebirge), Part A: Chemical composition. Contr. Mineral. Petrol. 27; 131-158
- Rockingham, J.E. 1951. Preliminary report on a lode near Kogo, Tibchi. Geol. Surv. Nigeria, Unpubl. Rep. 875
- Roedder, E. 1971. Metastability of fluid inclusions. Mining Geol (Japan) Spec. Issue 3, 327-334
- Roedder, E. 1984. Fluid inclusions. Reviews in Mineralogy Vol.12. Min. Soc. Amer. 644pp
- Roedder, E. and Coombs, D.S. 1967. Immiscibility in granite melts, indicated by fluid inclusions in ejected granite blocks from Ascension Island. J. Petrol. 8; 417-451
- Roedder, E. and Skinner, B.J. 1968. Experimental evidence that fluid inclusions do not leak. Econ. Geol., 63; 715-730.
- Rose, A.W. and Burt D.M. 1979. Hydrothermal alteration. In "Hydrothermal Ore Deposits." Ed. H.L. Barnes 173-235 John Wiley and Sons
- Rutherford, M.J. 1973. The phase relations of aluminous iron biotites in the system  $KAlSi_3O_8$ - $KAlSiO_4$ - $Al_2O_3$ -Fe-O-H. J. Petrol. 14; 159-80
- Rybach, L. 1976. Radioactive heat production; a physical property determined by the chemistry of rocks. In "The Physics and Chemistry of Minerals and Rocks." Ed. R.G.J. Strens 309-318 John Wiley and Sons.
- el Samani, Y. 1985. Microthermometric study of the Tungsten deposit at Jebel Eyob, Red Sea Hills Sudan. Abstract 306-307: 13th Colloquium of African Geology, St. Andrews Scotland September 1985. CIFEG publication occasionelle 1985/3. 397pp
- Savage, D., Cave, M.R. and Milodowski, A.E. 1985. Interaction of meteoric groundwater with Carnmenellis granite at 250°C and 50 MPa: an experimental study. In "High heat production (HHP) granites, hydrothermal circulation and ore genesis". Inst. Mining and Metall. 315-328
- Schlogl, H.U. 1984. The geology of the Krantzberg tungsten deposit, Omaruru, South West Africa. Unpubl. MSc thesis. Univ. Stellenbosch, South Africa.
- Shaw, D.M. 1980. Development of the early continental crust Part III. Depletion of incompatible elements in the mantle. Precambrian Research 10; 281-299
- Shepherd, T.J. 1981. Temperature-programmable, heating-freezing stage for

- microthermometric analysis of fluid inclusions. *Econ. Geol.* 76; 1244-1247
- Shepherd, T.J., Rankin, A.H. and Alderton, D.H.M. 1985. Fluid inclusion studies. Blackie, London 239pp
- Sheppard, S.F. 1977. Identification of the origin of ore-forming solutions by the use of stable isotopes. In "Volcanic processes in ore genesis" Spec. Publ. No. 7 Geol. Soc. Lond. 25-41
- Sheppard, S.M.F. 1986. Igneous Rocks: 111. Isotopic case studies of magmatism in Africa, Eurasia and Oceanic Islands. In "Stable isotopes in high temperature geological processes" Eds. J.W. Valley, H.P. Taylor Jr., and J.R. O'Neil
- Simonen, A. and Vormaa, A. 1969. Amphibole and biotite from Rapakivi. *Bull. Comm. Geol. Finlande* 238; 28pp
- Smithson, S.B. and Decker, E.R. 1973. K, U, and Th distribution between dry and wet facies of a syenitic intrusion and the role of fluid content. *Earth Planet. Sci. Lett.* 19; 131-134
- Smithson, S.B. and Heier, K.S. 1971. K, U, Th distribution between normal and charnockitic facies of a deep granitic intrusion. *Earth Planet. Sci. Lett.* 12; 325-326
- Stavrakis, P.K. 1975. A geochemical investigation of the granitoid and related rocks from the Southern Uplands, Scotland and northern Nigeria. Unpubl. MSc thesis, University of St. Andrews
- Stoeser, D.B. 1986. Distribution and tectonic setting of plutonic rocks of the Arabian Shield. In "Felsic plutonic rocks and associated mineralisation of the Kingdom of Saudi Arabia," Eds. A.R. Drysdall, C.R. Ramsay and D.B. Stoeser. Sp. Vol. *Journ. African Earth Sci.* Vol 4 pp21-46.
- Sun, S-S., Nesbitt, R.W. and Sharaskin, A.Ya. 1979. Geochemical characteristics of mid-ocean ridge basalts. *Earth Planet. Sci. Lett.*, 44: 119-138
- Suzuki, T. and Epstein, S. 1976. Hydrogen isotope fractionation between OH-bearing minerals and water. *Geochim. Cosmochim. Acta* 40; 1229-1240
- Swanenberg, H.E.C. 1980. Fluid inclusions in high-grade metamorphic rocks from S.W. Norway. *Geologica Ultraiectina, Univ. Utrecht*, 25; 147pp
- Sykes, L.R. 1978. Intraplate seismicity reactivation, reactivation of pre-existing zones of weakness, alkaline magmatism and other tectonism post-dating continental fragmentation. *Rev. Geophys. Space Phys.* 16; 621-688
- Tammemagi, H.Y. and Wheildon J. 1977 Further data on the south-west England heat flow anomaly. *Geophys. J. R. astr. Soc.* 49; 531-539
- Taylor, J. 1959. Occurrence of beryllium in the younger granites of northern Nigeria. Unpubl. Rep. Geol. Surv., UK Atom. Energ. Div. 221
- Taylor, J. 1961. Investigations on the economic potential of danalite-genthelvite occurrences in northern Nigeria. Unpubl. Rep. Geol. Surv.

U.K. Atom. Energy Div., No. 237.

Taylor, R.G. 1974. Metallogenic provinces as an approach to the problems of classification and genesis of tin deposits with special reference to eastern Australia. In "Metallization associated with acid magmatism" Ed. M. Stempok 74-78, Geological Survey, Prague

Taylor, H.P. 1974. The application of oxygen and hydrogen isotope studies to problems of hydrothermal alteration and ore deposition. *Econ. Geol.* 69; 843-883

Taylor, H.P. 1979. Oxygen and hydrogen isotope relationships in hydrothermal mineral deposits. In "Geochemistry of hydrothermal ore deposits", 2nd edition Ed. H.L. Barnes. J. Wiley and Sons, New York, 236-277

Thode, H.G., Monster, J. and Dunford, H.B. 1961. Sulphur isotope geochemistry. *Geochim. Cosmochim. Acta* 25; 159-174

Thornton, C.P. and Tuttle, O.F. 1960. Chemistry of igneous rocks, 1 Differentiation index. *Am. J. Sci.* 258; 664-684

Tugarinov, A.I., Kovalenko, V.I., Znamensky, E.B., Legeido, V.A., Sobatovich, E.V., Brandt, S.B. and Tsyhansky, V.D. 1968. Distribution of Pb-isotopes, Sn, Nb, Ta, Zr and Hf in granitoids from Nigeria. In "Origin and distribution of the elements," Ed. L.H. Ahrens. *Monographs in Earth Sciences*, 30: 687-699; Pergamon Press, Oxford

Turekian, K.L. and Wedepohl, K.H. 1961. Distribution of the elements in some major units of earth crust. *Geol. Soc. Am. Bull.*, 72; 641-664.

Turner, D.C. 1963. Ring structures in the Sara Fier complex, northern Nigeria. *Q. Journ. Geol. Soc. Lond.* 119; 345-366

Turner, D.C. and Bowden, P. 1979. The Ningi-Burra complex, Nigeria: dissected calderas and migrating magmatic centres. *Jl. Geol. Soc. Lond.* 136; 105-119

Tuttle, O.F. and Bowen, N.L. 1958. Origin of granite in the light of experimental studies in the system  $\text{NaAlSi}_3\text{O}_8$ - $\text{KAlSi}_3\text{O}_8$ - $\text{SiO}_2$ - $\text{H}_2\text{O}$ . *Geol. Soc. Am. Mem.* 74; 153pp

Vail, J.R. 1978. Outline of the geology and mineral deposits of the Democratic Republic of Sudan and adjacent areas. *Overseas Geol. Miner. resourc. Lond.* No 49.

Vail, J.R. 1979. Outline of geology and mineralisation of the Nubian shield east of the Nile valley, Sudan. In "Evolution and mineralization of the Arabian-nubian shield". *Inst. Applied Geol., King Adulaziz Univ, Jeddah, Vol. 1*, 97-107

Vail, J.R. 1985. Alkaline ring complexes in Sudan. *Journl. African Earth Sci.*, Vol 3 1/2 51-59

Valakovich, M.P. and Altunin, U.V. 1968. *Thermophysical Properties of carbon dioxide*. Colletts, London

- Varlamoff, N. 1972. Central and West African rare metal pegmatites, related aplites, quartz veins and mineral deposits. *Mineralium Deposita* 7, 202-216
- Vartiainen, R. and Woolley, A.R. 1976. The petrography, mineralogy and chemistry of the fenite of the Sokli carbonatite intrusion, Finland. *Geol. Surv. Finland Bull.* 280, 1-87
- Verheijen, P.J.T. and Ajakaiye, D.E. 1979. Heat flow measurements in the Ririwai ring complex, Nigeria. *Tectonophysics*, 54; 27-32
- Vidal, Ph., Dosso, L. Bowden, P and Lameyre, J. 1979. Strontium isotope geochemistry in syenite-alkaline granite complexes. In "Origin and distribution of the elements" Ed. L.H. Ahrens. *Phys. Chem. Earth*, 11; 223-231
- Webb, P.K. 1974. Roof modifications of a high level granite, Jos Bukuru complex, northern Nigeria. *Geol. Mag.* 111; No 1.
- Webb, P.C. and Brown, G.C. 1984a. The Eastern Highlands granites: heat production and related geochemistry. B.G.S. Investigation of the geothermal potential of the UK. 1-77
- Webb, P.C. and Brown, G.C. 1984b. Lake District granites: heat production and related geochemistry. B.G.S. Investigation of the geothermal potential of the U.K. 1-66
- Wedepohl, K.H. 1969,1970. Handbook of geochemistry. Springer Verlag
- Weisbrod, A. 1981. Fluid inclusions in shallow intrusives. In "Short course in fluid inclusions: applications to petrology" Min. Assoc. Canad., Short Course Handbook, Eds L.S. Hollister and M.L. Crawford. 241-267
- White, D.E. 1955. Thermal springs and epithermal ore deposits (50th Anniversary Volume): *Econ. Geol.* 50; 99-154
- Williams, P.A., Meehan, J.A., Paulo, K.L., John, T.U. and Rushton, H.G. 1956. Economic geology of the decomposed columbite-bearing granites, Jos Plateau, Nigeria. *Econ. Geol.* 51; 303-332
- Wilson, M. R. and Akerblom G.V. 1982. Uranium enriched granites in Sweden. In "Metallization associated with acid magmatism." Ed. A.M. Evans 367-385 John Wiley and Sons.
- Woolley, A.R. and Garson, M.S. 1970. Petrochemical and tectonic relationship of the Malawi carbonatite-alkaline province and the Luputa-Lebombo volcanics. In "African magmatism and tectonics" Eds. T.N. Clifford and I.G. Gass, 237-262. Oliver and Boyd, London.
- Wright, J.B. 1976. Origins of the Benue trough - a critical review. In "Geology of Nigeria." Ed. C.A. Kogbe, 309-318, Elizabethan press, Lagos
- Wright, J.B. 1981. Review of the origin and evolution of the Benue Trough, Nigeria. *EES*, 2, 98-103, Wiesbaden
- Wyllie, P.J. 1979. Magmas and volatile components. *Am. Mineral.* 64, 469-500

Wyllie, P.J. and Tuttle, O.F. 1964. Experimental investigations of silicate systems containing two volatile components. Part 111 The effects of  $\text{SO}_3$ ,  $\text{P}_2\text{O}_5$ ,  $\text{HCl}$  and  $\text{Li}_2\text{O}$  in addition to  $\text{H}_2\text{O}$  on the melting temperatures of albite and granite. *Am. J. Sci.* 262; 930-939

Ypma, J.M. and Simons, J.H. 1969. Genetic aspects of tin mineralisation in Durango, Mexico. A second technical conference on tin. Bangkok, 177-192

## Appendix 2 Method of XRF analysis in St. Andrews Geology Department

### Method of analysis

1) The sample is prepared from the solid rock specimen by first removing all obvious weathered portions using a grinding wheel. It is then split using a Lake and Elliot hydraulic splitter with stainless steel jaws. These blocks are then fed into a Sturtevant jaw crusher with steel jaws to reduce the rock to small chips. The chips are then ground in a Tema swing mill with tungsten carbide discs until the powder is less than 200 mesh.

2) Major elements are determined using a fused glass bead prepared from 0.5g of rock powder and 2.5g of Spectroflux 105 and ammonium nitrate as oxidant. The method is essentially that of Norrish and Hutton, 1968 (Geochimica et Cosmochimica Acta). X-ray analysis is performed on a Philips PW1212 using a Rh tube for primary excitation. Details of analytical conditions are given in the table below. Calibration is done by reference to a monitor (H12) supplied by K. Norrish, and using 25 international rock standards. The method uses a calculated regression line through apparent fluorescence values (AFV) as described by Harvey et al. (1973, X-ray Spectrometry). Matrix corrections are applied on an iterative basis using an on-line microcomputer and using coefficients for the Rh tube also supplied by K. Norrish. The methods and conditions are generally similar to those described by Norrish and Chappell (1977) p201-272 in Zussman, J "Physical Methods in Determinative Mineralogy", Academic Press. Iron is determined as total  $Fe_2O_3$  and FeO is determined independently by wet methods. The weight loss of the rock sample on fusion is measured and is used as an estimate of loss on ignition.

3) Trace elements are analysed on pressed powder discs, prepared for the better international standards by pressing to 5 tons a powder mixed with Moviol as binder. The elements are excited with a Rh tube and analysed with either LiF200 or LiF220 crystals. The apparent fluorescence values (AFV) are calculated for the better international standards by inverting the normal matrix correction procedure. These AFV values are then regressed against their intensities (already corrected for line overlap or blank values) and the coefficients of the line used in analysis. All intensities are calculated in terms ratios to a monitor in the first sample position to eliminate the effects of machine drift. For consistency all calculations are performed by an on-line microcomputer.

### Accuracy and precision

The precision estimates are based on six replicates each on six separate beads or pressed powder disks (trace elements and MnO) and the statistics are derived in the manner described by Harvey et al. (X-ray Spectrometry v2, 33-44, 1973). Oxides are quoted in %, elements as ppm. The apparently poor coefficient of variation (c.v.) for  $P_2O_5$  is due to the original sample being deficient in this component.

	Mean composition	Instrument precision		Pellet/Bead variation		overall st. dev.
		st. dev.	c. v. %	st. dev.	c. v. %	
SiO2	71.65	0.156	0.22	0.101	0.14	0.177
TiO2	0.39	0.001	0.33	0.006	1.49	0.006
Al2O3	14.52	0.052	0.36	0.016	0.11	0.042
Fe2O3	2.66	0.014	0.53	0.109	4.10	0.114
MgO	0.68	0.046	6.73	0.025	3.67	0.035
CaO	1.93	0.004	0.18	0.010	0.51	0.010
Na2O	3.61	0.118	3.27	0.027	0.75	0.099
K2O	3.52	0.003	0.10	0.014	0.40	0.013
P2O5	0.08	0.011	14.02	0.004	5.19	0.011
MnO	0.55	0.0002	0.29	0.00023	0.42	0.0003
V	34.5	0.8	2.27	0.5	1.45	0.9
Ba	908	9	0.96	2.7	0.30	8.0
La	105	1.3	1.25	1.1	1.05	1.3
Ce	129.4	2.1	1.63	1.1	0.86	2.0
Hf	5.83	0.35	6.00	0.26	4.46	0.41
Cr	60.7	0.6	1.04	1.3	2.19	1.4
Ni	106.0	0.7	0.68	1.1	1.00	1.2
Cu	34.5	0.7	1.94	0.5	1.57	0.8
Zn	62.5	0.8	1.19	0.2	0.37	0.7
Nb	27.3	1.18	4.30	1.59	5.81	2.0
Zr	216.8	0.92	0.43	6.93	3.20	6.9
Y	26.1	0.90	3.43	1.32	5.05	1.5
Sr	324.1	1.45	0.45	1.08	0.33	1.8
Rb	176.9	1.50	0.85	0.65	0.37	1.4
Th	24.4	3.03	12.42	0.55	2.27	4.2
Pb	23.8	0.97	4.08	0.19	0.83	0.8

Accuracy can only be estimated by reference to 'accepted' values, and the values given below are for the well-known USGS reference standards. The six standards were run 'blind' in a normal analytical session. The 'accepted' values are those given by Abbey, Geological Survey of Canada (1977) Paper 77-34.

USGS STANDARDS

	G-2		GSP-1		AGV-1		PCC-1		DTS-1		BCR-1	
	Abbey	St. A										
SiO2	69.19	69.08	67.31	67.21	59.72	59.10	42.15	42.18	40.68	40.76	54.85	54.30
TiO2	0.50	0.49	0.66	0.66	1.05	1.05	0.01	0.00	0.01	0.00	2.22	2.21
Al2O3	15.35	15.30	15.19	14.92	17.22	17.03	0.73	0.71	0.29	0.28	13.68	13.43
Fe2O3	2.67	2.67	4.33	4.52	6.84	6.94	8.28	8.32	8.60	8.96	13.52	13.63
MgO	0.77	0.54	0.96	0.82	1.55	1.66	43.63	43.63	49.83	50.01	3.49	3.87
CaO	1.98	2.00	2.02	2.06	5.00	5.02	0.53	0.53	0.15	0.09	6.98	6.98
Na2O	4.06	4.13	2.80	2.72	4.31	4.40	0.01	0.00	0.01	0.00	3.29	3.37
K2O	4.52	4.51	5.53	5.48	2.93	2.97	0.00	0.00	0.00	0.00	1.68	1.74
P2O5	0.14	0.13	0.28	0.27	0.50	0.50	0.00	0.01	0.00	0.01	0.33	0.35

Analytical conditions

Element	Line	Background	Time(s)	Crystal	Counter	Coll.	KV	mA
Si	K-alpha	-2.20	40	PE	Flow	C	50	32
Ti	K-alpha		20	LiF200	Flow	C	60	24
Al	K-alpha		40	PE	Flow	C	60	32
Fe	K-alpha		20	LiF200	Flow	C	60	24
Mn	K-alpha	+2.85	100	LiF200	Flow	C	60	32
Mg	K-alpha	+2.68	100	TAP	Flow	C	60	32
Ca	K-alpha		20	LiF200	Flow	C	60	24
Na	K-alpha	-2.25	100	TAP	Flow	C	60	32
K	K-alpha		40	PE	Flow	C	60	32
P	K-alpha	+1.93	100	PE	Flow	C	60	32
Nb	K-alpha	+2.88	100	LiF200	Scint	F	60	32
Zr	K-alpha	-1.55	100	LiF200	Scint	C	60	32
Y	K-alpha	+0.48	100	LiF200	Scint	C	60	32
Sr	K-alpha	+1.17	100	LiF200	Scint	C	60	32
Rb	K-alpha	+0.58	100	LiF200	Scint	C	60	32
Pb	L-beta(1)	+0.54	100	LiF200	Scint	F	60	32
Th	L-alpha(1)	-0.23	100	LiF200	Scint	F	60	32
Mn	K-alpha	+1.28	40	LiF220	Flow	C	60	32
V	K-alpha	-2.60	100	LiF220	Flow	F	60	32
Ba	L-beta(1)	+1.80	100	LiF220	Flow	F	60	32
Hf	L-alpha(1)	+1.00	100	LiF200	Flow	F	60	32
Ce	L-beta(1)	-0.90	100	LiF200	Flow	F	60	32
La	L-alpha(1)	+2.70	100	LiF220	Flow	C	60	32
Ti	K-beta(1+2)		20	LiF220	Flow	F	60	32
Zn	K-alpha	-1.27	40	LiF220	Flow	C	60	32
Cu	K-alpha	+1.84	20	LiF200	Flow	C	60	32
Ni	K-alpha	+1.30	40	LiF200	Flow	C	60	32
Cr	K-alpha	+1.40	20	LiF200	Flow	C	60	32

Appendix 3 Chemical analysis of selected major and trace elements by AAS techniques.

Selected major and trace elements were determined by a scheme which utilises a combination of published techniques and formed the basis for wet chemical analyses at St. Andrews. Details are available in:-

Batchelor, R.A. Analysis of major, minor and selected trace elements in silicate rocks and minerals. Int. Publ. 80/1. Dept. Geol. Univ. St. Andrews

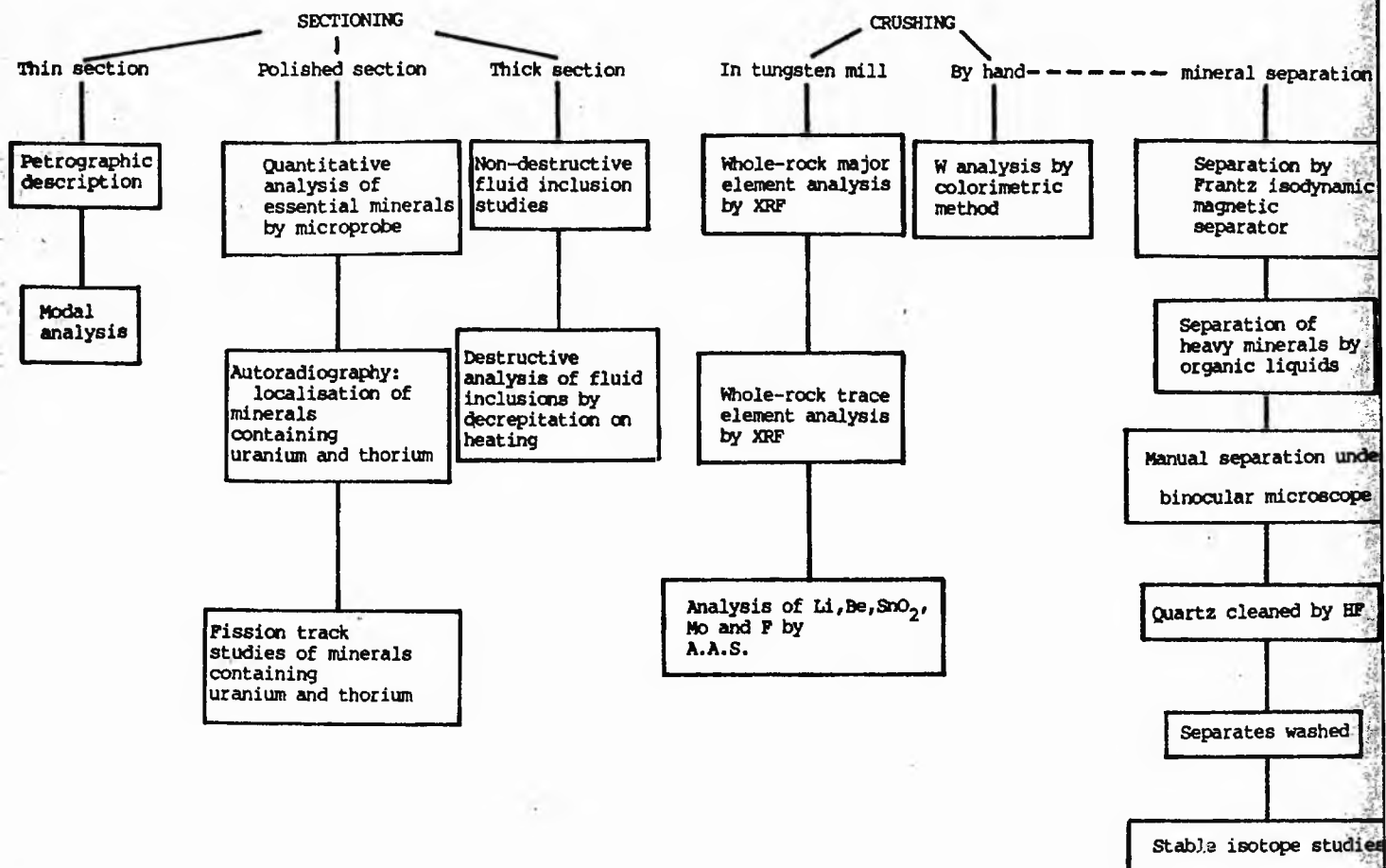
The precision of element analysis is as follows:

Standard deviations and coefficient of variance

Element	Mean	1SD	CV
Li	43	1.0	2.3
Zn	56	0.8	1.4
Cd	1970	43	2.2
Fe	10.6%	0.14	1.3
Zn	53.8%	1.06	1.9
Mn	0.95%	<0.01	<0.1
Sn	290	9	3.0

Appendix 4 Summary of the different methods of study of the rocks and mineral utilised in this work

ROCK SAMPLE



Appendix 5 Basic programme for the BBC microcomputer for the calculation of multicationic parameters R1-R2 and Q-F

$$R1 = 4Si - 11(Na+K) - 2(Fe+Ti)$$
$$R2 = 6Ca + 2Mg + Al$$

after de la Roche (1980)

$$Q = 1/3Si - (K+Na+2/3Ca)$$
$$F = K - (Na+Ca)$$

after de la Roche (1964)

```
10 REPEAT
20 CLS
30 INPUT "Si="Si, "Ti="Ti, "Al="Al, "Fe+++="Fe3, "Fe++="Fe2, "Mg="Mg, "Ca="Ca, "Na="Na, "K="K
40 Si=Si/60.09:Ti=Ti/79.9:Al=Al/101.96*2.0
50 Fe3=Fe3/159.69*2.0:Fe2=Fe2/71.85:Mg=Mg/40.3
60 Ca=Ca/56.08:Na=Na/61.98*2.0:K=K/94.2*2.0
70 R1=4*Si-11*(Na+K)-2*(Fe3+Fe2+Ti)
80 R2=6*Ca+2*Mg+Al
90 Q=Si/3-(K+Na+2/3*Ca)
100 F=K-(Na+Ca)
110 PRINT "R1=";R1*1000;"R2=";R2*1000;"Q=";Q*1000;"F=";F*1000
120 SILLY=GET
130 UNTIL FALSE
```

The instrument and its use

The JEOL JCA733 is a modern full function EPMA with 3 wavelength dispersive spectrometers (WDS) and controlled by a 28K word computer.

A beam of accelerated electrons is generated in an electron gun with W filament and focussed using electromagnetic condenser lenses. Normal accelerating voltages range from about 10 to 30 kV and beam currents of 1 to 25 nA. The beam may be focussed on a fixed point for microanalysis or scanned in raster fashion over a specified rectangle. Solid samples are presented to the beam horizontally, normal to the vertical beam axis, and resulting interactions are detected as secondary electrons, backscattered electrons, and X-rays.

In analytical terms it is one of the most sensitive of all analytical techniques and is capable of detecting  $10^{-15}$  g of a given element in a volume of approx. 1 cubic micron. This is an improvement on optical emission techniques ( $10^{-10}$  g), mass spectrometry ( $10^{-13}$  g), and is bettered only by radioactive tracer analysis and secondary ion mass spectrometry (both  $10^{-18}$  g) neither having the same spatial resolution in analysis. Thus for the analysis of points or areas on the micron scale EPMA is currently the best available technique and is widely used in materials analysis.

Imaging capabilities

Three basic types of image can be obtained in Scan mode depending on the detector selected.

1. SEI (scanning electron image) mode. Secondary electrons originating from interactions of the primary electron beam with the surface of the solid are collected by a scintillator-photomultiplier-collecting electrode system. This is capable of giving a very high resolution image of the surface features, as commonly used in electron microscopes.

2. BEI (backscattered electron image) mode. Backscattering of the electron beam by a target is principally a function of the atomic number of the target (or mean atomic number of a compound). By detecting this scatter using a Si, P-N junction detector small differences in materials of different composition can be detected. Thus an image reflecting composition may be generated. The method is sensitive to about 0.1 of an atomic number. The image is thus sometimes known as composition image or atomic number contrast image.

3. X-RAY (dot maps of X-ray sources) mode. The interaction of beam electrons with orbital electrons in the sample can give rise to X-ray emissions if the energy of the electron beam exceeds the X-ray excitation potential of an element in the sample. X-rays are detected using Bragg Law crystal spectrometers. By selecting an appropriate X-ray emission line for the sample and scanning over the surface an image is produced as a map of the sources of each X-ray emission. In this way the spatial distribution of an element in a solid may be observed. Spatial resolution is not very good using this method.

In all image modes scan rates and magnifications are easily varied and a split screen may be used to compare two images. Cameras (Polaroid and film) record the images and are used for accumulating multiple scans to give better image definition.

Analysis capabilities

The principal function of EPMA is accurate analysis of solid materials. X-rays from about boron upwards in the periodic table may be detected though detection limits for the light elements may be about 1% compared with about 0.01% or less for heavy elements. The method uses X-ray fluorescence spectrometry (XRFS). Two types of analysis are commonly performed:

1. Qualitative, achieved by scanning through the X-ray spectrum to record identifiable X-ray emissions. 2. Quantitative, in which the unknown is analysed by reference to analysed standards, mainly pure elements. In this case several corrections must be applied to the unknown to cater for differences between the matrix of the unknown and the standards. The principal corrections are for differences in Z for electron scattering, for differences in X-ray absorption, and for differences in secondary fluorescence characteristics. Such corrections typically adjust the initial estimate of composition as a function of intensity ratio to pure element by 10-20%. The method typically has a precision (2 sigma) of about 1%.

X-ray emissions arise from a volume typically 1 micron in diameter and about 1 micron deep into the sample and this is the limit to resolution of the method, though a diameter of up to 50 microns may be measured.

#### Specification

Accelerating voltage 5-50 kV

SEM resolution 7nm

Magnification 20-360,000

Working vacuum  $1.3 \times 10^{-3}$  Pa

Spectrometer crystals LiF (K-U)

PE (Si-Fe)

TAP (F-P)

STE (B-O)

Optical microscope x414 magnification, incident and transmitted light

Specimen stage 4 position, exchange through airlock

Specimen size typically 32 mm in maximum dimension

Computer DEC LSI11, 28K words.

## Appendix 7 Fluid inclusions studies

### Theoretical basis of inclusion studies

The most common constituent of fluid inclusions is water. In addition, gas or solid phases may co-exist. Most liquid and solid phases have separated out from a homogeneous liquid as it cooled. Fluid which filled the inclusion at high temperature, shrank in volume on cooling. Solid phases formed when the liquid became saturated in these phases as it cooled, resulting in the formation of daughter minerals. In this study it has usually been possible to distinguish between daughter minerals and captured minerals. Daughter minerals, despite the fact that they may not melt before the temperature of homogenisation, are recognised on the regularity of occurrence within inclusions and similarity of phase ratio of the solid in question. The most common daughter mineral is halite, since NaCl is the most common solute.  $K^+$ ,  $Ca^{++}$ ,  $SO_4^-$ ,  $CO_3^-$  and  $HCO_3^-$  are the next most abundant cations and anions respectively, and sylvite, carbonate and sulphate daughter minerals occur.

Heating experiments are designed to heat an inclusion to the temperature at which vapour, fluid and solid phases return to the one original phase. This is the homogenisation temperature ( $T_h$ ) and represents the true temperature of trapping only if the fluid was boiling at the time of trapping. If, however, the fluid was under sufficiently high pressure to prevent it boiling, it would have to cool to lower temperatures before the vapour began to form and the homogenisation temperature represents the minimum temperature of trapping. This can be corrected to the true temperature of formation provided that the total pressure at the time of trapping can be determined or estimated. Also on heating, daughter minerals will melt. The temperature at which the dissolution occurs can be used to determine the salinity of an inclusion and also helps to distinguish between halite and sylvite.

Freezing measurements are designed to determine the salinity of dilute inclusions that do not contain daughter minerals. Since dissolved salts depress the freezing point of water, the depression of the freezing point below  $0^\circ C$  is used to measure the salinity. This is measured in terms of equivalent wt% NaCl which is partly justified since NaCl is the principal solute in most aqueous inclusions. Since it is a measure of the total dissolved salt content the equivalent weight percent is therefore the amount of NaCl that would produce a similar depression of the freezing point. The higher the salt concentration, the lower the freezing point. Freezing measurements also help in the identification of dissolved organic compounds, particularly  $CO_2$  and  $CH_4$ , and from first melting temperature of the frozen fluid, indicate the main cationic species of the fluid (Crawford 1981).

### Equipment

The equipment used for microthermometric analysis is a Linkam TH600 system (Shepherd 1981). A temperature controlled chamber has been designed for experiments over the dynamic range  $-180^\circ C$  to  $+600^\circ C$  with a maximum resolution of  $0.1^\circ C$ .

The equipment (Appendix 7 Plate) consists of:-

- a) A heating/freezing chamber which is mounted on the stage of a Leitz microscope.
- b) A console with a digital temperature display and heating controls
- c) A console with an automatic temperature print-out linked to the temperature console
- d) A Dewar flask for cooling gas.

Organic and inorganic compounds were used to calibrate the equipment over the range -96 to + 398°C. Reproducibility of results is within +1% (MacDonald and Spooner 1981).

#### Calibration of the Linkam TH600 heating freezing stage

Selected compounds of spec. pure standards and organic liquids of known melting point were chosen on the basis of Rankin (1978) and MacDonald and Spooner (1981). After a number of different experimental techniques were used for a variety of compounds, the following were found to be most useful and were used for routine calibration:-

Compound	Melting temperature (°C)
potassium dichromate	398
sodium nitrate	307
4 chlorobenzoic acid	239
3-5 dinitrobenzoic acid	205
benzoic acid	122
acetanilide	115
phenyl benzoate	69
tetradecane	+5.86
water	0
n dodecane	-9.6
decane	-29.7
m-xylene	-47.86
pure CO <sub>2</sub> inclusion	-56.6
toluene	-95

Two different techniques were utilised for calibration, depending on the nature of the substance being used:-

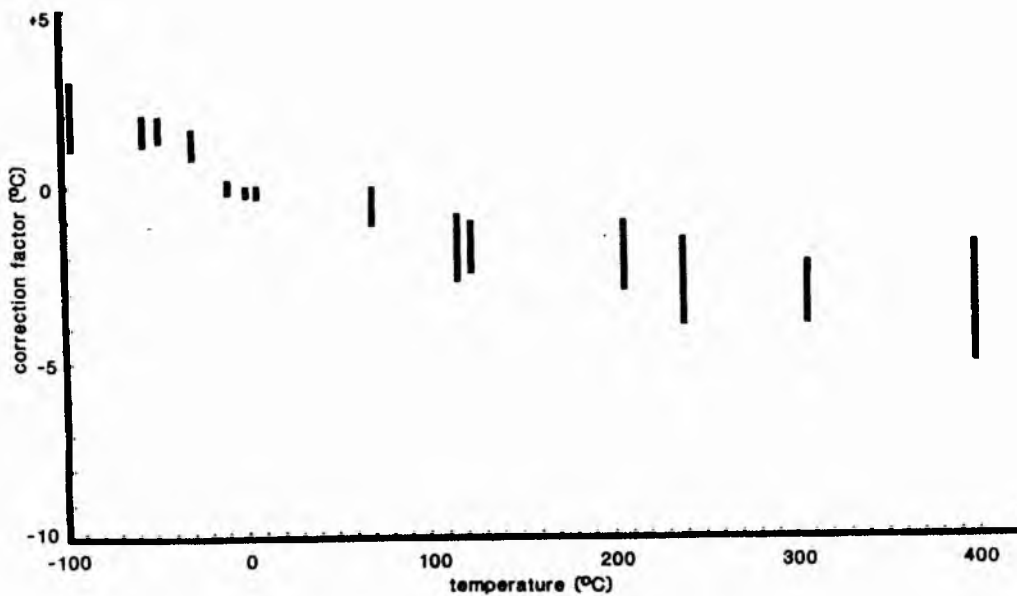
(1) For organic liquids a small droplet of liquid was placed on a glass plate by a micropipette and covered with a glass cover slip. This technique was also applied to certain solid compounds taking care to select only the smallest crystal grains for study. This was to ensure that the grains were as close as possible to the size of the fluid inclusions being studied.

(2) For compounds which sublime a sealed glass capillary tube was found to be the most successful. However, where possible such compounds were avoided.

The degree of care given to calibration of the stage varies depending on the

temperature range of the phase changes under consideration. For example errors of a few degrees at high temperature in the vapour-liquid homogenisation are unimportant. This is because uncertainties in the P-V-T properties of the fluid and from the estimate of pressure of entrapment are greater. However, for other studies, such as the effect of composition on the CO<sub>2</sub>-H<sub>2</sub>O solvus, accuracy of calibration is extremely important. Accuracy of measurement is generally more important for melting temperatures, than homogenisation temperatures. Errors in measuring temperatures of clathrate, hydrates and ice can also lead to significant errors in determining both amounts and presence of components dissolved in aqueous phases. For this reason, special care was taken for calibration in the range -30 to +30°C.

A typical calibration curve is presented in Appendix Fig 1.



calibration curve for the Linkam TH600 stage showing the relatively poor reproducibility of calibration standards

Pressure-density data from Haas 1971

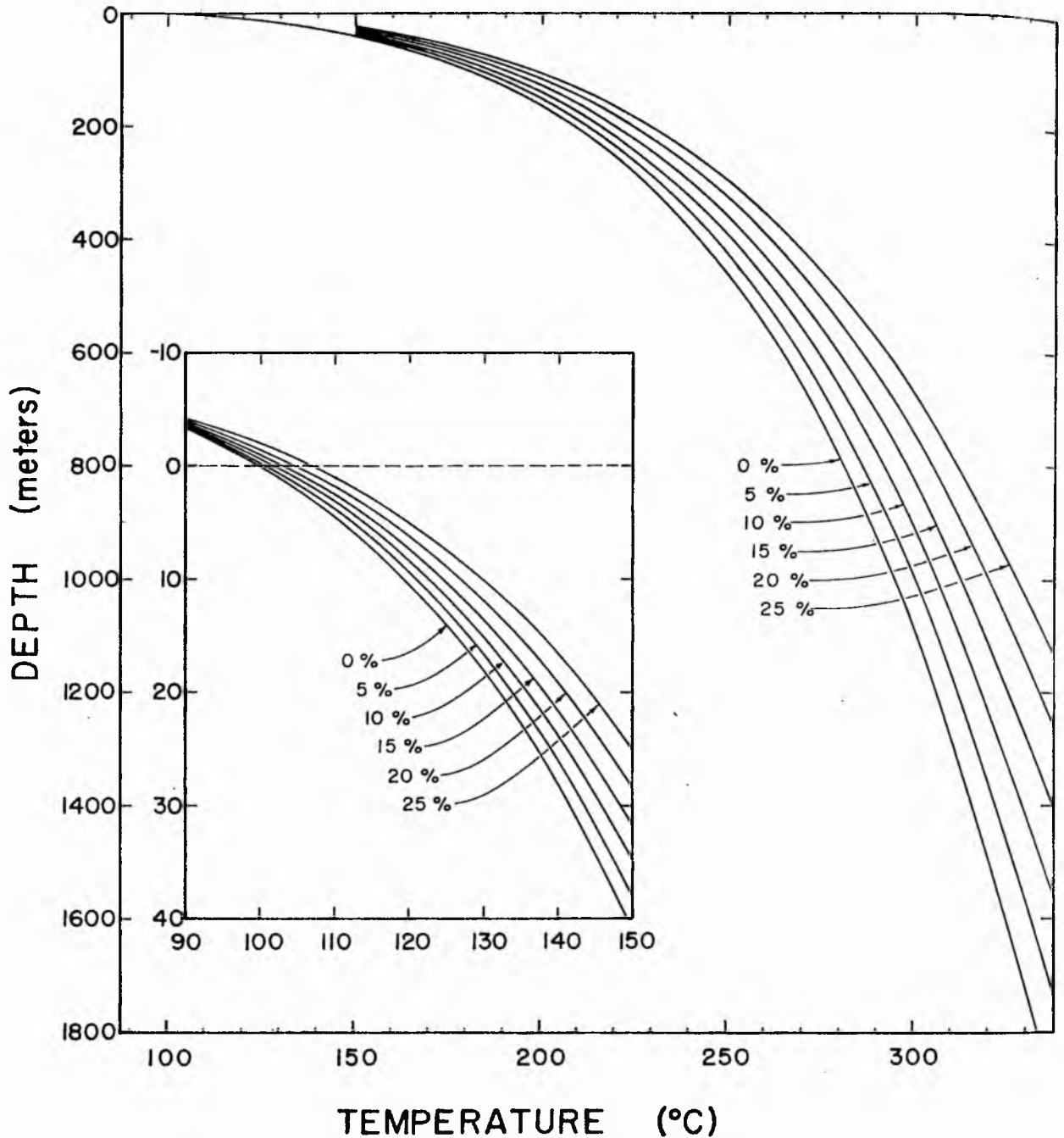
Thermal Profiles for Selected Compositions of NaCl-H<sub>2</sub>O Liquids  
With Corresponding Vapor Pressures and Densities<sup>2</sup>

The temperature at the water-table ( $P_0=1.013$  b) is given at the bottom of each profile.

Temp. (°C)	2.0 Wt Per Cent NaCl			5.0 Wt Per Cent NaCl			10.0 Wt Per Cent NaCl		
	Depth (meters)	Pressure (bars)	Density (g/cm <sup>3</sup> )	Depth (meters)	Pressure (bars)	Density (g/cm <sup>3</sup> )	Depth (meters)	Pressure (bars)	Density (g/cm <sup>3</sup> )
$T_b$	0.0	1.0	0.972	0.0	1.0	0.992	0.0	1.0	1.027
90.	-3.3	0.7	0.979	-3.4	0.7	1.000	-3.5	0.7	1.035
100.	-0.1	1.0	0.972	-0.3	1.0	0.993	-0.7	0.9	1.029
110.	4.2	1.4	0.965	3.9	1.4	0.986	3.2	1.3	1.022
120.	10.0	2.0	0.957	9.4	1.9	0.978	8.4	1.9	1.014
130.	17.6	2.7	0.949	16.7	2.6	0.970	15.2	2.5	1.007
140.	27.3	3.6	0.941	26.1	3.5	0.962	23.8	3.4	0.999
150.	39.7	4.7	0.932	37.9	4.6	0.953	34.8	4.4	0.990
160.	55.1	6.1	0.922	52.7	6.0	0.944	48.5	5.8	0.982
170.	74.3	7.8	0.913	71.0	7.7	0.935	65.6	7.4	0.973
180.	97.7	9.9	0.902	93.4	9.7	0.925	86.2	9.4	0.963
190.	126.0	12.4	0.892	120.5	12.2	0.915	111.3	11.7	0.954
200.	160.1	15.4	0.881	153.1	15.1	0.904	141.4	14.5	0.944
210.	200.8	18.9	0.869	191.9	18.5	0.893	177.2	17.8	0.934
220.	248.9	22.9	0.857	237.8	22.5	0.882	219.4	21.7	0.923
230.	305.5	27.7	0.845	291.7	27.1	0.870	269.0	26.1	0.912
240.	371.7	33.1	0.831	354.7	32.5	0.857	326.7	31.2	0.901
250.	448.6	39.3	0.817	427.8	38.6	0.844	393.6	37.1	0.889
260.	537.8	46.4	0.803	512.3	45.5	0.830	470.7	43.8	0.876
270.	640.5	54.4	0.787	609.6	53.3	0.816	559.3	51.3	0.863
280.	758.7	63.4	0.771	721.2	62.2	0.801	660.6	59.9	0.850
290.	894.3	73.6	0.753	849.0	72.1	0.784	776.0	69.4	0.835
300.	1049.5	84.9	0.734	994.9	83.2	0.767	907.3	80.0	0.820
310.	1227.2	97.5	0.714	1161.3	95.6	0.748	1056.2	91.9	0.804
320.	1430.7	111.5	0.691	1351.1	109.3	0.727	1225.0	105.1	0.787
330.	1664.3	127.1	0.666	1567.8	124.5	0.704	1416.3	119.1	0.768
	$T_b = 100.3^\circ\text{C}$			$T_b = 100.9^\circ\text{C}$			$T_b = 101.9^\circ\text{C}$		

Temp. (°C)	15.0 Wt Per Cent NaCl			20.0 Wt Per Cent NaCl			25.0 Wt Per Cent NaCl		
	Depth (meters)	Pressure (bars)	Density (g/cm <sup>3</sup> )	Depth (meters)	Pressure (bars)	Density (g/cm <sup>3</sup> )	Depth (meters)	Pressure (bars)	Density (g/cm <sup>3</sup> )
$T_b$	0.0	1.0	1.063	0.0	1.0	1.101	0.0	1.0	1.139
90.	-3.7	0.6	1.072	-3.9	0.6	1.110	-4.1	0.6	1.150
100.	-1.0	0.9	1.065	-1.4	0.9	1.104	-1.9	0.8	1.144
110.	2.6	1.3	1.059	1.9	1.2	1.097	1.1	1.1	1.137
120.	7.3	1.8	1.051	6.2	1.7	1.090	5.0	1.6	1.129
130.	13.6	2.4	1.044	11.9	2.3	1.082	10.2	2.1	1.122
140.	21.6	3.2	1.036	19.2	3.1	1.075	16.8	2.9	1.114
150.	31.7	4.3	1.028	28.5	4.0	1.067	25.2	3.8	1.106
160.	44.3	5.5	1.020	40.0	5.2	1.058	35.7	4.9	1.098
170.	59.9	7.1	1.011	54.3	6.7	1.050	48.6	6.3	1.089
180.	79.0	9.0	1.002	71.7	8.5	1.041	64.4	8.0	1.081
190.	102.0	11.2	0.993	92.7	10.6	1.033	83.5	10.0	1.072
200.	129.6	13.9	0.984	117.9	13.2	1.024	106.4	12.4	1.063
210.	162.4	17.0	0.974	147.8	16.2	1.015	133.6	15.2	1.055
220.	201.1	20.7	0.964	183.1	19.7	1.005	165.7	18.5	1.046
230.	246.4	25.0	0.954	224.3	23.7	0.996	203.1	22.3	1.037
240.	299.1	29.9	0.944	272.2	28.4	0.986	246.6	26.7	1.028
250.	360.1	35.5	0.933	327.6	33.7	0.977	296.8	31.8	1.019
260.	430.2	41.9	0.922	391.1	39.7	0.967	354.3	37.5	1.010
270.	510.5	49.1	0.910	463.8	46.6	0.957	420.0	44.0	1.002
280.	602.1	57.2	0.899	546.4	54.3	0.947	494.7	51.3	0.993
290.	706.1	66.3	0.887	639.9	62.9	0.937	579.0	59.5	0.985
300.	823.8	76.5	0.874	745.5	72.6	0.927	673.9	68.6	0.977
310.	956.8	87.8	0.861	864.2	83.3	0.916	780.4	78.7	0.969
320.	1106.7	100.3	0.847	997.3	95.2	0.906	899.3	90.0	0.962
330.	1275.3	114.2	0.832	1146.2	108.4	0.896	1031.7	102.4	0.954
	$T_b = 103.2^\circ\text{C}$			$T_b = 104.7^\circ\text{C}$			$T_b = 106.7^\circ\text{C}$		

Pressure-density data from Haas 1971



Boiling-point curves for H<sub>2</sub>O liquid (0 wt percent) and for brine of constant composition given in wt percent NaCl. Insert expands the relations between 100° and 150°C. The temperature at 0 meters of each curve is the boiling point for the liquid at 1.013 bars (1.0 atm) load pressure which is equivalent to the atmospheric pressure at sea level. The uncertainty is contained within the width of the lines.

## Appendix 8 Fluid extraction system

### Introduction

In addition to water in fluid inclusions, there are small amounts of volatile constituents which in relative order of abundance may include  $\text{CO}_2$ ,  $\text{CH}_4$ ,  $\text{N}_2$ ,  $\text{H}_2\text{S}$ ,  $\text{H}_2$ , and various other saturated hydrocarbons together with trace amounts of  $\text{CO}$ ,  $\text{NH}_3$ , Ar and other rare gases,  $\text{SO}_2$ , and S-rich hydrocarbons. The fluid extraction train has been designed and constructed for the isolation and analysis of the fluids trapped as inclusions in minerals by Professor T. Blackburn of St. Andrews College, North Carolina and has been funded by a Research grant from the University.

It was set up as an experimental system for gas chromatographic (GC) analysis of  $\text{CO}_2$ , hydrocarbons, sulphur-containing gases, together with  $\text{H}_2\text{O}$  released from the minerals. However, the design of the prototype is such that it only allows ~10% of the non-condensable gases to be sampled by the GC. This means that many gases ( $\text{CH}_4$ ,  $\text{N}_2$ ,  $\text{O}_2$ ) are below detection limits with the present system.

### Sample preparation

The sample is crushed sufficiently fine to produce individual grains of the required mineral, which will vary according to the sample to be studied. In practise grains within the size range 1.0mm and 0.5mm (mesh size BS+16 and -30) were found to be suitable. The mineral grains are then cleaned with dilute nitric acid followed by distilled water, to remove all admixed phases and ions adsorbed on the sample surface. Further details of sample preparation appear on pages 187-190 of Shepherd et al (1985).

### Analytical technique

The most versatile and inexpensive method for the analysis of volatile substances is Gas Chromatography, which has the ability to separate and characterise very small samples, such as the content of fluid inclusions in a typical geological sample of approximately 20-100 milligrams. It is particularly important to work with small samples, to avoid including anomalous and spurious sources of volatiles, because the results will have more geochemical significance if they are derived from a limited fluid inclusion population.

The Gas Chromatograph is fitted with a thermal conductivity detector and associated control circuits. The technique involves the separation of components of a mixture of substances by their differential movement through a porous medium of "carbosive" (carbon spherules) packed into chromatographic column. This differential movement is controlled by small differences in partitioning and adsorption-desorption properties between the individual gases and the solid within the column. The sample is transported by means of a carrier gas (helium) through the column in which the differential retardation takes place. The emergence of the gases on the other side of the column is monitored by the thermal conductivity detector.

The fluid is released from the minerals by decrepitation on heating to  $450^\circ\text{C} + 10^\circ$  under vacuum for 10 minutes. It is important to heat the sample quickly

without causing thermal decomposition of the released volatiles. The heating progress within the electrically heated tube furnace is monitored by a thermocouple.

Because the components of ordinary air ( $N_2, O_2, Ar, CO_2$ ) are important volatile constituents of fluid inclusions, the sample must be opened under vacuum which requires both a rotary oil forepump and a mercury diffusion pump. The system is equipped with high vacuum stopcocks throughout. The extraction train is therefore linked to a capacitance manometer which is a rugged and accurate device whose response is directly proportional to gas pressure and independent of the chemical identity of the gases. It is sensitive to  $10^{-3}$  torr.

### Analytical results

The analyses obtained are normally expressed as weight per volume  $H_2O$  although they can also be considered as mole concentrations. With regard to accuracy a sample of Carrock Fell quartz, previously analysed by Dr. Tom Sheppard of BGS, London on a Mass Spec. has been re-analysed by Richard Batchelor on the St. Andrews extraction train. The comparative results are shown below. Reproducibility of results has been based on analyses of Brazilian quartz which contains more  $CO_2$  than the Carrock Fell quartz. Reproducibility of results as shown below involves <10% error and the Brazilian quartz is now used as an internal standard.

### Accuracy - Carrock Fell Quartz (CF-77-77A)

	$(10^{-6} \text{ mole/g})$		
	$H_2O$	$CO_2$	Non condensibles
T. Shepherd analysis	7.47	0.15	0.03
St. Andrews	7.26	0.15	0.04
	7.53	0.14	0.04

### Reproducibility - Brazilian quartz

5.8	3.9	0.54	56.5	38.0	5.27
5.6	3.8	0.60	56	38	6
5.1	3.8	0.50	54.2	38.4	5.3
5.6	3.8	0.52	56.5	38.3	5.24

System error:  $0.05 \times 10^{-6}$  mole/g.

micromoles per g.

5.8.

3.9.

0.54.

1 micro  
mol.

Water

18 ppm.

1 micro mol CO<sub>2</sub>.

44 ppm

5.8  
3.9  
0.54  

---

10.24  

---

56.6  
38.0  
5.27  

---

99.87  

---

H<sub>2</sub>O  
CO<sub>2</sub>  
N.C.

10

56.0  
38.1  
2.6  

---

100.1  

---

9.41

~~59.8~~  
40.48  

---

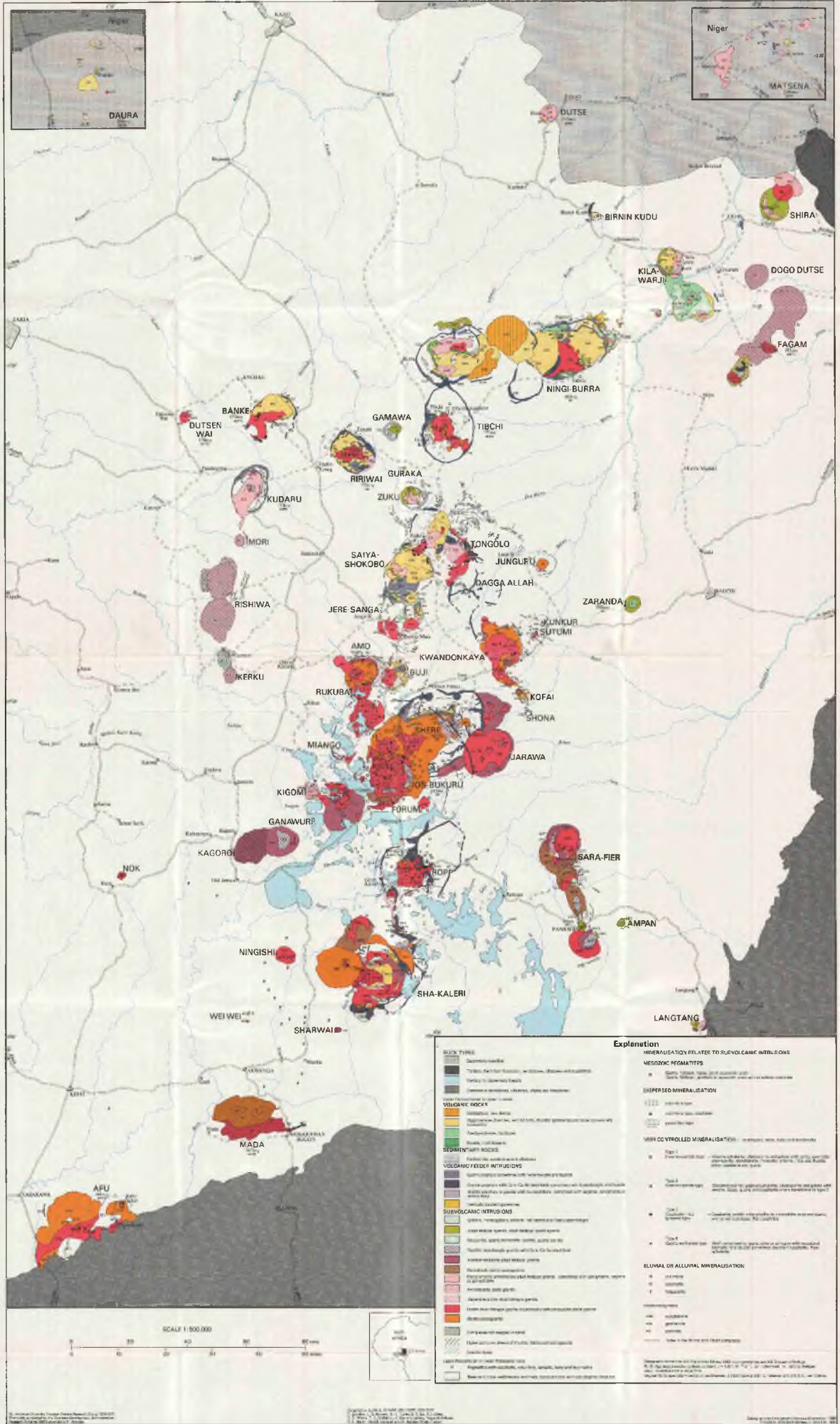
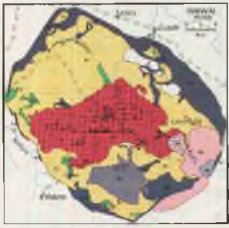
5.34  

---

100.  

---

9.92.



Index table listing various geological units, rock types, and symbols used on the map, organized in columns.

Explanation table detailing the symbols and colors used for different geological features, including Mesozoic pegmatites, dispersed mineralisation, and alluvial mineralisation.

